

A Field Study of Airflow in a High-Rise Multi-Unit Residential Building

by

Lorne Ricketts

A thesis
presented to the University of Waterloo
in fulfillment of the
thesis requirement for the degree of
Master of Applied Science
in
Civil Engineering

Waterloo, Ontario, Canada, 2014

© Lorne Ricketts 2014

Author's Declaration

I hereby declare that I am the sole author of this thesis. This is a true copy of the thesis, including any required final revisions, as accepted by my examiners.

I understand that my thesis may be made electronically available to the public.

Abstract

Airflow into, out of, and within buildings is fundamental to their design and operation as it can affect occupant health and comfort, building durability, and energy consumption. This thesis works to develop the understanding of airflow patterns and pressure regimes in high-rise multi-unit residential buildings which are both unique and complex due to the combination of their height, typical inclusion of operable windows, and compartmentalized layout. Specific attention is directed towards the performance of corridor pressurization based ventilation systems which are used pervasively within industry to ventilate and control contaminant transfer in these buildings.

Airflow is caused by pressure differences which for buildings are created by the driving forces of wind, stack effect, and mechanical ventilation systems. These airflows are resisted by the air permeance (i.e. airtightness) of building elements including the exterior enclosure and interior compartmentalizing elements. Using an experimental program at a case study building, this thesis assesses the interaction of these driving forces of airflow with the physical building to create the airflow patterns for a typical high-rise multi-unit residential building.

Perfluorocarbon tracer (PFT) testing was performed to measure in-service airflows into and out of the suites. This testing found that the air change rates of upper suites are significantly higher than that of lower suites and that most suites receive small fractions of modern ventilation rates or are over ventilated. Airflow measurements of the supply of ventilation air to each corridor indicate that these low flow rates are in part due to leakage of air from the supply duct. The PFT testing also found that significant airflow occurred from the parking garage below the building into the occupied building spaces indicating significant potential for transfer of harmful air contaminants.

The air permeance of the exterior enclosure and interior compartmentalizing elements were measured using neutralized fan pressurization and depressurization techniques and found to be within typical ranges. In particular this testing found that only 20% of the flow paths out of the corridor were to the adjacent suites through the suite entrance doors and that flows to the elevator shaft and stairwells could create a significant inefficiency in the ventilation system.

A long-term monitoring program was implemented at the case study building primarily to monitor exterior environmental conditions including wind and exterior temperature and to correlate these with measured pressure differences. A strong correlation was found between building pressure and exterior temperature. Nearly 70% of the theoretical stack effect pressure was measured to act across the corridor to suite pressure boundary which creates a significant pressure differences to be overcome by the ventilation system, likely contributing to the uneven distribution of ventilation rates. Both wind and stack effect pressures were found to often be of similar or greater magnitude than mechanically induced pressure differences and thus can overwhelm the ventilation system.

Overall, the corridor pressurization based ventilation system at the case study building does not effectively or efficiently ventilate the building and also does not provide sufficient control of air contaminants. As the case study building was found to be relatively representative of a typical multi-unit residential building, the findings from this building can be extended to many other buildings. Effective ventilation and airflow control in multi-unit residential buildings likely requires suite compartmentalization and direct supply of ventilation via ducted or in-suite systems.

Acknowledgements

Thank you to my supervisor, Dr. John Straube, for his guidance and trust in me throughout this project. His clarity of thought and wealth of building science knowledge enhanced this work, and what I have absorbed will serve me well.

Thank you to all of those at RDH Building Engineering that have helped with this work and contributed to my building science education over the years. In particular, thanks to Graham Finch and James Higgins for their thoughtful insights and continual hard work on this project; without them this work would have been much more difficult.

Thank you to my friends and colleagues in BEG, Emily Vance and Trevor Trainor, for their camaraderie, and to the staff at BSC for expanding my experience and being an excellent source of intelligent conversation and ever enjoyable building science banter.

Finally, thank you to my family for their continued support for whatever I decide to do, and to my girlfriend Linda for her support and patience while I completed my degree.

I would also like to gratefully acknowledge the funding support provided by NSERC and RDH.

Table of Contents

Author’s Declaration	iii
Abstract.....	v
Acknowledgements.....	vii
Table of Contents	ix
List of Figures.....	xv
List of Tables	xxix
Chapter 1 Introduction.....	1
1.1 Objectives	1
1.2 Approach.....	2
1.3 Scope.....	2
1.4 Organization of the Thesis.....	3
1.5 Disclaimer.....	4
Chapter 2 Pressure, Air Permeance, and Airflow Relationship.....	5
2.1 Airflow through Orifices.....	5
2.2 Airflow through Diffuse Media	5
2.3 Airflow through Cracks.....	6
2.4 Airflow through Building Pressure Boundaries	7
2.5 Density of Air	10
2.6 Nodal Analysis Approach.....	12
Chapter 3 Pressure Differences.....	17
3.1 Stack Effect.....	17
3.2 Wind	26
3.3 Mechanical Systems	40
3.3.1 ASHRAE Standard 62.1.....	40
3.3.2 Pressurized Corridor Ventilation System.....	43
3.3.3 Other Mechanical Systems.....	46
3.4 Combination of Driving Forces.....	46
Chapter 4 Air Permeance.....	55
4.1 Building Enclosure Air Barrier Systems	55
4.2 Compartmentalization	59
4.3 Airflow and Airtightness Metrics.....	60

4.3.1	Airflow Rate	60
4.3.2	Normalized Airflow Rate	60
4.3.2.1	Air Change Rate	61
4.3.3	Equivalent Leakage Area	61
4.3.4	Effective Leakage Area	62
4.3.5	Specific Leakage Area	62
4.3.6	Airflow per Unit Length	63
4.4	Airtightness Regulatory Requirements.....	63
4.5	Airflow Resistance of Materials, Components, and Assemblies.....	64
4.5.1	Airflow Resistance of Materials	64
4.5.2	Airflow Resistance of Building Components.....	65
4.5.3	Airflow Resistance of Stair Shafts.....	66
4.5.4	Airflow Resistance of Exterior Walls.....	66
4.6	Airtightness of Multi-Unit Residential Buildings Exterior Enclosure - Database	68
4.6.1	Airtightness of US Army Corps of Engineers Barracks	74
4.7	Airflow Resistance of Interior Compartmentalizing Elements	75
Chapter 5 Implications of Pressure Differences and Permeance for Ventilation		81
5.1	Dynamism of Natural Driving Forces.....	81
5.2	Occupant Controlled Dynamism	82
5.3	Ventilation Air Supply Flow Path	86
5.4	Movement of Air Contaminants	87
5.5	Changes in Flow Path Resistance.....	88
5.6	Fire and Smoke Control	90
5.7	Heat Recovery.....	91
Chapter 6 Testing and Measurement Techniques		93
6.1	Pressure Measurements.....	93
6.2	Airtightness Testing	95
6.2.1	Sequentially Neutralized Airtightness Testing.....	97
6.2.2	Alternative Multi-Zone Building Airtightness Testing Techniques	100
6.3	Airflow Measurements.....	101
6.3.1	Unpowered Flow Hood	101
6.3.2	Powered Flow Hood	102
6.3.3	Pitot Tube Traverse.....	103
6.3.4	Flow Velocity Measurement.....	103

6.3.5	Tracer Gas Testing	104
6.3.5.1	Concentration Decay	104
6.3.5.2	Constant Injection.....	104
6.3.5.3	Constant Concentration	104
6.3.5.4	Perfluorocarbon Tracer Testing.....	105
6.3.6	Visualization & Qualitative Techniques	105
6.3.6.1	Smoke	105
6.3.6.2	Sound Transmission.....	106
6.3.6.3	Infrared Thermography.....	106
6.4	Air Quality as an Indicator.....	107
Chapter 7 Testing and Monitoring of the Case Study Building.....		109
7.1	Introduction.....	109
7.1.1	Building and Project Overview	109
7.1.1.1	General Building Characteristics.....	111
7.1.1.2	Original Building Enclosure.....	113
7.1.1.3	Post-Retrofit Building Enclosure.....	114
7.1.1.4	Heating and Ventilation Systems	116
7.1.2	Objective.....	117
7.1.3	Approach.....	117
7.2	Measurement of Airflow between Zones	119
7.2.1	Objective.....	119
7.2.2	Approach.....	119
7.3	Mechanical Ventilation System Airflow Measurements	122
7.3.1	Bathroom Exhaust Fan Measurements	122
7.3.2	Make-up Air Unit Intake Testing.....	123
7.3.3	Make-up Air Unit Corridor Supply Measurements.....	123
7.4	Airtightness Testing.....	124
7.4.1	Objective.....	124
7.4.2	Approach.....	124
7.5	Pressure and Air Quality Monitoring Program.....	128
7.5.1	Objective.....	128
7.5.2	Approach.....	129
7.6	Weather Data	135
Chapter 8 Airflow Measurement and Testing Results.....		139

8.1	Make-Up Air Unit Intake.....	139
8.2	Make-Up Air Unit Supply to Corridor	142
8.3	Make-Up Air Unit Off.....	143
8.4	PFT Testing.....	144
8.4.1	Exterior Environmental Conditions During PFT Testing.....	144
8.4.2	Results of PFT Testing	147
8.5	Summary of Results.....	154
Chapter 9 Airtightness Testing Results		155
9.1	Suite Testing.....	155
9.2	Exterior Enclosure Testing of Floors 1 and 13	159
9.3	Floor 3 Suites versus Floor 11 Suites.....	160
9.4	Type -02 Suites versus Type -01 and -03.....	161
9.5	Demising Wall Comparison.....	162
9.6	Corridor Testing	163
9.6.1	Resistance to Airflow of Doors.....	165
9.7	Summary of Results.....	168
Chapter 10 Pressure Difference Monitoring Results.....		171
10.1	Guidance for Interpretation of the Monitoring Data	171
10.2	Exterior Enclosure Pressure Differences	173
10.2.1	Exterior Enclosure Pressure Differences and Exterior Temperature	173
10.2.2	Exterior Enclosure Pressure Differences and Wind.....	177
10.2.2.1	Minimal Wind	177
10.2.2.2	Light East Wind.....	180
10.2.2.3	Moderate East Wind	184
10.2.2.4	Moderate West Wind.....	189
10.2.2.5	Strong West Wind.....	192
10.2.3	Summary of Exterior Enclosure Results	197
10.3	Corridor-to-Corridor Pressure Differences.....	197
10.3.1	Corridor-to-Corridor Pressure Differences and Exterior Temperature	198
10.3.2	Corridor-to-Corridor Pressure Differences and Wind	201
10.3.3	Summary of Corridor-to-Corridor Results.....	202
10.4	Suite-to-Corridor Pressure Differences	202
10.4.1	Suite-to-Corridor Pressure Differences and Exterior Temperature	202
10.4.2	Suite-to-Corridor Pressure Differences and Wind.....	205

10.4.2.1	Moderate East Wind	206
10.4.2.2	Moderate West Wind.....	210
10.4.2.3	Strong West Wind.....	214
10.4.3	Summary of Suite-to-Corridor Results	218
10.5	Suite-to-Suite Pressure Differences.....	219
10.5.1	Suite-to-Suite Pressure Differences and Exterior Temperature.....	219
10.5.2	Suite-to-Suite Pressure Differences and Wind	223
10.5.2.1	Moderate East Wind	223
10.5.2.2	Moderate West Wind.....	226
10.5.2.3	Strong West Wind.....	230
10.5.3	Summary of Suite-to-Suite Results.....	234
10.6	Pressure Changes Due to Occupant Controlled Components	234
10.7	Location of the NPP and Thermal Draft Coefficient.....	243
10.8	Make-up Air Unit Pressures.....	250
10.9	Effect of the Retrofit.....	255
10.10	Summary of Results.....	255
Chapter 11	Airflows Calculated from Pressure and Air Permeance Measurements	257
11.1	Comparison of Measured and Calculated Airflow Rates.....	257
11.2	Calculated Airflow Rates	261
11.2.1	Calculated Airflow Rates and Exterior Temperature	261
11.2.2	Calculated Airflow Rates and Wind.....	263
Chapter 12	Indoor Air Quality Monitoring Results	269
12.1	Carbon Dioxide Concentrations	269
12.1.1	Periods of Vacancy	281
12.2	Dew Point Temperature	282
12.3	Summary of Results.....	290
Chapter 13	Conclusions and Recommendations.....	291
13.1	Conclusions.....	291
13.2	Recommendations	292
13.2.1	Recommendations for the Building Industry.....	294
13.2.2	Recommendations for Further Research.....	294
13.2.3	Recommendations for Implementation of Future Studies	295
References		297
Appendix A	Airflow Resistance of Building Elements	307

Appendix B Case Study Building Original Architectural and Mechanical Drawings	315
Appendix C Supplementary Airflow Measurement Information	335
Appendix D Supplementary Airtightness Testing Information	363
Appendix E Supplementary Monitoring Information.....	391
Appendix F Supplementary Calculated Airflow Graphs	471
Appendix G PFT Testing Report	485

List of Figures

Figure 2-1: Graph of flow rates across pressure boundary due to pressure difference for different flow exponent values assuming same flow rate at 75 Pa.....	9
Figure 2-2: Graph of Flow Rates through Pressure Boundary Due to Pressure Difference for Different Airtightness Values	10
Figure 2-3: Graph of impact on air density of changes in temperature, relative humidity, and atmospheric pressure	11
Figure 2-4: Schematic graphic of a high-rise multi-unit residential building illustrating the numerous zones and pressure boundaries.....	12
Figure 2-5: Graphic illustrating analogy of current flow between two points and airflow between two zones	13
Figure 2-6: Example building airflow nodal network for part of a building.....	14
Figure 2-7: Abstracted building illustrating nodal network concept	15
Figure 3-1: Graphic showing the development of pressure differences due to stack effect for a schematic building with no interior separations	18
Figure 3-2: Graph of pressure differences developed due to stack effect in a building.....	19
Figure 3-3: Graph of stack effect pressures overlaid on the number of hours different exterior temperatures occur in eight North American cities.....	20
Figure 3-4: Graphic showing a schematic building with significantly more air leakage paths at the bottom of the building than at the top thus shifting the NPP down to the bottom.....	21
Figure 3-5: Graphic showing a schematic building with significantly more air leakage paths at the top of the building than at the bottom thus shifting the NPP up to the top	22
Figure 3-6: Graphic showing a schematic building with interior zones having varying vertical distributions of leakage openings and thus different NPP locations	23
Figure 3-7: Graphics illustrating distribution of stack effect pressures in a building given different wall and floor air leakage configurations	24
Figure 3-8: Graphic illustrating thermal draft coefficient	25
Figure 3-9: Schematic representation of a stack effect pressures and flow within and through a building.....	26
Figure 3-10: Wind directional frequency and magnitude for Vancouver, BC from 2003 to 2012 at 10 meters above the ground	27
Figure 3-11: Wind directional frequency and magnitude for Calgary, AB from 2003 to 2012 at 10 meters above the ground	27
Figure 3-12: Wind directional frequency and magnitude for Winnipeg, MN from 2003 to 2012 at 10 meters above the ground	27
Figure 3-13: Wind directional frequency and magnitude for Toronto, ON from 2003 to 2012 at 10 meters above the ground	27

Figure 3-14: Wind directional frequency and magnitude for Montreal, QC from 2003 to 2012 at 10 meters above the ground	28
Figure 3-15: Wind directional frequency and magnitude for St. John's, NL from 2003 to 2011 at 10 meters above the ground	28
Figure 3-16: Probability Distribution of Wind Speeds at a Given Location According to a Weibull ($k = 2$).....	29
Figure 3-17: Boundary layer wind speed profiles with recognizable buildings for reference	30
Figure 3-18: Graph of wind stagnation pressure overlaid on the number of hours of various wind speeds in six Canadian cities.....	32
Figure 3-19: Local exterior wind pressure coefficients ($C_p \times 100$) for tall buildings (ASHRAE, 2009)	34
Figure 3-20: Roof pressure coefficient contours with wind from 0° (Brundrett, 1991)	35
Figure 3-21: Roof pressure coefficient contours with wind from 45° (Brundrett, 1991).....	35
Figure 3-22: Graphic showing distribution of wind pressure on the building enclosure	36
Figure 3-23: Graphic showing interior pressures due to wind with various different distributions of openings in a building enclosure (“p” denotes internal pressure coefficient) (Yeatts, 1992)	38
Figure 3-24: Schematic representation of wind pressures and flow within and through a building.....	39
Figure 3-25: Schematic representation corridor pressurization ventilation system	44
Figure 3-26: Graphic cross-section of a high-rise multi-unit residential building illustrating the operation of the corridor pressurization based ventilation approach.....	45
Figure 3-27: Graphic of a schematic building with a tilted neutral pressure plane created by wind pressure on the building.....	47
Figure 3-28: Graphic of a schematic building with a neutral pressure plane above the midpoint due to depressurization of the building created by the mechanical ventilation system.....	48
Figure 3-29: Graphic of a schematic building with neutral pressure plane below the midpoint due to pressurization of the building created by the mechanical ventilation system	48
Figure 3-30: Graphic of a schematic building with a neutral pressure plane above the building due to depressurization of the building created by the mechanical ventilation system.....	49
Figure 3-31: Graphic of a schematic building with neutral pressure plane below the building due to pressurization of the building created by the mechanical ventilation system	49
Figure 3-32: Schematic cumulative effect of driving forces of airflow on a tall MURB	50
Figure 3-33: Graph of proportion of total absolute pressure difference attributable to each of the driving forces for a 40 m tall building in Miami.....	51
Figure 3-34: Graph of proportion of total pressure difference attributable to each of the driving forces for a 40 m tall building in Vancouver	51
Figure 3-35: Graph of proportion of total pressure difference attributable to each of the driving forces for a 40 m tall building in Fairbanks.....	51
Figure 3-36: Graph of annual average proportion of total pressure difference attributable to each of the driving forces for various building heights in Vancouver.....	52

Figure 3-37: Graph of annual average proportion of total pressure difference attributable to each of the driving forces for a 40 m tall building in various North American cities	52
Figure 4-1: Exposed cast-in-place concrete wall assembly where the concrete is providing the air barrier. (Photo courtesy of RDH.)	56
Figure 4-2: Exterior gypsum sheathing sealed to provide the air barrier. (Photo courtesy of RDH.)	57
Figure 4-3: Interior plywood sheathing of pre-fabricated wall panel sealed with tape to provide the air barrier. (Photo courtesy of RDH.)	57
Figure 4-4: Exterior non-adhered sheathing membrane with seams taped to provide the air barrier. (Photo courtesy of RDH.).....	58
Figure 4-5: Exterior adhered sheathing membrane providing air barrier. (Photo courtesy of RDH.)	58
Figure 4-6: Closed cell spray foam insulation applied to exterior sheathing to provide air barrier with flexible membrane use at transitions and movement joints. (Photo courtesy of RDH.)	58
Figure 4-7: Building where curtain wall system provides the air barrier. (Photo courtesy of RDH.)	59
Figure 4-8: Chart of geographical distribution of buildings in the database	69
Figure 4-9: Chart of distribution of air barrier construction or modification date for buildings in the database	69
Figure 4-10: Chart of distribution of air barrier age when tested for buildings in the database	70
Figure 4-11: Chart of distribution of building height in storeys for buildings in the database	70
Figure 4-12: Graph of building enclosure airtightness value of buildings in the database	71
Figure 4-13: Graph of distribution of airtightness (q_{75}) of buildings in the database	71
Figure 4-14: Graph of exterior enclosure airtightness versus date of air barrier construction or modification for buildings in the database	72
Figure 4-15: Graph of exterior enclosure airtightness versus age of air barrier for buildings in the database	72
Figure 4-16: Graph of exterior enclosure airtightness versus building height for buildings in the database	73
Figure 4-17: Graph of distribution of flow exponent (n) values for buildings in the database	74
Figure 4-18: Graph of building enclosure airtightness value of USACE buildings in the database	75
Figure 4-19: Graph of distribution of airtightness (q_{75}) of USACE buildings in the database	75
Figure 5-1: Chart showing percent of operable window area open by floor (Proskiw & Phillips, 2008)	83
Figure 5-2: Unbalanced and balanced system reactions to a change in the flow path resistance	89
Figure 6-1: Graphic illustrating that there is no pressure difference between points in the same zone	94
Figure 6-2: Graphic illustrating that the pressure difference measured by a single gauge is equal to the sum of the pressure differences across the boundaries that the pressure measurement tubes cross for an uncompartimentalized building	94

Figure 6-3: Graphic illustrating how path of the tubes used for pressure measurement can impact the pressure measured because of stack effect.....	95
Figure 6-4: Graphic illustrating distribution of pressures during airtightness testing in cold weather	97
Figure 6-5: Typical Canvas Fan-Door Used for Airtightness Testing.....	98
Figure 6-6: Schematic showing sequentially neutralized pressurization/depressurization airtightness testing steps for a typical multi-unit residential building (Finch, Straube, & Genge, 2009)	99
Figure 6-7: Typical Unpowered Flow Hood apparatus.....	102
Figure 6-8: Typical Powered Flow Hood Apparatus.....	102
Figure 6-9: Typical hemispherical cup type anemometer used for measuring wind speed	103
Figure 6-10: Infrared thermographic images of a building from the exterior showing locations with no thermal anomaly in the left image and visible thermal anomalies in the right image once the building was pressurized indicating locations of airflow from the interior to the exterior (Images courtesy of RDH).....	106
Figure 7-1: North-east corner of the case study building post-retrofit (Photo courtesy of RDH)....	110
Figure 7-2: Typical floor the case study building.....	111
Figure 7-3: General geometric arrangement of buildings near to the case study building	112
Figure 7-4: Typical original exterior enclosure assembly below window	114
Figure 7-5: New wall assembly under construction at the case study building showing localized sealing with liquid applied membrane (red) at window head and sill, exterior mineral wool insulation, and fiberglass low conductivity clips (Photo courtesy of RDH).....	115
Figure 7-6: New wall assembly while under construction showing localized sealing at concrete slab cold joints, and cladding support system prior to installation of mineral wool insulation (Photo courtesy of RDH).....	115
Figure 7-7: Photo of outlet of in-slab exhaust duct at the case study building showing collapsed shape of the duct.....	117
Figure 7-8: Photo of interior of a duct at the case study building showing large pieces of debris within the duct.....	117
Figure 7-9: West elevation of the case study building indicating the primary, secondary, and tertiary monitoring and testing floors.....	118
Figure 7-10: PFT sources used at the case study building. Each colour is a different PFT tracer and the glass vials are “mega” sources of a distinct PFT used in the MAU.....	120
Figure 7-11: Typical CATS used for PFT testing at the case study building.....	120
Figure 7-12: Layout of PFT testing equipment on Floor 11 of the case study building	121
Figure 7-13: Photo of powered flow hood being used to test a bathroom fan at the case study building.....	122
Figure 7-14: MAU testing apparatus with green flex-duct to attach Retrotec fan to the MAU intake	123

Figure 7-15: A measurement of MAU airflow supplied to a corridor being made using a balometer	124
Figure 7-16: Airtightness testing schematic for Step 2 of pressurization of an -01 suite while pressure equalizing the floor above	126
Figure 7-17: Typical sealing of elevator doors for corridor airtightness testing using polyethylene sheet and PVC tape.....	127
Figure 7-18: Typical sealing of suite entrance door during corridor airtightness testing using polyethylene sheet and PVC tape.....	127
Figure 7-19: Two fan-doors used for airtightness testing of the case study building installed in a stairwell door (left) and a suite entrance door (right)	128
Figure 7-20: Laptop and four digital manometers used for controlling the airtightness testing fans and for making the pressure and airflow measurements during the test	128
Figure 7-21: Front face of a typical data acquisition unit used at the case study building showing the LCD screen to interact with the unit (top left), the carbon dioxide sensor (bottom left, round and white), and battery pack left.....	129
Figure 7-22: Front face of a typical data acquisition unit used at the case study building with the faceplate cover installed showing holes on the front of the cover to expose the temperature and relative humidity sensors (left) and pressure tube (top right).....	129
Figure 7-23: Typical SMT-A3 unit being installed in a wall above a suite entrance door	130
Figure 7-24: Typical data acquisition unit installed above a suite entrance door	130
Figure 7-25: Typical exterior pressure tap configuration	130
Figure 7-26: Legend of symbols used for interpretation of Figure 7-27 and Figure 7-28	131
Figure 7-27: Floor plan showing layout of monitoring equipment for Floors 3 and 11	132
Figure 7-28: North-south cross-section of the case study building illustrating how the pressure measurements are linked.....	133
Figure 7-29: Weather station installed on roof of the case study building	134
Figure 7-30: Elevation of case study building indicating location of the weather station and height of the anemometer and wind vane (weather station not to scale)	135
Figure 7-31: Graph of compiled exterior temperature, relative humidity, and dew point temperatures.....	136
Figure 7-32: Graph of compiled wind speed at the weather station (42.3 m above the ground)....	137
Figure 7-33: Graph of compiled wind direction	137
Figure 7-34: Chart of average wind speed and frequency during the monitoring and testing period	138
Figure 7-35: Graph of frequency of wind speeds during monitoring period and Weibull distribution based on the mean wind speed.....	138
Figure 8-1: Graph of MAU pitot tube pressure during the airflow testing of the MAU.....	139
Figure 8-2: Graph of MAU intake flow rate versus measured velocity pressure used to develop airflow versus measured pressure correlation.....	140

Figure 8-3: Graph of MAU intake flow rate based on pressure monitoring of pitot tube in duct	141
Figure 8-4: Graph of MAU supply airflow to corridors	142
Figure 8-5: Graph of airflow to and from MAU ventilation shaft with MAU off.....	144
Figure 8-6: Graph of wind speed and exterior temperature during PFT testing period	145
Figure 8-7: Graph of wind direction during PFT testing period	146
Figure 8-8: Chart of average wind speed and frequency during PFT testing period	147
Figure 8-9: Chart of airflow in to suites on Floor 3 and Floor 11 as determined by the PFT testing	148
Figure 8-10: Chart of airflow out of suites on Floor 3 and Floor 11 as determined by the PFT testing	148
Figure 8-11: Chart showing total air changes per hour of suite from all sources	150
Figure 8-12: Schematic cross section of the case study building showing the amount of PMCP tracer (which was released in the MAU duct on the roof) absorbed by the CATS in each zone	151
Figure 8-13: Chart showing the airflow rates from the parking garage to the lower zones of the building which were tagged with a PFT source	152
Figure 8-14: Schematic cross section of the case study building showing the amount of PDCB tracer (which was released in the parking garage) absorbed by the CATS in each zone	153
Figure 9-1: Graph of average airflow versus pressure difference relationship test results for the typical suites.....	155
Figure 9-2: Graph of average airflow versus pressure difference relationships for compartmentalizing elements of typical suites	156
Figure 9-3: Chart of distribution of airflow through compartmentalizing elements and exterior enclosure.....	156
Figure 9-4: Graph of average normalized airflow versus pressure difference relationships for compartmentalizing elements of typical suites	158
Figure 9-5: Graph of average normalized airflow rate for suite exterior enclosures pre- and post- retrofit.....	159
Figure 9-6: Graph of average normalized airflow rate for suite exterior enclosures on Floors 3 and 11 pre- and post-retrofit.....	161
Figure 9-7: Graph of average normalized airflow rate separated by suite type.....	162
Figure 9-8: Graph of average airflow versus pressure difference relationships for compartmentalizing elements of corridors	163
Figure 9-9: Chart of proportion of airflow through corridor compartmentalizing elements for each tested corridor	164
Figure 9-10: Chart of average proportion of airflow through corridor compartmentalizing elements	164
Figure 9-11: Graph of suite entrance door airflow rates at 75 Pa of the case study building compared to values from literature.....	166
Figure 9-12: Graph of airflow rate through suite entrance doors versus door undercut size	167

Figure 9-13: Graph of airflow rate through stairwell doors versus door undercut size.....	168
Figure 9-14: Floor plan of Floor 3 of the case study building showing the equivalent leakage areas of the measured pressure boundaries from the corridor and suite testing.....	169
Figure 9-15: Floor plan of Floor 11 of the case study building showing the equivalent leakage areas of the measured pressure boundaries from the corridor and suite testing.....	170
Figure 10-1: Floor plan of typical floor in the case study building schematically indicating the location of positive and negative pressure taps for the typical pressure sensors	172
Figure 10-2: Graph of 24 hour moving average of exterior enclosure pressure differences for Floor 3 and the exterior temperature.....	174
Figure 10-3: Graph of 24 hour moving average of exterior enclosure pressure differences for Floor 11 and the exterior temperature	174
Figure 10-4: Graph of 24 hour moving average of exterior enclosure pressure differences for Corridor 13 to roof and the exterior temperature.....	175
Figure 10-5: Graph of hourly exterior enclosure pressure differences for Floor 3 and the exterior temperature.....	176
Figure 10-6: Graph of hourly exterior enclosure pressure differences for Floor 11 and the exterior temperature.....	176
Figure 10-7: Graph of hourly exterior enclosure pressure differences from Corridor 13 to roof and the exterior temperature.....	177
Figure 10-8: Graph of wind speed and exterior temperature during period of minimal wind	178
Figure 10-9: Graph of wind speed squared during period of minimal wind	178
Figure 10-10: Graph of hourly pressure differences across exterior enclosure at Floor 3 during minimal wind	179
Figure 10-11: Graph of hourly pressure differences across exterior enclosure at Floor 11 during minimal wind	179
Figure 10-12: Graph of hourly pressure difference across exterior enclosure from Corridor 13 to roof during minimal wind.....	180
Figure 10-13: Graph of wind speed and exterior temperature during period of light east wind	181
Figure 10-14: Graph of wind direction during period of light east wind.....	181
Figure 10-15: Graph of wind speed squared during period of light east wind.....	182
Figure 10-16: Graph of hourly pressure differences across exterior enclosure at Floor 3 during light east wind.....	182
Figure 10-17: Graph of hourly pressure differences across exterior enclosure at Floor 11 during light east wind.....	183
Figure 10-18: Graph of hourly pressure difference across exterior enclosure from Corridor 13 to roof during light east wind	183
Figure 10-19: Graph of wind speed and exterior temperature during period of moderate east wind	184
Figure 10-20: Graph of wind direction during period of moderate east wind	185

Figure 10-21: Graph of wind speed squared during period of moderate east wind	185
Figure 10-22: Graph of hourly pressure differences across exterior enclosure at Floor 3 during moderate east wind	186
Figure 10-23: Graph of hourly pressure differences across exterior enclosure at Floor 11 during moderate east wind	186
Figure 10-24: Graph of hourly pressure difference across exterior enclosure from Corridor 13 to roof during moderate east wind.....	187
Figure 10-25: Image of North and East elevations of the case study building showing surrounding trees that provide local shielding with respect to wind	188
Figure 10-26: Graph of wind speed and exterior temperature during period of moderate west wind	189
Figure 10-27: Graph of wind direction during period of moderate west wind	190
Figure 10-28: Graph of wind speed squared during period of moderate west wind.....	190
Figure 10-29: Graph of hourly pressure differences across exterior enclosure at Floor 3 during moderate west wind.....	191
Figure 10-30: Graph of hourly pressure differences across exterior enclosure at Floor 11 during moderate west wind.....	191
Figure 10-31: Graph of hourly pressure difference across exterior enclosure from Corridor 13 to roof during moderate west wind	192
Figure 10-32: Graph of wind speed and exterior temperature during period of moderate west wind	193
Figure 10-33: Graph of wind direction during period of moderate west wind	193
Figure 10-34: Graph of wind speed squared during period of moderate west wind.....	194
Figure 10-35: Graph of hourly pressures differences across exterior enclosure at Floor 3 during moderate west wind.....	195
Figure 10-36: Graph of hourly pressure differences across exterior enclosure at Floor 11 during moderate west wind.....	195
Figure 10-37: Graph of hourly pressure difference across exterior enclosure from Corridor 13 to roof during moderate west wind	196
Figure 10-38: Graph of 24 hour moving average corridor pressures referenced to Corridor 13	198
Figure 10-39: Graph of 24 hour moving average corridor-to-corridor pressure differences.....	200
Figure 10-40: Graph of 24 hour moving average corridor pressures referenced to Corridor 13	200
Figure 10-41: Graph of hourly corridor pressure referenced to Corridor 13 during strong west wind	202
Figure 10-42: Graph of 24 hour moving average suite-to-corridor pressure differences averaged per floor and exterior temperature.....	203
Figure 10-43: Graph of hourly suite-to-corridor pressure differences averaged per floor and exterior temperature for one month.....	204

Figure 10-44: Graph of hourly suite-to-corridor pressure differences averaged per floor and exterior temperature for one week	204
Figure 10-45: Graph of hourly suite-to-corridor pressure differences averaged per floor during minimal wind	206
Figure 10-46: Graph of hourly suite-to-corridor pressure differences averaged per floor during light east wind.....	206
Figure 10-47: Graph of hourly suite-to-corridor pressure differences for Floor 2 during moderate east wind.....	207
Figure 10-48: Graph of hourly suite-to-corridor pressure differences for Floor 3 during moderate east wind.....	207
Figure 10-49: Graph of hourly suite-to-corridor pressure differences for Floor 4 during moderate east wind.....	208
Figure 10-50: Graph of hourly suite-to-corridor pressure differences for Floor 10 during moderate east wind.....	208
Figure 10-51: Graph of hourly suite-to-corridor pressure differences for Floor 11 during moderate east wind.....	209
Figure 10-52: Graph of hourly suite-to-corridor pressure differences for Floor 12 during moderate east wind.....	209
Figure 10-53: Graph of hourly suite-to-corridor pressure differences averaged per floor during moderate east wind.....	210
Figure 10-54: Graph of hourly suite-to-corridor pressure differences for Floor 2 during moderate west wind.....	211
Figure 10-55: Graph of hourly suite-to-corridor pressure differences for Floor 3 during moderate west wind.....	211
Figure 10-56: Graph of hourly suite-to-corridor pressure differences for Floor 4 during moderate west wind.....	212
Figure 10-57: Graph of hourly suite-to-corridor pressure differences for Floor 10 during moderate west wind.....	212
Figure 10-58: Graph of hourly suite-to-corridor pressure differences for Floor 11 during moderate west wind.....	213
Figure 10-59: Graph of hourly suite-to-corridor pressure differences for Floor 12 during moderate west wind.....	213
Figure 10-60: Graph of hourly suite-to-corridor pressure differences averaged per floor during moderate west wind.....	214
Figure 10-61: Graph of hourly suite-to-corridor pressure differences for Floor 2 during strong west wind	215
Figure 10-62: Graph of hourly suite-to-corridor pressure differences for Floor 3 during strong west wind	215

Figure 10-63: Graph of hourly suite-to-corridor pressure differences for Floor 4 during strong west wind	216
Figure 10-64: Graph of hourly suite-to-corridor pressure differences for Floor 10 during strong west wind.....	216
Figure 10-65: Graph of hourly suite-to-corridor pressure differences for Floor 11 during strong west wind.....	217
Figure 10-66: Graph of hourly suite-to-corridor pressure differences for Floor 12 during strong west wind.....	217
Figure 10-67: Graph of hourly suite-to-corridor pressure differences averaged per floor during strong west wind	218
Figure 10-68: Graph of 24 hour moving average suite-to-suite pressure differences for Floor 2 ...	220
Figure 10-69: Graph of 24 hour moving average suite-to-suite pressure differences for Floor 3 ...	220
Figure 10-70: Graph of 24 hour moving average suite-to-suite pressure differences for Floor 4 ...	221
Figure 10-71: Graph of 24 hour moving average suite-to-suite pressure differences for Floor 10.	221
Figure 10-72: Graph of 24 hour moving average suite-to-suite pressure differences for Floor 11.	222
Figure 10-73: Graph of 24 hour moving average suite-to-suite pressure differences for Floor 12.	222
Figure 10-74: Graph of hourly suite-to-suite pressure differences for Floor 2 and wind speed during moderate east wind	223
Figure 10-75: Graph of hourly suite-to-suite pressure differences for Floor 3 and wind during moderate east wind.....	224
Figure 10-76: Graph of hourly suite-to-suite pressure differences for Floor 4 and wind during moderate east wind.....	224
Figure 10-77: Graph of hourly suite-to-suite pressure differences for Floor 10 and wind during moderate east wind.....	225
Figure 10-78: Graph of hourly suite-to-suite pressure differences for Floor 11 and wind during moderate east wind.....	225
Figure 10-79: Graph of hourly suite-to-suite pressure differences for Floor 12 and wind during moderate east wind.....	226
Figure 10-80: Graph of hourly suite-to-suite pressure differences for Floor 2 and wind speed during moderate west wind.....	227
Figure 10-81: Graph of hourly suite-to-suite pressure differences for Floor 3 and wind during moderate west wind.....	227
Figure 10-82: Graph of hourly suite-to-suite pressure differences for Floor 4 and wind during moderate west wind.....	228
Figure 10-83: Graph of hourly suite-to-suite pressure differences for Floor 10 and wind during moderate west wind.....	228
Figure 10-84: Graph of hourly suite-to-suite pressure differences for Floor 11 and wind during moderate west wind.....	229

Figure 10-85: Graph of hourly suite-to-suite pressure differences for Floor 12 and wind during moderate west wind.....	229
Figure 10-86: Graph of hourly suite-to-suite pressure differences for Floor 2 and wind speed during strong west wind	230
Figure 10-87: Graph of hourly suite-to-suite pressure differences for Floor 3 and wind during strong west wind	231
Figure 10-88: Graph of hourly suite-to-suite pressure differences for Floor 4 and wind during strong west wind	231
Figure 10-89: Graph of hourly suite-to-suite pressure differences for Floor 10 and wind during strong west wind	232
Figure 10-90: Graph of hourly suite-to-suite pressure differences for Floor 11 and wind during strong west wind	232
Figure 10-91: Graph of hourly suite-to-suite pressure differences for Floor 12 and wind during strong west wind	233
Figure 10-92: Graph of hourly suite-to-suite pressure differences for Floor 2 showing occasions when suites became pressurized or depressurized relative to adjacent suites.....	235
Figure 10-93: Graph of hourly suite-to-suite pressure differences for Floor 3 showing occasions when suites became pressurized or depressurized relative to adjacent suites.....	236
Figure 10-94: Graph of hourly suite-to-suite pressure differences for Floor 4 showing occasions when suites became pressurized or depressurized relative to adjacent suites.....	236
Figure 10-95: Graph of hourly suite-to-suite pressure differences for Floor 10 showing occasions when suites became pressurized or depressurized relative to adjacent suites.....	237
Figure 10-96: Graph of hourly suite-to-suite pressure differences for Floor 11 showing occasions when suites became pressurized or depressurized relative to adjacent suites.....	237
Figure 10-97: Graph of hourly suite-to-suite pressure differences for Floor 12 showing occasions when suites became pressurized or depressurized relative to adjacent suites.....	238
Figure 10-98: Graph of hourly pressure across exterior enclosure at Suite 1102 (North elevation) showing depressurization	239
Figure 10-99: Graph of hourly pressure from Suite 1102 to Corridor 11 showing depressurization	239
Figure 10-100: Graph of hourly pressure versus airflow rate relationship for total of average suite pressure boundaries showing theoretical depressurization due to exhaust fan operation	240
Figure 10-101: Graph of hourly pressure differences between corridors for lower floors showing instances of depressurization	241
Figure 10-102: Graph of hourly pressure differences between corridors for upper floors showing instances of depressurization	241
Figure 10-103: Graph of hourly pressure difference between Corridor 13 and roof showing instances of depressurization	242
Figure 10-104: Figure showing calculation method for determination of the NPP location.....	244

Figure 10-105: Graph of 24 hour moving average location of the neutral pressure plane and exterior temperature.....	245
Figure 10-106: Graph of 24 hour moving average measured and theoretical stack effect gradients	246
Figure 10-107: Graph of 24 hour moving average of TDC across exterior enclosure of case study building.....	247
Figure 10-108: Graph of 24 hour moving average of TDC from corridor to exterior of case study building.....	247
Figure 10-109: Graph of 24 hour moving average of the pressure difference from Corridor 13 to the roof, the theoretical stack pressure, and exterior temperature.....	248
Figure 10-110: Graphic schematically illustrating the distribution of pressure difference due to stack effect at the case study building	250
Figure 10-111: Graph of hourly exterior enclosure pressure differences on Floor 3 when MAU off on February 6 th , 2013.....	251
Figure 10-112: Graph of hourly exterior enclosure pressure differences on Floor 11 when MAU off on February 6 th , 2013	252
Figure 10-113: Graph of hourly exterior enclosure pressure differences from Floor 13 to roof when MAU off on February 6 th , 2013.....	252
Figure 10-114: Graph of hourly corridor-to-corridor pressure differences when MAU off on February 6 th , 2013.....	253
Figure 10-115: Graph of hourly suite-to-corridor pressure differences when MAU off on February 6 th , 2013.....	254
Figure 11-1: Chart of airflow rates in to the suites on Floor 3 and Floor 11 as measured by the PFT testing.....	258
Figure 11-2: Chart of airflow rates in to the suites on Floor 3 and Floor 11 as determined using the airtightness testing results and monitored pressure differences	258
Figure 11-3: Chart of airflow rates out of the suites on Floor 3 and Floor 11 as measured by the PFT testing.....	259
Figure 11-4: Chart of airflow rates out of the suites on Floor 3 and Floor 11 as determined using the airtightness testing results and monitored pressure differences	259
Figure 11-5: Chart of average airflow rates in to the suites on Floor 3 and Floor 11 as measured by the PFT testing and as determined using the airtightness testing results and monitored pressure differences.....	260
Figure 11-6: Chart of average airflow rates out of the suites on Floor 3 and Floor 11 as measured by the PFT testing and as determined using the airtightness testing results and monitored pressure differences.....	261
Figure 11-7: Chart of the average flow into and out of the lower suites of the case study building during January and July	262
Figure 11-8: Chart of the average flow into and out of the upper suites of the case study building during January and July	262

Figure 11-9: Chart of the average flow into and out of Suite 303 during a moderate east wind	264
Figure 11-10: Chart of the average flow into and out of Suite 1103 during a moderate east wind.	264
Figure 11-11: Chart of the average flow into and out of Suite 301 during a moderate west wind ..	265
Figure 11-12: Chart of the average flow into and out of Suite 1101 during a moderate west wind	265
Figure 11-13: Chart of the average flow into and out of Suite 301 during a strong west wind.....	266
Figure 11-14: Chart of the average flow into and out of Suite 1101 during a strong west wind	266
Figure 12-1: Graph of corridor and MAU carbon dioxide concentrations.....	270
Figure 12-2: Graph of average suite carbon dioxide concentration by floor and MAU carbon dioxide concentration	272
Figure 12-3: Graph of 24 hour moving average suite and corridor CO ₂ concentration on Floor 2..	273
Figure 12-4: Graph of 24 hour moving average suite and corridor CO ₂ concentration on Floor 3..	273
Figure 12-5: Graph of 24 hour moving average suite and corridor CO ₂ concentration on Floor 4..	274
Figure 12-6: Graph of 24 hour moving average suite and corridor CO ₂ concentration on Floor 10	274
Figure 12-7: Graph of 24 hour moving average suite and corridor CO ₂ concentration on Floor 11	275
Figure 12-8: Graph of 24 hour moving average suite and corridor CO ₂ concentration on Floor 12	275
Figure 12-9: Graph of suite air changes rates versus average carbon dioxide concentrations during the PFT testing period	276
Figure 12-10: Graph of airflow rates into suites versus average carbon dioxide concentrations during the PFT testing period	277
Figure 12-11: Graph of 24 hour moving average CO ₂ concentration in Suite 301.....	278
Figure 12-12: Graph of 24 hour moving average CO ₂ concentration in Suite 302.....	278
Figure 12-13: Graph of 24 hour moving average CO ₂ concentration in Suite 303.....	279
Figure 12-14: Graph of 24 hour moving average CO ₂ concentration in Suite 1101	279
Figure 12-15: Graph of 24 hour moving average CO ₂ concentration in Suite 1102	280
Figure 12-16: Graph of 24 hour moving average CO ₂ concentration in Suite 1103	280
Figure 12-17: Graph of 24 hour moving average CO ₂ concentration in Suite 201 showing periods of vacancy	282
Figure 12-18: Graph of 24 hour moving average corridor and MAU intake air dew point temperatures.....	283
Figure 12-19: Graph of 24 hour moving average suite and corridor dew point temperature on Floor 2	283
Figure 12-20: Graph of 24 hour moving average suite and corridor dew point temperature on Floor 3	284
Figure 12-21: Graph of 24 hour moving average suite and corridor dew point temperature on Floor 4	284
Figure 12-22: Graph of 24 hour moving average suite and corridor dew point temperature on Floor 10.....	285

Figure 12-23: Graph of 24 hour moving average suite and corridor dew point temperature on Floor 11..... 285

Figure 12-24: Graph of 24 hour moving average suite and corridor dew point temperature on Floor 12..... 286

Figure 12-25: Graph of 24 hour moving average dew point temperatures in Suite 301 287

Figure 12-26: Graph of 24 hour moving average dew point temperatures in Suite 302 287

Figure 12-27: Graph of 24 hour moving average dew point temperatures in Suite 303 288

Figure 12-28: Graph of 24 hour moving average dew point temperatures in Suite 1101..... 288

Figure 12-29: Graph of 24 hour moving average dew point temperatures in Suite 1102..... 289

Figure 12-30: Graph of 24 hour moving average dew point temperatures in Suite 1103..... 289

List of Tables

Table 3-1: Atmospheric Boundary Layer Parameters (Reproduced from ASHRAE, 2009)	30
Table 3-2: Stagnation Pressure Statistics for Six Canadian Cities	33
Table 3-3: Excerpt of Minimum Ventilation Rates Table in ASHRAE 62.1-2010	41
Table 3-4: Excerpt of Minimum Exhaust Rates Table in ASHRAE 62.1-2010	42
Table 4-1: Airtightness Properties of Common Construction Materials	65
Table 4-2: Airflow Characteristics of Exterior Walls – Colliver et al (1994)	67
Table 4-3: Airflow Characteristics of Exterior Wall – Orne et al (1998)	67
Table 4-4: Airflow Characteristics of Interior Walls.....	77
Table 4-5: Airflow Characteristics Ceilings and Floors.....	77
Table 4-6: Airflow Distribution of Suites - (Gulay, Stewart, & Foley, 1993)	78
Table 4-7: Airflow Distribution of Suites – Finch (2007)	78
Table 4-8: Airflow Increased Due to Unsealing of Components during Whole Floor Airtightness Testing - (Gulay, Stewart, & Foley, 1993).....	79
Table 9-1: Summary of Suite Entrance Door Measurements and Observations.....	166

Chapter 1 Introduction

Airflow into, out of, and within buildings is a fundamental factor of building design and operation, as building airflow patterns impact occupant health and comfort, building durability, and energy consumption. The height, typical inclusion of operable windows, and compartmentalized nature of high-rise multi-unit residential buildings makes them both unique and complex, and to efficiently and effectively ventilate these types of buildings, an understanding of airflow within and through them is required. This understanding should include consideration of the driving forces of airflow and their interaction with the physical building including the building enclosure and interior compartmentalizing elements. While significant work has been conducted to understand airflows in houses and commercial buildings, multi-unit residential buildings pose unique challenges and are less well understood.

The majority of high-rise multi-unit residential buildings in Canada and the United States are ventilated using a corridor pressurization based ventilation system. This system is intended to pressurize the corridors to provide ventilation air to suites, and to control and dilute air contaminants. This supply air system is commonly supplemented with intermittent point source exhaust fans. Despite common anecdotal accounts of poor performance, and supporting research, the use of this ventilation system in high-rise multi-unit residential buildings is pervasive. Performance complaints include high humidity levels, sound transfer, and migration of cooking odours and vehicle exhaust fumes.

Historically, building enclosures have been sufficiently leaky to provide significant ventilation through infiltration which could help compensate for ventilation system performance issues; however, infiltration rates are being significantly reduced as the airtightness of building enclosures improves to meet more stringent comfort and health expectations, durability performance targets, and energy consumption targets. Additionally, changes in the distribution and magnitude of building airtightness can change the distribution of pressure differences thus altering airflow patterns. These types of complex interactions between building systems are seldom considered in design, including in particular the interaction between ventilation systems and the building enclosure and compartmentalizing elements.

Work in this field has been ongoing for many years, and much progress has been made; however, conclusions with direct implication for the building industry are limited. Through an extensive experimental program conducted at a case study building, this thesis focuses on measurements of airflows and factors which affect these airflows. It uses these measurements to assess in-service airflow patterns including the performance of the corridor pressurization ventilation system.

1.1 Objectives

This thesis seeks to contribute to the general understanding of airflow in high-rise compartmentalized buildings, and in particular multi-unit residential buildings. Specifically, this work aims to evaluate the interactions between the physical building, mechanical ventilation systems, interior and exterior environmental conditions, and building occupants, to develop an understanding of how these factors act together to create building airflow patterns. This includes

evaluation of pressurized corridor mechanical ventilation system performance. Based on the results of this analysis, this thesis aims to draw conclusions and to generate recommendations with respect to ventilation and airflow control for high-rise multi-unit residential buildings.

1.2 Approach

This thesis begins with a review of the physics of airflow within and through buildings and develops a nodal network model of airflow in buildings which provides a conceptual tool to facilitate subsequent discussion and analysis. A discussion of the causes of pressure differences in buildings is then provided followed by a discussion of the air permeance of building elements. The discussion of building air permeance includes the development of a multi-unit residential building exterior enclosure airtightness database to provide a benchmark for subsequent airtightness testing results. A review of previous findings with respect to airflow in buildings is then provided, and testing and measurement techniques are reviewed. This review of the relevant physics and available literature forms the base on which the main work of this thesis is founded.

The thesis work then uses this base to develop an experimental testing and monitoring program for a selected case study building located in Vancouver, British Columbia. This program includes measurements of airflow rates between zones and from the ventilation system, airtightness testing of both exterior and interior building elements, and long-term monitoring of building performance characteristics including pressure differences. Based on the results of the testing and monitoring program for the case study building, conclusions are developed regarding airflow in high-rise multi-unit residential buildings. An effort is made to extend these conclusions to recommendations for industry.

1.3 Scope

The findings of this work are based on a review of existing work in this field and new work performed at the case study building. Although the work focusses on airflow specifically within high-rise multi-unit residential buildings, parts of the work may be applicable to other building types. For the purposes of this work, “high-rise” buildings refers to buildings where wind and stack effect have the potential to be dominant driving forces of airflow due to the building height and wind exposure respectively. This definition typically includes buildings of 4 storeys or more in height.

While this work seeks to evaluate the performance of corridor pressurization ventilation systems in this type of building, a review of the various mechanical ventilation systems available and a detailed review of mechanical system components such as fans and motors is outside the scope of this work.

The results of this work are likely broadly applicable; however, as testing was conducted on a single building due to a combination of logistics and project budget, the results of this thesis work are not sufficient to provide a statistically significant sample. This is typical of experimental programs in this field of study due to the diversity of building design, geographic location, and climatic conditions in which buildings operate, as well as to relatively limited access to buildings for research.

1.4 Organization of the Thesis

The chapters of this thesis are introduced below with a brief outline of their content:

1. Introduction

Develops the premise of the research and provides an outline of the thesis work.

2. Pressure, Air Permeance, and Airflow Relationship

Provides discussion of the physics of airflow across pressure boundaries and develops the airflow nodal network approach to building airflow.

3. Pressure Differences

Provides discussion of the causes of pressure differences in high-rise multi-unit residential buildings: stack effect, wind, and mechanical systems.

4. Air Permeance

Describes various building assemblies designed to resist airflow and provides a summary of a multi-unit residential building exterior enclosure airtightness database.

5. Implications of Pressure Difference and Air Permeance for Ventilation

Provides a review of literature with respect to how pressure differences and air permeance interact with ventilation systems to create airflow patterns.

6. Testing and Measurement Techniques

Provides a review of testing and measurement techniques with respect to airflow, pressure differences, and air permeance for buildings.

7. Testing and Monitoring of the Case Study Building

Presents the objectives and methodology of the testing and monitoring program conducted at the case study building.

8. Airflow Measurement and Testing Results

Provides the results of airflow measurements at the case study building including PFT testing, and make-up air unit flow measurements.

9. Airtightness Testing Results

Presents results of the testing and monitoring program including analysis and synthesis.

10. Pressure Difference Monitoring Results

Provides analysis of the pressure difference monitoring data including consideration of the effect of each of the driving forces of airflow.

11. Reconciliation of the Nodal Network

Using the measured air permeance of the building elements and the monitored pressure differences, airflow rates are calculated and compared with the measured results.

12. Indoor Air Quality Monitoring Results

Provides analysis of the indicators of indoor air quality monitoring data.

13. Conclusions and Recommendations

Conclusions are drawn and then extended to recommendations for the implementation of future studies, for the building industry, and for further research.

Appendices are also included and provide supplementary information.

1.5 Disclaimer

This thesis work was performed in partnership with RDH Building Engineering Ltd. (RDH) and forms part of a larger study of multi-unit residential building energy use being led by RDH. Due to the nature of the funding arrangement and industry partnership, components of this work have been provided to RDH and may also appear in the associated RDH reports; however, all content of this thesis is the original work of this thesis' author and was originally created for this document.

Chapter 2

Pressure, Air Permeance, and Airflow Relationship

Airflow in all contexts is caused by pressure differences across a flow path. Both a pressure difference and flow path are necessary for airflow to occur, and the rate is governed by the magnitude of the pressure difference and the resistance to airflow provided by the flow path. For buildings, pressure differences are created by either the natural causes of wind and stack effect, or by mechanical ventilation systems, which collectively will be referred to as *driving forces* of airflow and are discussed in detail in Chapter 3. These driving forces move air within and through buildings. This airflow is resisted by various building elements including exterior and interior walls, doors, windows, floors, elevator doors, et cetera. For the purposes of this thesis, these building elements which resist airflow will be referred to as *pressure boundaries* because pressure differences can develop across these elements due the resistance to airflow.

Equations have been developed to describe the physics of airflow through different types of pressure boundaries, and these equations have been selected and applied to the topic of this thesis work, airflow within and through buildings. This chapter presents the relevant equations describing airflow across different pressure boundary types and then describes a conceptual model based on these equations which can be used as an aid to understand the complex interactions and airflow patterns developed in buildings.

2.1 Airflow through Orifices

When air flows through a sharp edged orifice the pressure-flow relationship can be described by a formula derived from Bernoulli's Equation which is shown in Eq. 2.1. This type of flow is considered to be completely turbulent and in a building may occur at flow paths such as open windows, where the depth of the flow path is small relative to the opening size.

$$Q = C_d \cdot A \cdot \sqrt{\frac{2 \cdot \Delta P}{\rho}} = \left[\frac{C_d \cdot A}{(\rho/2)^{0.5}} \right] \cdot \Delta P^{0.5} \quad \text{Eq. 2.1}$$

Where: Q = Airflow from High to Low Pressure [m³/s]
C_d = Discharge Coefficient [dimensionless]
A = Orifice Area [m²]
ΔP = Pressure Difference [Pa]
ρ = Air Density [kg/m³]

The discharge coefficient (C_d) is used to account for the resistance to flow as a result of turbulence, friction, and flow contraction. While most values of the discharge coefficient must be found experimentally for the given orifice geometry, a discharge coefficient of 0.611 ($\pi/(2+\pi)$) was calculated by Kirchhoff for flow through a circular sharp edged orifice, and this value is often used when experimental data is unavailable. (Retech; Straube & Burnett, 2005)

2.2 Airflow through Diffuse Media

The flow-pressure relationship of laminar air flow through diffuse media can be described by Darcy's Law as shown in Eq. 2.2. This type of flow is considered to be completely laminar.

$$Q = K \cdot A \cdot \Delta P \quad \text{Eq. 2.2}$$

Where: Q = Airflow from High to Low Pressure [m³/s]
K = Air Permeance of Media [m/s·Pa]
A = Flow Cross-Sectional Area [m²]
ΔP = Pressure Difference [Pa]

In building applications this type of flow may occur through the field of a material such as gypsum board or a sheet membrane product. The air permeance of the media through which the airflow occurs is a material property which must be determined experimentally.

2.3 Airflow through Cracks

Airflow through sharp edged orifices and airflow through diffuse media provide the completely turbulent and completely laminar bounds on airflow types; however, other types of flow paths exist that fall between these two bounds. For building pressure boundaries, these types of flow are typically considered to be crack flow, and combine the characteristics of flow through sharp edged orifices and flow through diffuse media. As an example, crack flow in buildings may occur between a closed door and its frame, or between two adjacent wood studs. Depending on the ratio between the length of the flow path through the crack and the opening cross-sectional dimensions (e.g. for a circle, the diameter), the flow through these types of openings can be more similar to turbulent flow (for a lower ratio) or more similar to laminar flow (for a higher ratio). (Straube & Burnett, 2005)

Airflow through cracks can be theoretically represented using a combination of orifice and diffuse flow as shown in Eq. 2.3. (Baker, Sharples, & Ward, 1987) This equation is Eq. 2.1 and Eq. 2.2 rearranged to solve for the pressure difference and then summed, and it indicates that the pressure drop across a crack can be represented by the sum of the pressure drops due to the turbulent and laminar flow components.

$$\Delta P = C_1 Q + C_2 Q^2 \quad \text{Eq. 2.3}$$

Where: ΔP = Pressure Difference [Pa]
Q = Airflow from High to Low Pressure [m³/s]
C₁ = Coefficient [Pa·s/m³]
C₂ = Coefficient [Pa·s²/m⁶]

While this equation is theoretically appropriate, the determination of the different types of flow with meaningful accuracy is not possible in many situations and adds complexity due to the inclusion of multiple coefficients. Consequently, this equation is primarily useful for academic study of airflow paths, and for general application a simplified form is more useful. Airflow through cracks has been empirically found to be well represented by Eq. 2.4. (Etheridge, 1977; Kronvall, 1991; Baker, Sharples, & Ward, 1987) This equation is not as theoretically accurate as Eq. 2.3 due to lack of dimensional consistency; however, it has gained general acceptance. (Etheridge, 1977)

$$Q = C_{crack} \cdot \Delta P^{n_{crack}} \quad \text{Eq. 2.4}$$

Where: Q = Airflow from High to Low Pressure [m³/s]
 C_{crack} = Crack Flow Coefficient [m³/s·Paⁿ]
 ΔP = Pressure Difference [Pa]
 n_{crack} = Crack Flow Exponent [dimensionless]

The crack flow exponent in this equation is bounded by the lower limit of 0.5 provided by turbulent sharp edged orifice flow and by the upper limit of 1.0 provided by laminar flow through diffuse media. It has been found to be approximately 0.63; however, the precise value depends on the crack geometry. (Etheridge, 1977; Kronvall, 1991; Baker, Sharples, & Ward, 1987)

2.4 Airflow through Building Pressure Boundaries

Airflow through building pressure boundaries is unlikely to be exclusively any one of the preceding three flow types and instead is likely a combination. Thus, theoretically, the flow through building assemblies can be described by summing the flows for each of these different types; however, any attempt to represent the broad range of flow types through building elements using this theoretical approach is unnecessarily complex and unlikely to succeed due the quantity and complexity of the flow paths. Consequently, similar to crack flow, a simplified empirical approach as shown in Eq. 2.5 has proved most useful and provides acceptable accuracy. (Sherman & Chan, 2004; ASHRAE, 2009; Tamura & Shaw, 1976; Straube & Burnett, 2005; Thorogood, 1979; Proskiw & Phillips, 2008) This equation is of the same form as the empirical crack flow equation (Eq. 2.4) except with a generalized flow coefficient and flow exponent.

$$Q = C \cdot \Delta P^n \quad \text{Eq. 2.5}$$

Where: Q = Airflow from High to Low Pressure [m³/s]
 C = Flow Coefficient [m³/s·Paⁿ]
 ΔP = Pressure Difference [Pa]
 n = Flow Exponent [dimensionless]

This equation is commonly referred to as the power law airflow relationship. The flow coefficient (C) and the flow exponent (n) are characteristics unique to each building pressure boundary and are experimentally determined through airtightness testing. As with crack flow, the flow exponent is limited to a range of 0.5 to 1.0 as these values correspond with completely turbulent and completely laminar flow respectively as shown in Eq. 2.1 and Eq. 2.2. When the flow coefficient is measured outside of this range it indicates that the physical characteristics of the pressure boundary changed during the test. For example, higher pressure differences may cause windows to seal more completely, or they may make laps in a membranes open wider, both of which change the physical properties of the associated pressure boundaries. Typically, the flow exponent for a building enclosure is approximately 0.65, and often if multi-point airtightness testing is not performed, this value is assumed. (Straube & Burnett, 2005; Orne, Liddament, & Wilson, 1998)

Eq. 2.5 is also sometimes provided in the normalized form shown in Eq. 2.6.

$$q = \frac{C \cdot (\Delta P)^n}{A} \quad \text{Eq. 2.6}$$

Where: q = Airflow from High to Low Pressure per Unit Area [$\text{m}^3/\text{s}\cdot\text{m}^2$]
 A = Area [m^2]
 C = Flow Coefficient [$\text{m}^3/\text{s}\cdot\text{Pa}^n$]
 ΔP = Pressure Difference [Pa]
 n = Flow Exponent [dimensionless]

There is some discrepancy in the literature regarding the flow coefficient (C). In some cases the flow coefficient is provided as it is in Eq. 2.5 and Eq. 2.6; however, in other cases it is presented as what this thesis will refer to as a *normalized flow coefficient*. The calculation of this coefficient is shown in Eq. 2.7.

$$C_N = \frac{C}{A} \quad \text{Eq. 2.7}$$

Where: C_N = Normalized Flow Coefficient [$\text{m}^3/\text{s}\cdot\text{Pa}^n$]
 C = Flow Coefficient [$\text{m}^3/\text{s}\cdot\text{Pa}^n$]
 A = Area [m^2]

While the flow coefficient provides information about the total flow that will occur through a pressure boundary, the normalized flow coefficient is useful as it provides a normalized metric that allows for comparison of the airflow resistance of pressure boundaries irrespective of boundary area. It is most suitable when comparing the air permeance of different pressure boundaries, or when predicting the amount of air that will flow through a pressure boundary for which measured data is not available.

To illustrate the impact of the flow coefficient on flow rates, Figure 2-1 shows the relationship between airflow and pressure difference for flow exponent values of 0.5, 0.65 and 1.0 assuming the same airtightness (also referred to as air permeance) of $1.5 \text{ L}/\text{s}\cdot\text{m}^2$ at 75 Pa. It is important to realize that while these curves all have the same airtightness at 75 Pa, at other pressure differences, including specifically at lower pressure differences more typical of pressure differences for buildings, there can be a significant difference in the airflow rates. As an example, this difference is illustrated at 20 Pa where the normalized flow rate for a flow exponent of 0.5 is nearly double the normalized flow rate for an exponent of 1.0.

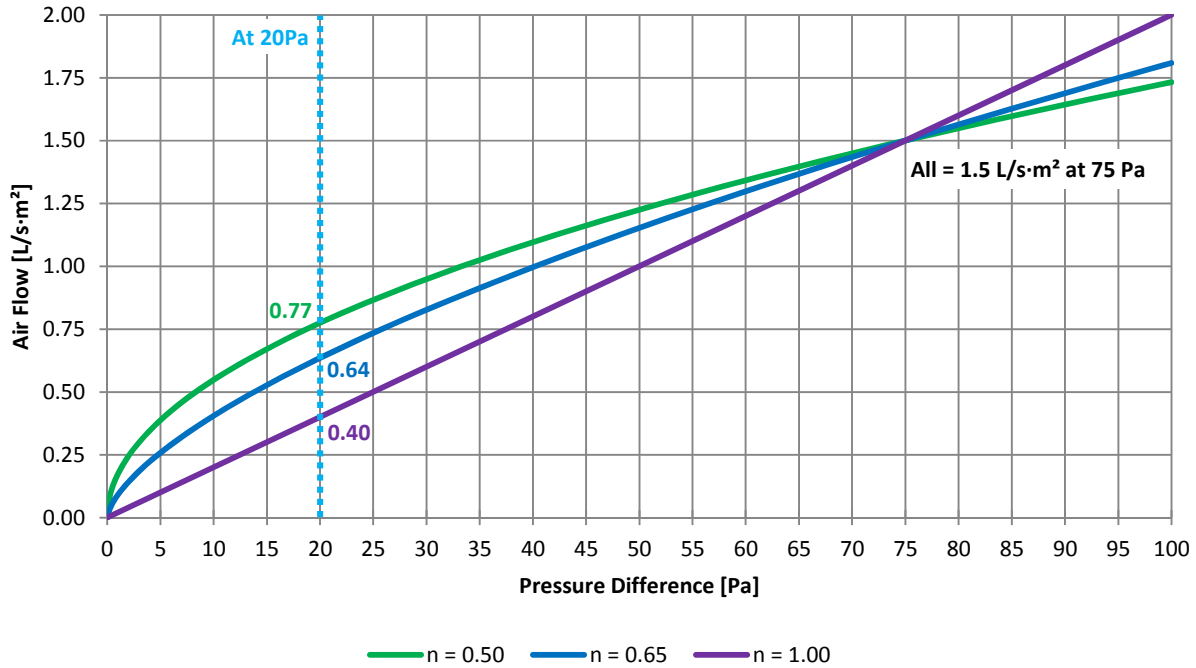


Figure 2-1: Graph of flow rates across pressure boundary due to pressure difference for different flow exponent values assuming same flow rate at 75 Pa

Typical airtightness values and testing methods and are discussed in Chapter 4 and Chapter 6 respectively; however, by assuming a flow exponent of 0.65 and using the tight, average, and leaky airtightness values (3.0, 1.5 and 0.5 L/s·m² at 75 Pa respectively) as suggested by ASHRAE (2009) based on Tamura & Shaw (1976), the graph in Figure 2-2 has been developed to show the amount of air flow that will occur across a separating element given a pressure difference. (These values may be somewhat antiquated based on current construction methods; however, they are still appropriate for this illustration of relative flow rates. Further discussion of airtightness values is provided in Chapter 4.)

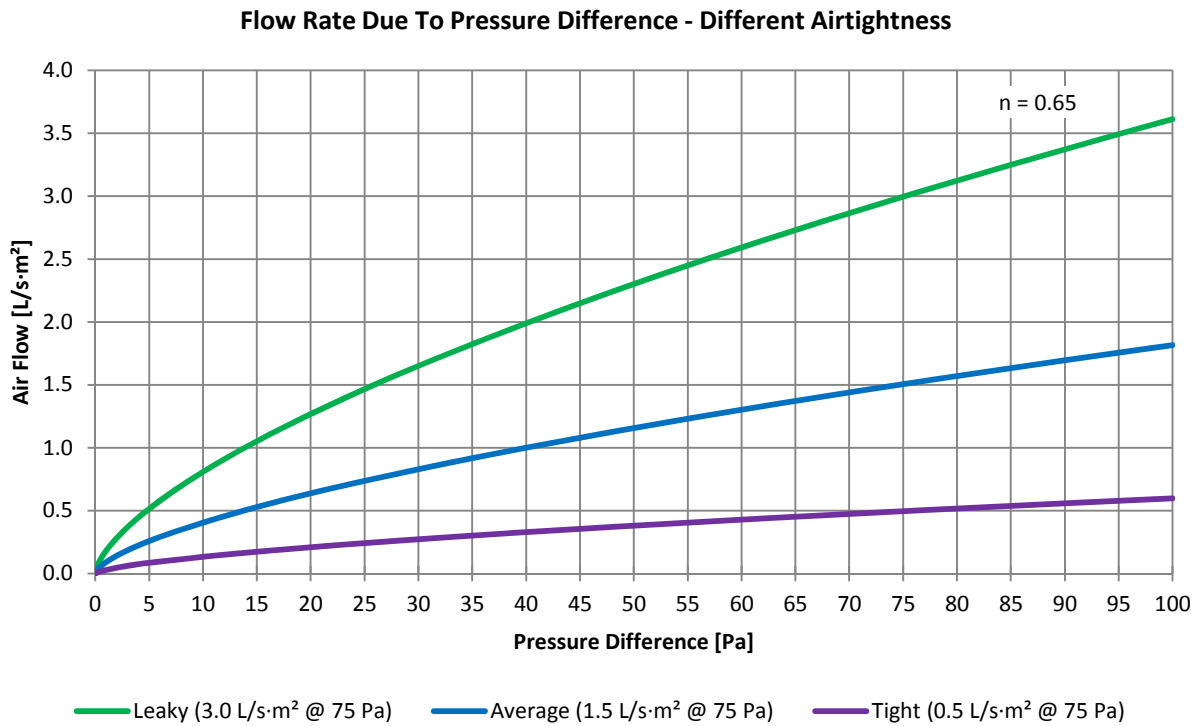


Figure 2-2: Graph of Flow Rates through Pressure Boundary Due to Pressure Difference for Different Airtightness Values

Fundamental to Eq. 2.5 is that to create airflow through a pressure boundary, a pressure difference must exist. Consequently, if air is forced into a space (e.g. by a fan), a pressure difference must develop across the pressure boundaries of that space to drive flow out of the space such that conservation of mass (airflow into the space equals airflow out of the space) is maintained. The development of this pressure difference to create flow is fundamental to the design intent of the corridor pressurization system.

2.5 Density of Air

The preceding airflow equations presented in this chapter are provided using volumetric flow rates as is common practice; however, fundamentally these airflow equations should be written as conservations of mass (rather than volume) to account for potential density differences. There are primarily three different causes of changes in density differences of air with respect to buildings and these are absolute (barometric) pressure, temperature, and humidity. A sensitivity analysis was performed to examine the change in air density due to changes in these parameters using a baseline condition of 20°C, 40% relative humidity, and atmospheric pressure of 101.325 kPa which are common values for air in buildings. The results of this analysis are provided in Figure 2-3. This figure shows the change in density compared to the percent change in these values to illustrate the relative sensitivity of air density to changes in these parameters. The ranges of these values used in the figure were selected to illustrate the changes in these parameters that could be reasonably expected with respect to buildings. The range of absolute pressures is from +500Pa to -500Pa from the baseline value is a conservatively large range for typical pressure differences at buildings. Note

that the range of absolute pressures selected is for consideration of conservation of volume versus conservation of mass; consequently, this range does not include larger fluctuations in absolute pressure which may occur due to weather or altitude as these changes would affect the pressure in all zones of a building as well as the exterior.

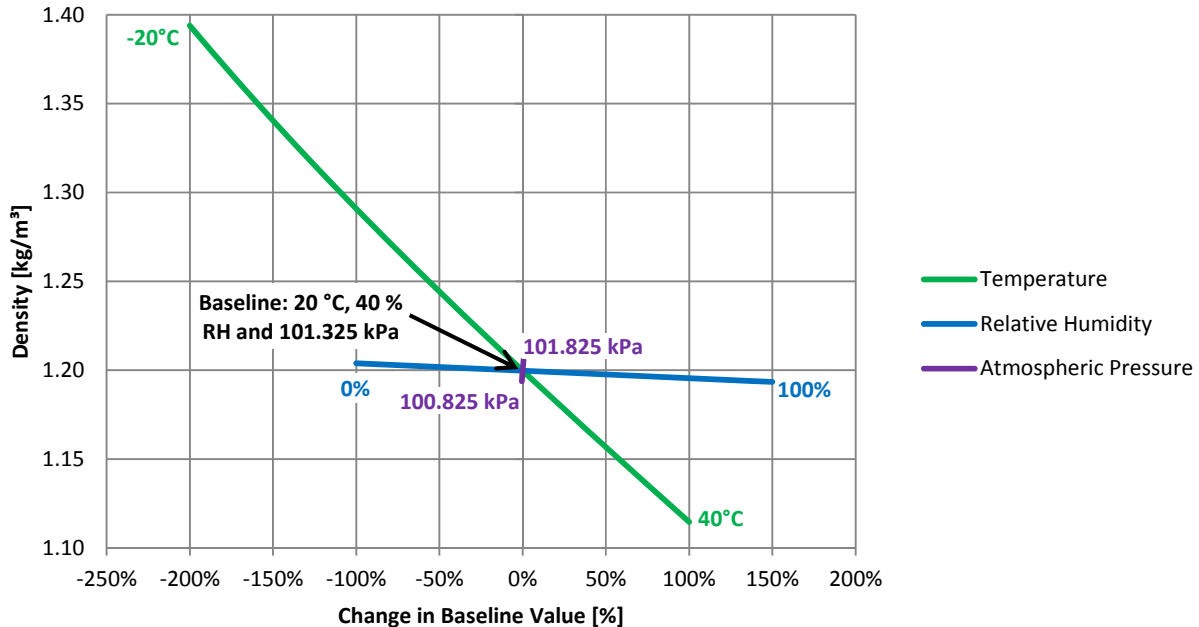


Figure 2-3: Graph of impact on air density of changes in temperature, relative humidity, and atmospheric pressure

The change in air density due to changes in relative humidity and absolute pressure over the selected ranges is less than 1%, so can generally be considered negligible when measuring airflow rates with respect to buildings; however, the change in density due to temperature is significant and should be considered when applicable. Additionally, air can be considered to act as an incompressible fluid with respect to airflows in buildings due to the relatively small change in density over the range typical operating pressure differences for buildings.

Given the bearing of air temperature on air density, an equation for calculating the density of dry air (0% relative humidity) is provided in Eq. 2.8 for reference.

$$\rho_{dry\ air} = \frac{351.99}{T} + \frac{344.84}{T^2} \quad \text{Eq. 2.8}$$

Where: $\rho_{dry\ air}$ = Density of Dry Air [kg/m³]
 T = Air Temperature [K]

(Straube & Burnett, 2005)

2.6 Nodal Analysis Approach

Buildings are complex three-dimensional assemblies of numerous zones and pressure boundaries as illustrated using a schematic high-rise multi-unit residential building in Figure 2-4.

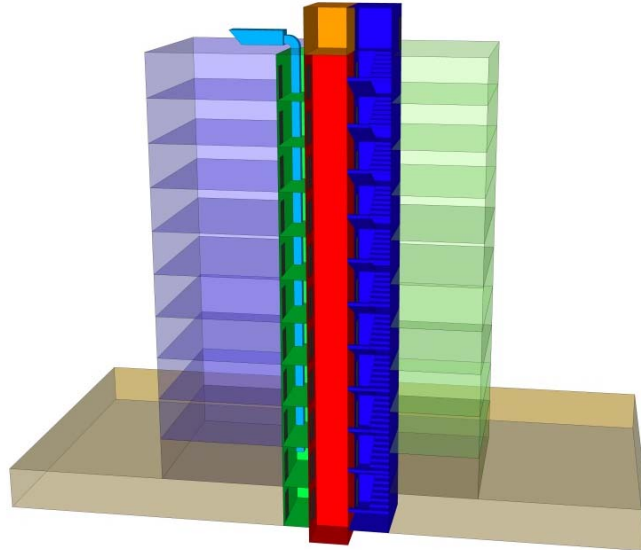


Figure 2-4: Schematic graphic of a high-rise multi-unit residential building illustrating the numerous zones and pressure boundaries

To assess the complex interaction between the driving forces and pressure boundaries, it is convenient to use a nodal analysis approach. For this thesis work, this nodal approach assumes that the air in each zone of a building is perfectly mixed and that the flow between the zones can be described by Eq. 2.5. This nodal approach has been applied on smaller scales to airflow through building elements such as in Kronvall (1991) and Listiburek (2000), and has also been applied in computational analysis of building airflows such as by Tamura (1969) and in software programs such as CONTAM (Walton & Dols, 2010) and COMIS (Feustel, 1998)

This type of nodal airflow network is akin to an electrical circuit where: airflow is analogous to electrical current (I , measured in Amps); pressure difference is analogous to voltage difference (V , measured in Volts); and airflow resistance is analogous to electrical resistance (R , measured in Ohms). Figure 2-2 illustrates how the airflow between two zones through a pressure boundary can be compared to the electrical current between two points across a resistor.

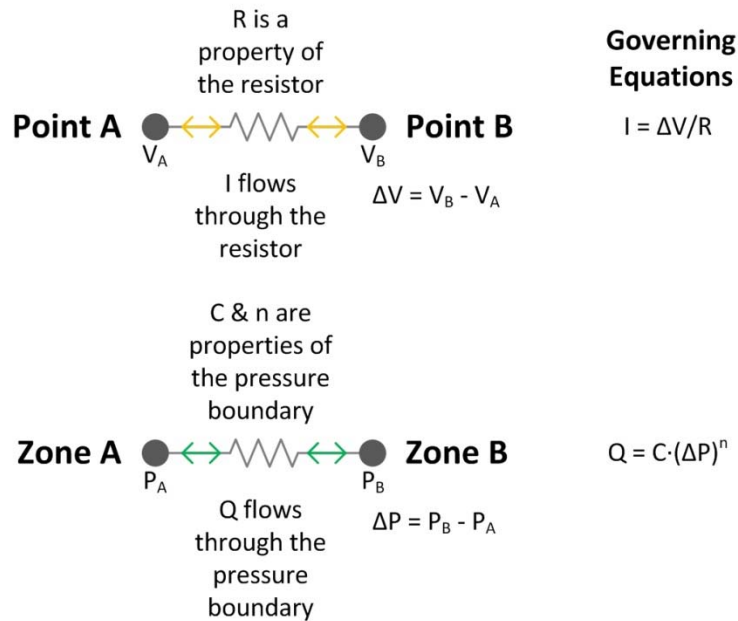


Figure 2-5: Graphic illustrating analogy of current flow between two points and airflow between two zones

An important difference between an electrical network and an airflow network is that while electrical current across a resistor is proportional to the voltage applied, airflow is not directly proportional to the pressure difference, as is apparent from Eq. 2.5. This equation forms the basis of the nodal network approach with each node having a given pressure, the resistance of each flow path being described by the flow coefficient and flow exponent, and these resulting in airflow between nodes.

Extending this analogy and considering each zone of the building as a node in the nodal network, and the walls, roofs, windows, doors, et cetera as pressure boundaries that resist airflow, this nodal network approach can be applied to a whole building. An example resistance network for part of a building is shown in Figure 2-6.

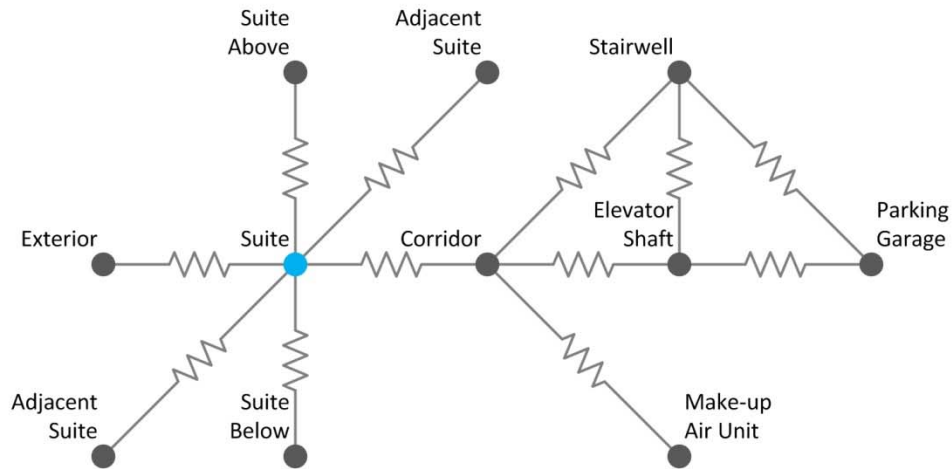


Figure 2-6: Example building airflow nodal network for part of a building

The network in Figure 2-6 is intended to provide a conceptual illustration for only one specific suite and factors that interact with that suite relatively directly. In actuality, the network for an entire building would consist of many of these types of networks connecting and overlapping with each other to create a much larger and extremely complicated network that is difficult to represent graphically. An abstracted three-dimensional building is shown in Figure 2-7 to illustrate this concept.

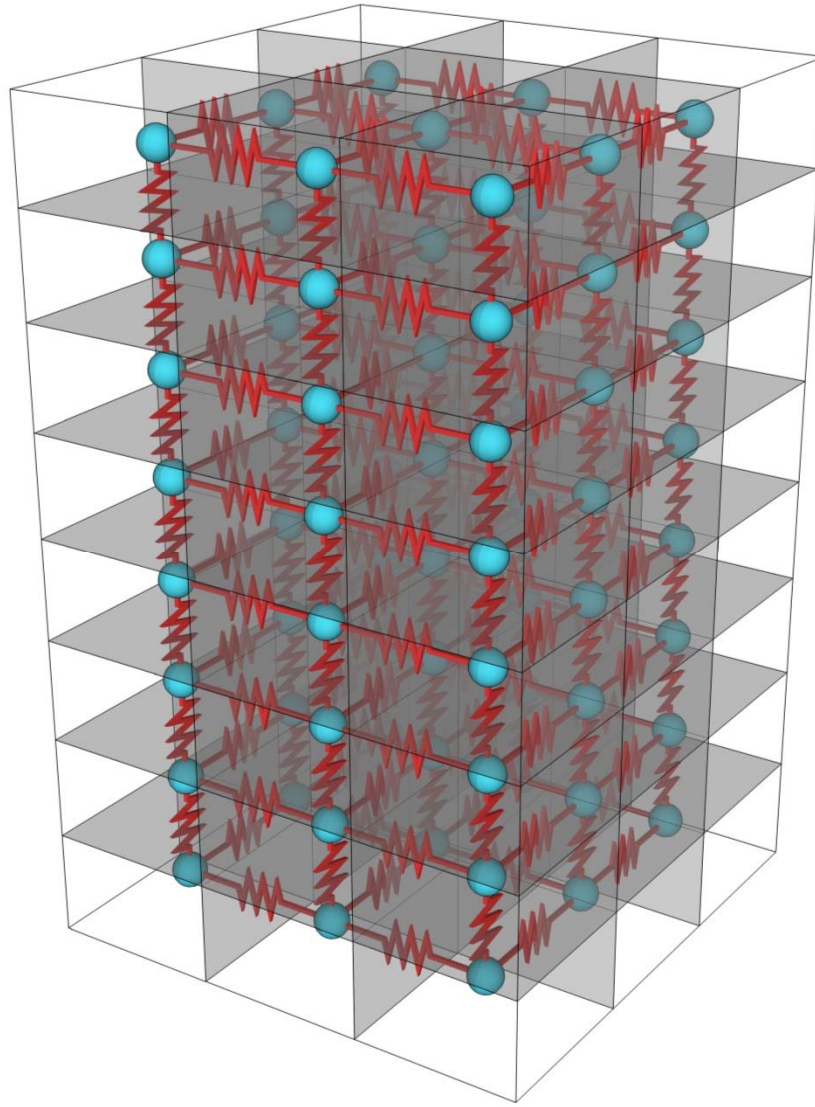


Figure 2-7: Abstracted building illustrating nodal network concept

The abstraction of a building to this type of airflow nodal network model does not provide an exact representation of airflow within an actual building. This model assumes airflow occurs only across boundaries between defined zones (nodes); however, airflow has been found to also occur within these boundaries (Lstiburek, 2000). Consideration of this level of detail would not provide significant benefit to this thesis work and would significantly increase the complexity of the analysis, so was not considered as part of this research.

This nodal airflow network approach to airflow into, out of, and within buildings provides a useful conceptual tool for understanding and analyzing airflow, and it forms the basis of the experimental procedure and analysis for this research.

Chapter 3

Pressure Differences

Airflow into, out of, and within buildings is created by pressure differences which are created by the natural forces of wind and stack effect, as well as by mechanical ventilation systems. These pressure differences may exist between the exterior and the interior of a building, and between internal building spaces. This chapter discusses how these driving forces create pressure differences and the typical magnitude of these pressure differences.

3.1 Stack Effect

Stack effect (sometimes also referred to as “chimney effect”) is a naturally occurring driving force of airflow created by the difference in air density between the interior of the building and the surrounding exterior environment due to the difference between exterior and interior temperature. As discussed in Section 2.5, warm air is less dense than cool air (of the same composition and atmospheric pressure). Consequently, a pressure differences develops as one travels up or down in two neighbouring columns of air of different temperature, and this difference in pressure acts on the boundary between the two air columns. The magnitude of stack effect can be calculated as shown in Eq. 3.1.

$$\Delta P_{stack} = g \cdot h \cdot (\rho_1 - \rho_2) \quad \text{Eq. 3.1}$$

Where: ΔP_{stack} = Total Pressure Difference Due to Stack Effect [Pa]
 g = Acceleration Due to Gravity [m/s^2]
 h = Stack Height [m]
 ρ_1 & ρ_2 = Density of Exterior and Interior Air Respectively [kg/m^3]

As air density depends primarily on the temperature of the air (as discussed in Section 2.5), this equation can be manipulated to the approximate form shown in Eq. 3.2 for ease of calculation.

$$\Delta P_{stack} = 3465 \cdot h \cdot \left(\frac{1}{T_o} - \frac{1}{T_i} \right) \quad \text{Eq. 3.2}$$

Where: ΔP_{stack} = Total Pressure Difference Due to Stack Effect [Pa]
 h = Stack Height [m]
 T_o & T_i = Outdoor and Indoor Temperatures Respectively [K]

(Straube & Burnett, 2005)

The development of pressure differences due to stack effect is illustrated in Figure 3-1 using a schematic building with no interior separations. This figure also identifies the neutral pressure plane (NPP) which is defined as the plane (horizontal in the absence of wind) at which there is no pressure difference between the interior and exterior of the building. The figure assumes a uniformly leaky building enclosure and that the interior of the building is warmer than the exterior which will tend to cause outward pressure at the top of the building and inward pressure at the bottom of the building which acts to force air into the building at the bottom and out of the building at the top. If the opposite temperature conditions were true (outside warmer than inside), stack

effect forces would be reversed thus forcing air into the building near the top and out of the building near the bottom.

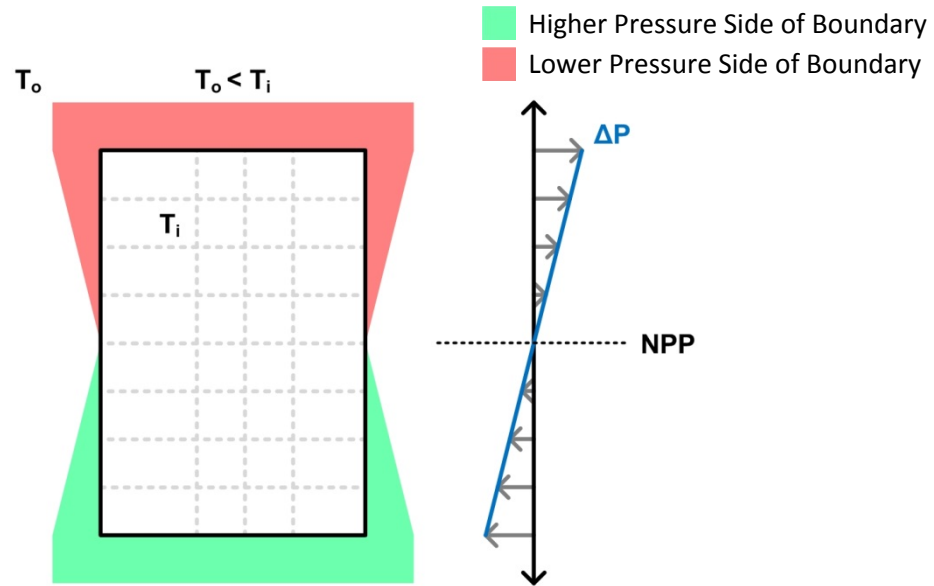


Figure 3-1: Graphic showing the development of pressure differences due to stack effect for a schematic building with no interior separations

The magnitude of the pressure developed by stack effect is determined by the interior temperature, the exterior temperature, and by the vertical distance from the NPP (stack height) as shown by Eq. 3.2. Figure 3-2 provides an indication of the magnitude of the pressure differences developed across the enclosure depending on the distance from the neutral pressure plane and the exterior temperature. Storeys are assumed to be 2.64 m (8' 8") in height and the interior temperature is set at 21°C for colder exterior temperatures, and at 24°C at warmer exterior temperatures.

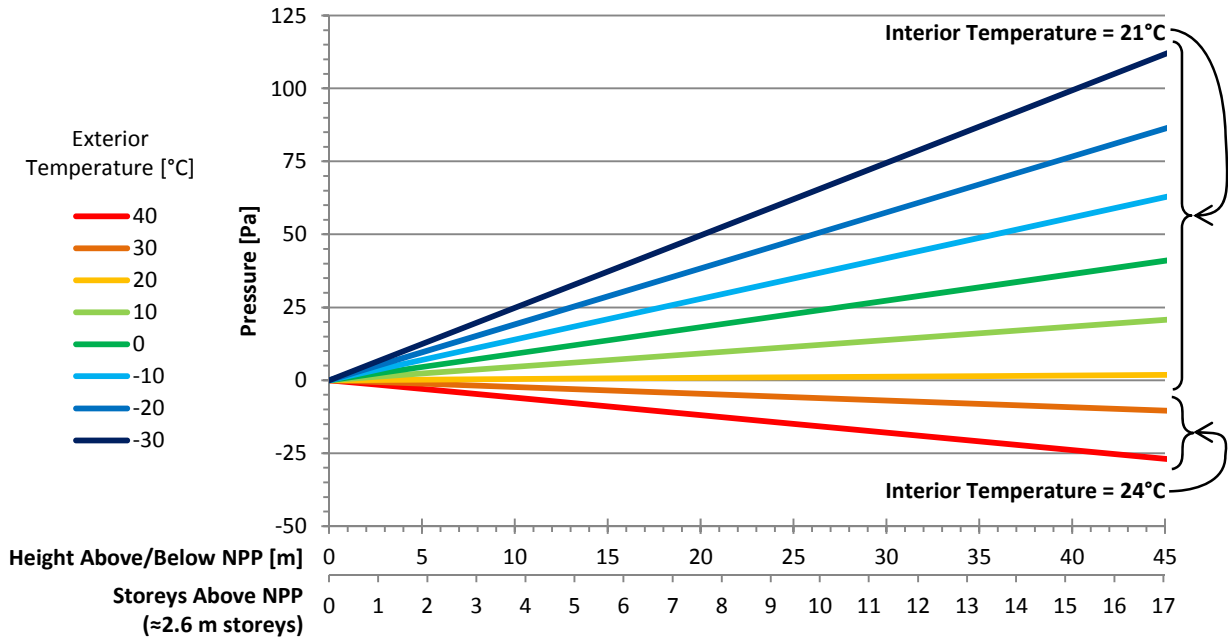


Figure 3-2: Graph of pressure differences developed due to stack effect in a building

To provide an indication of the how often these pressures occur, Figure 3-3 illustrates the number of hours per year that exterior temperatures typically occur in eight North American cities of varying climate. This figure is based on typical meteorological year (TMY) data for locations in the United States, and on Canadian Weather for Energy Calculations (CWEC) data for Canadian locations. Both types of data sets consist of compilations of months of data from various years that are determined to be most representative of typical conditions. The data sets were obtained through the U.S. Department of Energy (U.S. Department of Energy, 2013). The stack effect pressures for different distances from the NPP are overlaid on Figure 3-3 assuming an interior temperature of 21°C during cold periods and 24°C during warm periods.

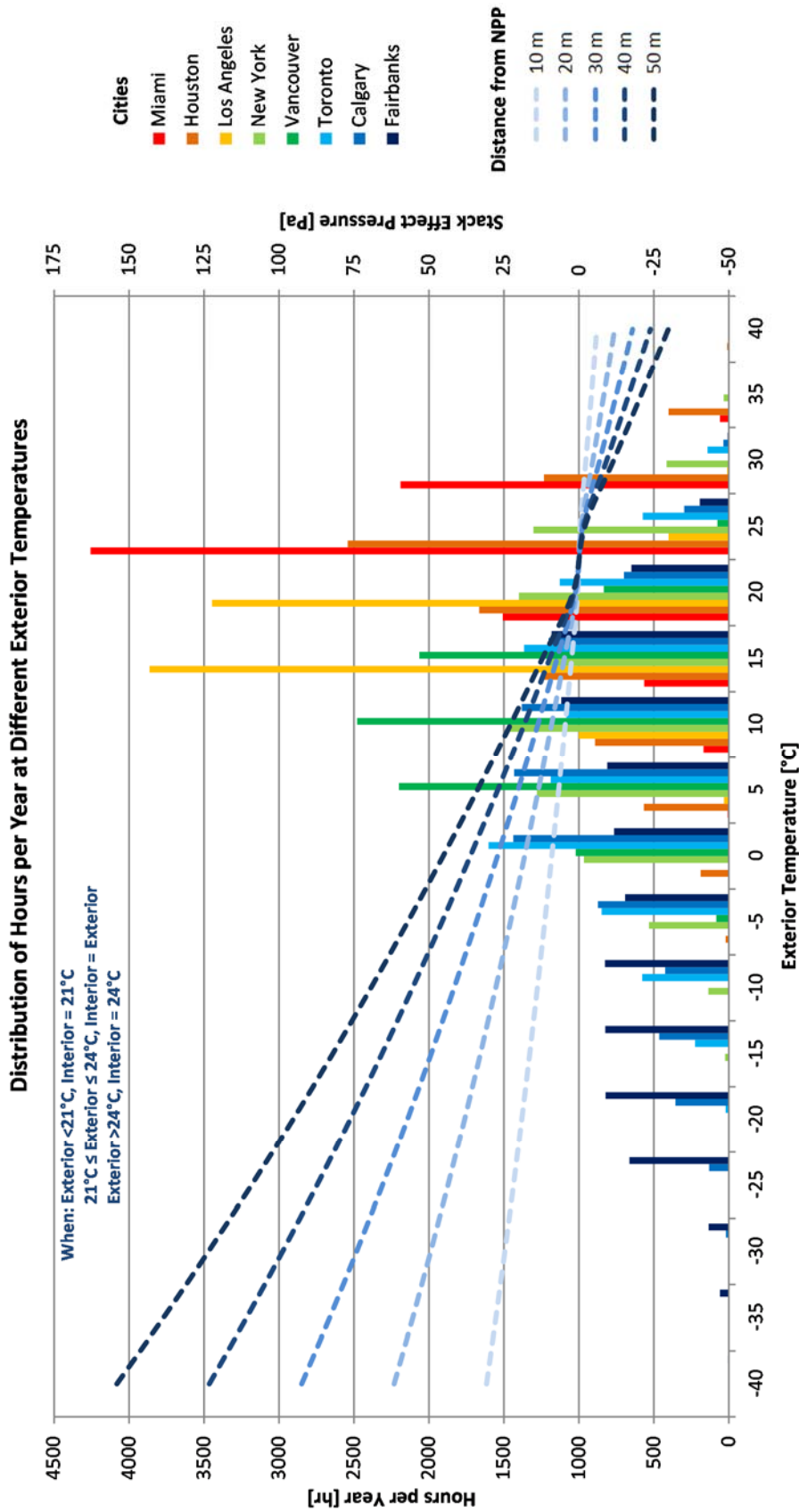


Figure 3-3: Graph of stack effect pressures overlaid on the number of hours different exterior temperatures occur in eight North American cities

Stack effect is typically most significant when exterior temperatures are colder than interior temperatures as these conditions are generally more common than periods of warmer exterior temperatures and typically create higher magnitude pressure differences. As stack pressures are also dependent on stack (or building) height, stack pressure are also more significant in high-rise buildings than in low-rise buildings. (Wilson & Tamura, 1968)

Unlike wind pressures which often fluctuate widely including both changes in direction and magnitude, as discussed later in Section 3.2, stack pressure are relatively consistent as they are based on temperatures differences which do not typically change rapidly over the short-term. Consequently, stack pressures are steady pressures which can significantly impact airflows into, out of, and within buildings. The relative influence of the driving forces is discussed further in Section 3.4.

The distribution of these pressure differences created by stack effect depends on the relative distribution of airflow resistance of the building pressure boundaries including the exterior enclosure and interior compartmentalizing elements. The location of the NPP varies depending on the vertical distribution of flow resistance of the building pressure boundaries. If there is less flow resistance towards the top of the building, the NPP will be above the mid-height of the building, and if there is less flow resistance towards the bottom of the building, it will be lower than the mid-height of the building as shown in Figure 3-4 and Figure 3-5. Overall, Proskiw and Phillips (2008) found that the location of the NPP in a building was highly variable, especially as a result of occupant operation of windows and exterior doors.

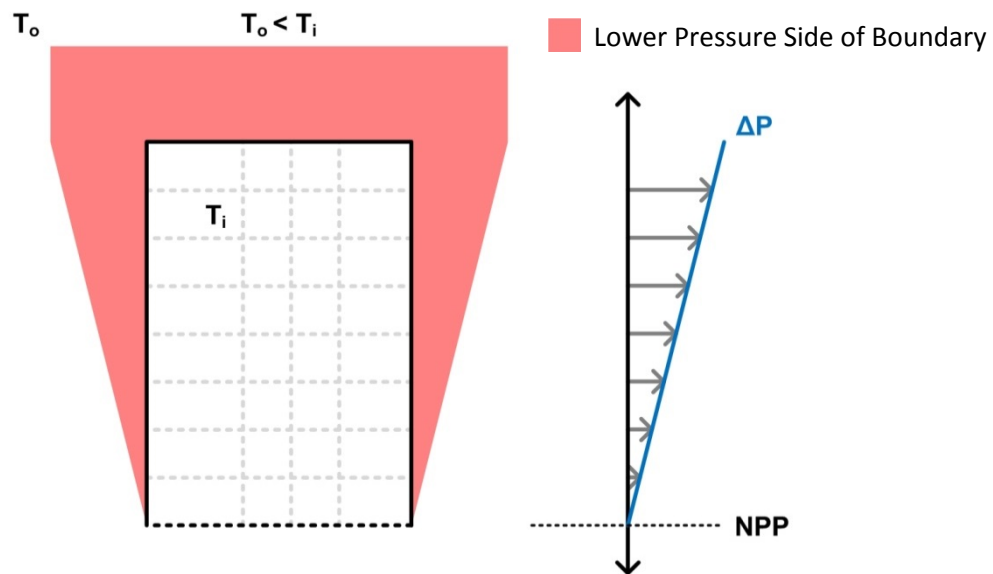


Figure 3-4: Graphic showing a schematic building with significantly more air leakage paths at the bottom of the building than at the top thus shifting the NPP down to the bottom

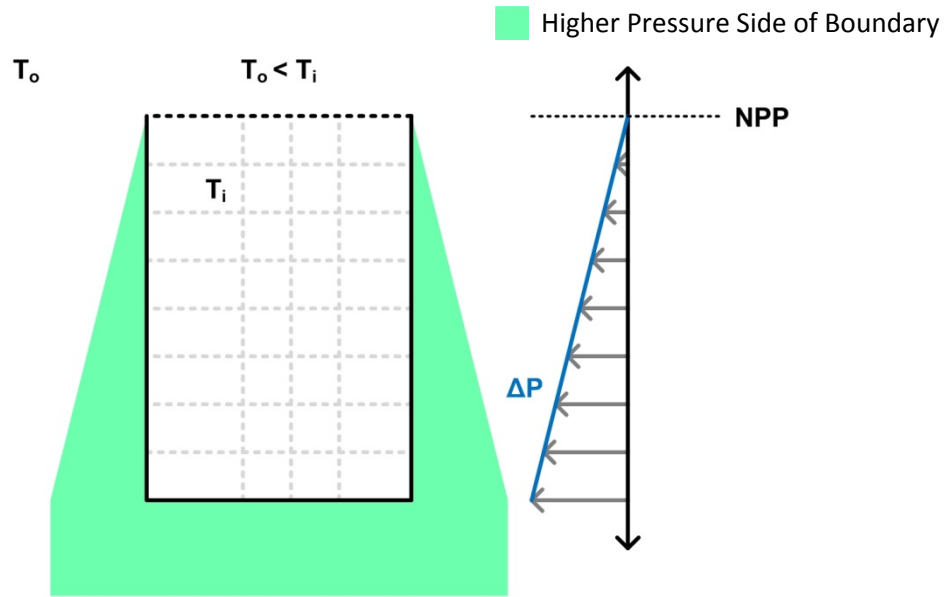


Figure 3-5: Graphic showing a schematic building with significantly more air leakage paths at the top of the building than at the bottom thus shifting the NPP up to the top

There can also be multiple NPPs in a building. For example, a stairwell with a door to the roof might have an NPP located higher in the building than an adjacent stairwell with no access to the roof. (Moffat, Theaker, & Wray, 1998) Or, floors of a building may be separated sufficiently that multiple NPPs are developed. This concept is illustrated in Figure 3-6 which demonstrates the complexity that develops as a result of multiple NPPs.

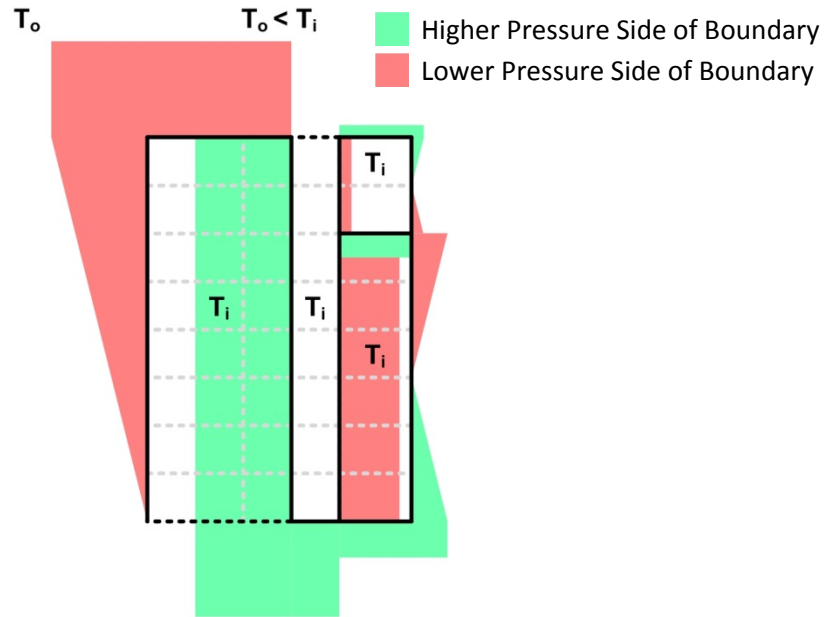


Figure 3-6: Graphic showing a schematic building with interior zones having varying vertical distributions of leakage openings and thus different NPP locations

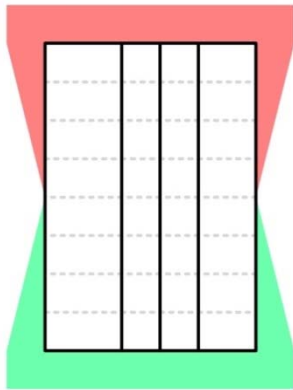
While the location of the NPP is controlled by the vertical distribution of airflow resistance, the distribution of pressure differences created by stack effect is also controlled by the airflow resistance of the various interior compartmentalizing elements. (Tamura & Shaw, 1976) Figure 3-7 illustrates various arrangements for the airtightness of these elements and how pressures differences would distribute within the building. This figure assumes that the enclosure is uniformly leaky and that it is warmer inside the building than it is outside.

Figure 3-7 a) shows the pressure differences developed across the exterior enclosure of a building due to stack effect if there are no internal horizontal separations.

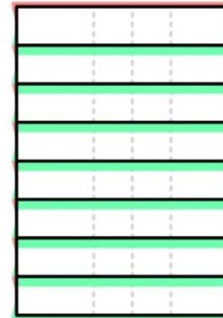
Figure 3-7 b) illustrates the pressure differences developed if the building is separated into floors that are perfectly air tight. By introducing these air tight separations, the building is essentially split into 8 sections that operate independently. Thus, a NPP is developed on each floor.

Figure 3-7 c) shows a building where each floor is equally air leaky, but does provide some resistance to airflow. This distribution of airflow resistance essentially creates a distribution of stack effect pressures that is a combination of a) and b) where some pressure drop occurs across the floors which moderates the stack effect, but because some airflow between floors is possible, stack effect does accumulate over the height of the building.

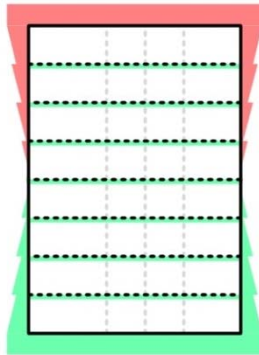
■ Higher Pressure Side of Boundary ■ Lower Pressure Side of Boundary
 Assumes uniformly leaky enclosure and warmer inside than outside.



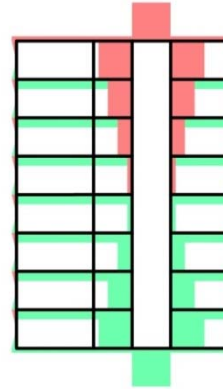
a) Airtight Walls and Very Leaky Floors



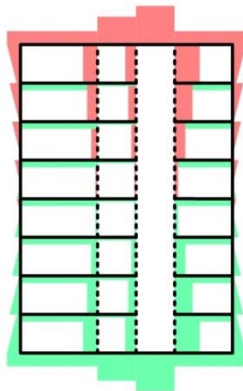
b) Very Leaky Walls and Airtight Floors



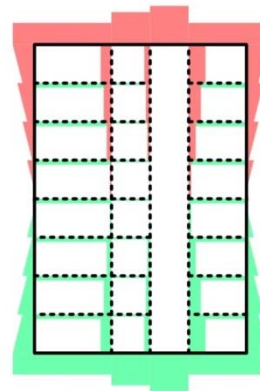
c) Very Leaky Walls and Uniformly Leaky Floors



d) Airtight Walls and Airtight Floors



e) Uniformly Leaky Walls and Airtight Floors



f) Uniformly Leaky Walls and Uniformly Leaky Floors

Figure 3-7: Graphics illustrating distribution of stack effect pressures in a building given different wall and floor air leakage configurations

Figure 3-7 d) shows the theoretical distribution of stack effect for a building which is perfectly split in to zones by airtight interior boundaries. In this case each zone acts as its own independent building. Notably, in this arrangement the majority of stack effect pressures act across the separations between interior shafts and adjacent zones.

In reality the interior walls of a building provide resistance to airflow, but are not perfectly airtight. Figure 3-7 e) illustrates a case where the interior walls are somewhat leaky and shows that the leakiness of these walls means that the stack effect now distributes across all of the interior compartmentalizing walls instead of just across the shaft walls. The distribution of these pressure differences depends on the relative airtightness of the walls.

Figure 3-7 f) shows a more realistic building where both walls and floors provide resistance to airflow but are not perfectly sealed. This arrangement distributes stack effect pressures across the interior compartmentalizing elements and the exterior enclosure, and also allows for accumulation of stack pressures between floors. This arrangement is the most realistic, and it is also the most complicated.

The ratio between the theoretical stack pressure developed if there were no interior separations and the actual stack pressure developed across the exterior enclosure is referred to as the *thermal draft coefficient* (TDC). (ASHRAE, 2009) The TDC for a building that is entirely open on the interior is 1.0 because all of the theoretical stack pressure occurs across the building enclosure. In an actual building with interior walls and floors, some of this stack pressure distributes across these other elements, so only a portion acts across the exterior enclosure and the TDC is less than one. The TDC concept is illustrated in Figure 3-8.

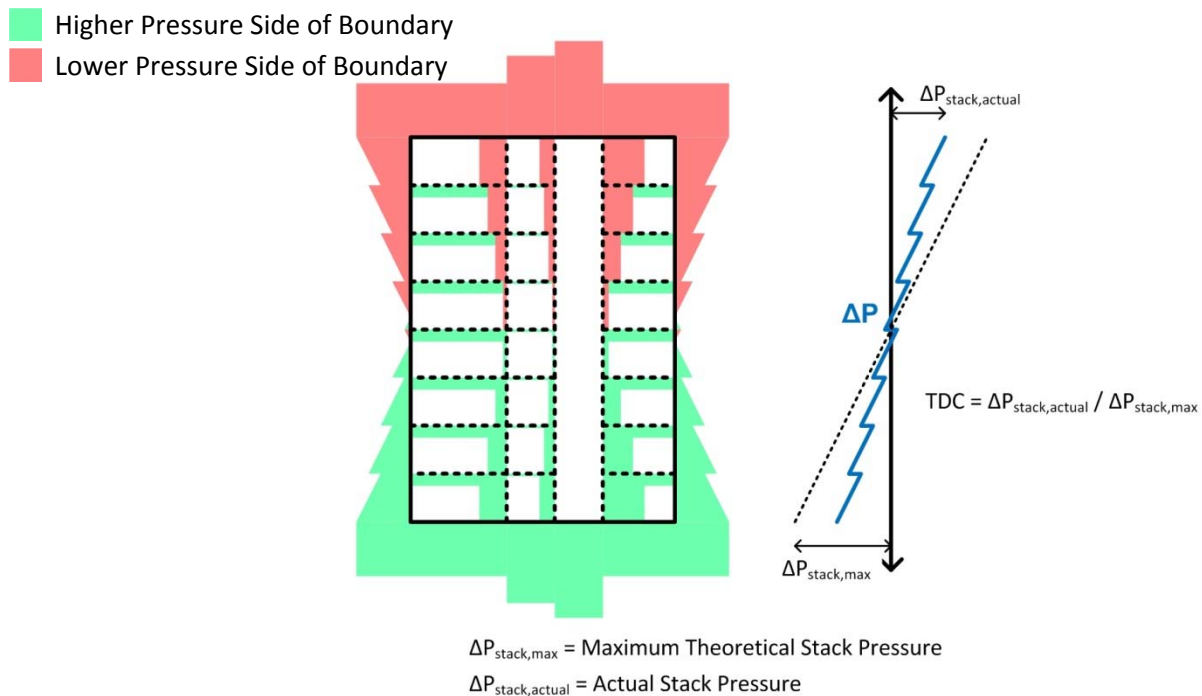


Figure 3-8: Graphic illustrating thermal draft coefficient

While the figure above shows the TDC for a whole building, it can also be calculated for individual floors. Tamura and Shaw (1976) found based on measurements of multi-storey office buildings that the TDC typically ranges from 0.63 to 0.88, and Moffat et al (1998) notes that multi-unit residential building would likely have lower TDC values than office buildings due to more interior compartmentalization.

Overall, the distribution of stack effect pressure differences in cold climates tend to create flows into the building near the bottom, vertically between floors and through shafts, and out of the building near the top as illustrated Figure 3-9.

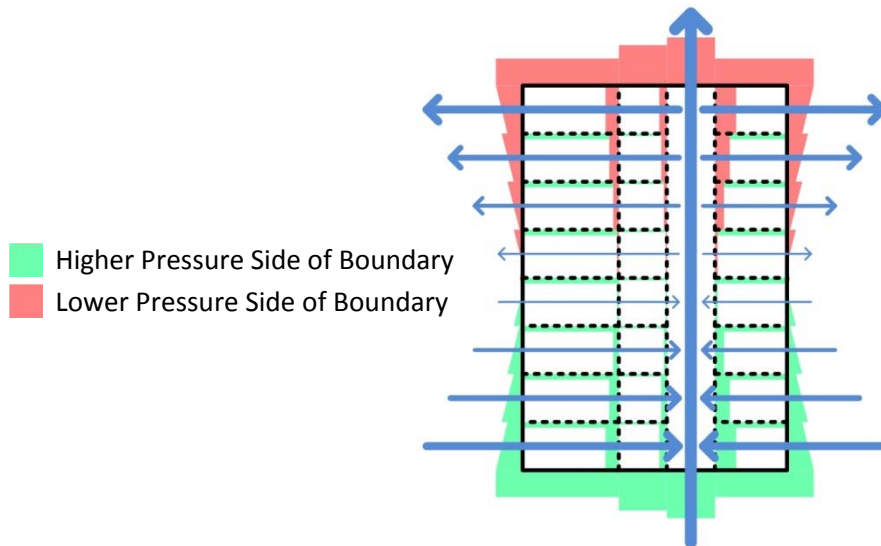


Figure 3-9: Schematic representation of a stack effect pressures and flow within and through a building

3.2 Wind

Wind typically creates the peak pressure differences across the building enclosure and as such is a primary consideration for building structural design and air barrier design including the strength and deformation of the air barrier system.

An important characteristic of wind with respect to its impact on building air flow is that it varies both temporally and spatially. The magnitude and the direction of the wind are constantly fluctuating which makes it difficult to predict the effect it will have on the building at any given moment in time. As a demonstration of the variability of wind speed and direction, the frequency of wind from each direction and the associated average wind speed are provided in Figure 3-10 to Figure 3-15 for the Canadian cities of Vancouver, Calgary, Winnipeg, Toronto, and Montreal based on ten year averages from 2003 to 2012 and for St. John's based on a nine year average from 2003 to 2011. The climate data was retrieved through Environment Canada and the wind speeds were measured at 10 m height above the ground at the main airport for each city. (Environment Canada, 2013) Note that the wind direction frequency is provided using percent divided by 4 for ease of presentation.

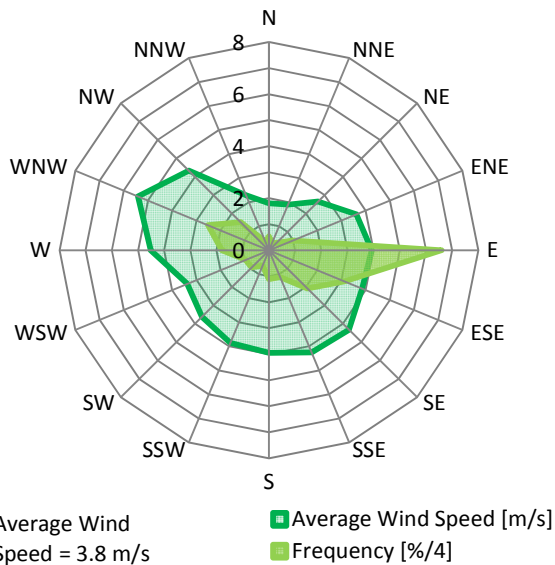


Figure 3-10: Wind directional frequency and magnitude for Vancouver, BC from 2003 to 2012 at 10 meters above the ground

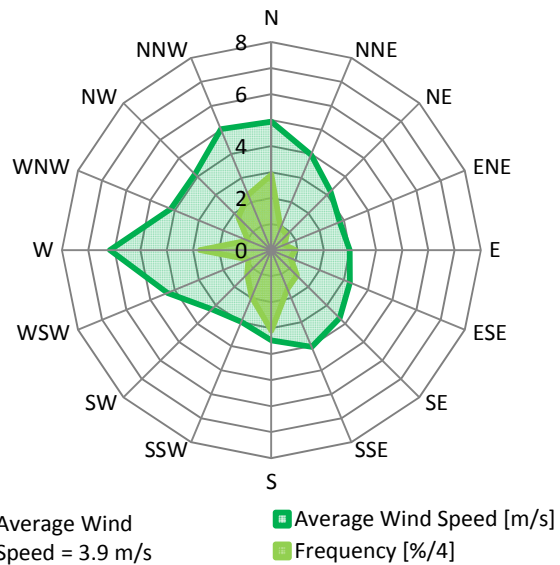


Figure 3-11: Wind directional frequency and magnitude for Calgary, AB from 2003 to 2012 at 10 meters above the ground

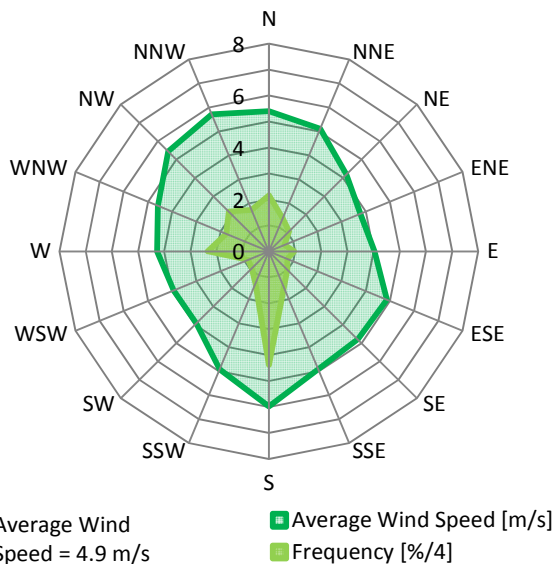


Figure 3-12: Wind directional frequency and magnitude for Winnipeg, MN from 2003 to 2012 at 10 meters above the ground

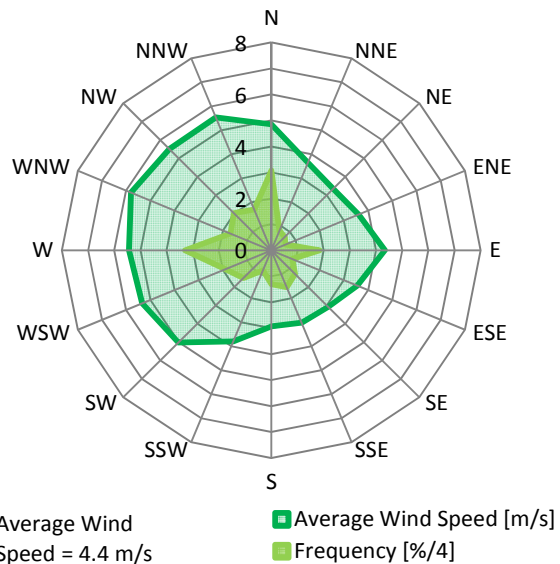


Figure 3-13: Wind directional frequency and magnitude for Toronto, ON from 2003 to 2012 at 10 meters above the ground

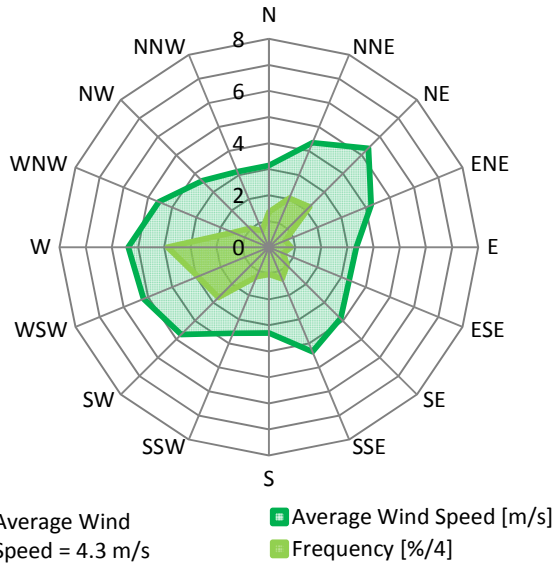


Figure 3-14: Wind directional frequency and magnitude for Montreal, QC from 2003 to 2012 at 10 meters above the ground

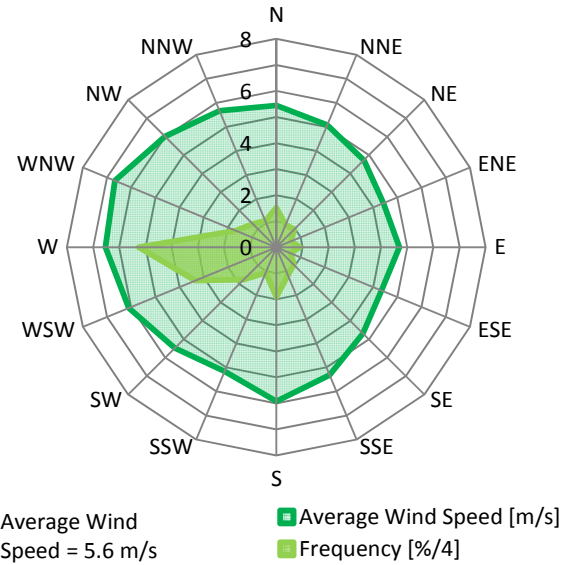


Figure 3-15: Wind directional frequency and magnitude for St. John's, NL from 2003 to 2011 at 10 meters above the ground

While wind direction and magnitude often fluctuate over short time periods (i.e. seconds or minutes), for the impact on exfiltration, infiltration, and ventilation, longer term average wind speeds and directions are most relevant. The distribution of the magnitude of hourly average wind speeds at a given location has been found to approximately follow a Weibull probability distribution function with a k value (shape parameter) of approximately 2 (Yilmax & Çelik, 2008). (A Weibull distribution with k equal to 2 is also known as a Rayleigh distribution.) The Weibull probability distribution function is shown in Eq. 3.3.

$$f(x) = \begin{cases} \frac{k}{\lambda} \cdot \left(\frac{x}{\lambda}\right)^{k-1} e^{-\left(\frac{x}{\lambda}\right)^k} & x \geq 0 \\ 0 & x < 0 \end{cases} \quad \text{Eq. 3.3}$$

Where: k = Shape Parameter
 λ = Scale Parameter (when $k = 2$, λ is the mean)

(Weisstein, 2013)

Weibull distributions with different mean averages and with a shape parameter of 2 are shown in Figure 3-16 to provide an indication of typically observed distributions of wind speed.

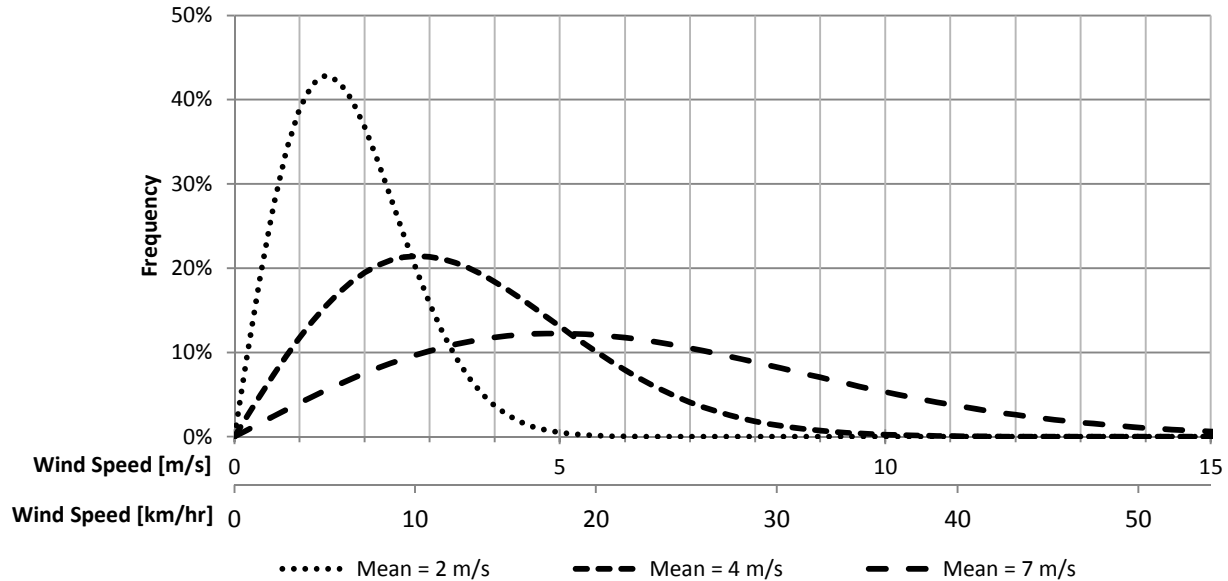


Figure 3-16: Probability Distribution of Wind Speeds at a Given Location According to a Weibull ($k = 2$)

The actual wind speed that occurs at a given building is highly dependent on both the relative roughness of the Earth’s surface in the surrounding area (Dalglish & Boyd, 1962), and local shielding effects (Dalglish & Schriever, 1968). As wind flows across the surface of the Earth, its flow is impeded by the aerodynamic drag of objects on the ground such as buildings and trees. Due to this aerodynamic drag, an atmospheric boundary layer (layer where the wind speed is affected by the roughness of the Earth’s surface) develops. The effect of the surface roughness of the Earth on wind speeds is dependent on surface terrain type. That is, areas with rougher terrain (i.e. larger obstructions) typically develop a larger surface boundary layer than areas with relatively smooth terrain. To determine the wind speed at a specific location, ASHRAE (2009) provides Eq. 3.4 which is intended to capture large scale atmospheric boundary layer effects on wind speed at the location of a building.

$$U_H = U_{met} \cdot \left(\frac{\delta_{met}}{H_{met}}\right)^{\alpha_{met}} \cdot \left(\frac{H}{\delta}\right)^{\alpha} \tag{Eq. 3.4}$$

- Where:
- U_H = Hourly Average Wind Speed at Building[m/s]
 - U_{met} = Hourly Average Wind Speed at Meteorological Station[m/s]
 - δ = Wind Boundary Layer Thickness at Building [m]
 - δ_{met} = Wind Boundary Layer Thickness at Meteorological Station [m]
 - H = Height Above Local Obstacles at Building [m]
 - H_{met} = Height Above Local Obstacles at Meteorological Station [m]
 - α = Wind Speed Profile Exponent at Building [dimensionless]
 - α_{met} = Wind Speed Profile Exponent at Building [dimensionless]

(ASHRAE, 2009)

The wind boundary layer thickness and wind speed profile exponent depend on the relative surface roughness of the Earth and are provided in Table 3-1.

Table 3-1: Atmospheric Boundary Layer Parameters (Reproduced from ASHRAE, 2009)

Terrain Category	Description	Exponent α	Layer Thickness δ [m]
1	Large city centers, in which at least 50% of buildings are higher than 25 m , over a distance of at least 0.8 km or 10 times the height of the structure upwind, whichever is greater	0.33	460
2	Urban and suburban areas, wooded areas, or other terrain with numerous closely spaced obstructions having the size of single-family dwellings or large, over a distance of at least 460 m or 10 times the height of the structure upwind, whichever is greater	0.22	370
3	Open terrain with scattered obstructions having heights generally less than 9 m including flat open country typical of meteorological station surroundings	0.14	270
4	Flat, unobstructed areas exposed to wind flowing over water for at least 1.6 km, over a distance of 460 m or 10 times the height of the structure inland, whichever is greater	0.10	210

Meteorological stations typically record wind speeds at 10 m above the ground ($H_{met} = 10$ m) and are also typically located in areas of terrain category 3. The wind boundary layer profiles described by Eq. 3.4 for each terrain category are provided in Figure 3-17.

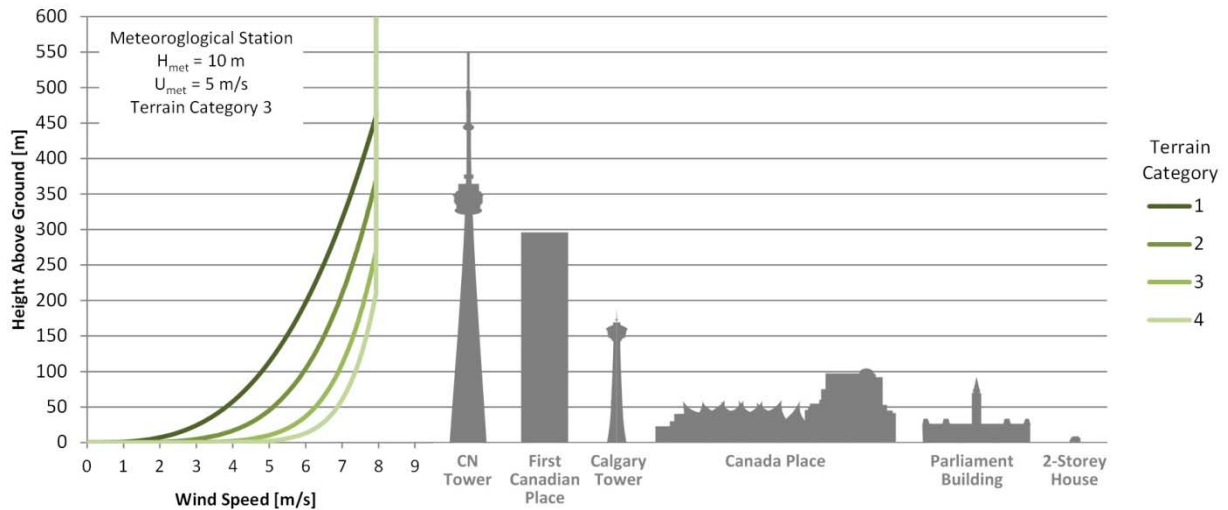


Figure 3-17: Boundary layer wind speed profiles with recognizable buildings for reference

The local effects of objects such as surrounding buildings, trees, and geographical features can also significantly alter the wind speed (and consequently pressures) at a building. While often these features reduce wind speeds at a building by providing shielding, it is also possible for features such as hills, valleys, or adjacent buildings to increase the local wind speed at the building by funneling. The local effects of shielding or funneling due to nearby objects must be considered on a case-by-case basis.

As wind flows around a building it creates pressures on the building enclosure. On the windward side of a building these pressures typically force air into the building, and on the leeward sides these pressures typically draw air out of a building (Shaw & Tamura, 1977). The pressures created on a building as a result of wind are typically measured as a proportion of stagnation pressure (Cóstola, Blocken, & Hensen, 2009). Stagnation pressure is the static pressure at a stagnation point (i.e. no air velocity) in the air. (Sometimes stagnation pressure it is also referred to as velocity pressure.) In these locations all kinetic energy has been converted into potential energy stored as pressure. This pressure acts on surfaces adjacent to the stagnation point, such as the walls of a building. The calculation of stagnation pressure is based on Bernoulli's Equation and is shown in Eq. 3.5.

$$\Delta P_{stag} = \frac{\rho \cdot v^2}{2} \quad \text{Eq. 3.5}$$

Where: ΔP_{stag} = Stagnation Pressure [Pa]
 ρ = Density of Air [kg/m^3] ($\approx 1.2 \text{ kg}/\text{m}^3$)
 v = Air Velocity [m/s]

The stagnation pressure of wind is provided Figure 3-18, overlaid on the number of hours for which the associated wind speed occurs for the same six Canadian cities previously discussed. Note that the distribution of hours is similar to that predicted by a Weibull distribution.

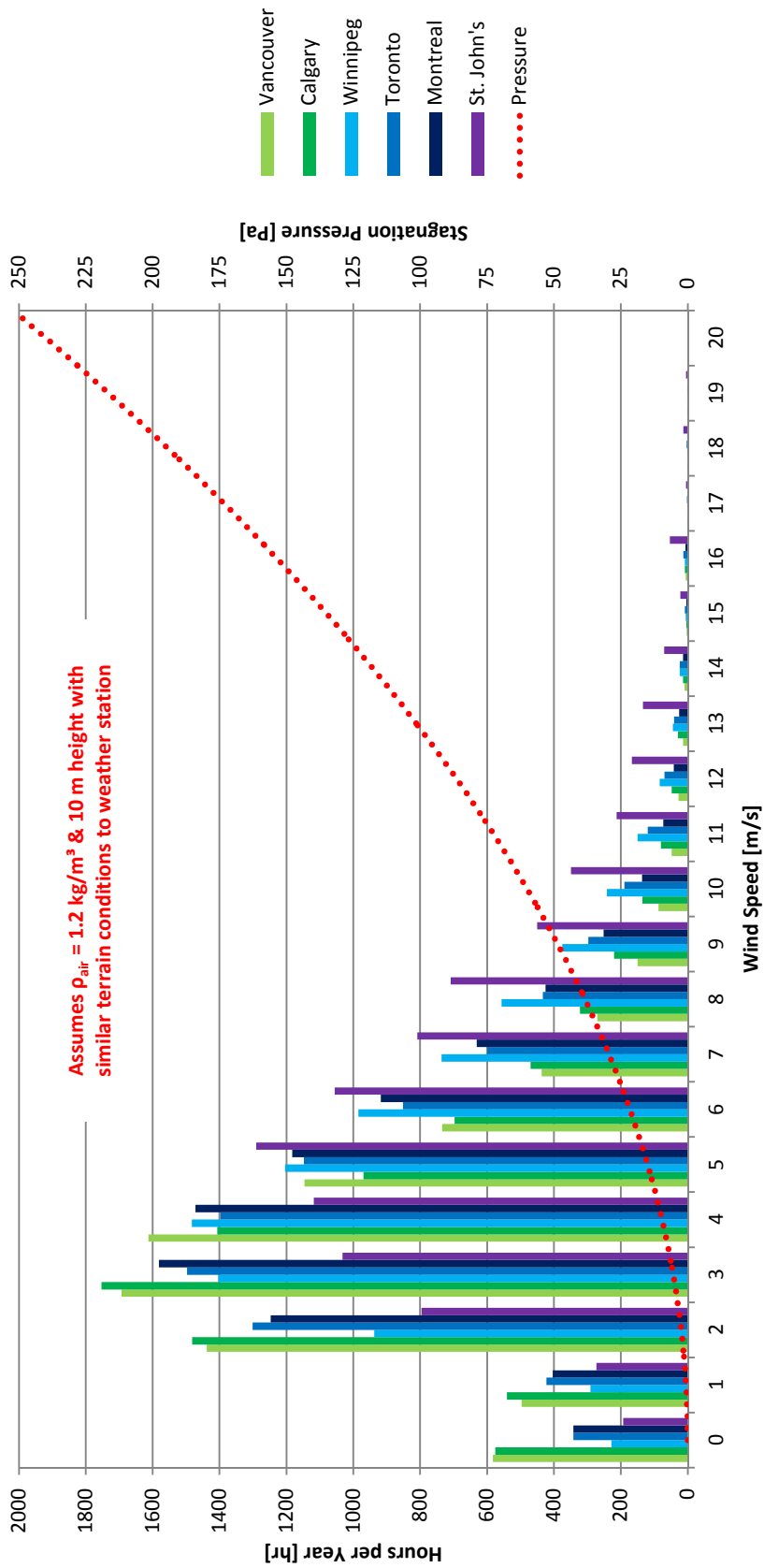


Figure 3-18: Graph of wind stagnation pressure overlaid on the number of hours of various wind speeds in six Canadian cities

Figure 3-18 illustrates that during the majority of hours, wind stagnation pressures are relatively low and this is reinforced by Table 3-2 which provides the mean average stagnation pressure, as well as 50th, 75th, 90th, and 95th percentile stagnation pressures for the same six Canadian cities. Note that these stagnation pressures have been calculated with an assumed air density of 1.2 kg/m³; however, as air temperatures vary with temperature, the stagnation pressure of the wind is increased when the air is colder. Consequently, cities in colder climates likely experience higher wind pressures than indicated and cities in warmer climates likely experience lower wind pressure than indicated.

Table 3-2: Stagnation Pressure Statistics for Six Canadian Cities

Percentile	Stagnation Pressure [Pa] (assuming $\rho_{air} = 1.2 \text{ kg/m}^3$)						
	Vancouver	Calgary	Winnipeg	Toronto	Montreal	St.John's	Average
50th (median)	7.8	7.8	13.4	10.4	10.4	16.7	11.1
75th	16.7	16.7	26.7	22.4	18.5	31.3	22.1
90th	26.7	31.3	47.4	41.7	36.3	56.7	40.0
95th	41.7	47.4	56.7	56.7	47.4	77.8	54.6
Mean Average	8.5	6.3	9.9	8.2	7.7	13.2	8.9

The pressure at a point on a building is indicated as a fraction of the stagnation pressure using a dimensionless local wind pressure coefficient (C_p) which is often assumed to be independent of the wind speed (Cóstola, Blocken, & Hensen, 2009). The calculation of this coefficient and its use to determine the wind pressure on a building are shown in Eq. 3.6 and Eq. 3.7.

$$C_p = \frac{P - P_0}{P_{stag}} \quad \text{Eq. 3.6}$$

- Where: C_p = Exterior Local Wind Pressure Coefficient [dimensionless]
 P = Pressure at Given Point on the Building [Pa]
 P_0 = Static Reference Pressure [Pa]
 P_{stag} = Stagnation Pressure [Pa]

$$P_{wind} = C_p \frac{\rho \cdot v^2}{2} \quad \text{Eq. 3.7}$$

- Where: P_{wind} = Wind Pressure at Point on Building [Pa]

The reference pressure for determination of the local wind coefficient is typically calculated using the wind speed at the roof height of the building (which can be adjusted from the measurement height to the roof height using Eq. 3.4) and is measured relative to local exterior atmospheric pressure, also at roof height. (ASHRAE, 2009)

An exterior wind pressure coefficient of one ($C_p = 1$) is typically not achieved for a large area of a building enclosure. Typical wind pressure coefficients range from -0.5 to 1.0 for the windward face of a building, -1.5 to 0.5 for faces of a building perpendicular to the wind, -0.5 to 0 for the leeward face of a building, and -6.0 to 0.5 for flat roofs of a building. (Brundrett, 1991) The local pressure

coefficient distributions on a typical tall building are shown in Figure 3-19. While the ranges described for pressure coefficients are typical, significantly higher and lower pressure coefficients can occur.

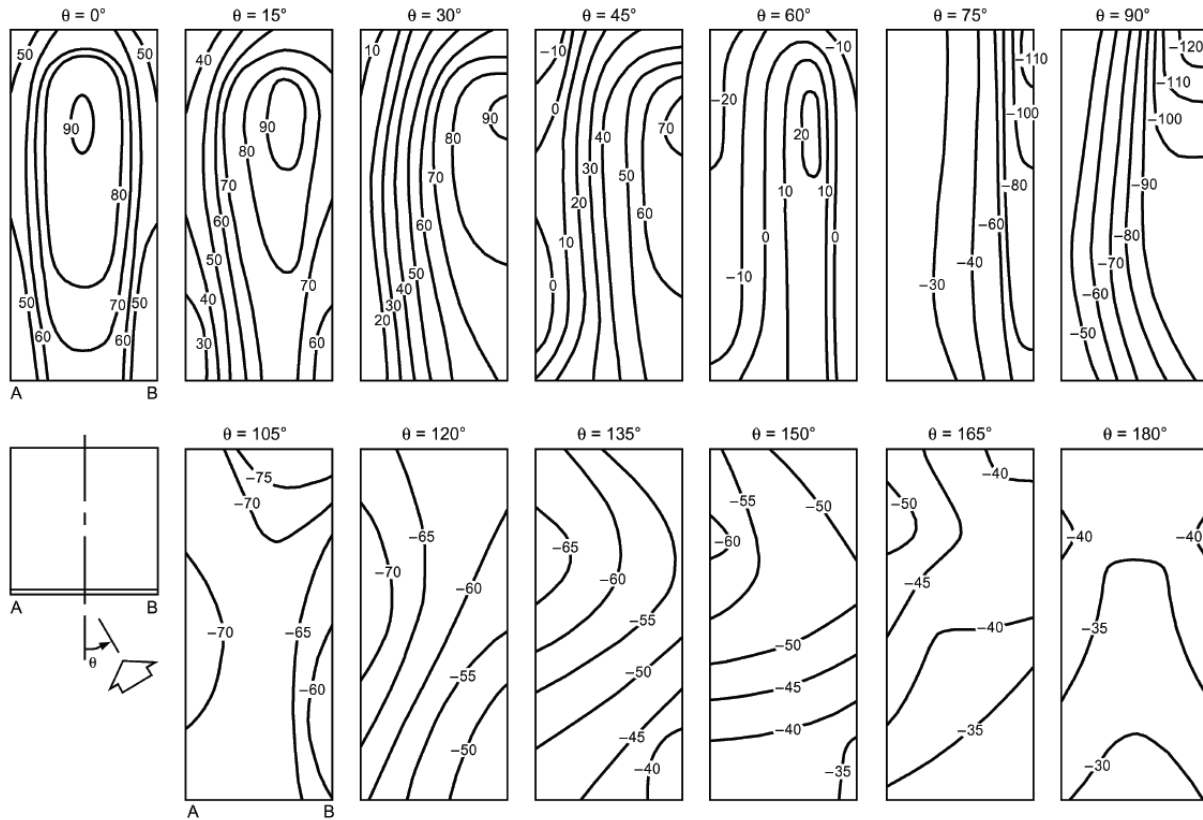


Figure 3-19: Local exterior wind pressure coefficients ($C_p \times 100$) for tall buildings (ASHRAE, 2009)

Brundrett, (1991) performed boundary layer wind tunnel testing of a cube and measured wind pressure coefficients across the top surface. His measured results from two cases are provided in Figure 3-20 and Figure 3-21.

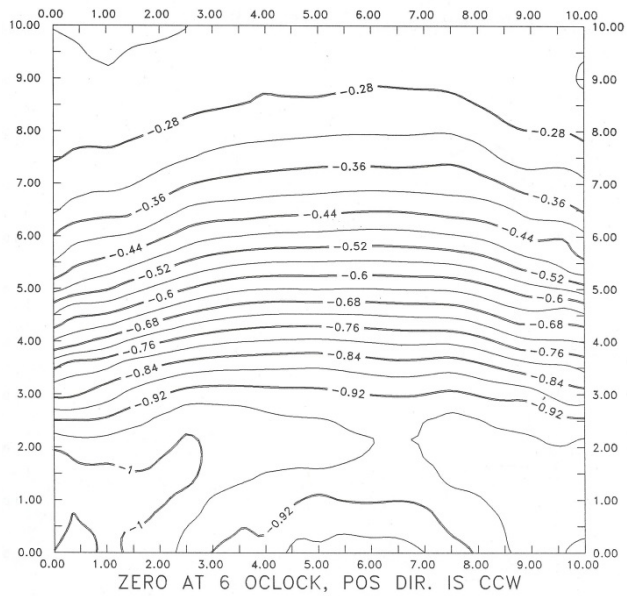


Figure 3-20: Roof pressure coefficient contours with wind from 0° (Brundrett, 1991)

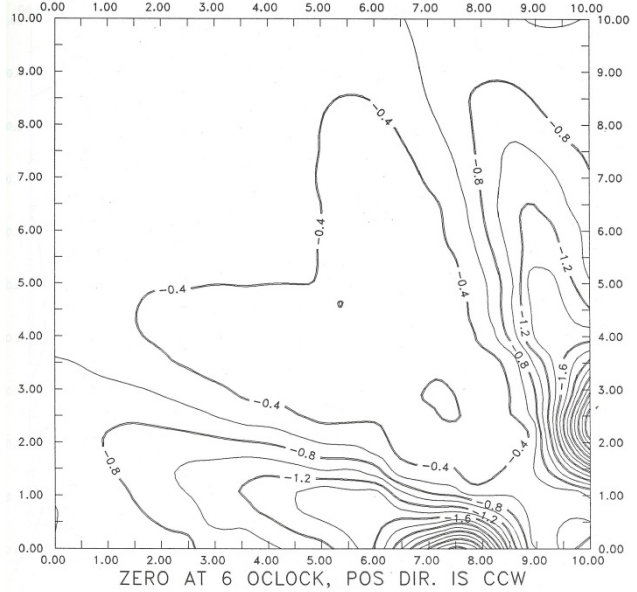


Figure 3-21: Roof pressure coefficient contours with wind from 45° (Brundrett, 1991)

A cross-section through the middle of a building with no interior separations and a perfectly airtight enclosure for the case with wind perpendicular to a face of the building ($\theta = 0^\circ$) is shown in Figure 3-22. Note that Figure 3-22 is based on the contours provided in Figure 3-19 by ASHRAE (2009) which do not account for some of the finer complexities of wind pressure distributions including in particular where outward acting pressures can occur on the windward side of a building near the corners because air can flow around the corners to connect to the large negative pressures on the side walls.

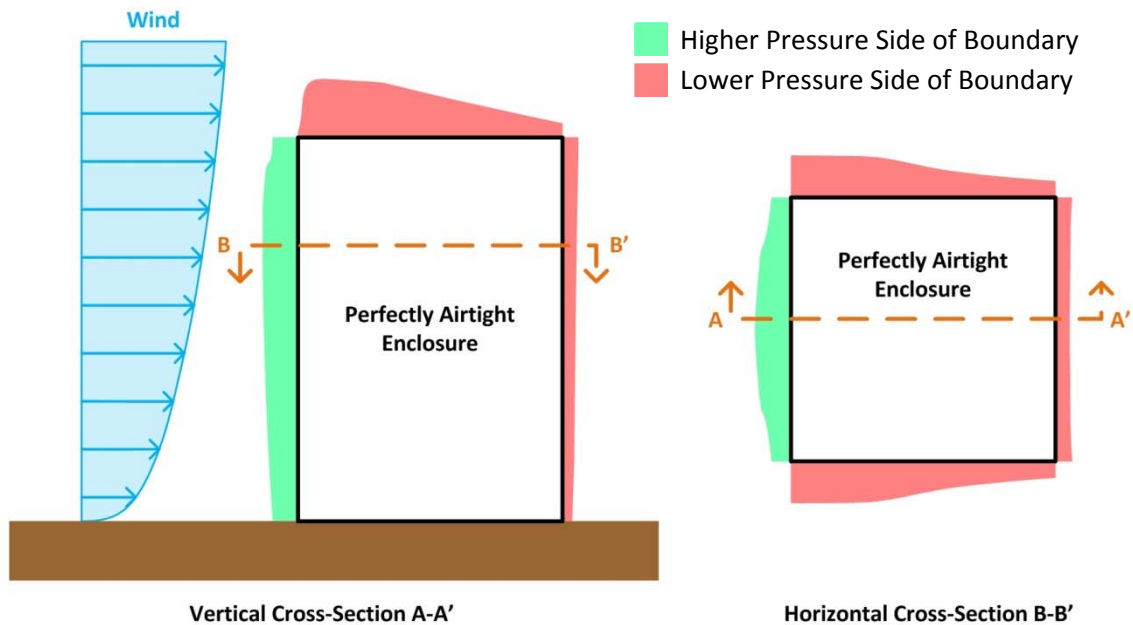


Figure 3-22: Graphic showing distribution of wind pressure on the building enclosure

The distribution of pressure coefficients becomes significantly more complicated and difficult to predict when non idealized building shapes (i.e. not rectangular prism) are considered. Protruding elements (e.g. balconies, wing walls, or roof parapets), alcoves, overhangs, and irregular building shapes (e.g. step backs or corners) will all impact the distribution of wind pressure on the building surfaces and can in many cases create wind pressure coefficients of significantly higher magnitude than those suggested by Brundret (1991) and ASHRAE (2009). To fully understand the distribution of wind pressures on buildings, measurements at existing buildings, scale boundary layer wind tunnel studies, or computational fluid dynamics models are required; however, these studies are costly and time consuming so are only rarely performed (Moffat, Theaker, & Wray, 1998; Cóstola, Blocken, & Hensen, 2009; Orne, Liddament, & Wilson, 1998; and Hill, 1999).

There are also various models available to estimate wind pressure coefficients and Cóstola et al (2009) provide a review of some of these models. Cóstola et al identify three separate analytical models for determining wind pressure coefficients that were developed based on analysis of testing and measurement data. They also note that instead of using these analytical models, values of wind pressure coefficients from various databases could also be used. Unfortunately, both analytical models and the databases are typically only capable of generating general wind pressure coefficient values, and determining high accuracy for specific sheltering and building geometries is not possible. Cóstola et al found that within databases the pressure coefficients vary by up to 0.4 even for relatively simple cube shaped buildings, which for a value that is usually in the range of -0.8 to 0.8 (Hill, 1999) is quite significant. For more complicated buildings with sheltering or complex geometry, Cóstola et al found that the wind pressure coefficient could vary by as much as 1.0 which is more than 50% of the expected range. Reliably predicting wind pressure coefficients on buildings without costly and time consuming wind tunnel or CFD modeling has been found to be challenging and inexact, making the prediction of pressure distributions on buildings difficult.

The exterior local wind pressure coefficient describes the distribution of wind pressures on the exterior surfaces of a building; however, the pressure of interior zones of a building can also change due to wind. Consequently, the pressure across the exterior enclosure of the building is not equal to P_{wind} as defined in Eq. 3.7. Instead, the pressure across the exterior enclosure is determined by the difference between P_{wind} and the pressure in the adjacent interior space. The distribution to the interior of pressure differences created wind depend on the relative airtightness of the pressure boundaries and is commonly described by an internal wind pressure coefficient as defined in Eq. 3.8.

$$C_{pi} = \frac{P - P_0}{P_{stag}} \quad \text{Eq. 3.8}$$

Where: C_{pi} = Interior Wind Pressure Coefficient [dimensionless]
 P = Pressure at Given Point in the Building [Pa]
 P_0 = Static Reference Pressure [Pa]
 P_{stag} = Stagnation Pressure [Pa]

Internal pressure coefficients are uniform throughout a building zone and are strongly dependent on openings in the exterior enclosure which makes them difficult to predict because it is difficult to predict whether exterior doors and windows will be open or closed. (Yeatts, 1992) Four simple scenarios created by Yeatts (1992) are provided in Figure 3-23 to illustrate how the location of openings in the exterior enclosure can affect the pressure of interior building zones. (Note that Yeatts uses “p” to denote the internal pressure coefficient and the arrows indicate only direction of pressure and not magnitude.)

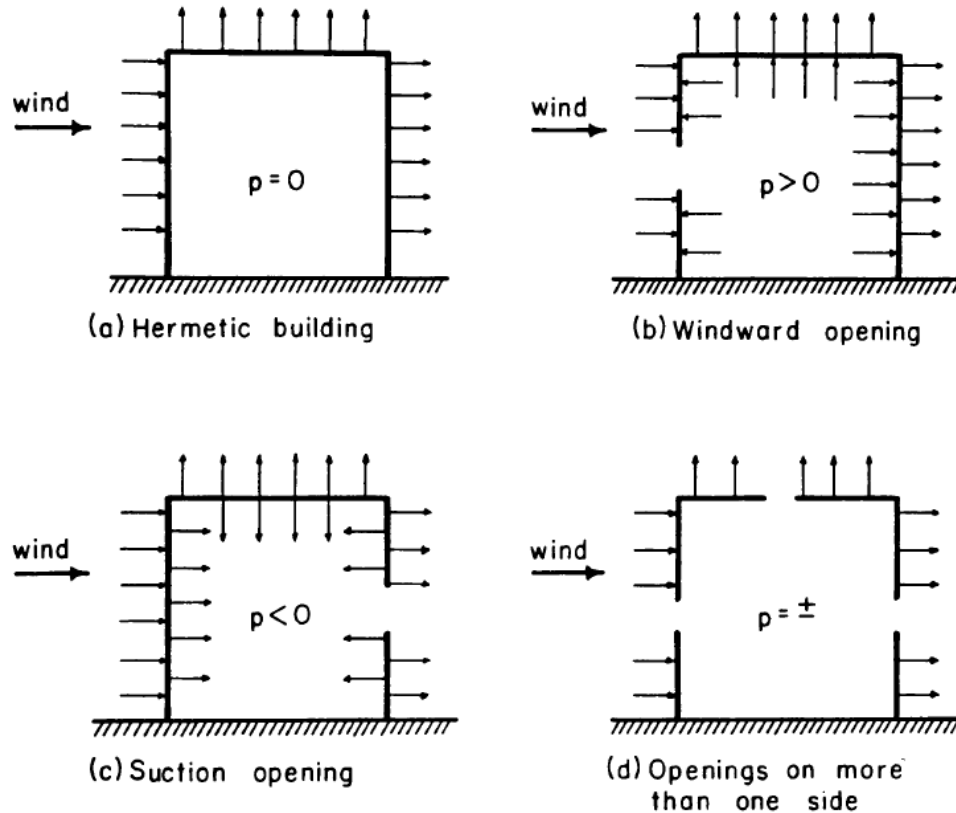


Figure 3-23: Graphic showing interior pressures due to wind with various different distributions of openings in a building enclosure (“p” denotes internal pressure coefficient) (Yeatts, 1992)

Liu (1975) developed an equation for predicting the internal pressure coefficient of a building zone based on the exterior pressure coefficients and the area of the openings under positive and negative pressures. This equation is provided in Eq. 3.9. Liu conducted wind tunnel studies to evaluate the accuracy of this equation and found that the predicted and measured results matched well.

$$C_{pi} = \frac{\overline{C_{p,l}} + r^2 \overline{C_{p,w}}}{1 + r^2} \quad \text{Eq. 3.9}$$

Where: C_{pi} = Interior Wind Pressure Coefficient [dimensionless]
 $\overline{C_{p,l}}$ = Mean C_p at leeward (suction) openings [dimensionless]
 $\overline{C_{p,w}}$ = Mean C_p at windward (positive) openings [dimensionless]
 r = Ratio of windward to leeward (suction) opening areas [dimensionless]

(Liu, 1975)

The majority of internal pressure coefficient research has been focused on either structural considerations or natural ventilation strategies and typically considers buildings with a single interior zone and different sizes and distributions of openings in the exterior building enclosure. For structural applications, typically the case of a sudden opening in the exterior enclosure on the windward side (e.g. broken window or door) is of primary concern as this can cause C_{pi} to temporarily overshoot the equilibrium (steady-state) C_{pi} and result in the greatest magnitude

pressures. For the airflow considerations of this thesis, however, average internal pressures are most relevant; unfortunately, results of this type directly applicable to typical building operations are limited. Yeatts (1992) found based on a literature review and boundary layer wind tunnel testing of an idealized single zone building that mean interior pressure coefficients are typically in the range of approximately 0 to 0.8 depending on a variety of variables. Yeatts also notes that there has been little to no work done investigating internal pressure coefficients for buildings with interior separations.

Importantly, both the interior pressure coefficient and the exterior local pressure coefficient describe the pressure increase of a location directly adjacent to a surface compared to ambient exterior pressure due to wind, and they do not directly describe the pressure difference across a pressure boundary. For example, the exterior pressure on the windward side of a building may increase ($C_p > 0$), but the pressure of the interior windward zones of that building may also increase ($C_{pi} > 0$); consequently, the pressure across the exterior enclosure is not defined by C_p as one might expect and instead is defined by the difference between C_p and C_{pi} .

Overall, the building pressure regime created by wind tends to cause air to flow through horizontally from the windward side towards the leeward side of a building and can have a significant effect on the rate and source of air supplied to spaces within the building (Moffat, Theaker, & Wray, 1998). A schematic representation of a building showing an example of airflow patterns created by wind is provided in Figure 3-24. Note that this figure does not include detailed consideration of localized wind pressures which can be created at building corners and projections as these pressures are relevant to structural design, but of limited relevance to general airflow patterns created by wind as discussed in this thesis.

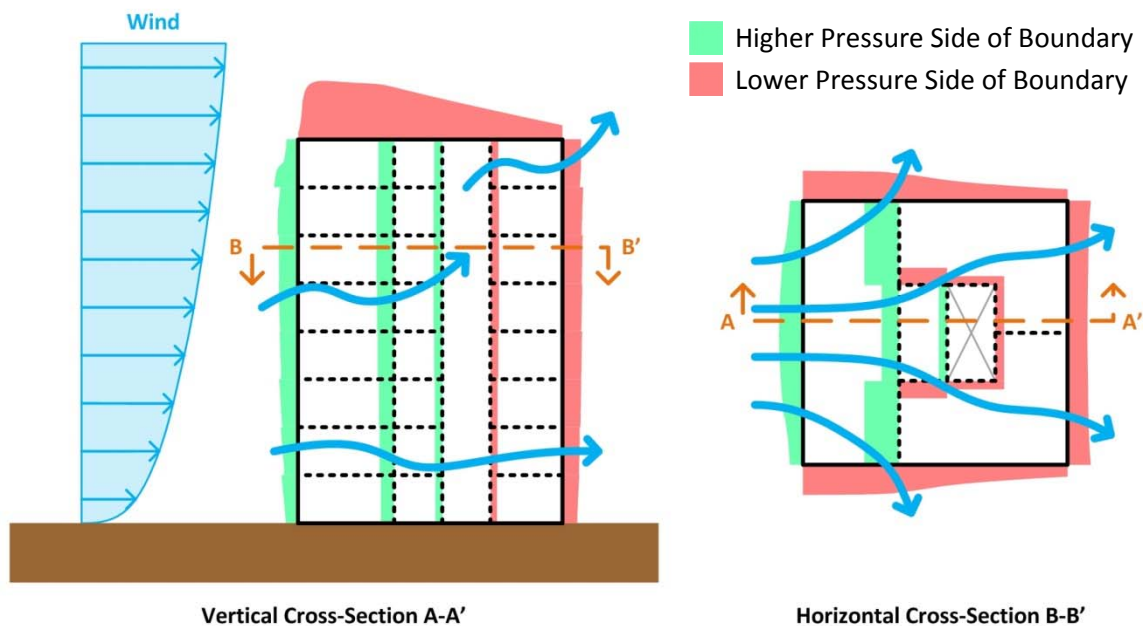


Figure 3-24: Schematic representation of wind pressures and flow within and through a building

3.3 Mechanical Systems

Mechanical ventilation systems use fans to create pressure differences to move air into, out of, and within building. These systems are intended to ensure that ventilation air of appropriate quantity and quality is provided to all areas of a building so that air contaminants are adequately diluted or removed, and they are also intended to control the flow of air contaminants between interior buildings zones. In some cases these systems also provide distribution for space heating and/or cooling systems.

A fundamental difference between mechanical systems and the natural driving forces of airflow is that mechanical systems are intentionally included as part of the building design. When properly implemented, mechanical ventilation systems can be used to control pressure differences and thus control both the direction and rate of airflows between zones. However, commonly the in-service effects of the operation of mechanical ventilation systems are not well understood or accounted for which can lead to the unintended development of pressure differences and consequently to unintended airflows.

This section provides an overview of typical ventilation requirements and design for multi-unit residential buildings, and the associated pressure differences which are developed and drive airflow.

3.3.1 ASHRAE Standard 62.1

The most commonly referenced ventilation standard in North America for ventilation of multi-unit residential buildings is *ASHRAE Standard 62.1 Ventilation for Acceptable Indoor Air Quality* (ASHRAE 62.1-2010), the most recent version of which was published in 2010 (ASHRAE, 2010). Versions of this standard are referenced in the National Building Code of Canada (NBC), and in the International Mechanical Code (IMC), which reproduces much of the standard, and is referenced in the International Building Code (IBC). (ICC, 2012; ICC, 2012; NRC, 2010) ASHRAE 62.1-2010 is intended to provide ventilation regulatory requirements “for all spaces intended for human occupancy except for those within single-family houses, [and] multi-family structures of three stories or fewer above grade.” (ASHRAE, 2010, p. 3) Multi-family structures of 3-storeys or less are covered by ASHRAE 62.2. (ASHRAE, 2010)

ASHRAE 62.1 is intended for use in situations of typical air contaminant loading and adherence to the standard does not guarantee acceptable indoor air quality (IAQ). Buildings which have particularly high concentrations of potentially hazardous air contaminants must be considered separately.

ASHRAE 62.1 provides three methods for determination of the ventilation requirements for a building zone: the Ventilation Rate procedure, the IAQ procedure; and the Natural Ventilation procedure.

The Ventilation Rate procedure uses a formula for the calculation of minimum outdoor air (ventilation air) supplied to a zone based on a combination of air to dilute occupancy related air contaminants and air to dilute building related sources of air contaminants. This formula is provided in Eq. 3.10.

$$V_{bz} = R_p \cdot P_z + R_a \cdot A_z \tag{Eq. 3.10}$$

Where: V_{bz} = Outdoor Air Supplied to Breathing Zone [L/s]
 R_p = Outdoor Airflow Rate Required per Person [L/s-person]
 P_z = Number of People Typically in Zone [person]
 R_a = Outdoor Airflow Rate Required per Unit Area [L/s-m²]
 A_z = Zone Floor Area [m²]

(ASHRAE, 2010)

ASHRAE 62.1-2010 provides a table of values for outdoor airflow rate required per person (R_p), outdoor airflow rate required per unit area (R_a), and for determining occupancy density, all for various different types of spaces. Sections of the minimum ventilation rates table provided in ASHREA 62.1 have been reproduced in Table 3-3 for reference.

Table 3-3: Excerpt of Minimum Ventilation Rates Table in ASHRAE 62.1-2010

Occupancy Category	People Outdoor Air Rate, R_p [L/s-person]	Area Outdoor Air Rate, R_p [L/s-m ²]	Occupant Density [persons/100 m ²]	Combined Outdoor Air Rate [L/s-person]
Daycare (through age 4)	5	0.9	25	8.6
Wood/metal shop	5	0.9	20	9.5
Conference/meeting	2.5	0.3	20	5.5
Residential Dwelling Unit	2.5	0.3	*	
Residential Common Corridor	-	0.3	-	-
Supermarket	3.8	0.3	8	7.6
Health club/weight rooms	10	0.3	10	13

*Occupancy for residential dwelling units is specified as two people for studios and one-bedroom units with one additional person for each additional bedroom. (For example a 3 bedroom unit would be 4 people)

The ventilation rates (as shown in Table 3-3) vary depending on predicted contaminant levels and types of contamination. Zones with relatively high area sources of air contaminants such as wood/metal shops require more area outdoor airflow, and zones with higher air contamination as a result of occupancy, such as weight rooms, require higher people outdoor airflow rates. Zones which typically contain no occupants such as residential common corridors only require area outdoor airflow.

The combined outdoor airflow rate is a simplification provided in the standard which combines the people outdoor air rate and area outdoor air rate using the occupant density. The combined outdoor airflow rate can be used as shown in Eq. 3.11.

$$V_{bz} = R_c \cdot P_z \tag{Eq. 3.11}$$

Where: V_{bz} = Outdoor Air Supplied to Breathing Zone [L/s]
 R_c = Combined Outdoor Airflow Rate Required per Person [L/s-person]
 P_z = Number of People Typically in Zone [person]

As an example, a 2 bedroom 100 m² dwelling unit would require 37.5 L/s of outdoor air supplied to the zone based on ASHRAE 62.1-2010. Rules of thumb for residential unit ventilation design are from 35 to 50 L/s.

The IAQ procedure for determination of minimum ventilation rates is based on the identification of contaminants of concern (COC). Source emission/generation rates for these contaminants are determined and then mass balance equations are used to determine the required ventilation rates to keep these COC concentrations below the limits specified in ASHRAE 62.1-2010. This approach also allows for determination of ventilation rates based on subjective evaluation of the zone or of a similar zone.

The Natural Ventilation procedure provided by ASHRAE 62.1-2010 allows for ventilation of spaces through natural means which in most cases means by use of operable windows. The standard provides requirements for the distribution and size of operable windows to provide sufficient ventilation and also notes that if a particular natural ventilation strategy is approved by the relevant authority then the building need not meet the requirements of ASHRAE 62.1-2010, which allows for some flexibility in design.

ASHRAE 62.1-2010 also provides requirements for minimum exhaust ventilation rates for different spaces to address point source contaminants such as odours and moisture generated in kitchens and bathrooms. These exhaust rates are applicable regardless of the approach selected for supply of ventilation air. An excerpt of the ASHRAE 62.1 table of minimum exhaust requirements is provided in Table 3-4. Note that not all of the occupancy categories provided are relevant to multi-unit residential buildings, but have been included for reference.

Table 3-4: Excerpt of Minimum Exhaust Rates Table in ASHRAE 62.1-2010

Occupancy Category	Exhaust Rate [L/s·unit]	Exhaust Rate [L/s·m ²]
Arenas	-	2.5*
Copy, printing rooms	-	2.5
Locker/dressing rooms	-	1.25
Parking garages	-	3.7
Residential kitchens	25/50†	-
Toilets - private	12.5/25†	-

*Note that the entry for this rate seems to have been unintentionally left blank in the metric column of ASHRAE 62.1-2010, so this value is a conversion from the IP units value.

†When exhaust is continuous, lower rate can be used, otherwise higher rate should be used.

ASHRAE 62.1-2010 also specifies that attached parking garages should be maintained at a negative pressure relative to adjacent zones to prevent the migration of vehicle exhaust fumes into the building. It also states that a vestibule must be used to provide separation between parking garages and adjacent spaces.

While ASHRAE 62.1-2010 focuses on requirements for building ventilation systems, it also provides some recognition of the interaction between building systems by specifying that the building enclosure be air sealed to provide a continuous air barrier. The standard also provides guidance for construction, maintenance, and operation, of ventilation systems as well as further details for their design.

3.3.2 Pressurized Corridor Ventilation System

To meet relevant ventilation requirements, most high-rise multi-unit residential buildings use a corridor pressurization based ventilation system. (Moffat, Theaker, & Wray, 1998; Morrison Hershfield Ltd, 1996; Ueno, Lstiburek, & Bergey, 2012) This section describes the design intent of this system.

To provide ventilation air, a corridor pressurization system uses a make-up air unit (MAU), usually located on the roof of the building, to draw fresh air in with a large fan either continuously or on a pre-set schedule. As the air is drawn in, it is usually filtered and then heated or cooled according to the temperature set point of the MAU. In heating mode, this set point is only intended to temper the air and make it an acceptable temperature for use in transition spaces such as corridors. In cooling mode this is often the only form of cooling for residential buildings in climates without long, hot summers. In both cases, the temperature set-point is typically approximately 15°C.

Once the air is drawn into the building it is distributed to each floor through a large vertical duct usually located in the building core. A grille is provided in this duct at each floor to allow air to flow from the duct to the corridors. Moffat et al (1998) found that in nine Canadian mid to high-rise multi-unit residential buildings the corridor supply airflow rate was designed to be in the range of 25 to 64 L/s per suite.

This flow of air into the corridor pressurizes the corridor relative to the surrounding spaces, thus giving the system its name. Edwards (1999) indicates that pressure that may result from the operation of mechanical systems in MURBs are typically in the range of 2 to 12 Pa, and Cooke (2005) found that the mechanical ventilation systems typically pressurized corridors relative to adjacent suites by 5 to 10 Pa.

The pressurization of the corridors relative to the surrounding suites forces air through gaps at the bottom of the suite entrance doors and into the suites. These gaps are called door undercuts and are intentionally created to allow the flow of ventilation air from the corridors to the suites. A less common alternative is to provide transfer grills either in the doors or through the adjacent wall in lieu of door undercuts.

As well as providing ventilation air to the corridor and suites, the pressurization of the corridors relative to the surrounding suites is intended to prevent the flow of contaminants such as cooking odours from suites to the corridor and from one suite to another via the corridor. (Moffat, Theaker, & Wray, 1998; Morrison Hershfield Ltd, 1996) The air that enters the suites is often also intended to pressurize the suites relative to the exterior to limit infiltration and associated comfort concerns. Figure 3-25 schematically illustrates the intended pressure regime as a result of the corridor pressurization system showing pressure differences between the corridor and suite, and suites and the exterior.

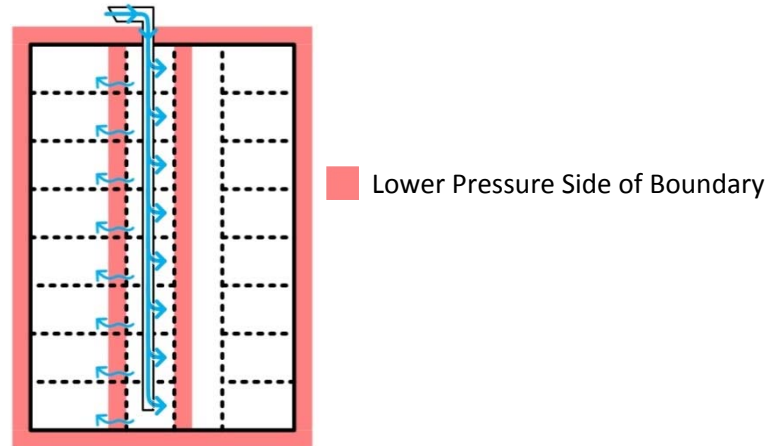


Figure 3-25: Schematic representation corridor pressurization ventilation system

The pressure distribution shown in Figure 3-25 is intended to be the net pressure pressure distribution from all driving forces; however, due to the dynamic nature of the natural driving forces of airflow (stack effect and wind) the net pressure distribution is likely to change significantly during building operation. To effectively implement airflow control using pressure differences, the control of mechanical ventilation systems using real-time measurement of operating pressure differences is likely necessary to maintain pressure differences at the desired magnitude and direction. This type of system is uncommon in multi-unit residential buildings and instead systems are typically balanced only during the initial commissioning of the building.

No provision is typically made for continuous exhaust systems as part of corridor pressurization ventilation systems. On-demand exhaust fans are usually included and are located in bathrooms, kitchen range hoods, and clothes dryers to exhaust point source air contaminants such as odours and water vapour. These fans are often installed to meet the exhaust requirements of ASHRAE 62.1 and the make-up air for this exhaust is intended to be provided through a combination of the corridor make-up air unit supply and infiltration. Exhaust fans are typically ducted from each fan directly to the exterior, or exhausts from multiple suites can also be ganged together and exhausted via a vertical shaft. In the ganged exhaust fan approach, a rooftop fan typically operates continuously to exhaust air, and in unusual cases this system may be supplemented by booster fans in suites or include balancing dampers to help control airflows. (Moffat, Theaker, & Wray, 1998; Ueno, Lstiburek, & Bergey, 2012; Edwards, 1999) Moffat et al (1998) found a large variation in the design exhaust capacity for suites ranging from 48 to 160 L/s with an average of 113 L/s, (1.22 to 4.91 ACH with an average of 2.88 ACH). Operation of these exhaust fans can also cause suites to become depressurized relative to surrounding zones which is discussed in more detail in Chapter 5.

The air that is provided to suites through door undercuts is only tempered by the MAU and may not be at the desired temperature for the suites. Heating and/or cooling is typically provided in the suites to offset heat losses/gains through the exterior enclosure, as well as to modify the temperature of the ventilation air. This additional conditioning of the air is typically provided by baseboard heaters, fan-coil units, fireplaces, or window mounted air conditioning units. The general arrangement of the corridor pressurization ventilation system is illustrated in Figure 3-26.

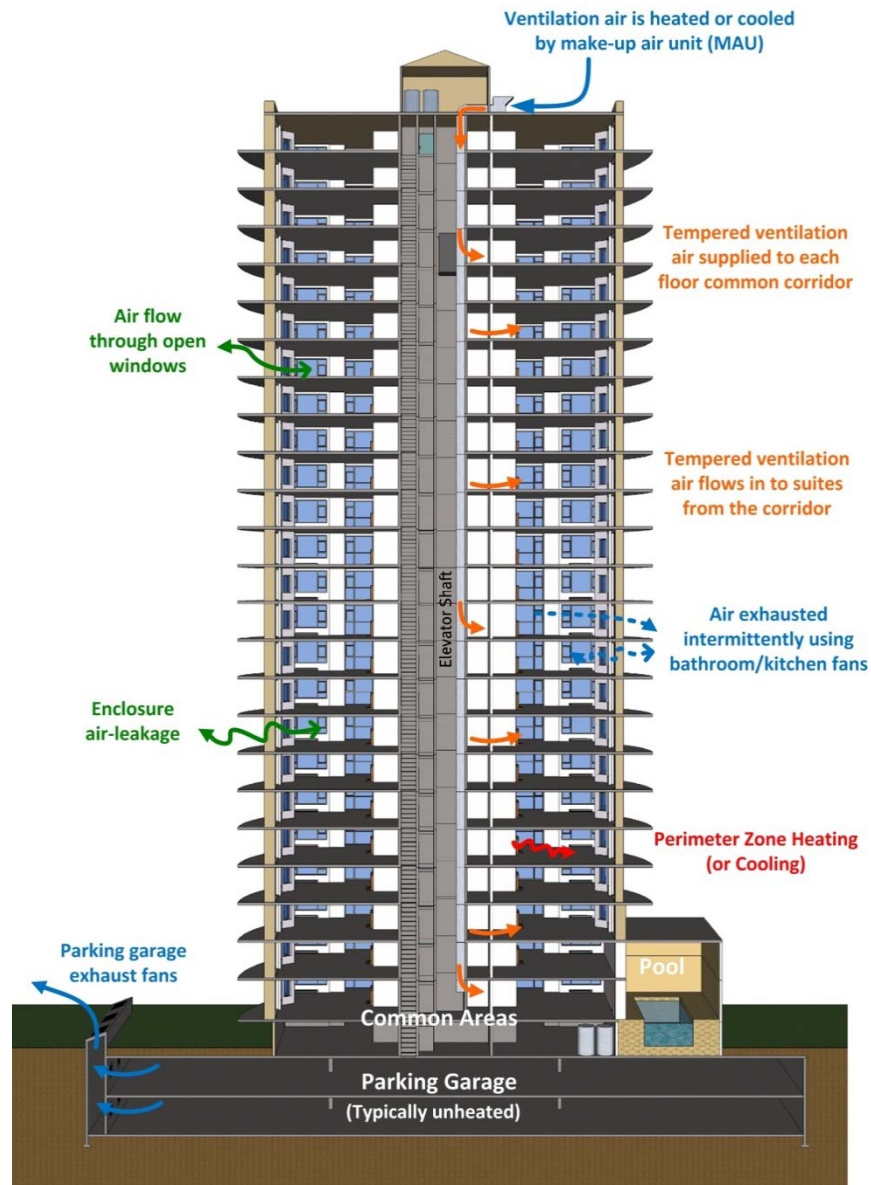


Figure 3-26: Graphic cross-section of a high-rise multi-unit residential building illustrating the operation of the corridor pressurization based ventilation approach

A standard addition to the corridor ventilation system is independent exhaust fans for any parking garage or garbage collection areas. These exhaust fans provide the additional ventilation required to adequately dilute the relatively high levels of air contaminants found in these areas.

Additionally, these exhaust fans may depressurize these spaces relative to the rest of the building which is intended to prevent the flow of air contaminants from these areas of high air contaminant concentration into the rest of the building.

Corridor pressurization ventilation systems are selected for a number of reasons. The primary and overriding driver for the selection of this system is industry familiarity. Corridor pressurization systems are widely used and system designers, installers, and equipment can be easily sourced.

Secondly, these systems use a single large MAU to provide air to the building instead of alternative systems which may use smaller equipment distributed throughout the building. Using a single piece of equipment and limited ducting is advantageous for building maintenance and simplifies design. Furthermore, a single piece of equipment allows for relatively straightforward commissioning and a single set of system controls. Finally, corridor pressurization systems are used because it is generally held that they are easy to design. Despite the apparent simplicity of this system, its actual behaviour is in fact quite complicated and often poorly understood with little design guidance literature available. (Edwards, 1999) The lack of awareness of how such systems actually behave can lead to performance problems as discussed in Chapter 5 and throughout this thesis.

3.3.3 Other Mechanical Systems

Operation of other mechanical equipment can also unintentionally drive airflow, and the primary example of this is the movement of elevators cars up and down within elevator shafts. Klote and Tamura (1986) found that in a 15-storey office building the pressures in the elevator lobbies (corridors) could change by up to approximately 15 Pa during elevator car movement which matched well with the computation model they developed. They also found that the effect is significantly reduced (on the order of 90%) for one car moving within a shaft containing two elevators.

3.4 Combination of Driving Forces

The pressure differences created by the driving forces of stack effect, wind, and mechanical ventilation systems can be summed to determine the actual pressure acting across a building element as shown in Eq. 3.12. (ASHRAE, 2009)

$$\Delta P_{total} = \Delta P_{stack} + \Delta P_{wind} + \Delta P_{mech} \quad \text{Eq. 3.12}$$

Where: ΔP_{total} = Total Pressure Difference
 ΔP_{stack} = Pressure Difference at Due to Stack Effect
 ΔP_{wind} = Pressure Difference at Due to Wind
 ΔP_{mech} = Pressure Difference Due to Mechanical Systems

Note that due to the non-linear relationship between airflow rate and pressure difference as defined in Equation 2.5, it is not correct to sum airflows caused by these forces to determine total airflow rates. Numerous methods exist for calculating total airflow based on the airflows caused by each of the driving forces individually. These include methods presented by Shaw and Tamura (1977), Sherman and Modera (1986) and Walker and Wilson (1998) (the Alberta Infiltration Model, AIM-2). These methods tend to focus on the airflows rather than the pressures because it is the airflow that is of consequence for energy calculations; however, both Shaw and Tamura (1977) and Sherman and Modera (1986) note that for more detailed analysis of flow within buildings, summation of the pressures at zones within the building is necessary. As consideration of pressure distributions within a building significantly complicates the calculation of infiltration rates (for which these models were developed), these models instead use empirical methods to combine the effects of the driving forces of airflow. However, it is more straightforward to understand the relationship as an addition of pressures rather than as a combination of flows, and is also more

fundamentally sound. The addition of pressure differences holds true for wind and stack effect induced pressures as they are generally independent (Sherman & Modera, 1986); however, the operation of mechanical ventilation system components is governed by flow curves, and changes in the backpressure as a result of stack effect and wind can potentially cause changes in the performance of the ventilation fans. This interaction between back pressure and flow rate makes that addition of pressures to determine total pressure somewhat inaccurate when considering mechanical systems; however, this addition is suitably accurate for general consideration of the interaction of these driving forces as is conducted for this thesis.

The interaction of the pressure differences created by stack effect and wind changes the location of the neutral pressure plane. The typically positive pressure created on the windward side of the building by wind causes the neutral pressure plane to move up and the typically negative pressure on the on the leeward side of the building causes the neutral pressure plane to move down resulting in a tilted neutral pressure plane for the building as shown in Figure 3-27. (Moffat, Theaker, & Wray, 1998)

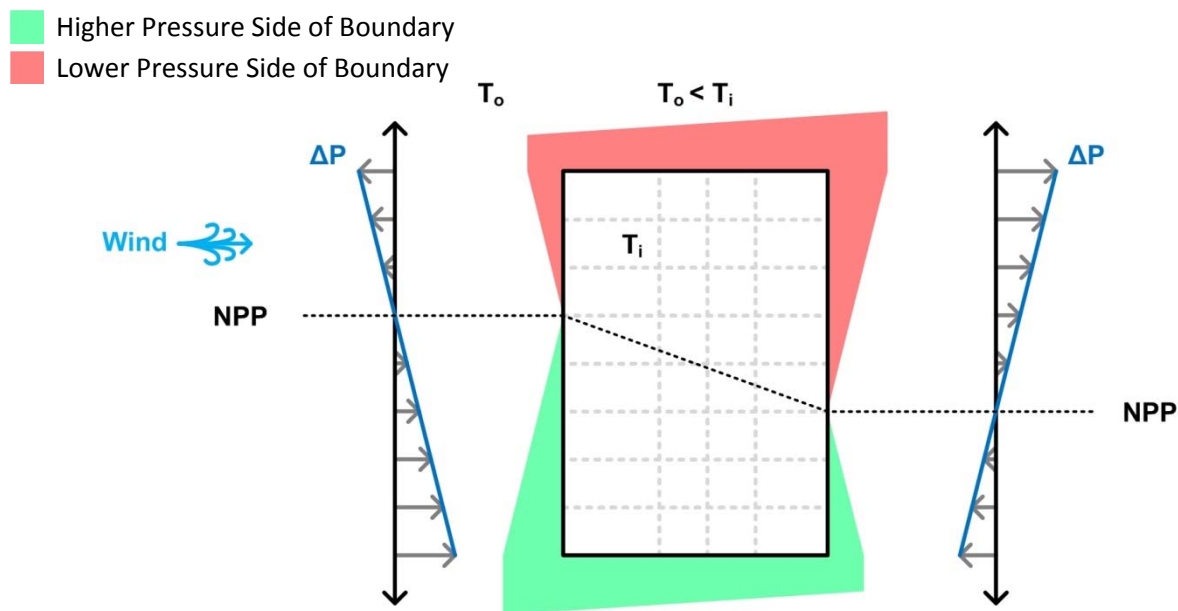


Figure 3-27: Graphic of a schematic building with a tilted neutral pressure plane created by wind pressure on the building

Mechanical ventilation systems can also impact the location of the neutral pressure plane. Depressurization of the building through more exhaust ventilation than supply causes the neutral pressure plane to move up, and pressurization of the building through more supply ventilation than exhaust causes the neutral pressure plane to move down as illustrate in Figure 3-28 and Figure 3-29 respectively.

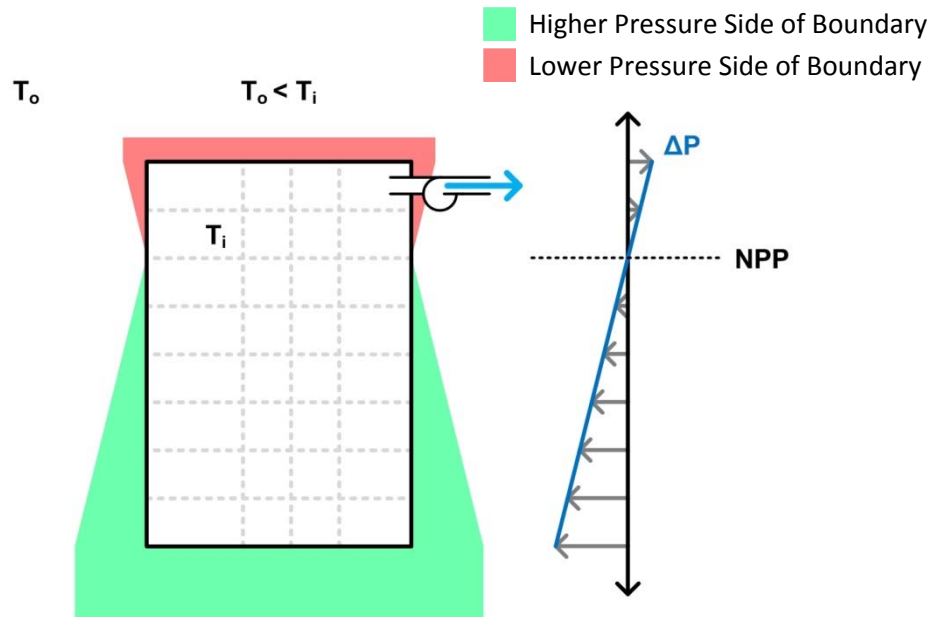


Figure 3-28: Graphic of a schematic building with a neutral pressure plane above the midpoint due to depressurization of the building created by the mechanical ventilation system

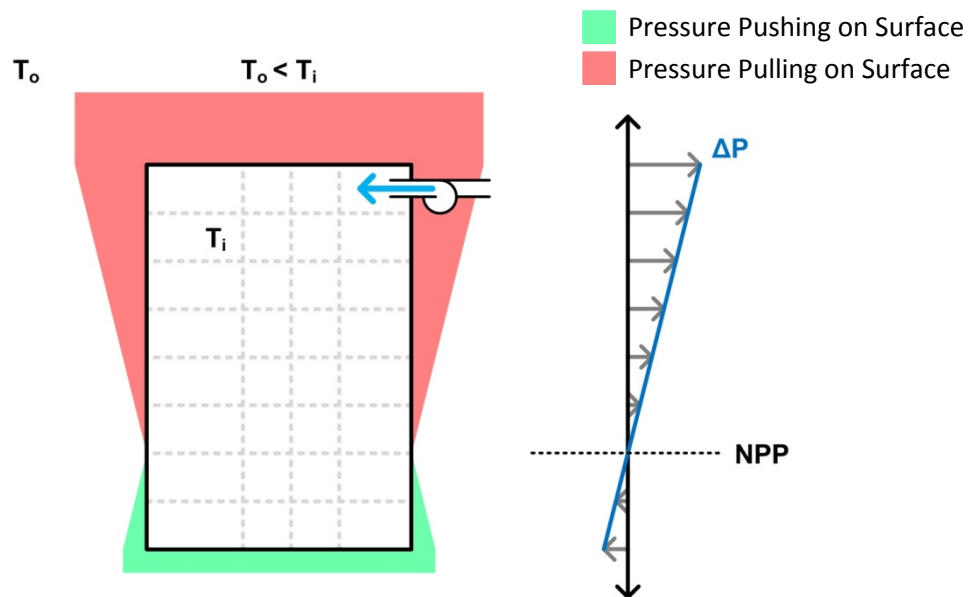


Figure 3-29: Graphic of a schematic building with neutral pressure plane below the midpoint due to pressurization of the building created by the mechanical ventilation system

If the pressure differences created by the mechanical ventilation system are of sufficient magnitude relative to the pressure difference created by stack effect, the neutral pressure plane can be moved above or below the physical extents of the building as shown in Figure 3-30 and Figure 3-31.

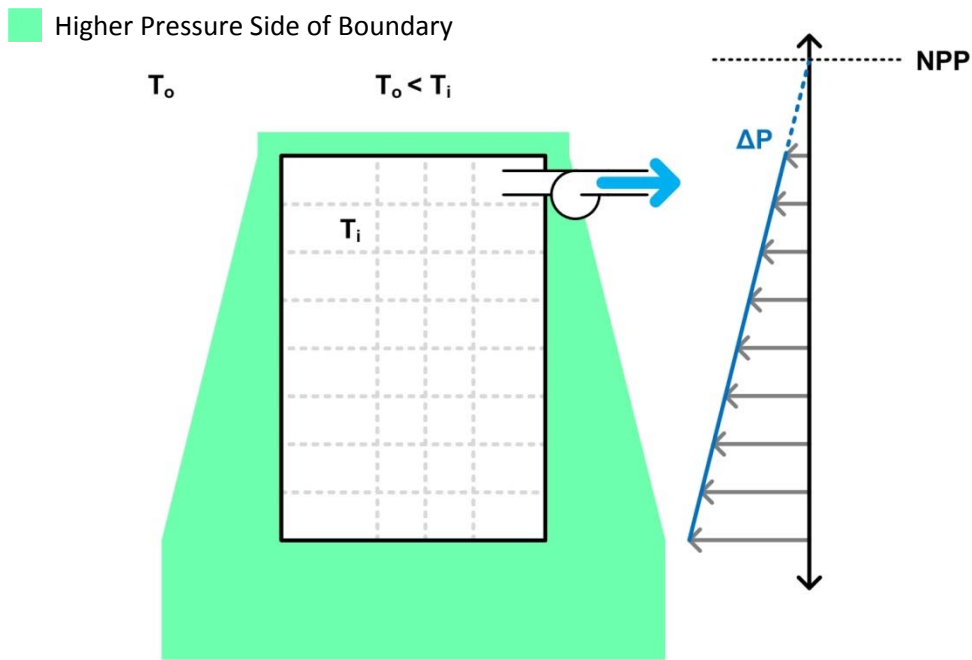


Figure 3-30: Graphic of a schematic building with a neutral pressure plane above the building due to depressurization of the building created by the mechanical ventilation system

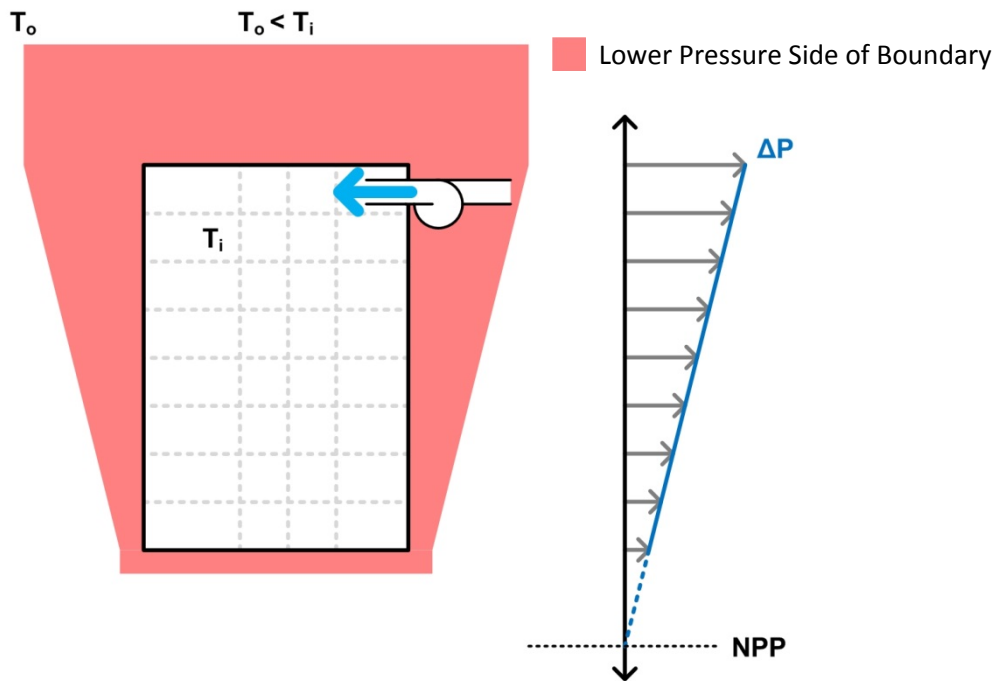


Figure 3-31: Graphic of a schematic building with neutral pressure plane below the building due to pressurization of the building created by the mechanical ventilation system

If the pressure differences created by wind are of sufficient magnitude relative to the magnitude of stack effect, wind can also cause the neutral pressure plane to be located beyond the physical extents of a building.

Overall, the distribution of pressure difference across the pressure boundaries of a building under steady state conditions is dependent on the driving forces of airflow and the relative airflow resistance of the pressure boundaries. Figure 3-32 schematically illustrates the cumulative effects of stack effect, wind, and mechanical ventilation systems on the total pressure regime acting on a building at a given instant in time. While the relative magnitudes of the forces for these conditions are represented accurately in the image for an outdoor temperature of -5°C , a wind speed of 4 m/s , and mechanical system that pressurizes the corridor relative to surrounding spaces by 5 Pa and the suites relative to the exterior by 5 Pa , the image is primarily intended to qualitatively illustrate the addition of these drivers and the resulting airflow regime. Also, different arrangements of airflow resistance would alter the pressure distribution. The implications of the combination of these pressures differences and their interaction with the airflow resistance of building pressure boundaries is discussed in Chapter 5 and throughout this thesis.

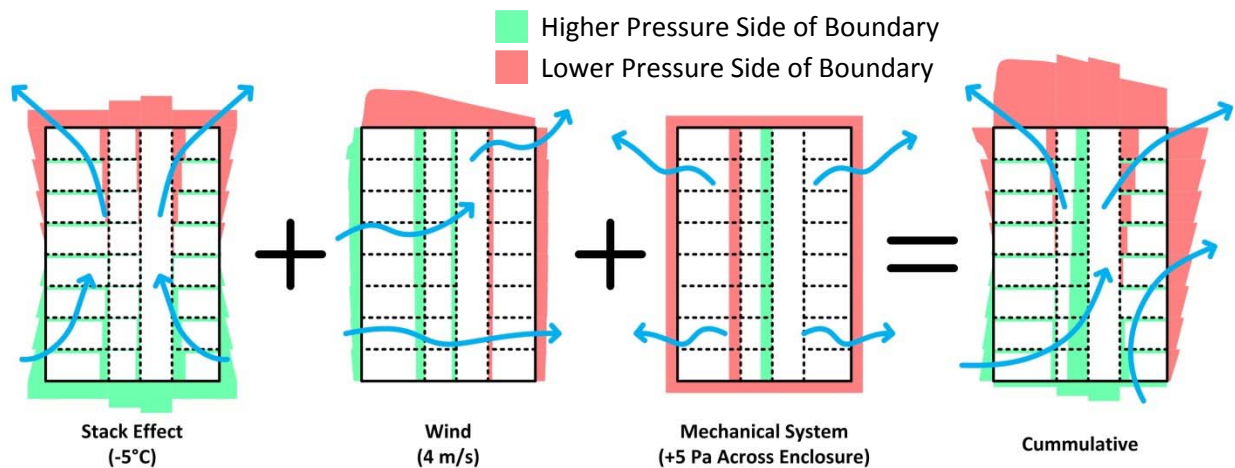


Figure 3-32: Schematic cumulative effect of driving forces of airflow on a tall MURB

To provide an indication of the relative magnitudes of the natural driving forces of airflow, the maximum pressure created by stack effect (assuming NPP at midheight of building) and the stagnation pressure of the wind ($C_p = 1$, and terrain category 2) at the roof of a building were calculated for building heights of 20 m , 40 m , 60 m , 80 m , and 100 m using a combination of CWEC and TMY data from the same sources as described for the stack effect pressure calculations in Section 3.1 (U.S. Department of Energy, 2013). The proportion of the total absolute magnitude of the driving forces attributable to stack effect, wind, and a mechanical pressure of 10 Pa was then determined on an hourly basis for each of eight cities in North America and plotted. A selection of these graphs is provided in Figure 3-33 to Figure 3-35. Figure 3-36 shows the annual average proportion of the absolute magnitude of the total pressure differences created by the driving forces for various building heights in Vancouver, and Figure 3-37 shows the proportions for a 40 m tall building in each of eight cities.

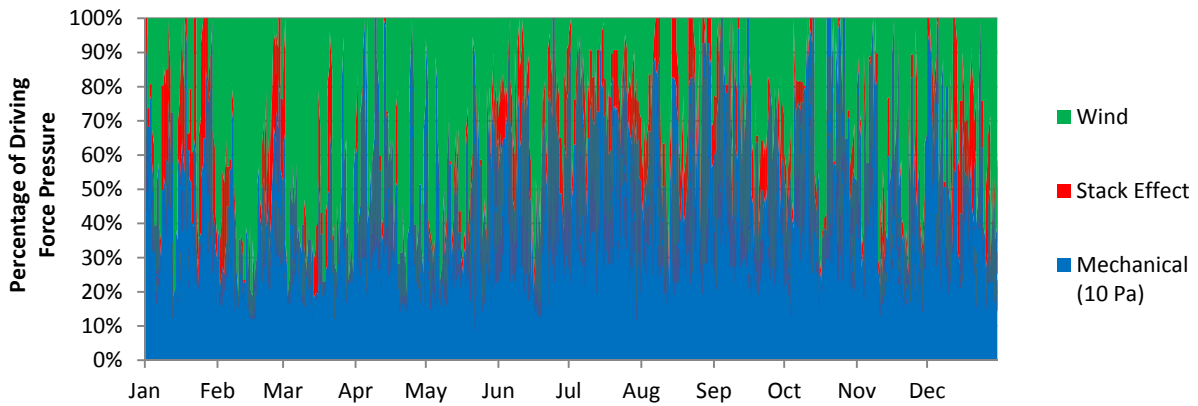


Figure 3-33: Graph of proportion of total absolute pressure difference attributable to each of the driving forces for a 40 m tall building in Miami

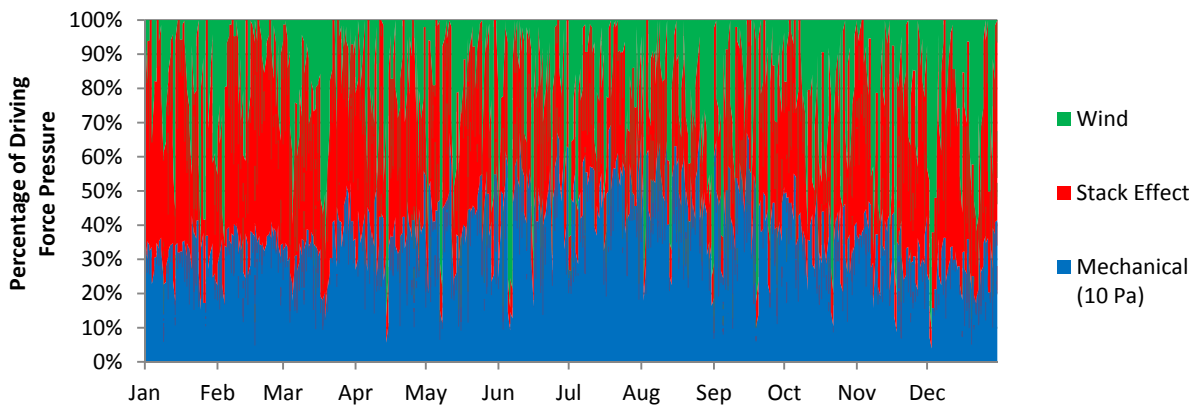


Figure 3-34: Graph of proportion of total pressure difference attributable to each of the driving forces for a 40 m tall building in Vancouver

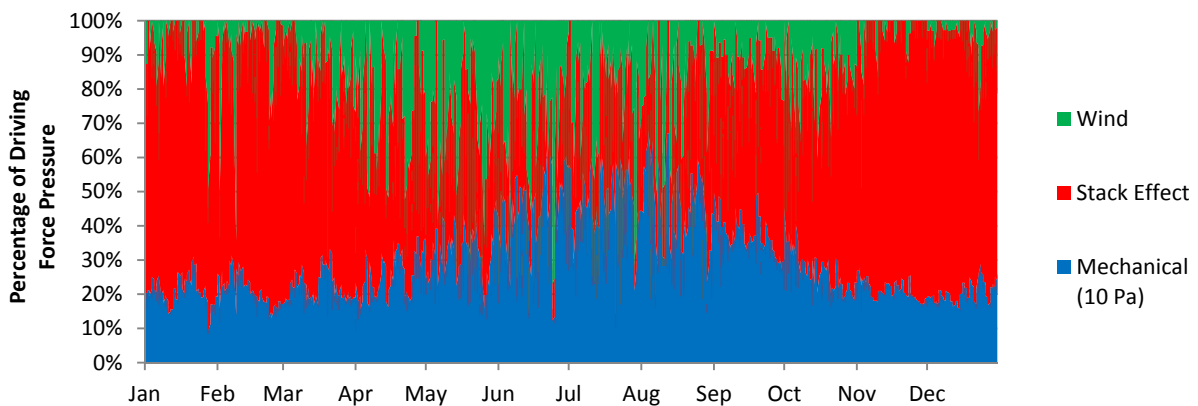


Figure 3-35: Graph of proportion of total pressure difference attributable to each of the driving forces for a 40 m tall building in Fairbanks

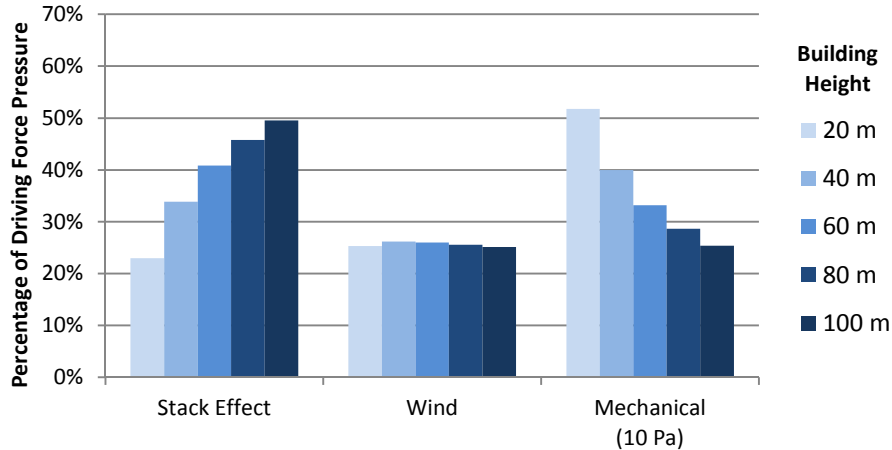


Figure 3-36: Graph of annual average proportion of total pressure difference attributable to each of the driving forces for various building heights in Vancouver

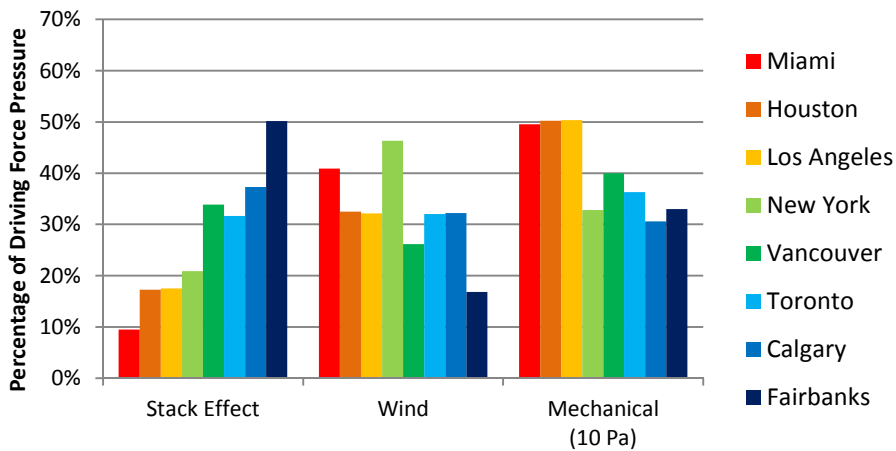


Figure 3-37: Graph of annual average proportion of total pressure difference attributable to each of the driving forces for a 40 m tall building in various North American cities

Note that the five preceding graphs do not indicate the direction of the pressure differences created (positive or negative) nor do they indicate the distribution of the pressure differences but instead are intended only to indicate relative magnitudes. As the mechanical ventilation pressure used for these graphs is always 10 Pa, this value can be used in interpreting the graphs to determine the approximate magnitudes of the driving forces.

The combination of the preceding graphs illustrates that, as one would expect, stack effect is a dominant driving force in colder climates and during colder periods of the year, but that in warmer climates wind and mechanical pressures are more likely to dominate. Also, the total magnitude of pressure differences created by stack effect and wind increases with building height, and thus the proportion of pressure difference due to the mechanical ventilation system decreases with building

height. Overall, it is possible that any one of the driving forces is dominant in both the short and long-term depending on climate and building height.

Chapter 4

Air Permeance

Air permeance, also called airtightness, describes the resistance to airflow provided by pressure boundaries and can be used to control airflow into, out of, and within buildings. The layer within a building assembly that is specifically designed to resist airflow is commonly referred to as the air control layer or air barrier. These airtight building elements separate the building into spaces which are relatively sealed with respect to air movement. This can include separation of the interior space from the exterior, as well as separation of interior spaces from each other, which is referred to as compartmentalization. To fully understand airflow within and through buildings, characterization of the air permeance of the building pressure boundaries is necessary.

This chapter provides a brief overview of common air barrier systems and discusses three different types of compartmentalization. It then provides a review of commonly used airtightness metrics and a summary of airtightness regulatory requirements, primarily with respect to the exterior building enclosure. Building material, component, assembly, and enclosure airtightness data collected from literature are then provided as a reference for subsequent comparison with airtightness testing performed as part of this thesis work. In particular, a database of multi-unit residential building airtightness testing results developed as part of this research work is summarized. The airtightness of interior compartmentalizing elements is also discussed.

A number of testing standards are referenced in this chapter and these are discussed in more detail in Chapter 5.

4.1 Building Enclosure Air Barrier Systems

Air control layers, or air barriers, are used to separate spaces with respect to airflow using a combination of airtight building components and materials to create a continuous relatively air impermeable layer that significantly reduces the flow of air across a pressure boundary for a given pressure difference. Air barrier systems must comply with a number of design requirements in order to function adequately and remain airtight over the life of the building, or building element. The following list has been generated based on guidance in Straube & Burnett (2005), and RDH Building Engineering Ltd. & FPIInnovations (2013).

- An air barrier system must be completely continuous over the boundary that it defines including at junctions with adjacent air barrier systems. This includes sealing at all penetrations and joints.
- An air barrier system must comprise elements which are adequately air impermeable. This is discussed further in subsequent sections.
- An air barrier system must be able to resist the air pressure forces imposed upon it by the driving forces of airflow (primarily wind) without deflection that compromises its performance. It should transfer these forces to the building along predictable load paths.
- The air barrier system should have a service life as long as that of components which would need to be removed to replace it, or alternatively should be easily accessible for repair or replacement.

The continuity requirement for air barrier systems is of particular importance. Many common materials used in the construction of buildings are airtight enough to meet the material requirements of an air barrier (discussed in Section 4.4); however, it is the interfaces and joints between these materials where significant airflow can occur. For this reason, the performance of an air barrier system is often highly dependent on the design of interface details and the quality of workmanship with which it is installed. To aid in achieving good workmanship, the constructability of an air barrier system is a key consideration. (Steffen, 2012) Additionally, during the selection and design of air barrier assemblies it is important to consider the location of penetrations such as for plumbing and electrical as these types of penetration can be difficult to seal and may compromise the continuity of an air barrier assembly.

Many strategies exist for the implementation of air barriers. While it is beyond the scope of this thesis to provide a detailed review of the various systems available, a brief overview of some common systems is provided here. The system types are discussed primarily with respect to the exterior enclosure; however, similar system types can be used for interior pressure boundaries.

Air barrier systems can be generally classified in to 5 categories:

- Monolithic Materials
- Sealed Sheathing (exterior or interior)
- Membranes
- Sprayfoam
- Window Wall and Curtain Wall

Monolithic material air barrier assemblies are formed by systems where the air barrier functionality of the system is integral to the material used to construct the assembly. A common example of this assembly type would be a cast-in-place concrete wall. Figure 4-1 shows an example of this type of air barrier system.

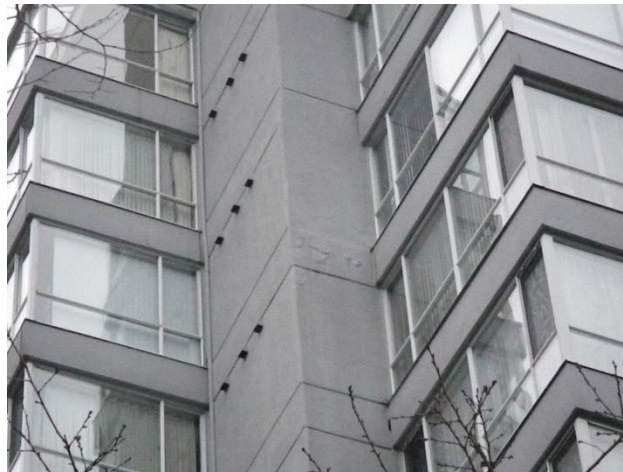


Figure 4-1: Exposed cast-in-place concrete wall assembly where the concrete is providing the air barrier. (Photo courtesy of RDH.)

Sealed sheathing air barrier assemblies consist of sealing the joints of rigid sheet products such as plywood, oriented strand board (OSB), gypsum wall board (drywall), exterior gypsum sheathing, or

extruded polystyrene insulation. Typically, exterior sheathing is sealed with sealant, liquid applied membranes, or tape. Interior sheathing, commonly in the form of drywall, can also be sealed. In the case of drywall this is known as the airtight drywall approach (ADA) (Building Science Corporation, 2009). Figure 4-2 and Figure 4-3 show examples of this type of air barrier system.



Figure 4-2: Exterior gypsum sheathing sealed to provide the air barrier.
(Photo courtesy of RDH.)



Figure 4-3: Interior plywood sheathing of pre-fabricated wall panel sealed with tape to provide the air barrier.
(Photo courtesy of RDH.)

Membranes are another common way to create an air barrier. Both sheet membranes and liquid applied membranes can be used as air barriers. In the case of sheet applied membranes, sealing of the joints between sheets is required. If the membrane is not adhered to the substrate, fastening and/or support is required to meet the structural requirement of an air barrier system. Figure 4-4 and Figure 4-5 show examples of this type of air barrier system.



Figure 4-4: Exterior non-adhered sheathing membrane with seams taped to provide the air barrier. (Photo courtesy of RDH.)



Figure 4-5: Exterior adhered sheathing membrane providing air barrier. (Photo courtesy of RDH.)

Sprayfoam is a unique material that can be used as an air barrier system. Both closed cell and open cell spray foams are appropriate for use as an air barrier (in appropriate thicknesses) and are commonly applied between studs or to the outside of exterior sheathing. Figure 4-6 shows an example of this type of air barrier system. Sprafoms are also used to provide air sealing at transitions between different air barrier systems.



Figure 4-6: Closed cell spray foam insulation applied to exterior sheathing to provide air barrier with flexible membrane use at transitions and movement joints. (Photo courtesy of RDH.)

Window wall and curtain wall assemblies can compose either part or the entirety of an air barrier system. The glass, seals, and metal of a curtain wall system can form an effective air barrier as in the building shown in Figure 4-7.



Figure 4-7: Building where curtain wall system provides the air barrier.
(Photo courtesy of RDH.)

In all cases, continuity of these air barrier systems at transitions is fundamental to their performance. At penetrations and transitions this continuity is typically provided through a combination of sealants, tapes, gaskets, and sprayfoams.

4.2 Compartmentalization

Air sealing between internal spaces or zones is often referred to as “compartmentalization” as it separates the building in to compartments. Compartmentalization is an important difference between multi-unit residential buildings and other types of building such as commercial buildings which typically have few separations on a floor. (Edwards, *Modelling of Ventilation and Infiltration Energy Impacts in Mid and High-Rise Apartment Buildings* 1999) In many cases this sealing is primarily for smoke control, but it can also form an important part of the ventilation strategy for a building.

Morrison Hershfield (1996) identifies three types of compartments within multi-unit residential buildings: suites, corridors, and vertical shafts such as elevator and stairwell shafts. They also identify three different types of compartmentalization: suite, floor-by-floor, and “double.” Suite compartmentalization refers to air sealing between adjacent suites on the same floor and between suites and the corridors. Floor-by-floor compartmentalization separate’s each floor by sealing between floors and also between vertical shafts and adjacent zones. Finally, double compartmentalization is suite and floor-by-floor compartmentalization combined.

As mentioned previously, intentional compartmentalization of high-rise multi-unit residential buildings is typically used as a fire and smoke control method. Floor levels are sealed with sealant around mechanical, electrical, and plumbing penetrations, and the walls between adjoining suites and the walls between suites and corridors are usually intended to be airtight. In cases where ducts

penetrate planes of airtightness it is often necessary to install fire dampers that will close in the event of a fire to prevent the distribution of smoke within the building.

In addition to its use as a fire and smoke control method, compartmentalization can also be used as part of building ventilation and airflow control strategies. Airtight interior pressure boundaries resist the flow of air between interior zones which reduces the quantity of airborne contaminant transfer and can also reduce acoustic transmission. Importantly, compartmentalizing interior spaces changes the distribution of pressure differences created by the driving forces of airflow. More airtight pressure boundaries tend to have larger pressure differences across them than do less airtight boundaries as larger pressure differences are required to create the same flow rate. In an assessment of ventilation rates and pressure differences in high-rise multi-unit residential buildings, Cooke (2005) concluded that it would be much easier to manage the pressure differences created within a building if it were compartmentalized.

4.3 Airflow and Airtightness Metrics

Common metrics used for reporting of airflow and airtightness are described in this section for reference.

4.3.1 Airflow Rate

The total airflow rate can be used to indicate the air leakage characteristics of a pressure boundary. This number can be useful for ventilation and energy calculations, and it is often known since it is directly measured as part of most airtightness testing procedures as discussed in Section 5.1. The airflow rate must be given at a specified pressure differential for it to have meaning. Typically airflow rates are reported at pressure differentials of 50 or 75 Pa. There is some discrepancy within industry as to which is preferable, and one of the common arguments for using 50 Pa is that it is a more easily achieved test pressure and it is usually possible to include this test pressure within the tested range so that extrapolation is not required to determine the result. However, as buildings become more airtight, 75 Pa is becoming a more easily achievable pressure difference for testing and typically the higher the pressure difference, the more stable and reliable the flow measurement. In either case, it is most useful to provide flow coefficients (or normalized flow coefficient) and flow exponents since these values can be used to calculate the flow rate at any pressure difference to allow for comparison. Flow rates are also often provided at lower pressures to represent in-service conditions. The airflow rate at a given pressure difference ΔP (in Pascals) is denoted $Q_{\Delta P}$ [m^3/s].

4.3.2 Normalized Airflow Rate

The normalized airflow rate, also known as the normalized leakage rate, is the airflow rate divided by a specific area. Typically the area used is the total area of the pressure boundary, which in many cases is the total enclosure area of the building. In some cases, only the above-grade area of the building enclosure is used. The equation for calculation of the normalized airflow rate is provided in Eq. 3.12.

$$q_{\Delta P} = \frac{Q_{\Delta P}}{A} \quad \text{Eq. 4.1}$$

Where: $q_{\Delta P}$ = Normalized Airflow Rate at ΔP [m/s]
 ΔP = Pressure Difference [Pa]
 $Q_{\Delta P}$ = Airflow Rate [m³/s]
 A = Area of Pressure Boundary [m²]

4.3.2.1 Air Change Rate

Air change rate, typically measured in air changes per hour (ACH), is a measure of how frequently the air volume in a space is replaced. This value is found by dividing the flow rate into a space by the volume of that space as shown in Eq. 4.2. The volume of the space used for this calculation is the entire volume enclosed by compartmentalizing elements or the building enclosure.

$$ACH_{\Delta P} = N_{\Delta P} = \frac{Q_{\Delta P}}{V} \cdot 3,600 \quad \text{Eq. 4.2}$$

Where: $ACH_{\Delta P}$ or $N_{\Delta P}$ = Air Changes Per Hour ΔP [h⁻¹]
 ΔP = Pressure Difference [Pa]
 $Q_{\Delta P}$ = Airflow Rate [m³/s]
 V = Volume of the Zone [m³]

ACH is not a fundamental indicator of resistance to airflow as it depends on the zone volume; however, it is commonly used as an indicator of airtightness, especially for houses. It is most useful when considering ventilation rates.

4.3.3 Equivalent Leakage Area

Equivalent leakage area (EqLA) represents the size of a sharp-edged orifice which would produce the same air flow at a given pressure differential as would occur cumulatively through all the leakage paths in a given pressure boundary. Flow through a sharp edged orifice is described in Eq. 2.1. While the concept behind this metric is to provide a tool for visualization of the airtightness of a pressure boundary (i.e. size of the hole), the hole size calculated does not actually provide a measurement of the cumulative size of the “holes” in the pressure boundary.

For the calculation of EqLA in accordance with *CGSB 149.10-M86 Determination of the Airtightness of Building Envelopes by the Fan Depressurization Method* (1986), a discharge coefficient of 0.611 (this corresponds with Kirchoff’s calculation for a round sharp-edged orifice) is assumed and a reference pressure difference of 10 Pa is used. A rearrangement of the sharp-edged orifice equation is provided in Eq. 2.1 to calculate EqLA according to CGSB 149.10-M86. By substituting Eq. 2.5 in to Eq. 2.1, Eq. 4.4 can be developed to calculate EqLA based on only the flow coefficient (C) and the flow exponent (n).

$$EqLA = \frac{Q_{10}}{0.611} \sqrt{\frac{\rho}{2 \cdot 10}} \cdot 10,000 \quad \text{Eq. 4.3}$$

Where: EqLA = Equivalent Leakage Area [cm²]
 Q_{10} = Airflow at 10 Pa [m³/s]
 ρ = Air Density [kg/m³]

$$EqLA = \frac{C \cdot 10^n}{0.611} \sqrt{\frac{\rho}{2 \cdot 10}} \cdot 10,000 \quad \text{Eq. 4.4}$$

Where: EqLA = Equivalent Leakage Area [cm²]
 C = Flow Coefficient of Pressure Boundary [m³/s·m²·Paⁿ]
 A = Area of Pressure Boundary [m²]
 n = Flow Exponent [dimensionless]
 ρ = Air Density [kg/m³]

4.3.4 Effective Leakage Area

Effective leakage area (EfLA) is a term commonly confused with EqLA. (Sometimes both of these are referred to as ELA.) EfLA is the measure used by the American Society for Testing and Materials (ASTM) and the calculation procedure is provided in ASTM E779-10 (2010). EfLA is calculated using the same procedure as EqLA except that the discharge coefficient is assumed to be 1.0 and a reference pressure of 4 Pa is used. Eq. 4.5 is used to calculate effective leakage area and was developed similarly to Eq. 4.4.

$$EfLA = \frac{Q_4}{1.0} \sqrt{\frac{\rho}{2 \cdot 4}} \cdot 10,000 = \frac{C \cdot 4^n}{1.0} \sqrt{\frac{\rho}{2 \cdot 4}} \cdot 10,000 \quad \text{Eq. 4.5}$$

Where: EfLA = Equivalent Leakage Area [cm²]
 Q₄ = Airflow at 4 Pa [m³/s]
 C = Flow Coefficient of Pressure Boundary [m³/s·m²·Paⁿ]
 A = Area of Pressure Boundary [m²]
 n = Flow Exponent [dimensionless]
 ρ = Air Density [kg/m³]

4.3.5 Specific Leakage Area

Specific leakage area (SLA) is either EqLA or EfLA normalized by the area of the pressure boundary. The calculation of SLA is provided in Eq. 4.6.

$$SLA = \frac{EqLA \text{ or } EfLA}{A} \cdot 100 \quad \text{Eq. 4.6}$$

Where: SLA = Specific Leakage Area [cm²/100 m²]
 EfLA = Equivalent Leakage Area [cm²]
 EqLA = Effective Leakage Area [cm²]
 A = Area of Pressure Boundary [m²]

Whether the calculation uses EqLA or EfLA can be specified with a subscript (e.g. SLA_{eq} or SLA_{ef}). In some cases SLA is calculated using the floor area of the zone instead of the enclosure area; however, similar to ACH, this metric does not provide a fundamental indication of the airtightness of a pressure boundary.

4.3.6 Airflow per Unit Length

The leakage per unit length is similar to the normalized airflow rate except that instead of dividing by the relevant area, a length is used. This measure is typically used in cases where a crack length is clearly identifiable, such as the perimeter of a window or door. The calculation of this metric is provided in Eq. 4.7.

$$q_{L,\Delta P} = \frac{Q_{\Delta P}}{L} \quad \text{Eq. 4.7}$$

Where: $q_{L,\Delta P}$ = Length Normalized Airflow Rate at ΔP [m/s]

ΔP = Pressure Difference [Pa]

Q_x = Airflow Rate [m³/s]

L = Crack Length [m]

4.4 Airtightness Regulatory Requirements

A variety of requirements and guidelines exist for air barrier materials, air barrier assemblies, and in some cases for the airtightness of the whole building enclosure. This section provides a brief summary of these as found in North American codes and third-party certification programs as they relate to multi-unit residential buildings.

The National Building Code of Canada (NBC) and National Energy Code for Buildings (NECB) include general requirements for the inclusion of a continuous air barrier as part of the exterior building enclosure. They specify that materials forming part of the air barrier systems must be air impermeable (less than 0.02 L/s·m² at 75 Pa) and continuity between air barrier components must be maintained. The airtightness requirements for components within the air barrier systems such as windows depend on the performance requirements and are in the range of 1.5 to 0.2 L/s·m² (AAMA/WDMA/CSA, 2008). There is no requirement in Canadian building codes for airtightness of the building enclosure as a whole. (NRC, 2010; NRC, 2011)

The International Building Code (IBC) specifies that buildings be built in accordance with the International Energy Conservation Code (IECC). (ICC, 2012; ICC, 2012) For high-rise multi-unit residential buildings the IECC requires that a continuous air barrier be installed. The materials used in the air barrier must be air impermeable (less than 0.02 L/s·m² at 75 Pa, same as the NBC), and assemblies of materials must be less air permeable than 0.20 L/s·m² at 75 Pa. This code also requires airtightness testing of the building enclosure in accordance with ASTM E779 (or an equivalent standard) and that the completed building enclosure be more airtight than 2.0 L/s·m² at 75 Pa. *ASHRAE Standard 189.1 – 2011 Standard for the Design of High-Performance, Green Buildings* has the same requirement for airtightness of the exterior building enclosure. (ASHRAE, 2011)

ASHRAE Standard 90.1-2010 Energy Standard for Buildings Except Low-Rise Residential Buildings requires a continuous exterior building enclosure air barrier, but provides no performance requirement. It requires testing of fenestration and doors in accordance with NFRC 400 and specifies airtightness that generally they must meet 2.0 L/s·m², but neglects to specify the test pressure at which components must meet the requirement. The test pressure for NFRC 400 is 75 Pa, so it is assumed that this airtightness of 2.0 L/s·m² is intended to be at a test pressure of 75 Pa. (NFRC, 2004)

Energy Star® is a rating system for buildings. It requires that buildings be tested in accordance with ASTM E779 or ASTM E1827 and be more airtight than $1.5 \text{ L/s}\cdot\text{m}^2$ at 50 Pa. Meeting this airtightness target is a requirement for both the prescriptive and performance paths of the Energy Star® rating system. (Energy Star, 2012)

Passivhaus (Passive House) is an energy efficient house program developed in Germany that has gained significant international recognition, and is also being applied to multi-unit residential buildings. This third-party certification requires that buildings be tested with a leakage rate of less than 0.6 ACH_{50} . (Passive House Institute, 2012)

Leadership in Energy and Environmental Design (LEED) is a sustainable building certification program which is one of the few standards to provide requirements for the airtightness of interior compartmentalizing elements. The LEED program requires that SLA_{eq} be less than $1.65 \text{ cm}^2/\text{m}^2$ for a combination of the exterior building enclosure and interior compartmentalizing elements when a suite is tested according to CGSB 149.10. (CaGBC, 2009) Assuming a flow exponent (n) of 0.65, this corresponds with $1.5 \text{ L/s}\cdot\text{m}^2$ at 75 Pa.

For the buildings over which it has jurisdiction, the United States Army Corps of Engineers sets a performance target of $1.27 \text{ L/s}\cdot\text{m}^2$ ($0.25 \text{ ft}^3/\text{min}\cdot\text{ft}^2$) at 75 Pa with required whole building testing to meet this target (US Army Corps of Engineers, 2012).

The newest update to the ASHRAE Standard 62.1 will include a compartmentalization airtightness requirement of $1.0 \text{ L/s}\cdot\text{m}^2$ at 50 Pa. (Lstiburek, 2013)

4.5 Airflow Resistance of Materials, Components, and Assemblies

This section provides the airflow resistance of various materials, components, and assemblies based on values found in literature. These values are provided primarily for reference and will be compared with the experimental results of the case study building in subsequent chapters.

4.5.1 Airflow Resistance of Materials

Many materials commonly used in building construction are relatively airtight. While it is most accurate to report material airtightness properties using normalized flow coefficients and flow exponents, it is easier to compare normalized flow rates reported at a given pressure difference, and this approach is more common. A sample of airtightness properties of materials are presented in Table 4-1 using both of these approaches whenever sufficient data was available.

Table 4-1: Airtightness Properties of Common Construction Materials

Material	Air Permeance [m/Pa ⁿ s]	Flow Exponent, n	q ₇₅ [L/s·m ² × 10 ⁻³]	Reference
Plywood Sheathing, 8mm	0.110	0.944	6.48	(AIR-INS, 1988)
Waferboard, 11mm	0.145	0.998	10.8	(AIR-INS, 1988)
Particle Board, 12.7mm	0.210	0.996	15.5	(AIR-INS, 1988)
Gypsum Wall Board (Moisture Resistant), 12.7mm	0.120	1.000	9.00	(AIR-INS, 1988)
Gypsum Wall Board (Interior), 12.7mm	0.266	0.995	19.5	(AIR-INS, 1988)
Fiber Board, 11mm	11.470	0.990	824	(AIR-INS, 1988)
Asphalt Impregnated Fiber Board, 11mm	11.266	0.995	827	(AIR-INS, 1988)
Expanded Polystyrene (EPS) - Type 1, 25.4mm	251.356	0.900	12,242	(AIR-INS, 1988)
Expanded Polystyrene (EPS) - Type 2, 25.4mm	1.630	0.993	119	(AIR-INS, 1988)
Fiberglass Insulation, 152mm	610.880	0.949	36,761	(AIR-INS, 1988)
30 lb Roofing Felt	2.535	0.996	187	(AIR-INS, 1988)
15 lb Non-Perforated Asphalt Felt	3.607	1.000	271	(AIR-INS, 1988)
15 lb Perforated Asphalt Felt	6.629	0.947	395	(AIR-INS, 1988)
Self-Adhered Membrane (polyethylene facer)	-	-	0.2	(ABAA, 2011)
Spray Polyurethane Foam (Closed Cell), 25mm	-	-	< 1.0	(ABAA, 2011)
Tyvek™	-	-	2	(ABAA, 2011)

As many common materials are relatively air impermeable (as shown in the table above), it is the combination of these materials in to building components (such as windows and doors) and assemblies which is more relevant to the airtightness performance of buildings.

4.5.2 Airflow Resistance of Building Components

Airflow characteristic data for components has been collected from Colliver, Murphy, & Sun (1994), Fang & Persily (1995), Gulay, Stewart, & Foley (1993), Moffat, Theaker, & Wray (1998), Tamura & Shaw (1976), Edwards (1999), Orne et al (1998), and Morrison Hershfield (1996). Due to the large nature of the data set, the collected data is presented Appendix A.

Data is also available through the CONTAM online database (NIST, 2013), and this data is also included in Persily & Ivy (2001). Much of the data relevant to multi-unit residential buildings that is available through this database is also included in Colliver et al (1994), so has already been included in Appendix A.

4.5.3 Airflow Resistance of Stair Shafts

While typically zones within a building are open and can be considered to have little to no pressure difference within them, vertical shafts have a high aspect ratio and thus can create non-negligible resistance to airflow. Achakji & Tamura (1988) performed testing of the resistance to airflow of stairwell shafts. They found that open tread stairs provide less resistance to airflow than do stairs with closed treads. The difference in resistance between the two stair types is exaggerated when the effect of occupants within the stairwell is considered. Additionally, they found that the effect of occupants in the stairwells was significant. In general they found that the SLA_{eq} (equivalent orifice area divided by the cross sectional shaft area) varied from 0.13 to 0.23 for closed treads depending on occupancy, and from 0.18 to 0.24 for open treads depending on occupancy. The stairwell model used in CONTAM is based on a power law fit to this experimental data. (Walton & Dols, 2010)

4.5.4 Airflow Resistance of Exterior Walls

The airtightness characteristics of exterior walls are presented in this section. These results are based on testing of walls which do not include interface details or penetrations. This type of testing can be performed in a laboratory or field setting, but requires that the effect of anomalies be eliminated. Values from Colliver et al (1994) and Orne et al (1998) are provided in Table 4-2 and Table 4-3 respectively.

Table 4-2: Airflow Characteristics of Exterior Walls – Colliver et al (1994)

Component	Best Estimate or Mean Average			Minimum q_{75} [L/s·m ²]	Maximum q_{75} [L/s·m ²]
	Flow Exponent, n	Normalized Flow Coefficient, C_{nl} [L/s·Pa ⁿ ·m ²]	q_{75} [L/s·m ²]		
Cast-in-Place Concrete	0.65*	0.052	0.86	0.08	3.10
Concrete block - unfinished	0.65*	0.364	6.02	2.24	6.88
Concrete block - painted or stucco	0.65*	0.114	1.89	0.89	1.89
Continuous Air Infiltration Barrier	0.65*	0.016	0.26	0.09	0.36
Rigid Sheathing	0.65*	0.036	0.60	0.50	0.71
Clay brick cavity wall - finished	0.65*	0.071	1.17	0.09	3.96
Pre cast Concrete Panel	0.65	0.125	2.07	0.48	2.84

* Assumed n when unknown to compare values

Table 4-3: Airflow Characteristics of Exterior Wall – Orne et al (1998)

Component	Median		Lower Quartile		Upper Quartile		Sample Size
	Flow Exponent, n	Normalized Flow Coefficient, C_{nl} [L/s·Pa ⁿ ·m ²]	Flow Exponent, n	Normalized Flow Coefficient, C_{nl} [L/s·Pa ⁿ ·m ²]	Flow Exponent, n	Normalized Flow Coefficient, C_{nl} [L/s·Pa ⁿ ·m ²]	
Brick (bare) - Laboratory and Field Tests	0.80	0.043	0.84	0.022	0.76	0.094	5
Brick (plastered)	0.85	0.018	0.86	0.016	0.84	0.021	3
Brick (wall board panelling) - Laboratory test	0.81	0.042	0.88	0.010	0.72	0.180	2
Cladding (ungasketed)	0.82	0.032	0.88	0.010	0.76	0.100	2
Cladding (gasketed) - Laboratory test	0.87	0.012	0.90	0.007	0.86	0.015	3
Concrete block (bare)	0.74	0.130	0.77	0.082	0.59	2.000	10
Concrete block (plastered internal) - Laboratory test	0.84	0.021	0.84	0.021	0.84	0.021	2
Concrete panels (pre cast)	0.75	0.110	0.80	0.050	0.74	0.120	6
Concrete panels (pre cast, gasketed) - Laboratory test	0.83	0.026	-	-	-	-	1
Metal panels (walls)	0.76	0.090	0.77	0.076	0.74	0.130	3
Curtain walling	0.74	0.120	0.76	0.089	0.74	0.140	3
Timber panel (with wall board)	0.75	0.520	0.70	0.270	0.58	2.700	6
Timber panel (with air barrier) - Laboratory test	0.76	0.066	-	-	-	-	1

4.6 Airtightness of Multi-Unit Residential Buildings Exterior Enclosure - Database

While testing of materials, components, and assemblies can provide some indication of the airtightness of actual completed buildings; the airtightness of buildings is largely dependent on workmanship and quality control, which is difficult to simulate. Airtightness testing of houses is common; however, airtightness testing of multi-unit residential buildings is still relatively rare (Sherman & Chan, 2004). Furthermore, results of this type of testing are largely not compiled.

As part of this thesis work, multi-unit residential building airtightness testing data has been collected and compiled in a database to enable the assessment of typical airtightness performance. The database is populated with data collected from various literature sources and from test results provided directly to the author from unpublished sources. In many cases, the unpublished data is recorded in reports that are not available publicly. Effort was made to collect information from Canada in particular, and some results from the United States are also included. As much information about these buildings as was available was collected including height, number of storeys, age (year of construction), age of the air barrier, and wall and/or air barrier type. Results were converted to a normalized flow coefficient and/or flow coefficient using either an experimentally determined flow exponent or an assumed flow coefficient of 0.65 if insufficient information was available to calculate the value. Using these values, various common metrics were calculated to allow for comparison.

The database includes a total of 55 unique multi-unit residential buildings, and there are results from 170 individual tests, as in many cases buildings were tested multiple times (e.g. different suites in the same building, or before and after air sealing). Note that when air sealing was performed, the building was only counted once; however, results are included for both pre and post air sealing since the air barrier of these buildings changed significantly. When multiple tests were performed on the same building without any changes to the air barrier, the average of these results was used for analysis, but the results of each test are included in the database to allow for comparison if desired. Counting before and after air sealing as separate buildings, there are testing results for 66 unique multi-unit residential buildings.

This database of buildings is not all encompassing. Sherman and Chan (2004) conducted a review of the testing data available for multi-unit residential buildings and identified a total of 44 buildings in Canada and approximately 100 buildings worldwide. These numbers have likely increased since 2004 in part due to required testing in some jurisdictions; however, these quantities generally indicate that this database includes a significant portion of the existing test results. Certainly, testing data exists that has not yet been included in the database, and it is intended that the database be continuously developed as additional testing results become available and as new tests are completed.

Also, the database of test results is likely not a representative sample of multi-unit residential buildings because buildings which are tested for airtightness are likely to be more airtight than the average building. Only in rare cases are buildings tested that are not associated with performance targets or air-sealing work. Testing of buildings prior to air sealing work also provides a non-representative sample as these buildings are likely less airtight than an average building as they have been identified as candidates for air sealing work.

The multi-unit residential buildings in the database are primarily located in Canada, with some also in the United States as shown in Figure 4-8. The buildings in the United States are primarily located in Washington State, where testing is required.

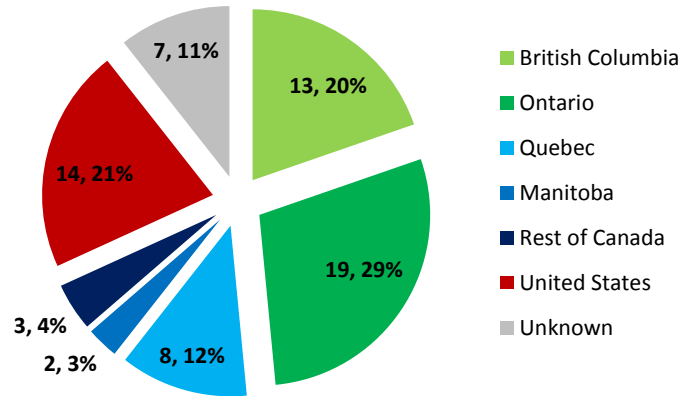


Figure 4-8: Chart of geographical distribution of buildings in the database

The distribution of the year of air barrier construction or modification (which is the year air sealing measures were completed where applicable) is provided in Figure 4-9, and the distribution of the age of the air barrier when it was tested are provided in Figure 4-10. The distribution of building heights is provided in Figure 4-11.

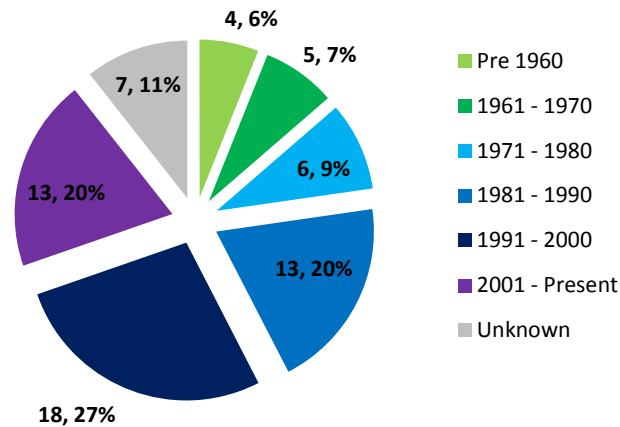


Figure 4-9: Chart of distribution of air barrier construction or modification date for buildings in the database

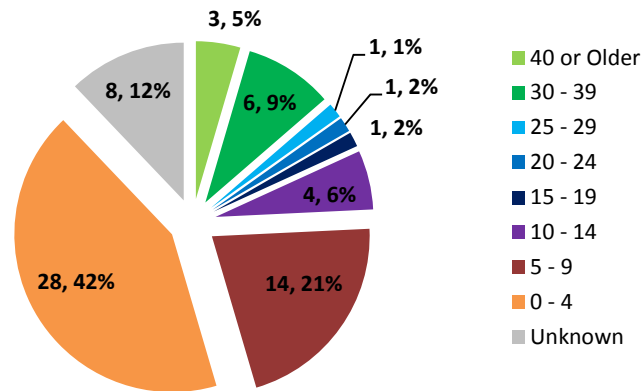


Figure 4-10: Chart of distribution of air barrier age when tested for buildings in the database

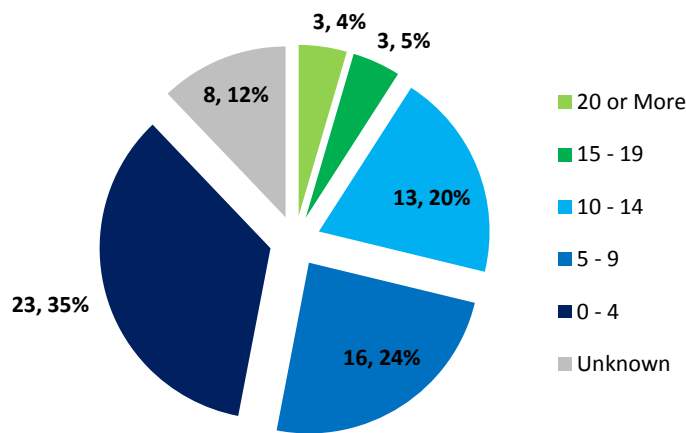


Figure 4-11: Chart of distribution of building height in storeys for buildings in the database

The mean average exterior enclosure airtightness of the buildings in the database is $3.81 \text{ L/s}\cdot\text{m}^2$ at 75 Pa based on data that was available for 45 buildings. The airtightness values (q_{75}) for the buildings in the database are plotted in Figure 4-12, and the distribution of these values is shown in Figure 4-13. The median and standard deviation are 3.02 and $3.23 \text{ L/s}\cdot\text{m}^2$ respectively at 75 Pa. The airtightness values of the buildings in the database vary by orders of magnitude with the lowest and highest values being 0.84 and $19.22 \text{ L/s}\cdot\text{m}^2$ at 75 Pa.

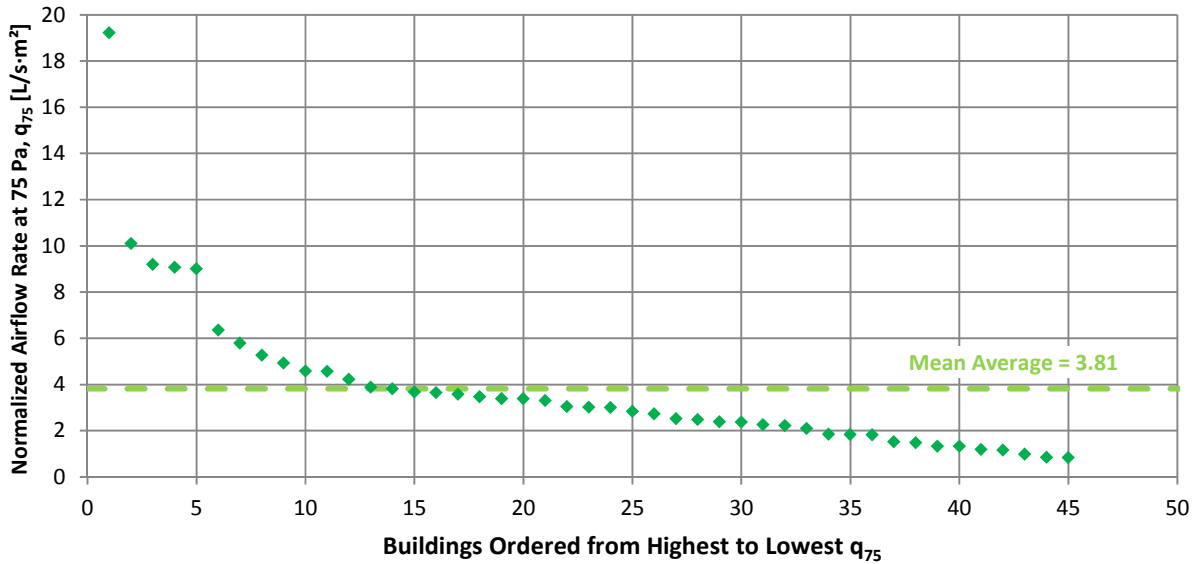


Figure 4-12: Graph of building enclosure airtightness value of buildings in the database

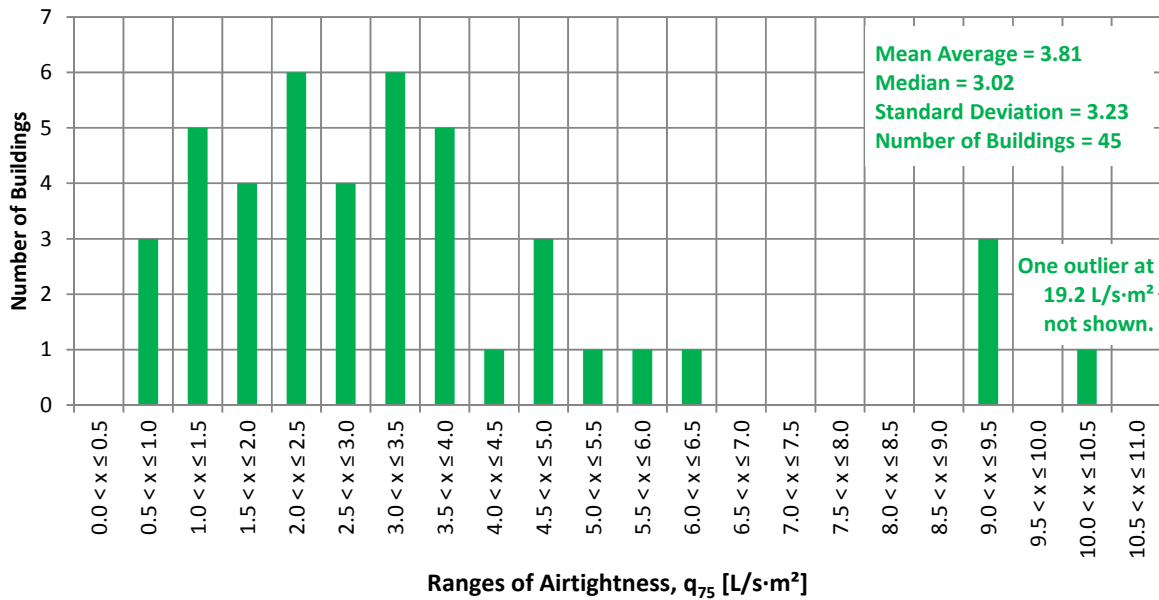


Figure 4-13: Graph of distribution of airtightness (q_{75}) of buildings in the database

To evaluate the relationship of the exterior enclosure airtightness values with the date of air barrier construction or modification, the age of the air barrier when tested, and building height, these values were plotted against each other in Figure 4-14, Figure 4-15, and Figure 4-16 respectively.

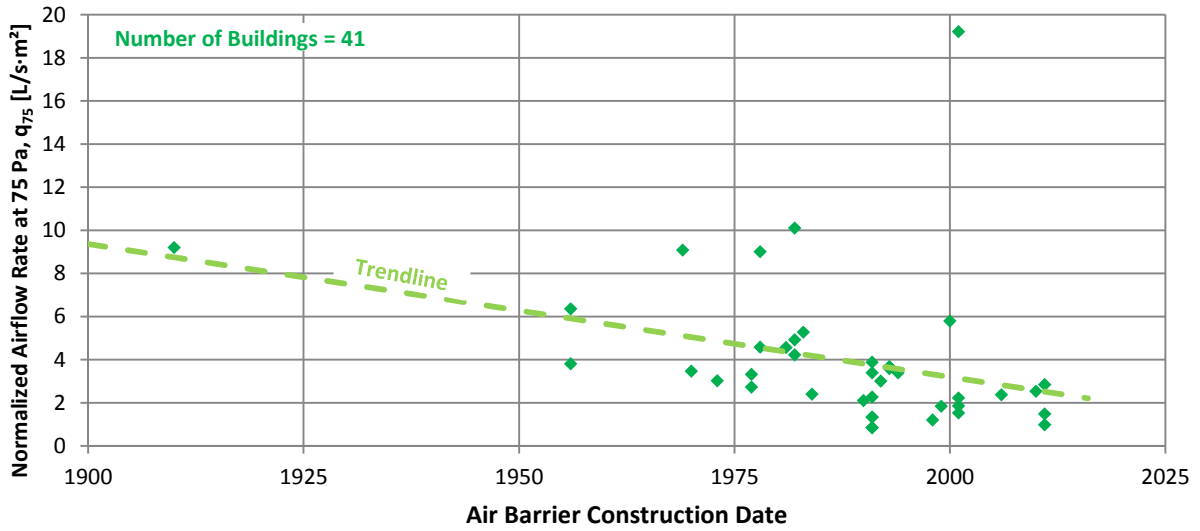


Figure 4-14: Graph of exterior enclosure airtightness versus date of air barrier construction or modification for buildings in the database

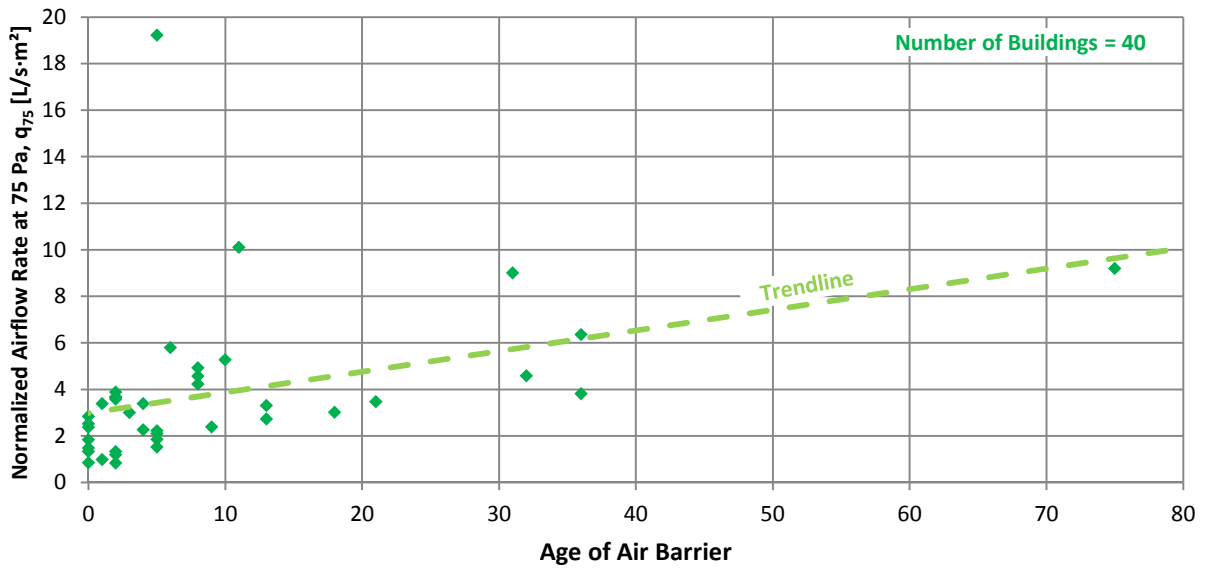


Figure 4-15: Graph of exterior enclosure airtightness versus age of air barrier for buildings in the database

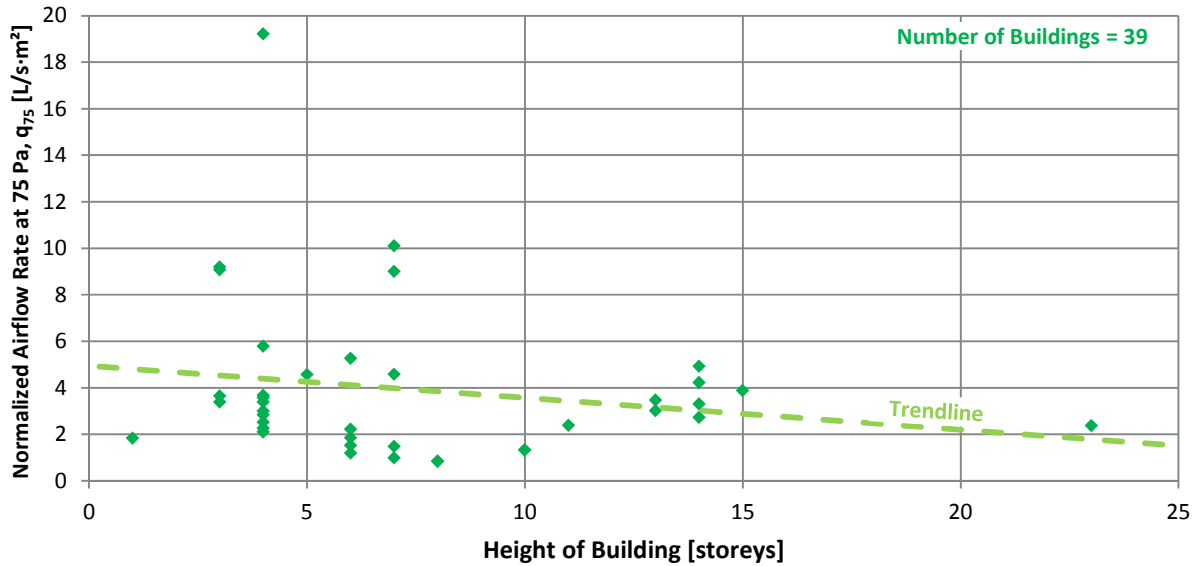


Figure 4-16: Graph of exterior enclosure airtightness versus building height for buildings in the database

Generally, buildings where the air barrier was constructed more recently are more airtight (lower normalized airflow rate) than building where the air barrier is older. This finding applies both to overall age and age of the air barrier at testing which indicates that air sealing practices are improving over time, but may also indicate that air barriers tend to degrade over time. It should be noted that in many cases the age of the air barrier is from original construction (i.e. no modifications to the air barrier were made), and consequently, the improved airtightness of younger air barriers when tested may not indicate degradation of the air barrier over time, but instead may simply indicate that older air barriers were less airtight when they were originally constructed.

A slight trend was found indicating that taller buildings are more airtight than shorter buildings. This may be as a result of typically more robust air barrier systems being used on taller buildings due to the higher wind speeds to which these buildings are often subjected.

For buildings where the flow exponent was found experimentally using multi-point testing, the mean average flow exponent value was found to be 0.63. This is consistent with literature values which suggest that the flow exponent typically ranges from 0.60 to 0.65. The distribution of the flow exponent values for buildings in the database is provided in Figure 4-17.

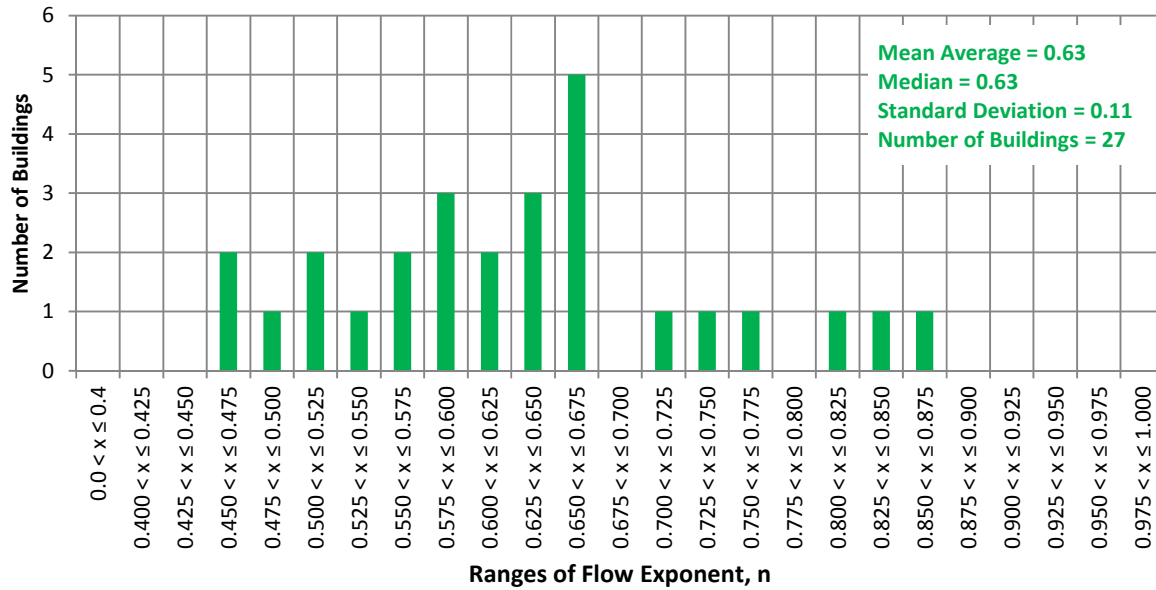


Figure 4-17: Graph of distribution of flow exponent (n) values for buildings in the database

Additional analysis of the airtightness of multi-unit residential buildings is possible based on the content of this database, but is beyond the scope of this thesis work.

Note that the case study building airtightness testing results presented in subsequent sections of this thesis are not included in the database since this database is intended to provide an independent benchmarking tool for comparison.

4.6.1 Airtightness of US Army Corps of Engineers Barracks

A separate section of the database also includes 52 United States Army Corps of Engineers (USACE) barracks type buildings which are similar in form to typical multi-unit residential buildings. USACE buildings are built to meet a target of 1.27 L/s·m² (0.25 ft³/min·ft²) at 75 Pa and tested in accordance with the *US Army Corps of Engineers Air Leakage Test Protocol for Building Envelopes* (US Army Corps of Engineers, 2012). These buildings provide a unique opportunity to assess the level of airtightness that is achievable when a performance target and required testing are implemented.

The airtightness of the exterior enclosures of these 52 buildings are graphed in descending order in Figure 4-18, and the distribution of airtightness values is provided in Figure 4-19. These figures show that despite the USACE setting a relatively airtight performance target, the vast majority of buildings were still able to meet the target and many buildings were significantly more airtight than required.

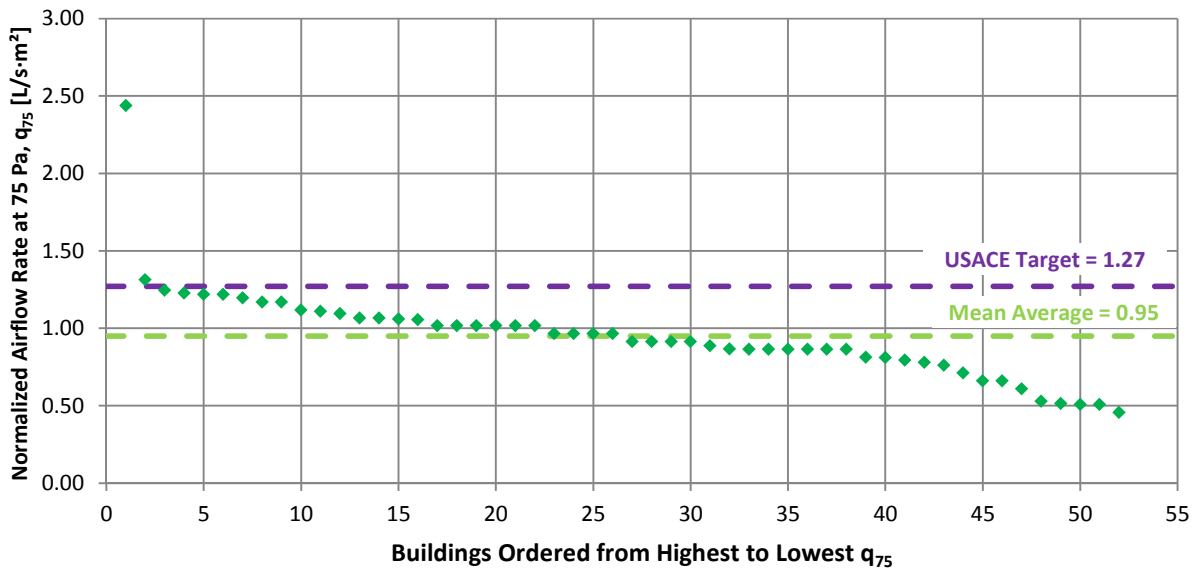


Figure 4-18: Graph of building enclosure airtightness value of USACE buildings in the database

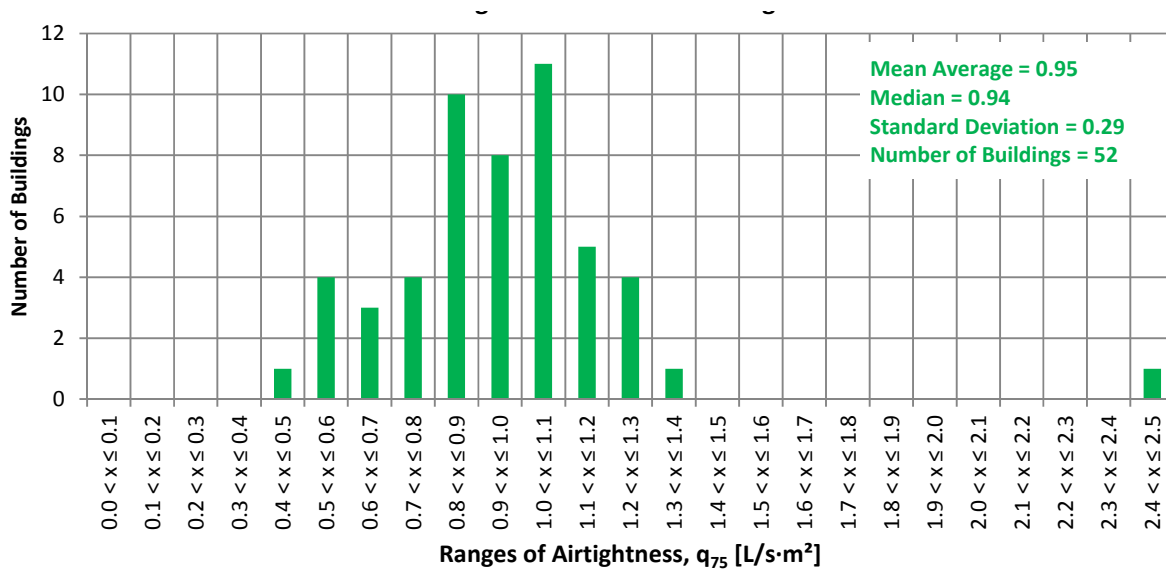


Figure 4-19: Graph of distribution of airtightness (q_{75}) of USACE buildings in the database

4.7 Airflow Resistance of Interior Compartmentalizing Elements

The airtightness characteristics of interior compartmentalizing elements are presented in this section as a reference for comparison with testing at the case study building. Compartmentalizing elements typically include interior walls, ceilings, and floors.

Shaw et al (1991) tested 4 floor/ceilings for whole floors, and more than 30 interior partition walls and floor/ceilings for specific suites at a multi-unit residential building that was constructed in

1981 and tested in 1989. The building was a concrete frame and the interior walls were 3 ½" steel stud with ½" interior gypsum wall board on each side and 1 ½" of insulation in the stud cavity. The results of this testing are summarized in Table 4-4 and Table 4-5 along with results from Fang & Persily (1995), and Colliver et al (1994).

Table 4-4: Airflow Characteristics of Interior Walls

Component	Best Estimate or Mean Average			Minimum	Maximum	Reference
	Flow Exponent, n	Normalized Flow Coefficient, C _n [L/s·Pa ⁿ ·m ²]	q ₇₅ [L/s·m ²]			
Interior Partition Walls - Apartment Building: Gypsum Board on Studs	0.65*	0.233	3.86	0.91	7.40	(Fang & Persily, 1995)
Interior Partition Walls - Multi-Unit Residential Building: Gypsum Board on Studs	0.65	0.147	2.43	0.86	4.73	(Shaw et al, 1991)

*As summed n when unknown to compare values

Table 4-5: Airflow Characteristics Ceilings and Floors

Component	Best Estimate or Mean Average			Minimum	Maximum	Reference
	Flow Exponent, n	Normalized Flow Coefficient, C _n [L/s·Pa ⁿ ·m ²]	q ₇₅ [L/s·m ²]			
Ceiling - General	0.65*	0.187	3.10	1.36	4.82	(Colliver, Murphy, & Sun, 1994)
Ceiling - Drop	0.65*	0.020	0.33	0.08	0.33	(Colliver, Murphy, & Sun, 1994)
Floors over Crawl Spaces	0.65*	0.229	3.79	0.69	8.43	(Colliver, Murphy, & Sun, 1994)
Floors over Crawl Spaces w/o ductwork in space	0.65*	0.206	3.41	-	-	(Colliver, Murphy, & Sun, 1994)
Floors over Crawl Spaces w/ ductwork in space	0.65*	0.234	3.87	-	-	(Colliver, Murphy, & Sun, 1994)
Floors - Office Buildings: Reinforced Concrete	0.65*	0.030	0.50	0.38	0.67	(Fang & Persily, 1995)
Floors - Apartment Buildings	0.65*	0.024	0.40	0.21	0.55	(Fang & Persily, 1995)
Floor/Ceiling - Multi-Unit Residential Building - Whole Floor	0.66	0.026	0.45	0.35	0.57	(Shaw et al, 1991)
Floor/Ceiling - Multi-Unit Residential Building - Individual Suite	0.65	0.032	0.53	0.25	0.74	(Shaw et al, 1991)

*Assumed n when unknown to compare values

Gulay, Stewart, & Foley (1993) provide a summary of five studies of airtightness, air movement and indoor air quality that were conducted across Canada including testing results for 11 high-rise multi-unit residential buildings. In some cases, measurements of interior compartmentalizing elements were also made. The distribution of air leakage that they found for four buildings is presented in Table 4-6

Table 4-6: Airflow Distribution of Suites - (Gulay, Stewart, & Foley, 1993)

	Prairie Region				Quebec			
	Building A		Building B		Building 1		Building 2	
	Q ₅₀ [L/s]	Percent of Leakage [%]	Q ₅₀ [L/s]	Percent of Leakage [%]	Q ₅₀ [L/s]	Percent of Leakage [%]	Q ₅₀ [L/s]	Percent of Leakage [%]
Entry Door	121	42	-	-	-	-	-	-
Left, Right, and Corridor Walls	72	25	48	27	39	14	37	20
Floor	6	2	29	16	54	18	33	18
Ceiling	17	6	25	14	82	29	-	-
Exterior Enclosure	71	25	78	43	115	39	115	62

Gulay et al’s results show that under test conditions a significant portion of the leakage occurs through the exterior enclosure; however, airflow through interior compartmentalizing elements is also significant. Modera et al (1985) found similar results in their testing, concluding that only 40% of the leakage area for a suite is through the exterior enclosure.

Bohac et al (2007) performed pressure neutralized airtightness testing of four multi-unit residential buildings of various types and found that on average 39% of suite airflow during the tests was to adjacent suites and the corridor. Additionally, they found that the normalized airflow rate of these interior compartmentalizing elements was on average 1.86 L/s·m² at 75 Pa with an average normalized equivalent leakage area of 201 cm²/100 m².

Finch (2007) performed pressure neutralized airtightness testing of 5 multi-unit residential buildings. Detailed results of that testing were provided to the author directly and are summarized in Table 4-7.

Table 4-7: Airflow Distribution of Suites – Finch (2007)

Normalized Airflow Rates at 50 Pa from Finch, 2007 [L/s·m ²]								
Adjacent Zone	Concrete Frame					Wood Frame		
	Building 3			Building A	Average	Building 2	Building 4	Average
	Suite 608	Suite 611	Suite 311	Suite 802		Suite 401	Suite 309	
Floor Above	-	-	0.04	0.32	0.18	-	0.00	0.00
Floor Below	-	0.05	0.07	0.09	0.07	0.65	0.00	0.33
Zone to Right	1.84	-	-	0.09	0.97	0.26	-	0.26
Zone to Left	1.11	2.36	1.05	0.21	1.18	2.86	0.23	1.55
Corridor (wall only)	-	13.32	10.23	6.13	9.89	6.62	11.46	9.04
Exterior Enclosure*	2.67	2.3	1.4	1.49	1.97	7.16	12.12	9.64
All 6 Sides	0.79	1.28	0.86	0.56	0.87	3.59	1.74	2.67

*Suites 608, 611, & 401 are on upper floors and include roofs in the enclosure area.

During testing of two other buildings also presented in Gulay et al (1993), whole floor airtightness testing was conducted on 5 floors at two different buildings. During the test certain building components were sealed so as not to measure the flow through these elements, and then measurements were made with each element unsealed individually and the results of this testing are presented in Table 4-8. Their results indicate that during normal building operation, there is significant potential for airflow within a building as airflow through various interior compartmentalizing elements is of similar magnitude to that through the exterior enclosure.

Table 4-8: Airflow Increased Due to Unsealing of Components during Whole Floor Airtightness Testing - (Gulay, Stewart, & Foley, 1993)

	Percent Increase in Airflow Due to Unsealing [%]				
	BC - Building B		BC - Building C		
	Floor		Floor		
	4	5	5	6	7
Elevator	80	78	128	264	323
Garbage Chute	13	23	n/a	n/a	n/a
Stairs	128	93	42	96	75
Fireplaces	n/a	n/a	2	n/a	n/a
Floor	n/a	n/a	80	173	n/a
Ceiling	n/a	n/a	n/a	253	n/a

Proskiw & Phillips (2006) performed airtightness testing of the seven corridors in two multi-unit residential buildings and determined that on average the suite entrance doors contributed approximately 49% of the leakage area of the corridor. In one test where the air leakage through the suite entrance doors and through the elevator doors was measured, it was found that the combination of the suite entrance doors and elevator doors was 77% of the total corridor leakage.

Limited test results for the airflow resistance of interior compartmentalizing elements are available in literature due to the relatively complex, time consuming, and costly nature of testing combined with a lack of regulatory requirement.

Chapter 5

Implications of Pressure Differences and Permeance for Ventilation

Wind, stack effect, mechanical ventilation systems, and the air permeance of building elements interact to create building pressure fields and resulting airflows into, out of, and within buildings. While the physics governing the relationship between these is relatively easily understood, the practical implications of the theory and the complex interactions that occur in real building are less well understood.

Despite the pervasive use of pressurized corridor based ventilation systems in multi-unit residential buildings to provide ventilation air and control airflows, it is well recognized that this approach frequently does not provide effective or efficient ventilation and that significant unintentional airflows occur. Some of the performance problems with the system are caused by poor application or misunderstanding of the design intent; however, other problems are inherent to the strategy itself. The following sections provide discussion of flow patterns and pressure distributions observed in high-rise multi-unit residential buildings with particular consideration of the performance of corridor pressurization based ventilation systems. In many cases there is overlap between sections; however, an attempt has been made to address specific interactions separately.

5.1 Dynamism of Natural Driving Forces

The nature of both wind and stack effect was described in Chapter 3; however, this section provides specific consideration of how these forces interact with corridor pressurization based ventilation systems.

As discussed in Chapter 3, wind tends to drive airflow horizontally through a building from the windward to the leeward side, and it has been noted that airflow due to wind can often be assessed independently for each floor (Shaw & Tamura, 1977). Stack effect, during the winter when it is typically most significant, tends to drive air into the building at the bottom, upward within the building, and outward near the top. Importantly, the direction and magnitude of these driving forces are dynamic over both short and long time scales, and this can significantly change both the direction and magnitude of the pressure differences and airflows they create.

The corridor pressurization system is typically a constant volume type ventilation system that is commissioned once during installation and has little to no ability to compensate for the dynamism of these driving forces either temporally or spatially within the building. These forces are of the same order of magnitude as the pressures created by the mechanical ventilation system, as discussed in Chapter 3, and can often overwhelm the system causing unintentional air flows. This can lead to some suites with higher ventilation rates than are needed, wasting energy, and others with less ventilation than is needed, potentially causing indoor air quality problems. In a heating climate, stack effect can frequently manifest as the over ventilation of lower and windward suites through infiltration and the under ventilation of upper and leeward suites (The Sheltair Group, 2003). Edward (1999) found that natural driving forces have the ability to create large air change rates in buildings, but that the distribution and reliability of these rates is poor.

Cooke (2005) measured corridor to exterior, and corridor to suite pressure differences on the 29th and 2nd floors of a multi-unit residential building during a period of 0°C exterior ambient air temperature. He found that with the corridor pressurization system on, the corridor was pressurized relative to the adjacent suites by 30 to 35 Pa on the 29th floors, and by 3 to -5 Pa on the 2nd floor indicating that stack effect is likely having a significant impact on the airflow patterns within the building and overwhelming the corridor ventilation system's ability to maintain the desired pressure distributions. The corridors were pressurized relative to the exterior by 35 to 45 Pa and 5 to 10 Pa for the 29th and 2nd floors respectively, also indicating the impact of stack effect. With the corridor ventilation system turned off, the corridor was pressurized relative to the suites by 10 to 15 Pa on the 29th floor, and was depressurized by 3 to 5 Pa on the 2nd floor. From the corridor to the exterior with the fans off, the pressure differences were 25 to 30 Pa on the 29th floor, and -30 to -40 Pa on the 2nd floor. The large difference in measured pressure between the 29th and 2nd floors when the ventilation system is turned off provides an indication of the stack effect forces that the corridor pressurization system must overcome.

The uneven distribution of pressures and thus airflow can also lead to an uneven distribution of energy use throughout the building as lower and windward suites essentially heat the air for upper and leeward suites. (Morrison Hershfield Ltd, 1996) Diamond et al (1996) measured energy consumption of suites within a 12 storey multi-unit residential building and noted that upper suites consumed 32% less energy than the average of all suites, and lower suites consumed 28% more. The authors attributed this distribution of energy consumption to stack effect.

Shaw et al (1991) found in a test using tracer gasses at a five storey multi-unit residential building that the corridor pressurization system was able to supply ventilation air to corridors, but that it was not capable of overpowering the driving forces of wind and stack to ensure that ventilation air reached all suites at all times.

5.2 Occupant Controlled Dynamism

Occupants have control of intermittent point-source exhaust fans as well as the opening and closing of windows and doors. Consequently, the state of these building components is dynamic, and can affect the distribution of airflow and pressure difference for high-rise multi-unit residential buildings.

When open, operable windows can significantly increase the leakage area of a building enclosure as the area of an open window is often of similar or greater magnitude than the total leakage area of the exterior enclosure with the windows and doors closed. Diamond et al (1986) identifies a number of reasons why occupants open windows and these are paraphrased below:

- To control interior temperature
- To control interior air quality including excess humidity
- To communicate with outdoors
- To follow tradition or custom

Diamond et al continue to note that often opening windows is for psychological motives as much as physical, and it is likely not possible to predict window operation based solely on indicators such as temperature, air movement, activity level, et cetera. This complicated motivation for the opening of

windows makes it difficult to predict their position at any given time and consequently makes theoretical simulation of the effect of window operation difficult..

Proskiw & Phillips (2008) found that at one building during periods of -25°C, 4°C, and 20°C exterior temperatures, 2.3%, 7.0% and 8.8% of the the building operable windows were open. They then calculated that based on the window areas, the normalized leakate rate (normalized airflow rate) at 75 Pa would be increased by 10.3, 31.3, and 39.4 L/s·m² respectively, which they found was very significant when compared to typical normalized leakage rates with the windows closed which they state are in the range of 1.18 to 6.37 L/s·m² at 75 Pa. Importantly, Proskiw & Philips found that windows were open even during periods of cold temperatures. During these cold periods they found that significantly more windows were open near the top of the building, as shown in Figure 5-1. This is likely caused by overheating or underventilation of upper suites due to stack effect in cold weather and occupants opening windows in an attempt to compensate.

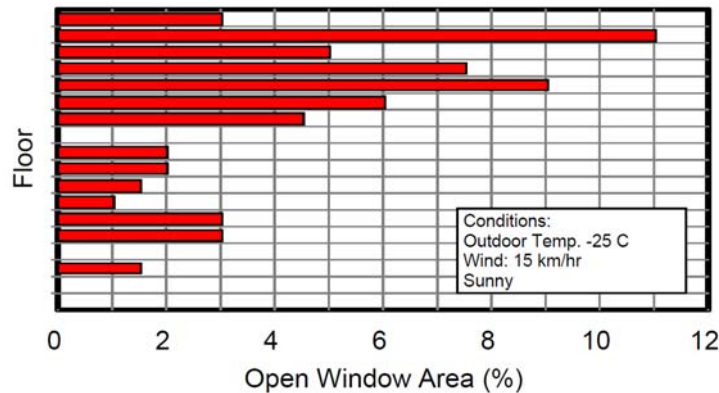


Figure 5-1: Chart showing percent of operable window area open by floor (Proskiw & Phillips, 2008)

Proskiw & Phillips also found that the operation of windows could move the neutral pressure plane towards the locations with open windows. Furthermore, they conclude that because windows can be opened, the airtightness of interior compartmentalizing elements is important as pressure differentials between the building core and the exterior now primarily act on these elements.

Moffat et al (1998) found that opening of windows, especially on the windward side, can significantly increase the effect of wind driving air horizontally through a building. They also found that simultaneously opening windows and the suite entrance doors of a suite increased the flow rate of ventilation air from the make-up air unit to the corridor by 100 to 150%, with an average of 111%. Moffat et al also found that prolonged opening of windows in upper suites to improve comfort can create a long-term upward shift of the building neutral pressure plane. Notably, they concluded that the less air permeable (more airtight) the building enclosure, the more opening windows and doors will affect the location of the neutral pressure plane because these operable openings comprise a larger proportion of the leakage area in relative airtight buildings. This finding can be extended to note that the tighter the building enclosure and compartmentalizing elements, the more operation of exterior and interior doors and windows will affect pressure and airflow patterns.

Morrison Hershfield (1996) notes that the ability for occupants to operate windows and doors in a multi-unit residential building is a key difference between this building type and other building types such as commercial and institutional, which often do not have operable exterior windows. Proskiw and Phillips (2008) came to a similar conclusion and noted that this feature makes multi-unit residential buildings unique among tall buildings and significantly complicates building airflow patterns. While enclosure and compartmentalizing elements can be designed as airtight, it is important to consider the ability of occupants to alter the airtightness of these pressure boundaries by orders of magnitude during normal building operation. Thus, approaches used in other types of high-rise buildings are not necessarily directly applicable to high-rise multi-unit residential buildings.

Building occupants also have control over intermittent exhaust fans such as range hood fans, clothes dryers, and bathroom fans. These fans are often oversized to compensate for underperformance. Moffat et al (1998) found that designed exhaust capacities typically exceeded ASHRAE 62.1 requirements by 126 to 295% (average of 189%); however, the measured exhaust capacities were typically in the range of 39 to 81% of ASHRAE 62.1 levels. Measured capacities were typically 19 to 54% of the design capacities. This practice of oversizing systems to compensate for poor performance wastes energy and demonstrates a lack of detailed design. Additionally, oversized equipment increases the capability of these exhaust fans to alter the pressure and flow regime within a building beyond the areas that they are intended to exhaust.

When on-demand exhaust fans are used, the suite can become depressurized relative to the exterior and/or adjacent suites (Cooke 2005). The magnitude of this depressurization increases as the number of exhaust appliances are operated. This can cause infiltration of air from the exterior through the building enclosure, which in a cooling climate can cause interstitial condensation problems, and can also cause flows from adjacent internal zones, potentially transferring air contaminants.

Moffat et al (1998) found that operating one of the exhaust devices in a suite decreased the suite pressure by 1 to 5 Pa relative to the corridors as compared to with no exhaust fans operating. With all exhaust fans operating they found that the suites became depressurized relative to the corridors by 1 to 10 Pa. They concluded that the development of these pressure differences indicated that insufficient make-up air was being provided by the corridor ventilation system (which they found was typically designed to supply a range of 20 to 80% of the exhaust capacity) or was infiltrating through the exterior enclosure. Tamura (1980) found that suites became depressurized by 2 to 20 Pa relative to the corridors due to bathroom exhaust fan operation.

In testing performed by Cooke (2005) of 6 suites in three buildings, significantly higher pressure differences as a result of exhaust fan operation were identified. They found that with two bathroom fans, the range hood fan, and the dryer exhaust fan operating, suites were depressurized relative to the exterior by 21 to 53 Pa.

In older buildings, the airtightness of the exterior building enclosure was relatively poor (approximately 5 to 15 L/s·m² at 75 Pa) which meant that while unintentional, a significant amount of air could flow in and out of the building through the enclosure, and these flows helped to moderate the magnitude of the pressure differences created by the building ventilation systems. As

air flow through the building enclosure can negatively affect its performance, in more recent construction the airtightness of the exterior enclosure has been significantly improved (to levels of 0.5 to 5 L/s·m² at 75 Pa). This improvement has reduced the amount of air flow through the building enclosure which can potentially reduce building energy consumption, improve air quality, and reduce the risk of moisture damage; however, it has also restricted the flow of air which used to alleviate the development of large pressure differentials. Higher pressure differentials must be developed and this can increase cross-contamination of air within a building and impact the performance of the exhaust fans. In some cases, depressurization of a suite can cause dangerous back drafting of combustion appliances that get their make-up air from the suite.

A similar effect can be noted when interior pressure boundaries are made more airtight. Cooke (2005) tested one suite before and after installing weather stripping on the suite entrance door. Prior to installation of the weather stripping, the suite was measured as depressurized by 35 to 40 Pa relative to the exterior during operation of the exhaust fans. Once weather stripped, this pressure difference increased to 65 to 75 Pa indicating that compartmentalization of suites without consideration for provision of adequate make-up air for exhaust devices can lead to the development of larger pressure differences and drive unintentional airflow.

Cooke also measured the flow rates for the exhaust devices before and after weather stripping. When all devices were operated simultaneously the flow rates through the fans decreased, in particular for the bathroom exhaust fans. Operating individually the two bathroom fans had measured exhaust flow rates of 33 and 38 L/s; however, when operating at the same time as the range hood and dryer these fan flow rates decreased to 7 and 17 L/s, which are 79% and 55% reductions in exhaust flow rate for these fans. Testing of this weather stripped suite with only the bathroom fans on, only the dryer on, and only the range hood on, found depressurization relative to the corridor of 30 to 40 Pa, 40 Pa, and 20 to 25 Pa respectively.

This significant reduction in flow rates is likely because, as Moffat et al (1998) notes, bathroom exhaust fans in multi-unit residential buildings are typically rated at relatively low static pressures of approximately 25 to 60 Pa which is of the same order of magnitude as the pressure differences developed during fan operation. Consequently, the pressure differences developed across the exterior enclosure and suite compartmentalizing elements have the potential to significantly impact fan performance and may be a significant cause of the typical underperformance of these exhaust fans.

Overall, the depressurization of suites due to exhaust fan operation can create significant pressure differences between building zones and across the exterior building enclosure. These pressure differences can be significant drivers of airflow and can overpower the corridor pressurization ventilation system.

A third dynamic factor of building operation controlled by occupants is the occupancy level itself. Occupancy levels in residential buildings often vary according to relatively predictable diurnal and weekly patterns, but can also change due to one-time events such as parties or changes in suite ownership. Different occupancy and usage characteristics are not accommodated by constant volume corridor pressurization based ventilation systems.

5.3 Ventilation Air Supply Flow Path

The relatively uncontrolled nature of the supply ventilation air flow can significantly reduce the efficacy and efficiency of the ventilation system. In many cases leakage of the vertical supply duct means that some portion of the air intake does not reach the corridors directly. In testing by Ueno et al (2012) of vertical ducts (in their case for a ganged exhaust system) at a multi-unit residential building, they found that approximately 15 to 20% of the airflow was leaked out of ducts. Moffat et al (1998) found based on measurements at nine buildings that the supply of air to the corridors was 34 to 81% (average of 59%) of the design flow rate.

Once the ventilation air is supplied to the corridors it is intended to flow into the suites through the suite entrance doors; however, frequently a large portion of this air does not flow directly to the suites and instead flows to other areas. These door undercuts also provide a path for sound transmission which can be of particular concern for suites adjacent to high traffic areas such as entrance lobbies.

A study by Cooke et al (2005) performed air leakage testing on the corridors of a multi-unit residential building and determined that the suite entrance doors represented only 59% of the air leakage from the corridor. Thus, 41% of the air flow out of the corridor during testing was through elevator doors, through the corridor walls, et cetera. The study actually concluded that likely less than 59% of leakage occurs through the suite doors in operation as some openings such as stairwell doors were sealed during the testing (Cooke, Kokko, & Greene, 2005).

While this leakage is inefficient with respect to providing ventilation air, it is even more inefficient if the system is also used to provide the space heating and/or cooling for the building. In this arrangement, the air that leaks from the intended flow path also takes with it the energy that was needed to condition it.

To evaluate the effectiveness of the corridor pressurization system at ventilating suites, Shaw et al (1991) released a tracer gas into the make-up air unit intake at a 5 store multi-unit residential and found that while the corridor pressurization system was relatively effective at distributing air to the corridors, it was not able to overcome other causes of pressure differences to supply adequate ventilation air to all suites. They found an uneven distribution of ventilation air, measuring much higher tracer concentration in leeward and upper suites than in windward and lower suites.

In some cases occupants can also impact the ability of air to reach the building spaces. Sometimes occupants do not realize that the gap under the suite entrance door is intentional and complain of drafts or noise from the corridor. Frequently, weather stripping or other draft stopping techniques are installed on these doors post occupancy which significantly impede the flow of air from the corridor to the suite and block the primary path for the system to provide ventilation air. Overall, using the airflow through suite entrance doors to provide ventilation air to suites has been found to be unreliable, and to often provide ventilation rates much lower than the design intent (Moffat, Theaker, & Wray, 1998).

Ventilation air that does reach the suites is uncontrolled. Ventilation air enters a suite through the door undercut into the main living space; however, it is not directed to side rooms such as bedrooms. In some cases air flow within the suite is sufficient to provide adequate air mixing which will ventilate these rooms, but closing interior doors can significantly limit the ability for air to

move within a suite. This can be a particular issue at night when occupants are sleeping and often close the doors to their bedrooms (Moffat, Theaker, & Wray, 1998).

Even if enough ventilation air does reach the building spaces, often the source of this air is a concern. Since the flow is largely uncontrolled and pressure and subsequent flow directions can be difficult to maintain, the air that reaches suites is often not directly fresh air from the exterior. The air may be coming partially or entirely from neighbouring spaces where it can be contaminated with odours, moisture, or other contaminants (The Sheltair Group, 2003).

Moffat et al (1998) summarized the performance of corridor pressurization ventilation systems. “The performance of mechanical ventilation systems in mid- and high-rise residential buildings is dependent on uncontrolled leakage areas, static pressures, and occupant interactions within the building and its suites. As a result, the performance of these systems is uncontrolled.” (Moffat, Theaker, & Wray, 1998, p. 25)

5.4 Movement of Air Contaminants

For many of the same reasons as discussed in preceding sections, the movement of contaminants within high-rise multi-unit residential buildings is not well controlled. Contaminants that are generated within a building space are moved between spaces by transfer air, which is air that moves from one space to another within a building. While the corridor pressurization system is intended to prevent the flow of transfer air between suites by pressurizing the corridor, designers often do not account for wind and stack effect pressures and also have little knowledge of the airtightness of the building enclosure and compartmentalizing elements (Edwards 1999). Consequently, maintaining the corridor pressurization consistently is unlikely, and as a result, significant flow of contaminants between spaces has been observed.

Bohac et al (2007) used perfluorocarbon tracer testing to measure the amount of air flow into suites that came from adjacent suites in five multi-unit residential buildings. They found that airflow from other suites was 1 to 26% of the total airflow into the suites with an average of approximately 7%. They also found that the average transfer air fractions varied with the height of the building. Lower suites, middle suites, and upper suites had 2%, 7%, and 19% transfer air flows respectively, which the researchers contributed to stack effect.

Moffat et al (1998) calculated the percent of air entering a suite that was transfer air based on carbon dioxide concentrations at 10 multi-unit residential buildings across Canada. They determined that 0 to 45% of air entering a suite was transferred from another suite, and also noted that the percentage of transfer air is likely higher in reality because the carbon dioxide based calculation method only accounts for transfer air from occupied suites (areas where carbon dioxide is produced) and does not account for transfer air from other sources such as garbage rooms and elevator shafts. They also found a fairly large range of transfer air fractions, which indicates limited control of airflow within the test buildings. They concluded that “corridor supply air systems do not always meet their primary design intent, because they are incapable of always preventing inter-suite airflows.” (Moffat, Theaker, & Wray, 1998, p. 93)

The most common occupant complaint with regards to transfer of air contaminants is of cooking odours from adjacent suites. Air transfer between zones of a building, and specifically between

suites, is forbidden by the National Building Code of Canada which states in Sentence 6.2.3.9.(1) that “air from one suite shall not be circulated to any other suite or to a public corridor.” (NRC, 2010)

Shaw et al (1991) found by releasing a tracer gas in a garbage room located at the bottom of the building that significant airflow occurred from the garbage room to all of the suites of the building. While the flow was more significant during the winter (stronger stack effect to drive airflow up garbage chute), it was also observed during a test performed in the summer.

Contaminants have also been found to infiltrate from the parking garage into the building. In some cases, ventilation systems are operated by timers or carbon monoxide sensors which can exacerbate this problem if there no independent pressurization of elevator vestibules in the parking garage which can cause problems as the pressure differences between occupied parts of the building and parking garage vary with time. (Moffat, Theaker, & Wray, 1998)

5.5 Changes in Flow Path Resistance

Because the supply of ventilation air is constant and the exhaust operation is intermittent, the corridor pressurization based ventilation is an unbalanced system which is inherently more sensitive to changes in flow path resistance than are balanced systems. This sensitivity to changes in flow path resistance can be explained using typical fan curve and system curves as shown in Figure 5-2. A fan curve is the relationship between the pressure and flow rate created by a fan, and the system curve is the relationship between the flow resistance created by the system (ducts et cetera) and the flow rate through the system. The flow rate through a given system can be determined by finding the point where the fan curve and the system curve intersect, and this point is referred to as the operating point. For simplicity, in Figure 5-2 Fan A and Fan B are assumed to be the same and the space is completely airtight.

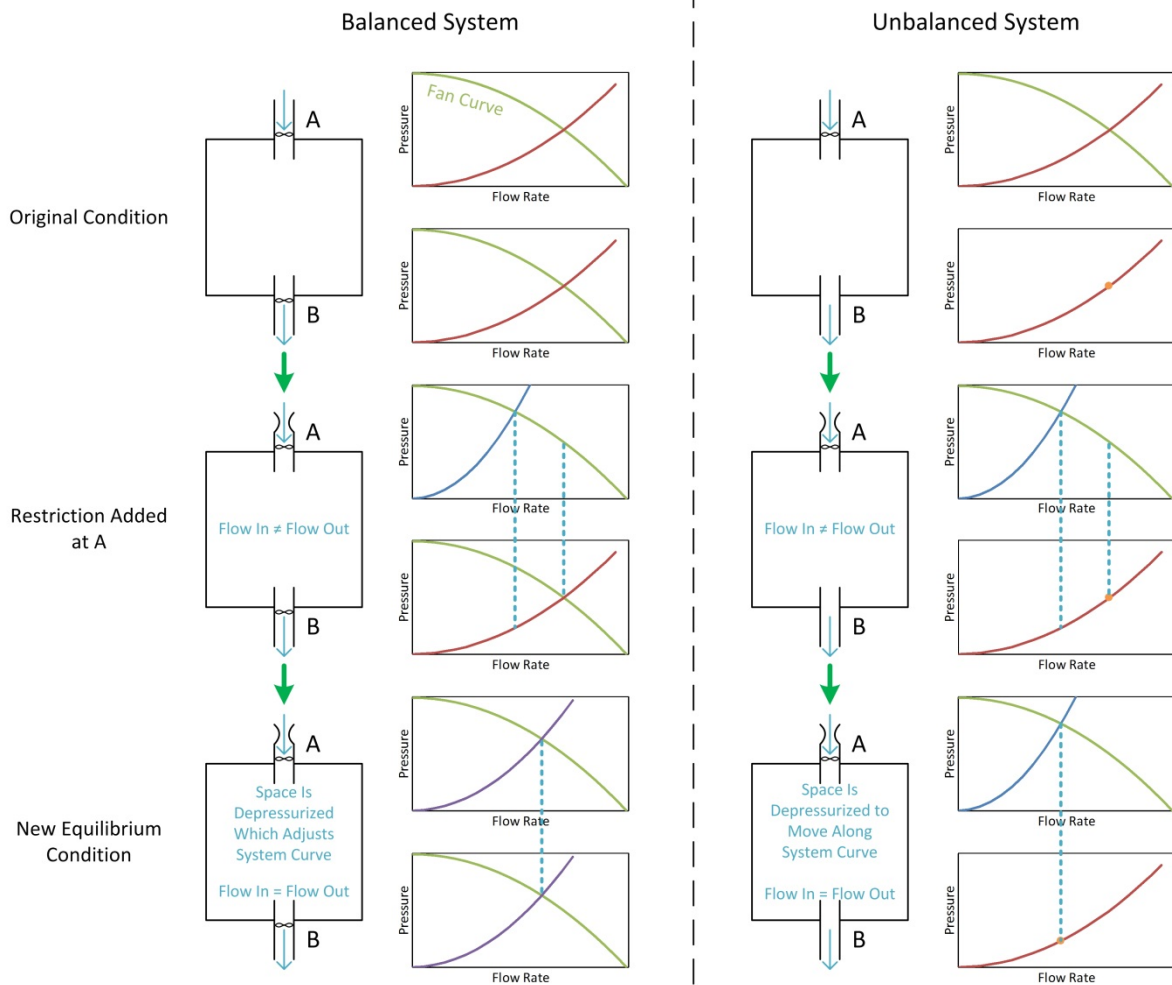


Figure 5-2: Unbalanced and balanced system reactions to a change in the flow path resistance

For the balanced system, when a restriction is added to the flow path of Fan A the immediate reaction is that Fan A is not able to provide as much air to the space; however, Fan B is still exhausting the same amount of air as before the restriction was added. Note that because air can be considered incompressible at the relevant pressure differences, this condition would only exist very briefly as Fan B would respond almost instantaneously to the addition of a restriction at Fan A. Due to this imbalance between the flow rates, the space becomes depressurized which adjusts the system curves for both A and B until the flow rates for both fans are equal. The point at which they reach equilibrium will be less than the flow rate prior to the restriction, but will not be as low as that of Fan A right when the restriction was added.

When the restriction is added to the unbalanced system, the flow through Fan A is reduced in the same way it was for the balanced system. In this system, however, there is no Fan B, so instead of the flow at B being restricted to a fan curve, it is only restricted to the system curve and thus the pressure difference across B simply drops to accommodate the now lower flow rate into the space.

Thus, in the unbalanced system (without the fan at B), the addition of a restriction to the flow path would reduce the air flow through the space more than in the balanced system.

As the pressurized corridor system is an unbalanced system that operates based on a pressure difference between the corridor and the suites, changes in the flow path resistance will also change the airflow rates and distribution of pressure differences. Changes in the flow path resistance may be in the form of operation of windows and doors, but may also include larger scale more permanent changes such as applying air sealing measures to the exterior enclosure.

As buildings are being built with more airtight exterior enclosures, higher pressure differentials must be developed to force air through the enclosure, which can impact the performance of fans and the distribution of pressure differences, as discussed previously with respect to exhaust fan operation. A more airtight building enclosure also impacts the supply of ventilation air by theoretically shifting the pressure differences created by the driving forces more towards this pressure boundary and away from other pressure boundaries such as interior compartmentalizing elements. This shift would theoretically reduce the pressure difference across suite entrance doors created by corridor pressurization based ventilation systems and thus reduce ventilation rates provided to suites. Despite guidance provided by ASHRAE (2009), the specification of building enclosure airtightness is not typically included in design of corridor pressurization ventilation systems, (Moffat, Theaker, & Wray, 1998) The actual impact of improved exterior enclosure airtightness on supply flow rates of ventilation systems has not been well investigated, but is assessed in subsequent chapters as part of this thesis work.

Overall, the unbalanced nature of the corridor pressurization ventilation system makes it potentially sensitive to changes in the airflow resistance of building pressure boundaries.

5.6 Fire and Smoke Control

A purported advantage of the pressurized corridor system is smoke and flame control in the event of a fire; however, it has been found that the pressure developed between the corridor and the adjacent suites is often insufficient to control the spread of smoke, especially when suite doors are left open during evacuation and near the bottom of a building during winter conditions (Tamura, 1980).

The large vertical ventilation shaft that travels the height of the building also provides concerns with respect to fire and smoke control. During a fire, the driving forces of stack effect are increased which can cause both fire and smoke to travel quickly vertically through a continuous open space like this ventilation shaft. Fire dampers are typically installed behind each of the grilles to this shaft to prevent the spread of fire and smoke. These dampers are relatively expensive, and in a survey these fire dampers were found to frequently be not working properly, installed incorrectly, or in some cases not installed at all (The Sheltair Group, 2003)

Generally, this thesis work will not consider fire and smoke control of corridor pressurization ventilation systems as in most cases these systems are intended to operate significantly differently in the event of a fire including the opening and/or closing of dampers and the turning off and/or on of fans. However, the door undercut required for supply of ventilation air to suites from the

corridor does create a potential conflict between ventilation, and fire and smoke control requirements, as this gap essentially always exceeds fire door requirements.

The National Fire Protection Association (NFPA) specifies the maximum door clearances for these doors in *NFPA 80: Standard for Fire Doors and Other Opening Protectives* (NFPA, 2013) which specifies that the clearance between the top and vertical edges of the door and the door frame must be less than 3.18 mm for wood and steel doors (a tolerance of ± 1.59 mm is allowed for steel doors). Interestingly this standard does not provide a maximum clearance for the sill which is likely in recognition of the potential conflict with ventilation requirements.

The International Building Code (IBC) requires testing of fire doors in accordance with *ANSI/UL 1794 Air Leakage Tests for Door Assemblies* and that the airflow rate through the doors not exceed $0.9 \text{ m}^3/\text{min}\cdot\text{m}^2$ at 25 Pa during tests conducted both at ambient temperature (approximately 21°C) and elevated temperature (approximately 200°C) (Walke, 2012). This test and performance requirement is also referenced by *NFPA 105 Standard for Smoke Door Assemblies and Other Opening Protectives* (NFPA, 2013).

The National Building Code of Canada (NBC) sentence 9.10.13.2.(2) indicates that doors separating a public corridor from a suite “shall have not more than 6 mm clearance beneath and not more than 3 mm at the sides and top.” (NRC, 2010)

Based on a survey of suite entrance doors it was found that typically the air flow through suite entrance doors is within the allowable limits set by the NFPA for fire doors (NFPA 80) but greater than the limits set by the NFPA for smoke doors (NFPA 105) and also greater than the limits set by National Building Code of Canada (Moffat, Theaker, & Wray, 1998). Moffat et al (1998) conducted this comparison by using a theoretical method to convert the allowable clearances of NFPA 80 to flow rates; however, it is not clear what clearance was used for the sill as none is specified by the standard. Moffat et al found that at 25 Pa the average suite door allowed $3.5 \text{ m}^3/\text{min}\cdot\text{m}^2$ which is significantly greater than the IBC, NFPA 105, and ANSI/UL 1794 (NFPA 105) requirement. The airflow through suite doors measured in this study was also much higher than these requirements (see Appendix A for measured data).

5.7 Heat Recovery

As the expectations for energy efficiency of buildings are being increased, the recovery of heat from exhaust ventilation air is becoming an expectation. The corridor pressurization system does not provide easy opportunities for heat recovery because its exhaust and supply points are often not in close proximity. (It should be noted that some buildings use grouped exhaust systems which exhaust on the roof relatively near to the air intake location, and application of heat recovery in these situations is more feasible.) As heat recovery more commonly becomes the expectation for ventilation systems, the lack of an easy way to integrate heat recovery in to corridor pressurization systems may prove to be an important factor limiting its continued use.

Chapter 6

Testing and Measurement Techniques

Various testing and measurement methods exist to quantitatively and qualitatively evaluate pressure differences, air permeance (i.e. airtightness), and airflow. This chapter provides a brief review of many techniques that are relevant to this research.

6.1 Pressure Measurements

Pressure differences can be measured using manometers (or micromanometers). It is important to note that the measure pressure differences are between two locations, and are not absolute pressures (also known as barometric pressure). The magnitude of the pressure differences being measured with respect to a building are usually too low to be measured accurately with a water filled manometer, so digital type manometers are most common. Digital manometers use a flexible membrane sensor to determine the pressure difference points. Digital manometers typically provide time averaging which can be useful when measuring fluctuating pressure differences such as those caused by wind.

A documented problem with membrane based sensors is that they often drift due to slight degradation of the sensor components. (Solinst Canada Ltd., 2012) Usually this drift occurs over relatively long time-periods (i.e. days to months) so is not a significant problem for most testing, but can be significant in monitoring applications. To compensate for this drift, some manometers incorporate a small valve which allows for automatic switching of the reference zone to facilitate automatic zeroing of the manometer.

When measuring pressure differences in a building it is important to understand some basic principles of pressure measurement. These measurement concepts are relatively straightforward when abstracted; however, when making measurements at a building it can sometimes be difficult to correctly apply these concepts to ensure that the pressures measured are in fact those intended for measurement.

There are a number of key principles to consider with respect to stack effect when making pressure measurements at buildings :

- There is no significant pressure difference between points in the same zone (vertical shafts can be an exception to this as discussed in Section 4.5.3)
- The pressure difference measured is equal to the sum of the pressure differences across the boundaries that the pressure measurement tubes cross
- The path of the pressure tubes used to measure pressure difference matters to the pressure measurement because temperature differences of the air in the tubes can cause pressure (i.e. cold air in exterior tubes is denser than warm air in interior tubes which can create stack effect pressures that do not actually exist between the two measurement points)

These concepts are illustrated graphically in Figure 6-1, Figure 6-2, and Figure 6-3 which consider a theoretical building with no interior separations (i.e. extremely leaky walls and floors) and different interior and exterior temperatures.

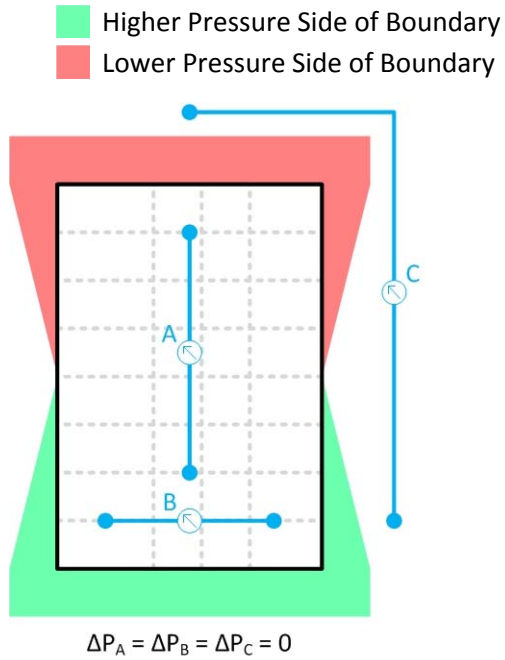


Figure 6-1: Graphic illustrating that there is no pressure difference between points in the same zone

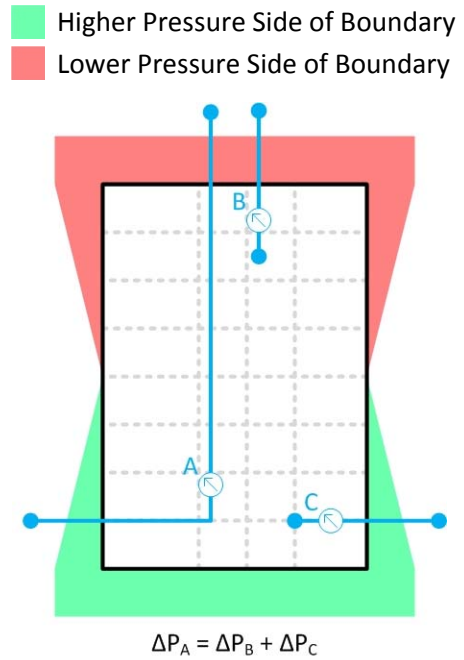


Figure 6-2: Graphic illustrating that the pressure difference measured by a single gauge is equal to the sum of the pressure differences across the boundaries that the pressure measurement tubes cross for an uncompartalized building

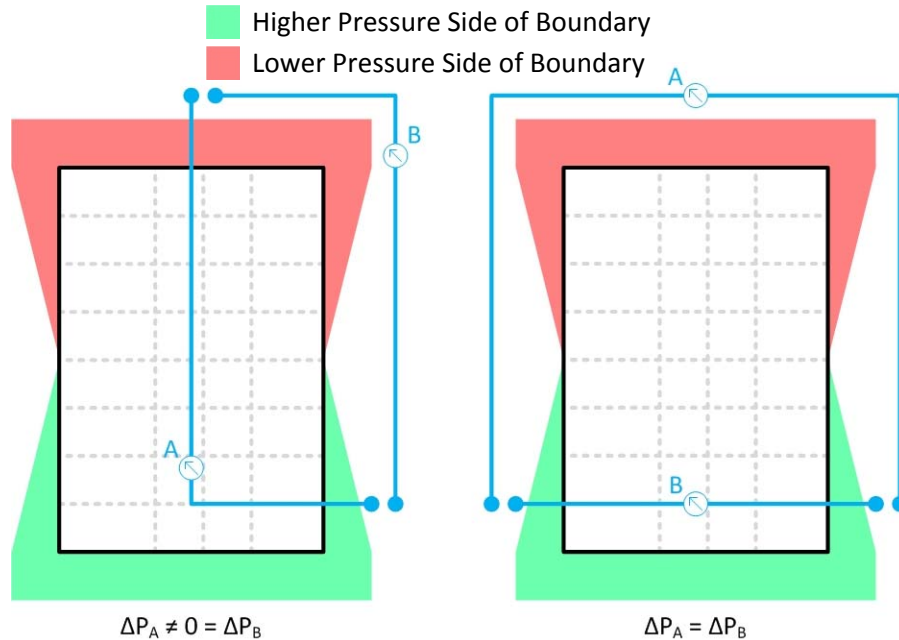


Figure 6-3: Graphic illustrating how path of the tubes used for pressure measurement can impact the pressure measured because of stack effect

When making measurements at buildings it also important to consider the effects of pressure from wind and mechanical ventilation systems; however, the measurement of these pressures is not affected by the arrangement of the pressure measurement tubes. The measurement of wind pressure, however, can be affected by the pressure tap, and it is important to ensure that when measuring moving air the orientation of the pressure tap relative to the flow direction is known and ideally is either pointed directly in to the airflow to measure the total pressure, or perpendicular to the flow to measure static pressure.

6.2 Airtightness Testing

Airtightness testing of buildings is one of the most common forms of measurements related to airflow. This type of testing is commonly performed on houses and is often required by energy efficient housing programs. The equipment and procedures for testing of houses are well developed and readily available. Airtightness testing of multi-unit residential buildings is relatively rare due the complexity of the test methods, the invasiveness of the test on building occupants, the time required to conduct the test, budget considerations, and a lack of regulatory requirements. However, as jurisdictions and programs have begun to require airtightness testing, it has become more common. (2009 Seattle Energy Code, 2009; Washington State Energy Code 2009, 2011)

Airtightness testing is performed by pressurizing or depressurizing a building, or zone of a building, relative to outdoors and/or to adjacent zones. The pressure difference is created by forcing air in or out of the test volume using a fan and is intended to be of sufficient magnitude to overcome and significantly outweigh naturally occurring pressure differentials. The flow rate through the fan is measured at a given pressure difference, and, by conservation of mass, the same amount of airflow must be occurring through the zone pressure boundaries.

Test procedures for this type of test include:

- CGSB 149.10-M86 Determination of the Airtightness of Building Envelopes by the Fan Depressurization Method (1986)
- CGSB 149.15-96 Determination of the Overall Envelope Airtightness of Buildings by the Fan Pressurization Method Using the Building's Air Handling Systems (1996)
- ASTM E779-10 Standard test method for Determining Air Leakage Rate by Fan Pressurization (2010)
- ASTM E1827-96 Standard Test Methods for Determining Airtightness of Buildings Using an Orifice Blower Door (2007)
- US Army Corps of Engineers Air Leakage Test Protocol for Building Envelopes (developed in conjunction with the Air Barrier Association of America (ABAA)) (US Army Corps of Engineers, 2012)
- ISO Standard 9972 Thermal Insulation – Determination of Building Airtightness – Fan Pressurization Method (2006)
- ATTMA Technical Standard L1-2010: Measuring Air Permeability of Building Enclosures (Dwellings) (2010)

Other test standards exist for laboratory testing of air barrier materials and assemblies.

The standards identified above are all similar in principle. The primary differences between them include:

- How the pressure difference is achieved (building mechanical system or fan specifically for testing)
- How the airflow rate is measured (calibrated fan or orifice plate)
- Whether the test volume is pressurized, depressurized, or both
- How many flow and pressure measurements are made (number of test points) and how long a time period each is made over (one reading, average over 10 seconds, et cetera)
- How the mechanical ventilation system is prepared for testing (are the ducts sealed and which ones?)
- The environmental conditions under which the test can be performed
- How the test results are reported

Averaging of both pressurization and depressurization testing doubles the amount of testing required; however, it has been observed that building enclosures can have different airtightness properties in different airflow directions. This characteristic is commonly attributed to physical changes in the pressure boundaries as a result of the pressurization or depressurization. For example, depressurization may pull an operable window more tightly closed and thus provide a better air seal, or pressurization may push open a loosely lapped sheathing membrane and consequently allow additional air flow.

The number of test points is important for developing the correlation which allows for the determination of the flow coefficient and flow exponent. For this correlation, measurements at at least 2 different pressure differences are required, and more than two are required to determine a correlation coefficient which indicates the quality of the correlation. The quality of the correlation

is commonly indicated using R-squared. There is some debate within industry as to whether it is generally more accurate to measure more points for a relatively short time or fewer points but for a relatively long time. Genge (2011) performed testing of the same building zone using multiple test methods and concluded that fewer test points measured over longer time periods provided the more accurate results; however, most standardized test procedures specify more points for less time.

Consideration of exterior environmental conditions during testing can also be important. While mechanical systems are almost always shut off during testing (or used as part of the test method), the driving forces of wind and stack effect continue to influence pressure differences during testing. Most testing standards provide limits on interior to exterior temperature difference and wind speed to mitigate these effects. In high-rise buildings, the magnitude of these forces can be higher than in low-rise buildings, and is of particular concern. As an example, Figure 6-4 schematically illustrates how testing of a high-rise building (8 storeys) at -5°C exterior temperature can significantly alter the distribution of pressures during the test with much higher pressure differences occurring at the top of the building than at the bottom.

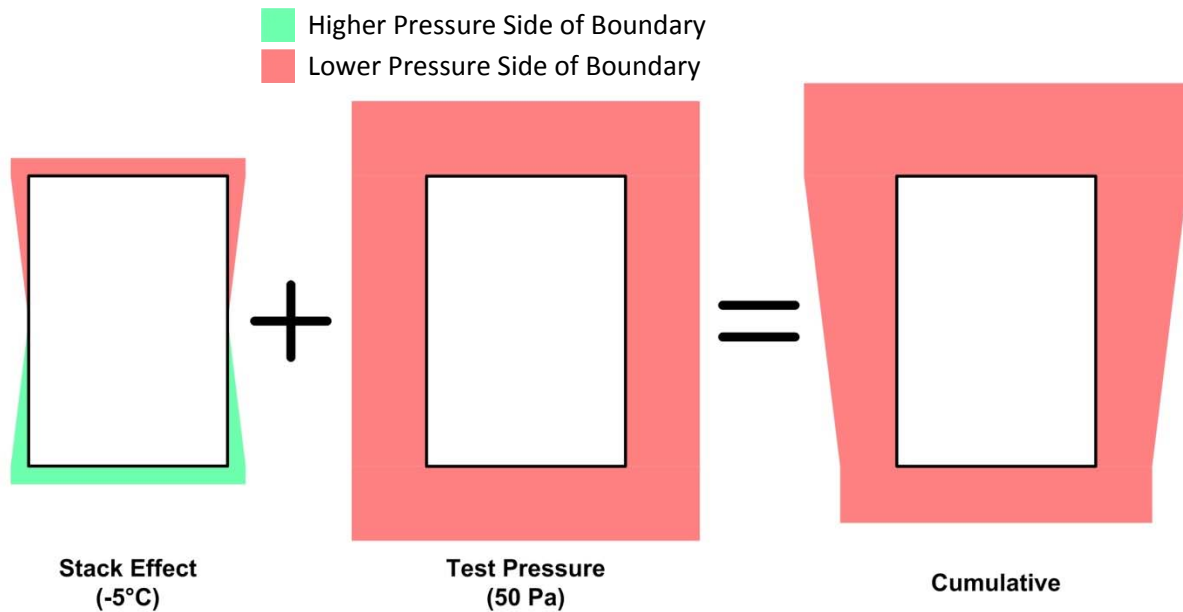


Figure 6-4: Graphic illustrating distribution of pressures during airtightness testing in cold weather

It is also important to note that the pressure differentials created during testing are significantly different in both magnitude and distribution than those that exist during normal building operation. This type of testing measures a property of the building (air permeance), but does not provide a measure of actual in-service airflows.

6.2.1 Sequentially Neutralized Airtightness Testing

The test procedures listed in the preceding section work well for single-zone non-compartmentalized buildings (or buildings that can have internal doors opened such that they act as a single zone); however, for compartmentalized multi-unit buildings it is often impractical or

impossible to equally or adequately pressurize (or depressurize) the entire building enclosure to perform an airtightness test in accordance with one of these test procedures.

To overcome these difficulties with testing of compartmentalized buildings, a sequentially neutralized pressurization/depressurization airtightness test method has been developed to allow for the airtightness testing of discrete spaces within a building, such as an individual suite in a multi-unit residential building. (Shaw, 1980; Reardon, Kim, & Shaw, 1987; Gulay, Stewart, & Foley, 1993; Finch, Straube, & Genge, 2009) This method provides for the isolation of each of the pressure boundaries of a zone (e.g. each of the six sides of a cube shaped zone) so that the airtightness properties of the interior compartmentalizing elements and of the exterior building enclosure can be determined. This can be of particular value when considering internal airflows.

Sequentially neutralized pressurization/depressurization airtightness testing is typically conducted using multiple blower-door fans similar the one shown in Figure 6-5. These fan-door units are made to seal into a standard doorway and are calibrated to measure the flow rate that they supply to or exhaust from a space.



Figure 6-5: Typical Canvas Fan-Door Used for Airtightness Testing

One of these fan door units is set-up to pressurize/depressurize the test zone. Additional fans are set-up to pressurize/depressurize zones adjacent to the test zone such that the pressure difference across the boundary between these zones can be neutralized (i.e. made equal to zero). In a test of a suite in a multi-unit residential building, typical adjacent zones might include the suites above and below the test suite, suites on the same floor adjacent to the test suite, and the corridor. By setting up the fans such that the pressure difference to each of the adjacent zones can be neutralized one adjacent zone at a time (sequentially), it is possible to determine the amount of airflow to those zones from the test zone and vice versa. Once all of the adjacent zones are pressure neutralized with respect to the test zone, the remaining airflow from the test zone must be with the outdoors.

The graphics in Figure 2-1 schematically illustrate this procedure for a typical compartmentalized multi-unit residential building.



Figure 6-6: Schematic showing sequentially neutralized pressurization/depressurization airtightness testing steps for a typical multi-unit residential building (Finch, Straube, & Genge, 2009)

One potential difficulty with the sequentially neutralized pressurization/depressurization technique is that controlling multiple fans distributed around a building can be logistically challenging. Access is required to multiple zones (often suites) within a building and doors must remain opened or closed as necessary during the test. Thus access to suites, stairwells, and

corridors is limited during testing which makes the cooperation of building occupants essential to the success of the test.

It can also be difficult to maintain consistent pressures in multiple zones controlled by multiple fans. The flow rate and pressures created by one fan affects the flow rates and pressures created by other fans which can make it difficult to maintain steady pressures in all zones. Automatic electronic controls and computer software aid significantly in this process and are available for commonly used blower-door systems. (Retrotec, 2012; The Energy Conservatory, 2009)

The largest potential for error in this test method is in the potential for zone bypasses. That is, any unmeasured air flow that occurs between zones other than the two intended zones will create measurement error. For this reason, care must be taken both prior to and during testing to identify any major airflow zone bypasses and address them. Often this can mean sealing them, or, if possible, neutralizing the pressure difference between the zones to which they connect. A vertical duct that connects multiple floors is an example of a typical zone bypass as it could potentially connect a zone not only with the floors above and below, but also with zones further up or down the building.

Despite some of the complications that arise as a result of the multiple fans required to perform this type of test, the advantages of this technique usually significantly outweigh the disadvantages and often this test method is the only feasible method for highly compartmentalized buildings such as multi-unit residential buildings.

6.2.2 Alternative Multi-Zone Building Airtightness Testing Techniques

Proskiw and Parekh (2001) developed a multi-zone test procedure which is similar to the sequentially neutralized pressurization/depressurization method except that it does not require that adjacent zones be completely pressure neutralized with the test zone. Instead this procedure requires that the pressure difference to adjacent zone be modified such that the air leakage at different magnitudes of pressure differences between the adjacent zone and the test zone can be determined. This method is most advantageous if the zones adjacent to the test zone are large or relatively air leaky and thus difficult to pressurize (or depressurize) to the same magnitude as the test zone.

The Nylund technique is based on the idea that internal building airflows between spaces can be determined by measuring the pressure field within the zones adjacent to the test zone. (Proskiw & Phillips, 2001) This method, however, assumes that the airtightness of every zone is the same and that the interior airflow between zones is much less than the airflow exchange with outdoors, that is, the exterior building enclosure is much less airtight than interior separators within a building. These assumptions are rarely true, and can cause significant errors in measurements if not true.

DePani and Fazio (2001) developed a technique such that the airtightness characteristics of a single zone can be determined with only a single fan-door unit by first pressurizing the test suite, and then each of the neighbouring suites one at a time. Using linear algebra, the flow coefficients and flow exponents for each component of the building can be determined. This technique was developed for a three zone building; consequently, it may have some limitations when used in buildings with

more zones as it may not be possible to solve the system of equations based on the available information.

Colliver et al (1992) developed a technique based on the creation of non-steady-state pressure differences which they refer to as AC pressurization. Instead of creating steady-state pressure differences and measuring airflow rates, this technique creates periodic pressure differences across pressure boundaries and then uses the magnitude of the pressure difference and the rate of change in pressure difference to determine airflow properties.

Lstiburek (2000) proposes a technique based on the idea of pressure perturbation. By increasing or decreasing the pressure in a zone and then monitoring how the pressure field within the building reacts to the change, conclusions can be drawn with regard to building airtightness characteristics.

6.3 Airflow Measurements

While measurements of pressure difference and airtightness provide indications of the airflow characteristics of a building, it is often most useful to directly measure in-service airflows. This section provides an overview of a number of flow measurement techniques relevant to the airflows in multi-unit residential buildings considered by this thesis.

6.3.1 Unpowered Flow Hood

An unpowered flow hood (also known as a balometer) is designed to measure flow rates of mechanical ventilation system intake and exhaust flow rates. This type of measurement apparatus is not able to compensate for the resistance of the apparatus itself (which is designed to be as small as practical), thus making the measurements less accurate. (Wray, Walker, & Sherman, 2002) A typical unpowered flow hood apparatus is shown in Figure 6-7.



Figure 6-7: Typical Unpowered Flow Hood apparatus

6.3.2 Powered Flow Hood

Powered flow hood measurements are used to measure flow rates of mechanical ventilation systems. Similar to an unpowered flow hood, the system is designed to seal over a ventilation grille. A typical system is shown in Figure 6-8



Figure 6-8: Typical Powered Flow Hood Apparatus

Unlike the unpowered flow hood, these systems incorporate a fan which can be used to compensate for the flow resistance added by the measurement apparatus. Alternatively, the test fan can be used to pressurize (or depressurize) a ventilation system and measure duct leakage or flow resistance.

Because of the active compensation for the flow resistance created by the measurement apparatus, Wray et al (2002) found that compared to unpowered flow hoods, powered flow hoods produce significantly more accurate and consistent results. This measurement technique has been used in many applications and systems for measuring relatively small flow rates are readily available. (The Energy Conservatory, 2012; Retrotec, 2012) Larger powered flow hood apparatus for measurement of larger flow rates can be custom designed for the specific application such as those used by Moffat et al (1998) and Ueno et al (2012).

6.3.3 Pitot Tube Traverse

ASTM D3154-00 Standard Test Method for Average Velocity in a Duct (Pitot Tube Method) (2000) provides a procedure for determining the average airflow velocity in a duct, which in turn can be used to calculate the airflow rate through the duct. This test method uses a pitot tube to measure the difference between velocity pressure and static pressure, and then from this measurement determines the airflow velocity. The standard splits the duct in to areas and then measures the pressure differences (flow velocity) in each of these areas and area weights them to determine the average flow velocity. This area weighting approach is necessary because of boundary effects on the flow velocity profile within ducts.

6.3.4 Flow Velocity Measurement

Anemometers are used measure airflow rates. Various types of anemometers exist including pinwheel, hemispherical cup, ultrasonic, and hot wire anemometers. (ASTM, 2003) A review of these different types of anemometers is beyond the scope of this thesis. An example of the type most commonly used in weather stations for wind speed measurements, the hemispherical cup type anemometer, is shown in Figure 6-9.



Figure 6-9: Typical hemispherical cup type anemometer used for measuring wind speed

Smaller anemometers can be used to detect airflow paths such as building enclosure air leakage during a pressurization/depressurization test.

6.3.5 Tracer Gas Testing

Tracer gas testing is a method of measuring in-service airflow rates by tagging the air in a given zone with a tracer gas and measuring concentrations of that gas in the air of the test zone and/or other zones in the building. Tracer gases must not be found naturally in air in significant concentrations and technology must exist to accurately measure the concentration of the gas in air. *ASTM E741-00 Standard Test Method for Determining Air Change in a Single Zone by Means of a Tracer Gas Dilution* (2006) provides test methods for performing three of the most common types of tracer gas testing: concentration decay, constant injection, and constant concentration. These methods are described in the subsequent sections. Other tracer gas testing methods exist and some use multiple different tracer gases at a time to measure multiple airflows during the same test period; however, these methods are essentially just adaptations of the three methods described in this section. (McWilliams, 2002) One such method using multiple tracers is perfluorocarbon tracer (PFT) testing which is also discussed.

For all of these methods it is important that the tracer gas be evenly distributed throughout the test zone. This is often accomplished by the use of small fans and/or by using multiple release points for the tracer gas. The primary advantage of tracer gas measurement techniques over other measurement techniques is that it can be conducted at in-service building conditions which allow the results to provide a more clear indication of airflows under realistic conditions.

6.3.5.1 Concentration Decay

The constant decay method releases an arbitrary quantity of tracer gas into a test zone (but an appropriate quantity such that the concentrations are within the measurable range) and then measures the concentration of the gas in the test zone over time. As air enters and leaves the space the tracer gas concentration is diluted, typically following an exponential decay. Using the curve generated from this test, the air change rate for the test zone during the testing period can be determined.

6.3.5.2 Constant Injection

The constant injection method releases a known steady amount of tracer gas into a space and measures the equilibrium concentration that is reached. Since the rate of release of the tracer gas into the space and the equilibrium concentration are both known, the air change rate for the test zone can be calculated.

6.3.5.3 Constant Concentration

The constant concentration technique is similar to the constant injection technique except that instead of releasing the gas into the space at a consistent known rate, the concentration in the space is specified and the rate of gas release is dynamically adjusted to maintain the concentration. This technique is more complicated to perform than the concentration decay and constant concentration techniques as it requires automated real time monitoring of tracer gas concentration and adjustment of release rate.

6.3.5.4 Perfluorocarbon Tracer Testing

Perfluorocarbon tracer (PFT) testing is another type of tracer testing and is similar in principle to constant injection tracer gas testing. The most commonly used method was developed by Brookhaven National Laboratory (BNL) as a result of its development of sensitive methods for measuring concentrations of these tracers. The PFT method as a whole consists of the tracers themselves, the release technique, the air samplers, and the analyzers. (Heiser & Sullivan, 2002)

To perform this type of testing, PFTs are released by sources in to the test zones. There are a variety of different types of PFTs available and BNL currently offers seven different types through its business branch of operations, Meadowbrook Partners Inc. These PFTs are nontoxic, nonreactive, and the concentrations of these tracers normally found in the air are negligible, which makes them excellent candidates for use as a tracer. Additionally, BNL has developed techniques to measure the concentration of these tracers very sensitively, in the range of parts per quadrillion. (Heiser & Sullivan, 2002) The PFTs are released in to the air using small vials of liquid PFT that are sealed with a PFT permeable material allowing diffusion of the PFT from the vial at a consistent rate.

Capillary Absorption Tube Samplers (CATS) are used to absorb the PFT from the air over a given test period using a charcoal-like material called Ambersorb. (Loss & Dietz, 1991) During the analysis phase, the PFTs are de-absorbed from the CATS so that the absorbed volume of PFT can be determined, and thus the average concentration of the PFT in the air of the associated zone during the test period can be determined. By placing both sources and CATS in various zones, the average airflow rates between those zones during the test period can be determined.

A single CATS can simultaneously absorb multiple types of PFTs, so multiple PFTs can be released during the same test period and thus multiple flow rates determined for the same test period. The ability to simultaneously measure multiple time averaged in-service airflow rates between zones is a significant advantage of this tracer technique. Airflow rates between multiple zones are determined based on linear algebra procedures outlined in D'Ottavio, Senum, & Dietz (1988).

This technique has been used successfully in previous studies of airflow in buildings such as by Flander and Song (1989) who assessed a two storey barracks building, by Bohac et al (2007) who tested six multi-unit residential buildings, and by D'Ottavio et al (1988) who performed testing in a three storey detached house.

6.3.6 Visualization & Qualitative Techniques

Visualization of airflows can provide a valuable diagnostic tool for evaluating airflows into, out of, and within buildings. In some cases recording these visualizations can allow for quantification of air movement; however, typically visualizations provide the basis of qualitative evaluation.

6.3.6.1 Smoke

Smoke generated from either a smoke machine or a smoke pencil can be used to visualize airflows. Smoke can also be generated using slow burning wicks; however, smoke released from burning is warmer than the air around it and tends to rise which can make determination of airflow patterns more difficult. Smoke released from smoke machines and smoke pencils is released with initial

momentum which can also make determining airflow patterns more difficult. This is one of the techniques described in ASTM E1186-03 (2003).

6.3.6.2 Sound Transmission

This test is described in the ASTM E1186-03 as a qualitative method for locating airflow paths. A sound generation device is placed in the building and then a sound detection device is moved over the exterior of the building. Locations where louder sound is identified indicate potential airflow path locations. The sound generation device could alternatively be placed on the exterior of the building and the survey performed on the interior.

6.3.6.3 Infrared Thermography

Infrared thermography uses an infrared camera to capture the infrared radiation emitted by an object and create a visual representation of that radiation. The infrared radiation emitted by an object is correlated with the surface temperature of that object, so this technique can be used to determine the surface temperature of an object.

With respect to building airflow, infrared thermography is useful for identifying locations of airflow from inside to outside or vice versa. To perform this type of assessment, infrared pictures are taken of the exterior of a building during a period when the interior and exterior temperatures are significantly different. (*ASTM E1186-03 Standard Practices for Air Leakage Site Detection in Building Envelopes and Air Barrier Systems* (2003) indicates that there must be a temperature difference of at least 5°C.) Initially, the building is pressurized and infrared pictures are taken identifying thermal anomalies which may be attributable to air leakage. Then, the building is depressurized and thermographic pictures are taken of the same locations. By comparing the differences between the two sets of images, airflow locations can be identified. Infrared thermographic images of a building that was tested in this manner are shown in Figure 6-10 with airflow locations identified.

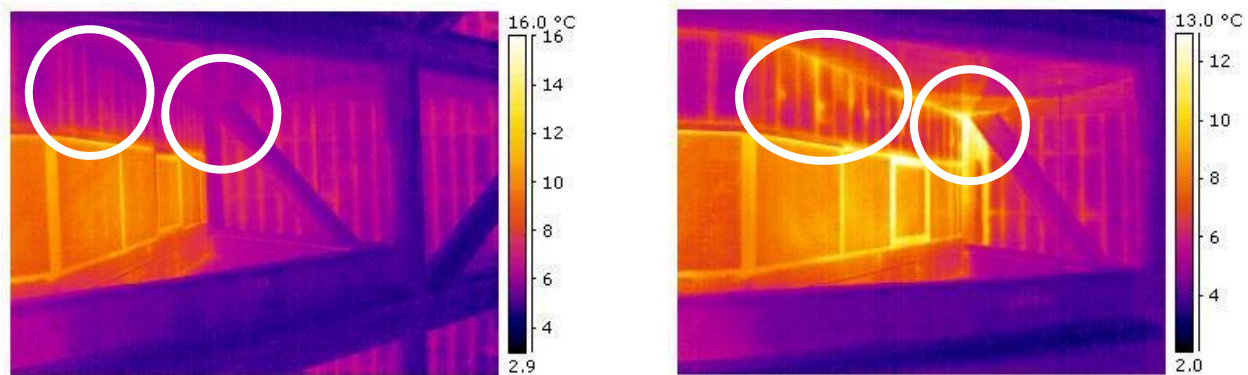


Figure 6-10: Infrared thermographic images of a building from the exterior showing locations with no thermal anomaly in the left image and visible thermal anomalies in the right image once the building was pressurized indicating locations of airflow from the interior to the exterior (Images courtesy of RDH)

Infrared thermography can also be performed without pressurizing or depressurizing the test zone (or building); however, it can be difficult to distinguish between thermal bridging and airflow when this procedure is used.

6.4 Air Quality as an Indicator

While not a direct measure of airflow or of parameters influencing airflow (pressure differences and air permeance), indoor air quality in buildings and zones of buildings can be used as an indicator of airflow rates. These types of measurements are similar in principle to the use of tracer gases or perfluorocarbons to determine airflow rates except they are based on naturally occurring substance in the air, usually contaminants. In most cases these types of measurements are used as qualitative indicators of airflow (e.g. higher contaminant levels in a zone might mean lower ventilation rates), and sometimes attempts are made to use measurements of indoor air contaminant to quantify airflow rates. These types of evaluations typically require numerous assumptions including most vitally the rate of the air contaminant generation.

For example, if using carbon dioxide concentration as a method of determining ventilation air flow rates into a zone, it would be necessary to know the concentration in the supply ventilation air, the concentration in the test zone, and then make an assumption about the generation of carbon dioxide in the test zone. (Moffat, Theaker, & Wray, 1998) Published data is available regarding the average production of carbon dioxide by humans based on activity level. (Persily, 1997) It would also be necessary to either quantify any other sources or sinks of carbon dioxide in a space. A similar approach would be taken if using an indicator other than carbon dioxide.

In many cases the number of assumptions required and the achievable accuracy of these assumptions makes using naturally occurring substances to determine airflow rates only qualitative.

Chapter 7

Testing and Monitoring of the Case Study Building

To evaluate airflow into, out of, and within high-rise multi-unit residential buildings, and in particular the performance of the corridor pressurization based ventilation system, a measurement program was developed and carried out at a case study building. This chapter presents the details the experimental program of this thesis work. The chapter provides a description of the case study building and details of the PFT airflow measurements, airtightness testing, monitoring, and supplementary testing programs. Results of this testing and monitoring program are provided in Chapter 8 to Chapter 11 with associated analysis and synthesis.

7.1 Introduction

7.1.1 Building and Project Overview

The case study building is a 13 storey multi-unit residential building located in Vancouver, British Columbia. The building was constructed in 1986, has a gross floor area of approximately 5,000 m², and contains 37 residential units. The building is strata owned which means that each suite occupant owns their unit and has joint ownership of common areas. A building bylaw requires that occupants must be 55 years of age or older to live in the building.

A photo of the north-east corner of the case study building is provided in Figure 7-1, and the floor plan for a typical floor is provided in Figure 7-2. A complete set of the original architectural and mechanical drawings for the building are provided in Appendix B.



Figure 7-1: North-east corner of the case study building post-retrofit (Photo courtesy of RDH)

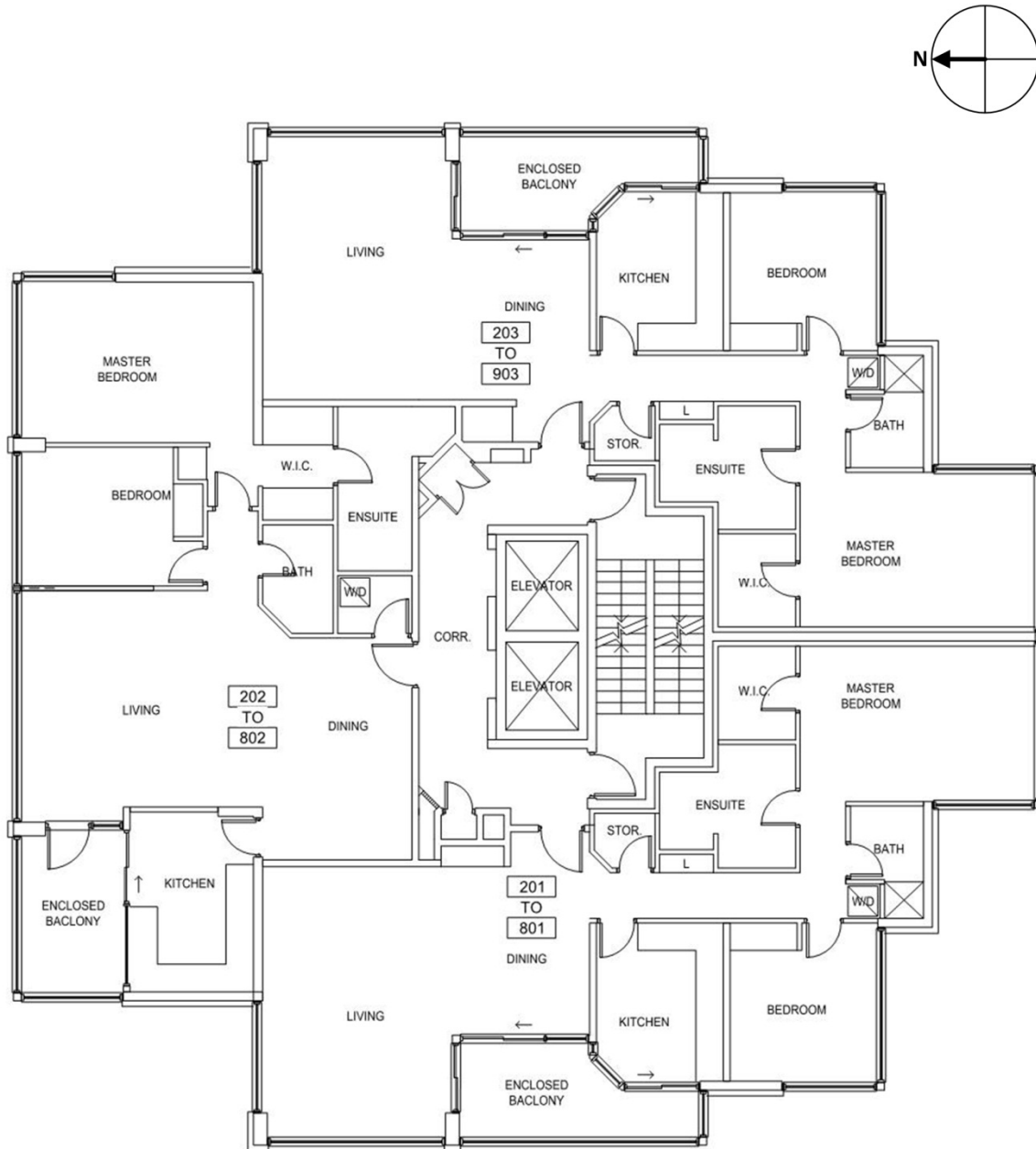


Figure 7-2: Typical floor the case study building

Through the partnership with RDH Building Engineering Ltd. (RDH), the author of this thesis was able to conduct the thesis work at the building as part of energy consumption focused research and rehabilitation work being conducted by RDH. The exterior enclosure of the building underwent a significant retrofit from approximately May to December 2012.

7.1.1.1 General Building Characteristics

The case study building is a cast-in-place concrete frame building with 7 ½" (191 mm) thick post-tensioned concrete floor slabs and a cast-in-place concrete elevator core and scissor style stairwell. It has a one level below grade parking garage that extends beyond the above grade building

footprint and is open to the outdoors through a vehicular access gate. There is an enclosed garbage room within the parking garage area and a garbage chute with a shaft that runs the full height of the building and has an access door at each corridor. The access to the garbage chute at each corridor is in a small room separated from the corridor with a door and the garbage chute itself also has a small access door for depositing garbage.

The walls between -01 and -03 suites are cast-in-place concrete. The walls between -01 and -02 suites, and between -02 and -03 suites are cast-in-place concrete in some areas, and in some areas consist of two rows of 2 ½" steel studs insulated with fiberglass batt insulation with 5/8" gypsum wall board on one side, and 5/8" and 1/2" gypsum wall board on the other side.

The walls between the corridor and the suites are a 3 5/8" steel stud walls insulated with fiberglass batts and have 5/8" gypsum wall board on both sides. The corridor walls are wallpapered.

The stairwell and elevator core walls are primarily 8" thick cast-in-place concrete with 8" concrete masonry unit infill sections around the elevator doors.

Most floors have an electrical services closet in the north-east corner of the corridor and electrical, telephone, and cable services run through the floor slabs in or near these closets. In some cases there is no closet and wiring runs in either an inaccessible space between the corridor and the suites or within the corridor walls.

The elevator vestibule in the parking garage is constructed with painted concrete masonry units and is separated from the parking garage with a weather stripped steel door. There are also electrical and fire suppression system rooms in the parking garage.

The case study building is located in an urban area with surrounding buildings of similar or lesser height. Figure 7-3 shows the general arrangement of nearby buildings that may cause wind shielding. Note that the bottom of the case study building is also surrounded by trees approximately 2 to 4 storeys in height.

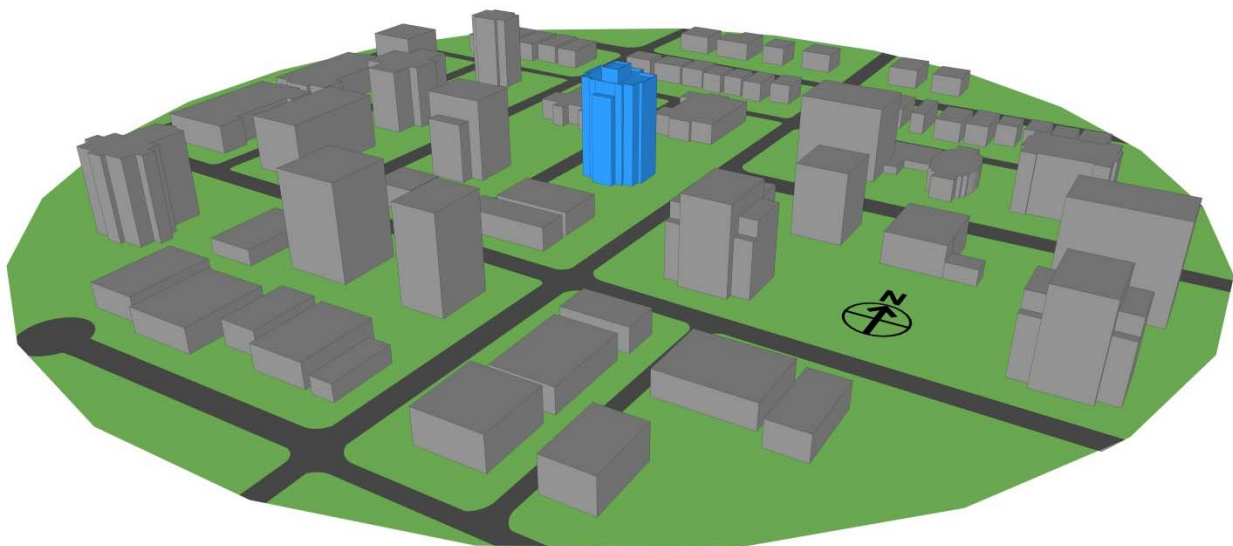


Figure 7-3: General geometric arrangement of buildings near to the case study building

7.1.1.2 Original Building Enclosure

Prior to the building enclosure retrofit, the case study building exterior enclosure was composed of exposed cast-in-place concrete walls which consisted of:

- Acrylic coating
- 5 ½" cast-in-place concrete
- 1 ½" steel studs with extruded polystyrene insulation
- Interior gypsum wall board

The effective R-value of these walls was determined by RDH to be approximately $0.70 \text{ m}^2\cdot\text{K}/\text{W}$ ($4.0 \text{ ft}^2\cdot\text{°F}\cdot\text{hr}/\text{Btu}$). There are also some small areas of stucco clad steel stud walls at the ground level and at the mechanical penthouses. A typical exterior wall assembly below a window is shown in Figure 7-4.

The original glazing was non-thermally broken aluminum frame with double glazed insulated glazing units. The exact specifications of the glazing units varied as many had been replaced by individual suite owners. RDH determined an effective U-value of $3.1 \text{ W}/\text{m}^2\cdot\text{K}$ ($R-1.8 \text{ ft}^2\cdot\text{°F}\cdot\text{hr}/\text{Btu}$) for these windows and doors. In some cases there are skylights above the windows in suites on Floor 13. The exterior building enclosure was approximately 45% glazing, 44% opaque wall, and 11% roofs and decks.

The original roof consisted of a protected membrane roof assembly with 1 ½" of extruded polystyrene insulation on top of a waterproofing membrane. This assembly was determined by RDH to have an R-value of approximately $1.67 \text{ m}^2\cdot\text{K}/\text{W}$ ($9.5 \text{ ft}^2\cdot\text{°F}\cdot\text{hr}/\text{Btu}$).

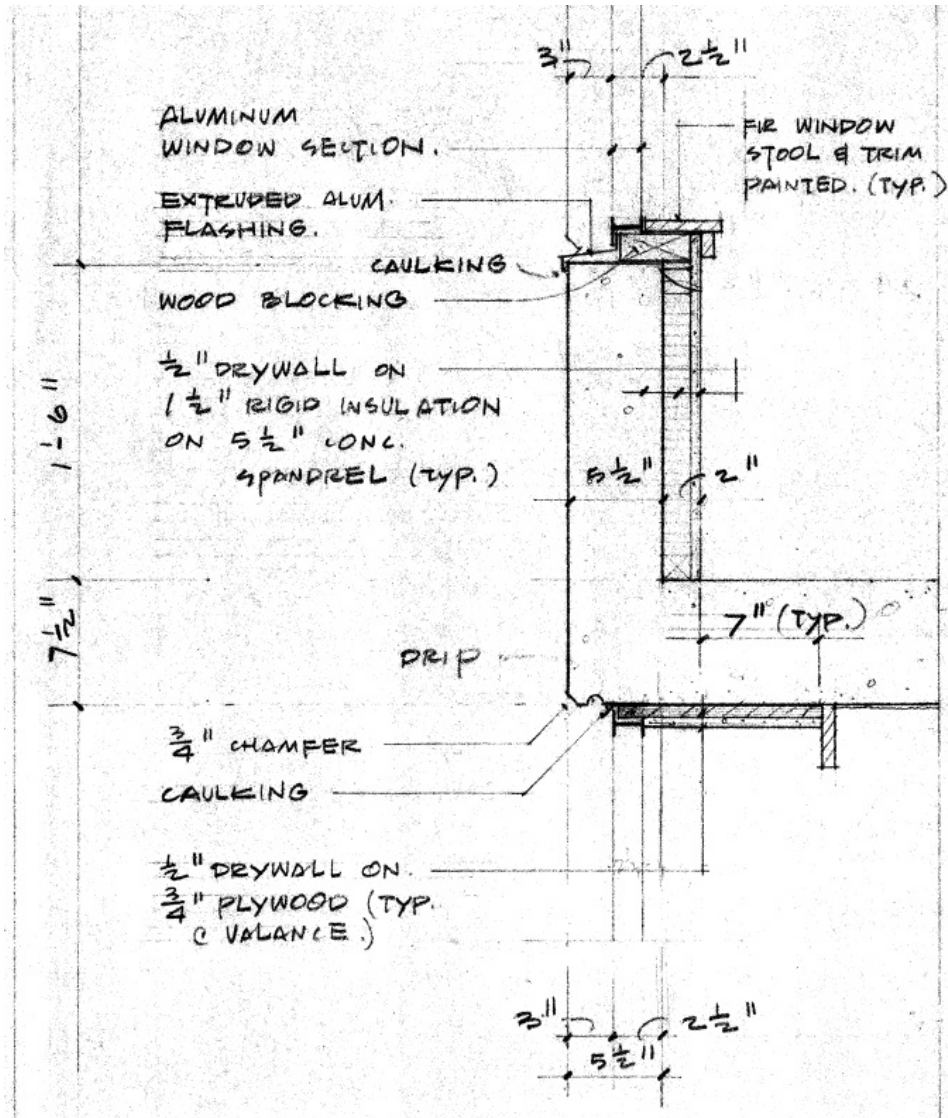


Figure 7-4: Typical original exterior enclosure assembly below window

7.1.1.3 Post-Retrofit Building Enclosure

The retrofit of the case study building was conducted from approximately May 2012 to December 2013 and included the installation of a new roof, replacement of windows and doors, and an over clad of the exposed concrete walls including the addition of exterior insulation. A detailed schedule of aspects of the retrofit likely to impact airflow patterns at the building is provided in Appendix E.

The upgraded wall assembly consists of:

- New metal panel cladding (or stucco in some locations)
- New 3 ½” of semi-rigid mineral wool insulation between a fiberglass clip low conductivity cladding support system
- New liquid applied vapour permeable membrane at cracks and transitions
- Existing cast-in-place concrete
- Existing 1 ½” steel studs with extruded polystyrene insulation
- Existing interior gypsum wall board

The effective R-value of these walls was determined by RDH to be approximately 2.8 m²·K/W (R-15.9 ft²·°F·hr/Btu). As part of the retrofit, localized sealing around penetrations and at cracks in the concrete was performed using a liquid applied membrane to improve water shedding and airtightness characteristics. Figure 7-5 and Figure 7-6 show the new wall assembly while under construction including example of localized sealing of the concrete.



Figure 7-5: New wall assembly under construction at the case study building showing localized sealing with liquid applied membrane (red) at window head and sill, exterior mineral wool insulation, and fiberglass low conductivity clips (Photo courtesy of RDH)



Figure 7-6: New wall assembly while under construction showing localized sealing at concrete slab cold joints, and cladding support system prior to installation of mineral wool insulation (Photo courtesy of RDH)

The new glazing consists of low conductivity fiberglass frames with triple-glazed insulating glazing units. RDH determined an effective U-value of 0.97 W/m²·K for these windows and doors. The glazing percentage of the building remained unchanged. As part of the installation of this new glazing, air sealing details at windows and doors was improved.

The new roof system is a protected membrane type roof assembly with 102 mm of extruded polystyrene insulation on top of a new waterproofing membrane. This assembly was determined by RDH to have an R-value of approximately 3.5 m²·K/W (19.9 ft²·°F·hr/Btu).

7.1.1.4 Heating and Ventilation Systems

Space heating at the case study building is provided by electric baseboard heaters located within the suites. Suites on the 9th through 13th floors also have gas fireplaces.

Ventilation air is supplied to the common corridors and suites using a corridor pressurization ventilation system. The ventilation air is brought in by a make-up air unit (MAU) located on the roof and then provided to each corridor by a vertical duct with a grille at each corridor. The MAU is manufactured by Reznor (model "HRPB250-8 S MV") and is a constant volume system with an airflow capacity of 1,560 L/s at a static pressure of 250 Pa which is approximately 42 L/s per suite (37 suites). The MAU heats the intake ventilation air via a stainless steel heat exchanger using a gas burner with a nominal efficiency of 80%. It is set to heat the air to 20°C and is controlled by a thermostat in the MAU duct downstream of the heat exchanger. Additional ventilation to the suites is assumed to be provided by operable windows which are operated by occupants according to their personal preference.

The main ventilation shaft is constructed of galvanized steel and incorporates fire dampers at each floor and on the roof. In the event of a fire, these dampers are intended to close on all floors except for the floor with the fire. A motorized damper opens at the top of the ventilation shaft at the roof to exhaust smoke from the corridor of the floor with the fire. Also, in the event of a fire the stairwell is designed to be pressurized by a dedicated fan located in the parking garage which is activated by the fire alarm system. The original smoke relief for the suites was designed to be achieved by opening balcony doors; however, these balconies are actually enclosed, so the current smoke relief strategy for the suites is unclear. It is not known when the balconies were enclosed.

Occupant controlled point source exhaust fans are installed in suite bathrooms (2 bathrooms per suite), kitchens, and are incorporated in in-suite clothes dryers. While in some cases the original fans have been replaced, the majority of bathroom fans are those originally installed and are rated at 70 ft³/min (33 L/s). Dryers and kitchen range hoods have often been replaced and specifications vary widely. The exhaust ducts for these systems are cast in the floor slab and do not include back-draft dampers unless incorporated in an updated fan unit. In many cases these ducts were observed to be partially blocked at the outlet, have debris within the duct, or be partially crushed as shown in Figure 7-7 and Figure 7-8.



Figure 7-7: Photo of outlet of in-slab exhaust duct at the case study building showing collapsed shape of the duct.



Figure 7-8: Photo of interior of a duct at the case study building showing large pieces of debris within the duct.

There is a separate ventilation air supply system for the elevator vestibule located in the parking garage. This system draws air from the exterior at the ground level and supplies it to the vestibule. Based on the original mechanical ventilation drawings this fan is rated to supply 118 L/s at 125 Pa of static pressure.

The parking garage has 2 large exhaust fans each rated for approximately 4,800 L/s at a static pressure of 31 Pa. The garbage room in the parking garage is ventilated with an exhaust fan that is rated at 94 L/s at 94 Pa of static pressure. Both the parking garage and garbage room exhaust fans have only manual on-off control and are on during typical building operation.

Original mechanical drawings for the case study building are provided in Appendix B.

7.1.2 Objective

The testing and measurement program at the case study building aims to quantify airflows at the case study building and to evaluate how these airflows are impacted by the air permeance of the building pressure boundaries and by pressure difference created by the driving forces of airflow. As part of this objective, this program also aims to quantify the natural driving forces of airflow, wind and stack effect, at the case study building to correlate their effect with the measured airflows and pressure differences. Measurements of indicators of indoor air quality were also made to provide an indication of the efficacy and appropriateness of the ventilation rates. Measuring these quantities provides a thorough understanding of airflow and factors affecting airflow at the case study building, and in particular allows for evaluation of the performance of the corridor pressurization based ventilation system.

7.1.3 Approach

To quantify airflow, air permeance, and pressure differences at the case study building a program of testing and measurement was developed. In general the testing and measurement program focuses on two representative floors near the bottom and top of the building (Floors 3 and 11). Due to timing, access, and budgetary considerations it was not possible to perform all of the testing and

measurement at every suite or every floor level. Carrying out the majority of the measurements and testing on the same two primary test floors allows for the results of the difference components of the experimental work to be directly compared. Some work was also carried out on other floors, notably including Floor 1 and Floor 13 to characterize the unique conditions of the bottom and top floors of the building. Floors adjacent to the primary testing and monitoring floors were designated as secondary testing and monitoring floors (which is most applicable for the monitoring program as discussed in Section 7.3) and other floors were designated as tertiary floors as shown in Figure 7-9.

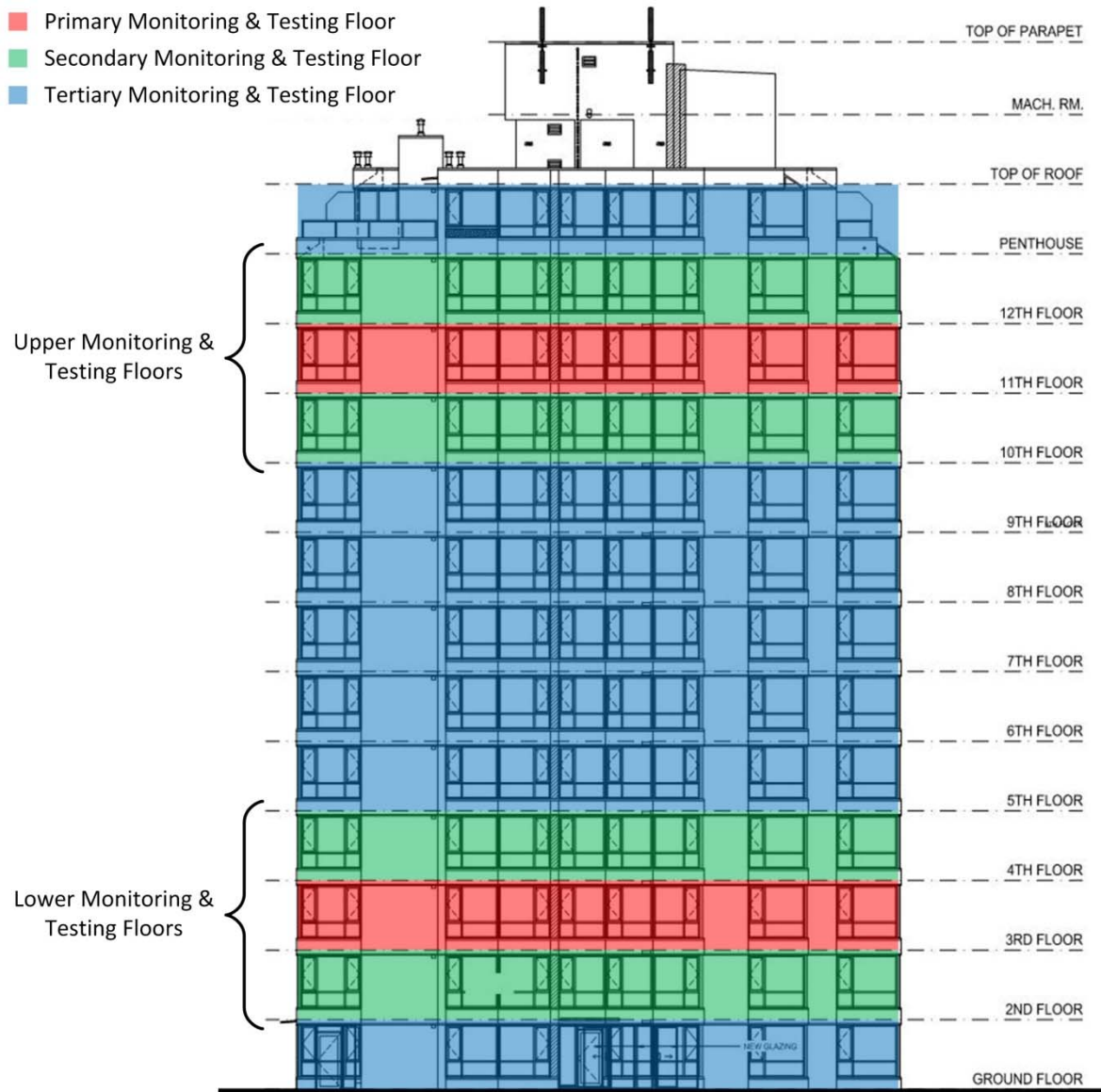


Figure 7-9: West elevation of the case study building indicating the primary, secondary, and tertiary monitoring and testing floors

Airflow rates between zones were measured using perfluorocarbon tracer testing which allows for the measurement of time averaged airflow. The airflow intake of the MAU was also measured using

a custom made powered flow hood, and the supply airflow rate of the MAU to each corridor was measured using a balometer. The airflow exhaust rates of bathroom fans were measured with a powered flow hood.

Airtightness testing using a sequentially neutralized pressurization technique was used to measure the air permeance (airtightness) of the exterior building enclosure and of interior compartmentalizing elements.

Pressure differences between interior zones and across the building enclosure were measured as part of a long-term monitoring program implemented at the case study building. This monitoring also included monitoring of exterior environmental conditions so that the interaction between exterior conditions (natural driving forces of airflow) and building airflow patterns could be assessed. Indicators of indoor air quality, carbon dioxide and dew point temperatures, were also measured as part of the monitoring program.

7.2 Measurement of Airflow between Zones

Airflow measurements between zones at the case study building were conducted using perfluorocarbon tracer (PFT) testing. This testing provides a direct measure of the airflow component of the airflow nodal network.

7.2.1 Objective

The objective of the PFT testing was to measure in-service airflows at the case study building. The airflows measured include:

- Airflow between corridors and suites
- Airflow between adjacent suites on the same floor, and on floors above and below
- Airflow from the parking garage to suites and corridors

The testing also provides qualitative results regarding the distribution of ventilation air from the make-up air unit and the flow of air from the parking garage into the occupied spaces of the building.

7.2.2 Approach

To measure the airflow between zones, PFT testing was conducted which provides time-averaged flow rates. This testing technique was discussed in Section 6.3.5.4; however, a brief review is provided here as well as discussion of its use for the thesis work.

The PFT test method used was developed by Brookhaven National Laboratory and uses seven distinct perfluorocarbon tracers. These tracers are released into the air and then absorbed by capillary absorption tube samplers (CATS). The laboratory is then able to determine the how much of the tracer the CATS absorbed. Using these absorbed volumes and the known release rates of the PFTs, the airflow between zones can be determined using the calculation procedure provided in D'Ottavio et al (1988). The PFT equipment and processing of the CATS samplers was provided by Brookhaven National Laboratory through Meadowbrook Partners Inc. (MPI). Figure 7-10 shows the PFT sources and Figure 7-11 shows a typical CATS used for this testing.



Figure 7-10: PFT sources used at the case study building. Each colour is a different PFT tracer and the glass vials are “mega” sources of a distinct PFT used in the MAU.



Figure 7-11: Typical CATS used for PFT testing at the case study building

This type of airflow measurement was selected because it provided for the ability to measure multiple airflows between zones during the same test period, and because it provided a time averaged measurement which is generally of the most interest with respect to airflow in buildings for indoor air quality and comfort considerations.

Consistent with the approach used in other components of the testing and measurement program, PFT testing focused on the primary test floors of the case study building. A unique tracer was also released in both the rooftop MAU and the parking garage so that airflow from these sources to zones of the building could be determined. Due to the limited number of PFTs available, some of the tracers were used in two locations within the building as suggested by MPI. Based on their previous experience with this type of testing, a separation of 3 floors between repeated tracers is typically sufficient to limit interference of the two source locations. (Based on the testing at the case study building, this assumption was subsequently found to be true.) Also, again due to the limited number of PFTs available, on each of the primary test floors a particular suite was identified as the primary test suite and tracers were installed in the suites above and below these suites. Suites 302 and 1103 were selected as the primary test suites. A CATS was installed in each suite on the primary test floors and the floors above and below the test floors, as well as in the corridor on each level of the building, in the MAU supply airflow duct (downstream of the PFT source), in the elevator lobby at the parking garage level. Three CATS were installed in the parking garage due to its large volume.

Detailed layouts and descriptions of the PFT testing equipment are provided in Appendix C, and, as an example, the layout of PFTs and CATS on Floor 11 is provided in Figure 7-12. Two sources of the same type were used in each tagged suite to provide a sufficiently high release rate of the tracers to achieve measurable concentrations and to evenly distribute the tracers within the suites.



Figure 7-12: Layout of PFT testing equipment on Floor 11 of the case study building

The PFT testing was conducted for a period of one week from April 10th, 2013 to April 17th, 2013 to capture the weekly occupancy pattern typical of a residential building. The duration of the test was also intended to average the effects of open windows, high and low wind speeds, intermittent operation of exhaust fans, et cetera. Results of the PFT testing are presented in Chapter 8.

7.3 Mechanical Ventilation System Airflow Measurements

The airflow rates associated with the building mechanical ventilation system were also measured including the flow rates of the bathroom exhaust fans, the intake flow rate of the make-up air unit, and the supply airflow rate from the make-up air unit to each corridor.

7.3.1 Bathroom Exhaust Fan Measurements

To determine the flow characteristics of the bathroom fans at the case study building, the flow rate of these fans was measured using a powered flow hood (and in some cases also using a balometer). The powered flow hood specifications are provided in Appendix C and the use of this equipment was discussed in Section 6.3.1 and Section 6.3.2. A typical arrangement of the powered flow hood equipment being used to measure the flow rate of a bathroom fan is shown in Figure 6-8.

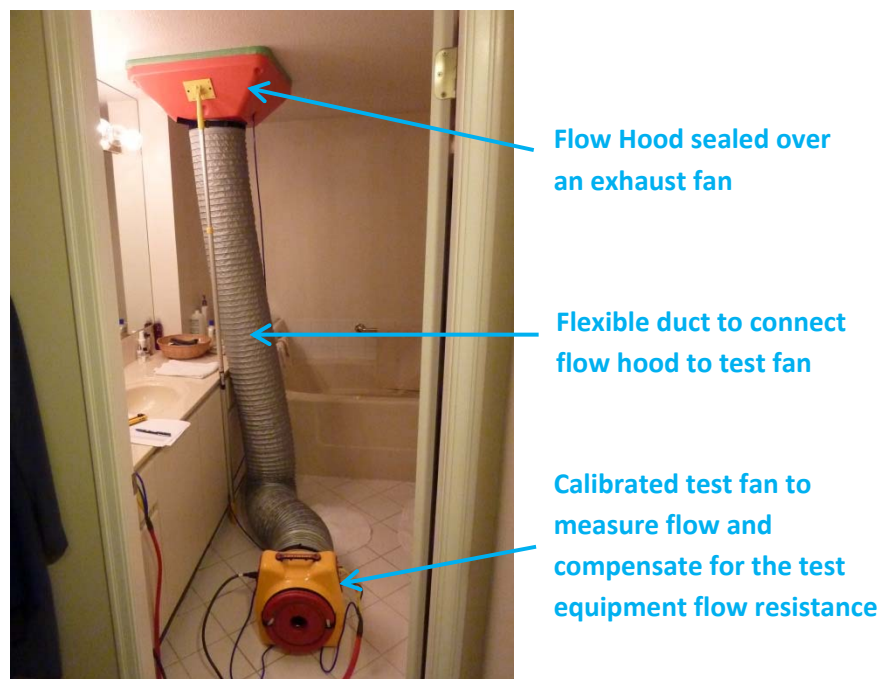


Figure 7-13: Photo of powered flow hood being used to test a bathroom fan at the case study building

This equipment was also used to artificially create pressure differences across the exhaust ducts (with the fan installed) and thus determine flow resistance properties of the duct including flow coefficients and flow exponents. The testing was performed with the bathroom fan off at test pressures of 25 Pa, 50 Pa, 75 Pa, and 100 Pa under pressurization (exhaust flow) only. As pressure differences and flow rates at each test pressure were relatively stable, and a large number of fans were tested, only one flow measurement was recorded at each test pressure. It is important to note that the pressure difference was measured from the inlet to the exhaust fan to the outlet on the exterior face of the building and included the exhaust fan, which when not operating as during the test, adds flow resistance that does not exist when the fan is running. This procedure was selected as removing the bathroom fans to perform the test was not feasible given the large number of fans being tested. Thus, the flow resistance of these ducts as determined by this test should be considered as an upper limit.

This testing was primarily performed as part of independent work being performed at the case study building by RDH that is outside the scope of this thesis; however, test results will be used as appropriate and are provided in Appendix C.

7.3.2 Make-up Air Unit Intake Testing

The airflow intake of the make-up air unit was measured on February 8, 2013 using a custom designed and built powered flow hood apparatus. This testing used a procedure similar to that used by Moffat et al (1998) and Ueno et al (2012). A large Retrotec fan of the same type used for airtightness testing (specifications provided in Appendix D) was used to measure airflow into the MAU and compensate for the flow resistance added by the testing apparatus. The fan was attached to the MAU by a custom made flexible duct which was also designed to be used for pitot tube traverse airflow rate measurements. An image of the testing set-up is shown in Figure 7-14. The results of these measurements are presented in Section 8.1.



Figure 7-14: MAU testing apparatus with green flex-duct to attach Retrotec fan to the MAU intake

7.3.3 Make-up Air Unit Corridor Supply Measurements

The air supplied to each corridor from the MAU was measured using a balometer (unpowered flow hood). The balometer specifications are provided in Appendix C. Due to the geometry of the supply grilles and corridor walls, the balometer was sealed around the grille with tape.

Flow measurements were made on July 27th, 2012, July 28th, 2012, February 8th, 2013, and July 11th, 2013. Measurements were made both with the MAU on and with the MAU off to measure in-service airflow and to indicate how the building would operate without the MAU. Only July 27th, 2013 measurements were only made with the MAU off, and on July 28th, 2012 measurements were only made with the MAU on. On February 8th, 2013 and July 11th, 2013 measurements were made with the MAU on and then again with the MAU off. A smoke pencil was also used to confirm the flow direction when the MAU was off. Figure 7-15 shows a corridor supply airflow rate measurement being made using a balometer. The results of these measurements are presented in Section 8.2 and Section 8.3.



Figure 7-15: A measurement of MAU airflow supplied to a corridor being made using a balometer

7.4 Airtightness Testing

Airtightness testing was conducted at the case study building to measure the air permeance (i.e airtightness) of the exterior building enclosure and of interior compartmentalizing elements.

7.4.1 Objective

This testing was conducted to quantify the resistance to airflow of interior compartmentalizing elements and of the exterior building enclosure pre- and post-retrofit. The results of this testing provide an understanding of the airflow resistance (flow coefficient and flow exponent) component of the airflow nodal network.

7.4.2 Approach

The airtightness testing was conducted using a sequentially neutralized pressurization/depressurization approach and focused on the primary testing and monitoring floors (Floor 3 and Floor 11), as well as the top and bottom floors (Floor 13 and Floor 1) of the case study building. This airtightness testing technique was selected because it provides the ability to measure the airtightness of the exterior enclosure in a highly compartmentalized building and to measure the airtightness of interior compartmentalizing elements whereas other commonly used techniques are not intended for this application. This method was used to determine the airtightness of the following:

- Suites on Floor 3 and Floor 11: Airtightness of the floors, ceilings, partition walls to adjacent suites on the right, partition walls to adjacent suites on the left, walls to the corridor, and pre- and post-retrofit exterior enclosure airtightness
- Suites on Floors 1 and 13: Pre- and post-retrofit exterior enclosure airtightness
- Whole Floor - Floor 1: Pre- and post-retrofit exterior enclosure airtightness
- Whole Floor - Floor 13: Post-retrofit exterior enclosure airtightness

- Corridors on Floors 3, 9, and 11: Airtightness testing of the corridor compartmentalizing elements including suite entrance doors, elevator doors, and stairwell doors.

Testing of the suites and corridors on Floors 3 and 11 provides measurements of the airtightness characteristics of the typical floors of the building. Testing of suites and whole floors on Floor 1 and Floor 13 provides the exterior enclosure airtightness characteristics of the top and bottom of the building which can be of particular importance. Testing of Corridor 9 was performed to increase the sample of tested corridors.

Pre-retrofit airtightness testing was generally performed with pressurization and depressurization to 10, 30, 50 and 60 Pa, with readings taken, using a computer and associated software, as frequently as the equipment would allow (minimum one reading per second) for 10 seconds. A multi-point test method was used so that the flow coefficient and flow exponent could both be determined. Measurement of the bias pressure was taken before and after testing for 30 seconds. The exterior reference pressure was measured as an average of pressure taps located at the east and west sides of the building at the level of the test.

Post-retrofit testing followed the same procedure except that pressurization and depressurization was conducted at 20, 30, 50, and 60 Pa. The change to the lowest test pressure (from 10 Pa to 20 Pa) was made because during testing it was difficult to maintain a consistent pressure difference at 10 Pa. To increase the stability of the pressure difference, the pressure magnitude was increased with the aim of making this lowest test pressure more consistent during the post-retrofit testing. Additionally, measurements for the post-retrofit testing were taken for 20 seconds (instead of 10 seconds) because the bias pressure was observed to be more variable and the longer measurement period was intended to compensate for this variability.

The airtightness testing did not follow a standardized test procedure such as those by ASTM, CGSB or USACE discussed in Section 6.2 and instead an alternate procedure was developed based on these standards. Testing was initially performed with approximately eight test points; however, a final methodology using four points was used as this method provided an appropriate combination of accuracy (strong correlation coefficients were typically determined based on the testing) and speed so that the large number of tests could be completed.

Airtightness testing of a suite was performed in 6 steps for pressurization and depressurization:

- Step 1 – All 6 Sides: Pressurize/Depressurize the test suite
- Step 2 – Floor Above: Pressurize/depressurize the test suite and the floor above
- Step 3 – Floor Below: Pressurize/depressurize all from Step 2 plus the floor below
- Step 4 – Corridor: Pressurize/Depressurize all from Step 3 plus the corridor on the same floor as the test suite
- Step 5 – Suite to Right: Pressurize/Depressurize all from Step 4 plus the suite to the right of the test suite
- Step 6 – Suite to Left: Pressurize/Depressurize all from Step 5 plus the suite to the left of the test suite

During each of these steps measurements were taken at each of the four test pressures.

Figure 2-1 shows a schematic of the airtightness testing layout for pressurizing a -01 suite while pressure equalizing the floor above (Step 2). Red and yellow fans show fans forcing air into the test suite and into the floor above. Doors are open to the non-test suites to allow for unimpeded air movement. Schematics for each of the testing steps for pressurization testing of an -01 suite are provided in Appendix D along with detailed descriptions of the test procedure. The test procedure for a -02 or -03 suite is similar.

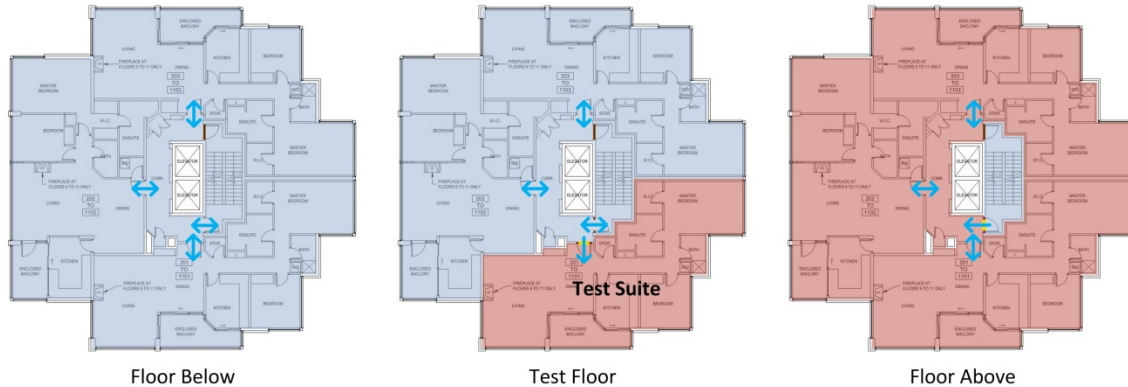


Figure 7-16: Airtightness testing schematic for Step 2 of pressurization of an -01 suite while pressure equalizing the floor above

Exterior enclosure only airtightness testing was performed on suites and whole floors for Floors 1 and 13. This testing was performed similarly to the suite testing on typical floors except only two steps were completed. The first step was pressurization and the second was depressurization, each with all adjacent zones pressure neutralized.

Testing of the exterior enclosure and suite compartmentalizing elements was performed with no sealing of mechanical systems or ducts such as those for bathroom fans, range hoods, clothes dryers, and fireplaces. This arrangement was selected to best represent in-service conditions as these fans are not normally operating (most of the time they are off). Exterior enclosure airtightness therefore includes walls, windows, roofs, and mechanical duct leakage.

Airtightness testing of the corridors was conducted by installing the test fan in the west stairwell door to the corridor. This fan was then used to pressurize/depressurize the corridor and measure flows. As the make-up air unit is on during typical building operation, during this testing the grille to the make-up air unit duct was sealed to prevent bypass airflows. Flows through compartmentalizing elements of the corridor were then sealed off one at a time (or pressure neutralized in the case of the floors above and below) and both pressurization and depressurization tests conducted. By determining the measured flow with each element sealed (or neutralized) compared to the measured flow without it sealed (or neutralized) the airflow through that component can be determined.

The compartmentalizing elements tested as part of the corridor testing includes:

- Suite entrance doors (3 per floor)
- Stairwell door (east door since fan installed in west stairwell door)
- Elevator doors

- Garbage chute room door
- Electrical closet door
- Floor above
- Floor below

Typical sealing practices for the elevator doors and for a suite entrance door are shown in Figure 7-17 and Figure 7-18 respectively.



Figure 7-17: Typical sealing of elevator doors for corridor airtightness testing using polyethylene sheet and PVC tape



Figure 7-18: Typical sealing of suite entrance door during corridor airtightness testing using polyethylene sheet and PVC tape

Door undercut sizes were measured for suite and stairwell doors and observations were also recorded of whether weather stripping was installed on the doors. These measurements and observations were made to determine typical door undercut sizing and to allow for correlation with suite entrance door airtightness testing results. The undercut measurements and observations are reported in Appendix D.

Images of the equipment used for the airtightness testing are provided in Figure 7-19 and Figure 7-20, and detailed equipment specifications are provided in Appendix D.



Figure 7-19: Two fan-doors used for airtightness testing of the case study building installed in a stairwell door (left) and a suite entrance door (right)



Figure 7-20: Laptop and four digital manometers used for controlling the airtightness testing fans and for making the pressure and airflow measurements during the test

It is important to note that the pressure regimes created during this type of airtightness testing are not representative of pressure regimes experienced at the building during normal operation. The test creates relatively high pressure differences (approximately 20 to 75 Pa) that are relatively consistent across all pressure boundaries. In operation, pressure differences are much lower (approximately 0 to 20 Pa) and would likely not be equally distributed across all building pressure boundaries. Thus, airtightness testing provides a measure of a physical property of the building (airtightness), but does not necessarily indicate actual in-service airflows and pressure regimes.

Supplementary airtightness testing information is provided in Appendix D.

7.5 Pressure and Air Quality Monitoring Program

To measure the pressure differences between zones within the case study building and across the exterior enclosure, a pressure monitoring program was implemented. While in-service pressure differences are the focus of the monitoring program, monitoring of temperature, relative humidity, and carbon dioxide concentrations was also implemented at various locations and will be used to supplement the pressure monitoring information. Exterior environmental conditions were also monitored. Energy consumption data including electricity and natural gas were monitored as part of the RDH research project but is not included in this thesis.

7.5.1 Objective

The monitoring program was primarily implemented to quantify in-service pressure differences and exterior environmental conditions at the case study building to allow for assessment of correlations between these pressures and the driving forces of airflow. The results of this monitoring provide an understanding of the pressure differences in building airflow nodal network. Additionally, this monitoring also aims to quantify interior temperatures, relative humidity levels, and carbon dioxide concentrations to provide information on operating conditions including indoor air quality.

The primary quantities of interest for this monitoring program are:

- Pressure differences across exterior building enclosure on each cardinal face of the building
- Pressure differences from the corridors to the suites
- Pressure differences across floors and ceiling to the zones above and below
- Pressure differences between adjacent suites
- Carbon dioxide concentration in ventilation air, corridors, and suites
- Dew point temperature (calculated from relative humidity and temperature) in ventilation air, corridors and suites
- Exterior temperature
- Wind speed and direction

The monitoring program also measured the airflow rate of the make-up air unit.

7.5.2 Approach

Wireless data acquisition units were used to record sensor measurements throughout the building. Two different types of these units are being used, the SMT-A2 and SMT-A3, both of which are supplied and manufactured by SMT Research Ltd. (SMT). These units communicate wirelessly with two SMT-BiG (Building Intelligence Gateway) systems within the building which act as central locations where data is stored and/or uploaded. The battery powered wireless data acquisition system was selected to limit both installation time and disruption to building occupants. The typical SMT-A3 units were designed to be mounted in a wall and have a faceplate cover. Photos of a typical SMT-A3 unit are provided in Figure 7-21 and Figure 7-22. Detailed data acquisition system and sensor specification information is provided in Appendix E.



Figure 7-21: Front face of a typical data acquisition unit used at the case study building showing the LCD screen to interact with the unit (top left), the carbon dioxide sensor (bottom left, round and white), and battery pack left



Figure 7-22: Front face of a typical data acquisition unit used at the case study building with the faceplate cover installed showing holes on the front of the cover to expose the temperature and relative humidity sensors (left) and pressure tube (top right)

A typical data acquisition unit being installed is shown in Figure 7-23 and the final appearance of the sensor unit installed above a suite entrance door is shown in Figure 7-24.



Figure 7-23: Typical SMT-A3 unit being installed in a wall above a suite entrance door



Figure 7-24: Typical data acquisition unit installed above a suite entrance door

One pressure port is on the front face of the unit (as shown in Figure 7-22), and the other pressure port is run from the back of the unit using 1/8" inner diameter tubing. In the case of a pressure sensor measuring pressure differences across a suite to corridor wall, the pressure port in the corridor was made by using 1/16" inner diameter copper tubing penetrating through the gypsum wall board.

Exterior pressure taps were installed by drilling a hole through the exterior concrete wall and running a 1/8" inner diameter tube to the exterior and then sealing around the tube on both the interior and exterior sides of the concrete wall. The exterior end of the tube is then covered by a custom made faceplate to protect the end of the tube from water and dirt. The faceplate cover has four holes to allow for pressure transfer, and the holes are sloped to the exterior to limit water ingress. A small notch was cut in the cover at the bottom to allow any water that does get behind the cover to drain. The relatively smooth contour of the exterior pressure tap faceplate is intended to minimize the impact of the pressure tap on the exterior pressure measurements. An example of the typical exterior pressure tap configuration is shown in Figure 7-25.



Figure 7-25: Typical exterior pressure tap configuration

A small number of other configurations of the monitoring units were also used for outdoor and portable applications and these are detailed in Appendix E. All monitoring units take readings simultaneously on the hour.

Floor 3 and Floor 11 of the case study building were selected as primary testing and monitoring floors to allow for direct comparison of data between different testing and monitoring programs. Consistent with this approach, monitoring equipment was primarily installed on these floors and adjacent floors.

Each data acquisition unit and sensor has been given a unique name which indicates its location and type, and these names are used in the presentation of results and analysis in this thesis. A list of all sensors and detailed monitoring equipment layouts are provided in Appendix E. Figure 7-27 provides the monitoring equipment layout for Floor 3 and Floor 11 as an example, and Figure 7-26 provides the legend for interpreting the layout. Figure 7-28 schematically illustrates how the pressure sensors can be referenced to each other because they are linked together.

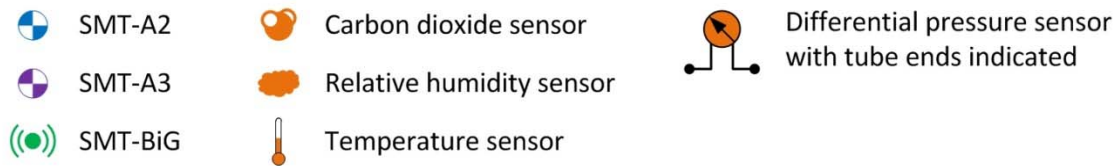


Figure 7-26: Legend of symbols used for interpretation of Figure 7-27 and Figure 7-28

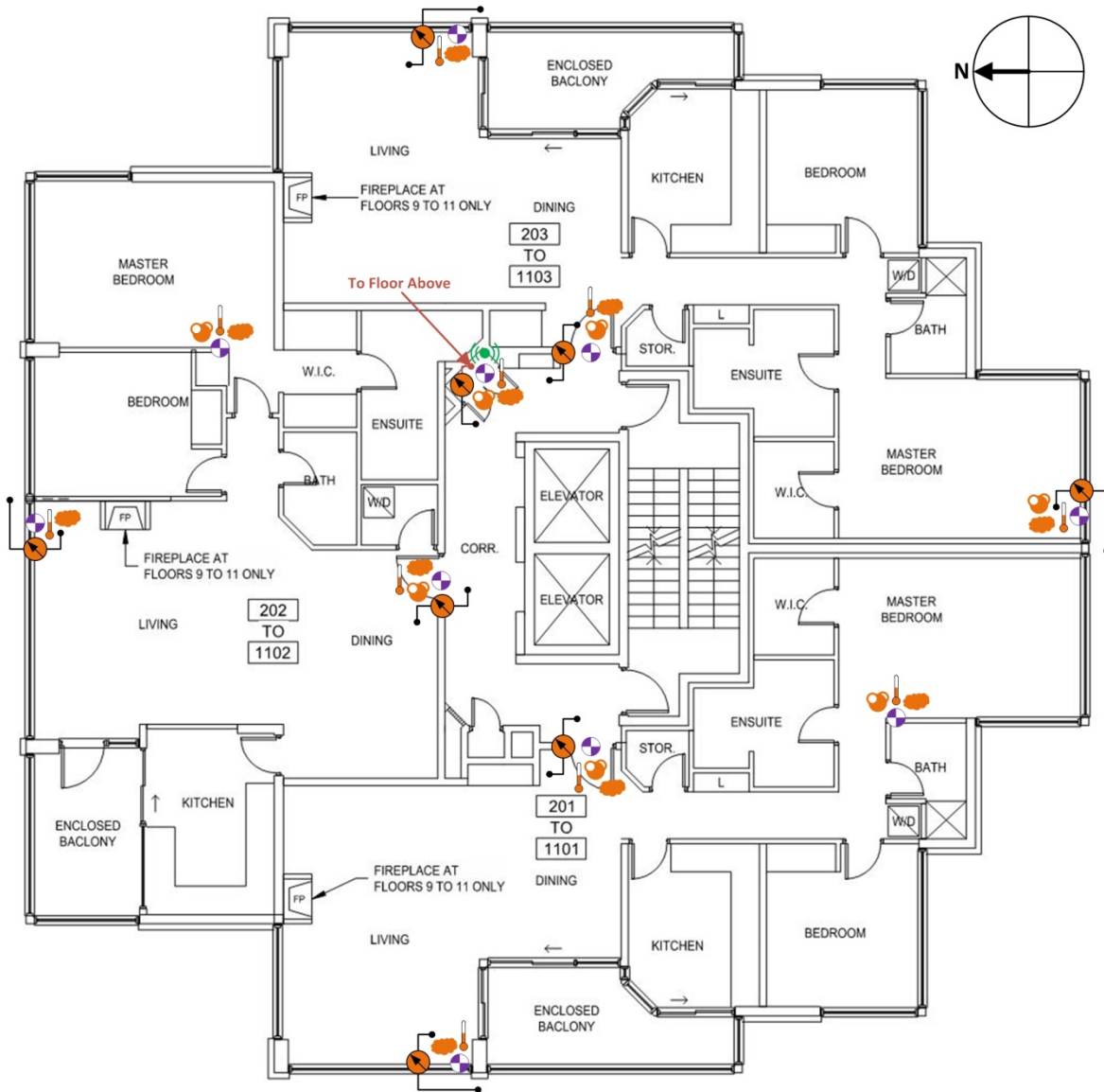


Figure 7-27: Floor plan showing layout of monitoring equipment for Floors 3 and 11



Figure 7-28: North-south cross-section of the case study building illustrating how the pressure measurements are linked

A weather station was installed on the middle of the roof of the upper mechanical penthouse to monitor exterior temperature, relative humidity, wind speed, wind direction, and barometric pressure. This system was manufactured by Davis Instruments Corp. and configured to communicate with the data acquisition system manufactured by SMT. The weather station

recorded exterior conditions every 5 minutes; however, for most analysis hourly averages of this data were used. The weather station is shown in Figure 7-29 and detailed specifications are provided in Appendix E. The wind vane and anemometer are located at approximately 2.1 m above the parapet edge of the upper mechanical penthouse and are a total of approximately 7.7 m above the parapet edge of the main roof of the building and 42.3 m above the ground. The location of the weather station is shown on a building elevation in Figure 7-30. There are some communication antennas that protrude above the mechanical penthouse and may cause some interference with the wind measurements, but given the relatively thin nature of these obstructions, their interference assumed to be small.



Figure 7-29: Weather station installed on roof of the case study building

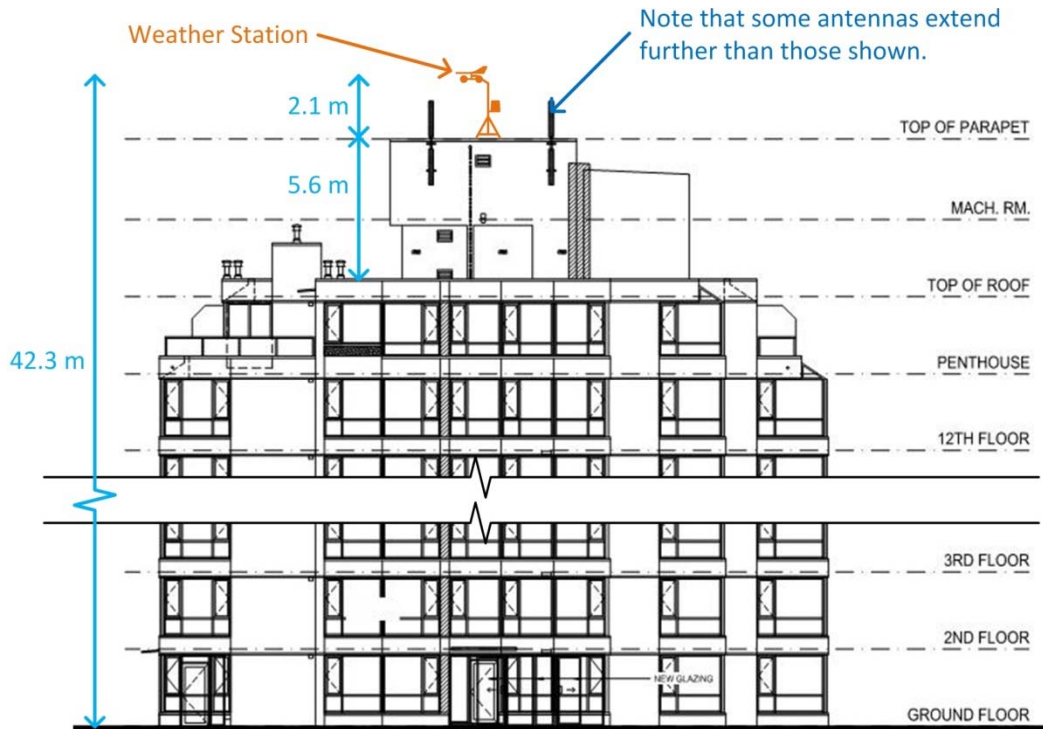


Figure 7-30: Elevation of case study building indicating location of the weather station and height of the anemometer and wind vane (weather station not to scale)

7.6 Weather Data

While the majority of monitoring and testing results are provided in subsequent chapters, an overview of the exterior environmental conditions during the testing and monitoring period is provided here for reference.

Various problems were encountered during the monitoring program and some of the most significant problems were with the weather station system. Upon periodic inspection of the data it was determined that the temperature, relative humidity, wind speed, and wind direction data were incorrect due to improper installation. Unfortunately, this resulted in a significant loss of data. The details of this data loss are discussed in Appendix E.

To overcome the loss of data, correlations were developed between Environment Canada weather data collected at Vancouver International Airport (YVR) and the weather data available from monitoring at the case study building. The YVR weather station is located approximately 5 km south of the case study building. Using these correlations, weather data from YVR was adjusted and used to fill in gaps in the available monitoring data. The development of the correlations is provided in Appendix E, and compiled relevant weather data that is used for analysis is provided in Figure 7-31, Figure 7-32, and Figure 7-33 to provide an indication of the typical exterior conditions during the testing and monitoring period. The compiled weather station data is denoted as WS' and all weather data used for analysis is from this compiled data set.

Prevailing winds in Vancouver are from the east, and stronger winds come from the west-north-west. The wind speeds during the testing period averaged 8.9 km/hr (2.5 m/s) which is lower than both the average based on CWEC data (11.9 km/hr, 3.3 m/s) and the 10 year average (13.7 km/hr, 3.8 m/s) presented in Chapter 3. The distribution of wind speeds closely followed a Weibull distribution based on the mean as shown in Figure 7-35.

For simplicity, the wind speed is always reported at the location of the weather station; however, in literature, the wind speed is often reported at the roof height. Using Eq. 3.4 with a terrain category of 2, the wind speed at the roof height can be calculated to be approximately 96% of the wind speed at the height of the weather station.

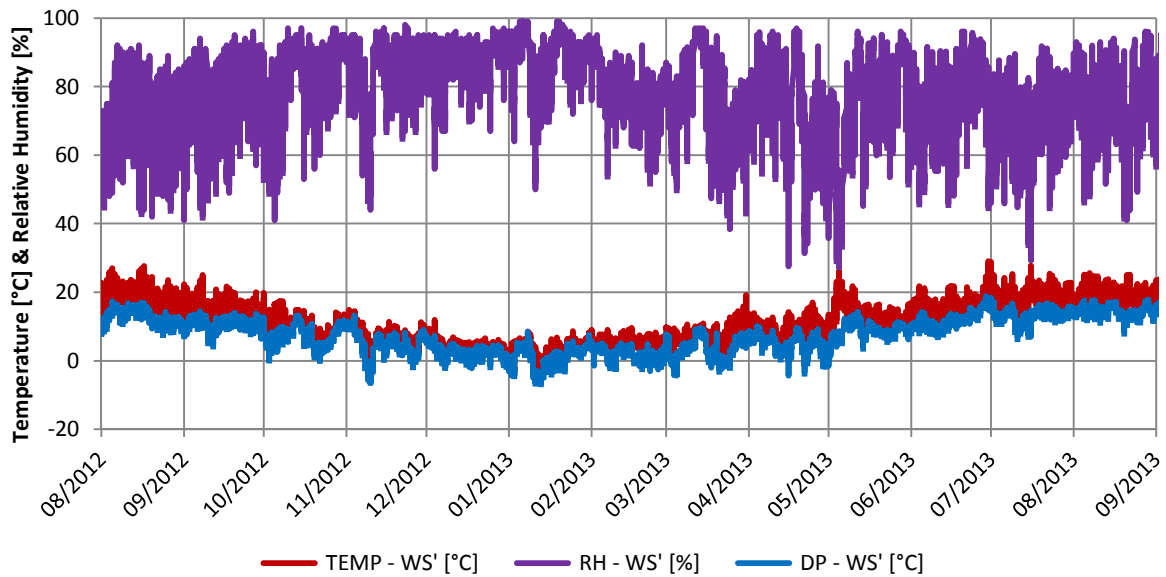


Figure 7-31: Graph of compiled exterior temperature, relative humidity, and dew point temperatures

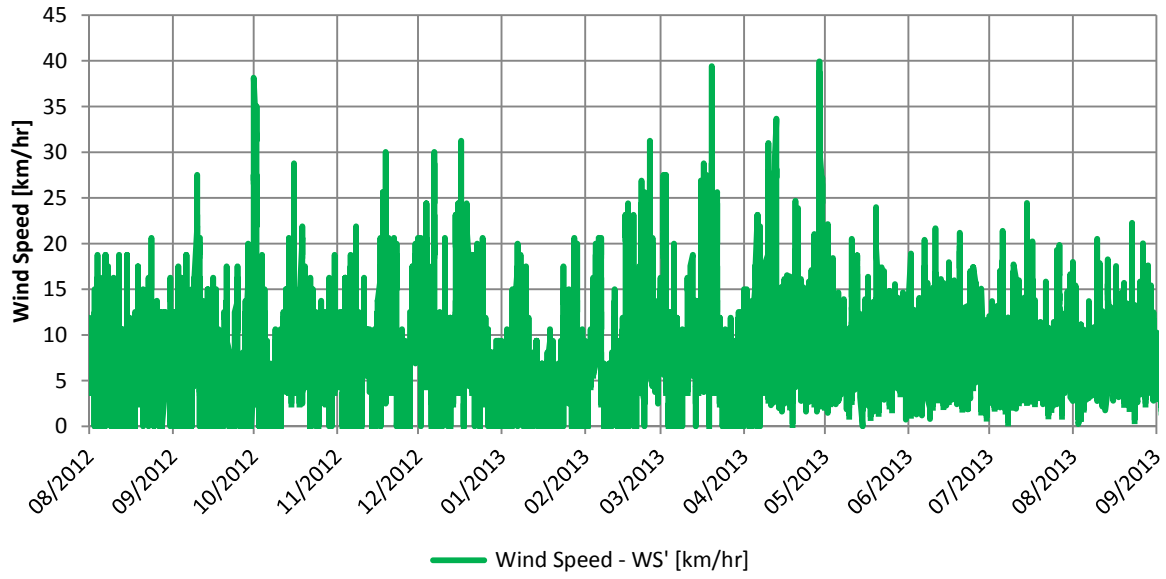


Figure 7-32: Graph of compiled wind speed at the weather station (42.3 m above the ground)

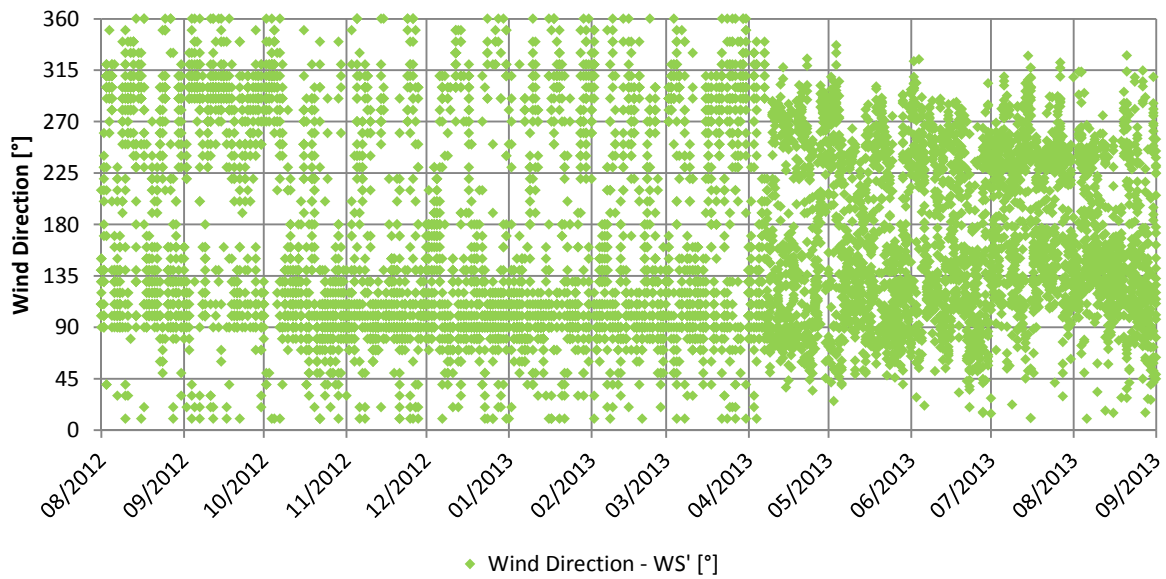


Figure 7-33: Graph of compiled wind direction

The change in wind direction data type starting approximately in April 2013 is due to the switch from YVR data to on-site monitoring data. The average wind speed and frequency of the wind by direction is provided in Figure 7-34.

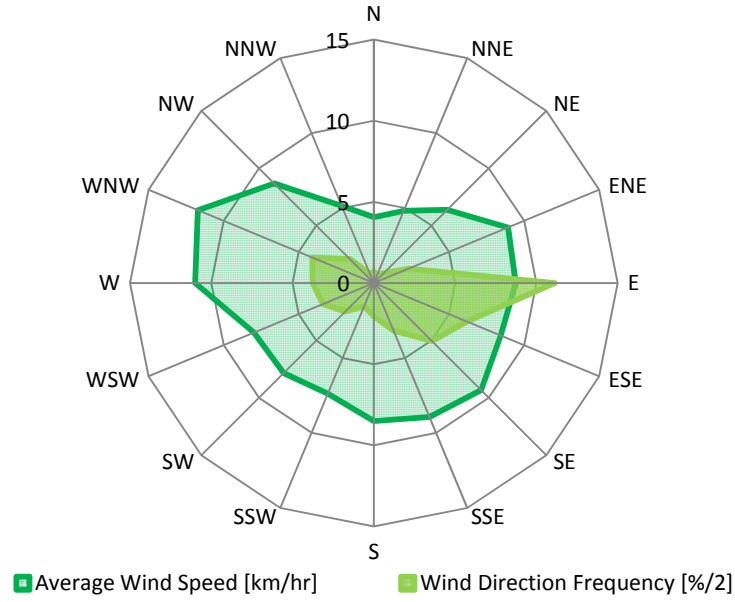


Figure 7-34: Chart of average wind speed and frequency during the monitoring and testing period

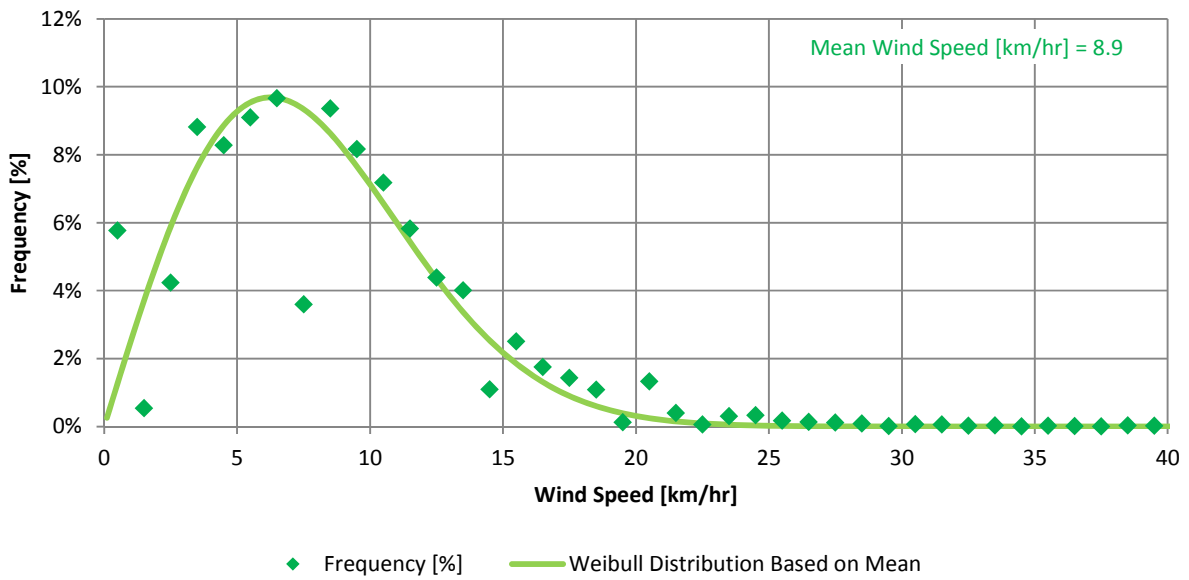


Figure 7-35: Graph of frequency of wind speeds during monitoring period and Weibull distribution based on the mean wind speed

Chapter 8 Airflow Measurement and Testing Results

To assess the airflow rates at various points along the supply air flow path, airflow measurements were made of the MAU intake and then of the supply to each corridor. To measure in-service airflows into and out of the suites, perfluorocarbon tracer (PFT) testing was performed. To provide an indication of building operation without the mechanical ventilation systems and to locate the natural neutral pressure plane, flow rates in to and out of the MAU supply duct at each corridor were also measured with the MAU off.

As context for the results presented in this chapter, a summary of general performance expectations for the building ventilation system are provided here. The ventilation system should consistently and evenly distribute adequate ventilation air to each corridor and suite in the building. ASHRAE 62.1-2010 is used throughout this chapter to provide an indication of typical modern ventilation rates. Additionally, the ventilation system should control the flow of air contaminants between zones. In particular, this includes preventing flow between suites and from the parking garage in to the occupied spaces of the building.

8.1 Make-Up Air Unit Intake

The MAU intake airflow was measured using the custom powered flow hood as described in Section 7.5.2 on February 8, 2013. During the test, the “PRES – MAU” sensor which is connected to a pitot tube pointing into the flow within the make-up air unit (MAU) duct was set to record measurements every 10 seconds. These measurements were then averaged over one minute time intervals and are plotted in Figure 8-1 to illustrate the performance of the MAU during the test.

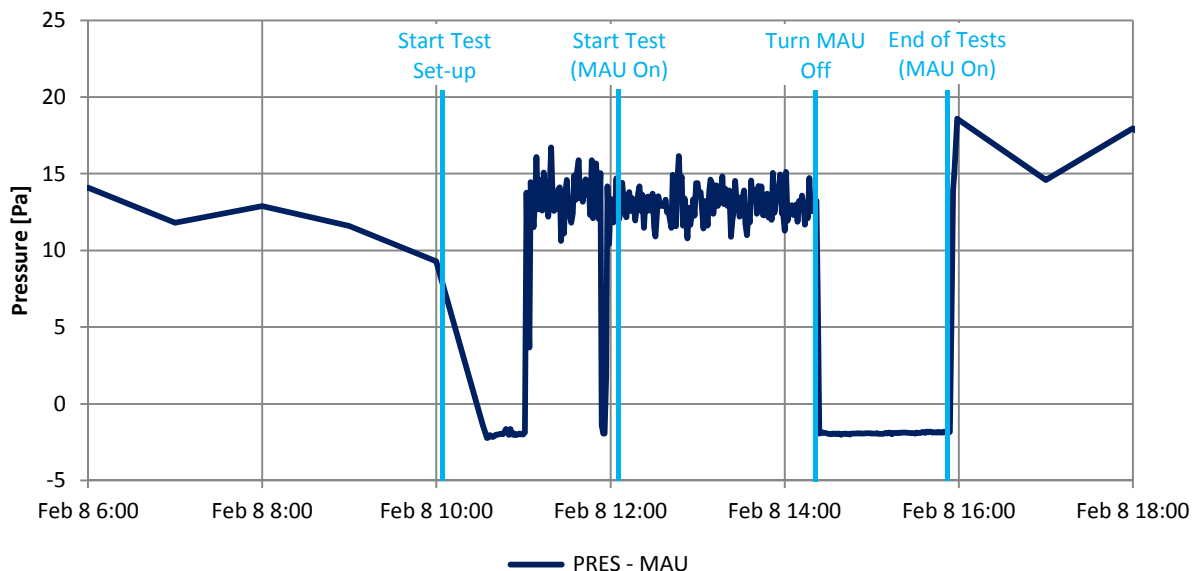


Figure 8-1: Graph of MAU pitot tube pressure during the airflow testing of the MAU

The post-retrofit balometer testing discussed in Section 8.2 was performed directly after the MAU intake measurements and the period when the MAU was off for this testing is clearly noticeable in Figure 8-1.

The MAU intake testing measured flow and flow resistance added by the testing apparatus 15 times over the course of the test. A table of the measurements is provided in Appendix C. These values showed relatively little variation and the average measured flow rate was approximately 1360 L/s, 87% of the 1,560 L/s specified for the unit on the original mechanical drawings. Unfortunately, the pressure rise across the MAU fan was not measured during testing, so it is unknown if the measured and specified flow rates are for the same static pressure. While the design intent is not known, for comparison the minimum ventilation airflow rate determined using the ASHRAE 62.1-2010 ventilation rate calculation method discussed in Section 3.3.1 is approximately 1,800 L/s. The measured flow rate and design flow rates are 25% and 13% less than this respectively.

The average velocity pressure measured by the monitoring equipment attached to a pitot tube in the MAU duct during the test was then used to develop a correlation between the airflow velocity (determined from the pressure using Eq. 3.1) and the measured flow rate so that the MAU flow rate could be determined from the monitored pressures throughout the monitoring period. This correlation is shown in Figure 8-2 and uses the assumption that there is no flow when no pressure difference is measured.

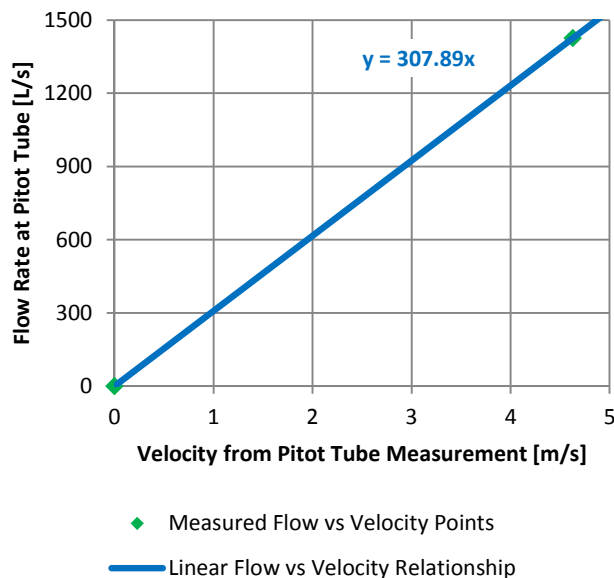


Figure 8-2: Graph of MAU intake flow rate versus measured velocity pressure used to develop airflow versus measured pressure correlation

The MAU intake air is heated between the fan and the pitot tube. Because of this, the density difference of the air was accounted for in the calculation of flow rate using the measured air temperature; however, accounting for this difference made only a 5% difference in the calculated flow rate.

Using the velocity flow rate correlation, a correlation between measured pressure and flow rate was developed based on Bernoulli’s equation and is provided in Eq. 3.5. The density difference of the air was found to have minimal impact on the flow rate, so a value of 1.2 kg/m³ was used which corresponds with 20°C and 40% relative humidity air, and is sufficiently accurate for this analysis.

$$Q_{MAU\ Intake} = 307.89 \sqrt{\frac{P_{MAU} \cdot 2}{1.2}} \quad \text{Eq. 8.1}$$

Where: $Q_{MAU\ Intake}$ = Make-up Air Unit Intake Airflow Rate [L/s]
 P_{MAU} = Make-up Air Unit Pitot Tube Velocity Pressure Difference [Pa]

Using the correlation in Eq. 3.5, pressure measurements of “PRES – MAU” were converted to flow rates and plotted during the monitoring period as shown in Figure 8-3. Note that the pitot tube sensor was not installed until November 20th, 2013, and unfortunately data was lost in a couple instances prior to December 4, 2013. Instances where the flow rate drops to zero or near zero are likely instances where the unit was turned off briefly. The reason for the MAU being turned off at these instances is unknown, and the instances where it was turned off for testing purposes associated with this thesis work have been removed.

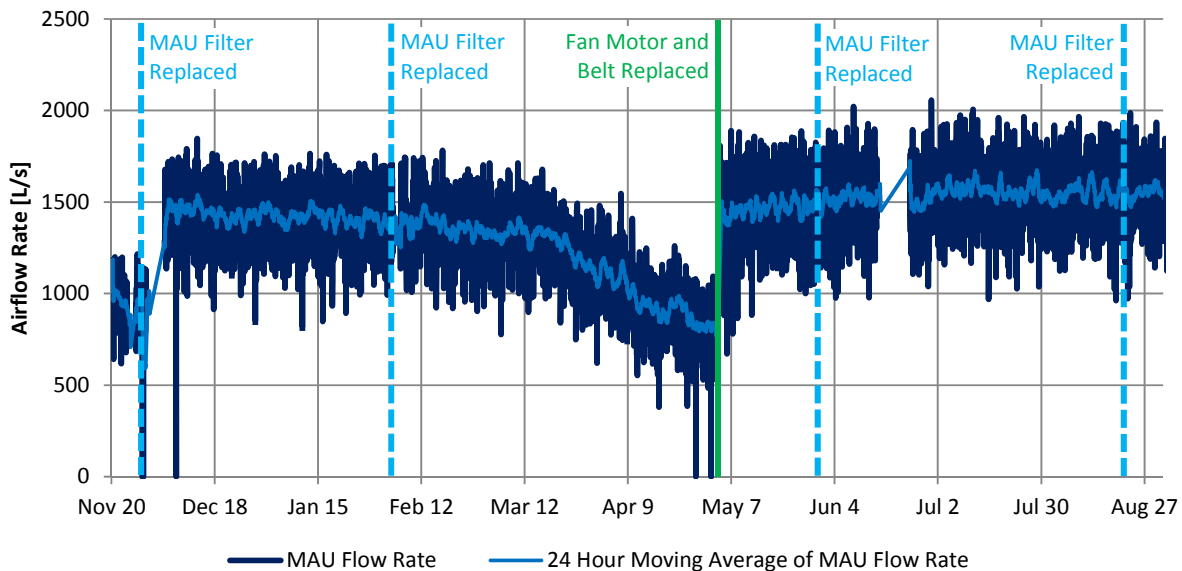


Figure 8-3: Graph of MAU intake flow rate based on pressure monitoring of pitot tube in duct

The MAU flow rate shows a significant increase near the end of November (exact date unclear due to data loss). The cause of this sudden increase is unknown and does not correspond with any activity in the maintenance log other than potentially with the replacement of the filters. It is possible that a belt connecting the motor to the fan was also replaced at this time and was not noted in the maintenance log. The flow rate then gradually decreases until May 3rd, 2013 when it suddenly increases again. The decrease of flow rate from the MAU during this period is likely due the gradual failing of the fan motor and wearing of the belt connecting the motor to the fan which are noted in the maintenance log as having been replaced on May 3rd, 2013.

With the possible exception of the filter change in November, changing of the MAU air filter was not found to have no noticeable impact on the flow rate through the MAU.

Overall, when operating correctly, the flow rate of the MAU is relatively consistent with the 1360 L/s measured using the powered flow hood apparatus, and in the months after repair of the motor it is frequently near the design flow rate of 1,560 L/s.

8.2 Make-Up Air Unit Supply to Corridor

The supply rate of air to each corridor from the make-up air unit were measured pre-retrofit on July 28, 2012, and post-retrofit on February 8, 2013 and July 11, 2013. The results of these measurements are provided in Figure 8-4.

During the pre-retrofit test, the exterior temperature was approximately 21°C and the wind was approximately 15 km/hr from the east-south-east. During the first post-retrofit test, the exterior temperature was approximately 6°C and the wind was approximately 4 km/hr from the west, and during the second post retrofit test the exterior temperature was approximately 16°C and the wind was approximately 13 km/hr from the west.

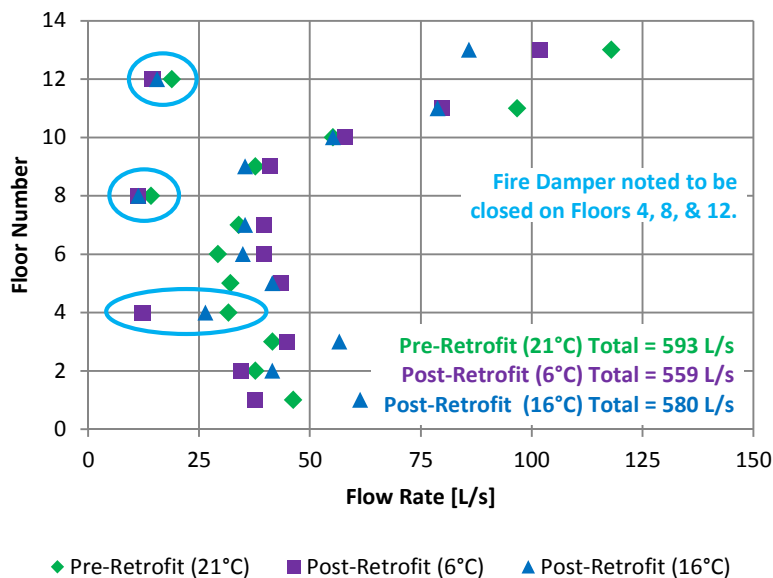


Figure 8-4: Graph of MAU supply airflow to corridors

All three times that these measurements were made show significantly higher flow rates on upper floors, and lower flow rates on lower floor with the exception of those floors where fire dampers were observed to be unintentionally closed (Floors 4, 8, and 12). A slight decrease in total airflow rate provided to the corridor from the MAU was noted during the colder period (post-retrofit at 6°C). This is likely as result of increased resistance created by the increased magnitude of stack effect pressure during these colder periods. This reduction in flow rate, however, is not large (6% less flow at 6°C than at 21°C), so is not likely to significantly change the amount of ventilation air provided to an individual floor or suite. This reduction in flow may be more significant in a climate with colder winter temperatures.

Using the ASHRAE 62.1-2010 ventilation rate calculation method for determining the minimum ventilation rate discussed in Section 3.3.1, the minimum recommended supply ventilation air to each floor was determined to be 142 L/s for a typical floor. (Note that floors 1 and 13 would have slightly different recommended minimum ventilation rates due their different arrangement, but as the calculated ventilation rate is only for general comparison purposes, this slight difference is insignificant in this context.) The calculated ventilation rate is higher than the ventilation rate supplied by the MAU to every floor in the building, and is approximately 250% higher than the ventilation rates supplied to lower floors of the building (floors 1 through 9). It should be noted that this building was not built to meet this ventilation standard and the specified make-up air unit intake rate of 1560 L/s would theoretically provide an average of 120 L/s of ventilation air per floor which is also significantly higher than nearly all of the measured corridor supply airflow rates.

The total of the post-retrofit corridor ventilation air supply rates measured at 6°C is 559 L/s which is only 40% of the measured MAU air intake (which was measured only a few hours earlier and under similar conditions). This indicates that a very significant loss of ventilation air occurs due to leakage from the ventilation duct which is a substantial inefficiency of the ventilation system.

It was noted that the fire damper on the MAU shaft at the roof which is intended to be closed during normal operation had a relatively high airflow rate leaking out of it. This flow rate was measured using the same balometer and found to be leaking approximately 66 L/s. While this leakage is significant, it only accounts for 5% of the intake flow rate of the MAU which indicates that the remaining 55% loss occurs at other, unidentified, locations.

8.3 Make-Up Air Unit Off

The airflow rates in to or out of the make-up air unit ventilation shaft on each floor were measured with the make-up air unit off. These measurements were taken to determine airflow within the building without the mechanical systems, and in particular to determine the location of the neutral pressure plane (NPP) for the ventilation shaft. The results of these measurements are provided in Figure 8-5. Testing was completed pre-retrofit on July 27, 2012 and post-retrofit on February 8, July 11, and July 26, 2013. Note that the measurements taken pre-retrofit were only completed down to the fourth floor (including the fourth floor but the measurements overlap exactly on the graph) because the tester had intended to measure the flow rates with the make-up air unit on and when it became apparent that it was off, stopped taking measurements. The results from these measurements, however, were found to be interesting, so measurements were taken intentionally with the make-up air unit off post-retrofit. The exterior conditions during these tests were similar to those of the tests performed with the MAU on and presented in Section 8.2, and the additional test on July 26th was performed with approximately 13 km/hr wind from the west and an exterior temperature of 19°C.

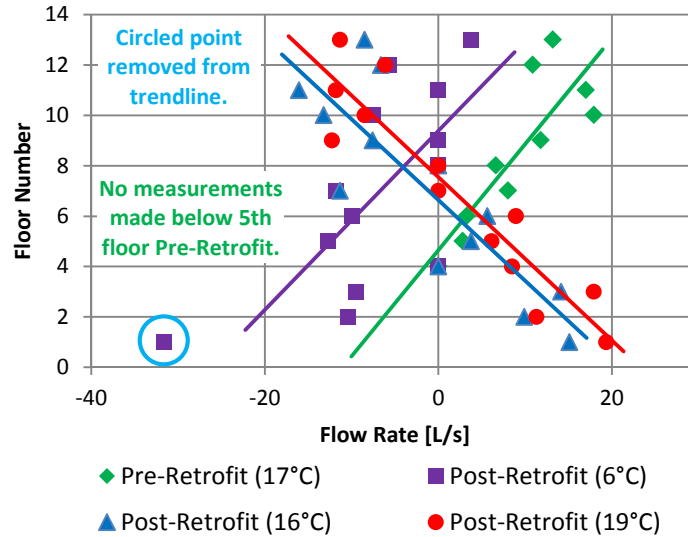


Figure 8-5: Graph of airflow to and from MAU ventilation shaft with MAU off

Each set of measurements indicates a clear trend in the flow rates in to and out of the MAU ventilation shaft and the approximate location of the NPP in each case is apparent; however, the direction of the stack effect is not consistent between the four measuring cases. It is unclear why this occurred, and in particular it is not clear why the post-retrofit measurements at exterior temperatures of 16°C and 19°C indicate a reversal in the direction of stack effect despite the interior temperature still being greater than the exterior temperature. It is theorized that because the flow rates in to and out of the ventilation shaft when the MAU is off are relatively low, relatively small changes in building operation between the tests may be sufficient to create the variation in flow direction that was observed. These operational differences may include, for example, the operation of exhaust fans, or the opening or closing of windows and exterior doors.

8.4 PFT Testing

The results of the perfluorocarbon tracer (PFT) testing are presented in this section including the exterior environmental conditions during the test period, airflow rates determined from the testing, and in comes cases PFT concentration measurements.

8.4.1 Exterior Environmental Conditions During PFT Testing

PFT testing was performed from approximately the morning of April 10th, 2013 to the morning of April 17th, 2013 to capture representative weekly occupancy pattern of the case study building over the course of a representative week (no holidays et cetera). The exterior temperature, wind speed, and wind direction during this period are provided in Figure 8-6 and Figure 8-7.

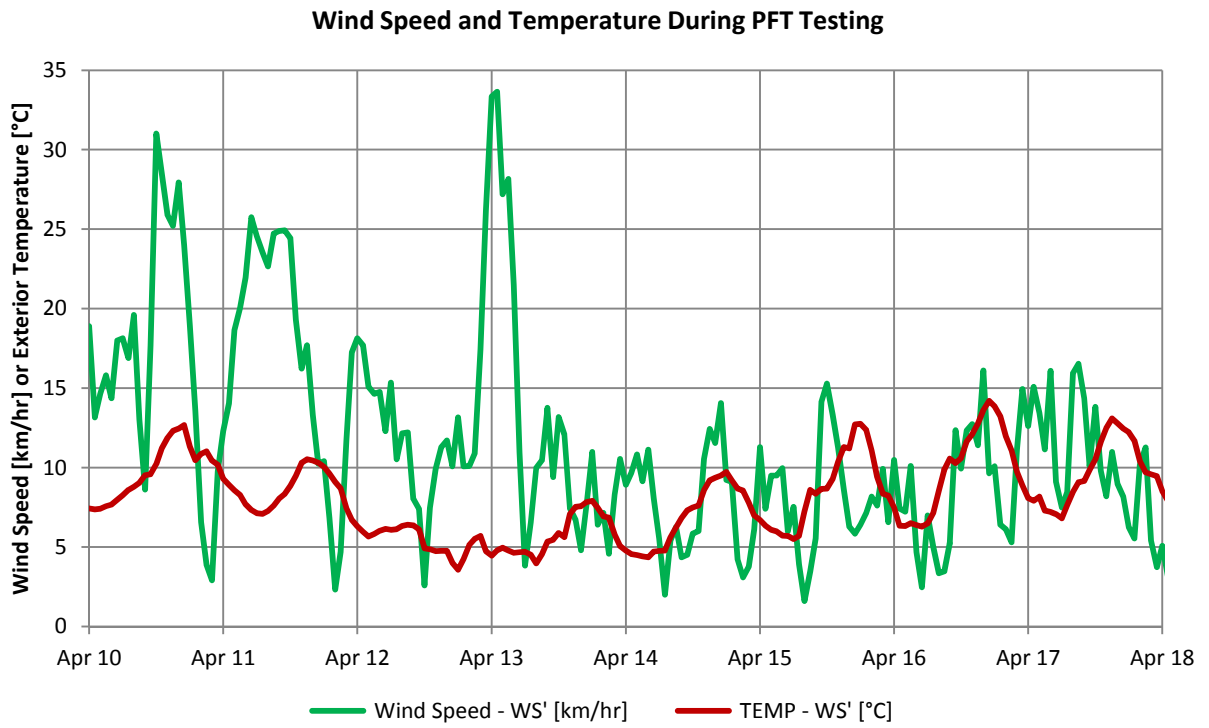


Figure 8-6: Graph of wind speed and exterior temperature during PFT testing period

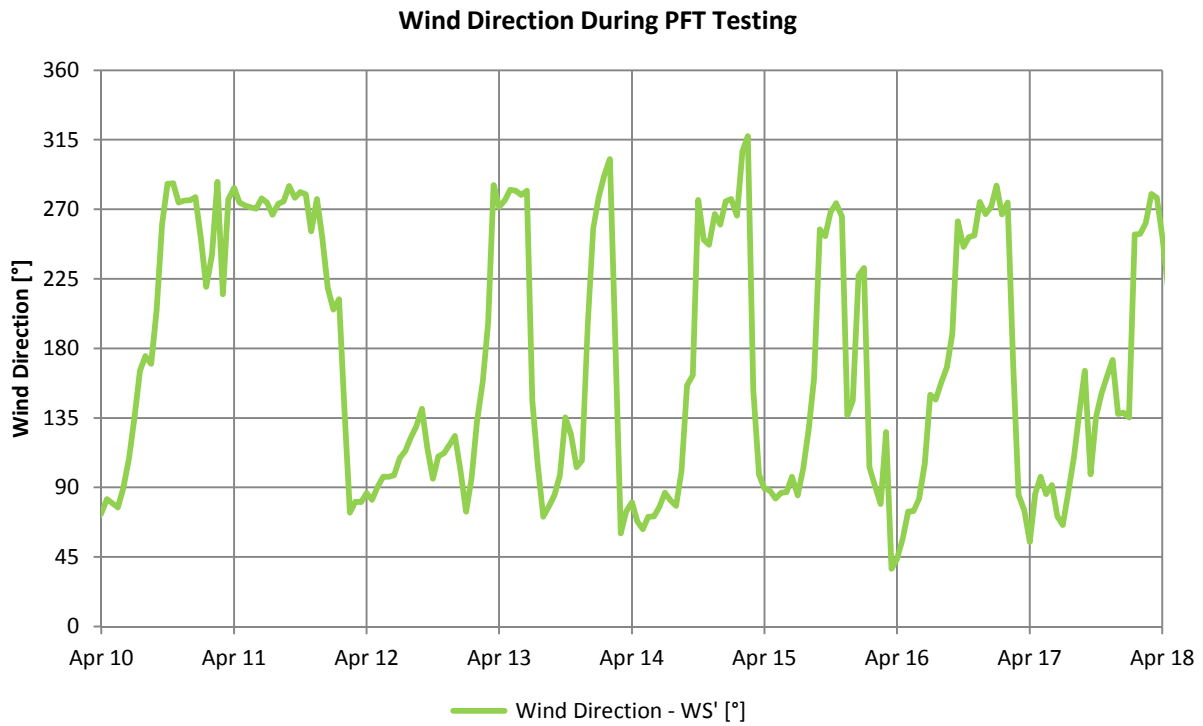


Figure 8-7: Graph of wind direction during PFT testing period

As shown in the preceding graphs, the temperature fluctuates by approximately 5°C over the course of a day, and ranges from approximately 4°C to 14°C over the course of the week. The average exterior temperature during the testing period was approximately 8°C.

The wind during the test period was primarily from the west during periods of the highest wind. The wind during approximately the first 3 days of testing is relatively strong, and during the last 4 days is relatively light to moderate. The average wind speed during the PFT testing period was 11.7 km/hr (3.3 m/s). The average wind speed and frequency from each direction during this period is provided in Figure 8-8.

**Compiled Average Wind Speed and Frequency by Direction
During PFT Testing Period**

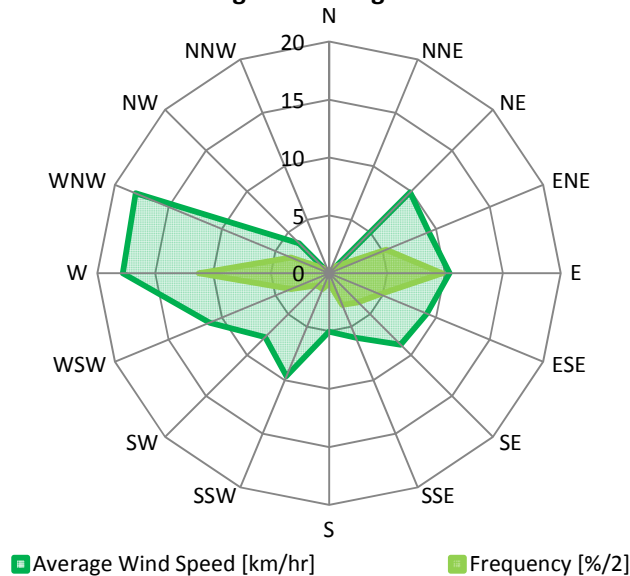


Figure 8-8: Chart of average wind speed and frequency during PFT testing period

In general, the exterior conditions during the PFT testing period were windier than the average conditions during the entire monitoring period and tended to be from the west more often as shown by comparison with the information provided in Section 7.6. The mean wind speed was, however, the same as the mean wind speed provided in by CWEC data as shown previously in Figure 3-7. Overall, the period of PFT testing is representative of a typical spring or fall week in Vancouver.

8.4.2 Results of PFT Testing

The volumes of PFT absorbed by the capillary absorption tube samplers (CATS) were used as inputs to system of equations to calculate various airflow rates at the case study building during the PFT testing period. Brookhaven National Laboratory performed these calculations and the associated report detailing the PFT results is provided in Appendix G. The report also provides discussion of the potential error in the determined results.

The airflow into and out of each of the suites on the primary test floor (Floor 3 and Floor 11) were measured using the PFT testing. This includes airflow to and from the corridors, adjacent suites, and exterior. In one suite on each of these two floors, the airflow to and from the suites above and below was also measured. Due to the potential for error in these results (as described by the report in Appendix G) the determined airflows should be primarily considered at an order of magnitude level. The results of the PFT testing are provide in Figure 8-9 and Figure 8-10.

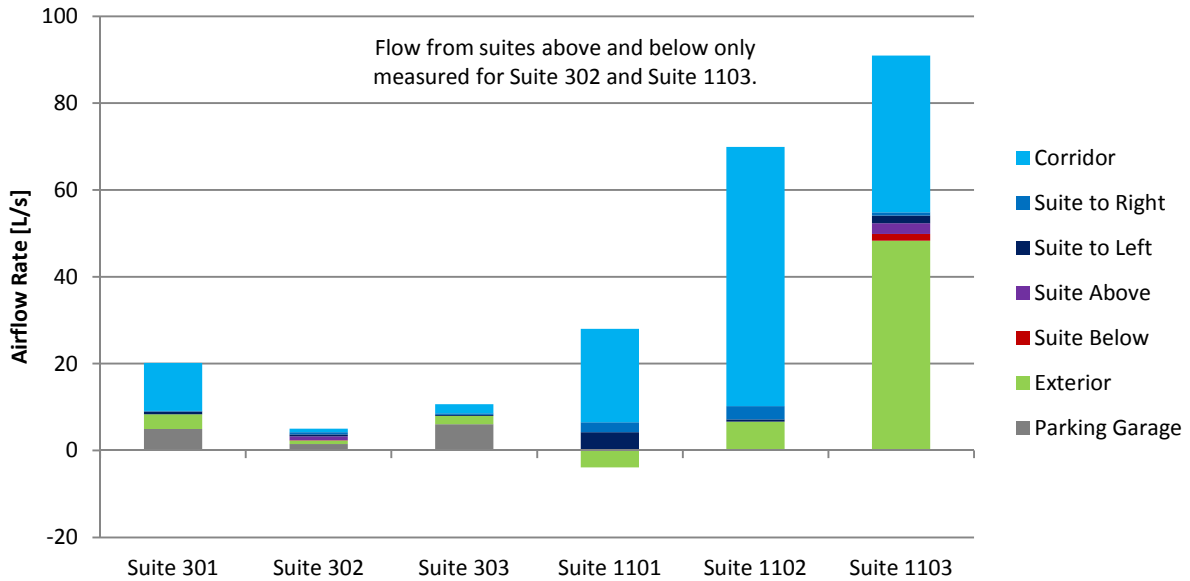


Figure 8-9: Chart of airflow in to suites on Floor 3 and Floor 11 as determined by the PFT testing

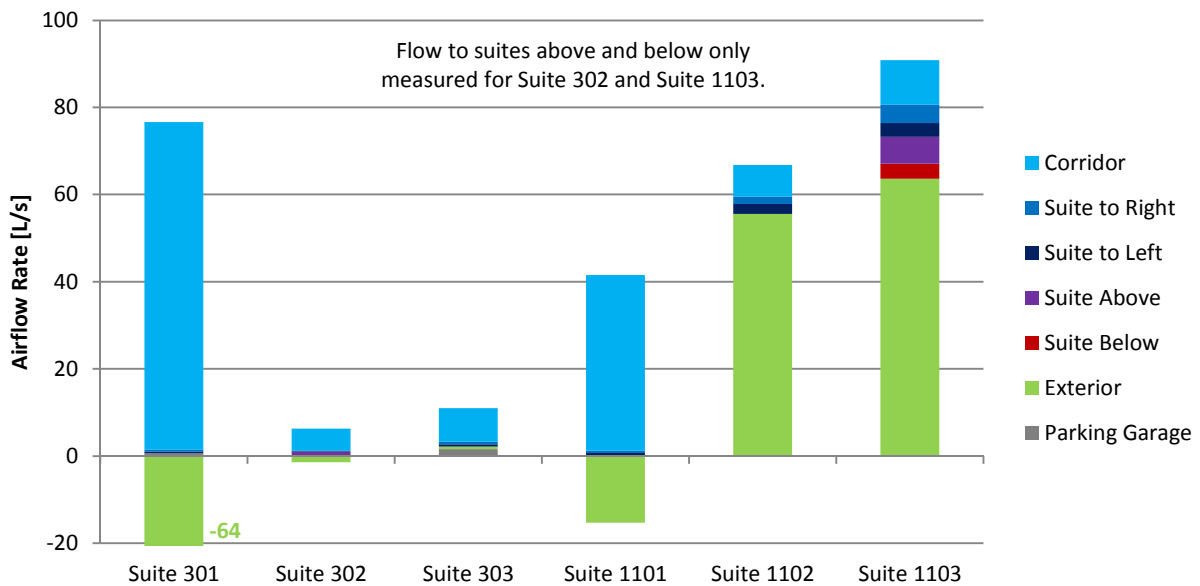


Figure 8-10: Chart of airflow out of suites on Floor 3 and Floor 11 as determined by the PFT testing

The determination of negative airflows indicates errors in solving the system of equations; however, in these cases the determined airflow rate is typically less than or of similar magnitude to the calculated standard deviation in the result, so it is likely that these cases indicate actual flow rates of approximately zero. Note that Suite 301 shows significant airflow out of the suite to the corridor but also shows significant negative airflow out of the suite to the exterior (that is flow in to the suite); however, it is likely that these are actually offsetting errors in the solving of the system of

equations and in reality there is near zero flow to the exterior from this suite and the flow to the corridor is similar to the flow to the corridors for Suites 302 and 303. This type of error is inherent to the solving of the system of equation which assumes internal consistency so in some cases an error in one measurement can create an offsetting error in another measurement when the system is solved. Because the calculation method assumes internal consistency, flows out of a suite and flows in to a suite must balance within the system of equations so total flows in to and out of building zones are equal. While this is also physically also true (flow in must equal flow out), the measurements may not satisfy this condition and can lead to these types of errors. Measurements may not satisfy this condition for a variety of reasons including, most likely, imperfect mixing of the air within a zone.

Generally, the PFT results for the test suites indicate that the order of magnitude of airflow rates for different suites in the building is highly variable. There is significantly more airflow both into and out of the suites on the upper floors, and the majority of this airflow occurs with the corridors and the exterior.

The suites on Floor 11 received much higher ventilation rates from the corridor than did the suites on lower floors with an average of approximately 40 L/s and 5 L/s respectively likely due to the closer proximity of Floor 11 to the MAU. This indicates that the corridor pressurization based ventilation system does not adequately or equally provide ventilation air to these suites. ASHRAE 62.1-2010 recommends a supply ventilation rate of approximately 42 L/s for the average suite at the case study building. By comparison, the supply of air from the corridor to the suites on Floor 11 is very close to this rate and on Floor 3 it is approximately 88% lower.

There was also found to be significantly higher airflow rates both to and from the exterior for the upper suite than the lower suites. It should be noted that due to the nature of this testing, airflow rates to and from the exterior are actually to and from any zone not tagged with a PFT source; however, as the majority of adjacent zones were tagged with sources and the associated measured flow rates are typically small, it is felt that it is appropriate to assume that the majority of this airflow is in fact with the exterior. (The exterior does not include air from the make-up air unit which is measured as air coming from the corridor.) This increase in air exchange with the exterior is theorized to be due to either increased exposure to wind on the upper floors than on the lower floors, or due to the presence of fireplaces in the upper suites and not the lower suites. The presence of fireplaces could increase both infiltration and exfiltration depending on whether the fireplace is on, causing exhaust, or off, in which case airflow in either direction could occur as there is no damper on the flue. It is also possible that these air exchange rates are due simply to a difference in window operation patterns (i.e. more open windows leading to more airflow).

The airflow measurements generally found that the flow rates from the corridor and the exterior were largest, with relatively low flow rates to and from adjacent suites and to and from the suites above and below. These findings are consistent with the airtightness testing findings (presented in Chapter 9) which found that the largest proportion of airflow pathways are from the suites to the corridors and from the suites to the exterior; however, despite these relatively low flow rates, some transfer of air between suites was measured and indicates the potential for transfer of air contaminants. Significantly less airflow can be required to transfer an air contaminant than to adequately ventilate a suite. On average, airflow to and from the adjacent suites on the same floor

was measured to be approximately 1 L/s, and to and from the suites below it was measured to be approximately 2 L/s. In particular, significant transfer air to and from Suite 1103 was measured with the suites above and below. No correlation beyond order of magnitude was found between the measured airtightness of a pressure boundary and the amount of airflow through that pressure boundary as measured by the PFT testing.

The total air changes per hour of each suite based on airflow from all sources was also found to vary significantly over the height of the building as shown in Figure 8-11. The average air changes per hour of the lower suites and upper suites respectively were found to be 0.2 and 0.7 respectively, and they varied from a low of 0.06 to a high of 1.07.

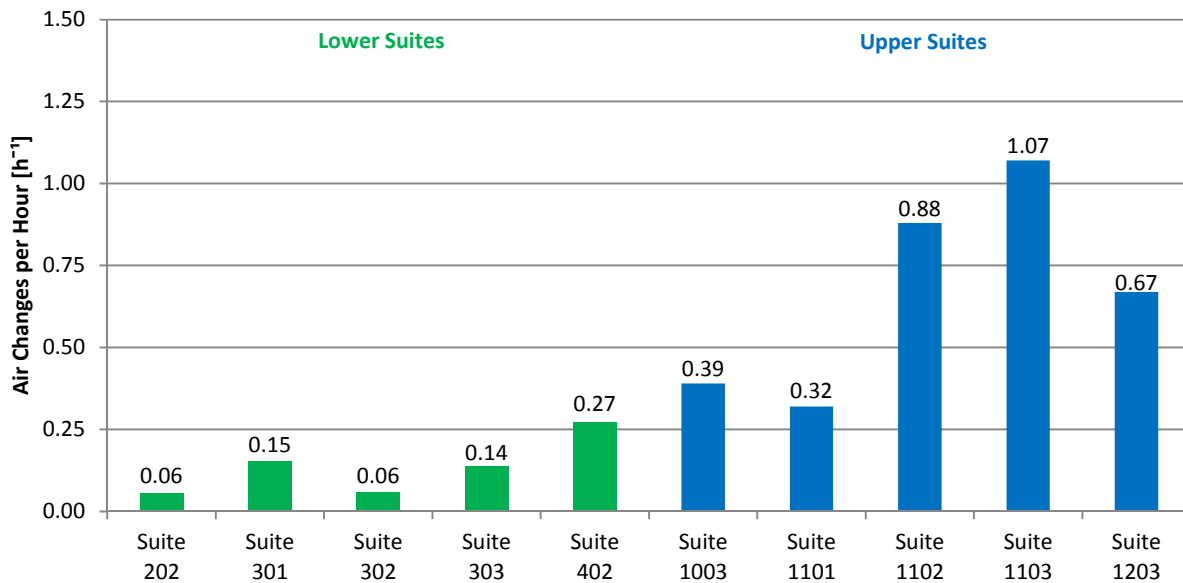


Figure 8-11: Chart showing total air changes per hour of suite from all sources

This difference in air change rates observed over the height of the building is due to the combination of the increased airflow rates from the corridor to the suites observed on the upper floors, and the increased air exchange with the exterior that was also observed on these upper floors. The increased air exchange at upper suites, as discussed previously, is likely a result of increased exposure to wind, increased stack effect pressure near the top of the building, and proximity to the MAU. Overall, the discrepancy in air change rates further supports the finding of uneven distribution of ventilation rates within the building.

The lack of even distribution of ventilation air observed in the suites is further reinforced by findings in the corridors. The amount of the PFT tracer released in the MAU (PMCP) that was absorbed by the CATS in each corridor was measured and provides an indication of the supply of airflow to each corridor. It is not possible to determine the airflow rate to the corridors as the total air change rate of these corridors is unknown. The amount of PMCP that was absorbed by the CATS in each zone of the case study building is shown graphically on schematic cross-section of the building in Figure 8-12 including the suites for which flows rates have been presented as well as other suites where there was no source installed but a CATS was installed to provide qualitative results.

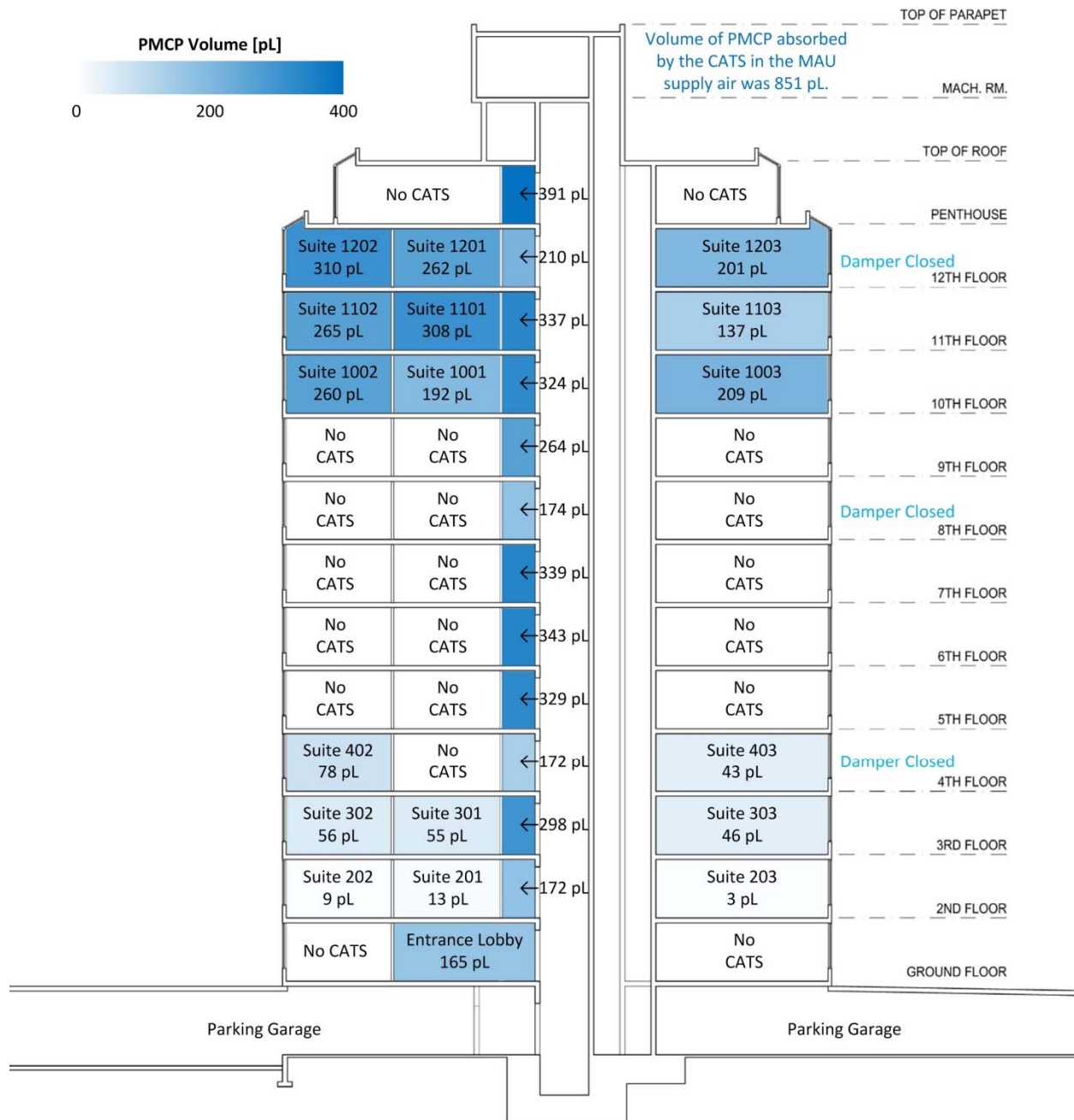


Figure 8-12: Schematic cross section of the case study building showing the amount of PMCP tracer (which was released in the MAU duct on the roof) absorbed by the CATS in each zone

Figure 8-3 illustrates that significantly less PMCP tracer was absorbed by the CATS in the lower zones of the building, including both the suites and corridors, which likely indicates that the ventilation system was not equally supplying ventilation air to each corridor and suite. It is also apparent that on floors where the fire damper in the MAU supply grille to the corridor were noted

to be unintentionally closed (Floors 4, 8, and 12), significantly less ventilation air was supplied to those corridors.

To assess the flow of air from the parking garage to the interior zones of the building a unique PFT (PDCB) was also released in the parking garage. The airflow rates to zones with sources in the lower part of the building are provided in Figure 8-13.

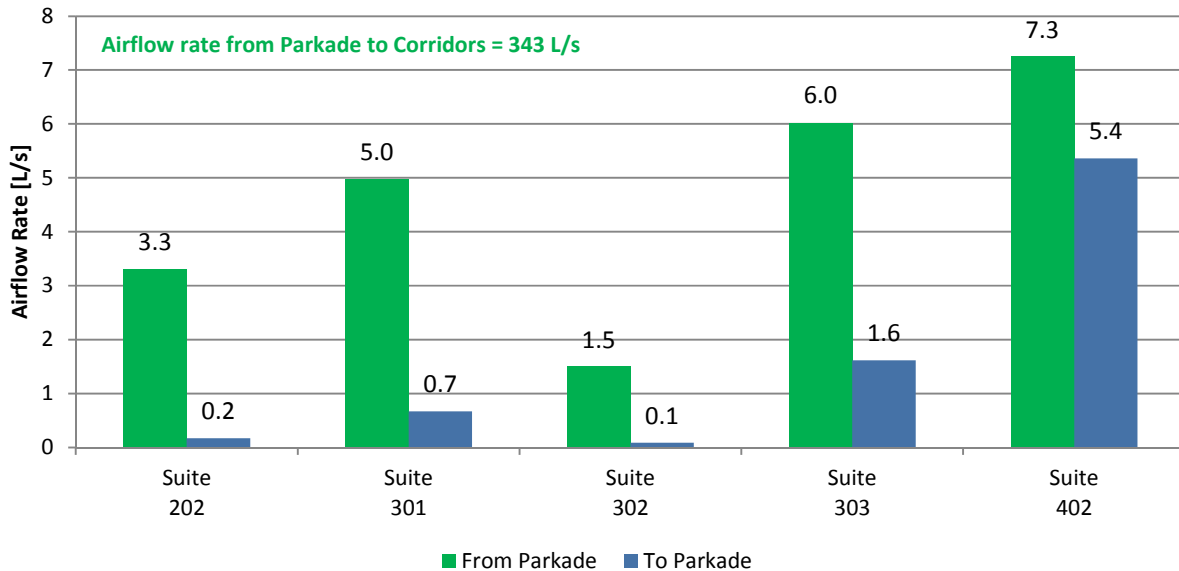


Figure 8-13: Chart showing the airflow rates from the parking garage to the lower zones of the building which were tagged with a PFT source

The total airflow from the parking garage to the corridors was 343 L/s, which is approximately 60% of the average total supply airflow to the corridor from the MAU (577 L/s). For many suites, significant airflow from the parking garage was measured, even four floors above the parking garage. Given the relatively low ventilation rates of these lower suites, this flow of air from the parking garage is a large portion of the total airflow in to a suite. This airflow from the parking garage is a serious concern because parking garage air can bring with it various contaminants including particulates, benzene, carbon monoxide, and various hydrocarbons from vehicle exhaust. These measurements were made during a period of relatively mild temperatures (average of 8°C), and the amount of airflow in to the building from the parking garage is likely to increase during periods of colder exterior temperatures due to the increased magnitude of pressure differences created by stack effect.

To illustrate graphically this flow of air from the parking garage in to the suites of the building, a schematic cross section is shown in Figure 8-14 which illustrates the quantity of PDCB (the PFT released in the parking garage) that was absorbed by the CATS in each of the lower zones of the building. No PDCB was measured in the CATS above Floor 4. Note that similar to the volumes of PFT from the MAU shown previously, these volumes do not correspond directly with airflow rates as in cases where zones did not have a source it was not possible to calculate the total air change rate of the zone and thus not possible to calculate the airflow rate from the parking garage to the

zone. Also, the result in Suite 302 is an outlier as the measured volume of PDCB is significantly higher than that of the parking garage, which is impossible.

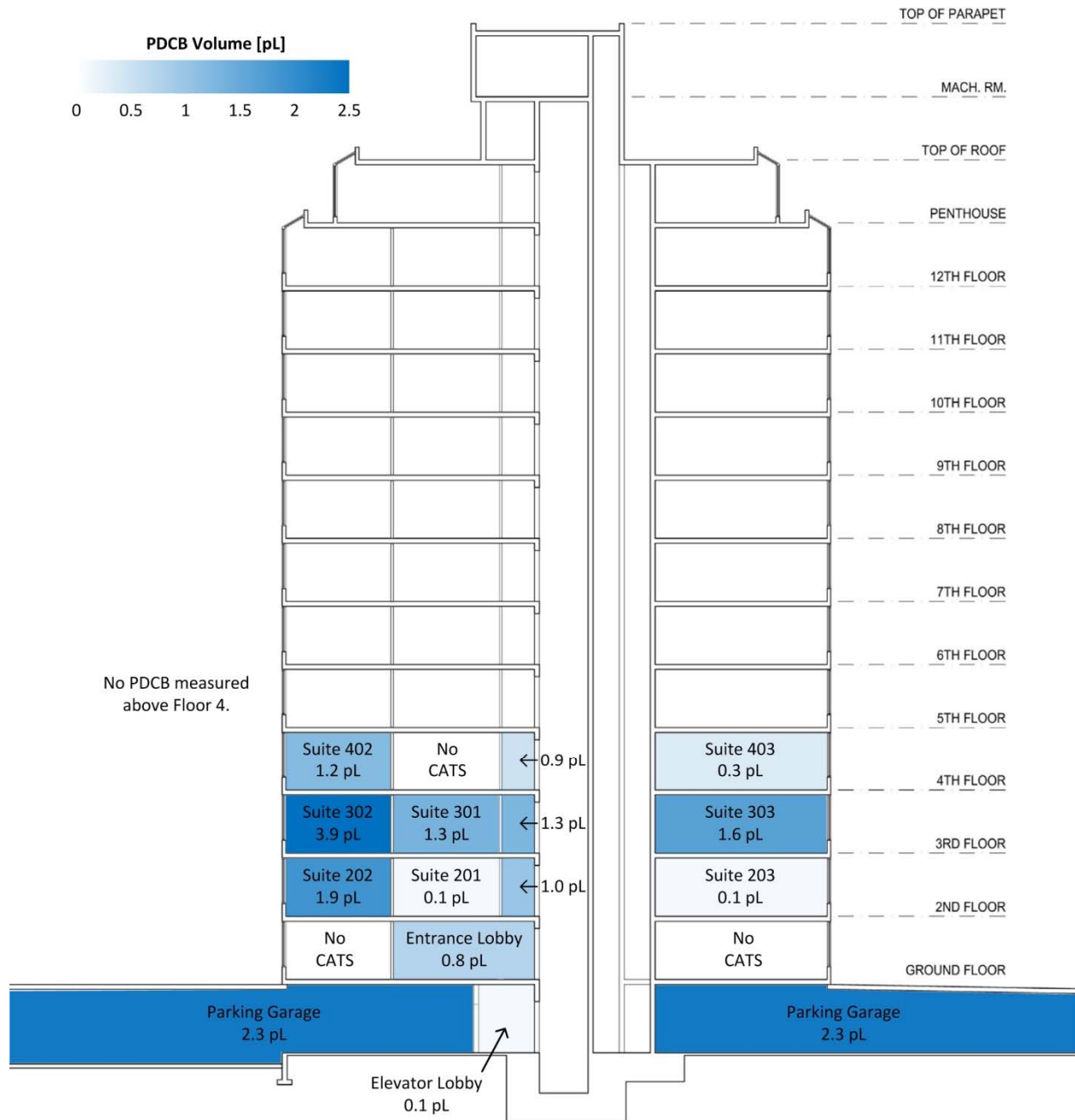


Figure 8-14: Schematic cross section of the case study building showing the amount of PDCB tracer (which was released in the parking garage) absorbed by the CATS in each zone

Brookhaven National Labs made a number of assumptions in determining the results presented in this section and their full report is provided in Appendix G. Most importantly, to determine the air change rates of the corridors they assumed that the PFT tracer released in the MAU was distributed

evenly throughout the building. This assumption is likely not appropriate as shown by some of the results of the testing which found typically lower concentrations of this tracer in lower zones of the building than in upper zones. Consequently, likely more of the tracer was distributed to the upper zones of the building and less was distributed to the lower zones. Thus, the air change rates for the upper corridors were likely calculated to be lower than they actually are, and the air change rates of the lower corridors were likely calculated to be higher than they actually are. As the corridor air change rates were not presented in this section, this inaccuracy is most relevant to the calculation of airflow rates out of the suites and in to the corridors. In upper zones where a lower air change rate was calculated than likely exists, the flow rates out of the suites and in to the corridors is likely higher than was calculated, and in lower zones the this airflow is likely lower than was calculated. It is not possible to know the magnitude of this discrepancy; however, it is anticipated that it is relatively low. Furthermore, higher air change rates in the upper corridors and lower air change rates in the lower corridors would only further exaggerate the uneven distribution of ventilation rates that was measured and would not change the conclusions drawn.

The other measurement that the inappropriate assumption of even distribution of ventilation air could impact is the calculation of airflow in to the building from the parking garage. Since this was calculated using the concentrations measured in the lower corridors it is likely that the calculated airflow rate into the building from the parking garage is higher than actually occurs and the magnitude of this error is unknown. While this may impact the exact flow rate determined, it is still clear that significant airflow from the parking garage in to the occupied spaces of the building occurs, and the flow rates determined from the parking garage in to the suites are accurate. Consequently, this error does not change the findings with respect to airflow from the parking garage into the building.

8.5 Summary of Results

The airflow measurement results at the case study building lead to numerous important conclusions. Primarily these results indicate a significantly uneven distribution of ventilation air to the corridors and suites of the building. Lower suites receive orders of magnitude less ventilation air from the MAU and also have less air exchange with the outdoors. Numerous suites receive small fractions of modern ventilation requirements primarily because the majority of the ventilation air brought in to the building by the MAU does not directly reach the suites and is unevenly distributed.

Furthermore, the ventilation system is not adequately controlling the migration of air contaminants within the building. While minimal flows were measured between suites, the potential for transfer of air contaminants exists. Flow of air from the parking garage in to the building, however, was measured to be significant and poses a risk for the transfer of harmful contaminants into occupied spaces of the building.

Overall, the measured flow rates indicate that the corridor pressurization based ventilation system at the case study building is not performing adequately with respect to its two primary functions: providing adequate ventilation air to all zones of the building, and controlling the migration of air contaminants.

Chapter 9 Airtightness Testing Results

Airflow into, out of, and within buildings is resisted by the air permeance (airtightness) of building boundaries. This chapter presents the results of the airtightness testing performed at the case study building and uses these results to contextualize the case study building relative to other buildings and to develop an understanding of the distribution of airflow resistance to aid in interpretation of the measured airflow results presented in Chapter 8. These results will also be used with monitored pressure differences in subsequent chapters to calculate in-service airflow rates.

This chapter presents average and typical results to highlight significant findings. Detailed airtightness testing results and descriptions of how the test measurements are used to determine airtightness are provided in their entirety in Appendix D including flow coefficients, flow exponents, and R-squared values for each test. All of the results presented in this section are an average of pressurization and depressurization test results.

9.1 Suite Testing

Test results from the six typical suites on Floor 3 and Floor 11 were averaged to create the airflow versus pressure curves for each of the six testing steps discussed in Section 7.2.2 and these curves are provided in Figure 7-1.

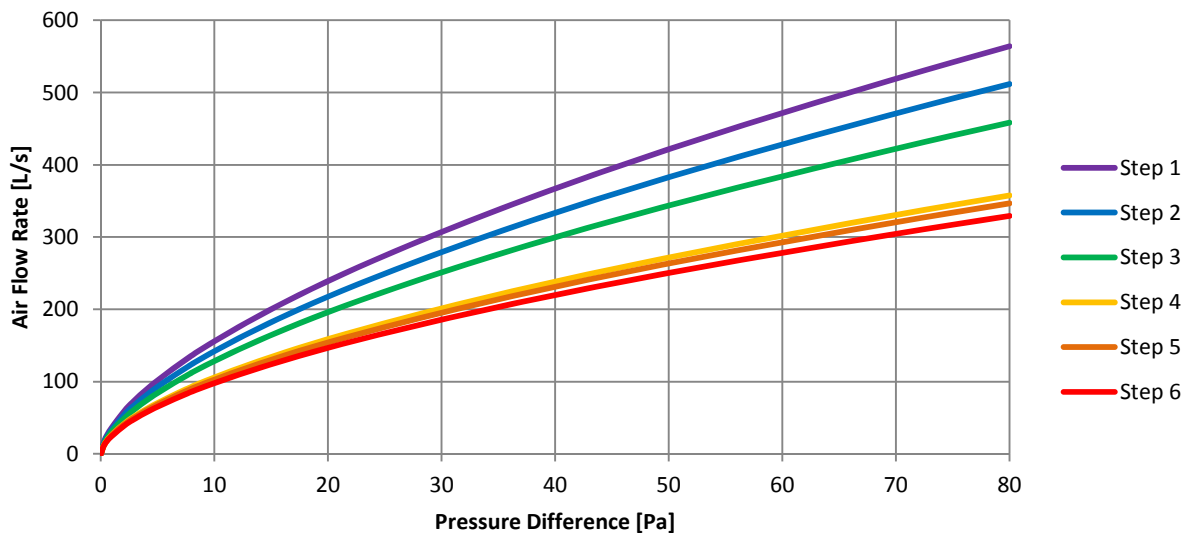


Figure 9-1: Graph of average airflow versus pressure difference relationship test results for the typical suites

Figure 7-1 indicates that the total flow rate decreased as adjacent zones were pressure neutralized, which is the expected result. The difference in airflow rates between each of these steps was then used to determine the airflow attributable to the exterior enclosure and to each of the compartmentalizing elements. Figure 9-2 shows the results of this analysis for the average of the

typical suites. Note that the graph includes the results of both pre- and post-retrofit airtightness testing of the exterior enclosure, and the airflow curve for “Suite Above” is not visible as it lies directly under the curve for “Suite Below.” Figure 9-2 also shows the airflow for an average suite entrance door which was determined based on the corridor airtightness testing described in Section 9.6.

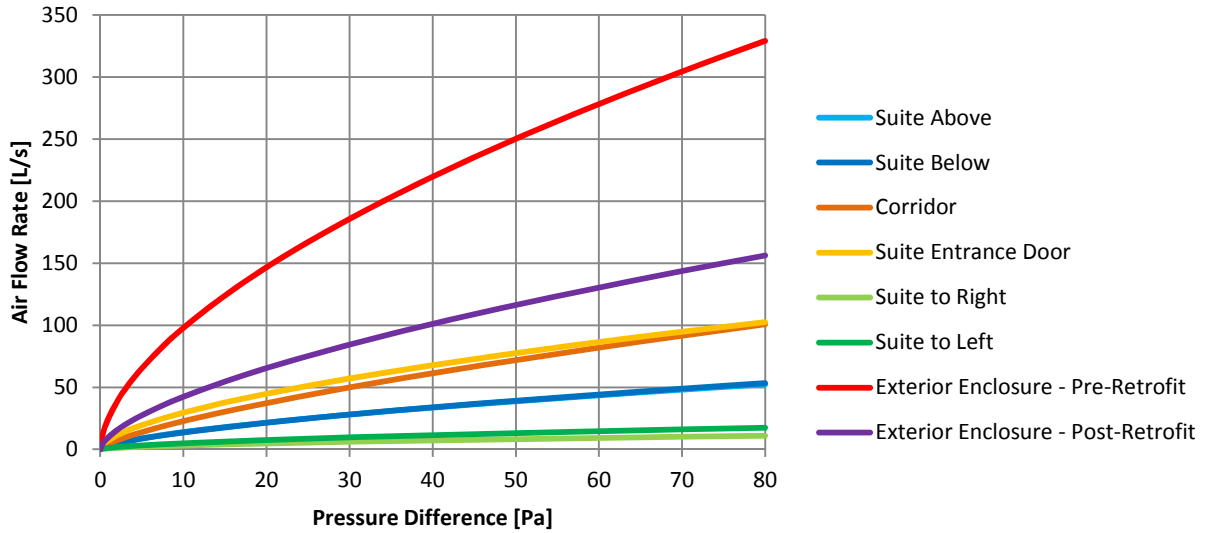


Figure 9-2: Graph of average airflow versus pressure difference relationships for compartmentalizing elements of typical suites

Figure 9-2 shows that the majority of airflow during the airtightness testing of these suites was through the exterior enclosure, but that this flow was reduced from 317 L/s at 75 Pa pre-retrofit to 150 L/s at 75 Pa post retrofit. This is a 53% improvement. The proportion of airflow attributable to each of the suite compartmentalizing elements and to the exterior enclosure is shown in Figure 9-3.

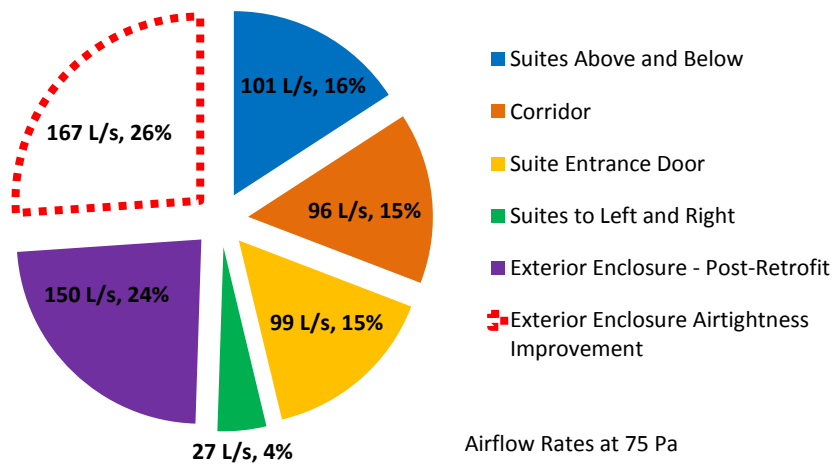


Figure 9-3: Chart of distribution of airflow through compartmentalizing elements and exterior enclosure

Figure 9-2 and Figure 9-3 indicate that when the typical suite is pressurized (or depressurized) relative to all adjacent zones equally, only a very small amount of airflow occurs through the partition walls to the adjacent suites to the left and right (4% total at 75 Pa). Airflow to the suites above and below; however, is significant and makes up 16% (101 L/s at 75 Pa) of the airflow into or out of the suite under test conditions. While the exact locations of the airflow through the slab are unconfirmed, it is suspected that the majority of the flow to suites above and below the test suite is through poorly sealed plumbing, electrical, and mechanical system penetrations. There is also a combined 195 L/s at 75 Pa (30%) of airflow from the suites to the corridors through the corridor-to-suite walls and the suite entrance door

For a similar construction type, Finch (2007) found based on testing of 4 suites in two buildings that flow to adjacent suites (left and right) was approximately 18% of the total flow, that flow to suites above and below was approximately 13% of the total flow, and that the flow through the corridor walls was approximately 45% of the total flow. Gulay et al (1993) found that flow to adjacent suites and the corridor during testing was approximately 22% of the total flow, and that airflow to the suites above and below the test suite was approximately 28% of the total flow. The findings at the case study building indicate relatively airtight walls between suites as compared to the values found in literature, while the airflow through the floors and ceilings of the suites is between the values from Guley at al (1993) and Finch (2007). The proportion of airflow through the suite to corridor walls at the case study building is similar to that found in Gulay et al (1993), but is significantly lower than the proportion found in Finch (2007).

It is also useful to examine the normalized airflow rates to determine relative airtightness. The average normalized airflow versus pressure relationships for the typical suites are provided in Figure 9-4. Again, the curve for "Suite Above" is not visible as it is directly under the curve for "Suite Below." The normalized airflow through the suite entrance door is not included in Figure 9-4 as the normalized airflow rate for the average suite entrance door is significantly higher than for other compartmentalizing elements. The normalized airflow for the average suite entrance door (normalized by the area of the door) is 55 L/s at 75 Pa.

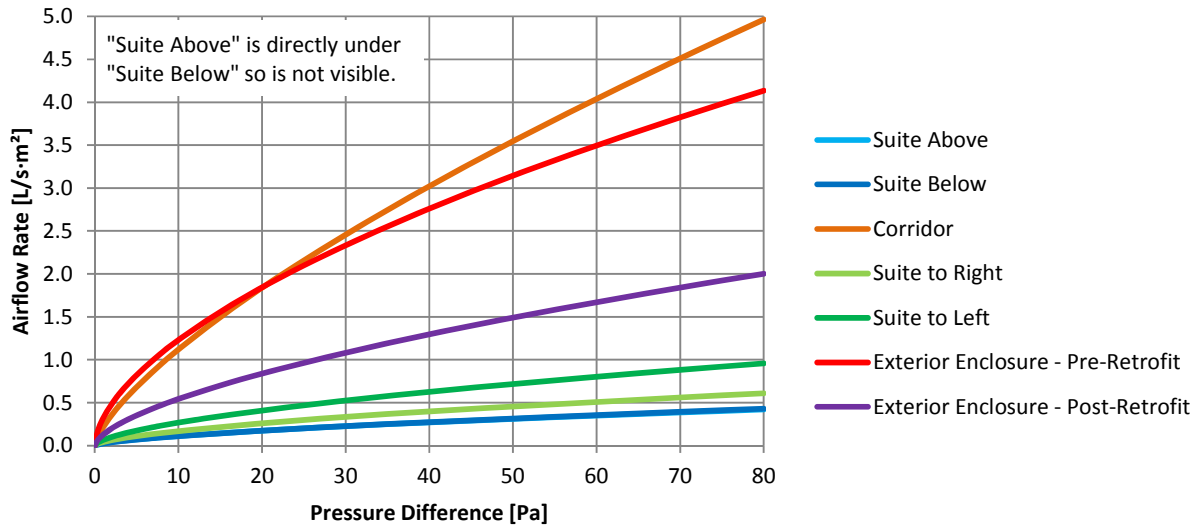


Figure 9-4: Graph of average normalized airflow versus pressure difference relationships for compartmentalizing elements of typical suites

The measured average normalized airtightness of the corridor walls at the case study building was found to be $4.7 \text{ L/s}\cdot\text{m}^2$ at 75 Pa which is of the same magnitude as values found in literature (provided in Appendix A), except for Finch (2007) who found corridor walls to be much less airtight.

The average normalized airflow rate at 75 Pa for the floors and ceilings was found to be $0.4 \text{ L/s}\cdot\text{m}^2$ which is within the ranges provided by both Fang & Persily (1995) and Shaw et al (1991) and close to the average of both of these ranges of 0.4 and $0.5 \text{ L/s}\cdot\text{m}^2$ at 75 Pa , respectively. Finch (2007) found more airtight values.

The average normalized airflow rate at 75 Pa for the walls separating suites was found to be $0.8 \text{ L/s}\cdot\text{m}^2$ which is within the ranges provide by Fang & Persily (1995) and Shaw et al (1991), but near the minimum (most airtight) end of both ranges. The measured airtightness for these walls at the case study building is also approximately twice as airtight (half the flow at 75 Pa) as the average determined for similar walls by Finch (2007).

The exterior enclosure airtightness was also measured for suites on the first and thirteenth floors pre- and post-retrofit. The airtightness of the exterior enclosure of these suites along with the airtightness of the exterior enclosures for the typical suites is provided in Figure 9-5. This figure includes the average of all of the tested suites pre- and post- retrofit which are respectively $3.6 \text{ L/s}\cdot\text{m}^2$ and $1.6 \text{ L/s}\cdot\text{m}^2$ at 75 Pa . The averages for just the typical suites (suites on Floors 3 and 11) are higher and are $4.0 \text{ L/s}\cdot\text{m}^2$ and $1.8 \text{ L/s}\cdot\text{m}^2$ at 75 Pa pre- and post-retrofit respectively. Based on these averages for the typical suites, the retrofit improved the airtightness of the exterior enclosure by 55%. It is also possible to determine the airtightness improvement for all of the suites of the building by weighting the airflow for typical suites by the number of typical suites and then adding the airflow for the upper and lower suites. Using this method the airtightness improvement was also determined to be 55%.

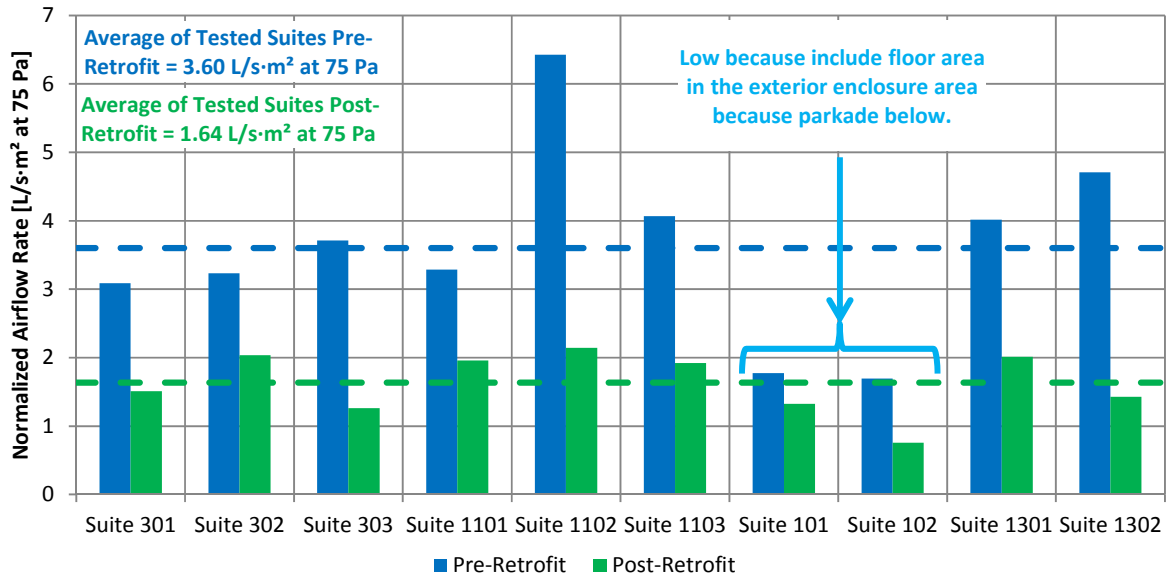


Figure 9-5: Graph of average normalized airflow rate for suite exterior enclosures pre- and post-retrofit

The exterior enclosure airtightness values for suites on the first floor are significantly lower than those for the other suites. This is likely because these values were normalized using a larger area than the typical suites because the floor of these suites is above the parking garage and is thus included in the exterior enclosure airtightness. As shown in the testing of the compartmentalizing elements of the typical suites, the floor slab is significantly more airtight than the vertical exterior enclosure, so including this area could cause the more airtight values determined for the suites on the first floor. One would expect a similar result for the suites on Floor 13 as the roof is included as part of the enclosure area of these suites; however, the airtightness testing did not find this result. The increased airflow of Floor 13 suites compared to Floor 1 suites under test conditions is likely attributable to details specific to these suites such as the presence of fireplace flue penetrations through the roof and of skylights which are located above some windows in the upper suites. Also, the fireplace flue penetration air sealing detailing was improved as part of the retrofit which may explain the significant airtightness improvement of these suites.

Both the pre- and post-retrofit exterior enclosure values are consistent with the range of values provided in the multi-unit residential building data compiled as part of this thesis work. The pre-retrofit airtightness for the typical suites (4.0 L/s·m² at 75 Pa) is similar to the average of MURBs in the database, which is 3.8 L/s·m² at 75 Pa. The post-retrofit airtightness of the typical suites (1.8 L/s·m² at 75 Pa) is in the lower quartile of results in the multi-unit residential building database.

9.2 Exterior Enclosure Testing of Floors 1 and 13

The exterior enclosure airtightness of the entire floor was measured pre-retrofit for Floor 1, and post-retrofit for Floor 1 and Floor 13. The exterior enclosure airtightness of these tests were determined to be 16, 10, and 117 L/s·m² at 75 Pa respectively.

These values are significantly higher than the average exterior enclosure airtightness testing values. Higher values for the upper and lower floors of the building are not unexpected because these floors have additional details that could allow for significant airflow to and from the exterior. For example, the first floor has the entrance lobby and entrance doors which were not well sealed. On the thirteenth floor, various mechanical and plumbing services penetrate the ceiling of the corridor to the mechanical penthouses above and are also not well sealed. In some cases it is possible to visually see through the holes from below and in to the mechanical rooms above. These mechanical rooms are directly open to the exterior through passive vents, so the poorly sealed penetrations that enter these rooms provide a direct path for airflow to and from outdoors.

Despite anticipating relatively high leakage rates, the measured leakage rates are even higher than anticipated. One potential cause of this finding may be due to a difference in testing technique between the suite and whole floor tests. Importantly, when testing the suites the elevator shaft is separated from the test zone by the corridor, so there is no concern of bypass airflow within the elevator shaft that may compromise the integrity of test. However, when testing a whole floor the elevator door is a boundary of the test area, so it is possible that significant airflow is occurring through the elevator shaft directly to and from the exterior or other floors. This could be further exacerbated by a relatively air leaky top and bottom of the elevator shaft. These bypass flows can cause full floor airtightness testing results to overstate the airflow through the exterior enclosure.

9.3 Floor 3 Suites versus Floor 11 Suites

Suites on Floor 11 have decorative gas fireplaces with open flues (un-sealed combustion) which are ducted to the roof of the building, and Floor 3 suites do not have these fireplaces. As mechanical penetrations were not sealed during testing and these fireplaces flues do not include a damper, it is likely the fireplace flues increase the measured leakage through the exterior enclosure for these suites. The average measured exterior enclosure airtightness for Floors 3 and 11 are shown in Figure 9-6.

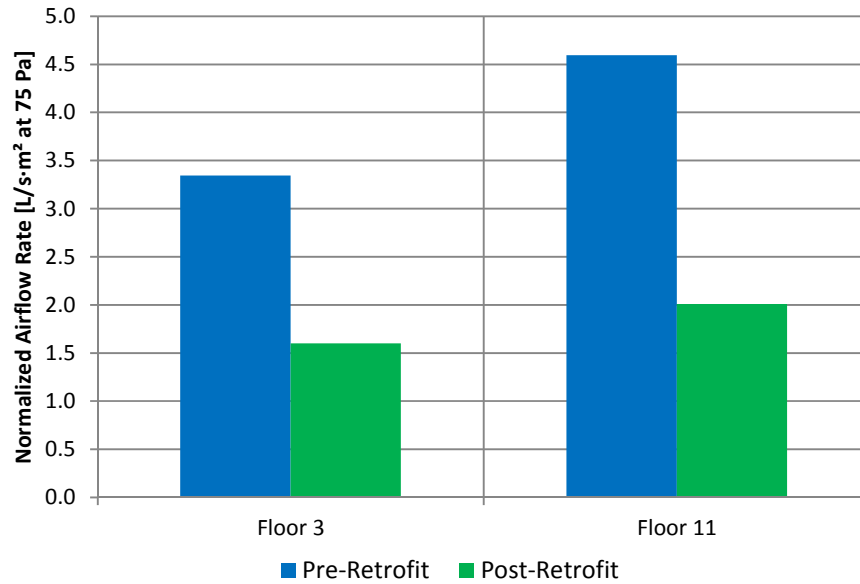


Figure 9-6: Graph of average normalized airflow rate for suite exterior enclosures on Floors 3 and 11 pre- and post-retrofit

The measured normalized airflow rates at 75 Pa show that the exterior enclosure of suites on Floor 11 were on average 40% (1.37 L/s·m²) higher than the rates on the Floor 3 pre-retrofit, and 26% higher post-retrofit. This finding supports the conclusion that the fireplaces are a significant airflow path.

One would expect that the airflow contribution of the fireplaces will remain unchanged as a result of the retrofit since no changes were made to these appliances or flues; however, the difference in flow rate for the exterior enclosure pre- and post-retrofit are 91 L/s and 33 L/s respectively, measured at 75 Pa. This change in the difference in flow rate between the floors suggests that there is another difference between Floor 3 and Floor 11 which has not been identified and which was made more airtight as a result of the retrofit. Upon closer inspection, it is possible that this is due in large part to the large improvement in airtightness of Suite 1102 as it had a particularly high leakage rate pre-retrofit.

9.4 Type -02 Suites versus Type -01 and -03

Type -01 and Type -03 suites are mirror images of each other, and Type -02 suites have a different layout as shown by the architectural drawings in Appendix B. Since these suite types differ, there may be observable differences in the airtightness characteristics. The average normalized airflow rate at 75 Pa for the compartmentalizing elements of these two suite types are provided in Figure 9-7.

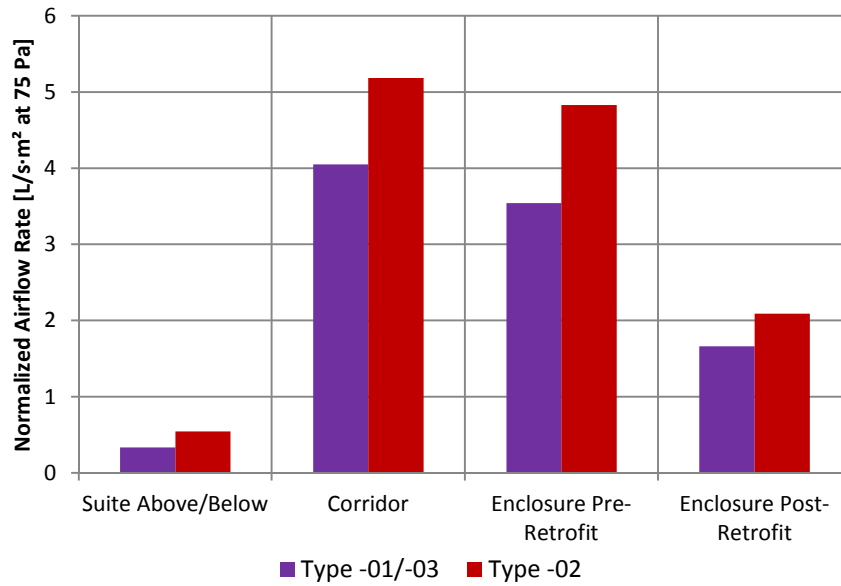


Figure 9-7: Graph of average normalized airflow rate separated by suite type

These normalized airflow rates show that in general the Type -02 suites have higher normalized airflow rates than the Type -01 and Type -03 suites. While the exact cause of the difference airtightness for these suite types is unknown, some potential causes are provided.

The cause of the increased normalized flow rate to the suites above and below may be as a result of the closer proximity of the Type -02 suites to the electrical closet in the corridor which may allow more airflow through penetrations in the slab. The higher normalized airflow rate for the corridor may also be due to proximity of these suites to the electrical closet as in some cases the electrical conduits and associated equipment enter the stud cavity through the gypsum wall board and are not sealed. Also, the gypsum wall board is not well finished in the electrical closets because it is not necessary for aesthetics. It is also possible that the increased normalized airflow rate for Type -02 suites to the corridor is due the larger wall area between the corridor and these suites which increases the likelihood of a significant defect within this area. The cause of higher normalized flow rates for the exterior enclosure both pre- and post-retrofit is unknown.

9.5 Demising Wall Comparison

The demising walls between -01 and -02 type suites and between -02 and -03 type suites are partly cast-in-place concrete and partly double steel stud walls with gypsum wall board as described in Section 7.1.1.1. The demising walls between -01 and -03 suites are entirely cast-in-place concrete. The difference in construction is expected to create different airflow resistance characteristics. Consistent with this expectation, suite to suite demising walls which are partially steel studs had an average normalized flow rate at 75 Pa of 0.90 L/s·m² (8 tests of 4 walls) while the entirely cast-in-place concrete walls had an average of 0.48 L/s·m² (4 tests of 2 walls). This finding shows that cast-in-place concrete walls are more airtight than interior steel stud walls with gypsum wall board.

As each demising wall was tested twice, once for each suite it encloses, it is possible to compare the results of the tests. This comparison showed that the results from the two tests are usually similar;

however, in some cases there was a significant difference between the two test results. This is likely because the flow rates determined for these demising walls is low compared to the total airflow measurement, so there is significant potential for error. Additional information regarding the comparison of demising wall test results is provided in Appendix D.

9.6 Corridor Testing

Airtightness testing of the corridors on Floors 3, 9, and 11 was conducted to determine the airtightness of the corridor compartmentalizing elements. The average airflow to pressure relationship curves for these elements are provided in Figure 9-8. Note that airflow measurements for the stairwell doors were only made for the east stairwell door in each corridor as the test fan was installed in the west stairwell door. Consequently, the stairwell door values presented in Figure 9-8 are actually the values for the east stairwell door doubled to represent the total airflow in to the stairwell through both doors. This is thought to be a reasonable approach as the east and west stairwell doors are generally of the same arrangement including dimensions, undercut measurements, and lack of weather stripping.

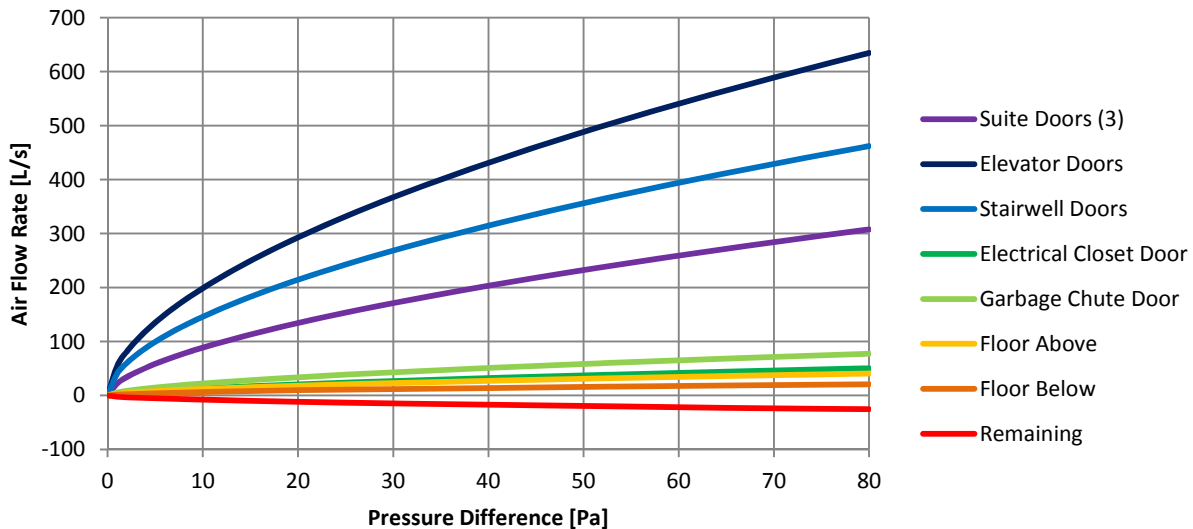


Figure 9-8: Graph of average airflow versus pressure difference relationships for compartmentalizing elements of corridors

The “remaining” leakage includes air leakage through elements that were not sealed during the testing such as corridor walls and it was calculated by subtracting the flows attributable to each compartmentalizing element of the corridors from the total flow measured with none of these elements sealed. Using this subtraction method, the remaining leakage was calculated to be negative which is impossible and is likely due to some double counting of airflows. For example, it is likely that airflow in to the electrical closet actually makes its way to the floors above and below through the electrical penetrations in the floor and ceiling and thus would have been measured for both tests and subtracted twice from the total airflow. To mitigate this double counting, the airflows measured for the electrical closet, garbage chute door, floor above, and floor below, were added together. This was deemed appropriate as the airflow rates through these elements are low

compared to the flow rates through the suite doors, elevator doors, and stairwell doors, which is the primarily important finding. The proportion of corridor leakage attributable to each component is shown in Figure 9-9 for each corridor test, and the average is shown in Figure 9-10.

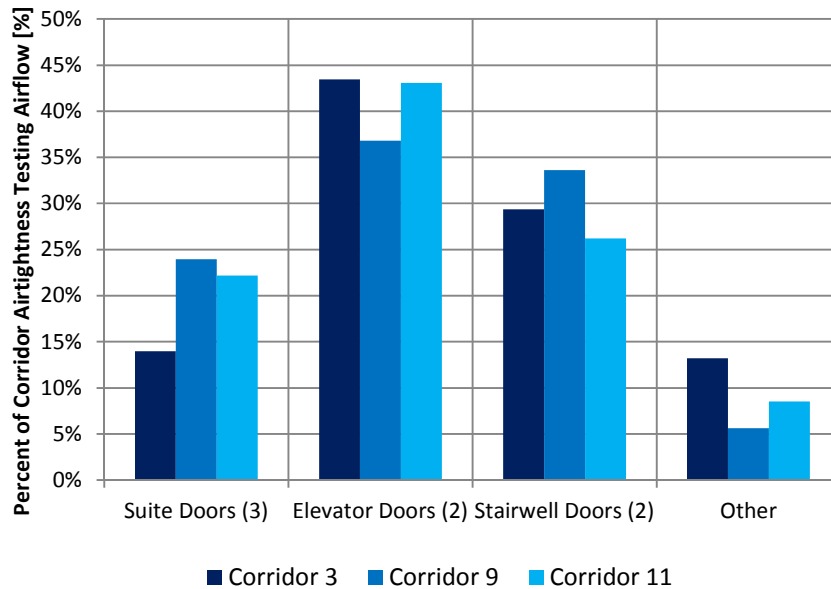


Figure 9-9: Chart of proportion of airflow through corridor compartmentalizing elements for each tested corridor

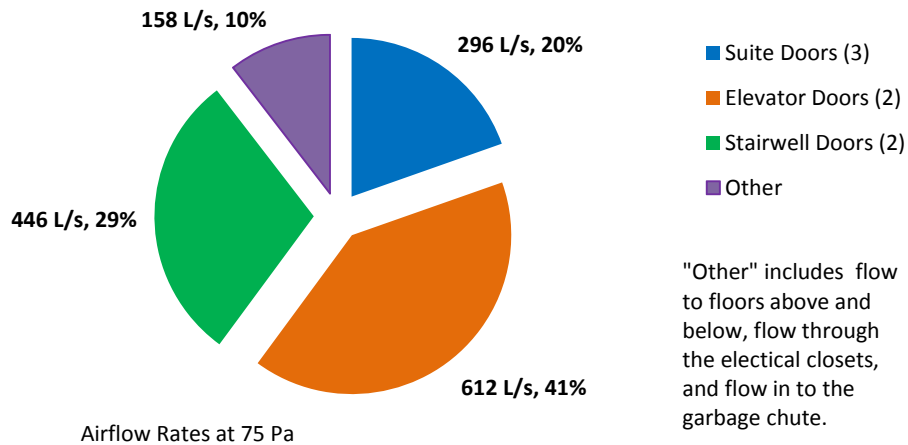


Figure 9-10: Chart of average proportion of airflow through corridor compartmentalizing elements

Figure 9-10 indicates that if a corridor were pressurized equally relative to all adjacent zones, 41% of the airflow would be to the elevator shaft through the two elevator doors, 29% would be to the stairwell, and only 20% would be to the suites through the entrance doors. Figure 9-9 indicates that the results from are consistent for the three corridors that were tested.

Gulay et al (1993) found that unsealing the elevator increased airflow from the corridor during testing by 78 to 323%, and that unsealing the stairwell doors increased flow by 42 to 128%. These percent increases are consistent with the findings at the case study building which determined an average percent increase in flow rate for the elevator doors and stairwell doors of approximately 134 and 98%, respectively.

Given that the corridor pressurization ventilation system is based on the principle of supplying ventilation air to suites and controlling airflows by pressurizing the corridor relative to adjacent zones, this finding represents a significant inefficiency in the ventilation system. Theoretically, approximately 80% of air supplied to the corridor would not directly enter the suites. Based on the airflow rates presented in Chapter 8, it was determined that approximately 40% of the make-up air unit (MAU) intake flow rate of approximately 1,500 L/s is supplied to the corridors directly. Consequently, if 60% of the ventilation air is lost from the duct, and 80% of the flow that reaches the corridors flows through paths other than under the suite entrance doors, then only approximately 8% of air brought in to the building by the MAU reaches the suites directly. 8% of 1,500 L/s is approximately 3 L/s per suite. For comparison, ASHRAE 62.1-201 recommends a ventilation rate of 42 L/s for the average suite at the case study building. While this calculation provides only a rough measure of in service ventilation rates, it does indicate that the pressurized corridor based ventilation system provides poor air flow path control at the case study building, which can lead to very low ventilation rates.

It is important to realize that this airtightness finding does not necessarily indicate in-service flows of ventilation air. Due to actual operating pressure differences (that are not necessarily similar to distribution of pressures during testing), more or less airflow may occur to and from certain zones and the measured results of airflows for the case study building were presented in Chapter 8. However, the lack of airflow control that is indicated by this testing does strongly indicate a significant obstacle to the effective implementation of corridor pressurization systems.

9.6.1 Resistance to Airflow of Doors

Suite entrance door flow coefficients, flow exponents, door undercut measurements, and observations regarding weather stripping are provided in Table 4-1.

Table 9-1: Summary of Suite Entrance Door Measurements and Observations

Suite Entrance Door Testing					
Door	Flow Coefficient, C [L/s·Pa ⁿ]	Flow Exponent, n	Q ₇₅ [L/s]	Door Undercut	Notes
Door 301	7.9	0.56	88	11	No weather stripping.
Door 302	3.4	0.58	42	4	No weather stripping.
Door 303	4.2	0.64	65	9	No weather stripping.
Door 901	16.8	0.55	185	22	No weather stripping.
Door 902	6.4	0.61	91	3	Weather stripping on left jamb from door handle to ground.
Door 903	8.6	0.55	95	3	Weather stripping on bottom.
Door 1101	2.4	0.58	30	0	Weather stripping on bottom.
Door 1102	9.5	0.72	213	9	No weather stripping.
Door 1103	8.0	0.58	98	4	No weather stripping.

The measured flow rate through the suite entrance doors ranged from 30 to 213 L/s at 75 Pa with an average of 101 L/s. The majority of these doors were not weather stripped. These values are compared to the ranges provided by Orne et al’s (1998), Moffat et al (1998), and Morrison Hershfield (1996) in Figure 9-11. Generally these ranges from literature are consistent with the range of values found for the suite entrance doors at the case study building.

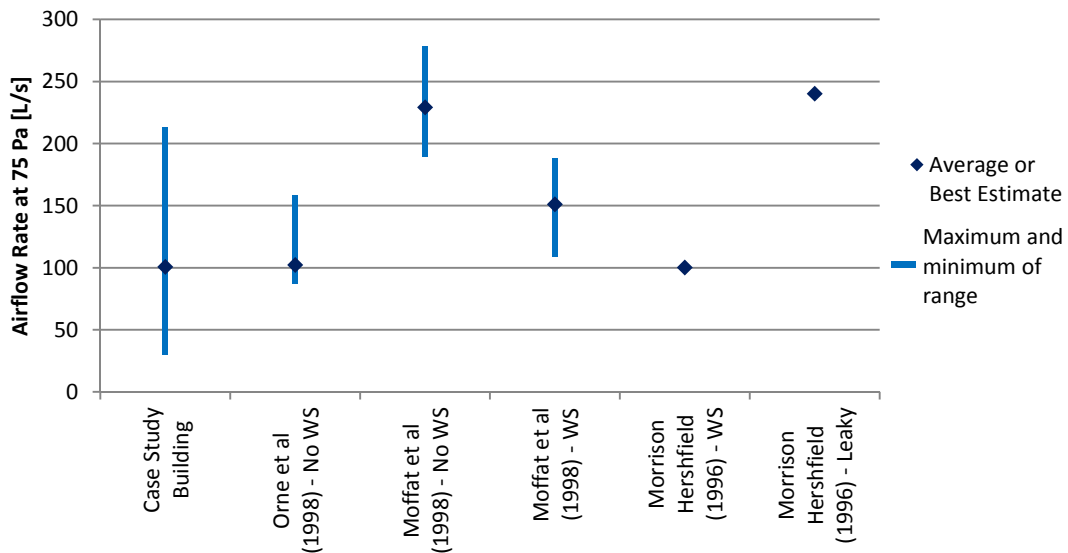


Figure 9-11: Graph of suite entrance door airflow rates at 75 Pa of the case study building compared to values from literature

To determine whether the size of the door undercut or the presence of weather stripping would provide a good indicator of suite door airtightness, the door undercut measurements were compared with the airflow measurements at 75 Pa and are shown graphically in Figure 9-12. This graph shows undercut size and the airflow measured through the doors with larger undercuts

correspond to with higher airflow rates; however, there is significant scatter, so prediction of airflow rates based only on door undercut size is not possible.

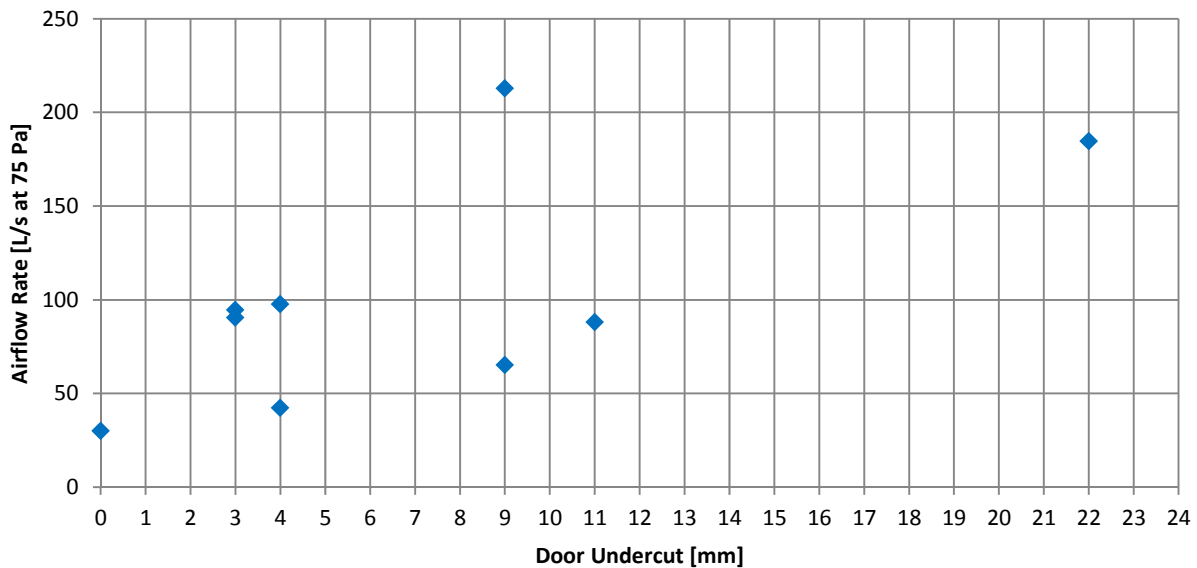


Figure 9-12: Graph of airflow rate through suite entrance doors versus door undercut size

The requirement for a door undercut to provide ventilation can conflict with fire code requirements. The door undercuts measured for the suite entrance doors at the case study building often significantly exceeded the 6 mm requirement of the 2010 National Building Code of Canada (NRC, 2010) as shown by the values provided in this section as well as the additional undercut measurements provided in Appendix D. Based on the average suite entrance door flow coefficient and exponent, the average of the measured suite entrance doors permits approximately $1.7 \text{ m}^3/\text{min}\cdot\text{m}^2$ at 25 Pa which is significantly higher than the maximum flow rate of $0.9 \text{ m}^3/\text{min}\cdot\text{m}^2$ required by the International Building Code and NFPA Standard 105. (ICC, 2012; FPA, 2013)

The stairwell doors, which are 89 cm by 200 cm, were measured to allow 201 L/s to 260 L/s at 75 Pa, with an average of 223 L/s. This is consistent with the values in Moffat et al (1998) which provides a range from 113 L/s to 271 L/s at 75 Pa with an average of 172 L/s, and is also consistent with the values for non-weather-stripped doors provided by Orne et al (1998). The airflow at 75 Pa for these doors is plotted versus door undercut size in Figure 9-13 which shows that the undercut size likely does provide some indication of flow rate for these types of doors, but more measurements would be required to confirm this correlation.

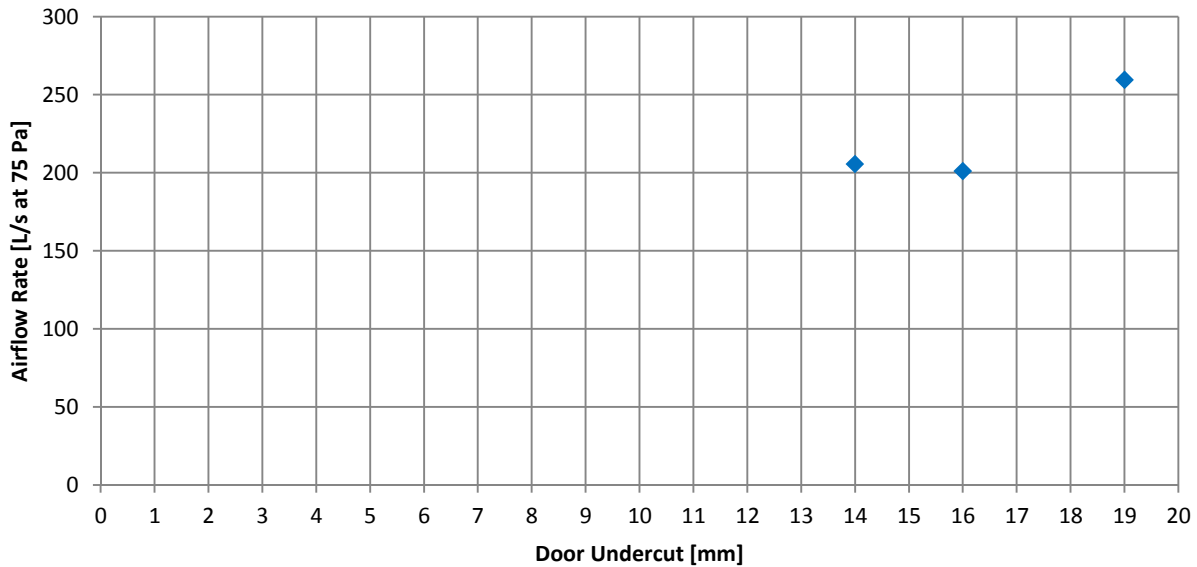


Figure 9-13: Graph of airflow rate through stairwell doors versus door undercut size

These stairwell doors allow significantly more airflow than the suite entrance doors, even for the same undercut size. This is consistent with the qualitative observation that the stairwell doors fit less tightly in their frames than do the suite entrance doors. This finding also suggests that significant airflow occurs around all edges of the door and not just through the undercut at the bottom, so a simple measurement of the door undercut does not necessarily provide a good method for predicting the airflow characteristics of a door.

The elevator doors (2 per floor), which measure 91 cm by 213 cm, were determined to be a major component of the airflow to and from the corridor during testing. A range of 284 L/s to 331 L/s for each door at 75 Pa was measured for these doors, with an average of 306 L/s. Tamura & Shaw (1976) found a range from 307 L/s to 448 L/s with an average of 360 L/s which is consistent with the measurements at the case study building.

9.7 Summary of Results

Overall, the airflow resistance of the various compartmentalizing elements measured at the case study building are within the expected range for multi-unit residential buildings as compared with values in literature. Thus, the airtightness of the case study building is representative of a typical building of this type. Based on comparison with the compiled database of multi-unit residential building airtightness performance, the pre-retrofit exterior enclosure is representative of a typical building of this type, and the post-retrofit exterior enclosure is representative of a moderately more airtight building, typical of more modern buildings.

The corridor airtightness testing found that a significant fraction of the corridor leakage area is to the stairwell and the elevator shafts. These airflow paths potentially create a significant inefficiency in the corridor pressurization ventilation system strategy as they provide a path for ventilation air to flow out of the corridor and in to the elevator shaft and stairwells instead of into the suites.

To help visualize the overall distribution of airflow paths in the case study building, circles representing the equivalent leakage area of each compartmentalizing element of the exterior enclosure have been drawn on floor plans for Floor 3 and Floor 11 based on a combination of the results of the suite and corridor airtightness testing. These floor plans are provided in Figure 9-14 and Figure 9-15. Notably, the largest flow paths are typically through the exterior enclosure, through the combination of corridor to suite walls and entrance doors, through elevator doors, and through stairwell doors. Other flow paths are comparatively small.

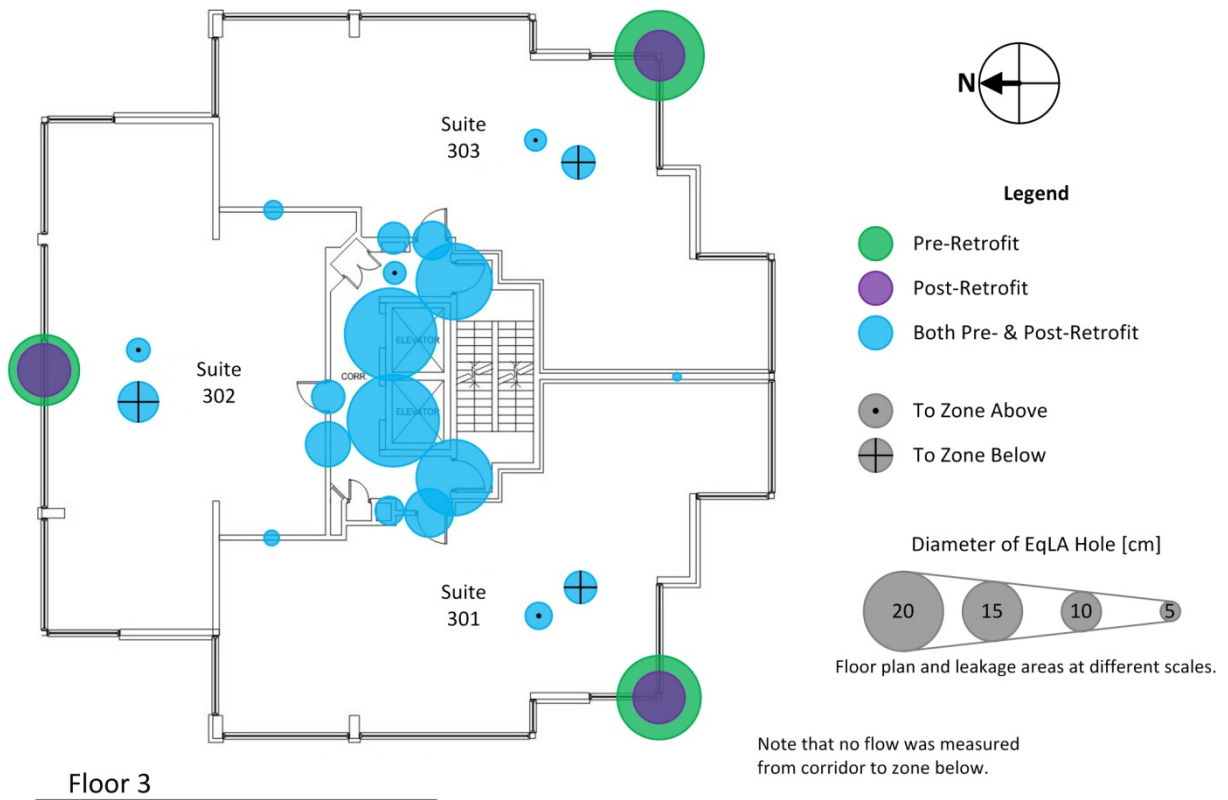


Figure 9-14: Floor plan of Floor 3 of the case study building showing the equivalent leakage areas of the measured pressure boundaries from the corridor and suite testing

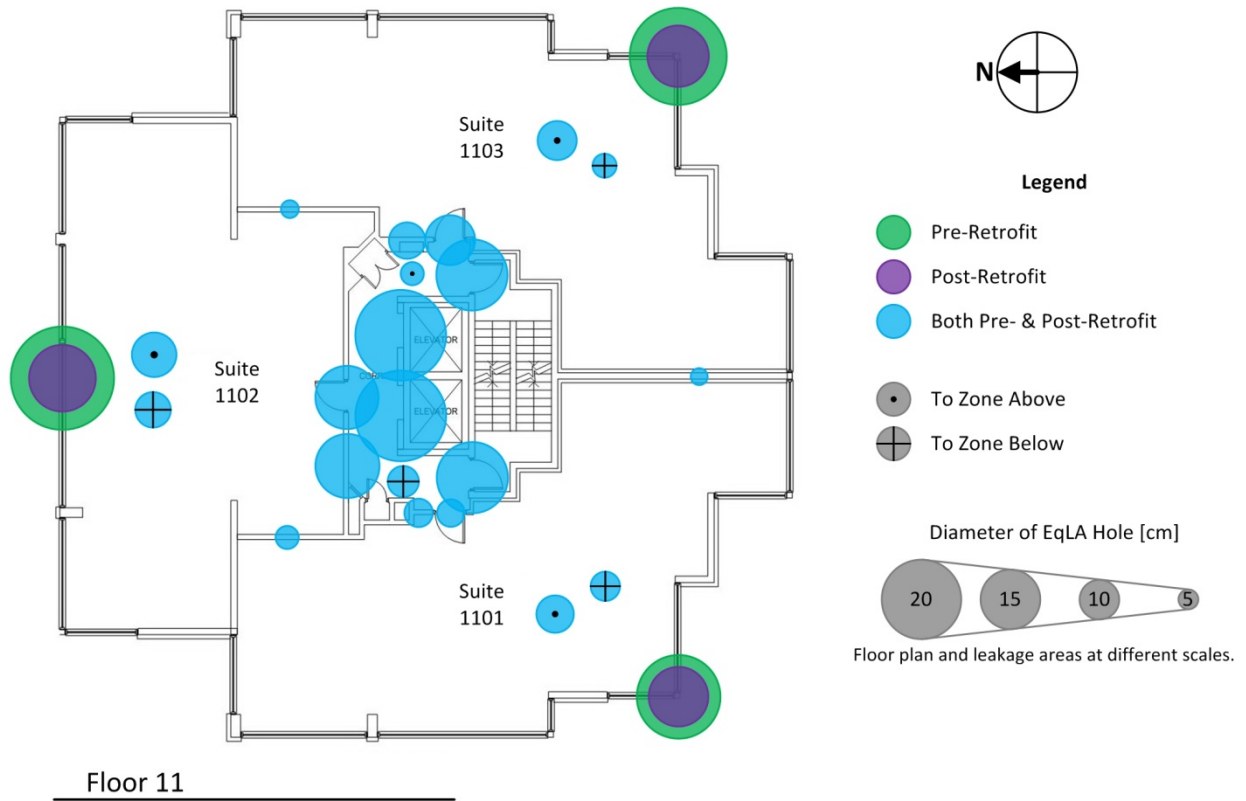


Figure 9-15: Floor plan of Floor 11 of the case study building showing the equivalent leakage areas of the measured pressure boundaries from the corridor and suite testing

Chapter 10

Pressure Difference Monitoring Results

This chapter presents the measured pressure difference at the case study building created by wind, stack effect, and mechanical ventilation systems. These measured pressure differences are used to interpret the measured airflow results presented in Chapter 8.

In some cases sensors and data acquisition units malfunctioned and provided incorrect measurements. These instances are identified where appropriate and discussed in detail in Appendix E.

10.1 Guidance for Interpretation of the Monitoring Data

All of the pressure sensors used in for this project measured pressure differences and do not measure absolute pressure. To be able to interpret the pressure monitoring data it is necessary to define which pressure will be used as a reference (defined as zero) for each sensor. A convention has been adopted such that in all cases the second zone listed will be the reference zone. That is, if a pressure is measured from Zone A to Zone B, then Zone B is the reference zone and is defined as zero pressure. Consequently, if a positive pressure is measured from Zone A to Zone B, then Zone A is pressurized relative to Zone B.

Figure 10-1 identifies the reference pressure tap locations for each of the pressure sensors. This figure indicates the zones in which the pressure taps are located; however, the exact location of the sensors and the pressure taps has been modified for clarity. Virtual pressure sensors indicated in the figure are locations where there is no physical sensor and pressure differences were determined by adding the measurements of other sensors. Generally, the corridors and the exterior are used as the reference pressure. For corridor-to-corridor pressure measurements, the upper of the two corridors is the reference location.

As an example, if the pressure sensor identified by an “A” in Figure 10-1 measures a positive pressure, it indicates that the east suite is at a higher pressure than the west suite.

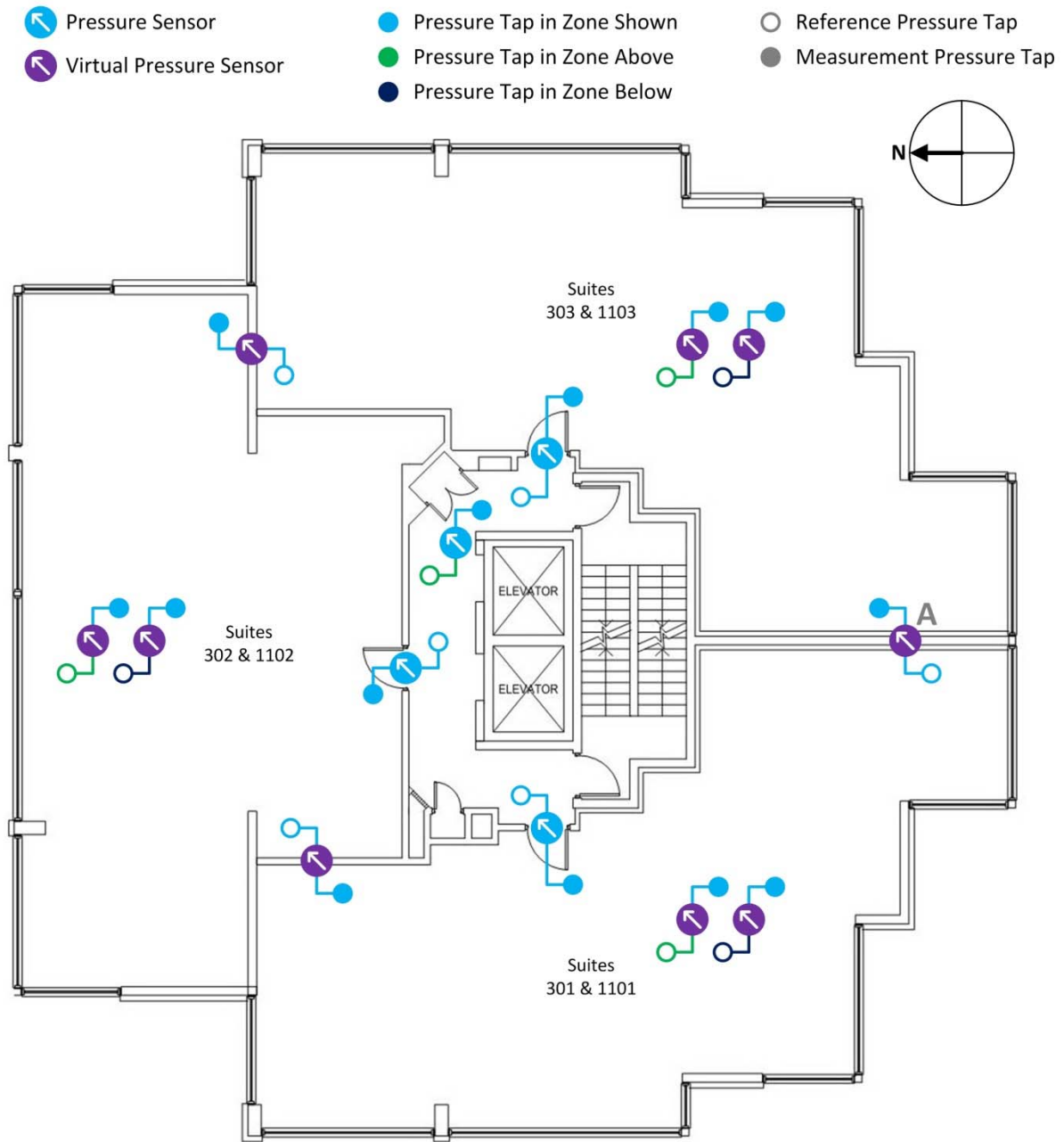


Figure 10-1: Floor plan of typical floor in the case study building schematically indicating the location of positive and negative pressure taps for the typical pressure sensors

A convention is also used for wind direction. Wind is referred to by the direction from which it originates. For example, an east wind is from the east (as opposed to towards to the east).

Pressure differences were only sampled once per hour, and given the inherent variability of wind pressures on buildings may not capture the hourly average pressure, and instead may measure maxima or minima.

When examining the results of the monitoring program it is important to consider the potential effect of the building retrofit. Changes to the air barrier were completed in September 2012 when the last of the new windows were installed. Work on installation of exterior cladding continued after this date up to the end of January 2013; however, the cladding likely has limited influence on the building airflow patterns. Scaffolding with netting remained installed on some elevations up to the end of January to facilitate the cladding work and this would likely act to slightly dampen wind pressures, but would have no impact on stack effect pressures. Prior to completion of the cladding, the exterior pressure taps could not be completely installed and instead hung along the side of the building near their final installation locations. The arrangement of these pressure taps likely had little to no impact on the pressure measurements.

The exterior pressure tap on the roof was not completely installed until March 8, 2013 because the installation could have potentially interfered with ongoing work at the roof of the mechanical penthouse. Prior to attachment to the exterior pressure tap, the pressure tube from “1300 – CO” (also referred to as “Floor 13 to Roof”) was installed such that it was protruding from the west facing wall of a mechanical room on the roof. Consequently, prior to attachment to the pressure tap, westward winds create a negative pressure reading (pressure higher outside than inside); however, it is likely that in reality the pressure across the roof was positive. Once the pressure tap was fully installed, positive pressures were typically recorded during westward winds.

For reference, a more detailed schedule of the rehabilitation process is provided in Appendix E.

Generally, monitoring results are presented for the post-retrofit condition as the condition of the building is difficult to determine while the retrofit is on-going and is likely not representative of typical building operation. However, in some cases data that was collected during the retrofit is used, and the potential for impact of the ongoing work on the results should be noted. The impact of the retrofit on airflow patterns within and through the case study building is discussed in Section 10.9.

10.2 Exterior Enclosure Pressure Differences

The pressures across the exterior enclosure were monitored near the middle of each of the cardinal elevations of the building at the third and eleventh floors, and across the roof of the building from the 13th floor corridor to a pressure tap attached to the weather station.

The arrangement of the pressure taps for measurements across the exterior enclosure is such that the reference pressure tap is located on the exterior. Thus, based on physics and results in literature, one would expect the pressure across the exterior enclosure to decrease on the windward side of the building and to increase on the leeward side. In literature, the reference pressure for these types of measurements is commonly the interior; consequently, measurements would be expected to have the opposite sense. The reader should refer to Figure 10-1 as needed to aid in interpretation of the pressure measurements.

10.2.1 Exterior Enclosure Pressure Differences and Exterior Temperature

To assess the relationship between exterior temperature and pressures across the exterior enclosure, 24 hour moving averages of the pressure differences were plotted versus temperature for the monitoring period. These graphs are provided in Figure 10-2, Figure 10-3, and Figure 10-4.

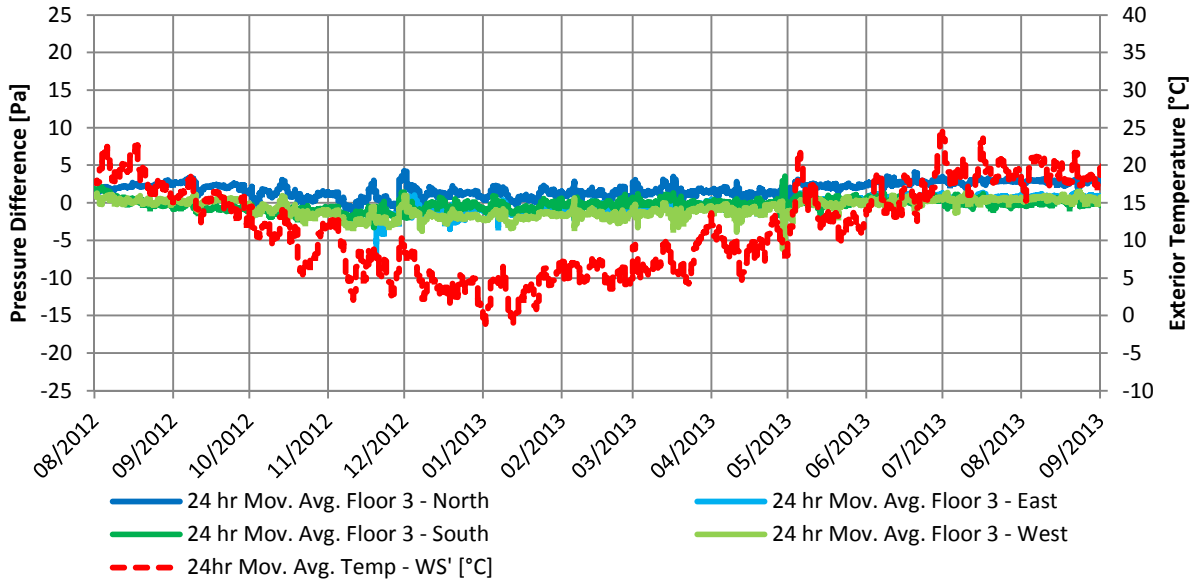


Figure 10-2: Graph of 24 hour moving average of exterior enclosure pressure differences for Floor 3 and the exterior temperature

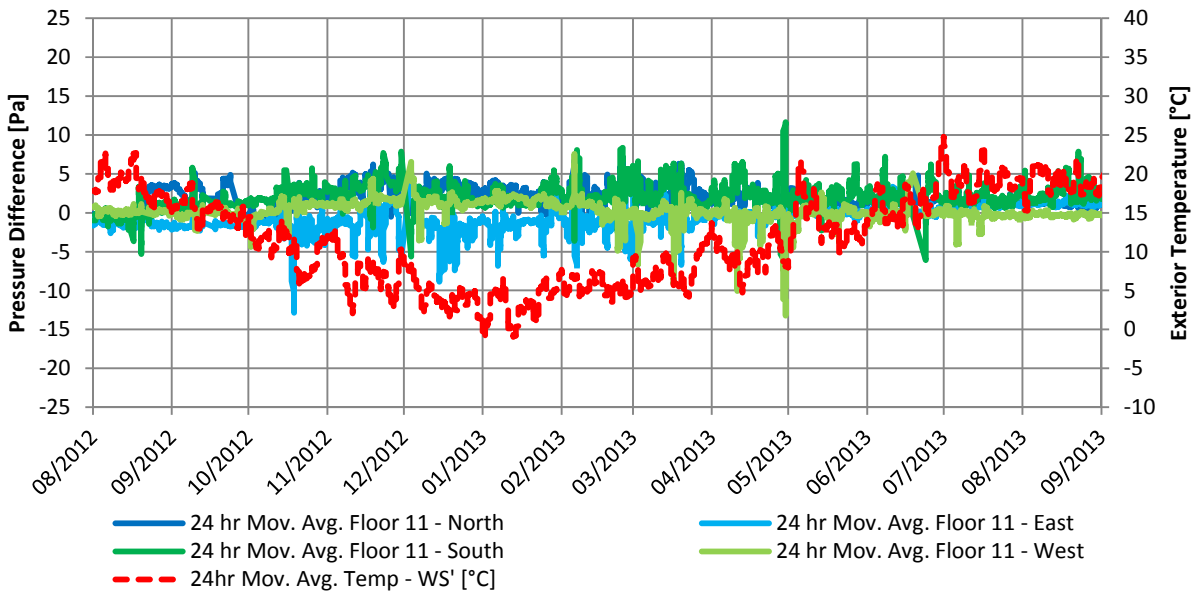


Figure 10-3: Graph of 24 hour moving average of exterior enclosure pressure differences for Floor 11 and the exterior temperature

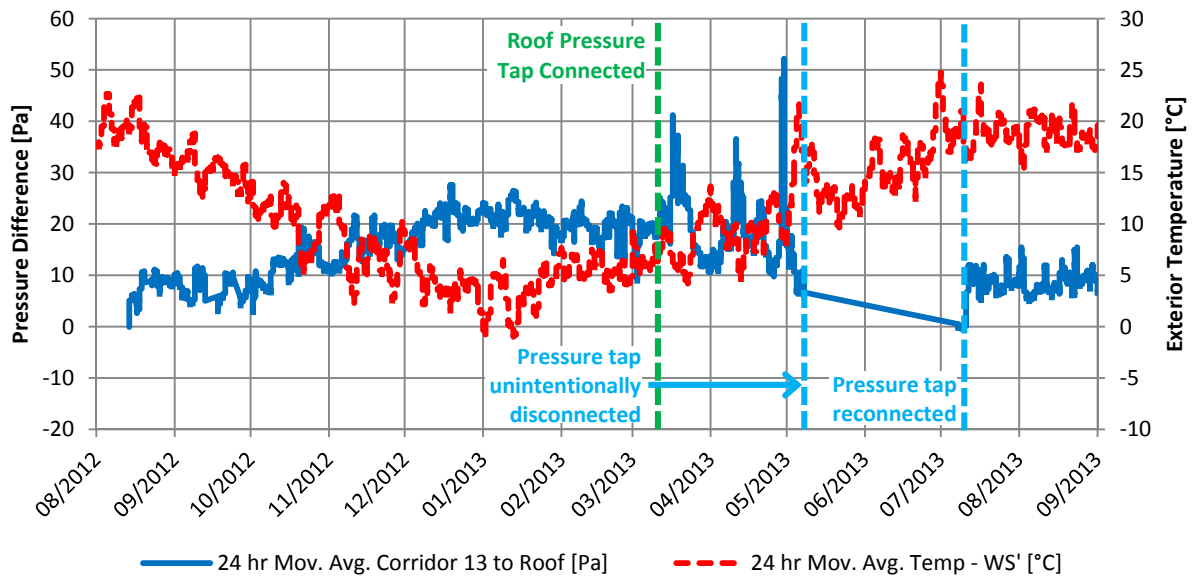


Figure 10-4: Graph of 24 hour moving average of exterior enclosure pressure differences for Corridor 13 to roof and the exterior temperature

Inspection of Figure 10-2 and Figure 10-3 shows that the 24 hour moving average pressures from the suites to the exterior are relatively low (almost always under 5 Pa) and do not vary significantly with outdoor temperature. However, the pressure across the exterior enclosure on Floor 11 shows larger variations and higher peak pressures due to increased wind exposure.

Conversely, Figure 10-4 (note the change in scale compared to the two preceding figures) indicates a strong relationship between exterior temperature and the pressure difference across the roof of Corridor 13. This pressure increases as the temperature decreases, and then decreases as the temperature increases. This relationship corresponds with what would be predicted given increased stack effect pressures at lower temperatures. 24 hour average exterior temperatures ranged from approximately 0°C to 20°C and corresponded with a range of approximately a 25 Pa to 0 Pa pressure difference from Corridor 13 to the roof.

The predicted impact of stack effect is not observed at the exterior enclosure pressure sensors on Floors 3 and 11 likely because the stack pressure distributes more across interior compartmentalizing elements within the building than it does across the enclosure. Distribution of stack pressures across interior compartmentalizing elements will be discussed further in Section 10.3 and Section 10.4 and the relative distribution across different pressure boundaries is discussed in Section 10.7.

Pressure differences between Corridor 13 and the roof of the building were also found to be related to the exterior temperature over the course of a day or week, and pressure differences between the suites and the exterior at Floors 3 and 11 were not found to be significantly related to exterior temperature. This is shown in Figure 10-5, Figure 10-6, and Figure 10-7.

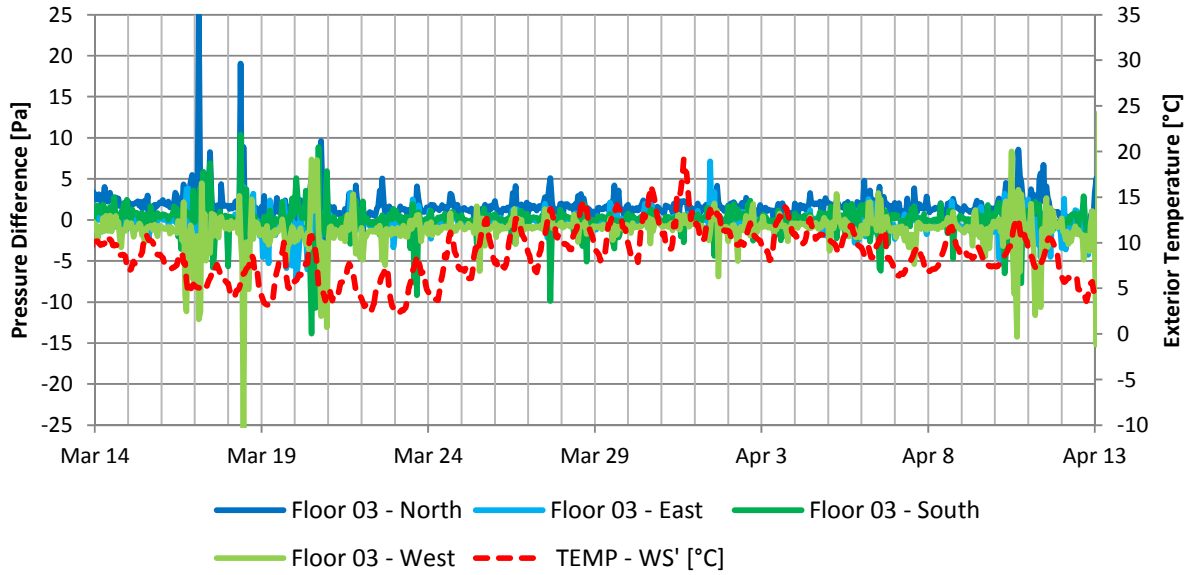


Figure 10-5: Graph of hourly exterior enclosure pressure differences for Floor 3 and the exterior temperature

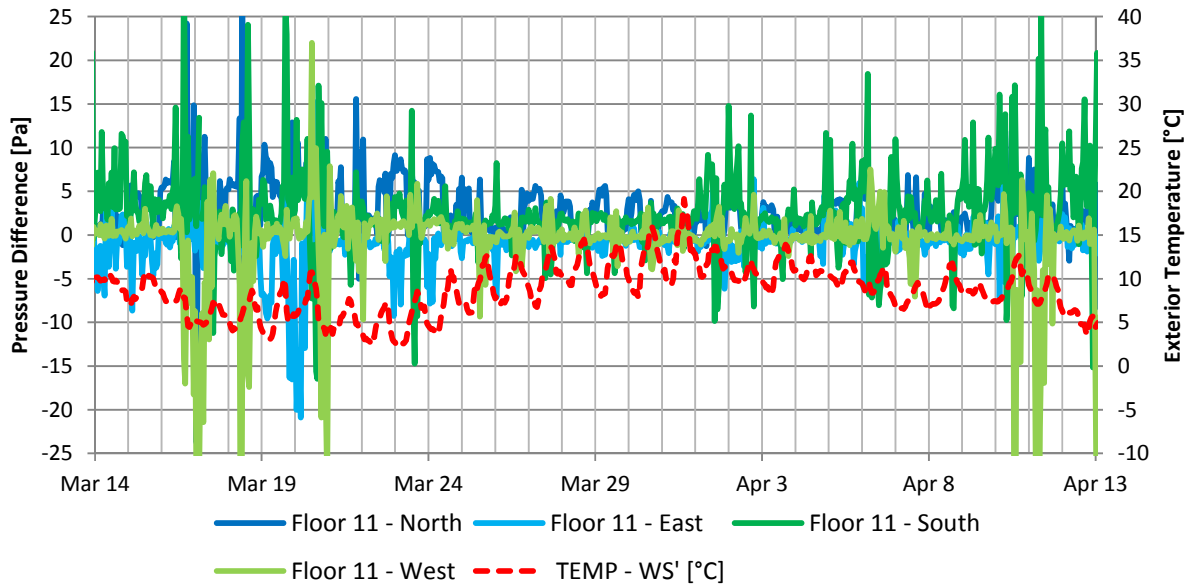


Figure 10-6: Graph of hourly exterior enclosure pressure differences for Floor 11 and the exterior temperature

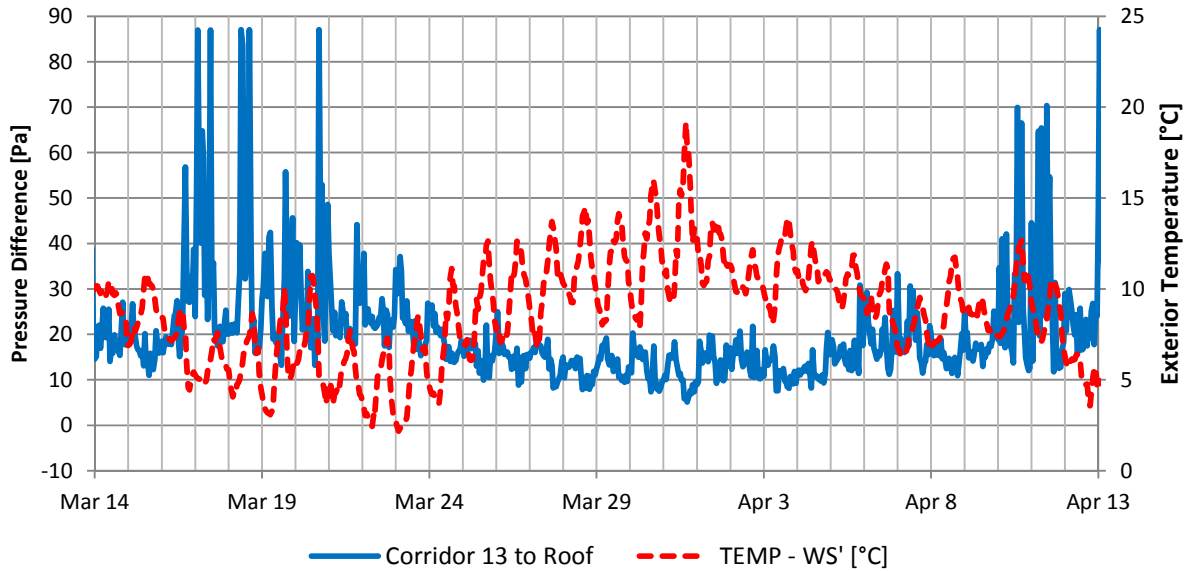


Figure 10-7: Graph of hourly exterior enclosure pressure differences from Corridor 13 to roof and the exterior temperature

Figure 10-7 shows a strong relationship between exterior temperature and the measured pressure between the corridor and the roof over the course of approximately a month with pressure changes related to temperature also apparent over the course of a day. (Note the change in scale between Figure 10-7 and the two preceding figures.) Typically, a change in temperature of approximately 5°C corresponds with a change in pressure difference of approximately 10 Pa. The large spikes in pressure measurements observed in these figures are not a result of temperature changes, and instead are more likely caused by wind as discussed in subsequent sections.

10.2.2 Exterior Enclosure Pressure Differences and Wind

Spikes in the exterior pressure differences are thought to be a result of increased wind speeds, and to evaluate the relationship between wind speed, wind direction, and exterior enclosure pressures at the case study building, a number of shorter periods were selected during periods of minimal, light, moderate, and strong wind. The two primary directions of concern for wind at the case study building are approximately east and west as shown previously in Chapter 7, so these directions have been selected for analysis in the subsequent sections. Note that the scale of the graphs in these sections may appear inappropriate in some cases; however, this was done to keep the scale consistent between cases to facilitate direct comparison.

10.2.2.1 Minimal Wind

A period with minimal wind (approximately less than 10 km/hr) was identified from January 15th to January 23rd, 2013 and the wind speed and exterior temperature during this period are provided in Figure 10-8. During this period the scaffolding was still in place at the building; however, this case is primarily used as reference for comparison with subsequent wind events and given the low wind speeds during this period, the scaffolding likely had little effect on pressure differences.

Wind speed squared is a useful quantity as it is theoretically linearly related to enclosure pressure differences according to Eq. 3.5 and it is provided during the period of minimal wind in Figure 10-9. It is important to appreciate that because of the relationship between wind speed and pressure defined by Eq. 3.5, a doubling in wind speed creates a quadrupling in the potential pressure created.

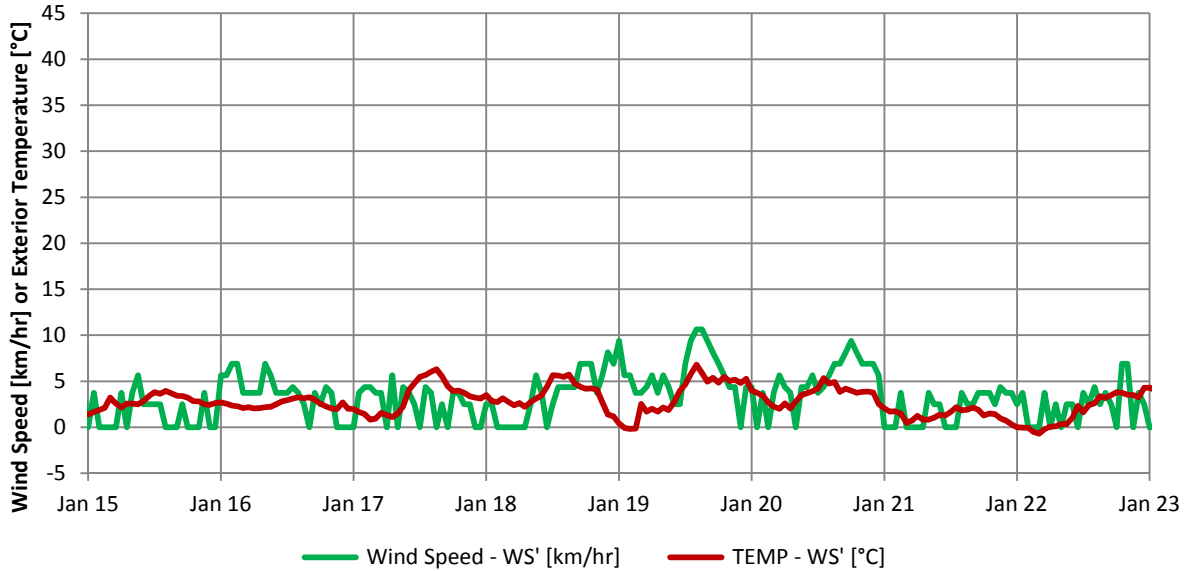


Figure 10-8: Graph of wind speed and exterior temperature during period of minimal wind

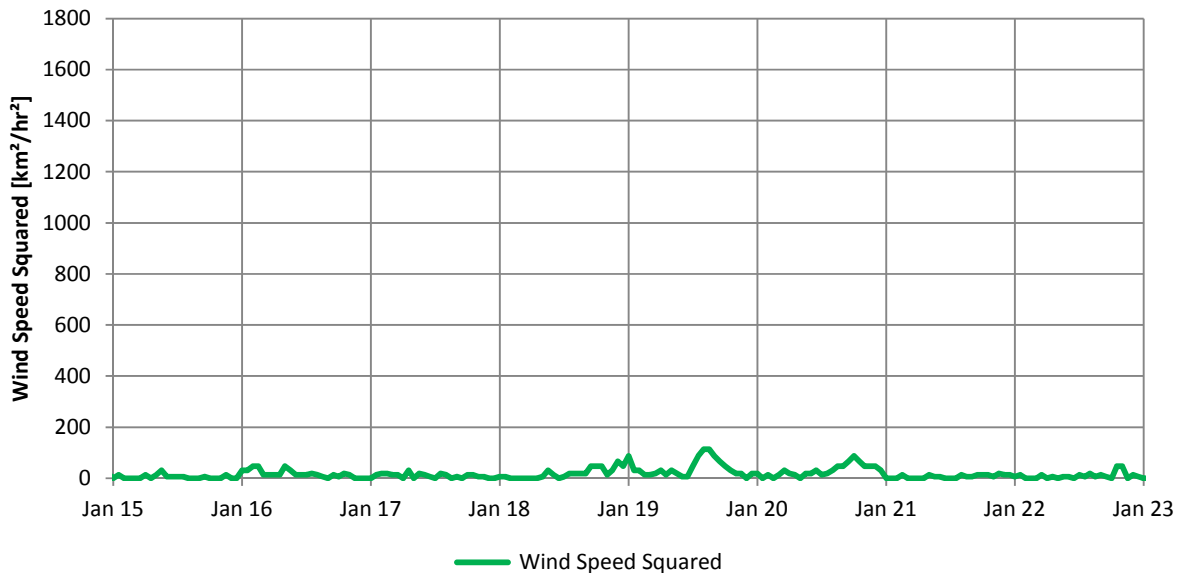


Figure 10-9: Graph of wind speed squared during period of minimal wind

The pressures measured across the exterior enclosure at Floors 3, 11, and 13 are provided in Figure 10-10, Figure 10-11, and Figure 10-12 respectively.

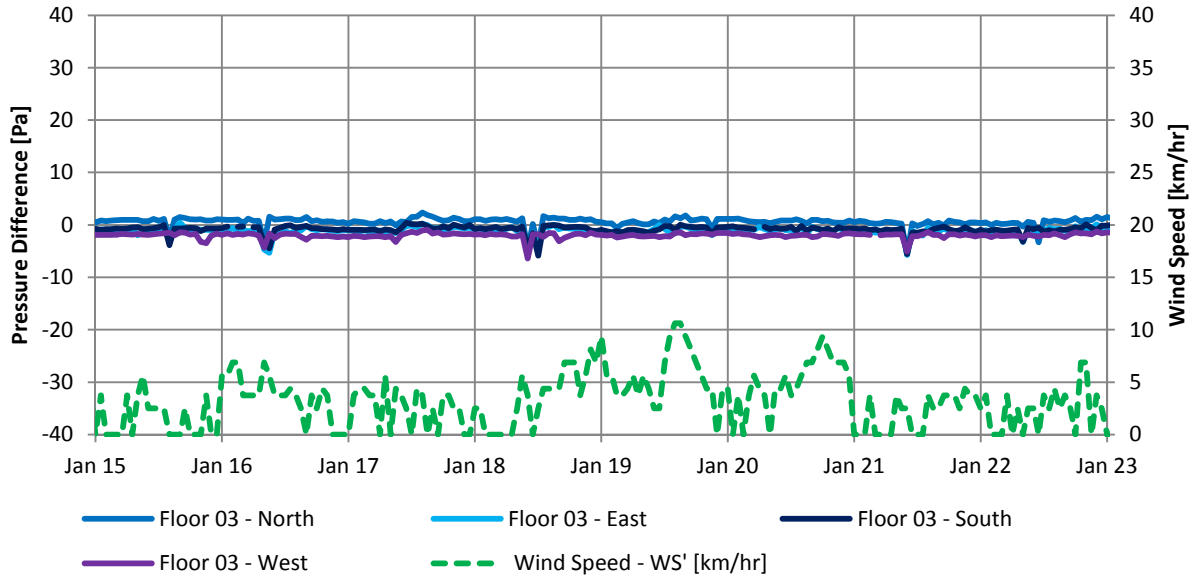


Figure 10-10: Graph of hourly pressure differences across exterior enclosure at Floor 3 during minimal wind

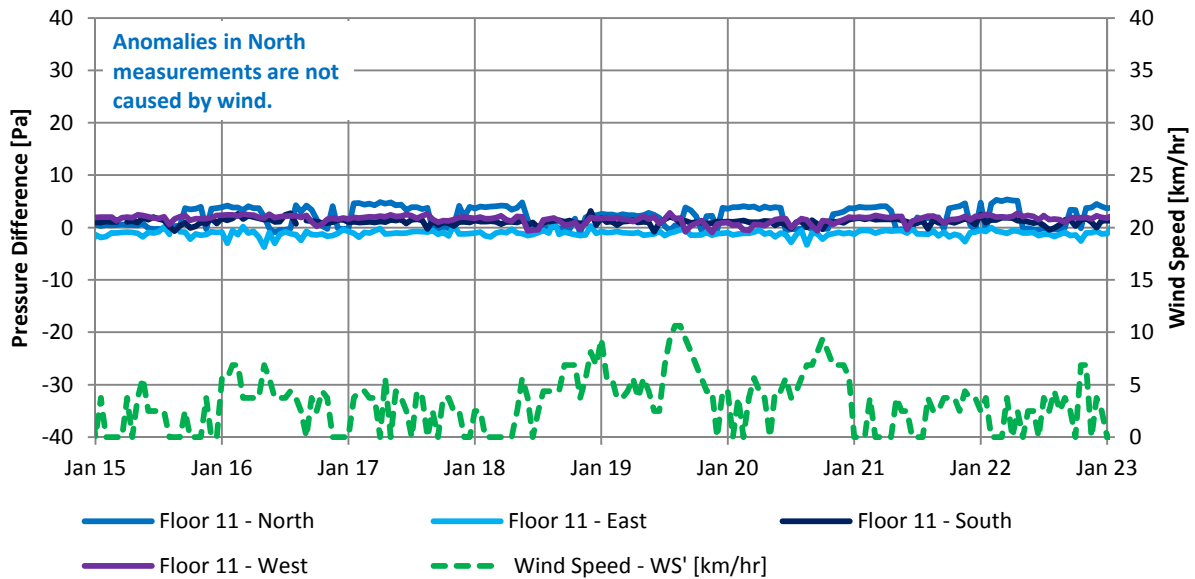


Figure 10-11: Graph of hourly pressure differences across exterior enclosure at Floor 11 during minimal wind

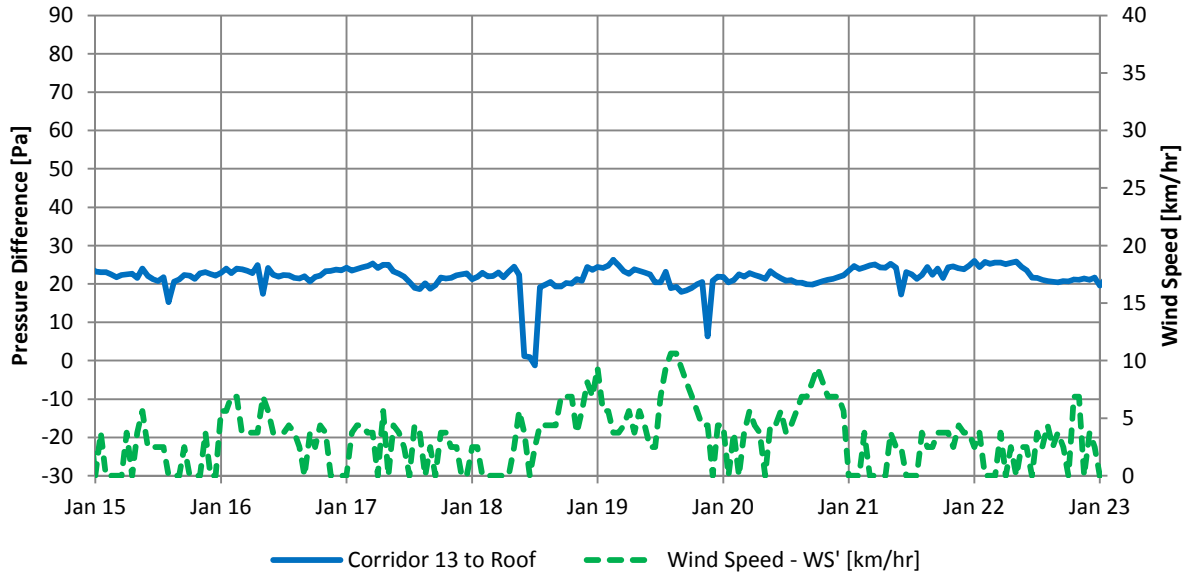


Figure 10-12: Graph of hourly pressure difference across exterior enclosure from Corridor 13 to roof during minimal wind

The three preceding graphs show that during minimal wind the pressure differences across the enclosure of the building are relative stable. Furthermore, the pressure differences across the exterior walls are nearly zero. The approximately 5 Pa magnitude flat increases in pressure observed in the “Floor 11 – North” readings shown in Figure 10-11 are likely as a result of driving forces other than wind.

10.2.2.2 Light East Wind

A period of light easterly wind speeds (approximately between 5 and 10 km/hr) was identified from January 13th to January 15th, 2013. The wind speed and exterior temperature during this period are provided in Figure 10-13, the wind direction is provided in Figure 10-14, and the wind speed squared is provided in Figure 10-15. During this period, scaffolding was still in place on some of the building; however, similar effects were noted during other periods of light east wind after the scaffolding was removed.

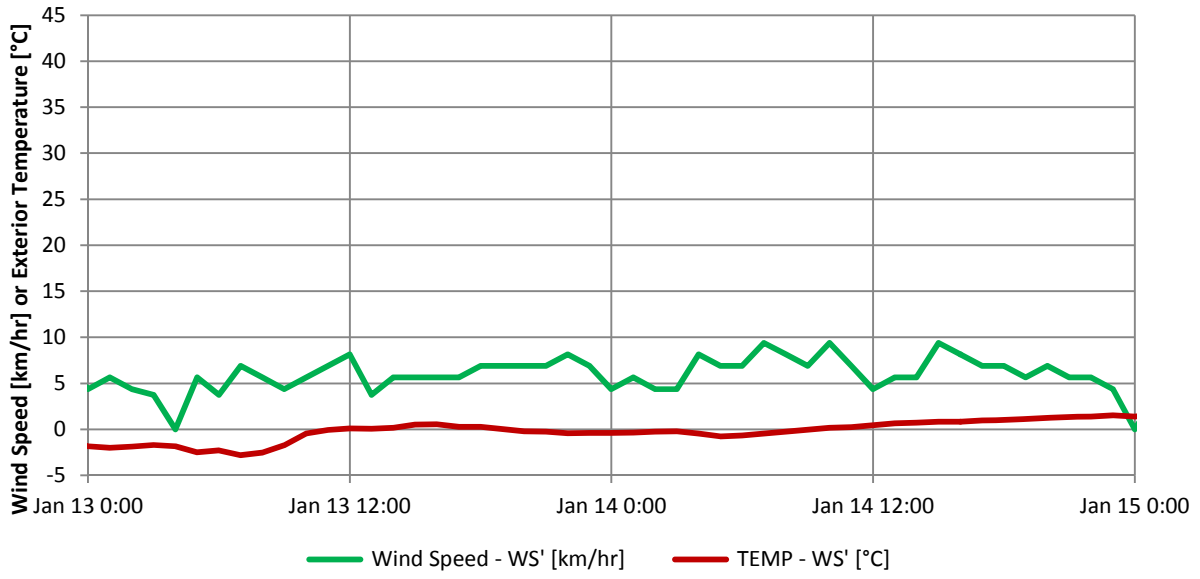


Figure 10-13: Graph of wind speed and exterior temperature during period of light east wind

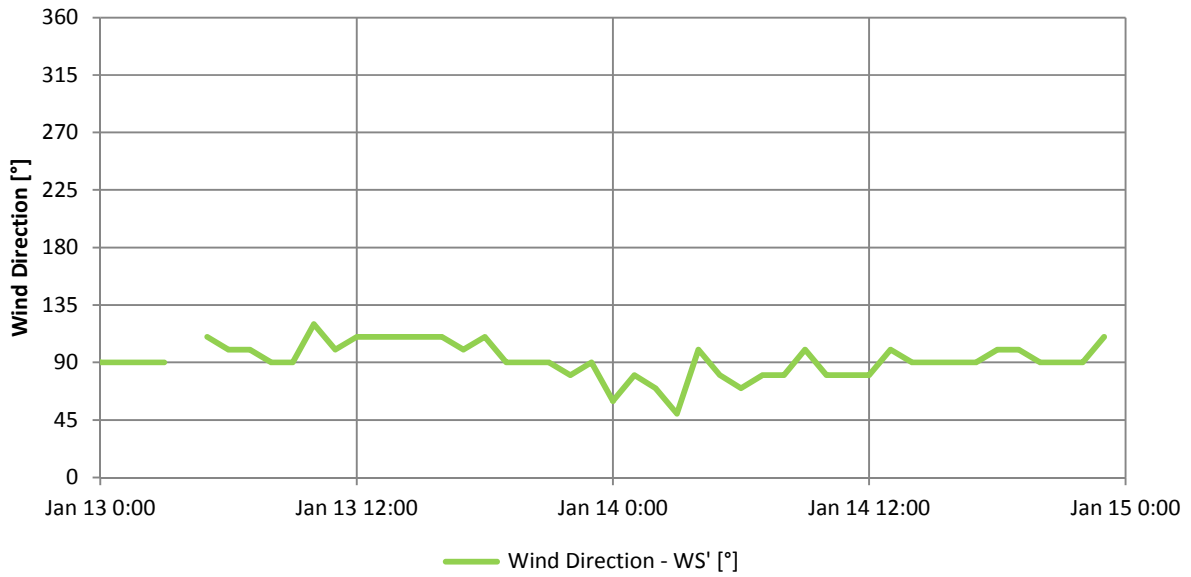


Figure 10-14: Graph of wind direction during period of light east wind

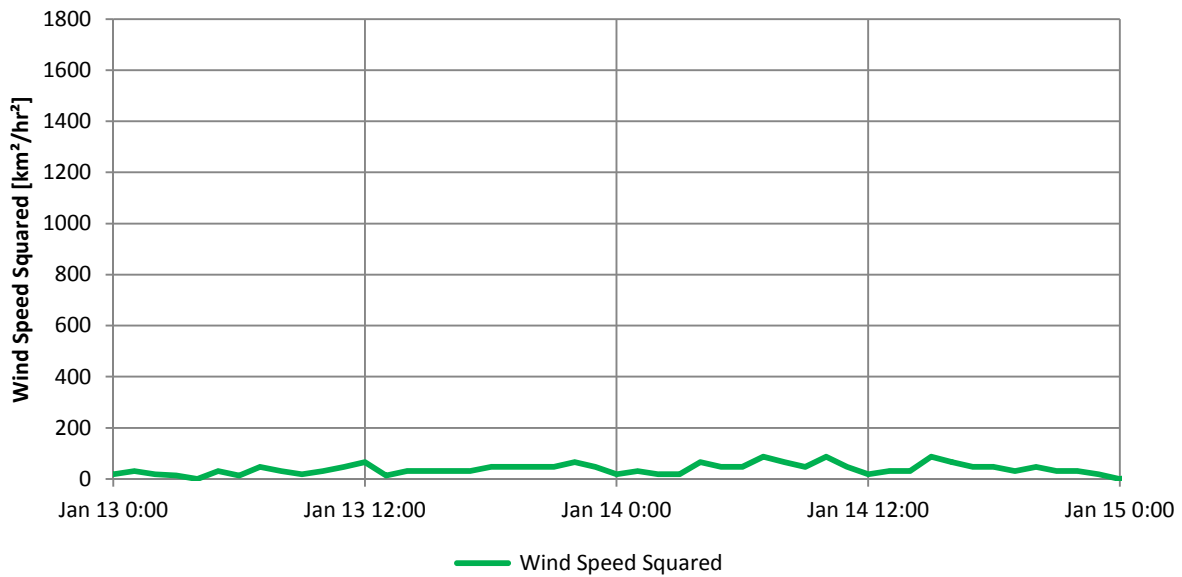


Figure 10-15: Graph of wind speed squared during period of light east wind

The pressures measured across the exterior enclosure at Floors 3, 11, and 13 are provided in Figure 10-16, Figure 10-17, and Figure 10-18 respectively.

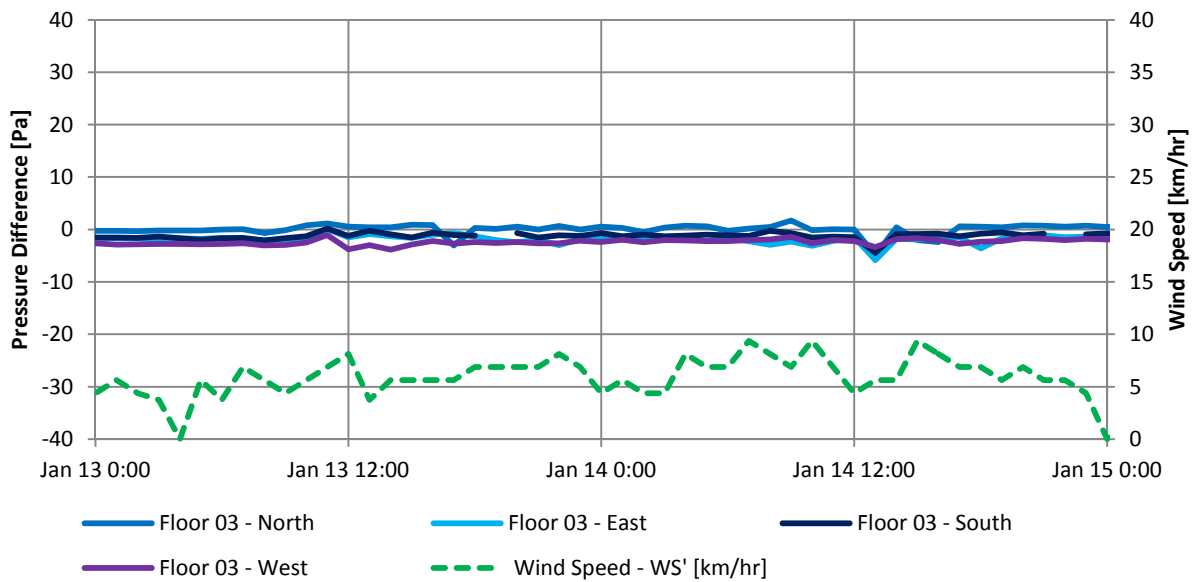


Figure 10-16: Graph of hourly pressure differences across exterior enclosure at Floor 3 during light east wind

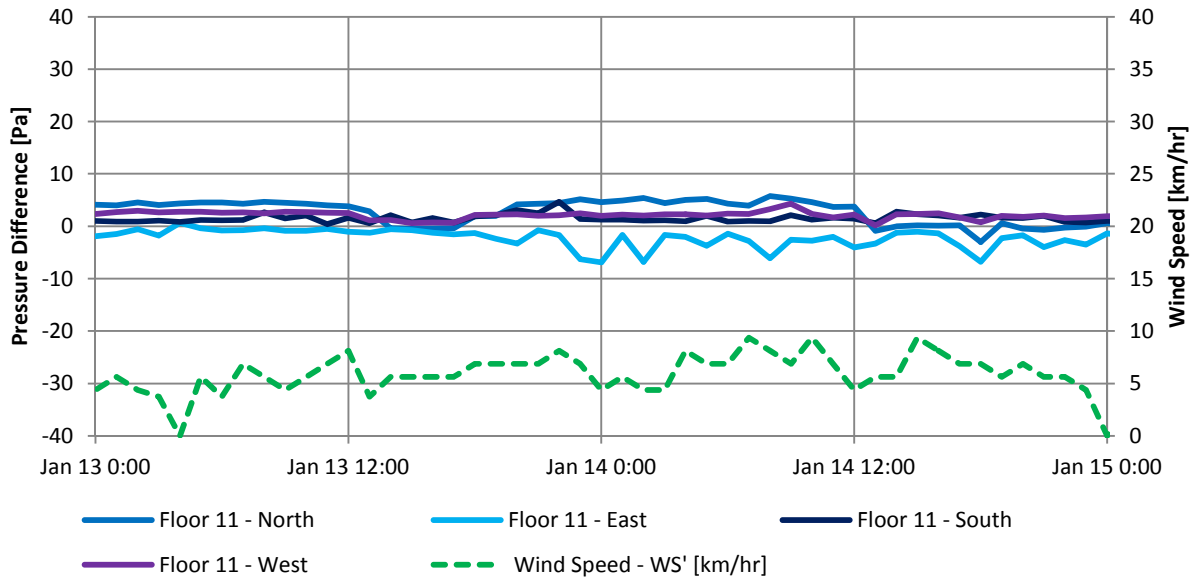


Figure 10-17: Graph of hourly pressure differences across exterior enclosure at Floor 11 during light east wind

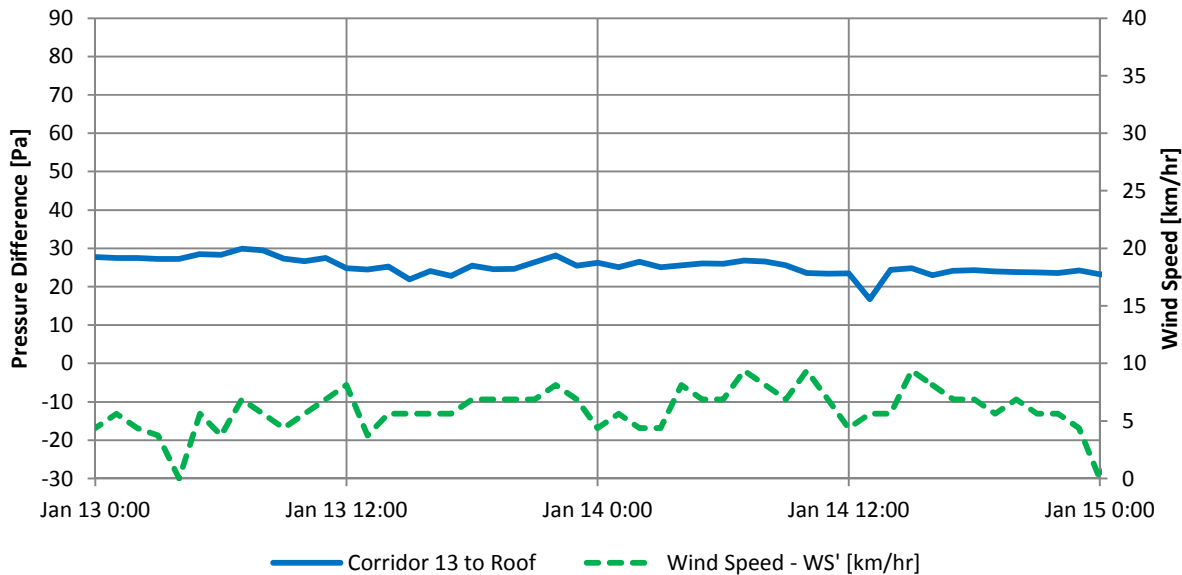


Figure 10-18: Graph of hourly pressure difference across exterior enclosure from Corridor 13 to roof during light east wind

The three preceding graphs show that during light east wind the pressure differences across the enclosure of the building are relatively stable; however, the pressure measured across the enclosure on the east elevation on Floor 11 is slightly lower (more negative) reaching pressures of approximately -7 Pa. This negative pressure reading is consistent with a light easterly wind.

The results for this particular time period are typical of results for periods of light easterly winds at the case study building.

10.2.2.3 Moderate East Wind

A period of moderate easterly wind speeds (approximately 10 km/hr with peak hourly average wind speeds up to 20 km/hr) was identified from December 24th, 2012 at noon, to December 26th, 2012 at noon. The wind speed and exterior temperature during this period are provided in Figure 10-19, the wind direction is provided in Figure 10-20, and the wind speed squared is provided in Figure 10-21. During this period, scaffolding was still in place on much of the building; however, similar effects were noted during other periods of moderate east wind after the scaffolding was removed.

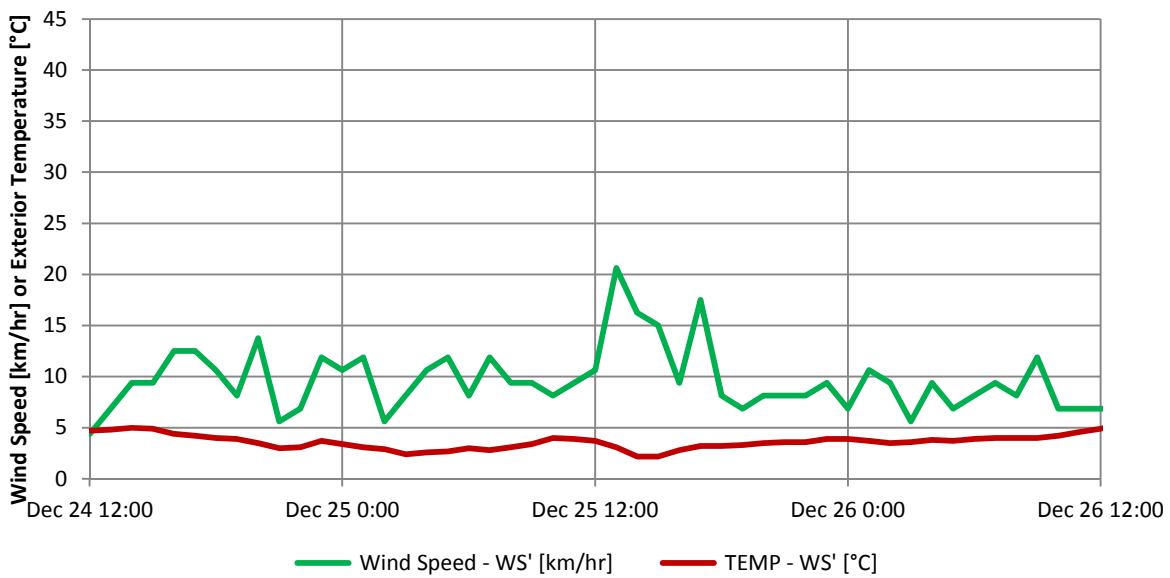


Figure 10-19: Graph of wind speed and exterior temperature during period of moderate east wind

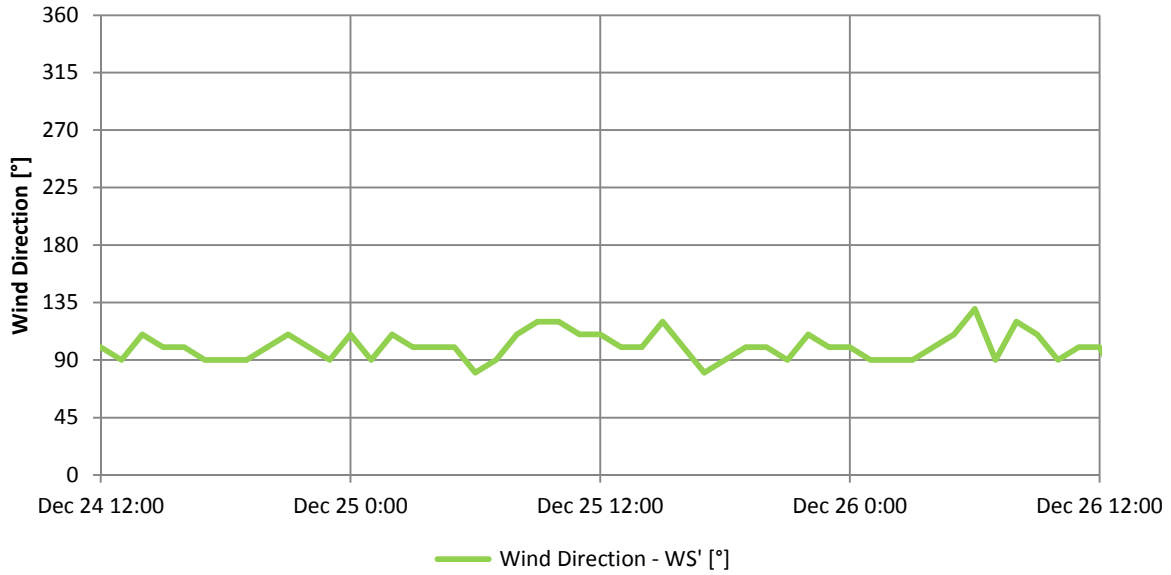


Figure 10-20: Graph of wind direction during period of moderate east wind

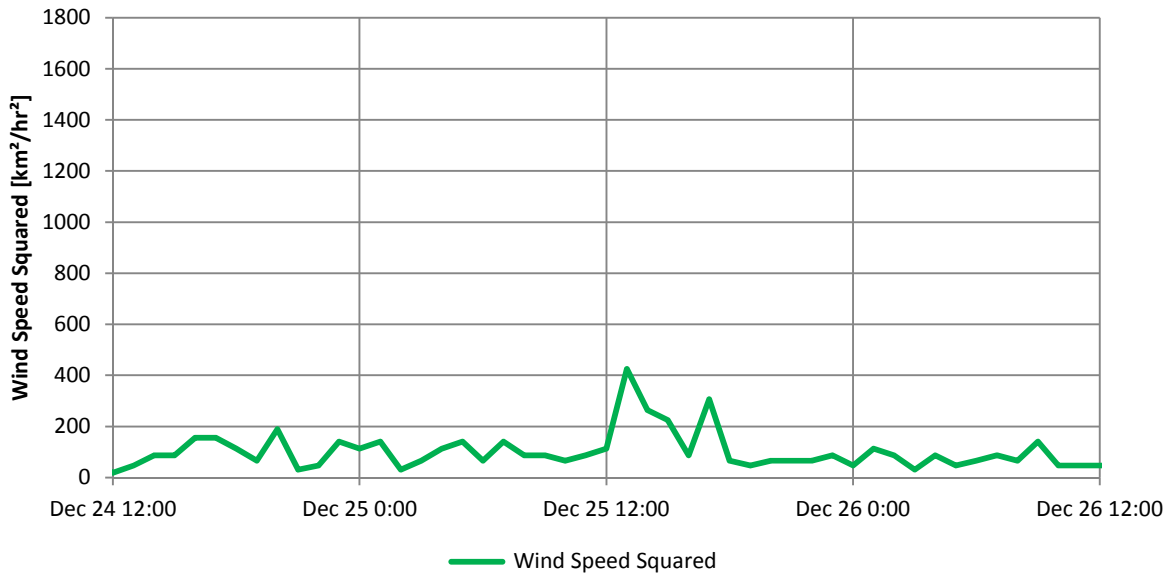


Figure 10-21: Graph of wind speed squared during period of moderate east wind

The pressures measured across the exterior enclosure at Floors 3, 11, and 13 are provided in Figure 10-22, Figure 10-23, and Figure 10-24 respectively.

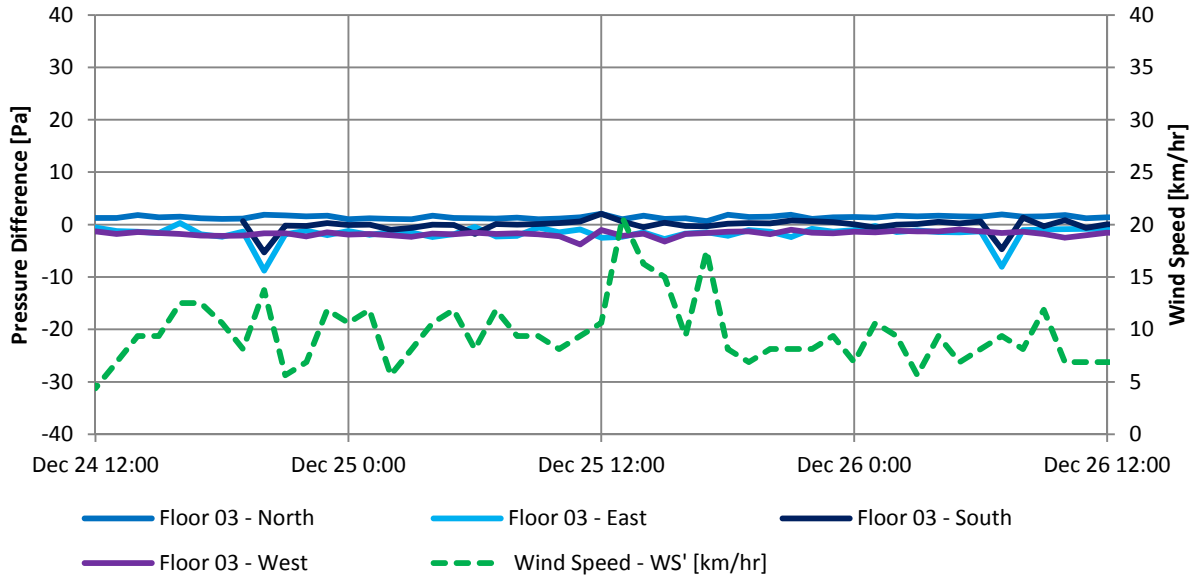


Figure 10-22: Graph of hourly pressure differences across exterior enclosure at Floor 3 during moderate east wind

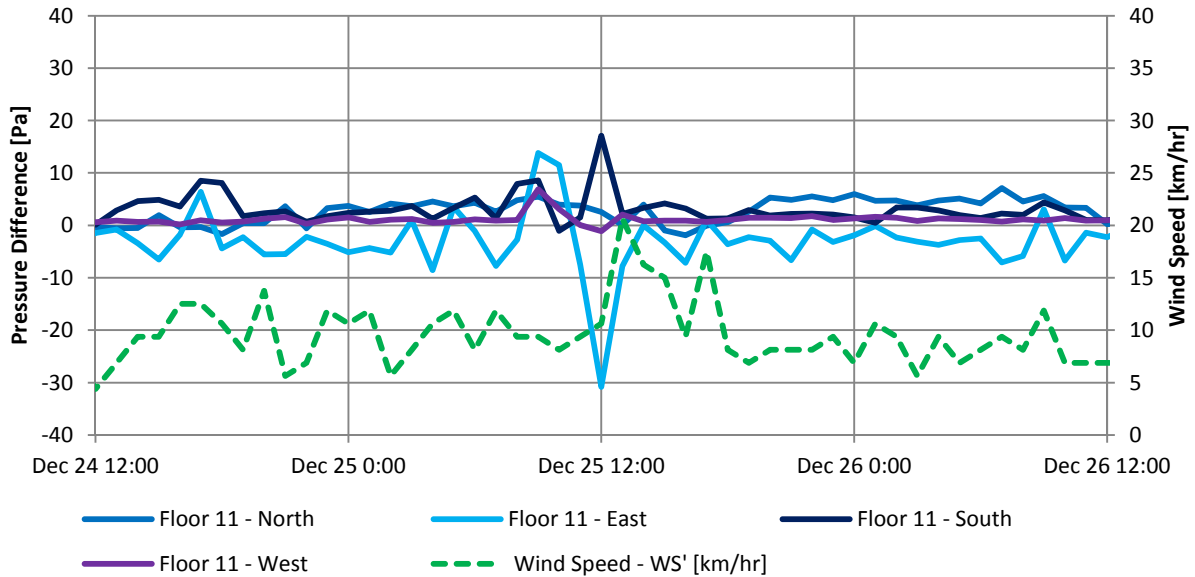


Figure 10-23: Graph of hourly pressure differences across exterior enclosure at Floor 11 during moderate east wind

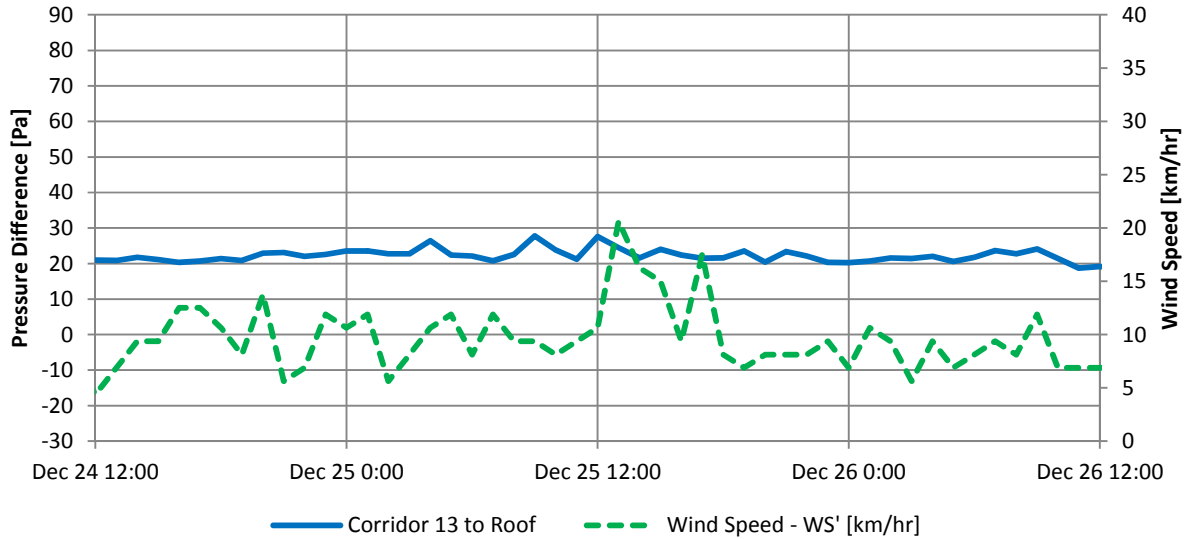


Figure 10-24: Graph of hourly pressure difference across exterior enclosure from Corridor 13 to roof during moderate east wind

The three preceding graphs show that, as one would expect, during moderate east wind the pressure differences across the enclosure of the building are less stable than during light and minimal wind conditions. Additionally, the pressure differences measured across the enclosure increase in magnitude with the east elevation experiencing the peak pressure magnitude. Very little change in the pressure difference across the enclosure is observed at Floor 3 during this period of moderate east wind, and this is likely a result of the lower floor of the building being more sheltered by surrounding buildings, trees, et cetera, and the lower wind speeds at lower heights due to the atmospheric boundary layer. The local shielding of the case study building is shown in Figure 10-25.



Figure 10-25: Image of North and East elevations of the case study building showing surrounding trees that provide local shielding with respect to wind

The peak negative pressure (outside higher than inside) observed on the east elevation at Floor 11 is approximately -31 Pa, and the peak positive pressure is observed on the south elevation and is approximately 17 Pa. Both of these spikes in pressures correspond approximately with the peak hourly average wind speed of 20 km/hr.

It is important to note the significant increase in pressure differences observed due to the increase in wind speeds from approximately 10 km/hr to 20 km/hr. The east elevations pressure differences change from approximately -6 Pa to -30 Pa as a result of this increase in wind speed. This is a reflection of the proportional relationship between the square of the wind velocity and potential pressure created by the wind. Since the wind doubles in speed, one would expect the pressures observed to increase by approximately a factor of 4. In this case they have increased by approximately a factor of 5. Because this factor is greater than 4, it suggests that at lower wind pressures, other driving forces may have a larger impact on the pressure across the building enclosure, and at higher wind speeds, wind becomes the dominant driving force.

Some fluctuation in the pressure across the roof is noticeable with the pressure from the corridor on Floor 13 to the exterior above the roof increasing by approximately 8 Pa during the periods of peak hourly wind speeds (which means the interior became more pressurized relative to the exterior). This period, however, is during the time that the exterior pressure tap was not connected to the pressure tube; consequently, it is likely that the measured pressure difference is less than the

actual pressure difference across the roof in some areas, as the pressure tap during this monitoring was located on the west side of a mechanical penthouse.

The results of this time period are typical of the results observed for moderate easterly winds at the case study building.

No instances of strong east winds were observed during the monitoring period.

10.2.2.4 Moderate West Wind

A period of moderate westerly wind speeds (ranging from approximately 5 km/hr to peak average hourly wind speeds up to approximately 20 km/hr) was identified from January 28th, 2013 to January 22nd, 2013. The wind speed and exterior temperature during this period are provided in Figure 10-26, the wind direction is provided in Figure 10-27, and the wind speed squared is provided in Figure 10-28.

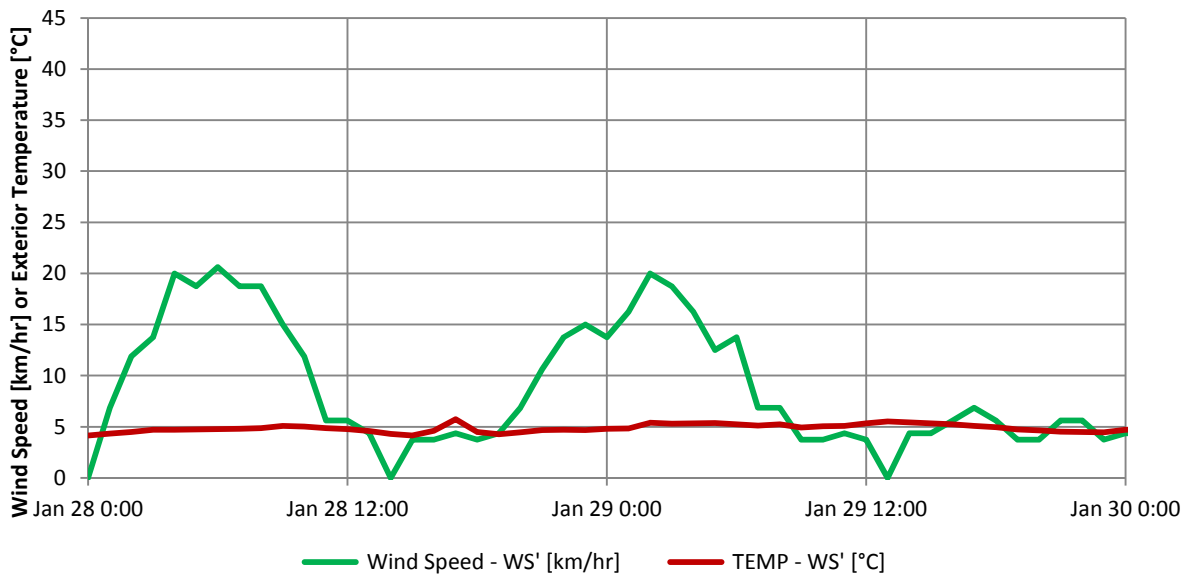


Figure 10-26: Graph of wind speed and exterior temperature during period of moderate west wind

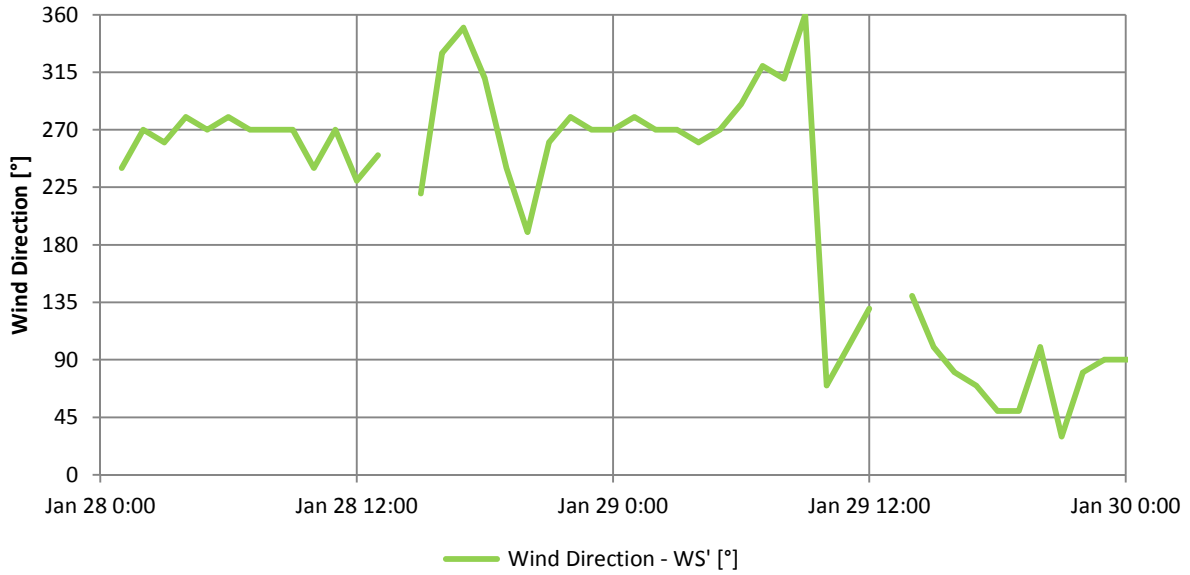


Figure 10-27: Graph of wind direction during period of moderate west wind

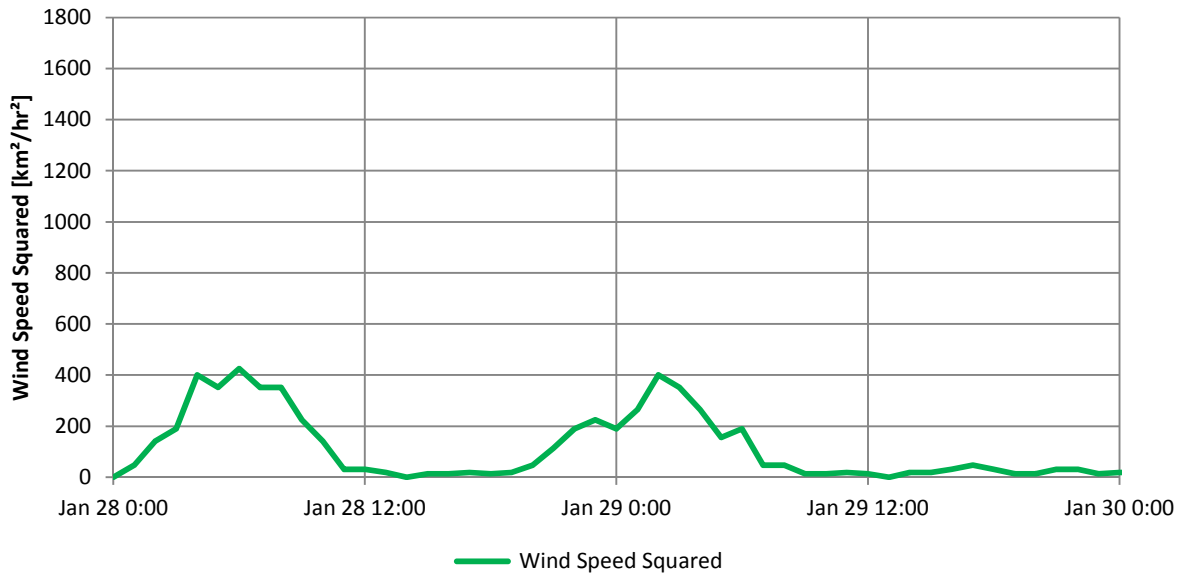


Figure 10-28: Graph of wind speed squared during period of moderate west wind

The pressures measured across the exterior enclosure at Floors 3, 11, and 13 are provided in Figure 10-29, Figure 10-30, and Figure 10-31 respectively.

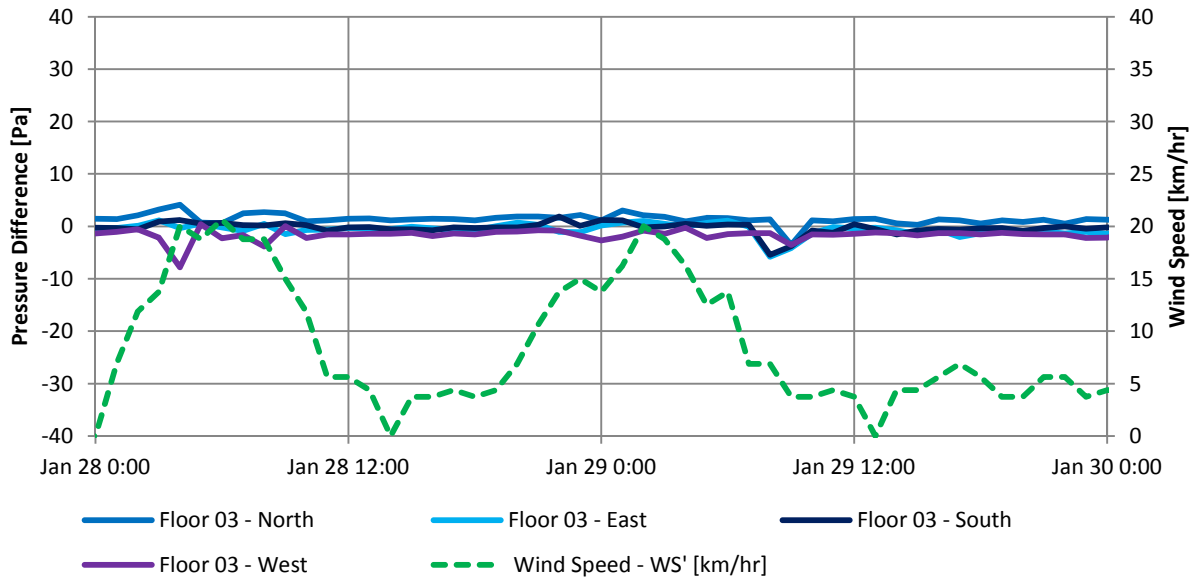


Figure 10-29: Graph of hourly pressure differences across exterior enclosure at Floor 3 during moderate west wind

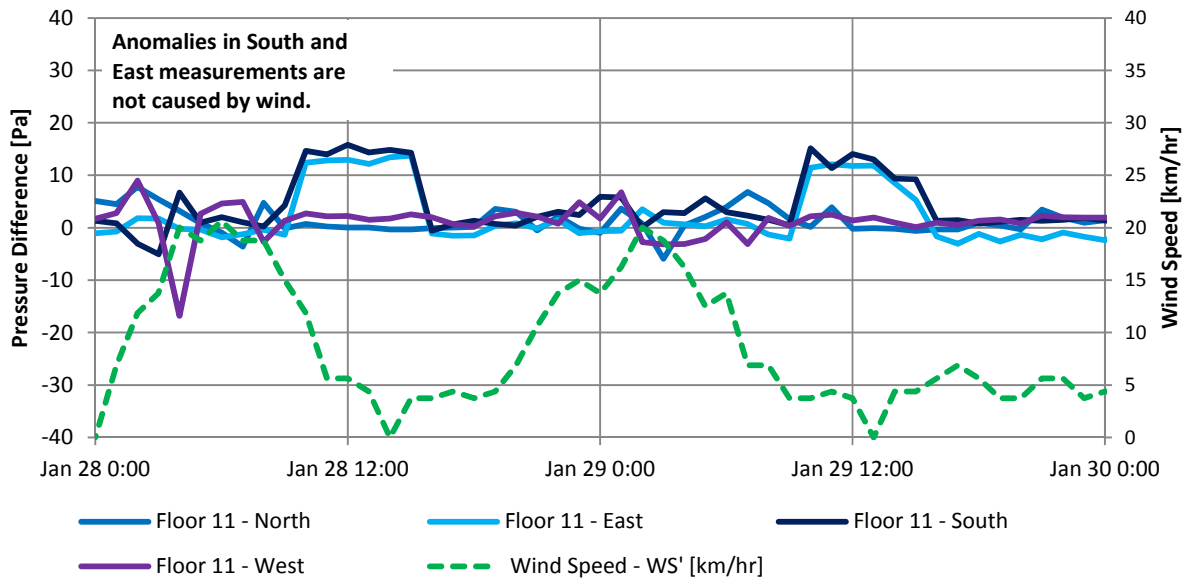


Figure 10-30: Graph of hourly pressure differences across exterior enclosure at Floor 11 during moderate west wind

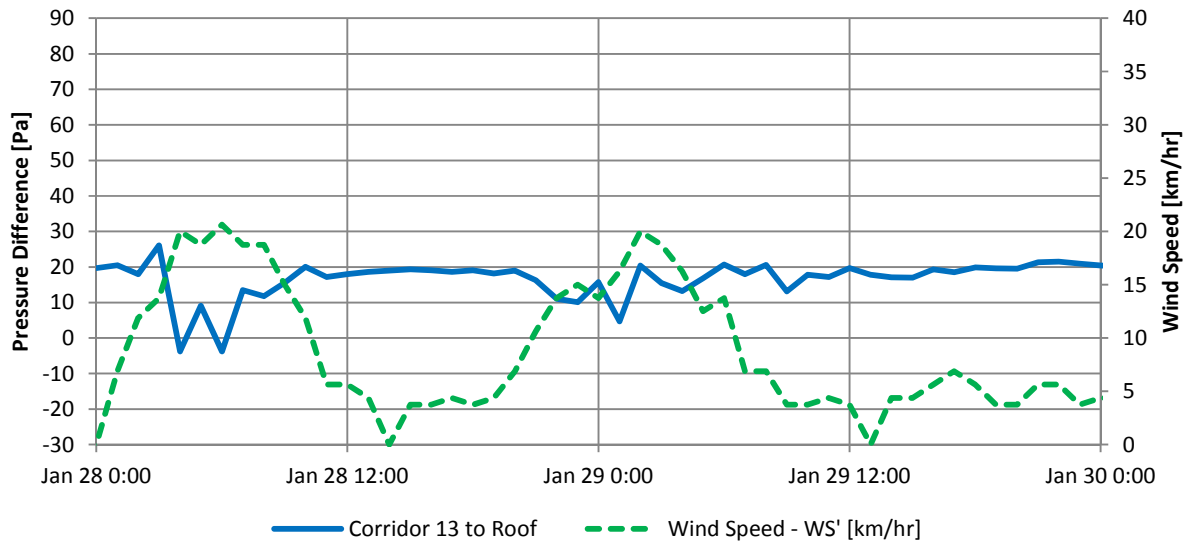


Figure 10-31: Graph of hourly pressure difference across exterior enclosure from Corridor 13 to roof during moderate west wind

The three preceding graphs illustrate that during a moderate west wind the pressure differences across the enclosure of the building are less stable than in periods of light and minimal wind conditions which is consistent with the findings during easterly winds. In the interval during which the peak hourly average wind speed was approximately 20 km/hr, the pressure across the building enclosure on the west elevation of the building decreased by approximately 15 Pa at Floor 11, and a smaller decrease of approximately 6 Pa occurred at Floor 3. This is similar to the results for a moderate east wind where it was observed that likely local shielding and less height resulted in the lessened influence of the wind on pressures at the lower part of the building.

The exterior pressure tap was not yet installed on the roof during this period; consequently, west winds were recorded as creating a more negative pressure reading (outside higher pressure than inside); however, this is likely a result of the pressure tube being located on the west (windward) side of a mechanical penthouse. In actuality, the pressure across the roof of the building likely became more positive as a result of the wind as shown in Section 10.2.2.5 for a strong west wind case.

Note that the increased pressures of the “Floor 11 – East” and “Floor 11 – South” sensors are a result of an anomaly discussed in Appendix E, and are not due to wind.

The results of this particular time period are typical of the results observed for moderate westerly winds at the case study building.

10.2.2.5 Strong West Wind

A period of strong westerly wind speeds (approximately ranging from 5 km/hr to peak average hourly wind speeds up to approximately 40 km/hr) was identified from April 25th, 2013 to May 2nd, 2013. The wind speed and exterior temperature during this period are provided in Figure 10-32,

the wind direction is provided in Figure 10-33, and the wind speed squared is provided in Figure 10-34. Note that the strong west wind occurs primarily on April 29th, 2013.

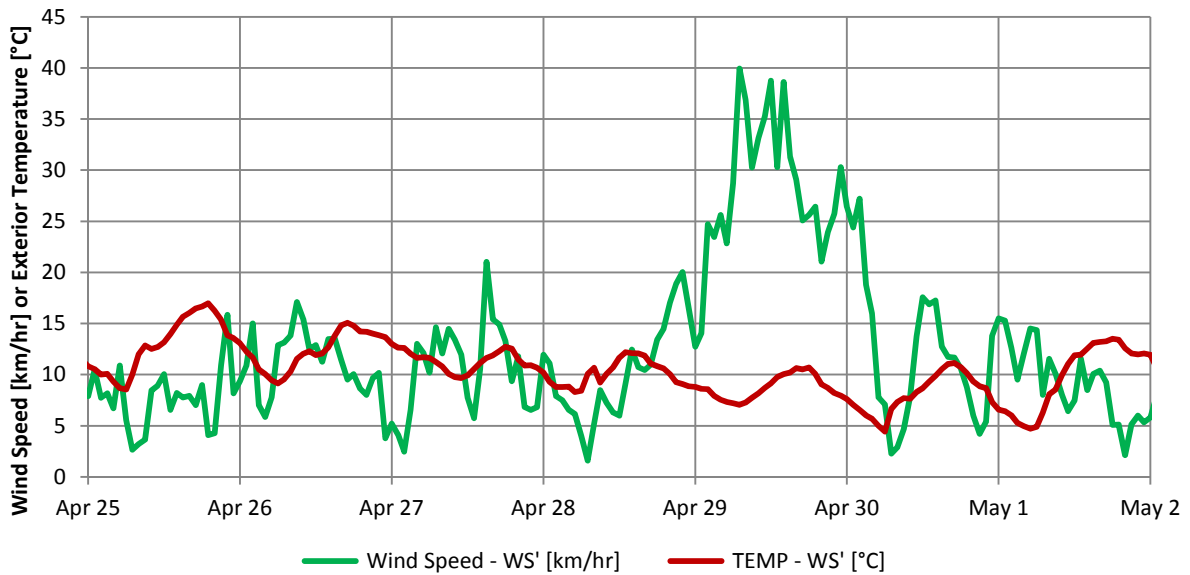


Figure 10-32: Graph of wind speed and exterior temperature during period of moderate west wind

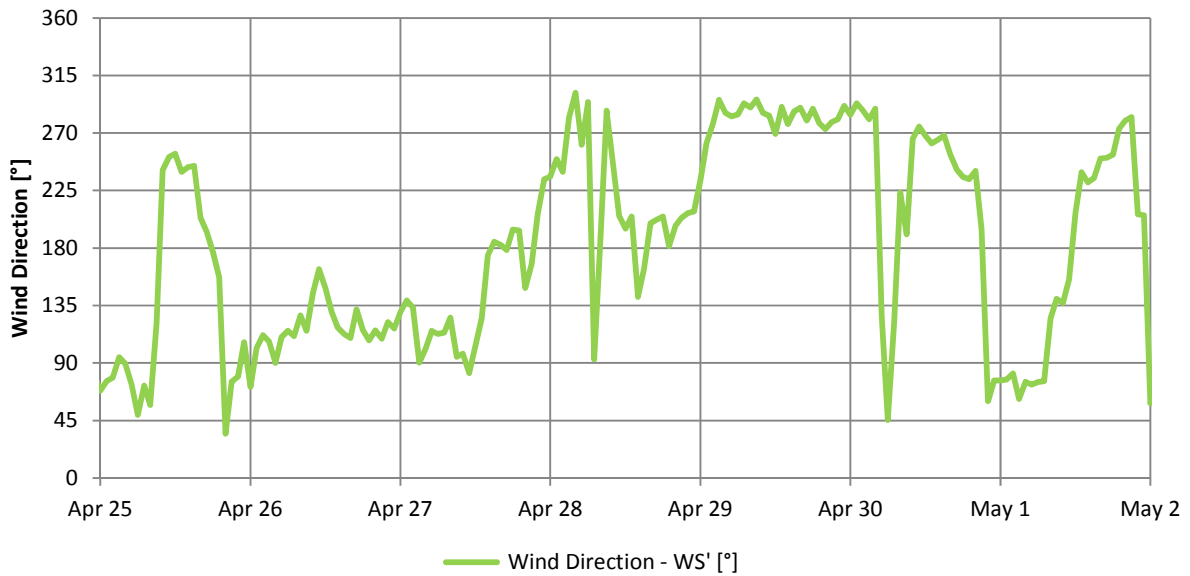


Figure 10-33: Graph of wind direction during period of moderate west wind

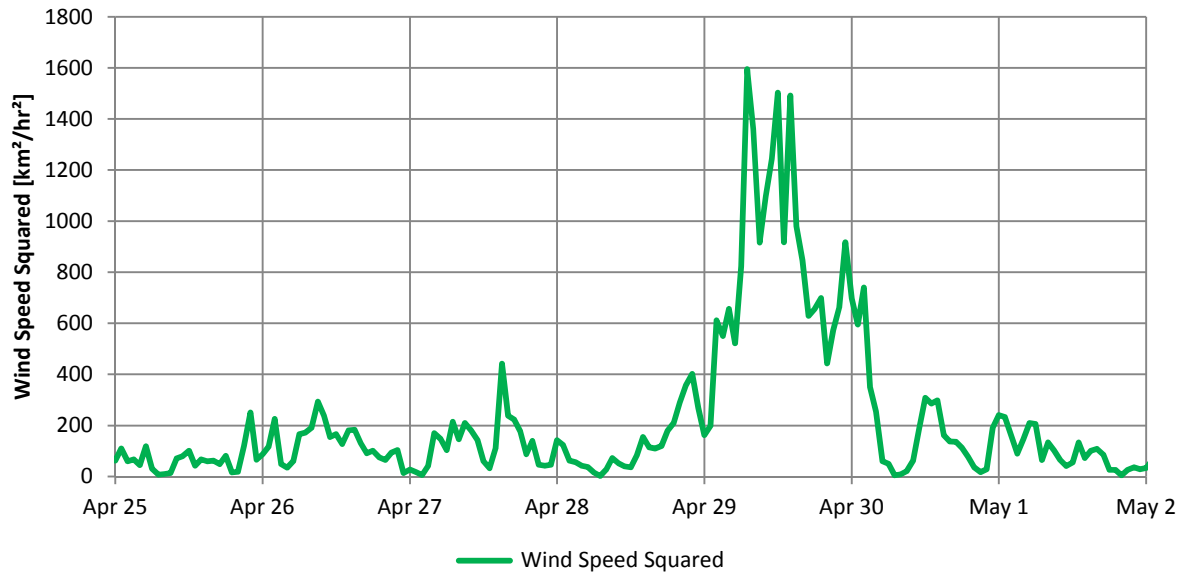


Figure 10-34: Graph of wind speed squared during period of moderate west wind

It is important to note the significant increase in wind energy available to create pressures as a result of the higher wind speeds. The 40 km/hr winds provide 4 times more potential for creating pressures than the “moderate” wind speeds of 20 km/hr, and 16 times more than the “light” wind speeds of 10 km/hr. This is reflected in the observed pressure results, especially those across the roof.

The pressures measured across the exterior enclosure at Floors 3, 11, and 13 are provided in Figure 10-29, Figure 10-30, and Figure 10-31 respectively.

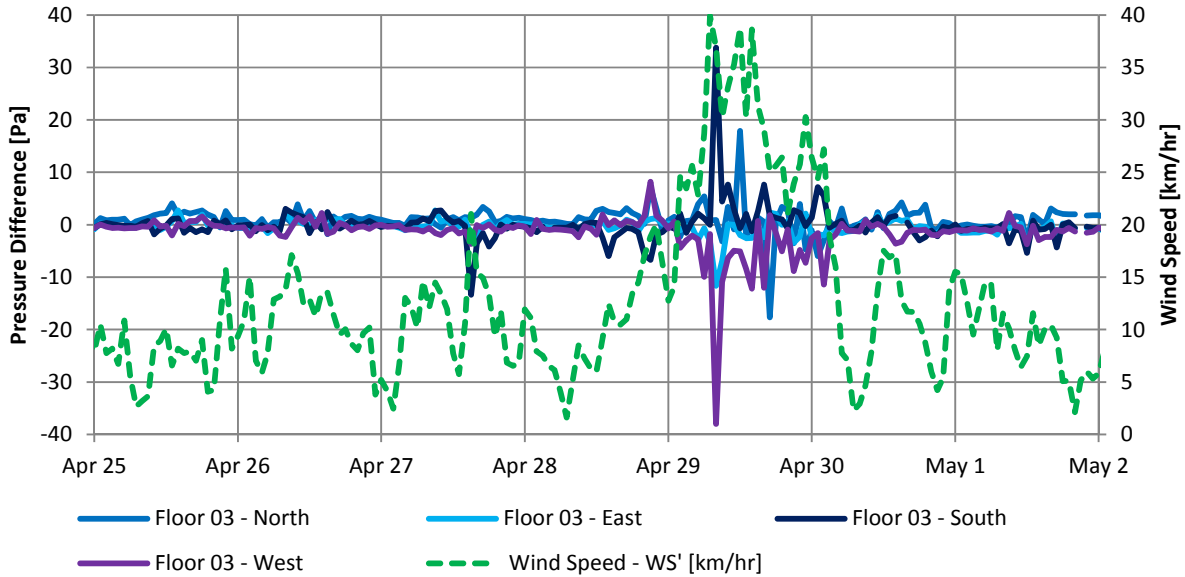


Figure 10-35: Graph of hourly pressures differences across exterior enclosure at Floor 3 during moderate west wind

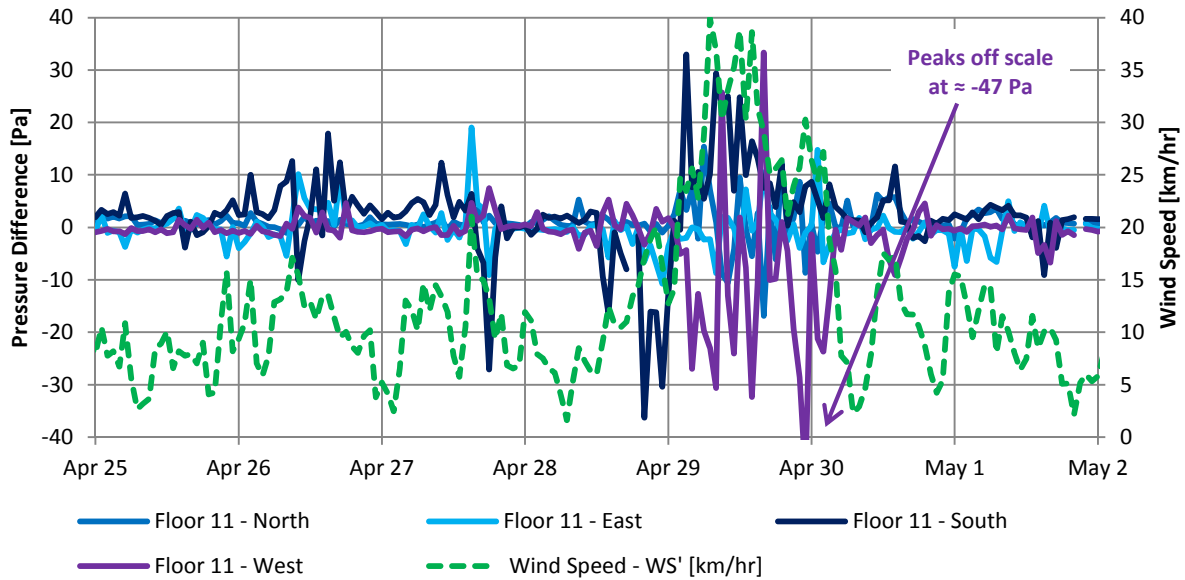


Figure 10-36: Graph of hourly pressure differences across exterior enclosure at Floor 11 during moderate west wind

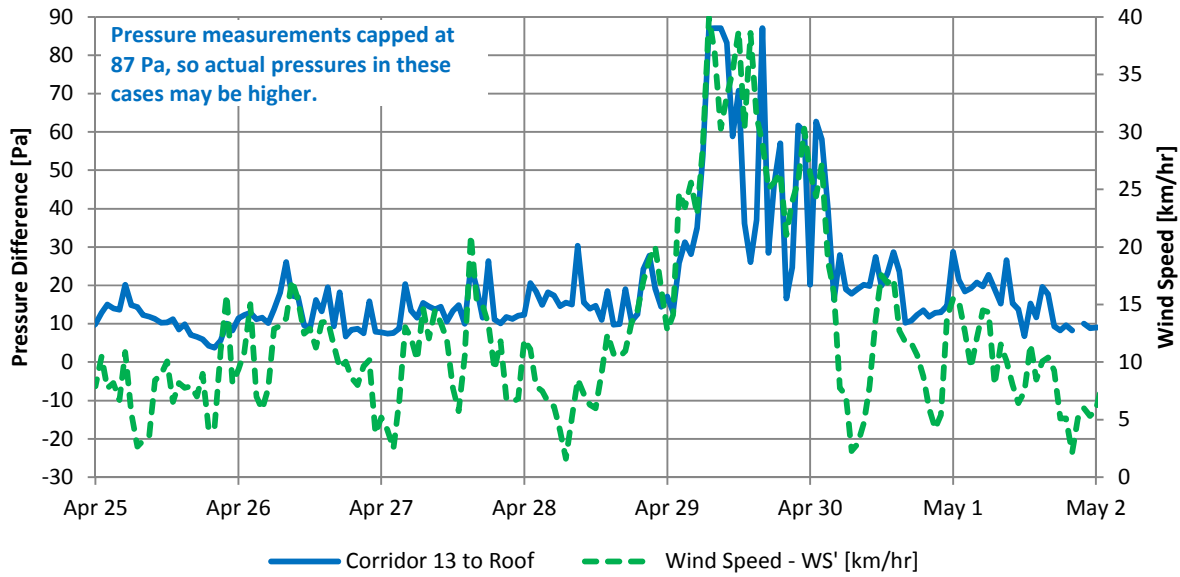


Figure 10-37: Graph of hourly pressure difference across exterior enclosure from Corridor 13 to roof during moderate west wind

The three preceding graphs illustrate that during periods of strong west winds the pressure differences across the building enclosure can change significantly and have large variability. During periods corresponding with the peak average hourly wind speeds of approximately 39 km/hr, pressure spikes can be noted at Floor 3, Floor 11, and the roof.

At Floor 3, the pressure difference across the west elevation decreases to approximately -40 Pa and the pressure difference on the south elevation increases (interior pressurized relative to exterior) up to approximately 34 Pa during this period of moderate west wind. Given that the wind is from a west-north-west direction, the significant positive pressure difference measured at the south elevation is expected. One would expect to measure a decrease in the pressure difference across the east face; however, this was not observed in this case.

At Floor 11 the pressure difference across the west elevation of the enclosure peaks at a -47 Pa (which drives infiltration of air) and reaches pressures of -20 Pa to -30 Pa multiple times throughout the day on April 29th. During a brief period when the wind is from the south at the end of the day on April 28th, suction pressures on the south elevation peak at approximately 30 to 35 Pa and these correspond with wind speeds of approximately 15 to 20 km/hr. There is significant variability in the pressures measured across the enclosure during this windy period, with positive pressures up to approximately the 25 to 33 Pa range on both the west and south elevations.

At the roof, the pressure measurements spike very positive reaching 87 Pa multiple times during the day. The calibrated operating range of the pressure sensors is less than a 63 Pa pressure difference, and the monitoring equipment caps the reading at 87 Pa. Consequently, the reliability of the measurements at this high a pressure difference is uncertain and the actual pressures may in fact be higher than recorded. These sensors were selected for their accuracy at lower pressures rather than their ability to measure high pressures as pressure differences of lower magnitude are of primary concern for this research.

The pressure in Corridor 13 is significantly higher than above the roof during period of high winds. This is the only case presented here for which the roof pressure tap was mounted correctly to the weather station tripod; however, similar pressure differences were also measured across the roof during other periods of moderate and strong westerly winds, which reinforce the findings here.

The large pressure differences created by the strong westerly wind have the potential to drive significant short-term airflow into, out of, and within the building, and can affect the interior building pressure regime.

The results of this particular time period are typical of the results observed for strong westerly winds at the case study building.

10.2.3 Summary of Exterior Enclosure Results

Overall, pressure differences across the vertical elements of the exterior enclosure (i.e. walls) were found to be low (typically under 10 Pa) and highly dependent on wind speed and direction, whereas exterior temperature (i.e. stack effect) had little to no influence (much less than 5 Pa). During periods of moderate to high wind speeds larger pressure differences (of not more than approximately 100 Pa) were developed across the exterior enclosure with windward elevations typically experiencing pressure that acted from the exterior to the suites (inward), and leeward and perpendicular elevations experiencing pressures acting from the suites to the exterior (outward). This is consistent with predictions based on previously discussed physics and findings in literature. However, the pressure differences were also found to be highly variable with respect to wind with periods of strong and moderate winds often creating significant fluctuations in pressure difference, both positive and negative. The high pressures created by wind on the exterior enclosure have significant potential to drive exfiltration and infiltration. Given that the pressure differences due to wind were typically higher at the upper parts of the case study building than at lower parts (likely due to a combination of local shielding and atmospheric boundary layer effects), wind likely causes significantly more infiltration and exfiltration at upper parts of the building than lower parts of the building. This supports findings of higher exfiltration and infiltration rates measured as part of the PFT testing presented in Chapter 8.

The pressure differences measured across the roof of the case study building were found to typically be positive (higher pressure in corridor than above roof) and these pressure differences were strongly correlated with the exterior temperature. Colder exterior temperatures created higher pressure differences, and the pressure differences were found to be near zero when exterior temperatures were approximately the same as interior temperatures. Wind typically created positive pressure differences across the roof (outward acting) and in moderate and strong wind conditions these pressure differences were often large (up to approximately 100 Pa) creating a significant driver of exfiltration from upper zones of the building.

10.3 Corridor-to-Corridor Pressure Differences

The pressure differences between corridors are discussed in this section including their relationship to the natural driving forces of airflow.

10.3.1 Corridor-to-Corridor Pressure Differences and Exterior Temperature

To assess the relationship between exterior temperature and the pressure differences observed between corridors, Figure 10-38 graphs the 24-hour moving average exterior temperature with the pressure differences from each of the corridors to Corridor 13.

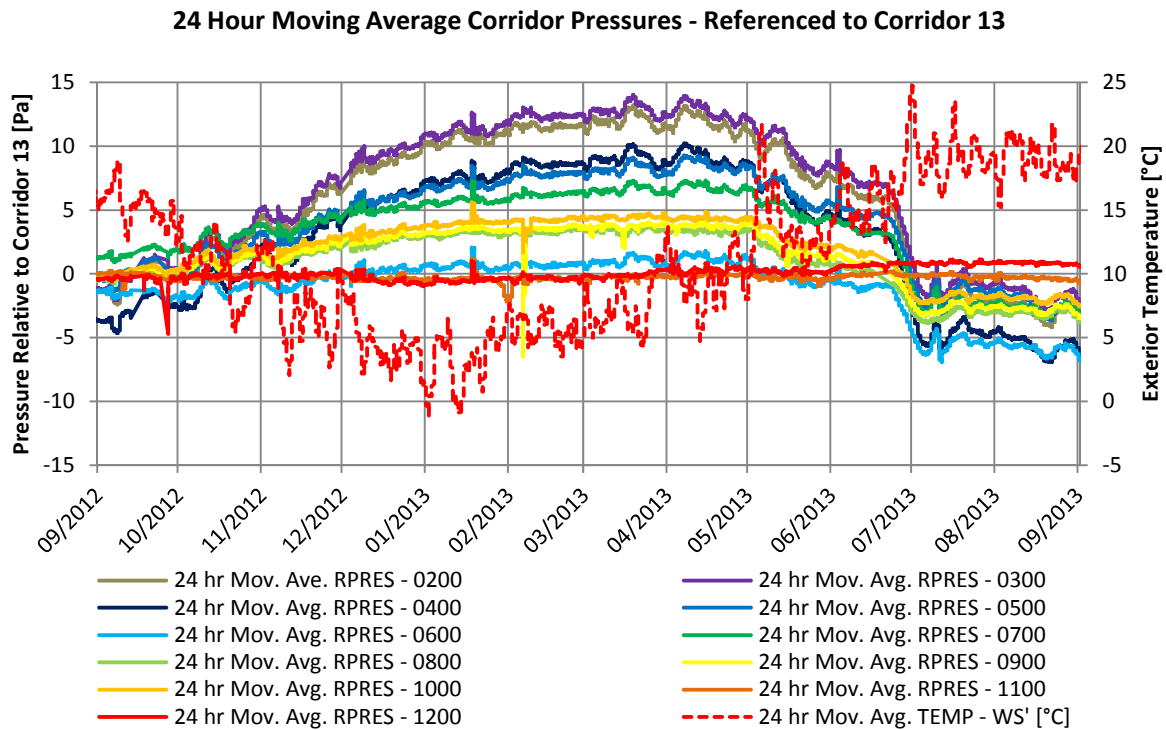


Figure 10-38: Graph of 24 hour moving average corridor pressures referenced to Corridor 13

This figure illustrates a seasonal correlation between the corridor pressure distribution and exterior temperature with decreases in exterior temperatures typically creating an increase in pressure on lower floors relative to upper floors, and the opposite response occurs for increases in temperature which is consistent with stack effect. Seasonally, the 24 hour moving average temperature varied from approximately 25°C to -1°C and the pressure differences from approximately -6 Pa to 14 Pa for the lower corridors relative to Corridor 13. This corresponds with approximately 0.8 Pa change in pressure per 1°C change in temperature for the lower floors, and less for higher floors.

The seasonal change in pressure differences appears to lag changes in exterior temperature as peak pressure differences occurred in March and April whereas the lowest exterior temperatures occurred in January. The cause of this seasonal lag is unknown and is particularly unclear as later sections of this chapter establish a relationship between exterior temperature and corridor-to-corridor pressure on a shorter time scale of weeks and days. Also, the change of the direction of stack effect due to the increase in exterior temperature at the beginning of July 2013 is unexpectedly fast with no apparent lag.

One theory for explaining this lag is that there may be some drift in the pressure sensors over time when subjected to a consistent pressure difference. This could cause the measured pressure to continue to increase after the actual peak pressure difference has occurred. The direction and magnitude of the corridor-to-corridor pressure differences are more consistent than many of the other pressure measurements in this study which may also increase the likelihood of drift in these sensors. Also, these pressure differences are determined by addition of multiple sensors which potentially makes the measurements more sensitive to drift if multiple sensors drift in the same direction. Based on field checks of the pressure sensors, significant drift was only noticed in some sensors while others demonstrated little to no drift. It was not possible to determine whether this was the cause of the observed lag in pressure differences, but it is important to recognize this potential source of error. While drift in the sensors may be a cause of the lag, it is unlikely that drift would significantly affect the general conclusions regarding the relationship of corridor-to-corridor pressure differences and exterior temperature.

Another possible explanation for the lag is that as the building retrofit was completed it changed the characteristics of the building leading to increased stack effect pressures between floors; however, work on the air barrier was completed in September 2012 and the scaffolding was removed by the end of January 2013, approximately 2 months before the peak recorded pressure differences. Additionally, increased airtightness of the exterior enclosure would more likely decrease the pressure differences acting across the floors of the building. Consequently, it is unlikely that the retrofit caused the lag in pressure differences.

A number of the corridor-to-corridor pressure sensors exhibited unusual measurement trends as shown Figure 10-39 which plots the corridor-to-corridor pressure differences. PRES-0400, PRES-0500, PRES-0700, and PRES-1000 all measured a similar seasonal pressure difference pattern, and PRES-0600 measured a similar but opposite pattern. These sensors all measured pressure changes seemingly correlated with exterior temperature (except for the noted lag). At the start of July 2013 all of these sensors measured a relatively quick change in pressure difference and then measured a nearly constant pressure differences for the remainder of the monitoring period. While this trend may be due to changes in exterior temperature, the constant pressure difference measured starting in July indicates that other factors may be influencing these measurements. Overall, the cause of this anomalous pressure trend is unknown.

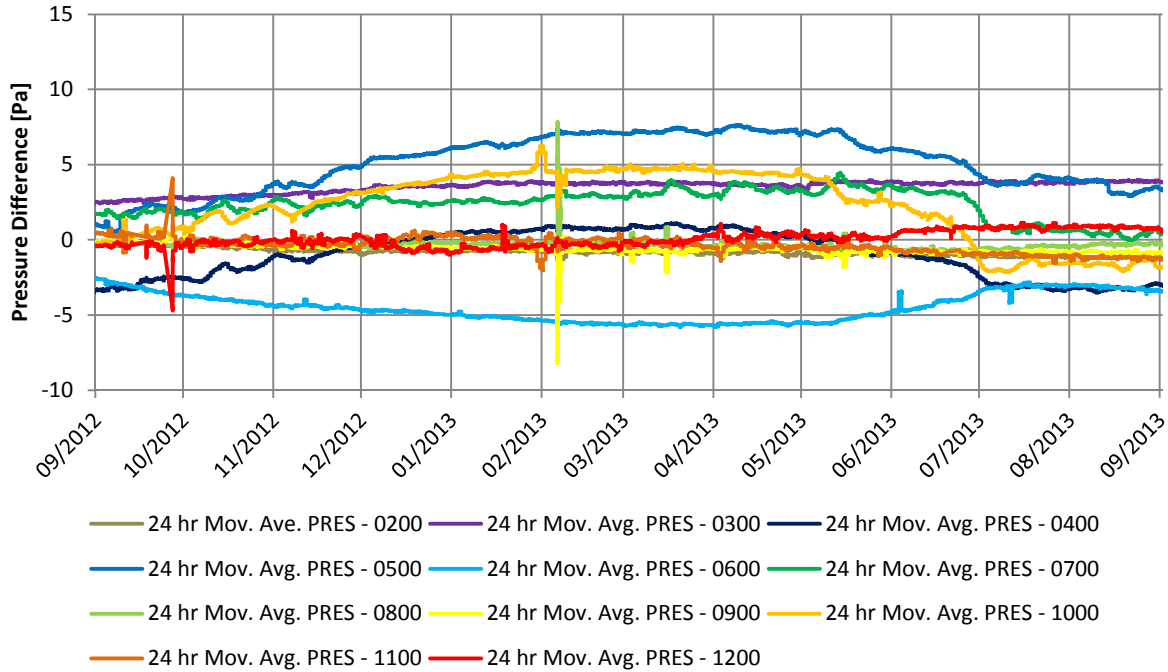


Figure 10-39: Graph of 24 hour moving average corridor-to-corridor pressure differences

The correlation between exterior temperature and the corridor pressures relative to Floor 13 is also apparent on a weekly basis as shown in Figure 10-40 which shows the exterior temperature and 24 hour moving average of pressure differences relative to Corridor 13.

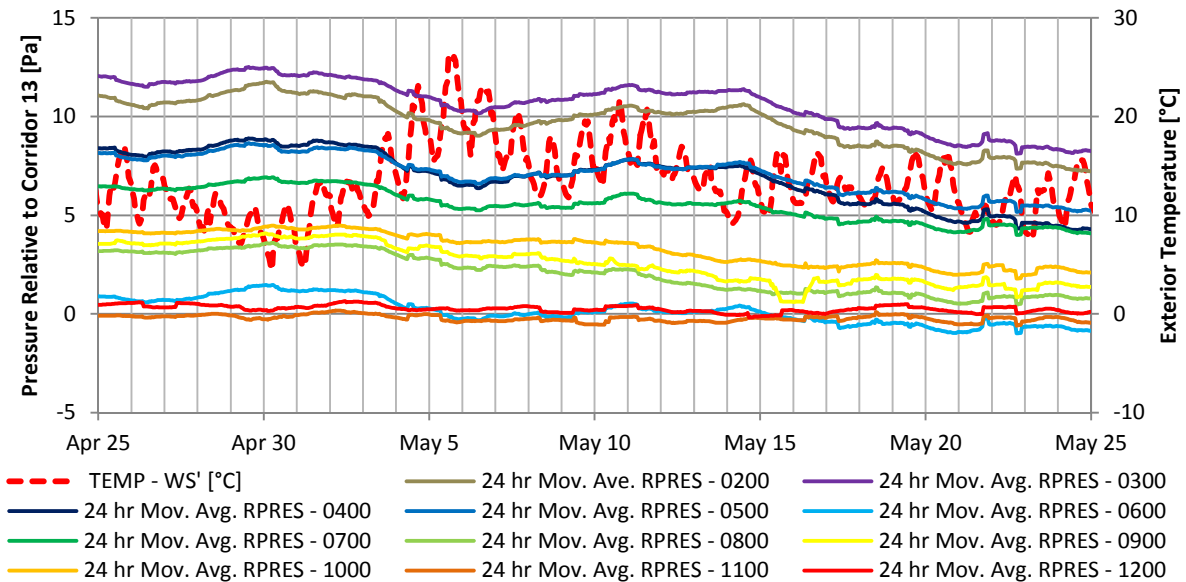


Figure 10-40: Graph of 24 hour moving average corridor pressures referenced to Corridor 13

Figure 10-40 shows that the pressure differences between corridors vary with exterior temperature over the short-term with no lag. Despite this short-term correlation, the lag can be

noted over a longer time as the pressure differences at the start of the period (April 25, 2013) are generally of larger magnitude than the pressure differences at the end of the period shown (May 25, 2013) even though the exterior temperature at these points is approximately equal, and this is an indication of the noted seasonal lag.

No correlation between exterior temperature and corridor pressures distribution is apparent over the course of a day. This lack of correlation is likely in part due to the relatively small changes in pressures that are observed as a result of exterior temperature changes. On a daily basis, changes in temperature rarely exceeded 7 to 8°C and may not be large enough to create a noticeable change in pressure. However, even with the relatively small change in temperatures observed over the course of a day, one would still expect to see some correlation on a daily basis, but none was measured.

Additional consideration of the distribution of stack effect pressure differences across the exterior enclosure and the corridor to suite boundaries including the location of the neutral pressure plane and calculation of the thermal draft coefficient is provided in Section 10.7.

10.3.2 Corridor-to-Corridor Pressure Differences and Wind

As shown earlier, the exterior enclosure exhibited relatively strong relationships between wind speed, wind direction, and pressure differences; however, little to no correlation was observed between wind speed, wind direction, and corridor pressures. This is consistent with findings in literature that suggested that in general floors can be considered to act independently with respect to wind. (Shaw & Tamura, 1977)

The same wind events were examined as were examined for the exterior enclosure (Sections 10.2.2.1 to 10.2.2.5), and the only case which showed a noticeable change in pressure distribution as a result of wind was the case with strong west winds. The wind speed and direction for this case were shown previously in Figure 10-32 and Figure 10-33. The pressure differences from each corridor relative to Corridor 13 during this period are shown in Figure 10-41.

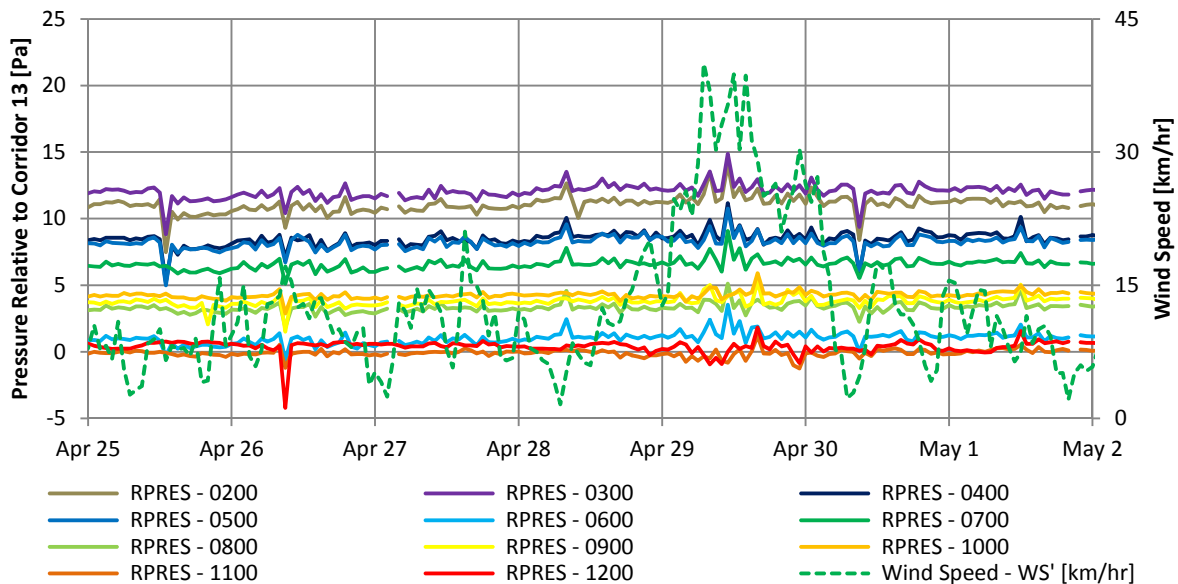


Figure 10-41: Graph of hourly corridor pressure referenced to Corridor 13 during strong west wind

During the strong west winds the corridor pressures of the lower floors becomes more variable with increases of approximately 3 Pa corresponding with the periods of strongest wind. Even at these relatively high wind speeds (approximately 40 km/hr), the variation in pressure is relatively low. Thus, wind is likely not a strong driver of airflow between floors of the building.

10.3.3 Summary of Corridor-to-Corridor Results

Corridor-to-corridor pressure differences at the case study building were found to be correlated with exterior temperature on a seasonal basis and to be less impacted by wind events. Consequently, the pressure measurements support the finding that floor to floor airflows at the case study building are primarily driven by stack effect. Generally, the pressure difference between two adjacent floors was found to be of relatively low magnitude which likely indicates that the corridors are well connected with respect to airflow. Based on the airtightness testing results presented earlier in Chapter 9, this connection is most likely through the elevator shaft and stairwells as the doors to these zones were found to be relatively air leaky.

10.4 Suite-to-Corridor Pressure Differences

This section assesses the pressures between the corridors and the suites at the case study building including the relationship with exterior temperature (stack effect) and wind. The pressure differences between suites and corridors were monitored on Floors 2, 3, 4, 10, 11, and 12. Note that positive pressure measurements reported here indicate that the suite is pressurized relative to the corridor.

10.4.1 Suite-to-Corridor Pressure Differences and Exterior Temperature

To assess the relationship between exterior temperature and the pressure differences observed between the suites corridors and the suites across floors between corridors, the 24 hour moving

average exterior temperature has been graphed with average suite-to-corridor pressures of the monitored floors in Figure 10-42.

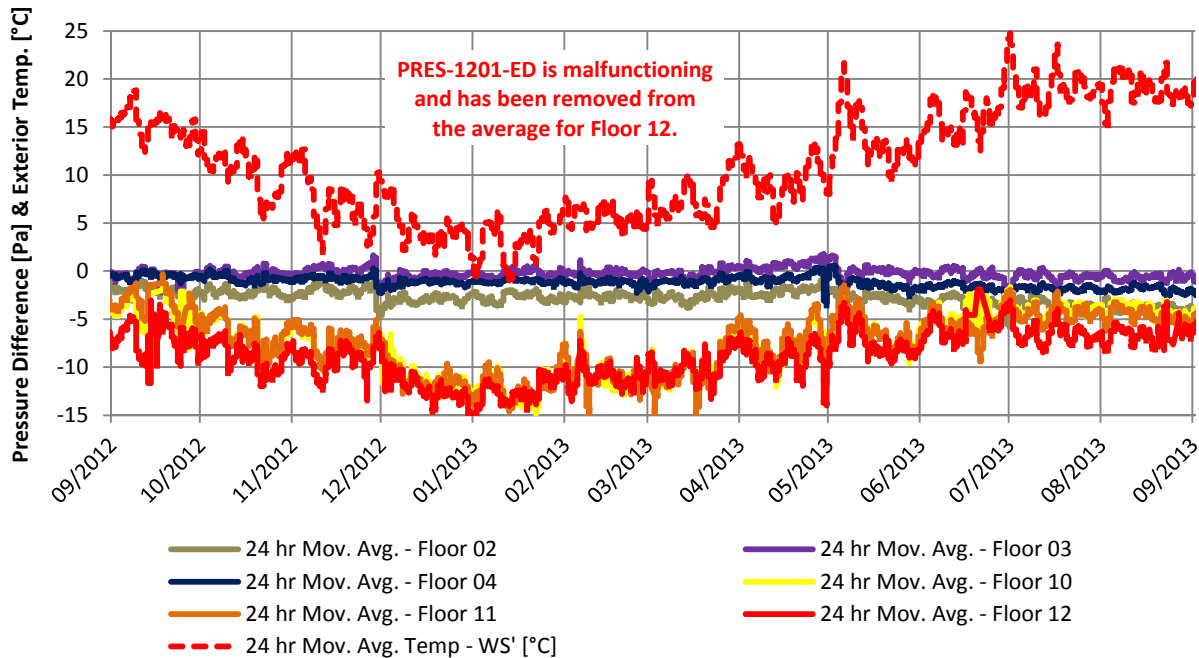


Figure 10-42: Graph of 24 hour moving average suite-to-corridor pressure differences averaged per floor and exterior temperature

Based on these monitoring results, it was found that the pressure differences from suites to corridors on upper floors show a strong seasonal correlation with exterior temperature. Suites become more depressurized relative to corridors during periods of colder temperatures. A seasonal change in 24 hour average temperature from approximately 20°C to near 0°C resulted in a decrease in the pressure of the suites on upper floors relative to the corridor by approximately 5 to 10 Pa. This is consistent with stack effect acting on the building's central stacks.

Note that the suite-to-corridor pressure sensor for Suite 1201 malfunctioned and its measurements have been removed from the average.

The pressure differences from suites to corridors on lower floors can also be observed to change with the exterior temperature; however, these changes are of relatively small magnitude so are primarily noticeable over shorter time periods as shown in Figure 10-43 and Figure 10-44.

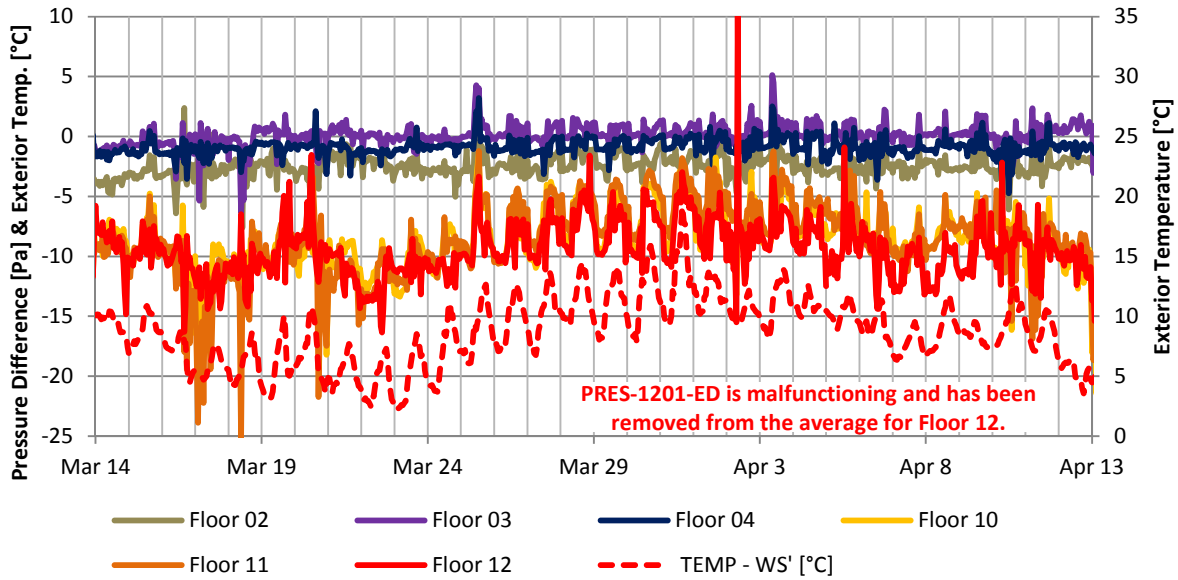


Figure 10-43: Graph of hourly suite-to-corridor pressure differences averaged per floor and exterior temperature for one month

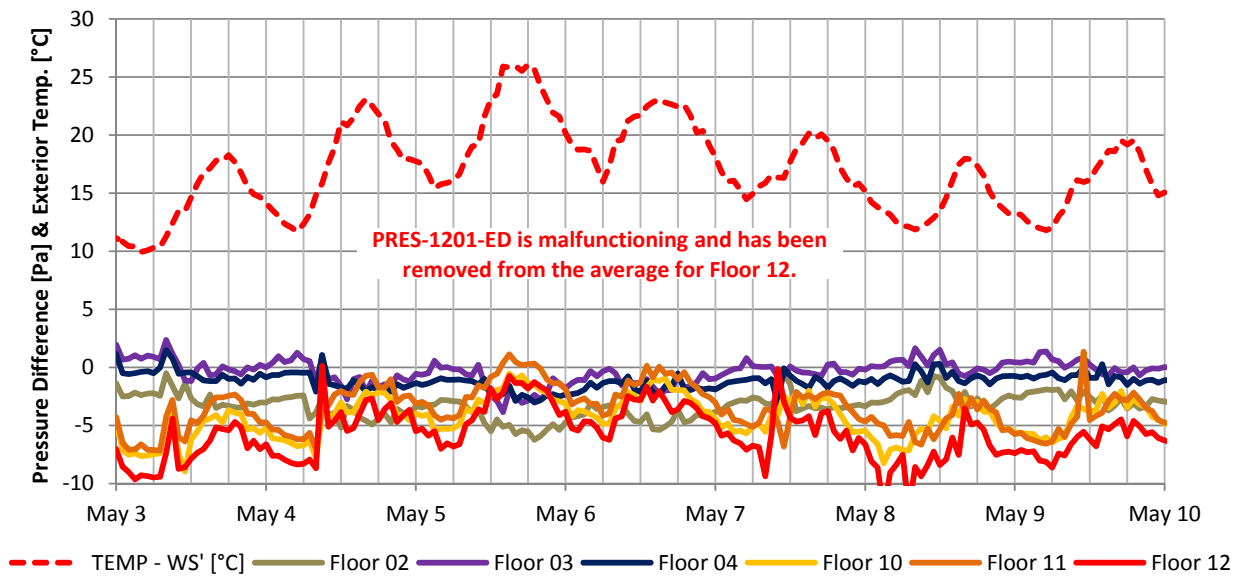


Figure 10-44: Graph of hourly suite-to-corridor pressure differences averaged per floor and exterior temperature for one week

In Figure 10-43 the pressure from the suites to the corridors on the upper floors can clearly be seen to vary with the exterior temperature on a daily and hourly time scale with decreases in temperature creating increases in the pressure acting from the corridors to the suites. On Floor 2, the opposite relationship was measured with increases in exterior temperature creating increases in the pressure acting from the corridors to the suites. This finding is consistent with the physics of

stack effect and likely indicates that Floor 2 is below the neutral pressure plane of the building during this period. The suite-to-corridor pressure differences on Floors 3 and 4 have little to no relationship with exterior temperature.

Later in this thesis (Section 10.7) analysis is performed to determine the location of the neutral pressure plane at the case study building and it is determined to be located on approximately the third or fourth floor of the building during relatively cold exterior temperatures. The closer neutral pressure plane is to a given floor, the less stack effect pressure is created. This is consistent with the finding that changes in exterior temperature create little to no change in pressure on Floors 3 and 4, some change in pressure on Floor 2, and larger changes in pressure on upper floors.

10.4.2 Suite-to-Corridor Pressure Differences and Wind

The relationship between wind speed, wind direction, and suite-to-corridor pressure differences was evaluated using the same periods of different wind magnitudes and directions as used with respect to the exterior enclosure. Consequently, graphs of wind speeds, direction, and exterior temperatures during these periods were provided in Section 10.2.2 and are not repeated here; however, wind speeds are overlaid on the pressure graphs.

Typically, during periods of minimal and light winds pressure differences between the suites and the corridors are relatively stable; however, the pressure differences from suites to corridors on upper floors are typically more variable than the pressure differences on the lower floors during these periods with little wind. These pressure differences are illustrated graphically in Figure 10-45 and Figure 10-46. The pressure spikes apparent in these figures are not likely as a result of wind, and are more likely as a result of window, door, and exhaust fan operation as discuss in Section 10.6.

During these periods, scaffolding was still in place on some of the building; however, similar effects were noted during other periods of similar wind conditions after the scaffolding was removed.

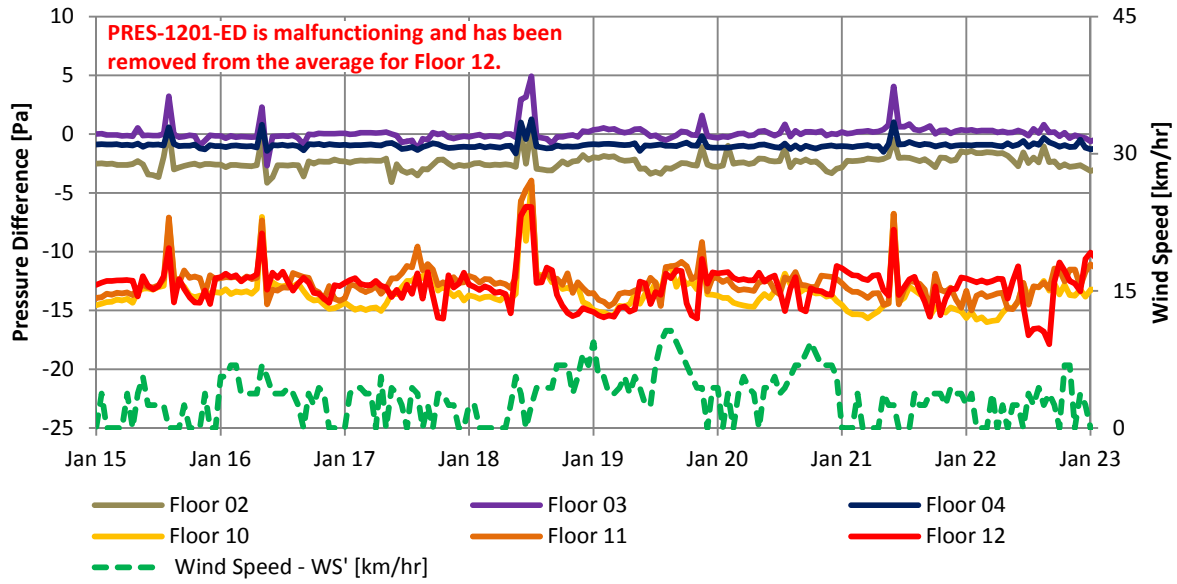


Figure 10-45: Graph of hourly suite-to-corridor pressure differences averaged per floor during minimal wind

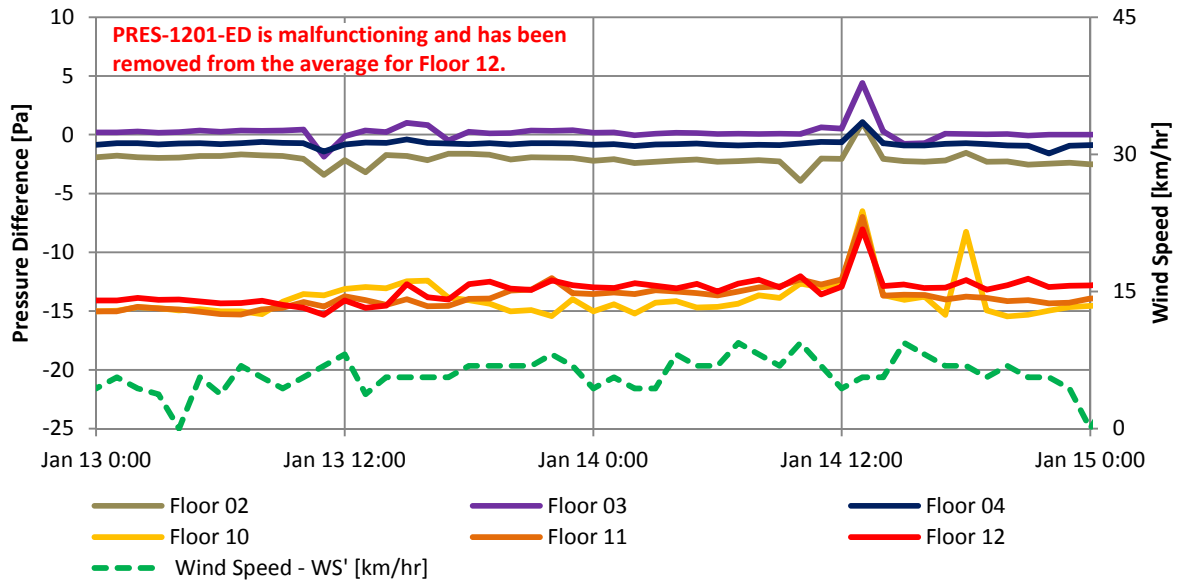


Figure 10-46: Graph of hourly suite-to-corridor pressure differences averaged per floor during light east wind

10.4.2.1 Moderate East Wind

A period of moderate easterly wind speeds (approximately 10 km/hr with peak hourly average wind speeds up to 20 km/hr) was identified from December 24th, 2012 at noon, to December 26th, 2012 at noon. The suite-to-corridor pressure differences for each floor are provided in Figure

10-47 to Figure 10-52, and the average suite-to-corridor pressure by floor are provided in Figure 10-53. During this period, scaffolding was still in place on much of the building; however, similar effects were noted during other periods of moderate east wind after the scaffolding was removed.

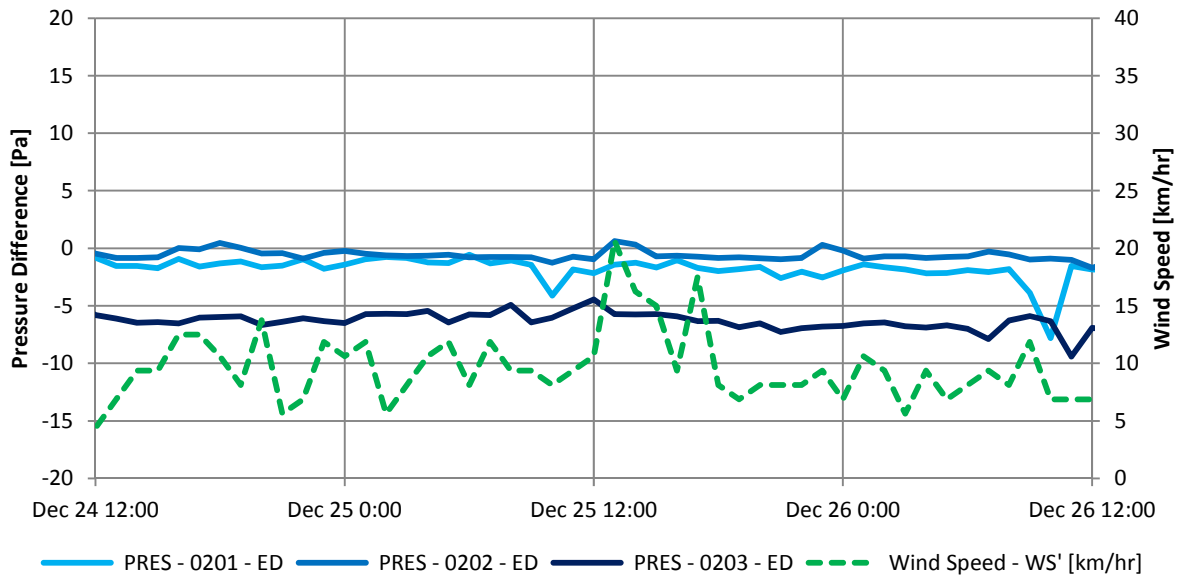


Figure 10-47: Graph of hourly suite-to-corridor pressure differences for Floor 2 during moderate east wind

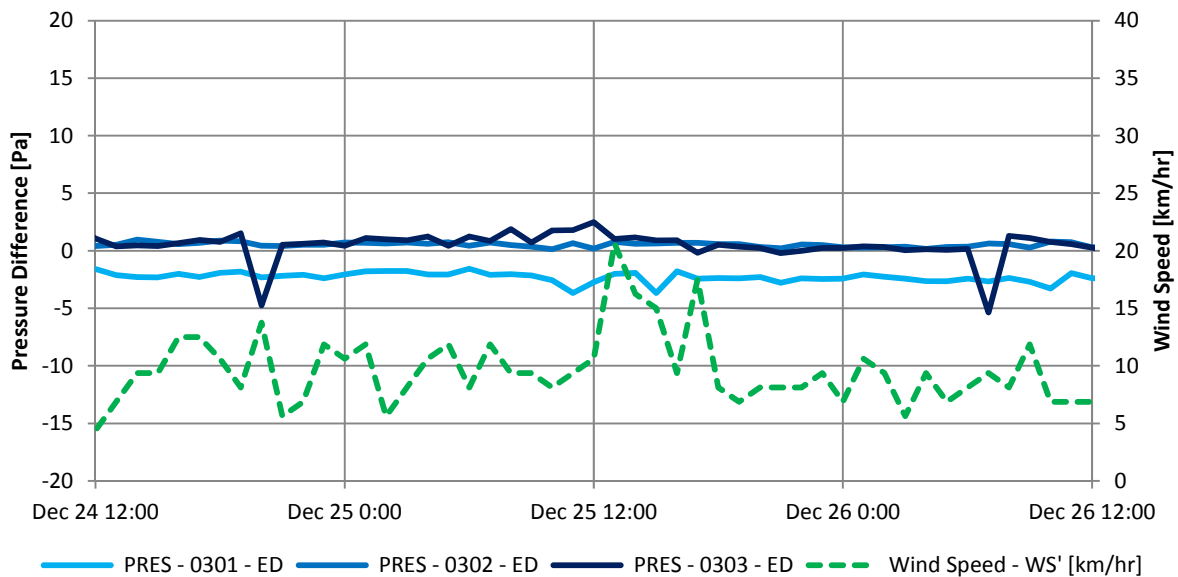


Figure 10-48: Graph of hourly suite-to-corridor pressure differences for Floor 3 during moderate east wind

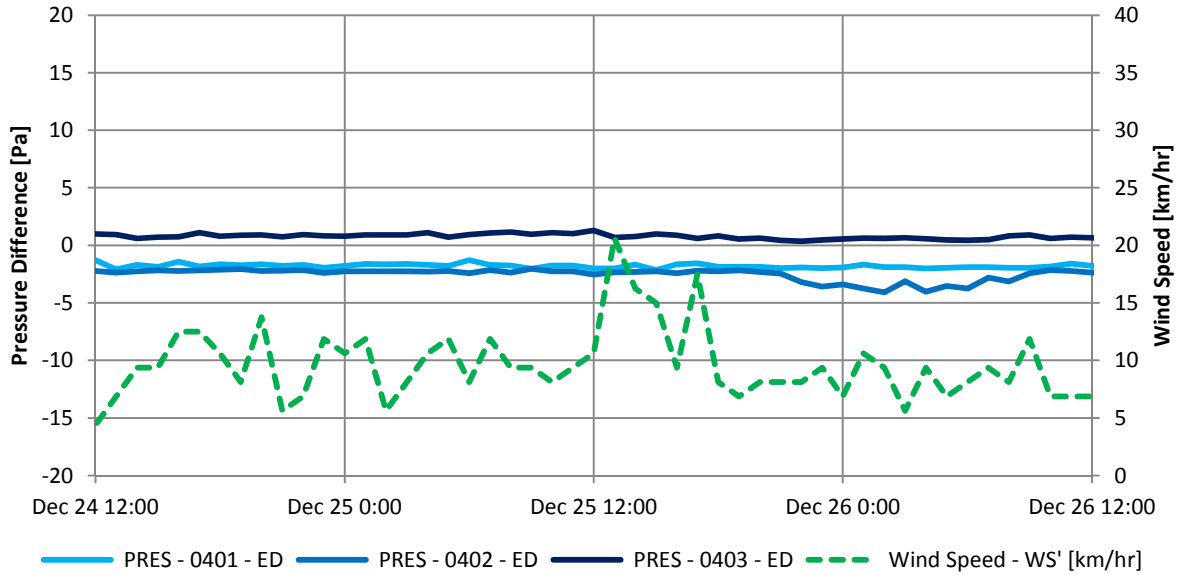


Figure 10-49: Graph of hourly suite-to-corridor pressure differences for Floor 4 during moderate east wind

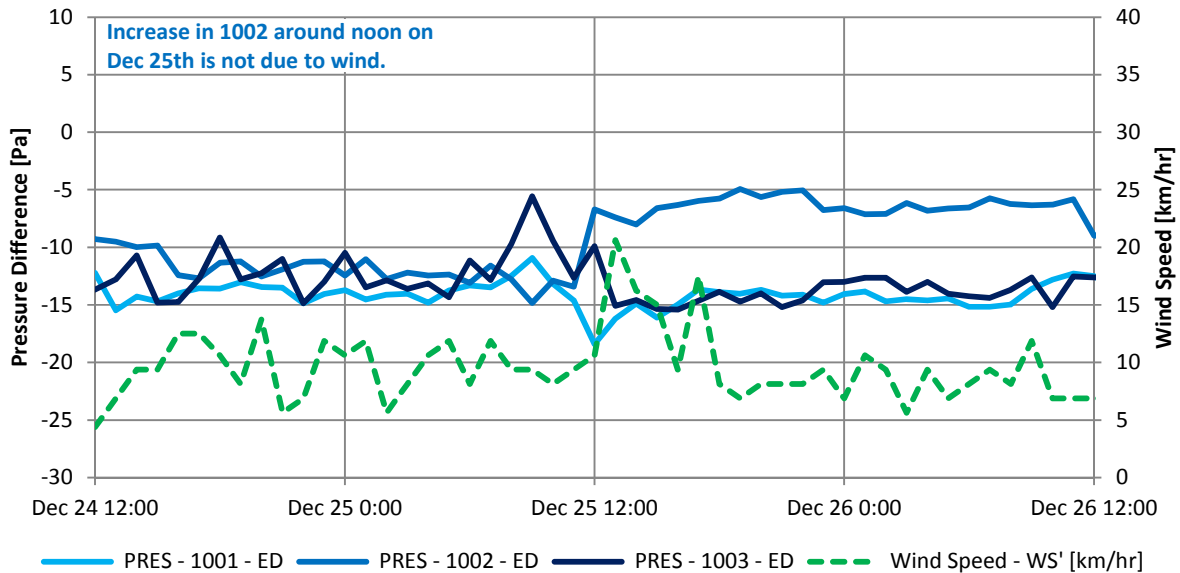


Figure 10-50: Graph of hourly suite-to-corridor pressure differences for Floor 10 during moderate east wind

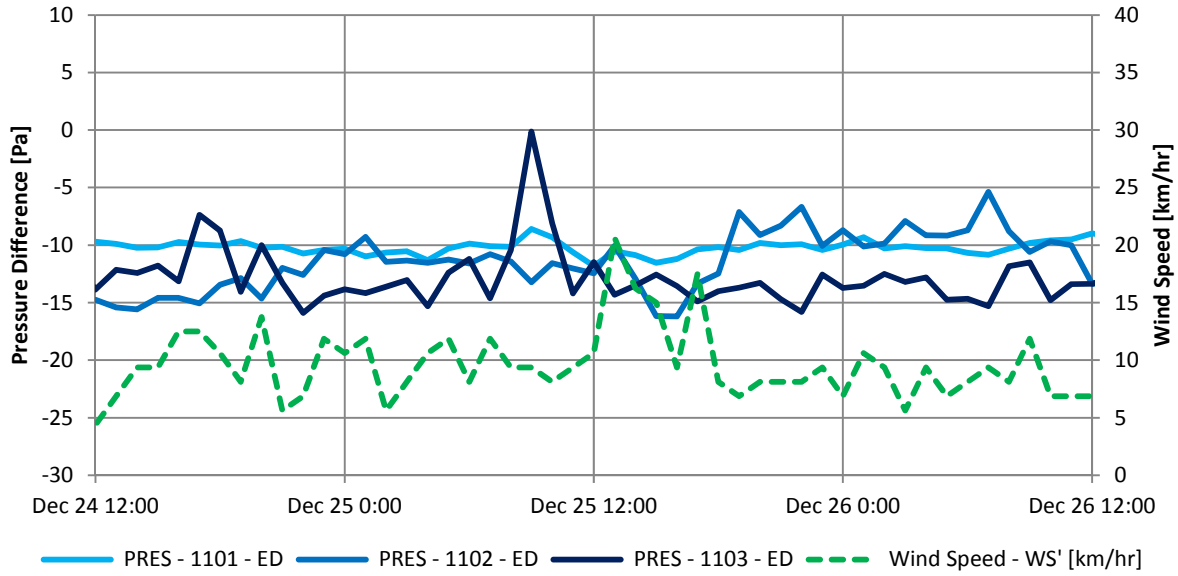


Figure 10-51: Graph of hourly suite-to-corridor pressure differences for Floor 11 during moderate east wind

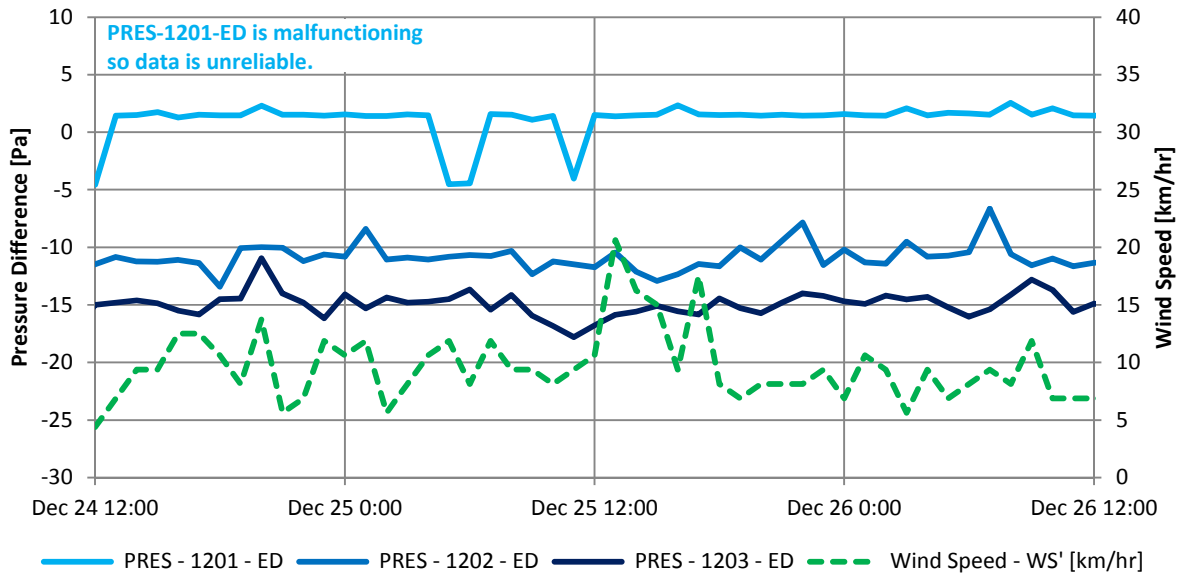


Figure 10-52: Graph of hourly suite-to-corridor pressure differences for Floor 12 during moderate east wind

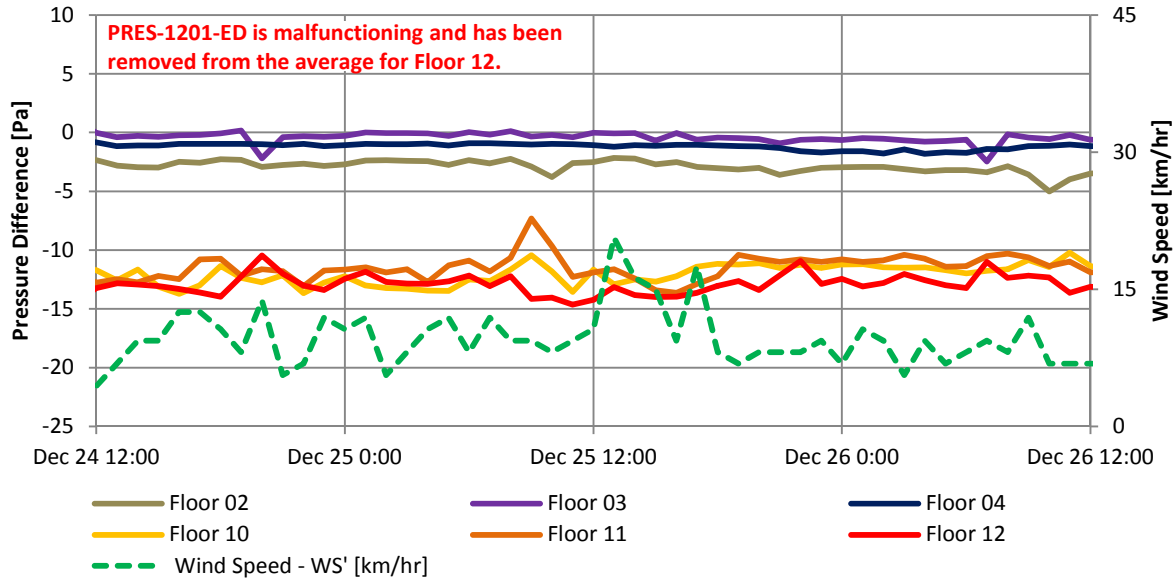


Figure 10-53: Graph of hourly suite-to-corridor pressure differences averaged per floor during moderate east wind

During this period of moderate east wind, the pressure difference from the suite to the corridor is noted to increase on east facing upper suites (-03 type suites), and little to no change is noted on lower floors which is consistent with findings for the exterior enclosure which suggested that sheltering of lower suites reduced the pressure differences created at these suites by wind. In Suite 1103 the pressure increases by approximately 14 Pa and in 1003 by approximately 8 Pa. Little to no change is noted in the pressure difference of 1203. It is likely that suites with more windward windows open would become more pressurized relative to the corridor.

The main increase in pressure during this period of moderate east wind occurred slightly before the period of strongest wind speeds. The cause of this is uncertain; however, it is possible that these readings were coincidentally taken during a gusty period prior to the main wind event that was not captured in the average hourly wind speed.

10.4.2.2 Moderate West Wind

A period of moderate west wind (approximately ranging from 5 km/hr to peak average hourly wind speeds up to approximately 20 km/hr) was identified from January 28th, 2013 to January 22nd, 2013. The suite-to-corridor pressure differences for each floor are provided in Figure 10-54 to Figure 10-59, and the average suite-to-corridor pressure by floor are provided in Figure 10-60.

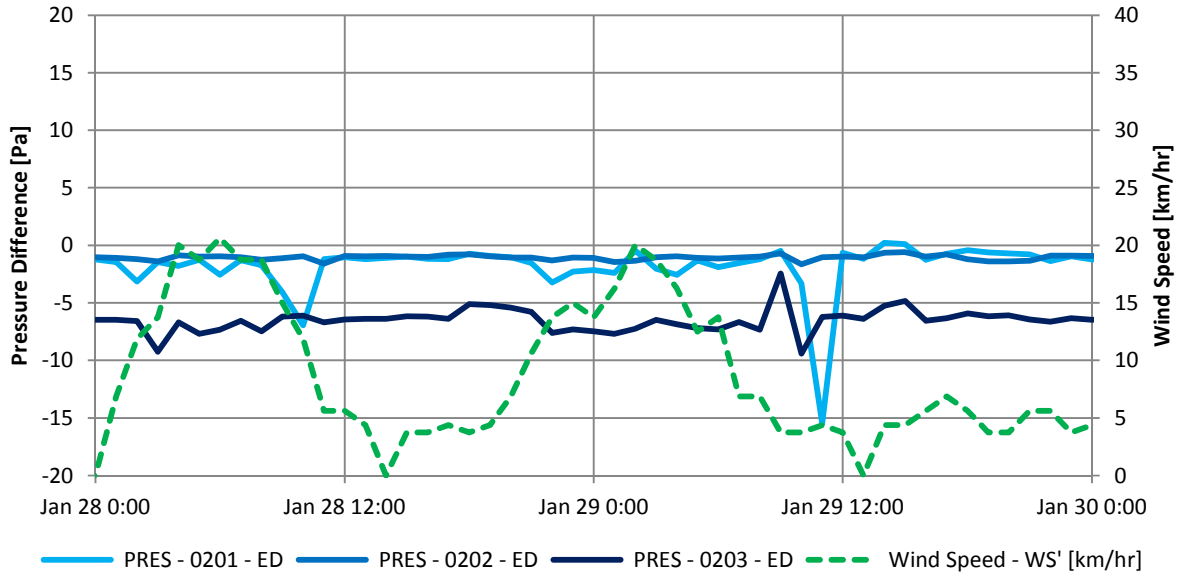


Figure 10-54: Graph of hourly suite-to-corridor pressure differences for Floor 2 during moderate west wind

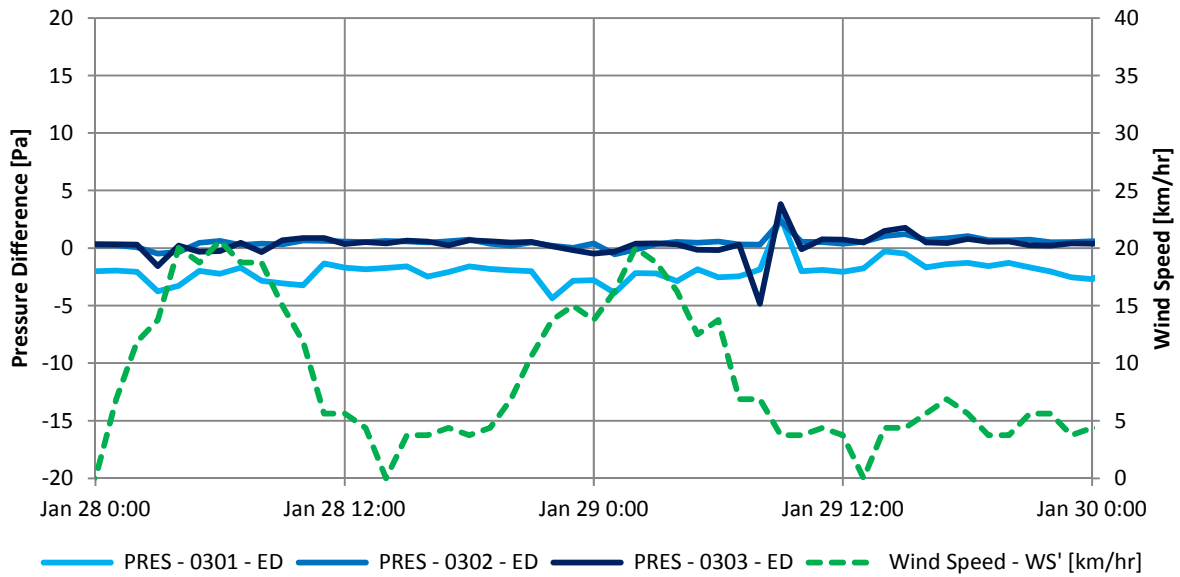


Figure 10-55: Graph of hourly suite-to-corridor pressure differences for Floor 3 during moderate west wind

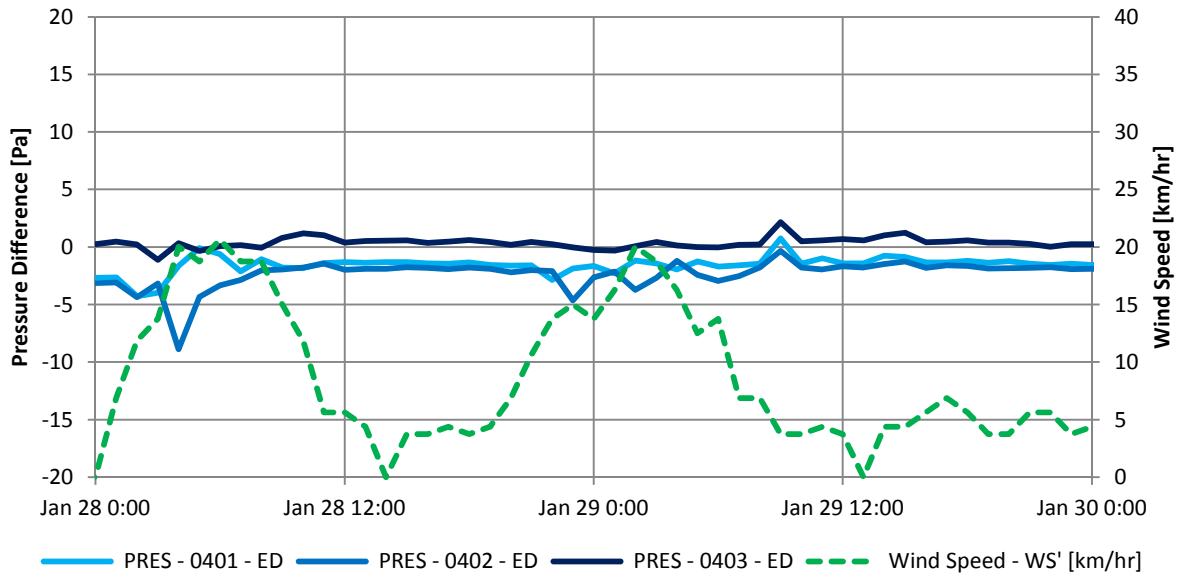


Figure 10-56: Graph of hourly suite-to-corridor pressure differences for Floor 4 during moderate west wind

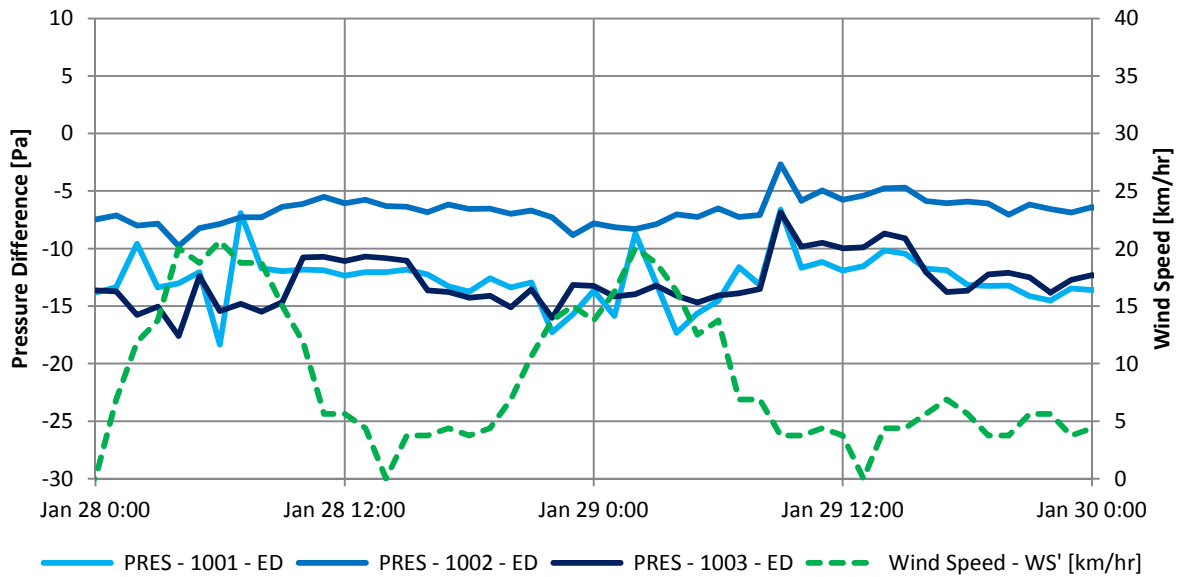


Figure 10-57: Graph of hourly suite-to-corridor pressure differences for Floor 10 during moderate west wind

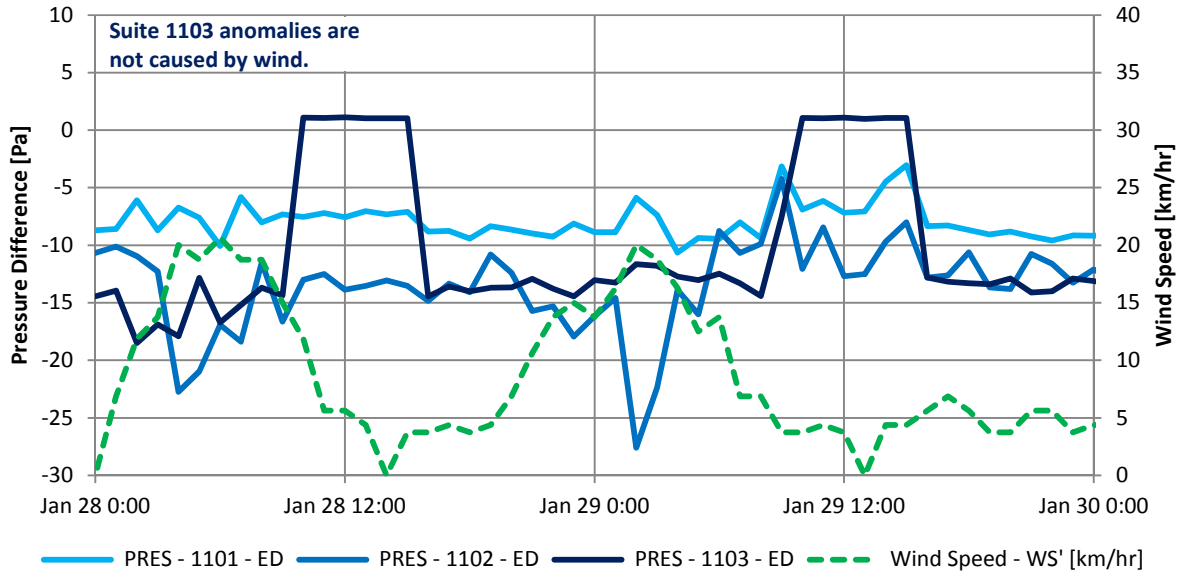


Figure 10-58: Graph of hourly suite-to-corridor pressure differences for Floor 11 during moderate west wind

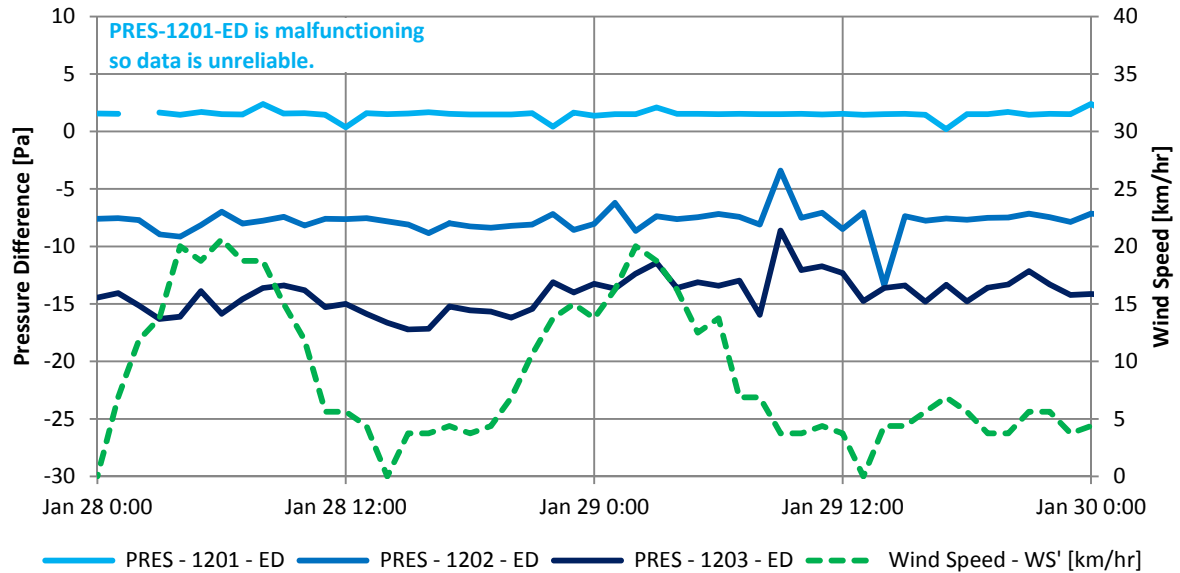


Figure 10-59: Graph of hourly suite-to-corridor pressure differences for Floor 12 during moderate west wind

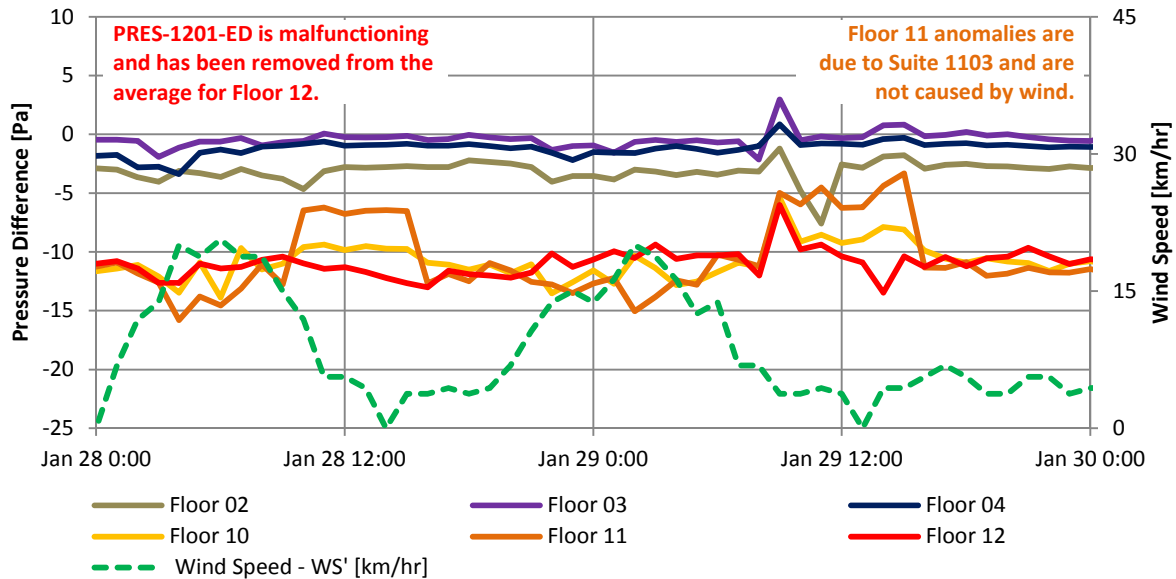


Figure 10-60: Graph of hourly suite-to-corridor pressure differences averaged per floor during moderate west wind

During the moderate west wind, which is strongest at approximately 6 am on January 28th and 3 am on January 29th, little to no effect is again noted on the lower floors. On upper floors it is difficult to notice any major pressure changes from -01 type suites to corridors as would be expected. This may indicate that these suites have their windows closed during these periods which may mitigate the transfer of wind pressures to the suite-to-corridor pressure boundary.

Significant depressurization of Suite 1102 is noted during the periods of moderate west wind with the peaks in wind speed corresponding with additional depressurization of the suite by approximately 7 to 12 Pa. Depressurization of this suite is consistent with the distribution of pressures predicted by standard wind pressure coefficients which indicate that the building face perpendicular to the wind direction can become significantly depressurized.

10.4.2.3 Strong West Wind

A period of strong westerly wind speeds (approximately ranging from 5 km/hr to peak average hourly wind speeds up to approximately 40 km/hr) was identified from April 25th, 2013 to May 2nd, 2013., with the main peak in wind speeds occurring on April 29th. The suite-to-corridor pressure differences for each floor are provided in Figure 10-61 to Figure 10-66, and the average suite-to-corridor pressure by floor are provided in Figure 10-67.

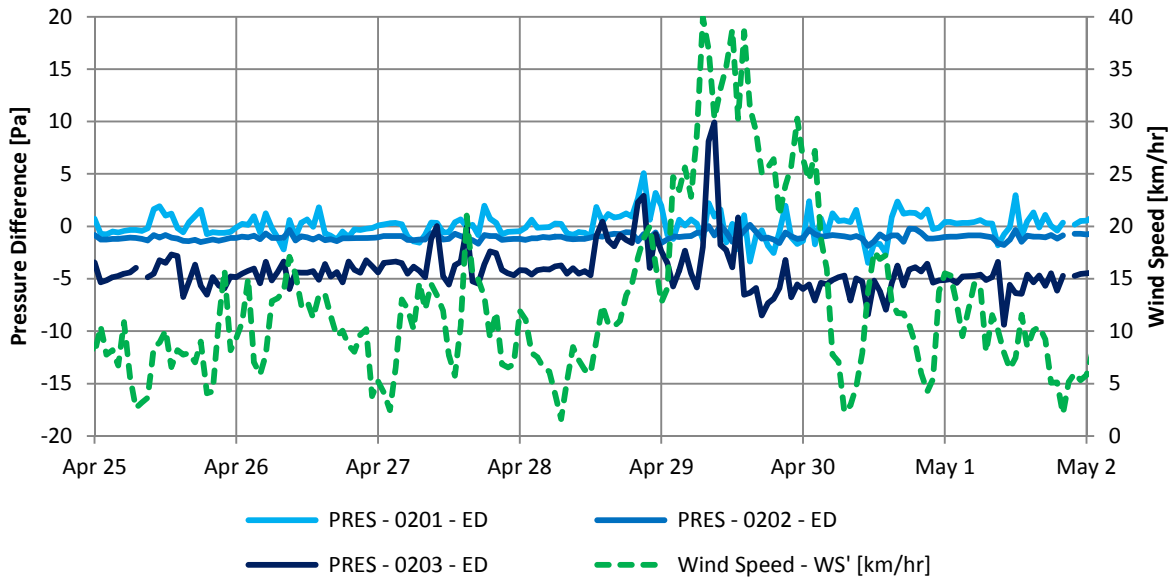


Figure 10-61: Graph of hourly suite-to-corridor pressure differences for Floor 2 during strong west wind

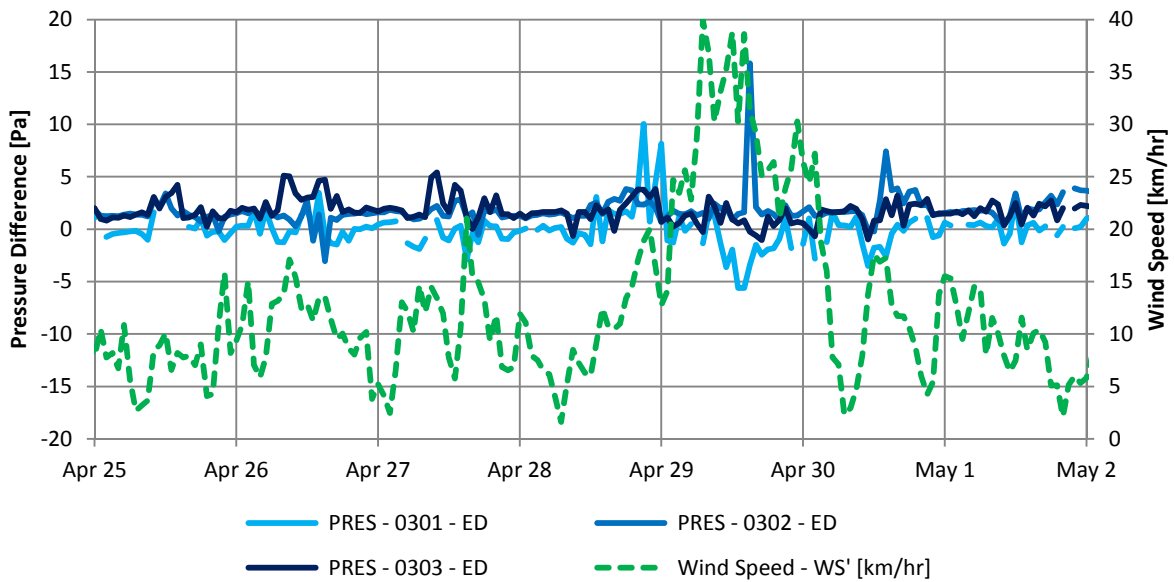


Figure 10-62: Graph of hourly suite-to-corridor pressure differences for Floor 3 during strong west wind

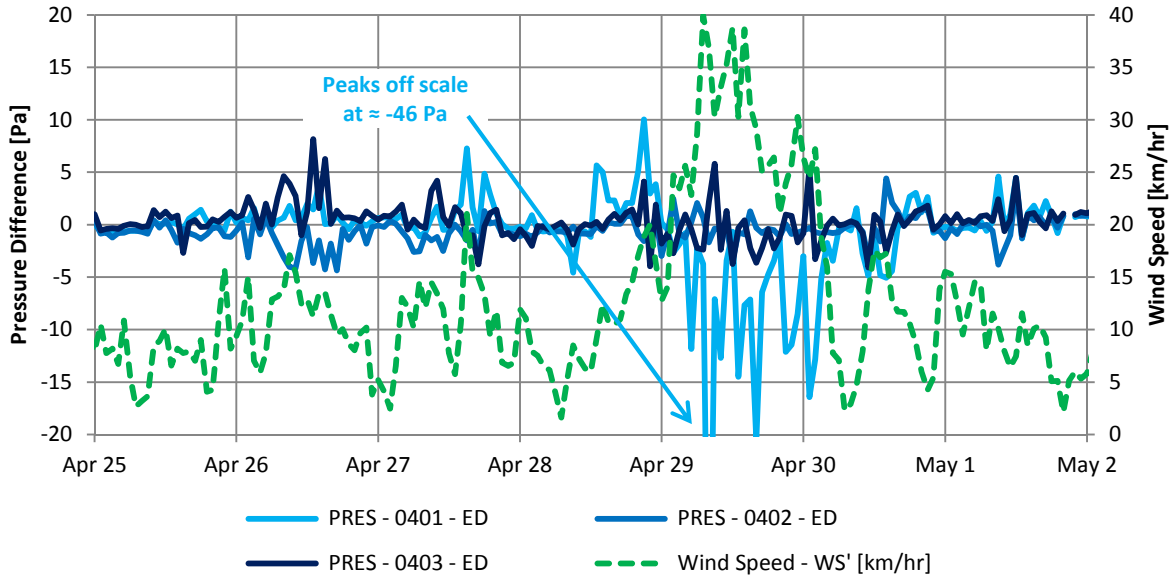


Figure 10-63: Graph of hourly suite-to-corridor pressure differences for Floor 4 during strong west wind

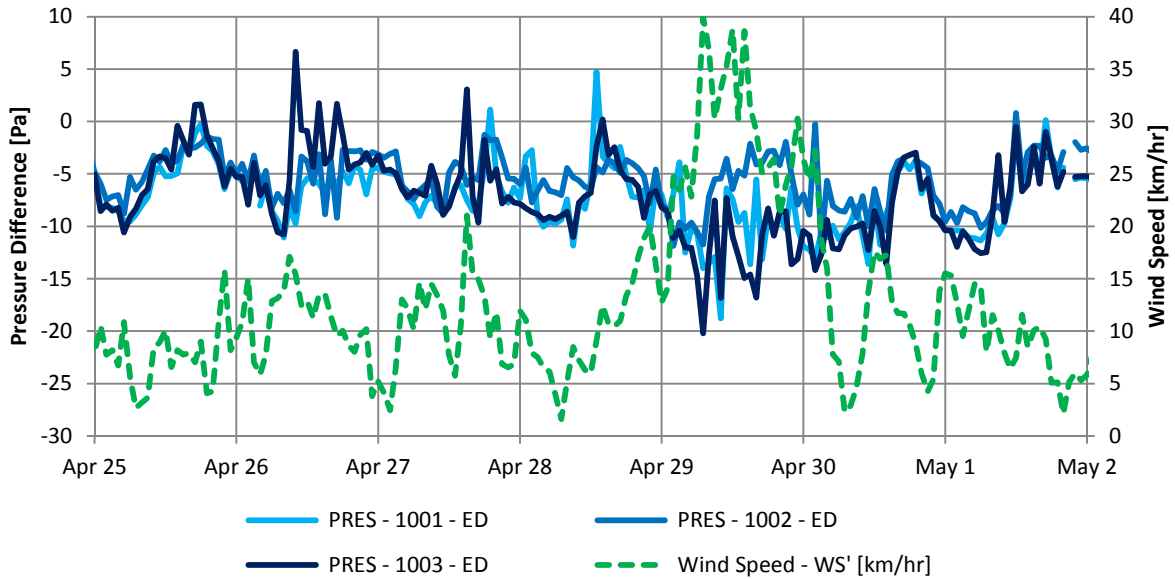


Figure 10-64: Graph of hourly suite-to-corridor pressure differences for Floor 10 during strong west wind

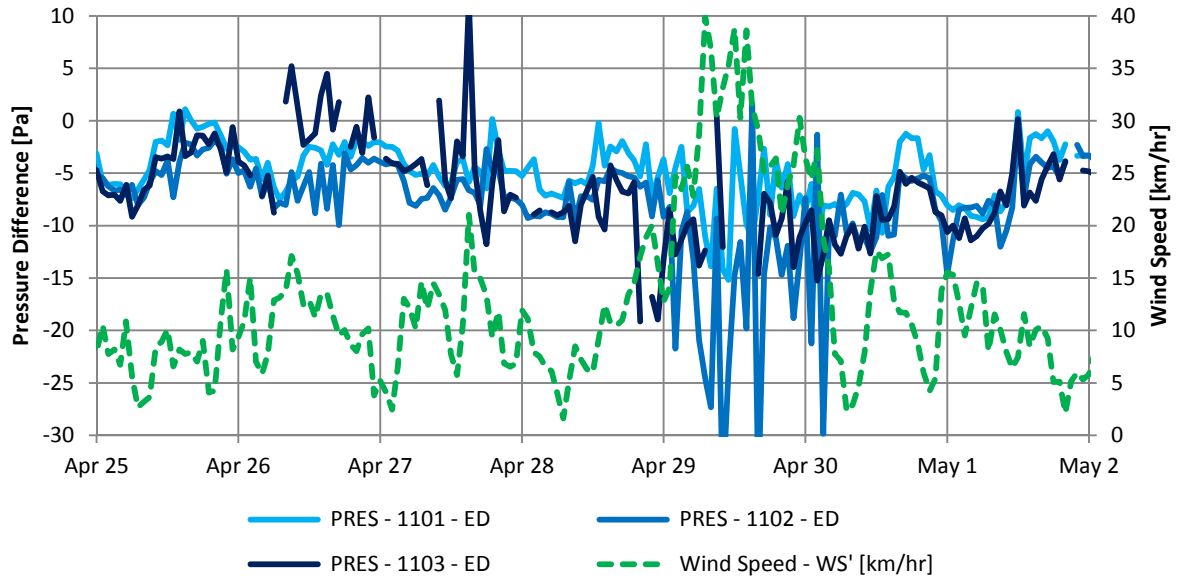


Figure 10-65: Graph of hourly suite-to-corridor pressure differences for Floor 11 during strong west wind

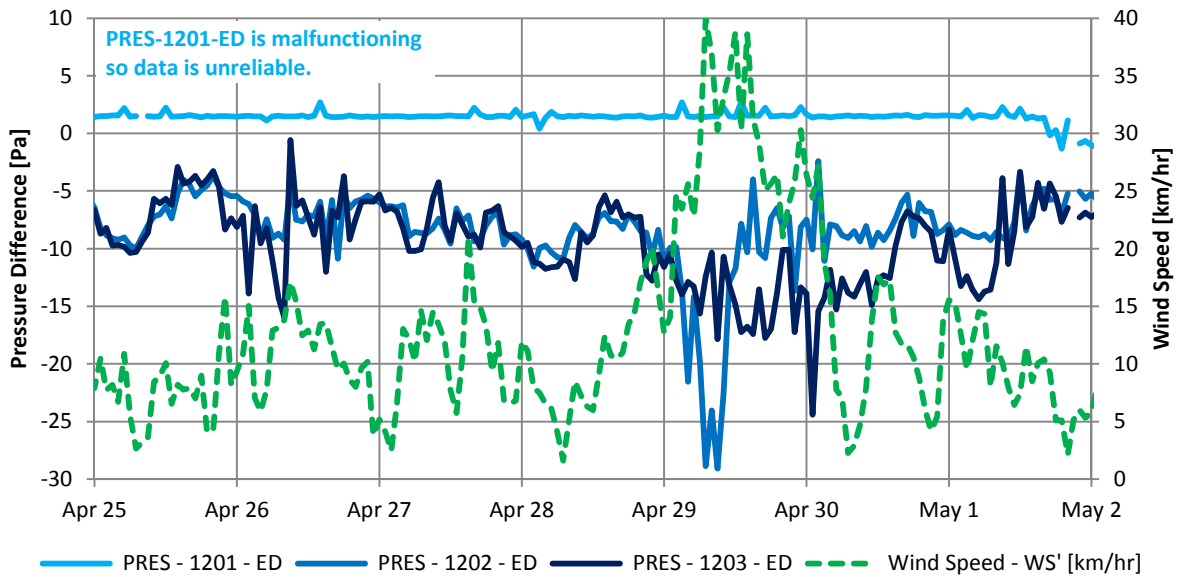


Figure 10-66: Graph of hourly suite-to-corridor pressure differences for Floor 12 during strong west wind

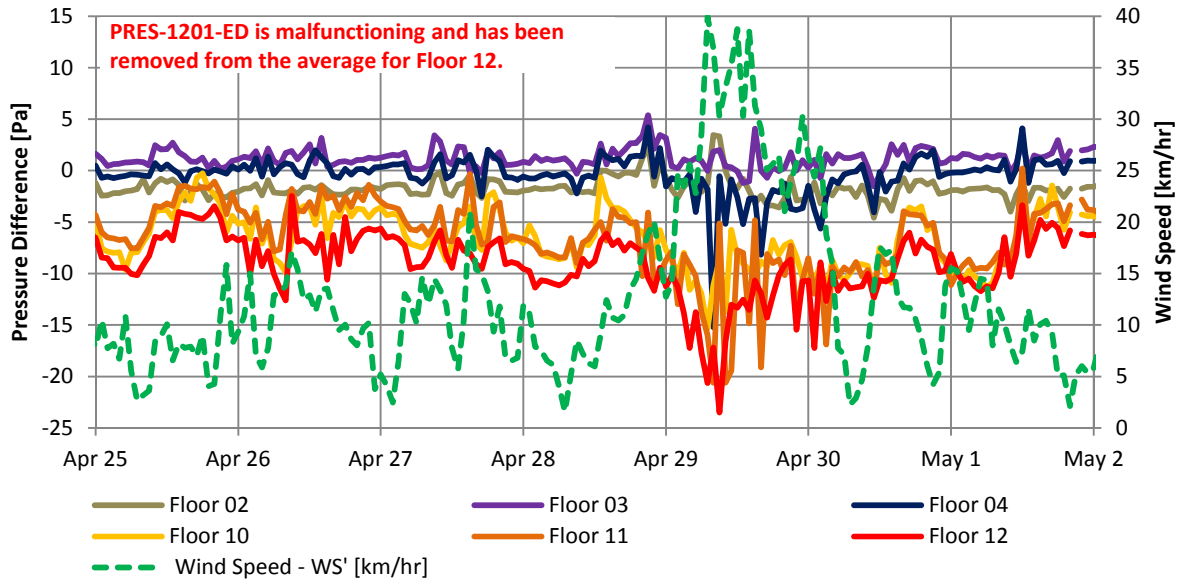


Figure 10-67: Graph of hourly suite-to-corridor pressure differences averaged per floor during strong west wind

Significant changes in suite-to-corridor pressures were measured during this period of strong west wind. Consistent with other findings, pressure fluctuations were of larger magnitude on upper floors than lower floors, likely due to shielding effects reducing the exposure to wind of lower floors of the buildings.

Notably, in most cases suites were measured to become significantly more depressurized relative to the corridor during the strong west wind. While one would expect suites on the sides of the building perpendicular to the wind and on the leeward side (-02 and -03 types suites) to become more depressurized due to a strong west wind, significant depressurization was also measured in a number of -01 type suites including Suite 401 which recorded a minima of 46 Pa below the corridor. Generally, the 35 to 40 km/hr west winds were associated with decreases in the pressure of suites relative to the corridor by approximately 10 to 25 Pa on upper floors, and, with the exception of Suite 401, 0 to 5 Pa on lower floors.

Suite 203 increased in pressure relative to the corridor by approximately 15 Pa during this period of strong west wind. This is opposite of the expected relationship, and the cause is unknown.

Overall the pressures from suites to the corridors during this period of high wind were found to be of significant magnitude and were highly variable in direction making the associated flows difficult to predict.

10.4.3 Summary of Suite-to-Corridor Results

Typically suite-to-corridor pressure differences were found to be negative indicating that the corridors are pressurized relative to the suites; however, significant variation in these pressures was noted. The most significant correlation was found to be with exterior temperatures which correlated well with the measured suite-to-corridor pressure both long-term and short-term.

Larger changes in pressure due to changes in exterior temperature were noted on floors that are located farther from the neutral pressure plane.

Wind pressures were also found to distribute across the suite-to-corridor pressure boundary, but the direction and magnitude of these pressures was found to be highly variable and difficult to predict. In some cases little to no pressure difference due to wind was observed possibly indicating that building occupants tend to keep their windows closed during moderate and strong wind events.

Overall, the pressure differences from the suite to the corridors were found to be highly variable, based primarily on exterior temperature. The net result being that the corridor was not found to be consistently or evenly pressurized relative to the suites and thus likely an uneven amount of ventilation air from the corridors is supplied to the suites of the building. These pressure measurements found that upper corridors of the building were typically more pressurized relative to the adjacent suites than were lower corridors and thus likely were receiving more ventilation air. This is consistent with the findings of the PFT airflow measurements presented in Chapter 8.

The uneven and inconsistent distribution of pressure differences also indicates that in some cases the natural driving forces overcome the mechanical ventilation system and create positive suite-to-corridor pressures. This change in direction of pressure creates the potential for migration of air contaminants from the suites to the corridors and subsequently to other suites.

10.5 Suite-to-Suite Pressure Differences

The pressure differences between adjacent suites on the same floor were determined using the suite-to-corridor pressure measurements. The relationship between these pressure differences, and exterior temperature and wind are considered in this section. As these pressure differences are calculated using the suite-to-corridor pressure measurements, many of the observations are similar.

Note that a positive suite-to-suite pressure measurement indicates that the first suite listed is at a higher pressure than the second suite listed. The reader should refer to Figure 10-1 for further clarification if required.

10.5.1 Suite-to-Suite Pressure Differences and Exterior Temperature

Stack effect due to the difference between interior and exterior temperatures is not anticipated to create pressure differences between suites on the same floor, as there is no vertical distance between these suites. To assess whether exterior temperature impacts the pressure differences between adjacent suites, these pressures are provided over the course of the monitoring period in Figure 10-68 to Figure 10-73.

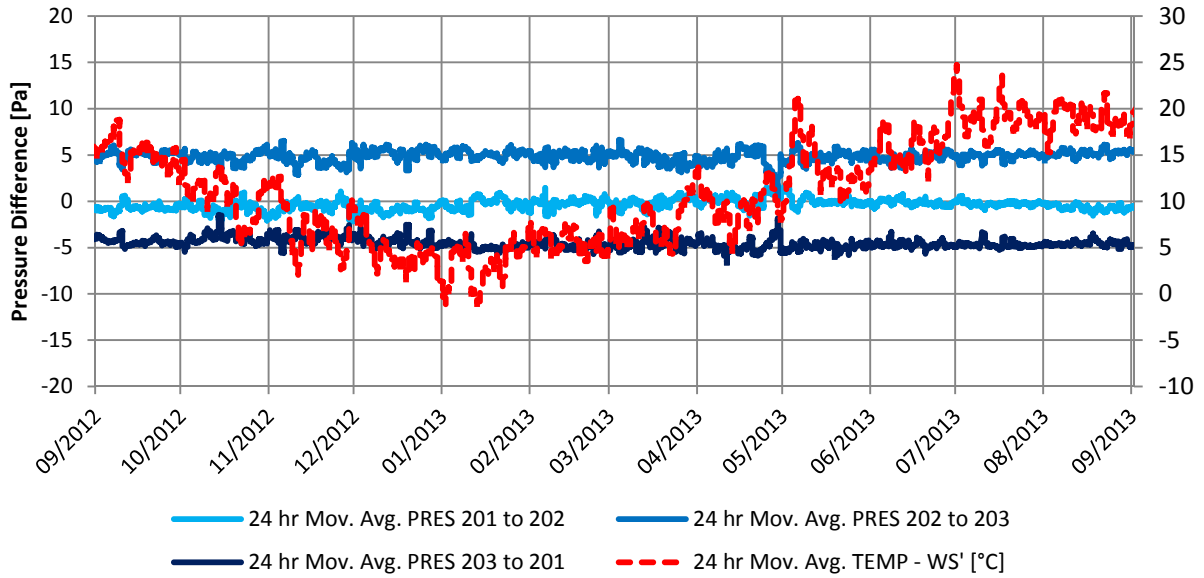


Figure 10-68: Graph of 24 hour moving average suite-to-suite pressure differences for Floor 2

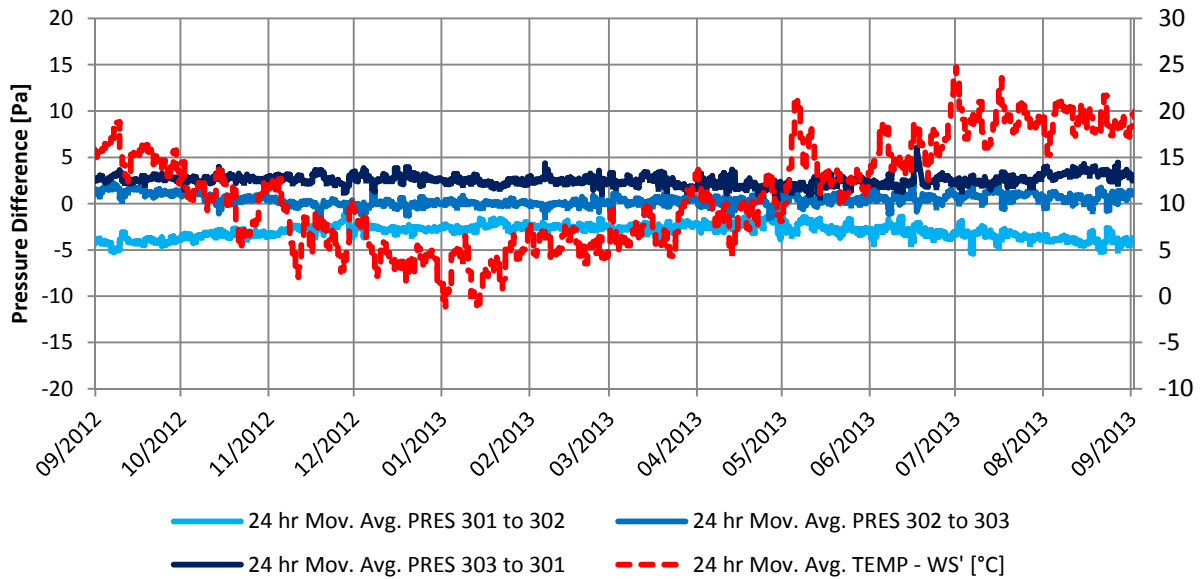


Figure 10-69: Graph of 24 hour moving average suite-to-suite pressure differences for Floor 3

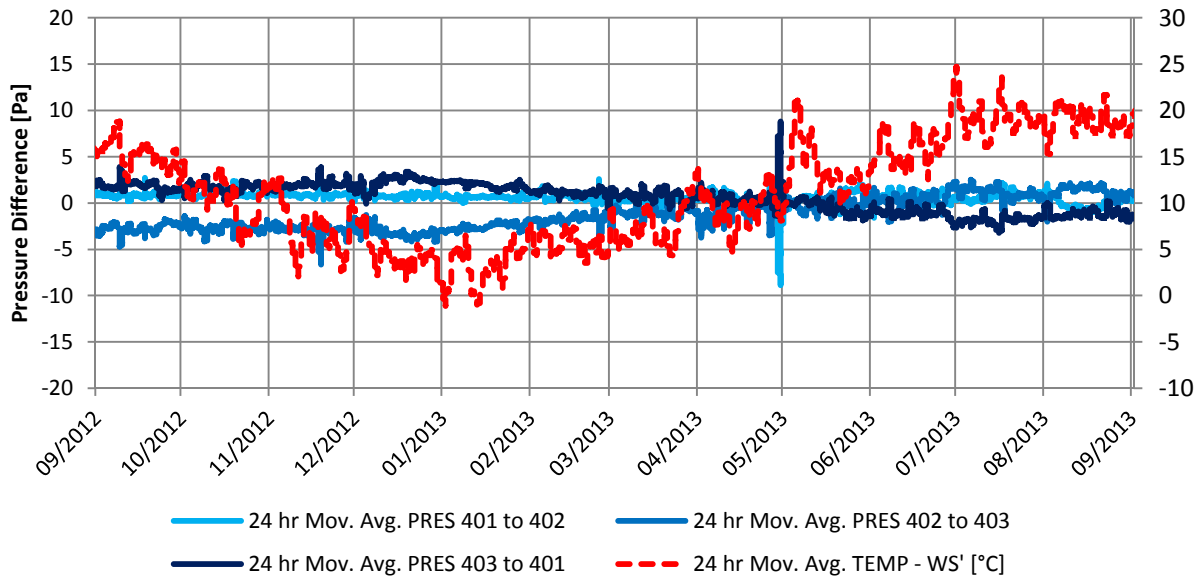


Figure 10-70: Graph of 24 hour moving average suite-to-suite pressure differences for Floor 4

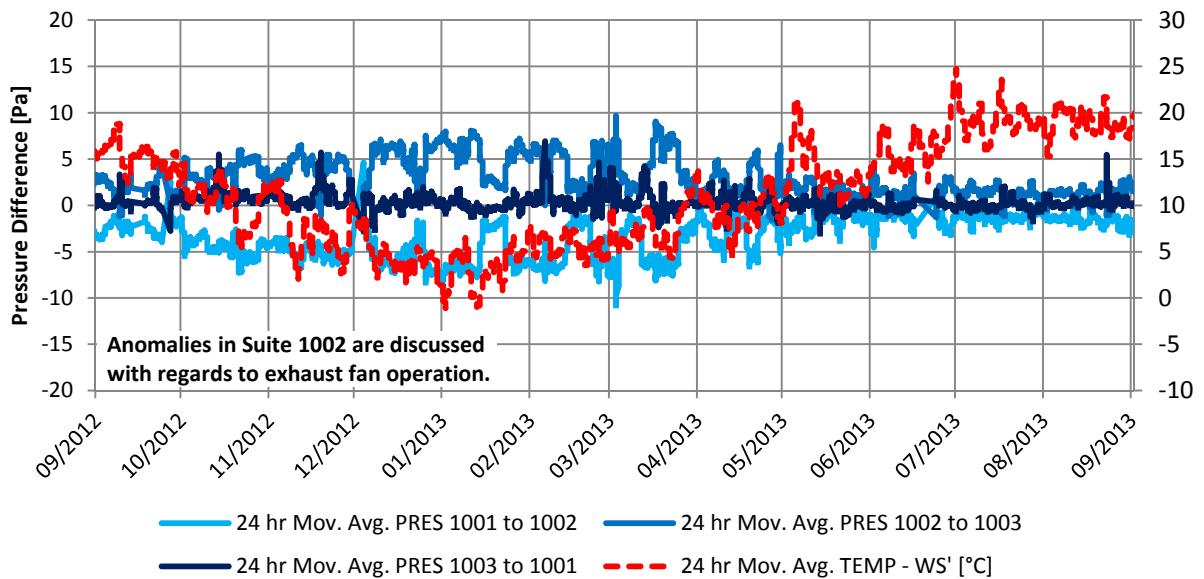


Figure 10-71: Graph of 24 hour moving average suite-to-suite pressure differences for Floor 10

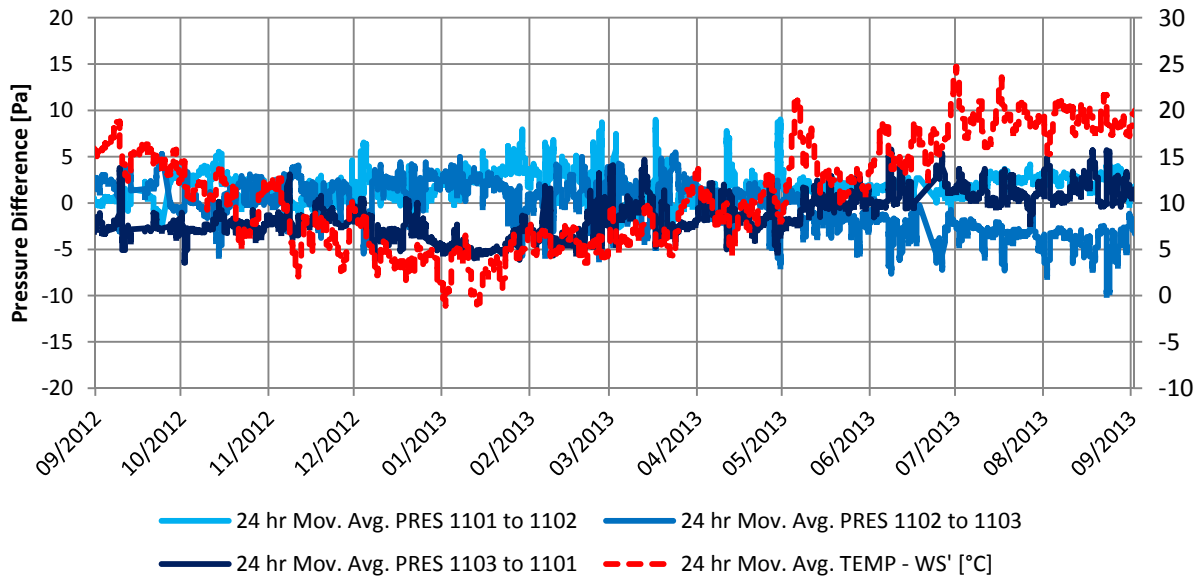


Figure 10-72: Graph of 24 hour moving average suite-to-suite pressure differences for Floor 11

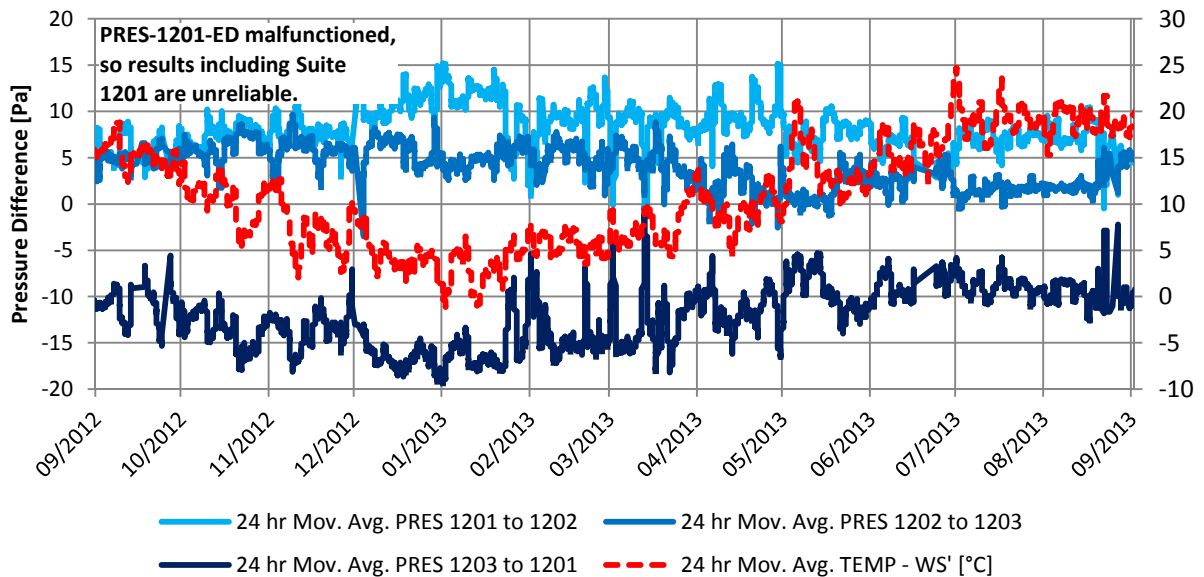


Figure 10-73: Graph of 24 hour moving average suite-to-suite pressure differences for Floor 12

As expected, the preceding figures illustrate that there is little to no relationship between exterior temperature and the suite-to-suite pressure differences. The potential exception to this is Floor 10 where decreasing exterior temperature is correlated with a decrease in the pressure difference from Suite 1001 to Suite 1002 and an increase in the pressure difference from Suite 1002 to Suite 1003. During the coldest periods of the year these pressure differences are approximately a magnitude of 5 Pa. This indicates that the pressure in Suite 1002 increases relative to adjacent suites as the temperature decreases. This may be a result of Suite 1002 having a leakier suite

entrance door, leakier corridor to suite walls, or a more airtight exterior enclosure than is typical as this would cause stack effect to have more influence on the suite pressure. Airtightness testing was not conducted at this suite, so the characteristics of these pressure boundaries are unknown. A more airtight exterior enclosure could also be caused by the occupant keeping more windows closed than other the occupants of other suites on the floor.

10.5.2 Suite-to-Suite Pressure Differences and Wind

The relationship between wind speed, wind direction, and suite-to-corridor pressure differences was evaluated using the same periods of different wind magnitudes and directions as used with respect to the exterior enclosure. Graphs of wind speeds, direction, and exterior temperatures during these periods were provided in Section 10.2.2 are not repeated here; however, for reference, wind speed is overlaid with the pressure data on the graphs.

Similar to suite-to-corridor pressures, little to no relationship between wind speed and suite-to-suite pressures was noted during periods of minimal wind and light east winds. Consequently, only moderate and strong wind events are presented.

10.5.2.1 Moderate East Wind

A period of moderate easterly wind speeds (approximately 10 km/hr with peak hourly average wind speeds up to 20 km/hr) was identified from December 24th, 2012 at noon, to December 26th, 2012 at noon. The suite-to-suite pressure differences for each floor are provided in Figure 10-74 to Figure 10-79. During this period, scaffolding was still in place on much of the building; however, similar effects were noted during other periods of moderate east wind after the scaffolding was removed.

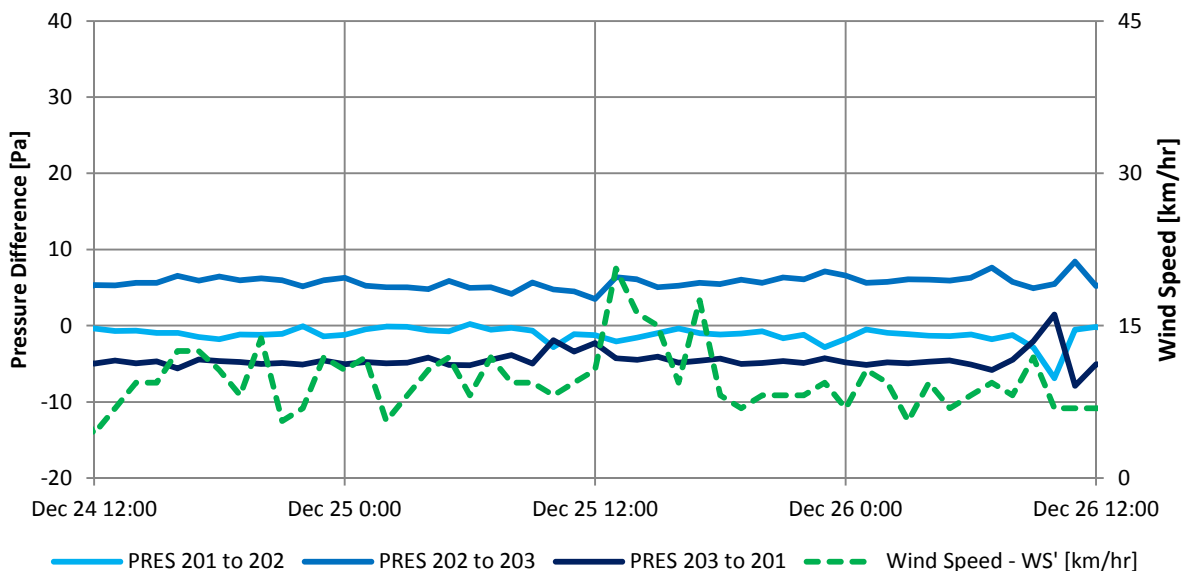


Figure 10-74: Graph of hourly suite-to-suite pressure differences for Floor 2 and wind speed during moderate east wind

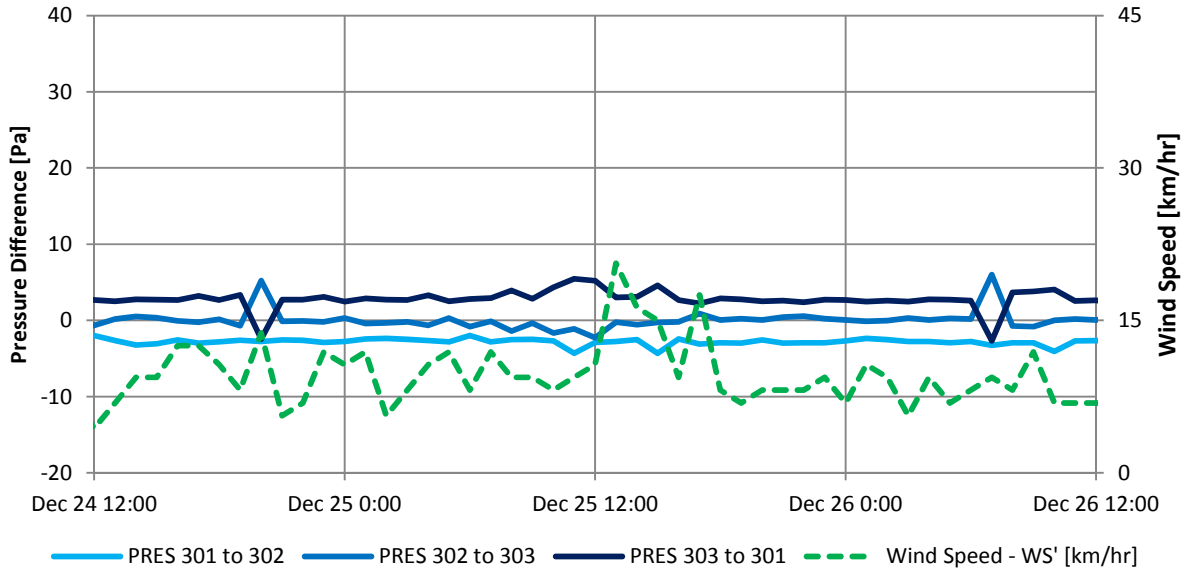


Figure 10-75: Graph of hourly suite-to-suite pressure differences for Floor 3 and wind during moderate east wind

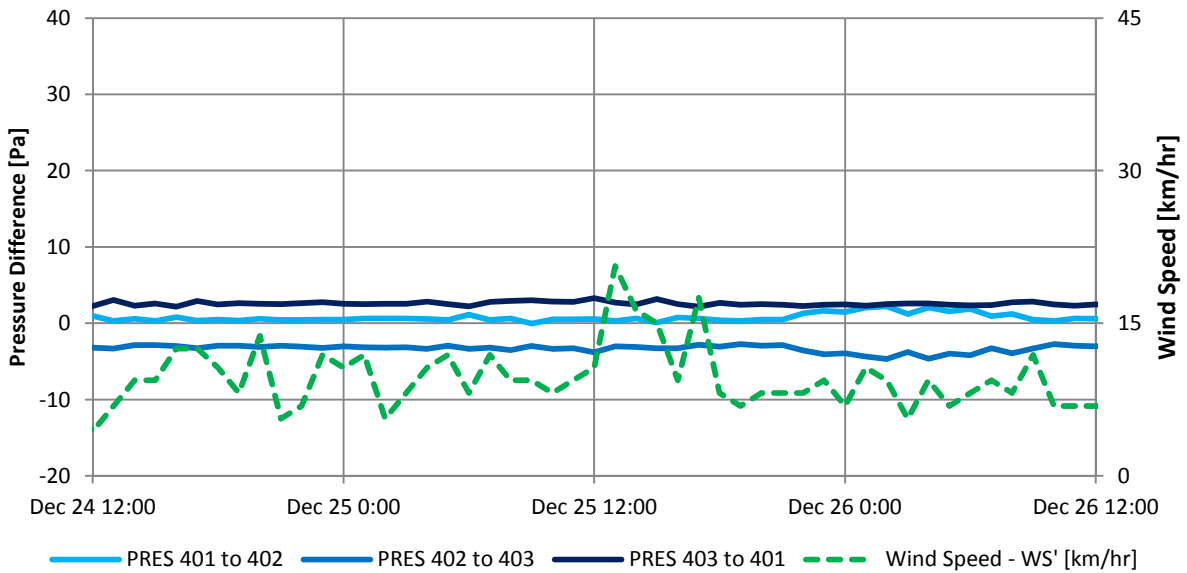


Figure 10-76: Graph of hourly suite-to-suite pressure differences for Floor 4 and wind during moderate east wind

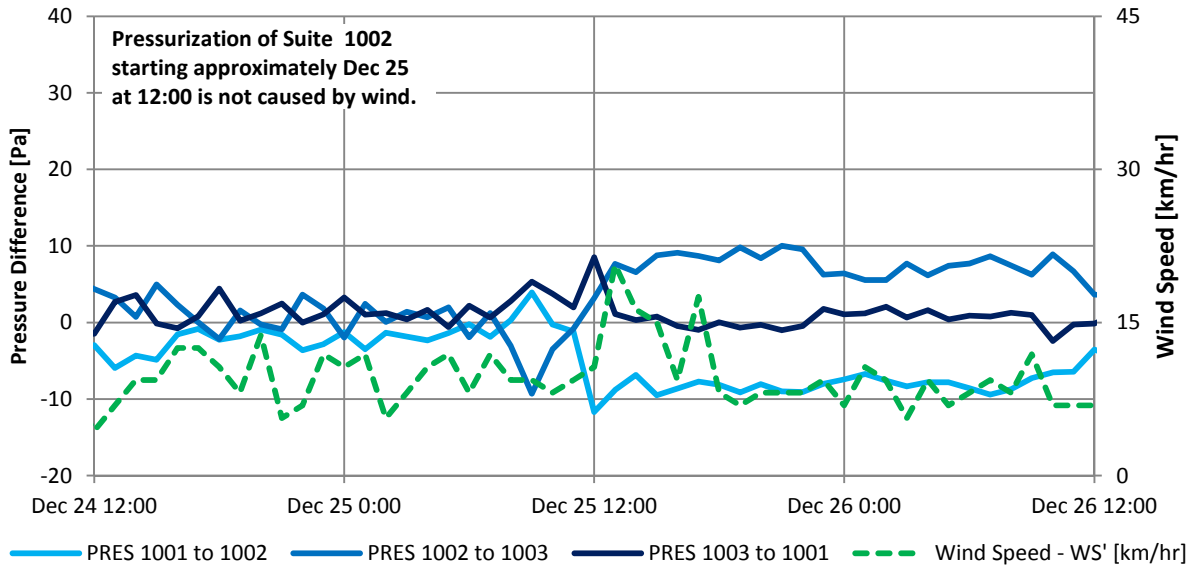


Figure 10-77: Graph of hourly suite-to-suite pressure differences for Floor 10 and wind during moderate east wind

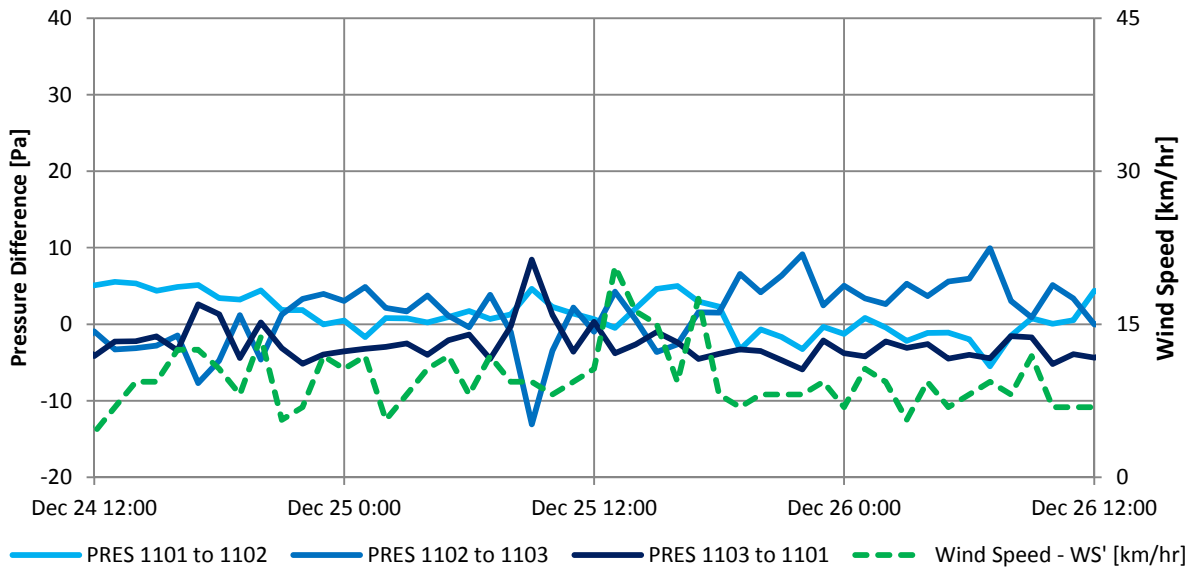


Figure 10-78: Graph of hourly suite-to-suite pressure differences for Floor 11 and wind during moderate east wind

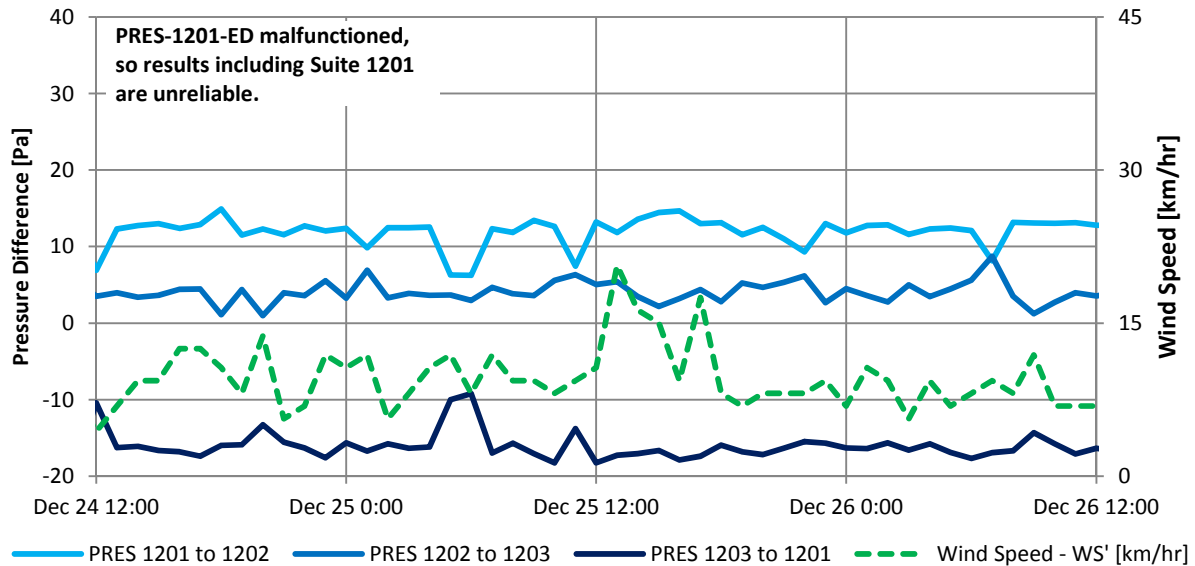


Figure 10-79: Graph of hourly suite-to-suite pressure differences for Floor 12 and wind during moderate east wind

There is little to no relationship between suite-to-suite pressure differences and wind speed on lower floors. On upper floors, pressure differences are more variable during this moderately windy period than during periods of less wind.

Suite 1103 (east suite) becomes pressurized relative to the adjacent suites by approximately 8 to 10 Pa slightly before the main period of moderate east winds shown in the graphs. This change in pressure corresponds with the suite-to-corridor pressure for this suite spiking to 0 Pa; consequently, it is likely that this spike was not a result of wind but rather is a result of the suite entrance door being open at the time of the pressure measurement. Opening the suite entrance door would effectively equalize the pressure in the suite with that of the corridor and likely cause the measured effects. The effect of opening suite entrance doors on pressure distributions is discussed in Section 10.6.

10.5.2.2 Moderate West Wind

A period of moderate westerly wind speeds (approximately ranging from 5 km/hr to peak average hourly wind speeds up to approximately 20 km/hr) was identified from January 28th, 2013 to January 22nd, 2013. The suite-to-suite pressure differences for each floor are provided in Figure 10-80 to Figure 10-85.

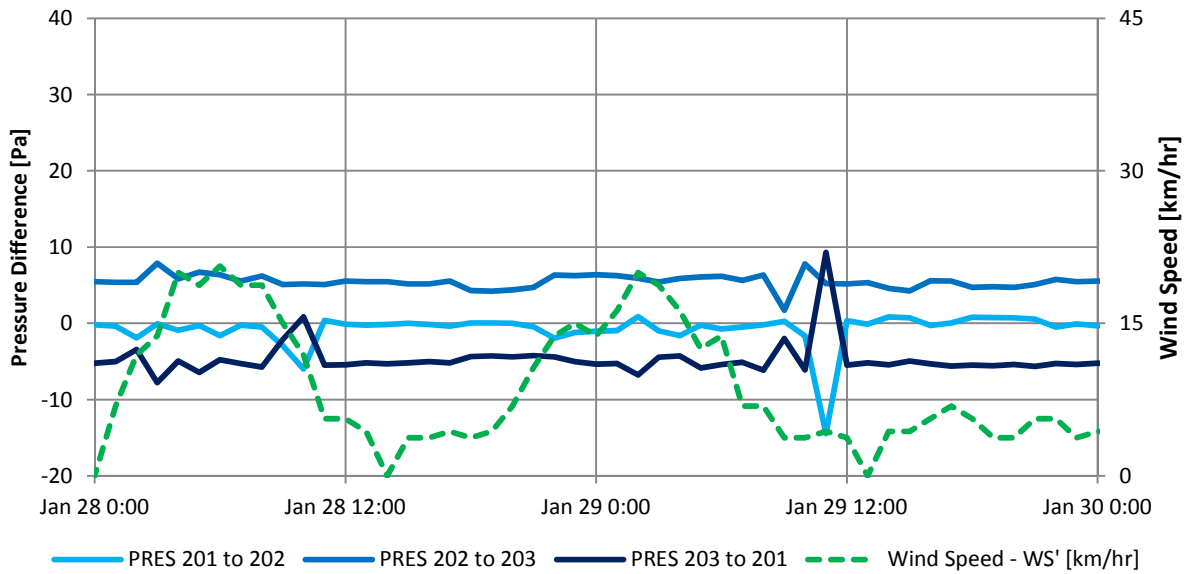


Figure 10-80: Graph of hourly suite-to-suite pressure differences for Floor 2 and wind speed during moderate west wind

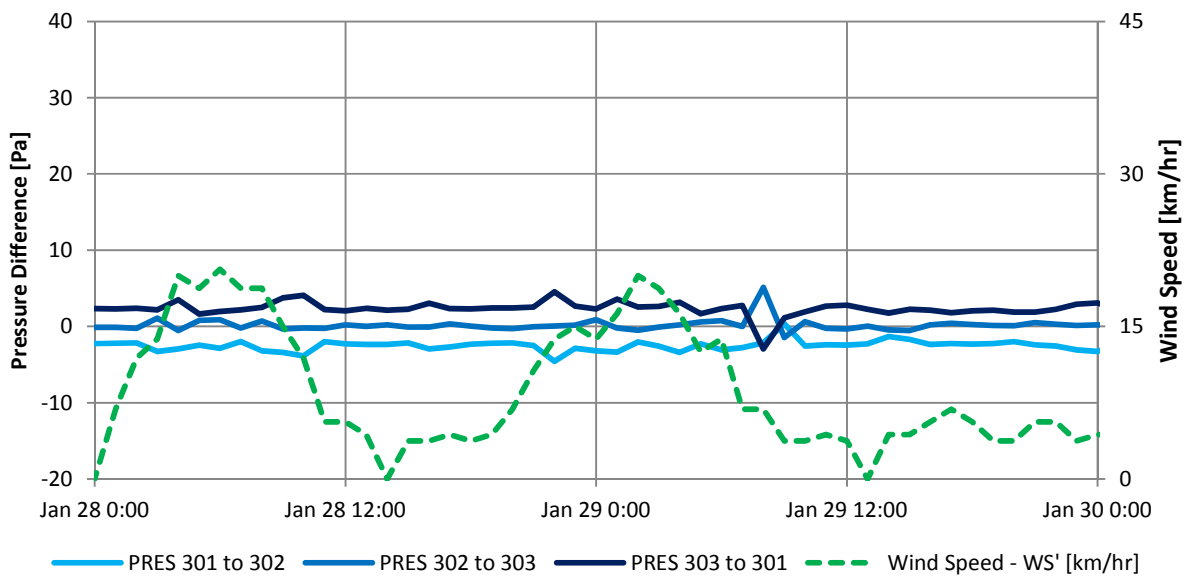


Figure 10-81: Graph of hourly suite-to-suite pressure differences for Floor 3 and wind during moderate west wind

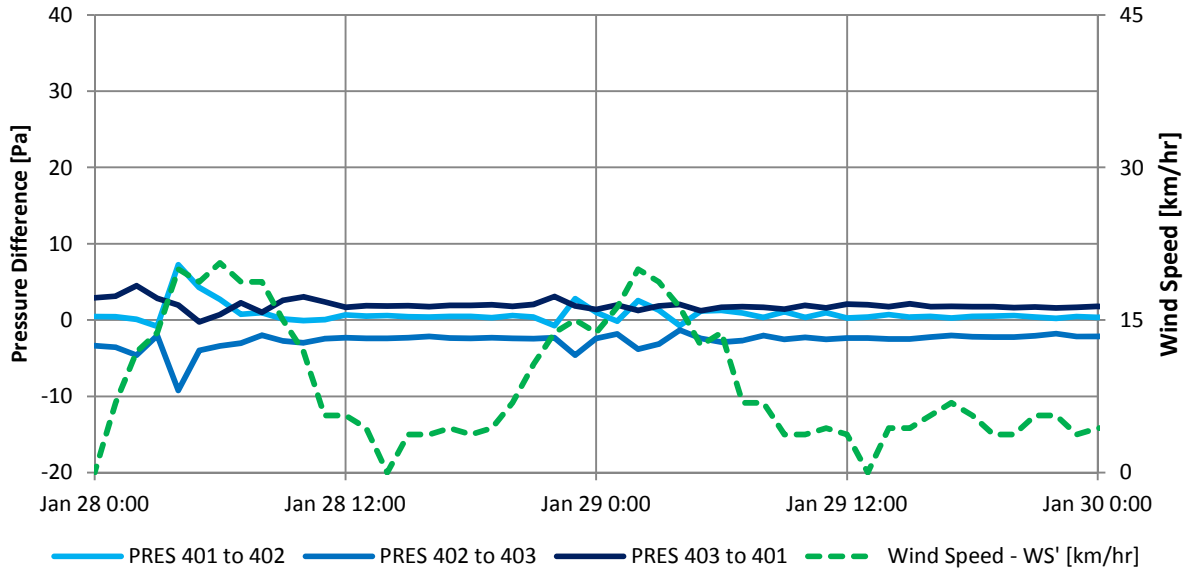


Figure 10-82: Graph of hourly suite-to-suite pressure differences for Floor 4 and wind during moderate west wind

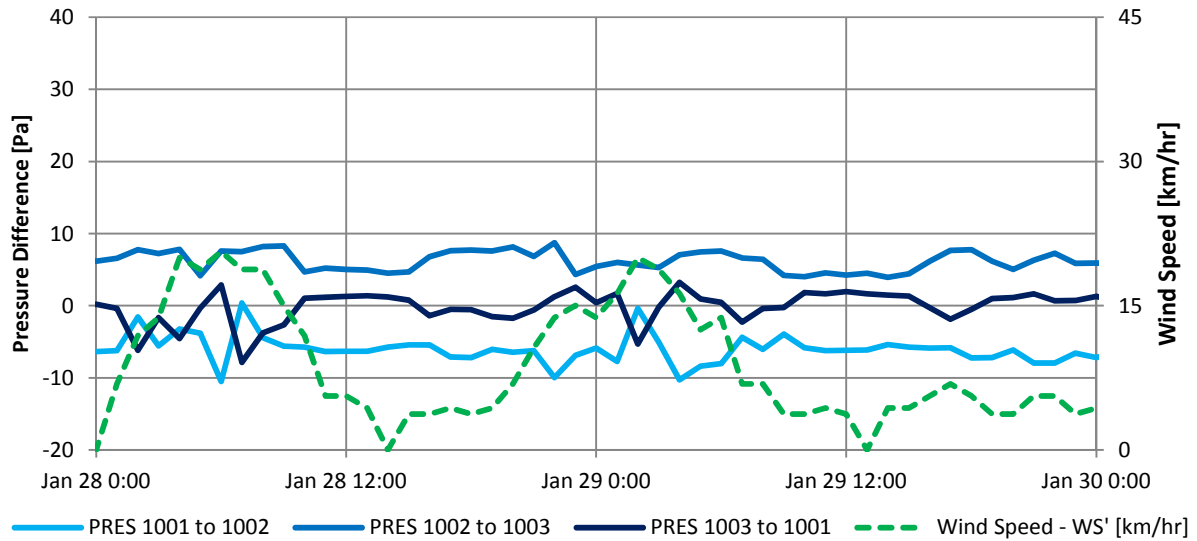


Figure 10-83: Graph of hourly suite-to-suite pressure differences for Floor 10 and wind during moderate west wind

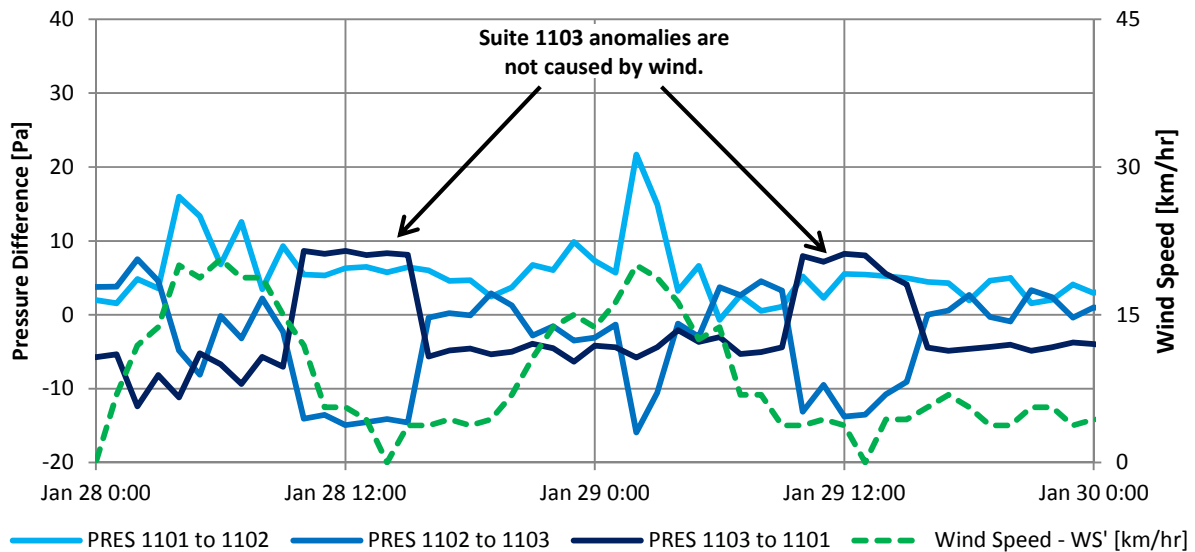


Figure 10-84: Graph of hourly suite-to-suite pressure differences for Floor 11 and wind during moderate west wind

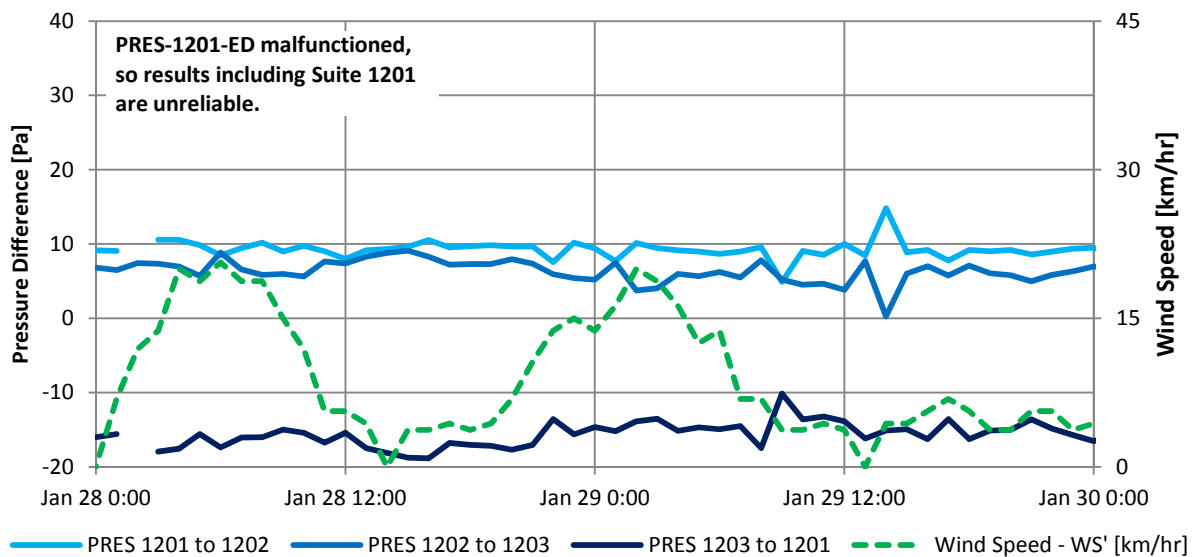


Figure 10-85: Graph of hourly suite-to-suite pressure differences for Floor 12 and wind during moderate west wind

During this period of moderate west winds, -01 type suites typically became pressurized relative to adjacent suites, which is consistent with the effects predicted by wind physics. In some cases (Floor 4 and Floor 11) the pressure in -02 suites decreased relative to adjacent suites, which is also expected based on theory as the wind pressure coefficients for elevations perpendicular to the wind direction are typically negative.

The magnitude of these pressure changes varies with building height with lower floors typically exhibiting lesser changes in pressure than upper floors. On Floor 11, the floor with the maximum suite-to-suite pressure difference due to the moderate west wind, the magnitude of the suite-to-suite pressure difference increased by approximately 15 to 20 Pa whereas changes on lower floors were typically less than 5 Pa. Floor 12 may have experienced similar pressure distribution to Floor 11; however, the Suite 1201 sensor malfunctioned so accurate measurements are not available..

10.5.2.3 Strong West Wind

A period of strong westerly wind speeds (approximately ranging from 5 km/hr to peak average hourly wind speeds up to approximately 40 km/hr) was identified from April 25th, 2013 to May 2nd, 2013, with the strongest winds occurring on April 29th. The suite-to-suite pressure differences for each floor are provided in Figure 10-86 to Figure 10-91. Unfortunately some Floor 11 data was lost during this windy period due to a monitoring equipment malfunction.

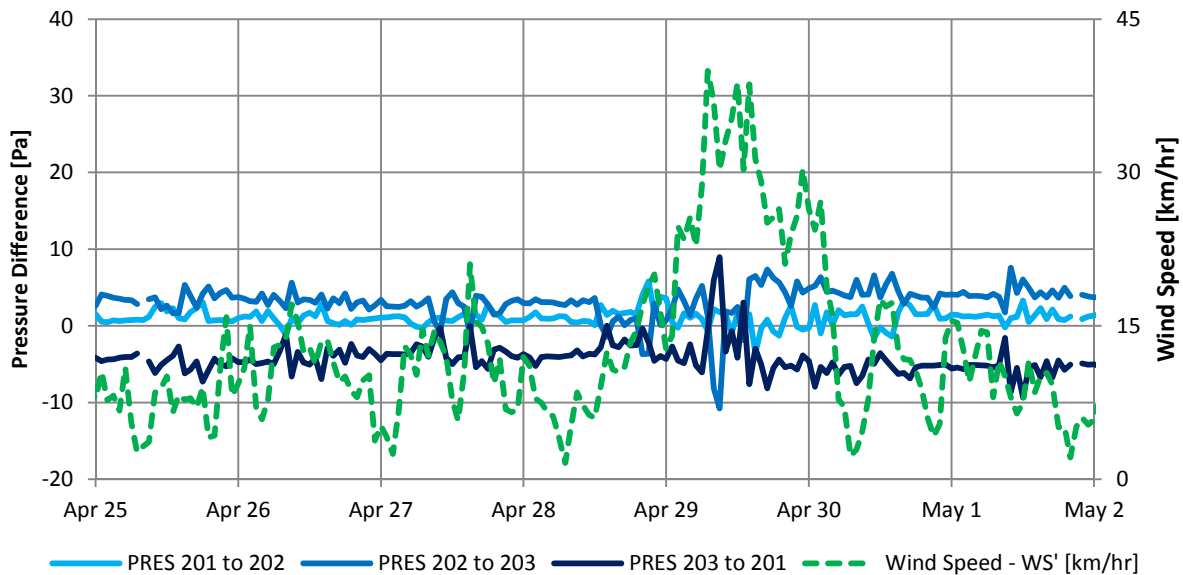


Figure 10-86: Graph of hourly suite-to-suite pressure differences for Floor 2 and wind speed during strong west wind

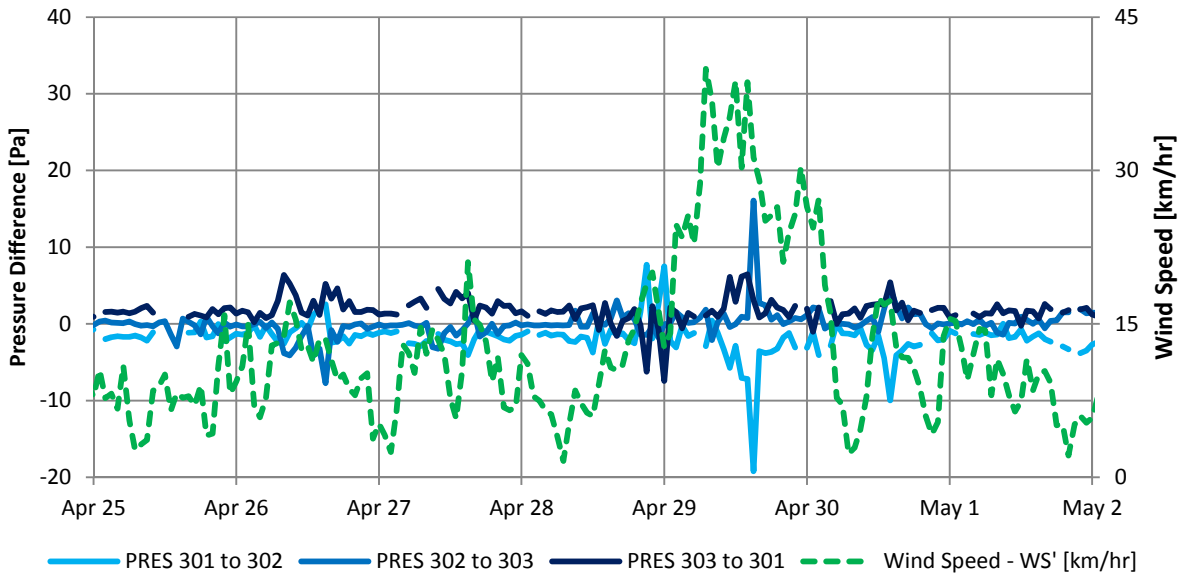


Figure 10-87: Graph of hourly suite-to-suite pressure differences for Floor 3 and wind during strong west wind

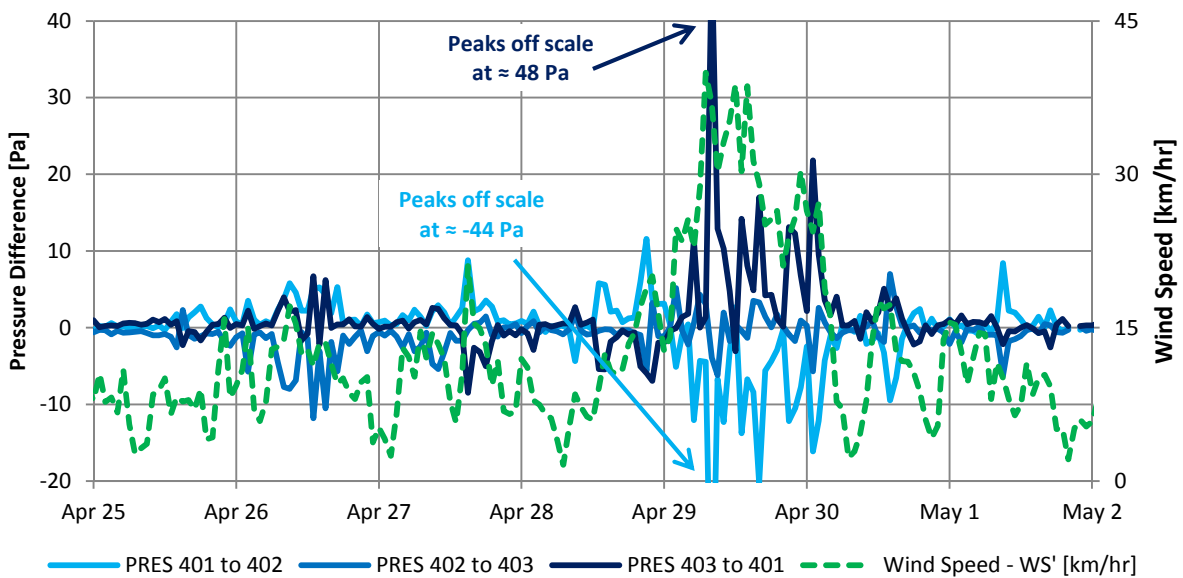


Figure 10-88: Graph of hourly suite-to-suite pressure differences for Floor 4 and wind during strong west wind

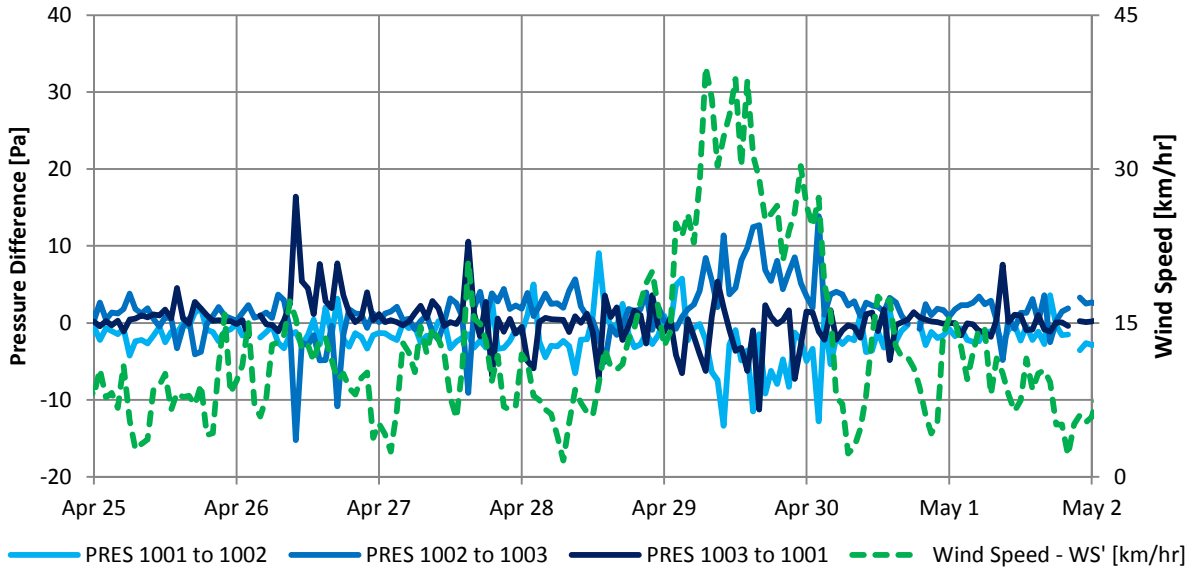


Figure 10-89: Graph of hourly suite-to-suite pressure differences for Floor 10 and wind during strong west wind

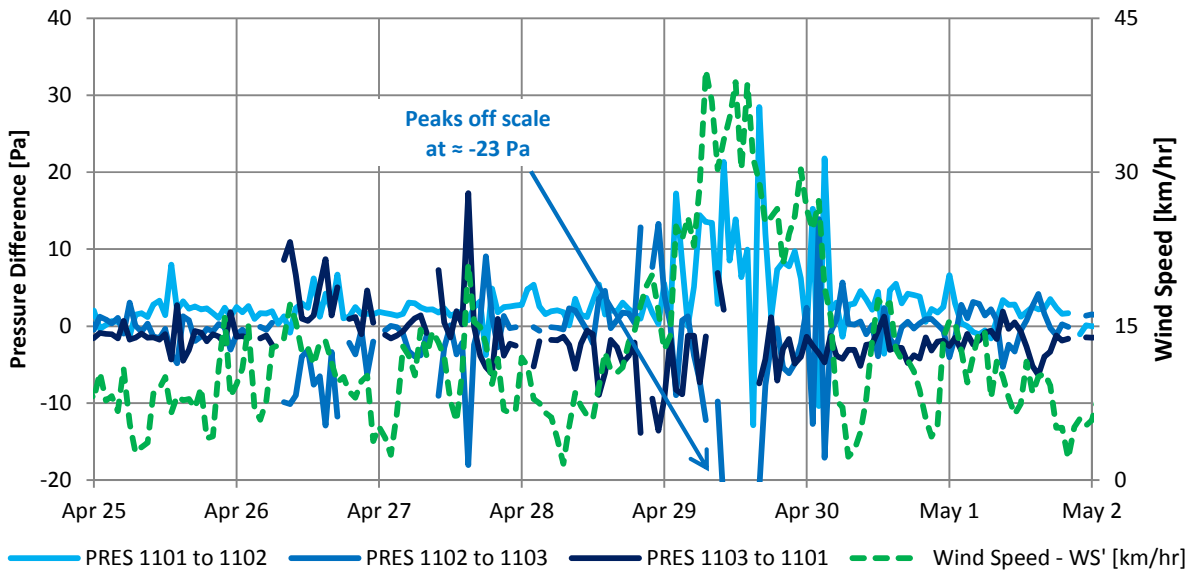


Figure 10-90: Graph of hourly suite-to-suite pressure differences for Floor 11 and wind during strong west wind

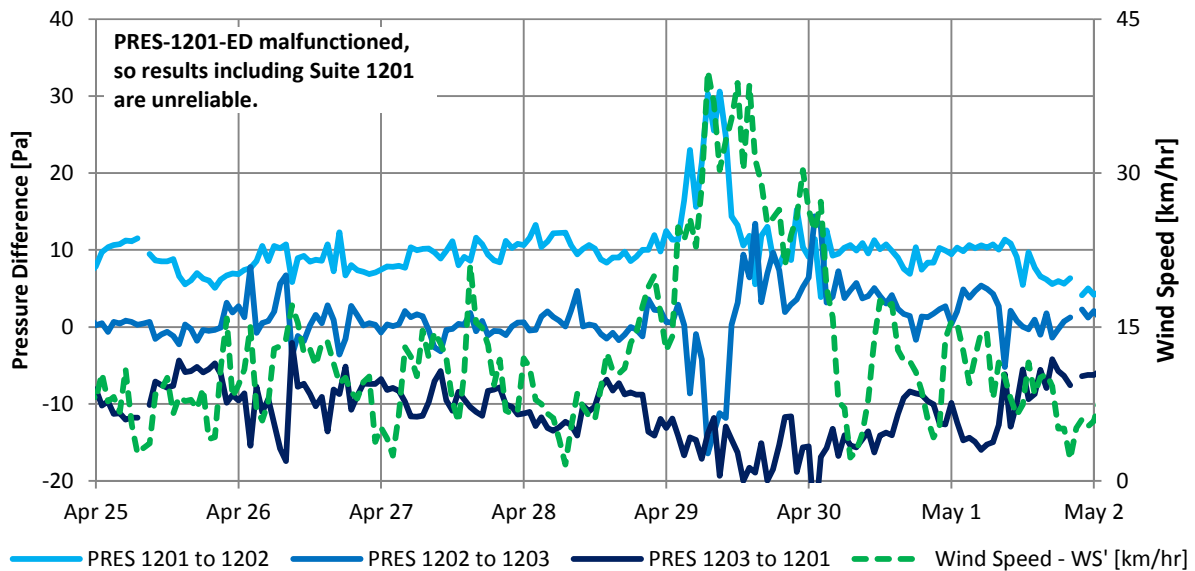


Figure 10-91: Graph of hourly suite-to-suite pressure differences for Floor 12 and wind during strong west wind

Changes in suite-to-suite pressure differences during the period of strong west wind are apparent at both lower and upper floors. The changes in pressures created are highly unpredictable and are summarized below.

- Floor 2 – The pressure in Suite 203 decreases relative to adjacent suites on the same floor by 10 to 14 Pa
- Floor 3 – The pressure in Suite 302 increases relative to adjacent suites on the same floor by 16 to 19 Pa.
- Floor 4 – The pressure in Suite 403 increases relative to adjacent suites on the same floor by up to 45 Pa.
- Floor 10 – The pressure in Suite 1002 and 1001 both increase relative to Suite 1003, by 12 Pa and 10 Pa respectively.
- Floor 11 – The pressure in Suite 1102 decreases relative to adjacent suites on the same floor by up to 30 Pa.
- Floor 12 – The pressure in Suite 1202 decreases relative to adjacent suites on the same floor by up to 15 to 20 Pa. (Note that the corridor-to-suite pressure sensor for Suite 1201 malfunctioned, so results using this sensor are unreliable.)

There is little consistency in the reaction of suite pressures to this strong west wind. An increase in pressure of -01 type suites would be anticipated for a strong west wind, and fluctuations in pressures of -02 types suites may also be anticipated as relatively small changes in wind direction (e.g. from west to north-west) could significantly change the pressure on the north elevation. Furthermore, the pressure of -02 type suites may depend largely on how many windows are open and which ones (windward windows, leeward windows et cetera) and this could cause different suites to have different reactions to the same wind event. However, the significant pressurization

of Suite 403 that was measured is unexpected and highlights the complex nature of pressures created by wind within the building.

In general, the pressure differences created between suites due to wind can be of significant magnitude (up to nearly 50 Pa) and thus can generate significant airflow between suites. The magnitude and direction with which the pressure differences act are highly complex.

10.5.3 Summary of Suite-to-Suite Results

Overall, suite-to-suite pressure differences have little to no relationship with exterior temperatures but can be significantly altered by wind. In some cases windward suites become pressurized relative to adjacent suites, as would be predicted, but generally the magnitude and direction of the suite-to-suite pressure differences created by wind are difficult to predict beyond the general finding that stronger winds typically create higher magnitude pressure differences. These pressure differences can range up to 50 Pa for strong winds. The suite-to-suite pressure differences created by wind have the potential to create significant airflow between suites if the demising walls are not adequately air sealed.

10.6 Pressure Changes Due to Occupant Controlled Components

Occupants have direct control over a number of building components that can change pressure differences and airflow patterns into, out of, and within the case study building. These include operation of point source exhaust fans (e.g. bathroom exhaust fans, range hood exhaust fans, and clothes dryers), operating unsealed combustion type gas fireplaces, opening and closing exterior windows and doors, opening and closing of suite entrance doors, and movement of the elevator including opening and closing of elevator doors. It is anticipated that these types of relatively short-term events would be apparent as fast and short changes in pressure (i.e. pressure spikes) that occur independent of driving forces such as temperature and wind. It is also possible that these types of events could occur over longer time periods such as the opening of windows. To assess the changes in pressures due occupant operation of these building components a period of minimal wind from January 15, 2013 to January 23, 2013 was selected as the low magnitude of the wind combined with the relatively stable exterior temperatures during this period make the pressure differences stable and should make pressure spikes due to occupant operation of building components more apparent. The exterior temperature during this period is relatively cold compared to typical exterior temperatures at the case study building and ranged from approximately 0 to 5°C. As pressure differences were only sampled once per hour and operation of these occupant controlled building components is expected to be for relatively short durations, it is likely that many operation events were not captured by these measurements.

Figure 10-92 to Figure 10-97 show the suite-to-suite pressures during this period identifying occasions when suites became pressurized or depressurized relative to adjacent suites on the same floor. (Note that not all suite pressurization and depressurization events are identified in these figures, but samples of the most easily distinguishable events are identified.) Using suite-to-suite pressure differences proved to be the easiest method for identifying pressure changes in one suite relative to the other suites on the floor as these quantities are largely unaffected by short term effects of the natural driving forces which makes the pressure spikes more easily noticed.

Depressurization and pressurization of suites relative to adjacent suites can be noted by identifying instances where two pressure differences spike and then by determining the suite common to both measurements.

The identification of instances where individual suites become pressurized or depressurized relative to adjacent suites is easier on the lower floors of the building where the general variation in pressure differences is relatively small, while on upper floors the variation is large enough that it can make the identification of pressure spikes caused by exhaust fans et cetera to be much more difficult.

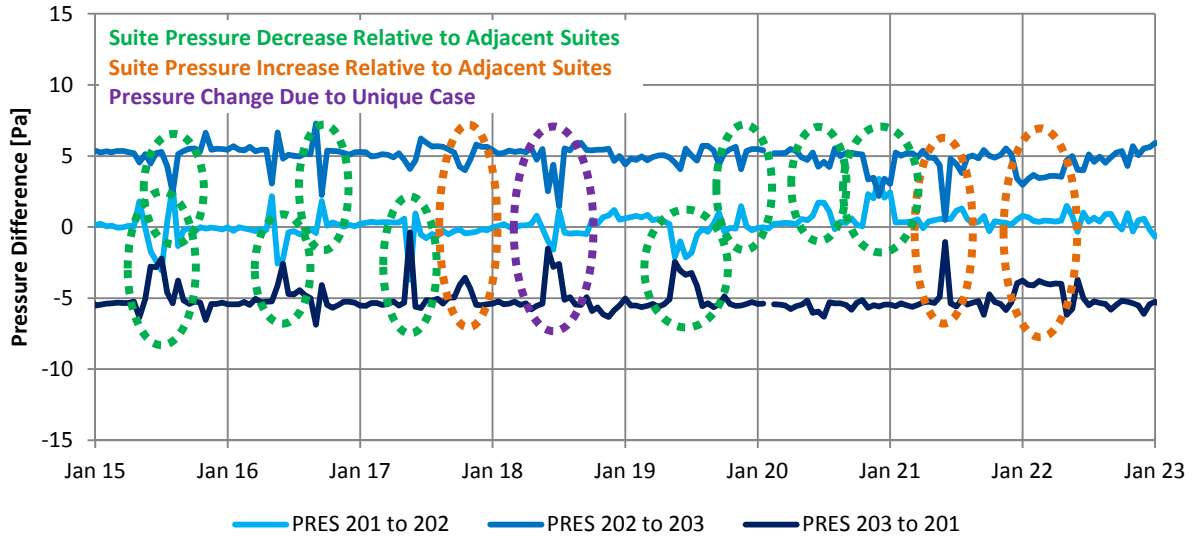


Figure 10-92: Graph of hourly suite-to-suite pressure differences for Floor 2 showing occasions when suites became pressurized or depressurized relative to adjacent suites

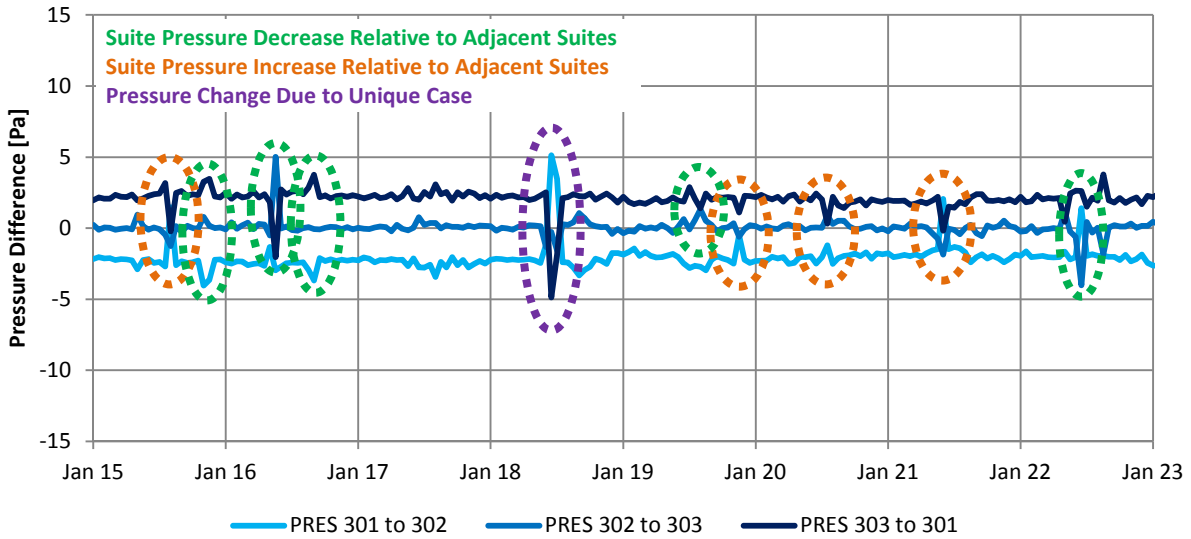


Figure 10-93: Graph of hourly suite-to-suite pressure differences for Floor 3 showing occasions when suites became pressurized or depressurized relative to adjacent suites

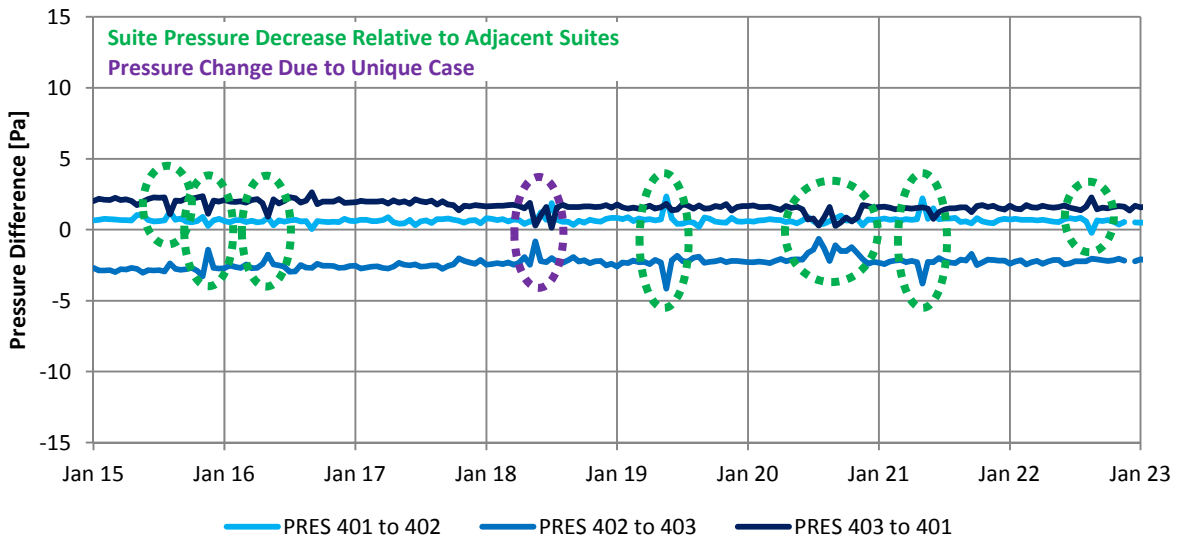


Figure 10-94: Graph of hourly suite-to-suite pressure differences for Floor 4 showing occasions when suites became pressurized or depressurized relative to adjacent suites

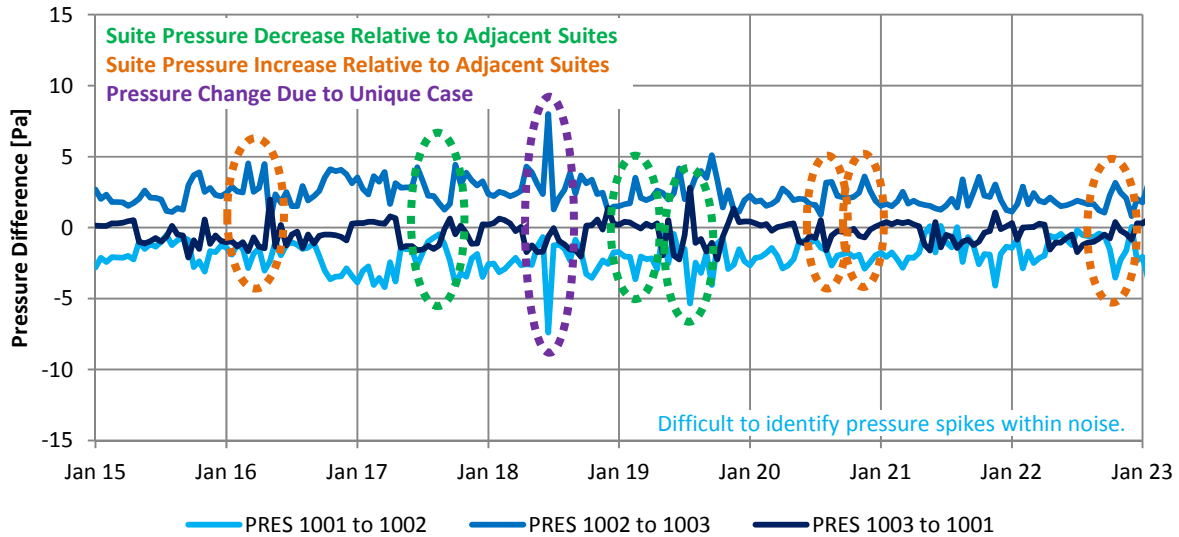


Figure 10-95: Graph of hourly suite-to-suite pressure differences for Floor 10 showing occasions when suites became pressurized or depressurized relative to adjacent suites

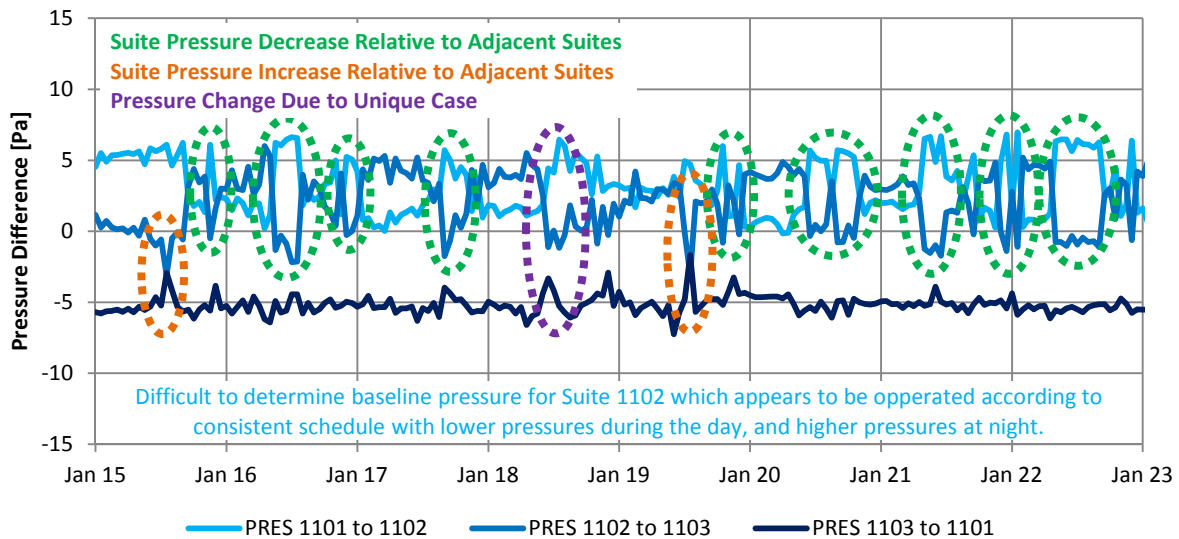


Figure 10-96: Graph of hourly suite-to-suite pressure differences for Floor 11 showing occasions when suites became pressurized or depressurized relative to adjacent suites

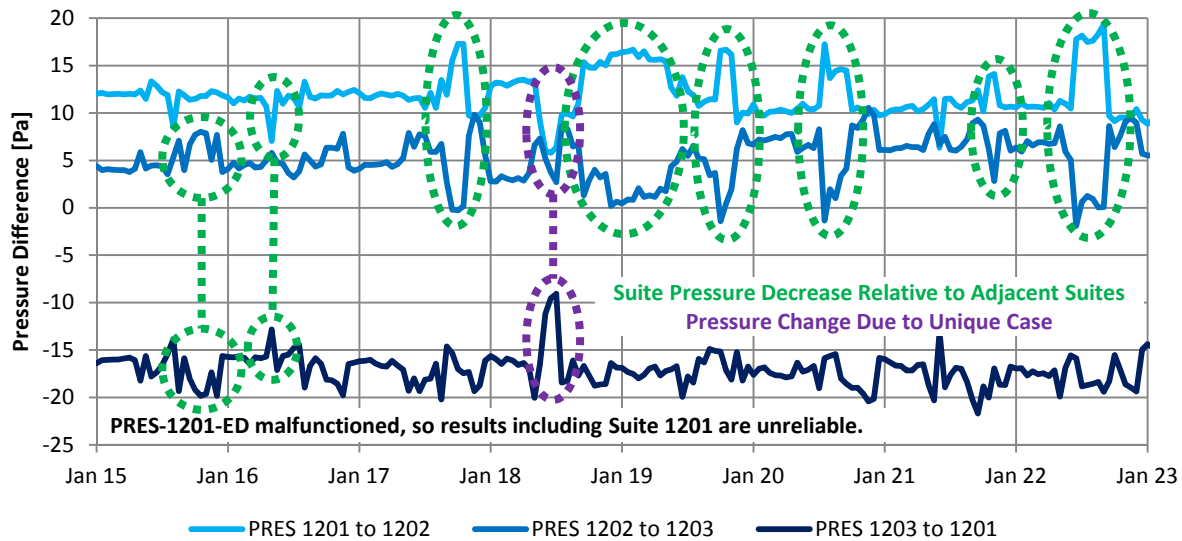


Figure 10-97: Graph of hourly suite-to-suite pressure differences for Floor 12 showing occasions when suites became pressurized or depressurized relative to adjacent suites

When suites become depressurized relative to adjacent suites it is likely that this is caused by the operation of point source exhaust fans. The depressurization relative to adjacent suites as a result of exhaust fan operation ranges in magnitude from 1 Pa to 5 Pa, and in some limited cases up to approximately 10 Pa. The larger changes in pressure may be due to simultaneous operation of multiple fans. The changes in pressures measured from the suite to the corridor and from the suite to the exterior are of similar magnitude. This is shown for Suite 1102 in Figure 10-98 which identifies many of the same periods of depressurization as in Figure 10-96.

The depressurization of Suite 1102 relative to adjacent suites is typically 4 Pa, and the depressurization relative to the exterior is also approximately 4 Pa. The change in pressure differences from the suite to the corridor during the same periods is 3 to 4 Pa, which is slightly less and indicates that the corridor may be depressurized slightly (on the order of 1 Pa) by the suite exhaust fans in this case. This finding that changes in suite to adjacent zone (corridor, exterior, and adjacent suites) pressure differences as a result of exhaust fan operation are all of similar magnitude is typical for pressure differences caused by exhaust fan operation at the case study building.

Suite 1102 is a unique because the occupant operates an exhaust fan (or multiple exhaust fans) during large proportions of the day. This makes it difficult to determine whether the suite is being depressurized by an exhaust fan or whether it is being pressurized by some other means during the other time periods; however, examination of the pressure differences for this suite during time periods other than those shown in Figure 10-98 and Figure 10-96 made it more apparent that it was being depressurized.

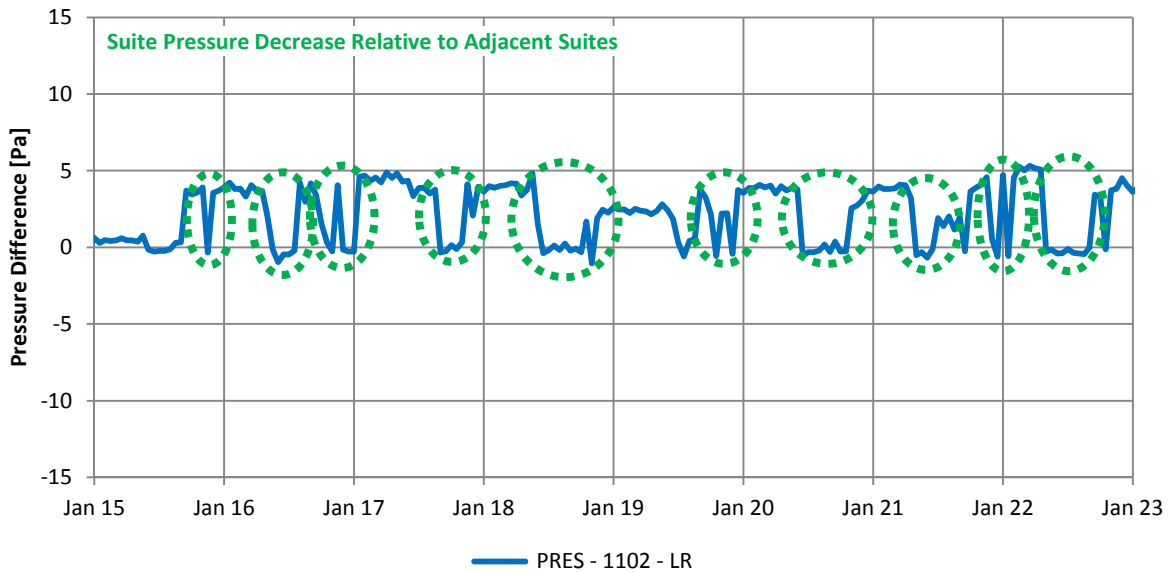


Figure 10-98: Graph of hourly pressure across exterior enclosure at Suite 1102 (North elevation) showing depressurization

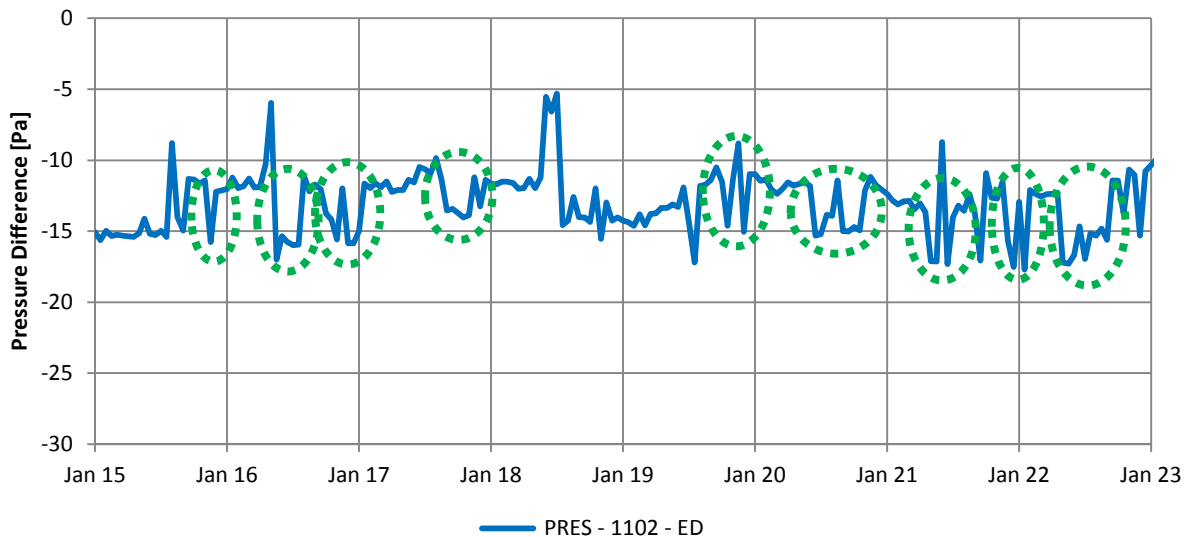


Figure 10-99: Graph of hourly pressure from Suite 1102 to Corridor 11 showing depressurization

It is also possible to calculate the theoretical pressure differences created by the operation of exhaust fans using a combination of the measured exhaust flow rates and the total airflow characteristics of the suite pressure boundaries from the airtightness testing. The range of exhaust fan flow rates that were measured at the case study building are plotted with the total pressure versus airflow rate curves for the average of the typical suites in Figure 10-100. The measured airflow rates for the exhaust fans are provided in Appendix C and the airtightness testing results were presented in Chapter 9.

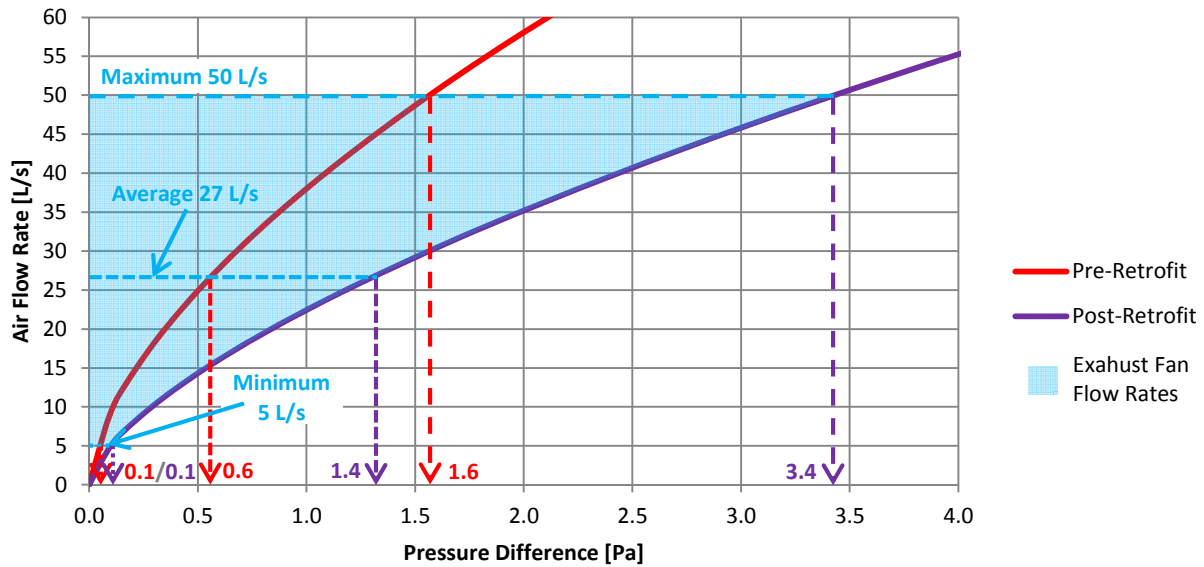


Figure 10-100: Graph of hourly pressure versus airflow rate relationship for total of average suite pressure boundaries showing theoretical depressurization due to exhaust fan operation

Figure 10-100 shows that the theoretical depressurization of a typical suite created by the operation of bathroom exhaust fans pre-retrofit ranged from essentially 0 Pa to approximately 1.6 Pa, and post-retrofit the theoretical pressure differences ranged from approximately 0 Pa to 3.4 Pa. The measured results presented earlier in this section are during the post-retrofit conditions. This level of depressurization is slightly less than the measured pressures; however, the magnitude is similar. This finding like indicates that the pressure identified in the measured data are the instances where suites were most depressurized, and instances where suites were not as significantly affected by operation of exhaust fans were not identified as the pressure differences are not noticeable within the general variation in pressures. The slightly higher pressure differences measured may also be due to operation of higher capacity exhaust fans such as kitchen range hoods or by the simultaneous operation of multiple exhaust fans in the same suite.

In some cases the effect of exhaust fan operation can also be noted to depressurize the corridor to the corridors on the floors above and below. Typically these changes in pressures are either very small (1 Pa or less) or not apparent; however, in some cases these changes in pressures are apparent across multiple floors. The corridor-to-corridor pressure differences are shown in Figure 10-101 and Figure 10-102 for lower and upper floors respectively with instances of depressurization that coincide with depressurization of a single suite identified. These events are likely due to the operation of exhaust fans in suites.

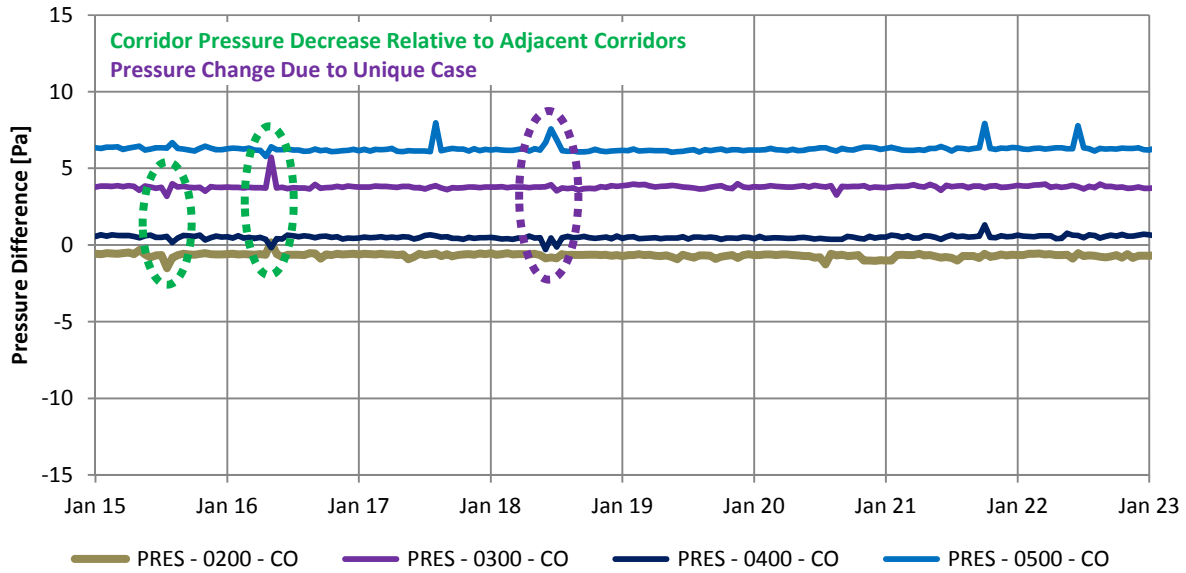


Figure 10-101: Graph of hourly pressure differences between corridors for lower floors showing instances of depressurization

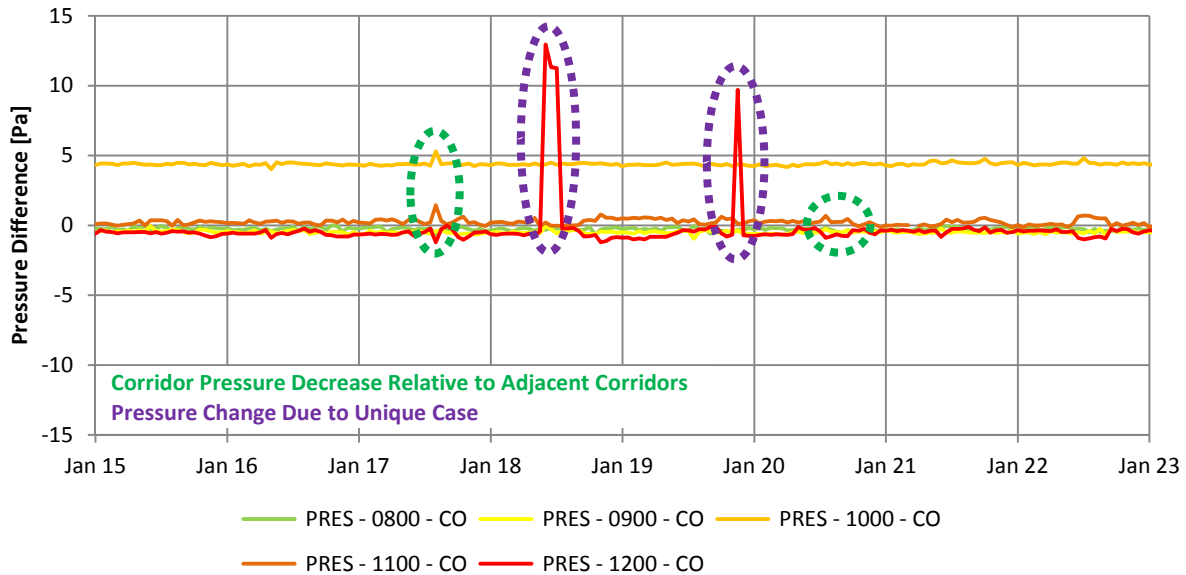


Figure 10-102: Graph of hourly pressure differences between corridors for upper floors showing instances of depressurization

In some less common cases, suites were also noted to increase in pressure relative to adjacent suites. When this occurs, typically all of the suites on a floor are measured to increase in pressure relative to the corridor, and this is likely due to the elevator doors opening on that floor. It is possible that the elevator doors opening could provide a path for ventilation air supplied by the

make-up air unit to the corridor to flow out of the corridor more easily, thus temporarily dropping the pressure in the corridor relative to normal operation.

It is theorized that these cases where only one suite on the floor is measured to increase in pressure relative to the corridor are due to opening of the suite entrance door. Typically suites are at a lower pressure than the corridor; consequently, opening the suite entrance door would effectively equalize the pressure between the corridor and that suite and could cause the observed pressure increases.

The large pressure spikes on January 18th and January 19th which are identified as “Unique Case” throughout the graphs in this section are a result of strong depressurization of Floor 13. These relatively large changes in pressure are also noticeable in the Corridor 13 to exterior pressure measurements as shown in Figure 10-103. This strong depressurization is anomalous and not typical of pressure patterns observed at the case study building. The cause of these strong changes in pressure is unknown, but it is theorized that because the depressurization occurred on the thirteenth floor these spikes may have been caused by opening the door to the roof at the top of the stairwell. Opening of this door would likely equalize the Corridor 13 pressure with the exterior and, given the pressurized nature of this corridor relative to the exterior, this equalization would appear as a negative pressure spike towards 0 Pa which is consistent with the observed pressure measurements. While the data is consistent with someone opening the roof door, there is no information available about the position of the door to support or refute this theory.

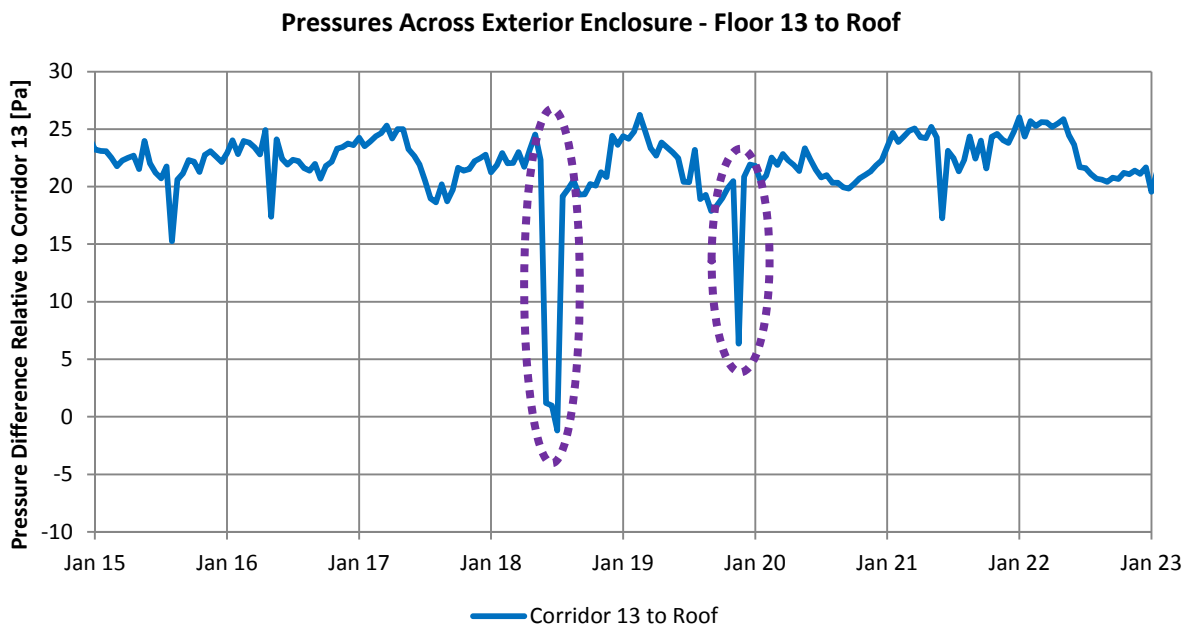


Figure 10-103: Graph of hourly pressure difference between Corridor 13 and roof showing instances of depressurization

During this significant decrease in the pressure of Corridor 13, the corridor to suite pressure differences decreased. The magnitude of this decrease was less for lower floors than for upper floors, likely due to relative proximity to Floor 13. For the spike which occurred on January 18th,

Floor 13 decreased in pressure by approximately 13 Pa relative to Corridor 12 and by 20 Pa relative to the exterior. The depressurization of Corridor 12 relative to adjacent suites was approximately 7 to 9 Pa, and the depressurization of Corridor 2 relative to adjacent suites was approximately 2 to 5 Pa. If this phenomenon was in fact caused by operation of the stairwell to roof door, this instance clearly indicates the strong impact that operation of exterior windows and doors can have on the airflow patterns and pressure regimes within the building.

Analysis of pressure spikes due to occupant operation of building components was also attempted during a warmer periods; however, the variability of the pressures during warmer periods was too great to be able to identify pressure spikes due to occupant operation of building components. This is likely due to typically higher wind speeds and less stable stack effect pressures during these warmer periods. This in itself is a useful finding. That is, that during periods with even light to moderate winds, the pressure differences due to occupant operations of building components such as exhaust fans become small compared to the pressure differences created by other driving forces of airflow.

Overall, occupant controlled building components can alter the pressure regime and thus airflow patterns within the case study building. Exhaust fans were measured to depressurize suites by approximately 1 to 5 Pa, and the opening of suite entrance doors can increase suite pressures by a similar magnitude. Given that these pressures are of similar magnitude to the pressure differences created by wind and stack effect, the operation of these building components has the potential to significantly alter the magnitude and direction of pressure differences in the case study building. While the changes in pressure due to operation of these components is significant, these components likely have a relatively smaller impact on building airflow patterns than stack effect, wind, and the make-up air unit due to the relatively short duration of their operation.

10.7 Location of the NPP and Thermal Draft Coefficient

The pressure monitoring data can be used to calculate the location of the neutral pressure plane (NPP) of the building. As the majority of the pressure difference due to stack effect was measured across the corridor to suite boundary, the location of the NPP for the corridors has been calculated. The calculation uses the procedure provided in Proskiw & Phillips (2008) which assumes a linear relationship between the pressure difference and the elevation within the building and then calculates the location of the NPP using the pressure measurements from interior to exterior at two different elevations. This technique is shown graphically in Figure 10-104. As the pressure differences due to stack effect do not follow a strictly linear relationship as is assumed by this technique, there is some potential for error in calculation of the NPP location. If the pressure differences between floors are the same for every level, this error is limited to approximately half a floor; however, if these pressure differences are not the same, the error can be larger. This level of accuracy is sufficient for this assessment as it provides only an approximation of the location of the NPP.

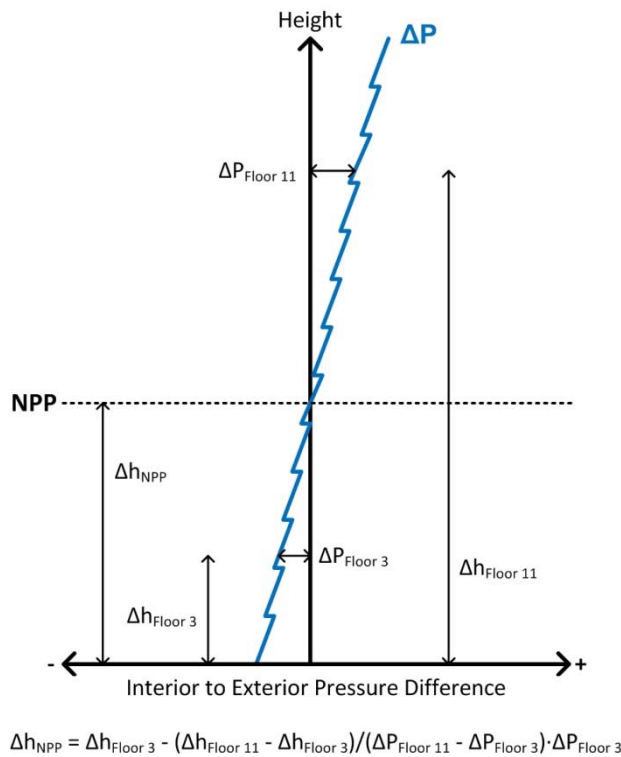


Figure 10-104: Figure showing calculation method for determination of the NPP location

For the case study building, the average pressure differences measured from the corridor to the exterior on Floor 3 and Floor 11 (determined using the average of the sum of corridor-to-suite and suite-to-exterior pressures on each of the two floors) were used for this calculation. The location of the NPP is provided graphically in Figure 5-1. This figure shows that the location of the NPP is relatively stable near Floor 3 and Floor 4 during periods where the 24 hour moving average exterior temperature is below approximately 15°C. The location of the NPP is most stable during periods of cold exterior temperatures. This is consistent with the anticipated findings based on physics as the stability of the NPP will largely depend on the magnitude of the stack pressure. The stronger the pressures created by stack effect (i.e. the colder the exterior temperatures), the more stable the location of the NPP becomes because the pressures needed to overcome stack effect are larger. During relatively warm periods of the year the NPP location is highly variable and often is calculated to be located significantly above or below the building. This is likely because the pressure differences created due to stack effect during these periods are relatively low and are easily overcome by other driving forces. The retrofit appears to have had no impact on the location of the NPP.

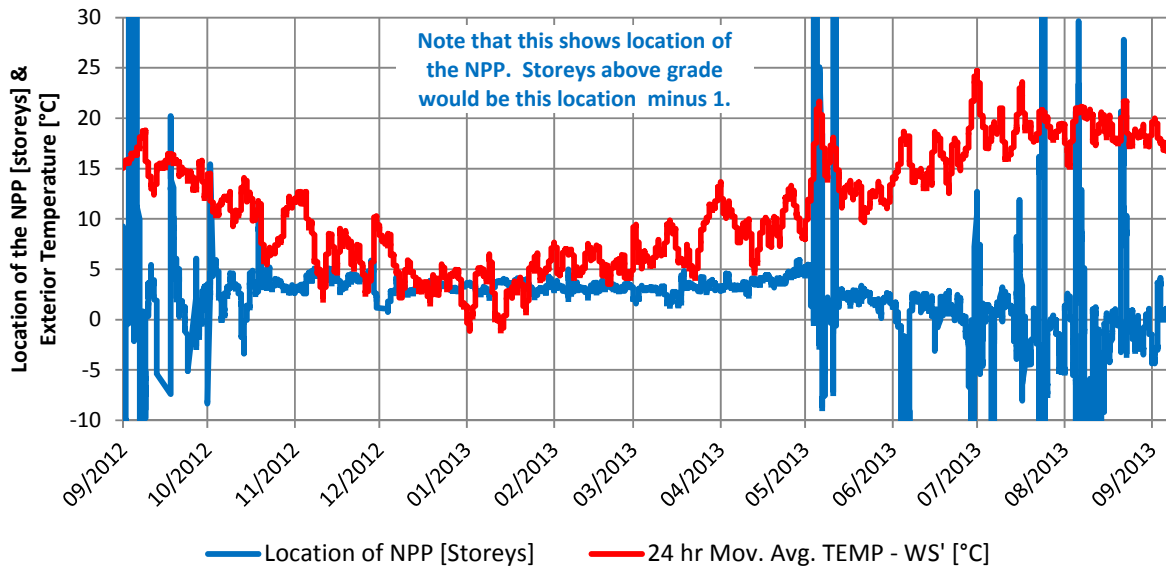


Figure 10-105: Graph of 24 hour moving average location of the neutral pressure plane and exterior temperature

Section 10.2.1 showed that exterior temperature had very little observable effect on the pressure differences measured across the exterior enclosure of the case study building. To determine how much of the pressure difference created by stack effect distributes across different building elements, the thermal draft coefficient (TDC) has been calculated using the average of pressure differences measured on Floor 3 and Floor 11, which are the floors where pressure differences across the exterior enclosure were measured. These pressures were used to determine the measured stack effect gradient (i.e. the pressure difference developed per meter of height) which was then compared to the theoretical stack effect gradient calculated using the outdoor temperature and average of the corridor temperatures. The measured stack effect gradient from the suites to the exterior (across the exterior enclosure), the measured stack effect gradient from the corridors to the exterior (across the exterior enclosure and the corridor to suite boundary), and theoretical stack effect gradient are plotted in Figure 10-106.

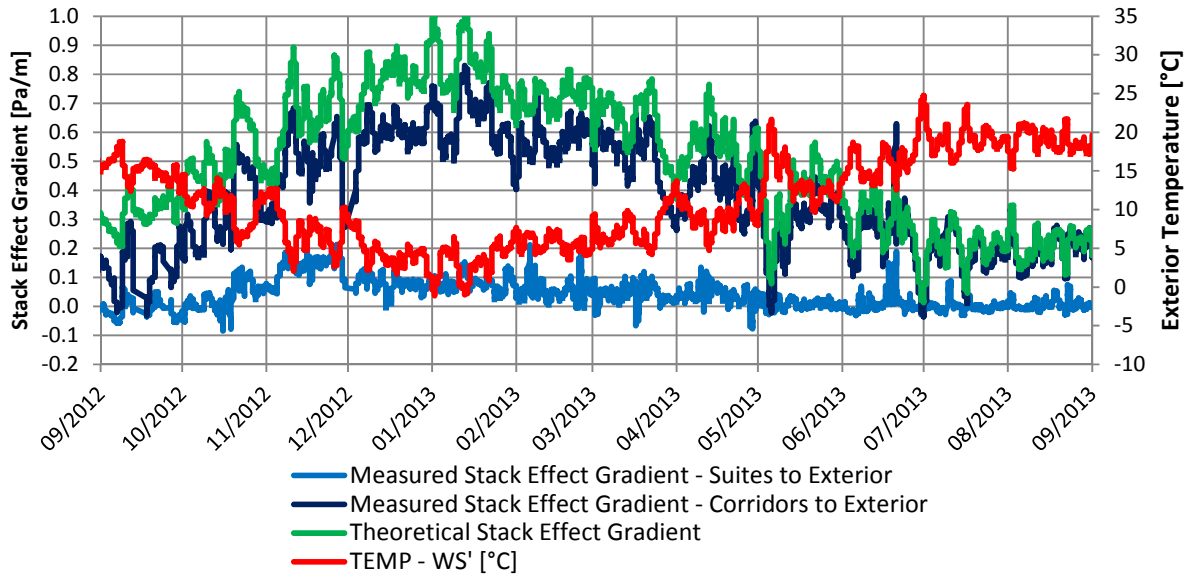


Figure 10-106: Graph of 24 hour moving average measured and theoretical stack effect gradients

This figure shows that only a small amount pressure difference created by stack effect acts across the exterior enclosure; however, a very large portion of the theoretical stack effect pressure difference acts across the corridor to suite pressure boundary. During the period of relatively stable NPP location from December 1, 2012 to Mar 31, 2013, 9% (i.e. a TDC of 0.09) of the pressure difference due to stack effect acts across the exterior enclosure, and 69% (i.e. a TDC of 0.69) acts across the corridor to suite boundary. These values are shown in Figure 10-107 and Figure 10-108 respectively which plot the distribution of stack pressures for these suite-to-exterior and corridor-to-exterior respectively.

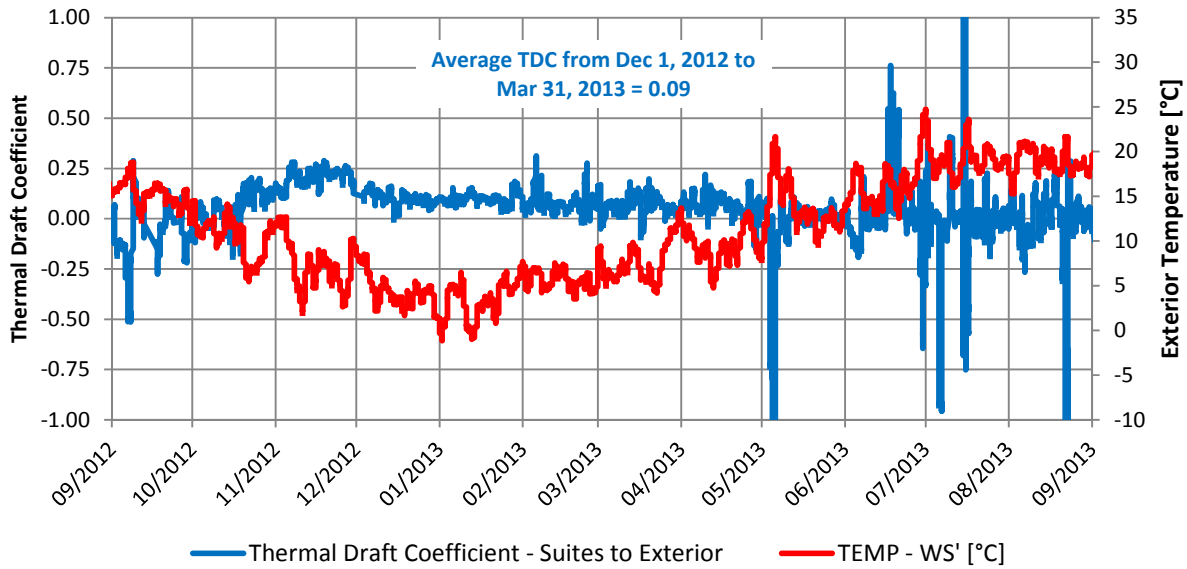


Figure 10-107: Graph of 24 hour moving average of TDC across exterior enclosure of case study building

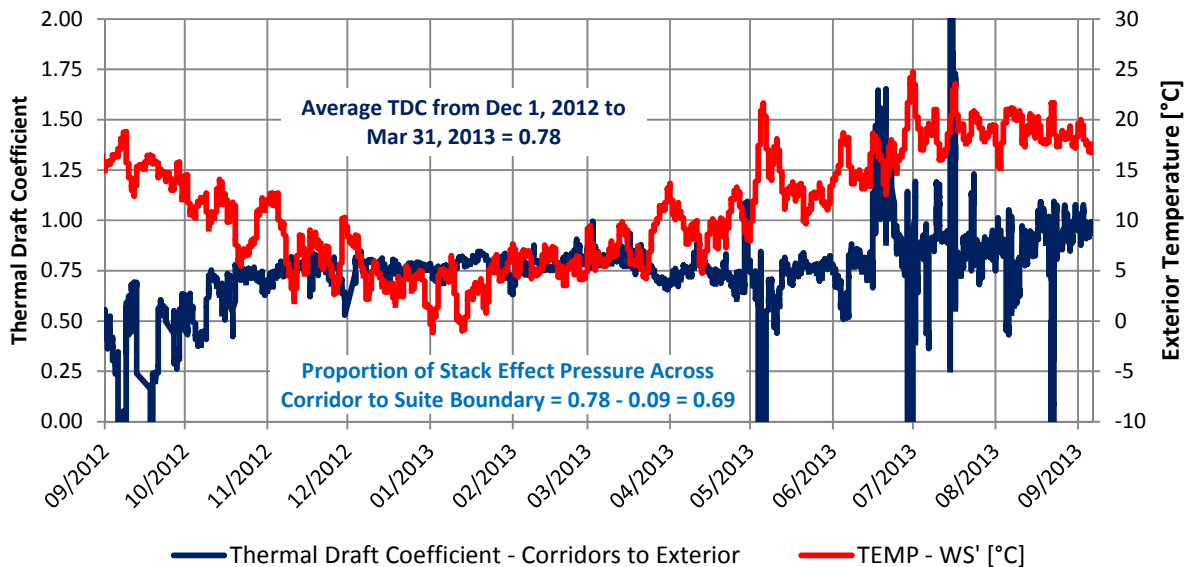


Figure 10-108: Graph of 24 hour moving average of TDC from corridor to exterior of case study building

The pressurized corridor ventilation system is intended to control pressure differences between the corridors and the adjacent suites to provide ventilation air and to control the flow of air contaminants. Because stack effect pressure differences act primarily across this corridor to suite pressure boundaries, pressure differences created by the ventilation system and by stack effect potentially directly conflict. This is a major contributor to the uneven vertical distribution of ventilation air.

This distribution of pressure difference created by stack effect also indicates that the corridors are relatively well connected vertically with respect to airflow and allow for the development of a large fraction of the theoretical stack effect pressures. This is consistent with the finding that the pressures across individual floors from corridor-to-corridor are relatively low in magnitude. The connection of the corridors to each other is likely primarily provided by the elevator shaft and stairwells through relatively air leaky doors as determined by the corridor airtightness testing.

The finding that a large proportion of the theoretical stack effect is developed and distributes across the corridor-to-suite boundary is reinforced by the finding that the pressure from Corridor 13 to the roof are typically very similar to the calculated theoretical total stack effect pressure. This is shown in Figure 10-109. Based on the average from Dec 1, 2012 to Feb 28, 2013, when stack effect is most stable for the roof pressure tap, the proportion of the total stack pressure which was found to distribute across the roof is 0.77. This proportion is very similar to proportion of the pressure difference that occurs from the corridor the exterior across the vertical enclosure (0.78) as shown earlier. As these proportions should theoretically be equal, this similarity helps to validate the measurement and calculation methodology used to determine the distribution of stack effect and location of the NPP.

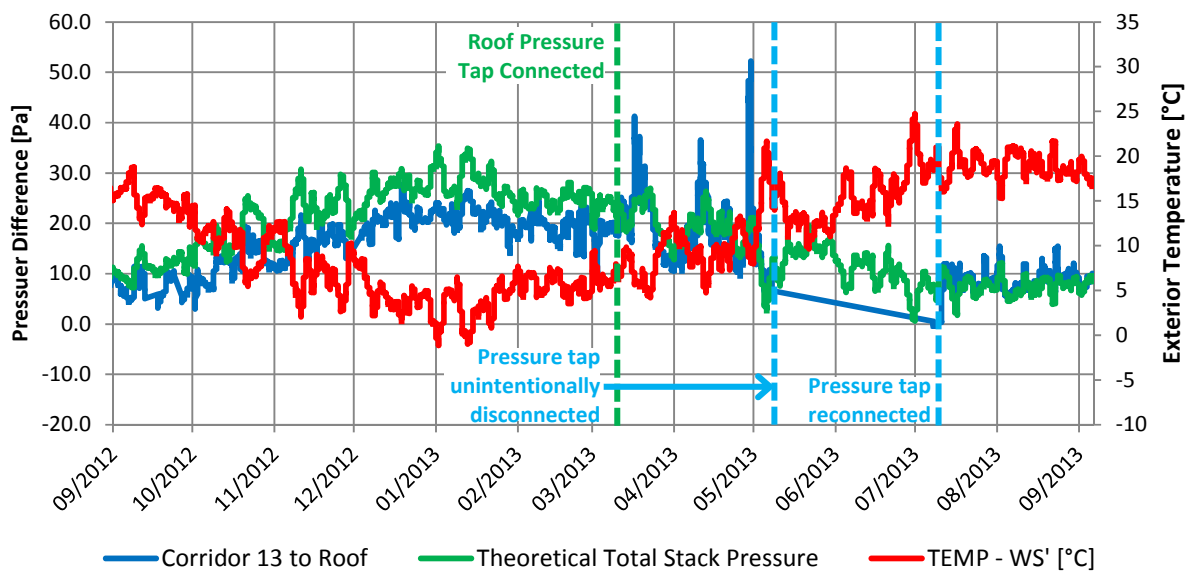


Figure 10-109: Graph of 24 hour moving average of the pressure difference from Corridor 13 to the roof, the theoretical stack pressure, and exterior temperature

The 0.77 proportion of theoretical stack effect pressure that acts across the roof is higher than expected as the theoretical maximum proportion is the proportion of the building height that is above the neutral pressure plane, which is approximately 0.73. While these values are similar and within the expected range of error, it is also likely that the proportion is higher due to pressurization of Corridor 13 by the mechanical ventilation system which would create a higher pressure difference across the roof than would be generated by stack effect alone. If the pressure differences created by mechanical system were evenly distributed, this would not be a potential explanation for the higher proportion; however, because the upper parts of the building were

measured to receive more ventilation air (Chapter 8) and to be more pressurized by the MAU than lower floors (Section 10.8), it is likely that Corridor 13 is pressurized by the MAU more than other corridors of the building.

The high proportion of stack effect pressure which acts across the corridor to suite pressure boundary indicates that this boundary is more airtight than the exterior enclosure. However, the airtightness testing found that post-retrofit (during the majority of the monitoring period) the exterior enclosure for a typical suite allows approximately 156 L/s at 75 Pa, while the corridor walls of a typical suite plus a typical suite entrance door allow 200 L/s at 75 Pa. Based on this distribution of airtightness, one would expect that more stack pressure would distribute across the exterior enclosure than across the suite-to-corridor wall and suite entrance door. It is theorized that the observed distribution occurs as a result of occupant operation of windows which create a relatively unobstructed airflow path between the suite and the exterior mitigating pressures across the exterior enclosure, and instead redistributing these pressure differences to interior compartmentalizing elements such as the corridor to suite walls and suite entrance doors. This distribution of pressure differences reinforces previous findings in literature which note the significant impact that operation of exterior windows can have on the distribution of building pressures. (Proskiw & Phillips, 2008)

To aid in the understanding of the distribution of pressure differences due to stack effect at the case study building, the distribution of these pressures has been schematically illustrated on a cross-section of the building in Figure 10-110. This distribution of pressure differences in this graphic has been developed based on the determined location of the neutral pressure plane and the approximate distribution of stack effect pressures across the corridor to suite pressure boundary and the exterior enclosure. It is intended to represent the order of magnitude distribution rather than an accurate distribution as it does not take into account unique characteristics of each floor, suite, wall, et cetera. Note that the pressure differences are not shown for below grade pressure boundaries (bottom of the elevator and stair shafts) as the distribution of the pressure differences at these locations are overly complex. For the purposes of this graphic, it was also assumed that there is no pressure difference between the stair shaft and the elevator shaft.

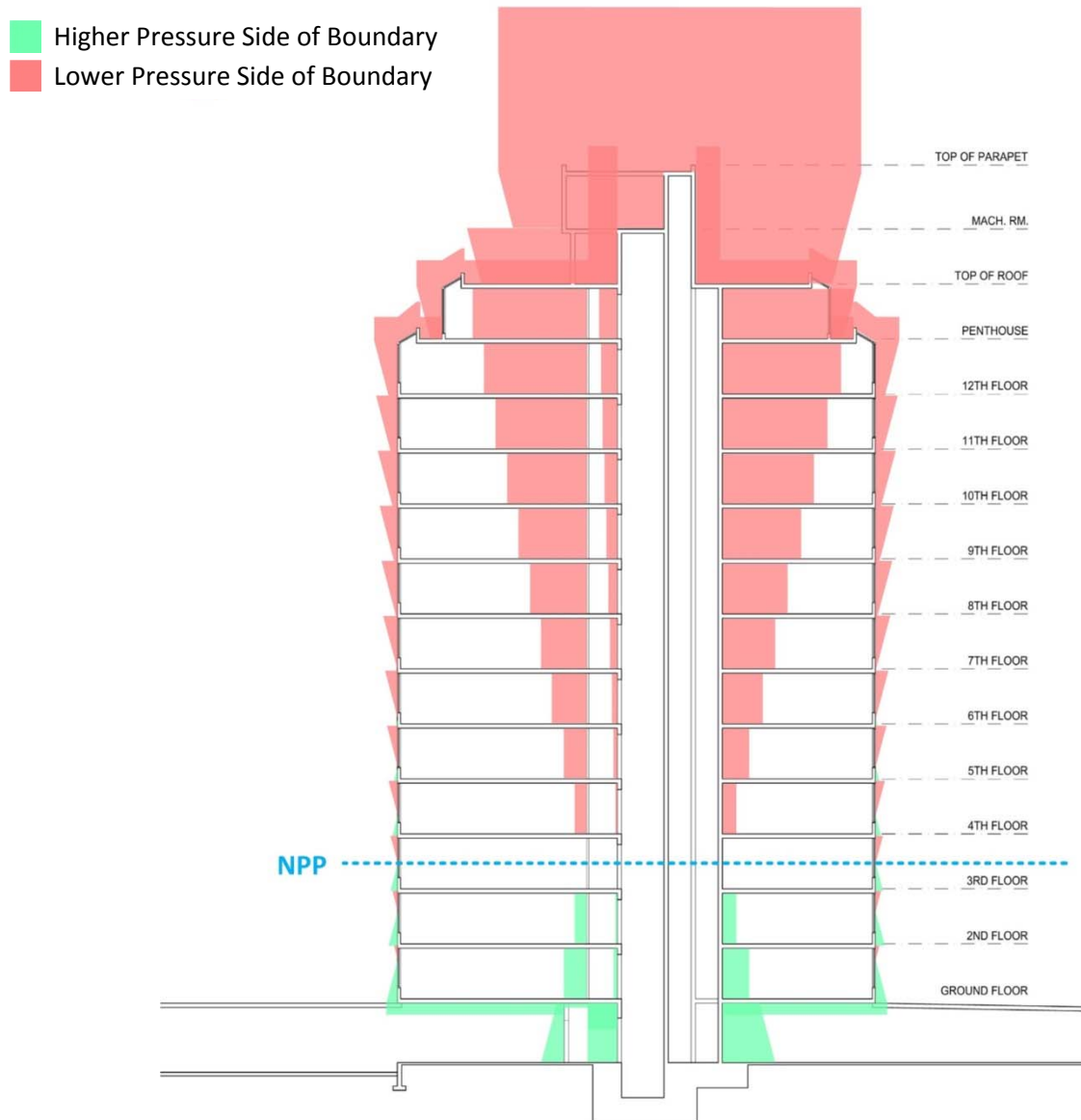


Figure 10-110: Graphic schematically illustrating the distribution of pressure difference due to stack effect at the case study building

10.8 Make-up Air Unit Pressures

As discussed in Chapter 8, the MAU was turned off multiple times to measure the airflow into or out of the MAU duct on each floor. During these flow measurements, the pressure monitoring equipment measured the pressure differences at the building. Comparing these measurements made when the MAU was off to measurements with it on provides an indication of the impact of the MAU of the building pressure regime. These periods with the MAU off and the monitoring equipment installed occurred on three separate dates: February 6, July 11, and July 26, 2013. The

monitoring results from February 6th are presented in this section as examples, and the measurements on July 11th and 26th are provided in Appendix E.

To illustrate the impact of the MAU on pressure differences across the exterior enclosure the measured pressure differences for February 6th, 2013 are plotted in Figure 10-111 to Figure 10-113.

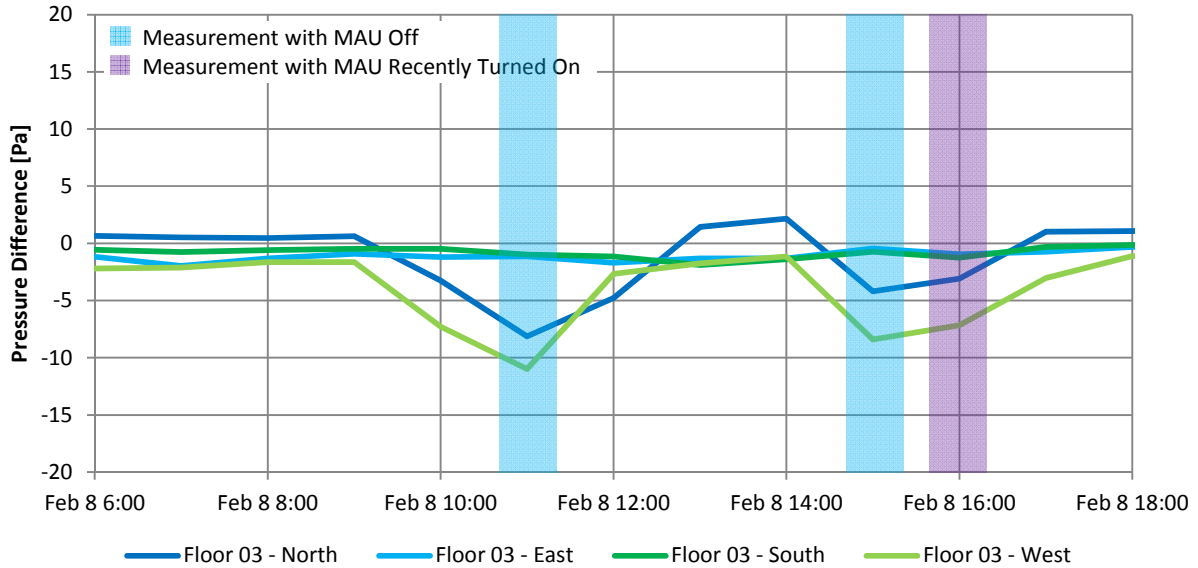


Figure 10-111: Graph of hourly exterior enclosure pressure differences on Floor 3 when MAU off on February 6th, 2013

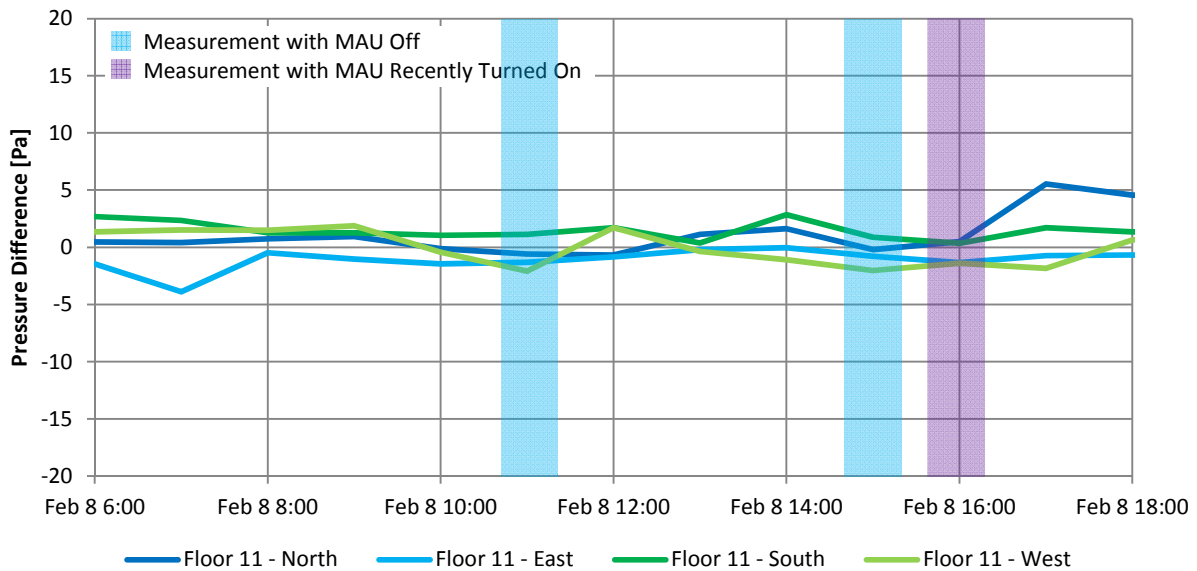


Figure 10-112: Graph of hourly exterior enclosure pressure differences on Floor 11 when MAU off on February 6th, 2013

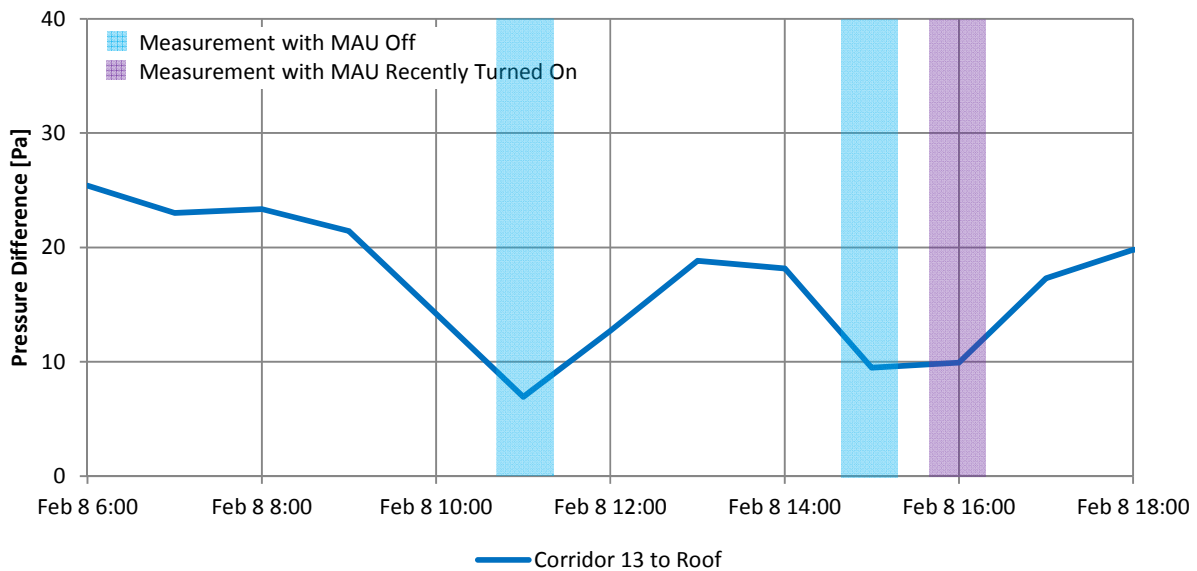


Figure 10-113: Graph of hourly exterior enclosure pressure differences from Floor 13 to roof when MAU off on February 6th, 2013

These figures show that in two cases (Floor 3 – West and Floor 3 – North) the suite pressures decreased by approximately 8 to 10 Pa relative to the exterior when the MAU was turned off. The other exterior enclosure pressure measurements show no noticeable change due to the MAU being turned off. The measurements for the two times in July that the MAU was turned off found similar results with some measurements on the third floor decreasing by less than 5 Pa, but the majority of

measurements remaining essentially unchanged. Since cases where no change was observed generally correspond with pressures of approximately 0 Pa, it is theorized that in these cases the pressure difference across the enclosure was negated by open windows.

The pressure difference across the roof for the measurements in February showed decreases of approximately 10 Pa due to the MAU being turned off, and the measurements in July show no change in one case and a decrease in pressure of approximately 5 Pa in the other case.

To assess the pressure difference between corridors that is created by the MAU, the corridor-to-corridor pressure differences are graphed in Figure 10-114 for the measurements taken in February. While there is a noticeable impact due to turning off the MAU, it is less than 2 Pa which suggests that the MAU does not create significant pressure differences between floors. This is consistent with the findings for the measurements made in July which found typically that the changes in pressure between floors due to the MAU were approximately 1 Pa.

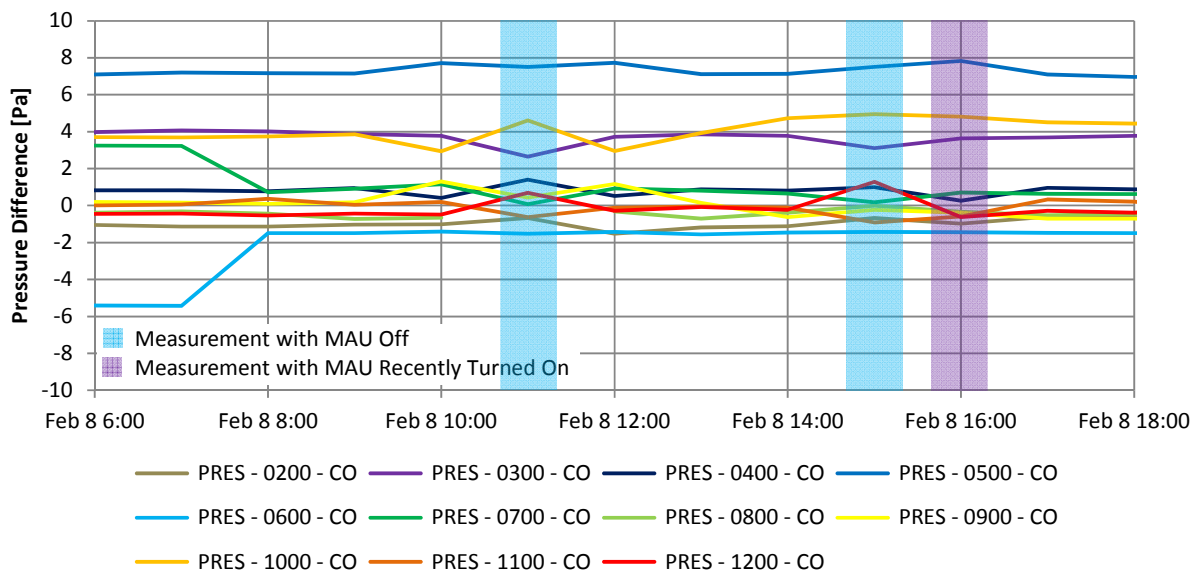


Figure 10-114: Graph of hourly corridor-to-corridor pressure differences when MAU off on February 6th, 2013

The pressurized corridor ventilation system is designed to control pressure differences from the corridors to the suites. To assess the pressures created due to MAU operation, the average suite-to-corridor pressure by floor are graphed in Figure 10-115 for the periods with the MAU off on February 8th.

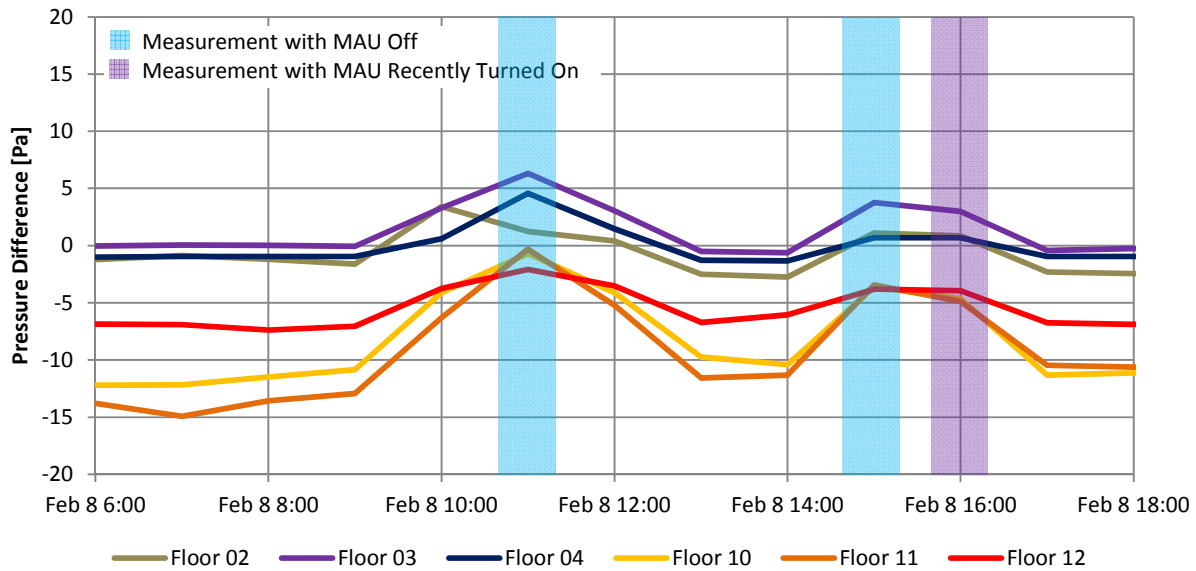


Figure 10-115: Graph of hourly suite-to-corridor pressure differences when MAU off on February 6th, 2013

When the MAU was turned off, suite-to-corridor pressure differences were approximately 2 to 12 Pa higher on lower floors than when the MAU was on, and were an average of approximately 5 Pa higher. On upper floors the pressures increased in the range of 5 to 13 Pa, and were an average of approximately 10 Pa higher. The July measurements (provided in Appendix E) found that the suite-to-corridor pressures typically increased by 5 Pa on all floors when the MAU was turned off. These measurements indicate that the MAU pressurizes the corridors relative to the adjacent suites; however, during periods of colder exterior temperatures the pressure differences created by the MAU are approximately 5 Pa higher on upper floors than on lower floors, likely due to a combination of proximity to the MAU and increased flow resistance caused by stack effect. In many cases the pressure difference from the suites to the corridors with the MAU operating are low and can be overwhelmed by other driving forces including stack effect, wind, and suite exhaust fans.

The ventilation airflow rate to the suites from the corridors through the suite entrance doors can be determined using the typical pressurization of the corridors relative to the suites of 5 Pa and 10 Pa presented here, and the flow characteristics of the suite entrance doors as determined by the airtightness testing protocol and presented in Chapter 9. It is difficult to assign airflow rates through the suite entrance doors due to the operation of the MAU as the pressures created by the MAU do not operate in isolation (i.e. the flow created by a change in pressure from 0 to 5 Pa is not the same as the flow created by a change in pressure from 5 to 10 Pa); however, if one assumes that the corridor to suite pressures are 0 Pa when the MAU is not operating, the flow rate into a suite due to operation of that MAU can be approximated. This assumption is not entirely accurate as shown by the suite-to-corridor pressures in Section 10.4, but is reasonable for this application. The average flow coefficient and flow exponent for the nine suite entrance doors tested are 7.5 L/s·Paⁿ and 0.60 respectively. The flow rates at 5 Pa and 10 Pa determined using these quantities are 20 and 30 L/s respectively. For comparison, ASHRAE 62.1-2010 recommends a ventilation rate of approximately 42 L/s for the average suite in the case study building. As the ASHRAE 62.1-2010

rate is generally recognized to be a relatively high ventilation rate (Lstiburek, 2011) the theoretical amount of airflow that the MAU creates from the corridor the suites may be sufficient to ventilate the suites; however, as determined previously, the pressure differences developed from the corridor to the suites can be overwhelmed by other driving forces, and typically significantly lower airflow rate from the corridors to the suites were measured by the PFT testing results presented in Chapter 8.

Overall, the MAU typically increased the pressure of the corridors relative to adjacent suites by 5 to 10 Pa. The distribution of these pressures was uneven during measurements made in colder weather (the pressure differences on higher floor were higher in magnitude than on lower floors). This uneven distribution is likely due to a combination of stack effect and proximity to the MAU. In some cases pressure differences of approximately 5 Pa were measured across the exterior enclosure due to operation of the MAU; however, in many cases there was no observable pressure difference and it is theorized that often pressure differences across the enclosure are neutralized by the opening of the operable windows. Generally, the pressures created by the MAU are within the anticipated range. The measured pressure differences are of similar magnitude to pressures created by other driving forces. Consequently, there is significant potential for the pressures created by the MAU to be overwhelmed thereby significantly reducing its ability to effectively distribute ventilation air and control the movement of air contaminants.

10.9 Effect of the Retrofit

The results of the pressure monitoring at the case study building indicate that the building enclosure retrofit had no observable impact on the building pressure field. While the building industry commonly suggests that airtightness of the exterior enclosure may restrict airflow and thus provide additional resistance to both supply and exhaust of ventilation air as well as change the distribution of pressure differences within the building, this has not been found to be the case for this building. It is theorized that this lack of measurable impact is largely due to the operation of windows effectively negating the improved airtightness of the exterior enclosure and thus allowing the building to operate very similarly pre- and post-retrofit. It is also possible that no change was observed because the building was sufficiently tight both before and after the retrofit, or because the building was sufficiently leaky before and after the retrofit.

10.10 Summary of Results

During cold periods of the year, lower floors of the building are at a higher pressure than upper floors as predicted by the physics of stack effect. The measured stack effect pressures were similar to the theoretical stack pressures for a building with no vertical separation. This result indicates that the floors of the case study building are relatively well connected with respect to airflow. This connection is theorized to occur primarily through the elevator shaft and stairwells which are well connected to the corridors via relatively air leaky elevator and stairwell doors.

Stack effect pressure acted primarily across the corridor to suite pressure boundary with 69% of the theoretical pressure difference acting across this pressure boundary whereas only 9% acts across the exterior enclosure. This distribution of pressure differences suggests that operation of windows significantly alters the airtightness of the exterior enclosure and mitigates the

development of stack effect pressures across the enclosure pressure boundary. It also indicates that the pressure boundaries of the vertical shafts in the building (e.g. elevator doors and stairwell doors) provide little resistance to airflow.

Since a large portion of the stack effect pressures occur across the corridor to suite pressure boundary, control of the pressure difference from corridors to suites is difficult. The make-up air unit increases corridor to suite pressures differences by approximately 5 to 10 Pa depending on vertical location within the building and the exterior temperature. Upper corridors were found to be more pressurized relative to the adjacent suites than lower corridors, likely due to a combination of stack effect and proximity to the make-up air unit. This pressurization would likely provide increased ventilation flow rates to these suites which is consistent with the airflow findings presented in Chapter 8.

Wind typically creates the peak pressure difference at the case study building; however, the direction and magnitude of these pressures is difficult to predict and the duration of these higher pressures is measured in only a few hours per month. Significant pressure differences were measured across all of the pressure boundaries of the building due to wind except for corridor-to-corridor where the pressure differences were found to be relatively independent of wind. For the other pressure boundaries, wind pressures created in moderate and strong winds were often of sufficient magnitude to overcome other driving forces and may facilitate the unintentional flow of air between building zones, potentially causing transfer of air contaminants and associated indoor air quality issues.

Exhaust fans typically created pressure differences of 5 Pa or less, but in some cases higher pressures were measured. It was difficult to identify these pressure differences except in periods when other driving forces (in particular wind) were consistent and of low magnitude because the magnitude of the changes created by the operation of exhaust fans or other occupant controlled components are relatively low and the majority of measurements were made in hourly increments. While in the short-term exhaust fans and operation of doors et cetera change pressure distributions enough to alter airflow patterns, these components likely have a relatively small impact on building airflow patterns compared to stack effect, wind, and the make-up air unit due to the relatively short duration of their operation. A more significant impact may be possible if more powerful fans were installed or if they were operated more frequently.

Overall, all three categories of driving forces of airflow play a significant role in creating the pressure and airflow patterns at the case study building. The inability of the mechanical ventilation system to adequately control the building pressure field and evenly distribute ventilation air creates significant potential for the transfer of contaminants between zones and for the uneven and inadequate ventilation of building zones. These findings are consistent with and identify causes of the measured airflow results presented in Chapter 8.

Chapter 11

Airflows Calculated from Pressure and Air Permeance Measurements

The results of the experimental program measuring airflow, air permeance (airtightness), and pressure differences, have been presented in Chapters 8, 9 and 10 respectively. Using the measurement of airtightness and pressure differences it is possible to calculate the theoretical flow rate that would occur across each pressure boundary and then to compare these airflow rates with the airflow rates that were measured directly. This redundancy in the testing and monitoring plan is intentional and allows for comparison and reconciliation of the two methods.

This chapter initially compares the calculated and measured flow rates during the PFT testing period, and then having established the relatively validity of this approach, presents the calculated flow rates for other time periods.

11.1 Comparison of Measured and Calculated Airflow Rates

The airflow rates in to the suites on Floor 3 and Floor 11 as measured by the PFT testing and as determined by calculation using the airtightness testing results and monitored pressure differences are provided in Figure 11-1 and Figure 11-2 respectively. The airflow rates out of these suites as determined by the two difference methods are provided in Figure 11-3 and Figure 11-4 respectively. Note that charts of the airflows measured by PFT flows are repeated from Section 8.4 to facilitate comparison of the results. (Note that airflows to and from the parking garage for the lower suites have been removed as it is not possible to calculate these flow rates with the available pressure and airtightness information.)

Figure 11-1 to Figure 11-4 illustrate that the calculated airflow rates using these two different methods are similar for airflows in to the suites, but are significantly different for airflows out of the suites. There are many potential causes for discrepancies between the two methods.

The airtightness testing of the pressure boundaries of these suites does not account for the operation of suite entrance doors, or of exterior doors and windows. The operation of these building components significantly alters the resistance to airflow of the given pressure boundary and allows for much greater airflow at the same pressure difference. Additionally, airtightness testing is performed at pressures significantly higher than the operating pressures and extrapolation of the test results down to these lower operating pressures can be a source of significant error. (Genge, 2011)

Operation of exhaust fans is a likely explanation for the significant differences in measured and calculated airflows out of the suites. The measured results using the PFT testing found significantly larger airflow rates from the suites to the exterior on upper floors than did the calculation method. Airflows out of the building due to exhaust fan operation are not accounted for in the calculation method, so it is likely that these flows account for at least part of this discrepancy. This discrepancy primarily occurs on the upper floors, so it is possible that exhaust through the fireplaces is also contributing to this discrepancy.

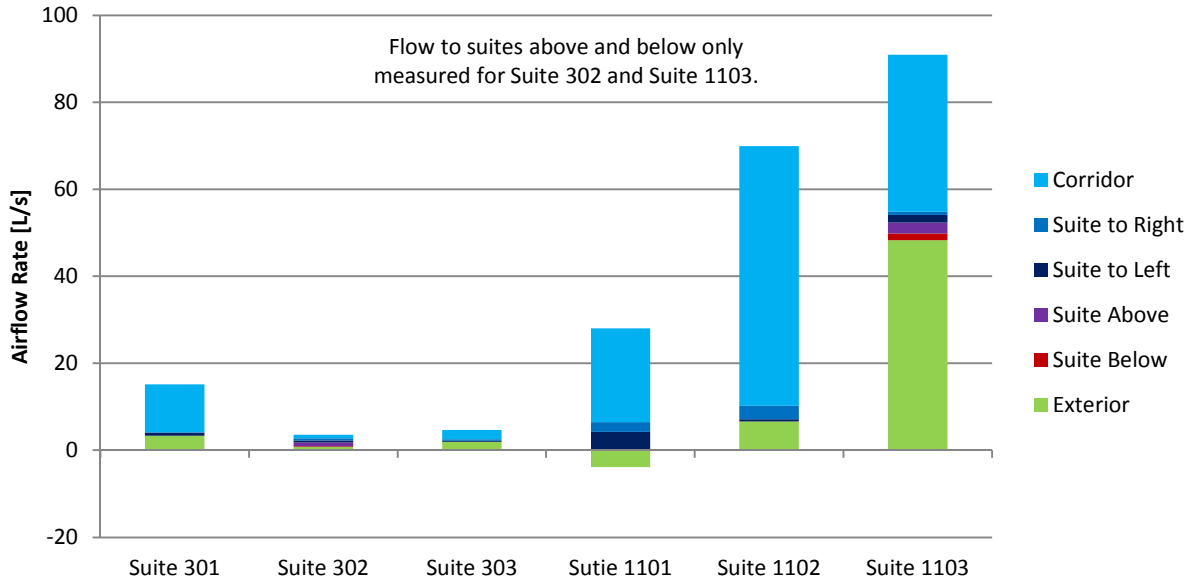


Figure 11-1: Chart of airflow rates in to the suites on Floor 3 and Floor 11 as measured by the PFT testing

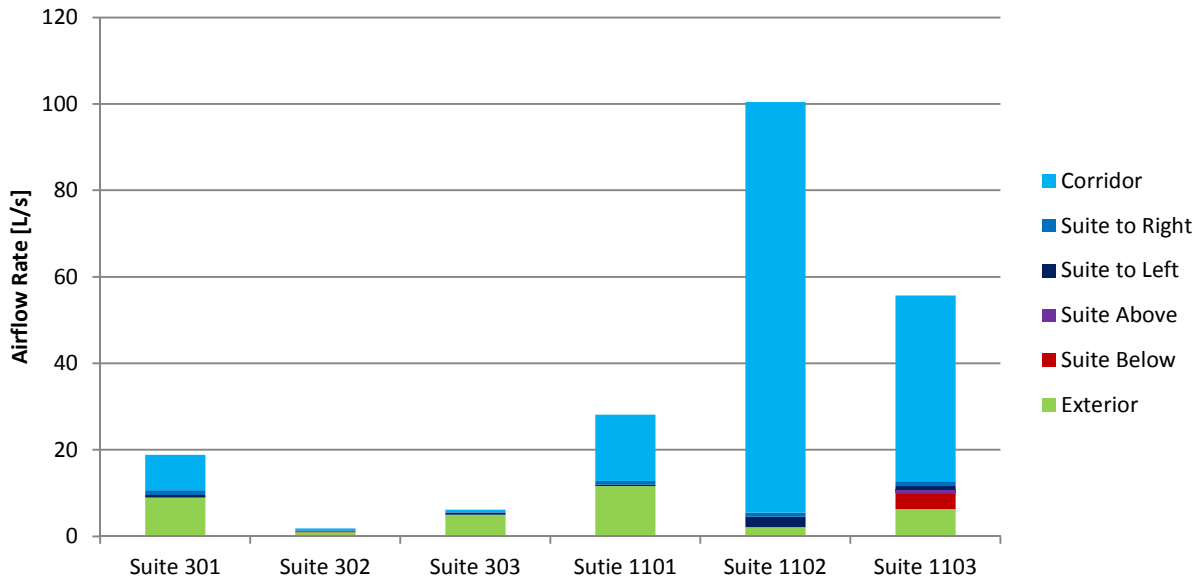


Figure 11-2: Chart of airflow rates in to the suites on Floor 3 and Floor 11 as determined using the airtightness testing results and monitored pressure differences

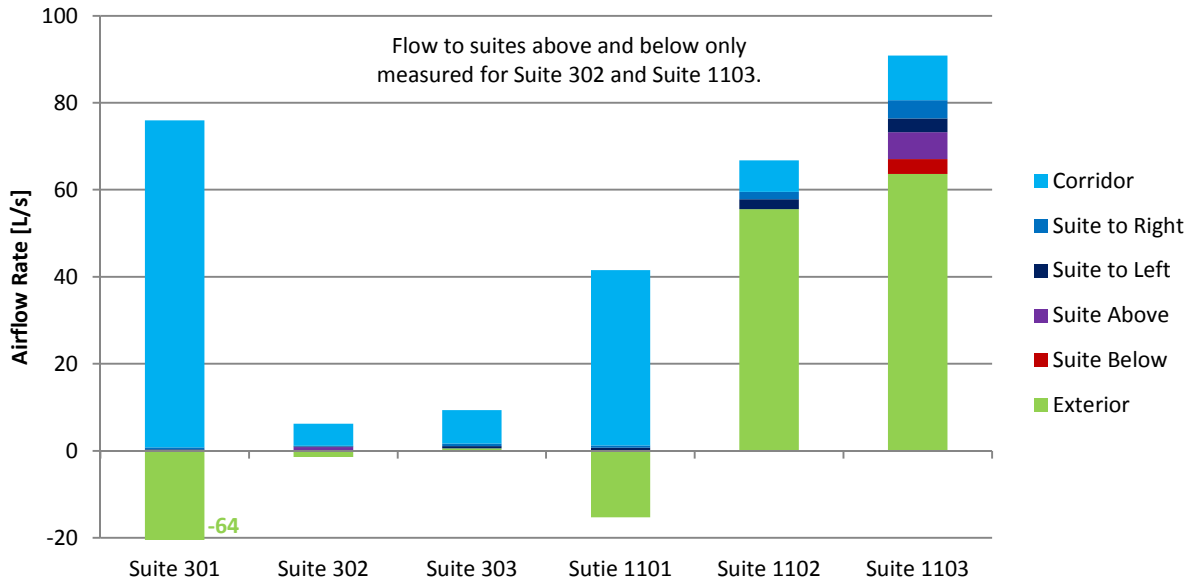


Figure 11-3: Chart of airflow rates out of the suites on Floor 3 and Floor 11 as measured by the PFT testing

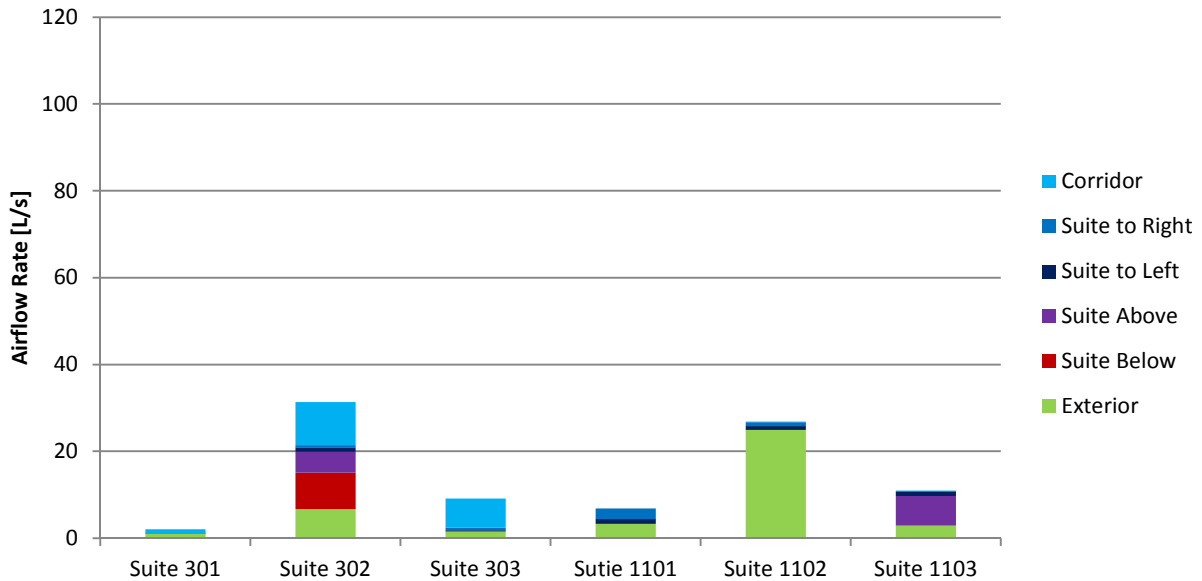


Figure 11-4: Chart of airflow rates out of the suites on Floor 3 and Floor 11 as determined using the airtightness testing results and monitored pressure differences

It is also possible that uneven distribution of pressures, especially across the exterior enclosure, were not captured by the arrangement of monitoring equipment, or that the one hour monitoring interval was too long to capture short term pressure events.

Finally, the results of the PFT measurements are calculated using a system of equations; however, this system of equations does not come to an exact solution and instead the most likely outcome is

determined and then standard deviations generated for each result. In some cases these standard deviations are relatively high and could explain the discrepancies, but this is not thought to be a large source of error other than in specific cases where offsetting airflow errors were determined as discussed in Section 8.4. The standard deviations of the PFT results are provided as part of the PFT testing report in Appendix G.

Despite the generally poor relationship between the flow rates for each suite, when the flow rates as determined by each method are averaged for the six suites, the correlation between the two methods is significantly improved as shown in Figure 11-5 and Figure 11-6.

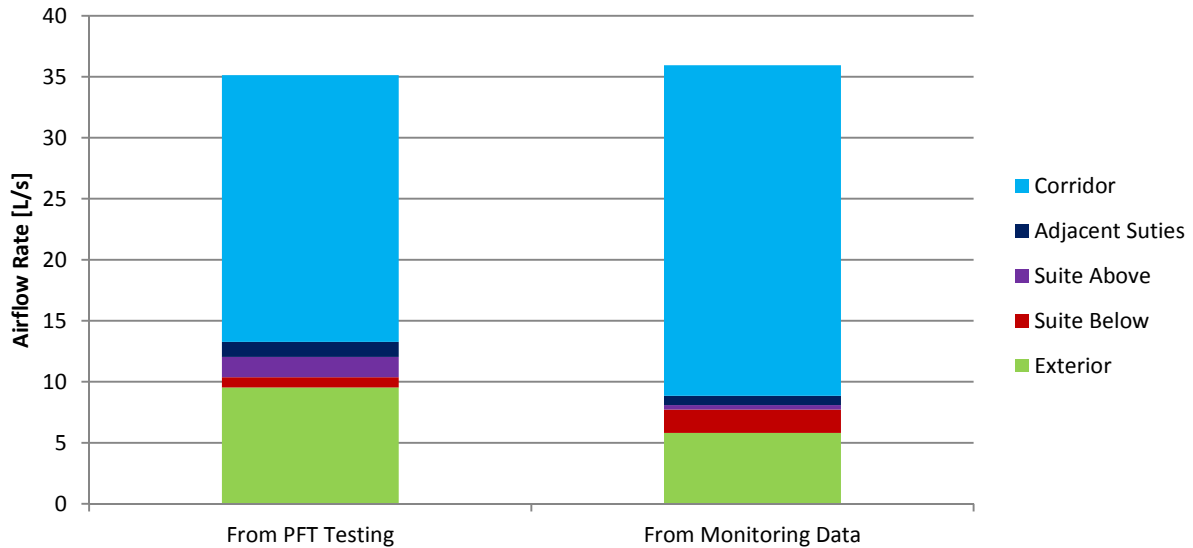


Figure 11-5: Chart of average airflow rates in to the suites on Floor 3 and Floor 11 as measured by the PFT testing and as determined using the airtightness testing results and monitored pressure differences

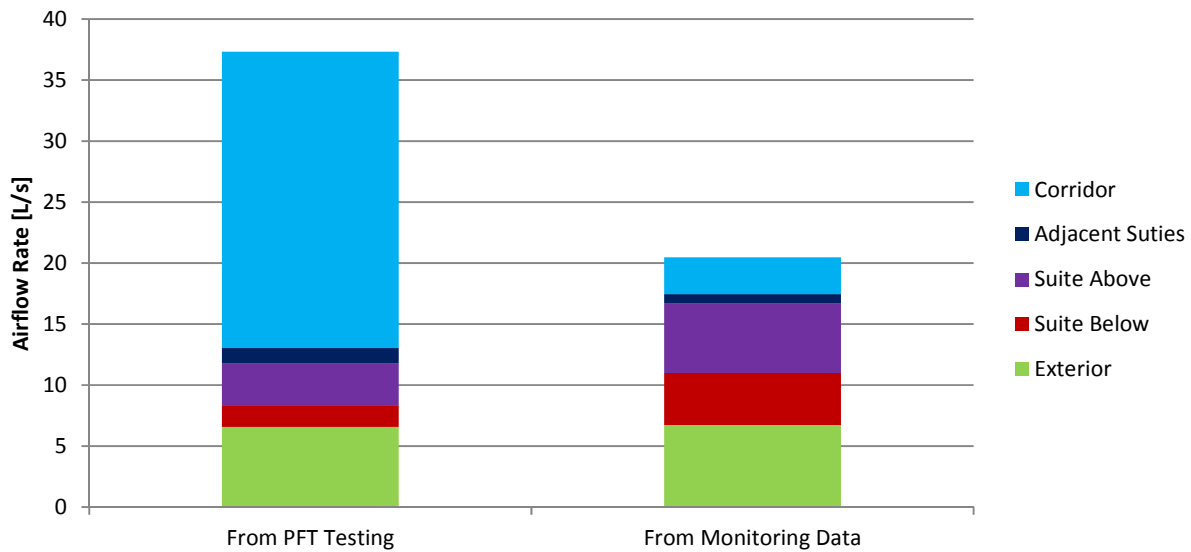


Figure 11-6: Chart of average airflow rates out of the suites on Floor 3 and Floor 11 as measured by the PFT testing and as determined using the airtightness testing results and monitored pressure differences

The difference in airflow out of the suites into the corridor between the PFT testing and that calculated from the monitoring data may be due to the inappropriate assumption of even distribution of the PFT tracer released in the MAU duct as discussed in Section 8.4.2. The magnitude of this potential error is unknown.

Overall it is felt that the PFT testing likely provides a more accurate indication of the airflow rates at the case study building than does the method using the airtightness testing results and monitored pressure difference because the PFT method provides a direct measurement of the airflow.

11.2 Calculated Airflow Rates

Despite the relatively poor correlation between the two airflow measurement techniques, it has still been deemed worthwhile to use the monitored pressure difference and airtightness testing results to determine order of magnitude airflow rates under various conditions. Given that the calculated airflow rates depend on the measured pressure differences, airflow rates versus time graphs appear very similar to those provided for monitored pressure differences in Chapter 10.

Consequently, this section instead provides average flow rates into and out of the suites under various conditions which is appropriate because average (e.g. daily, weekly, monthly) flow rates are of primary importance with respect to ventilation and indoor air quality. This method, however, does not provide information with regards to short-term contaminant transfer such as of cooking odours between suites.

11.2.1 Calculated Airflow Rates and Exterior Temperature

To assess the impact of exterior temperature on the flow rates into and out of the suites of the case study building, the average flow rates were determined for the coldest month, January, and the hottest month, July, which had average exterior temperatures of 3.3°C and 19.1°C respectively.

Charts of the average flow rates for upper and lower suites during these two periods are provided in Figure 11-7 and Figure 11-8.

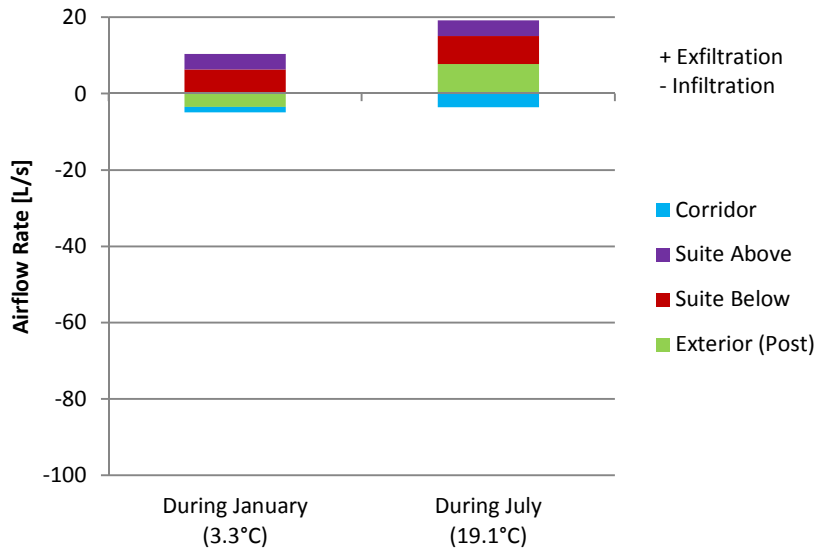


Figure 11-7: Chart of the average flow into and out of the lower suites of the case study building during January and July

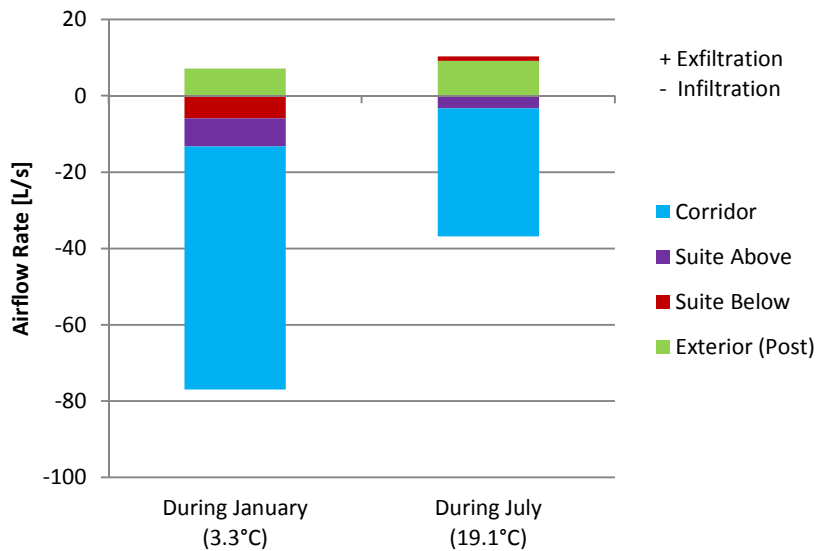


Figure 11-8: Chart of the average flow into and out of the upper suites of the case study building during January and July

These figures illustrate the previously noted lack of airflow from the corridors to the suites on lower floors. On upper floors, the flow rate from the corridor to the suites changes significantly due to the change in exterior temperature with average flow rates of 64 L/s and 34 L/s for the cold and

hot months respectively. This is further confirmation of the significant impact of stack effect on ventilation of the building.

11.2.2 Calculated Airflow Rates and Wind

To determine the effect of wind independent from stack effect, pairs of comparable periods have been selected. The first period of each of the pairs is during a wind event, and the second period is during relatively lower wind speeds but with other parameters similar to the first period, in particular exterior temperature. Typically, the effects of the wind events are most apparent for the windward suites in moderate and strong wind events; consequently, the graphs for those suites are provided in this section. Graphs for the average airflow for each of the suites during each of the selected wind events are provided in Appendix F. The wind events selected for this analysis are the same events as those discussed previously in Chapter 10.

Figure 11-9 to Figure 11-14 provide the average airflow rates for the windward suites during a moderate east wind, a moderate west wind, and strong west wind. As discussed, each of these figures also includes a baseline wind case during a similar time of the year with relatively lower wind speeds and with similar exterior temperature.

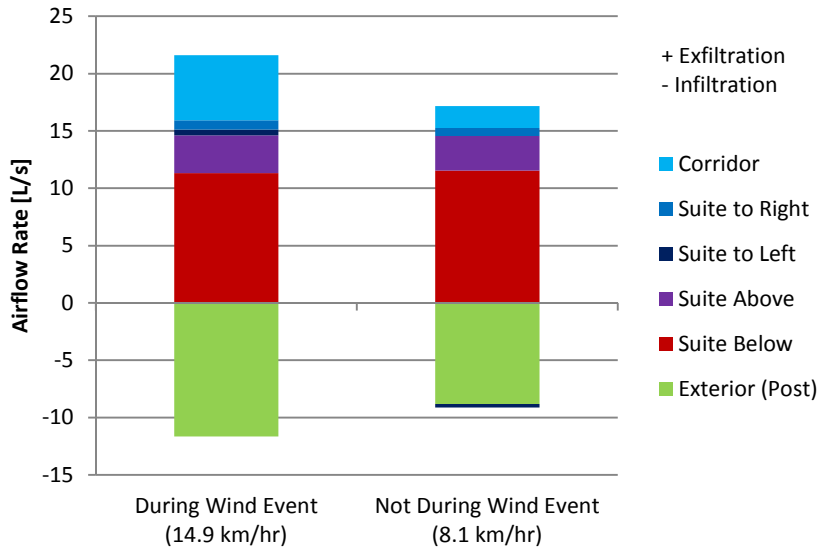


Figure 11-9: Chart of the average flow into and out of Suite 303 during a moderate east wind

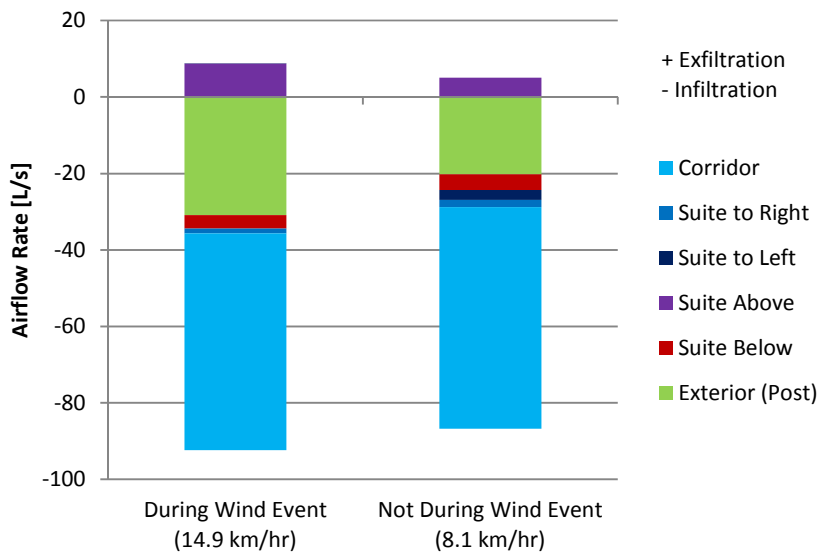


Figure 11-10: Chart of the average flow into and out of Suite 1103 during a moderate east wind

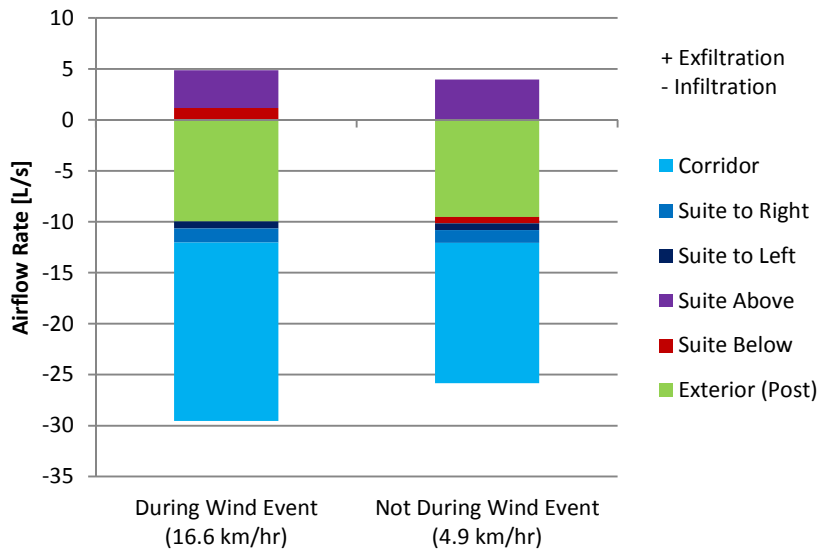


Figure 11-11: Chart of the average flow into and out of Suite 301 during a moderate west wind

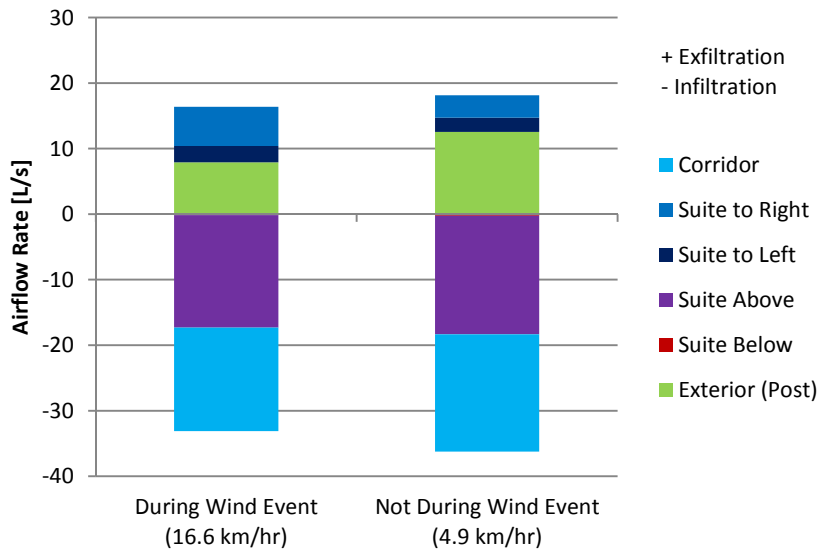


Figure 11-12: Chart of the average flow into and out of Suite 1101 during a moderate west wind

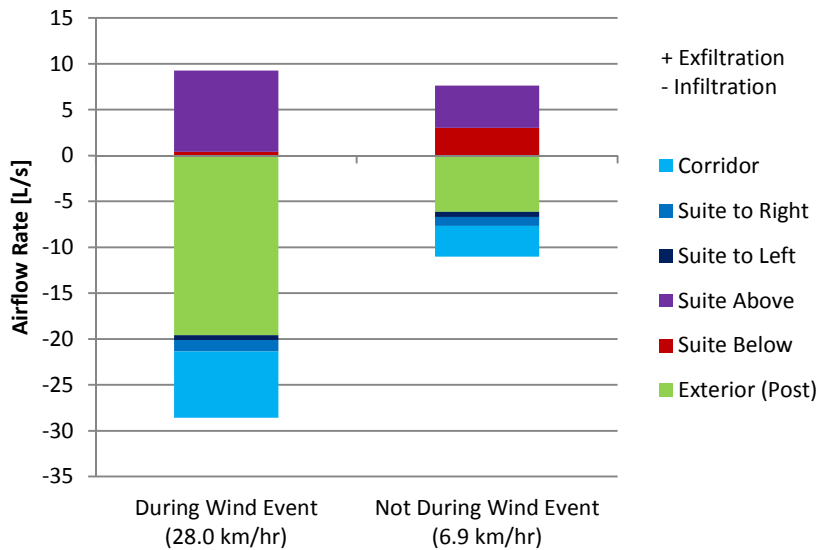


Figure 11-13: Chart of the average flow into and out of Suite 301 during a strong west wind

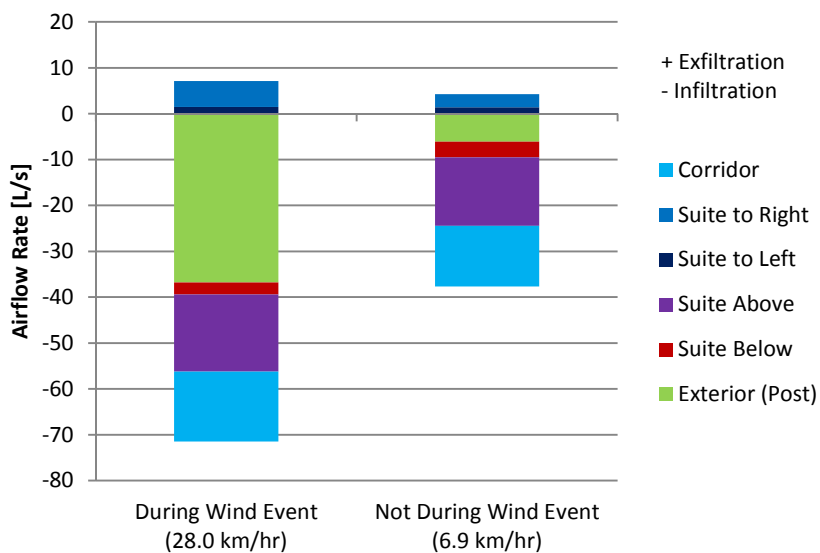


Figure 11-14: Chart of the average flow into and out of Suite 1101 during a strong west wind

The preceding figures show that typically the windward suites experience increased infiltration through the exterior enclosure during wind events and the magnitude of the increase is correlated with the strength of the wind. Also, the airflow rates caused by wind are typically higher for the upper suites, which is consistent with the finding of increased pressure magnitudes due to wind on upper suites. This is likely due to the increased exposure of the upper floors and higher wind speeds at higher elevations due to surface boundary layer effects. Overall, however, it is difficult to predict both the direction and magnitude of the flow changes due to wind and this is reflected in the high variability observed both in the graphs provided here, and in the additional graphs provided in

Appendix F. This finding is consistent with the findings with respect to measured pressure differences due to wind discussed in Chapter 10.

Chapter 12

Indoor Air Quality Monitoring Results

The indoor air quality of a space is determined by the balance of air contaminant generation and air contaminant removal or dilution, and consequently provides an indirect method to evaluate ventilation rates. While many air contaminants exist, carbon dioxide and dew point temperature were selected as indicators of indoor air quality for use in this thesis work. As the primary source of carbon dioxide in buildings is the occupants, concentrations are typically correlated with occupancy and activity levels. Dew point temperature is a measure of the moisture in the air and correlates with occupancy and activity levels as well as with other sources of water vapour such as showering and cooking. This chapter presents the measurements of these two indicators made as part of the monitoring program at the case study building. The results are used to evaluate airflow patterns at the case study building and to compare these results with the results of other aspects of the experimental program.

12.1 Carbon Dioxide Concentrations

As part of the monitoring program, carbon dioxide (CO₂) concentrations were measured in suites on floors 2, 3, 4, 10, 11, and 12. Concentrations were also measured in each corridor, and in the air intake of the MAU. As previously stated, the main source of carbon dioxide generation is from occupant respiration, so carbon dioxide concentrations provide an indication of occupancy level. For reference, ASHRAE 62.1-2010 does not provide a limit on carbon dioxide concentrations; however, it does note that typically concentrations of approximately 700 ppm above outdoor air concentration will satisfy most occupants. This would typically correspond with interior carbon dioxide concentrations of 1000 to 1200 ppm.

During the course of the monitoring program the accuracy of a number of the carbon dioxide sensors was called into question. There are some unique cases where sensors appear to have been initially calibrated incorrectly; however, more widespread issues were also identified. A recently calibrated handheld carbon dioxide sensor (specifications and calibration date provided in Appendix E) was used to check the measurements of the installed carbon dioxide sensors. While typically the installed sensors were found to be measuring higher than the concentration measured by the handheld unit, this upward drift was inconsistent. Usually the measured drift was approximately 200 to 300 ppm; however, more drift was measured in some sensors. Typically, drift of carbon dioxide sensors readings is caused by accumulation of dirt within the sensor and degradation of the sensor components which cause them to indicate lower concentrations than are actually present. (CO2Meter.com, 2013) This is the opposite of the error in the measurements for the sensors at the case study building. Despite effort to determine potential causes of the drift or a consistent relationship so that data could be appropriately adjusted, no resolution to this issue was found. Fortunately, the measured error in the sensors is typically low enough relative to the measured concentrations that it does not significantly affect the findings; however, the carbon dioxide measurements should generally be considered as qualitative relative indicators as the precise concentrations may not be reliable. Specific sensor errors not attributable to this drift are identified where appropriate.

Carbon dioxide concentrations in the corridors were found to be consistent with concentrations measured in the MAU intake for the majority of corridors as shown in Figure 12-1. Note that the higher concentrations measured in Corridors 5 and the lower concentrations measured in Corridor 11 are a result of miscalibration of the monitoring equipment. This miscalibration was confirmed with a handheld sensor unit; however, adjustment of the data was not possible.

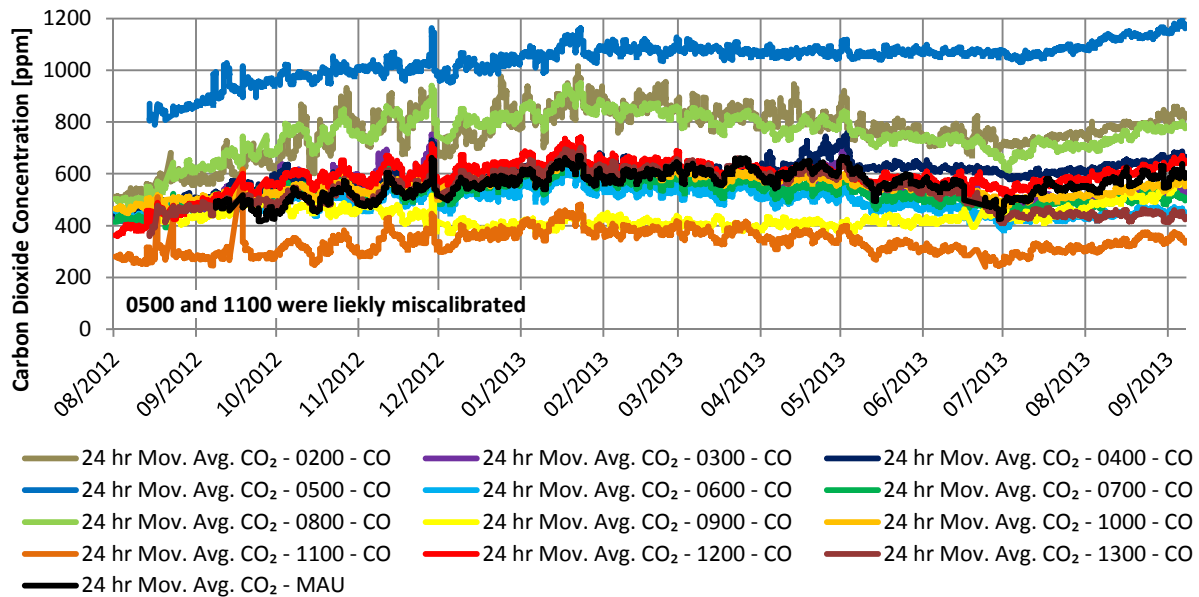


Figure 12-1: Graph of corridor and MAU carbon dioxide concentrations

Generally, the carbon dioxide concentrations in the corridors are similar to the outdoor carbon dioxide concentration (i.e. concentration in the MAU). This could either indicate relatively consistent supply of ventilation air to the corridors or be a result of limited carbon dioxide generation in the corridors because they are typically unoccupied. Given that the airflow measurements presented in Chapter 8 indicate inconsistent ventilation of the corridors, it is likely that the similarity between carbon dioxide concentrations in the corridors and the outdoors is primarily due to low carbon dioxide generation rates in the corridors.

The measured concentrations in the corridors tend to increase by approximately 100 to 500 ppm during colder months. This increase is likely due in part to occupants keeping their windows closed more during colder periods of the year. When occupants keep their windows closed they receive less natural ventilation from the exterior which can lead to increased carbon dioxide concentrations in the suites. It is possible that occupants spend more time indoors during colder periods of the year and that this increased occupancy leads to increased carbon dioxide concentrations. Given that the airflow measurements presented in Chapter 8 showed that there is significant airflow from the suites to the corridors, corridor carbon dioxide concentrations would increase due to increased concentrations in the suites.

During the colder months of the year, the carbon dioxide concentration in Corridor 9 was measured to decrease in absolute concentration and relative to the concentration in other corridors and the MAU. It is not clear why this decrease would occur, but it is theorized that a suite occupant (or multiple suite occupants) on this floor may keep many of their windows open during these colder

periods and this may provide outdoor air to the corridor through the suites. This potential cause was not confirmed.

In Corridors 2 and 8 the carbon dioxide concentrations are significantly higher than that measured in the air of the MAU. It is likely that the higher concentration in Corridor 8 is due to reduced ventilation air supply from the MAU because the fire damper in the MAU duct grille is closed on that floor. The increased carbon dioxide concentration in Corridor 2 may be a result of its location below the neutral pressure plane of the building as discussed in Chapter 10. As the neutral pressure plane is consistently located above Floor 2, air from suites with relatively higher concentrations of carbon dioxide (due to the occupants) tends to flow in to the corridor due to stack effect and consequently increase the carbon dioxide concentration in the corridor. As only Floors 1 and 2 are typically entirely below the neutral pressure plane, this effect would only be observed on these floors. The carbon dioxide concentration in Corridor 1 (i.e. the entrance lobby) was not monitored. The concentration in Corridor 1 would likely be lower than in Corridor 2 due to increased ventilation through operation of the entrance doors.

Carbon dioxide concentrations were also measured in the suites on Floors 2, 3, 4, 10, 11, & 12. The average concentrations for the suites on each of these floors are graphed in Figure 12-2.

The carbon dioxide measurements presented in Figure 12-1 and in subsequent graphs in this chapter are all approximately 500 ppm at the beginning of August, 2012, near the start of the monitoring program. The building enclosure retrofit work was ongoing during this time leading to extended periods with windows uninstalled, doors open to provide access, et cetera. Additionally, likely more windows were open during the summer due to warm outdoor temperatures. It is theorized that the combination of increased activity and more open windows significantly increased building ventilation rates and caused interior carbon dioxide concentrations to be nearly the same as outdoors during the beginning of August, 2012.

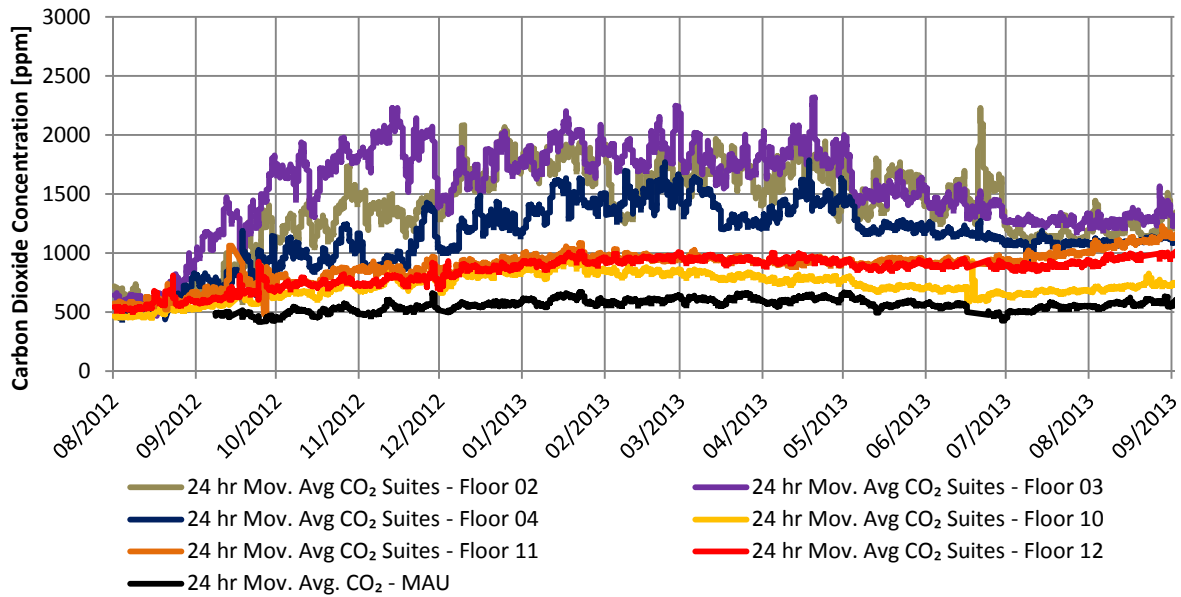


Figure 12-2: Graph of average suite carbon dioxide concentration by floor and MAU carbon dioxide concentration

This graph shows that typically suites on lower floors of the building have higher carbon dioxide concentrations than suites on higher floors, and that the average suite concentration on each floor is higher than the concentration measured in the MAU. The difference in carbon dioxide concentrations on lower and upper floors is greatest during the colder months of the year. This is likely due to a combination of lower ventilation rates on the lower floors (as shown by the airflow measurements discussed in Chapter 8) and occupants keeping their windows closed during colder exterior temperatures thereby reducing the ability of natural ventilation to supplement ventilation provided by the mechanical ventilation system.

Different carbon dioxide concentrations were also measured for suites on the same floors as shown in Figure 12-3 to Figure 12-8. As stack effect would tend to act equally for all suites on a floor, it is likely that this uneven distribution of carbon dioxide concentrations between suites on the same floor is a result of window operation.

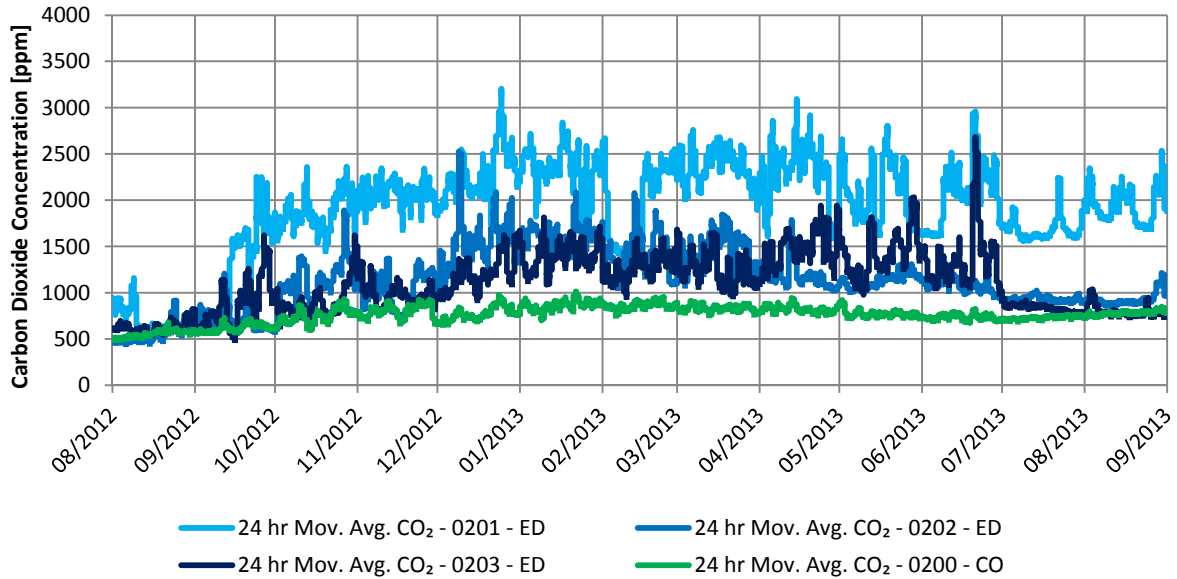


Figure 12-3: Graph of 24 hour moving average suite and corridor CO₂ concentration on Floor 2

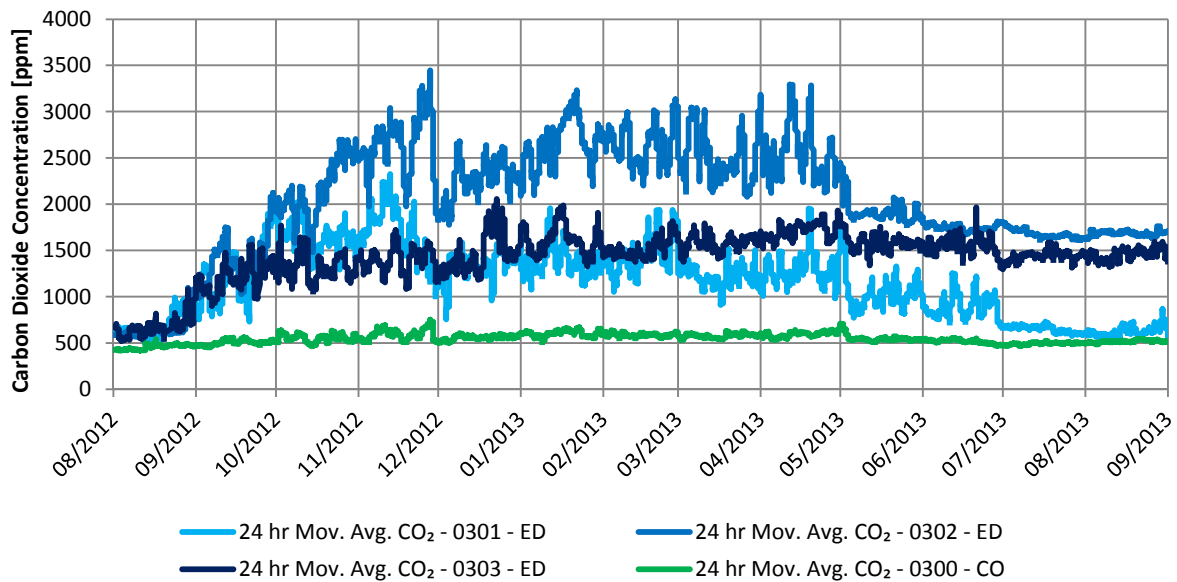


Figure 12-4: Graph of 24 hour moving average suite and corridor CO₂ concentration on Floor 3

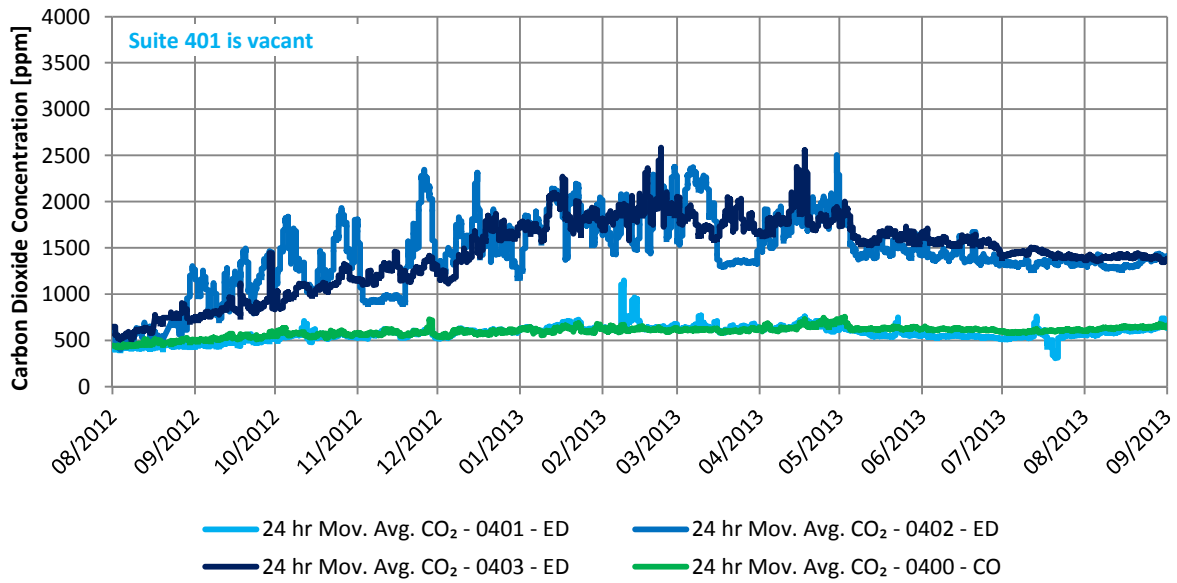


Figure 12-5: Graph of 24 hour moving average suite and corridor CO₂ concentration on Floor 4

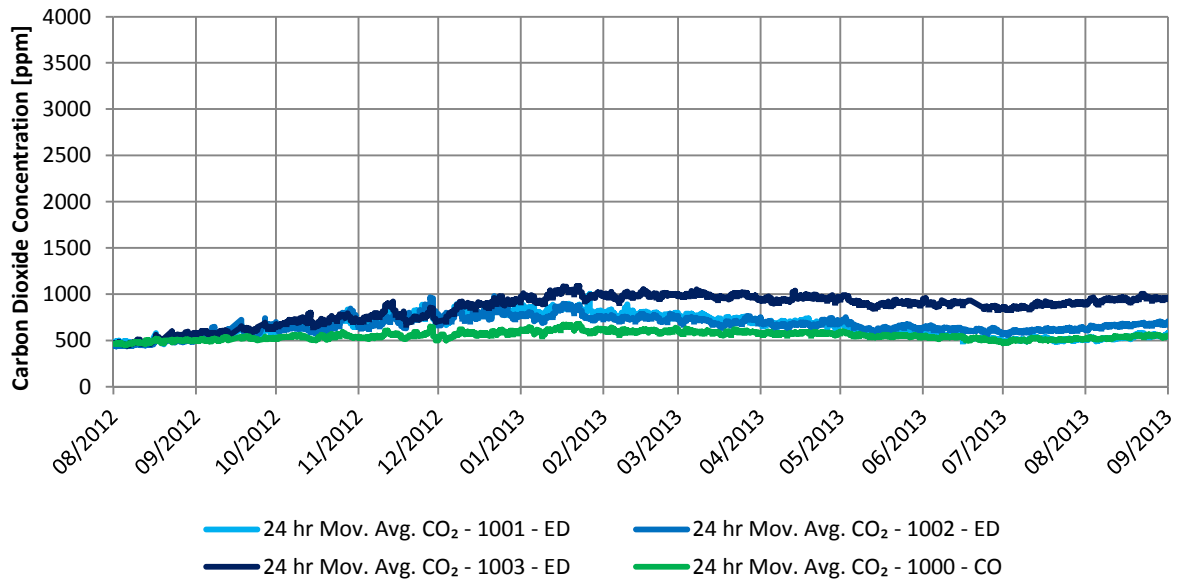


Figure 12-6: Graph of 24 hour moving average suite and corridor CO₂ concentration on Floor 10

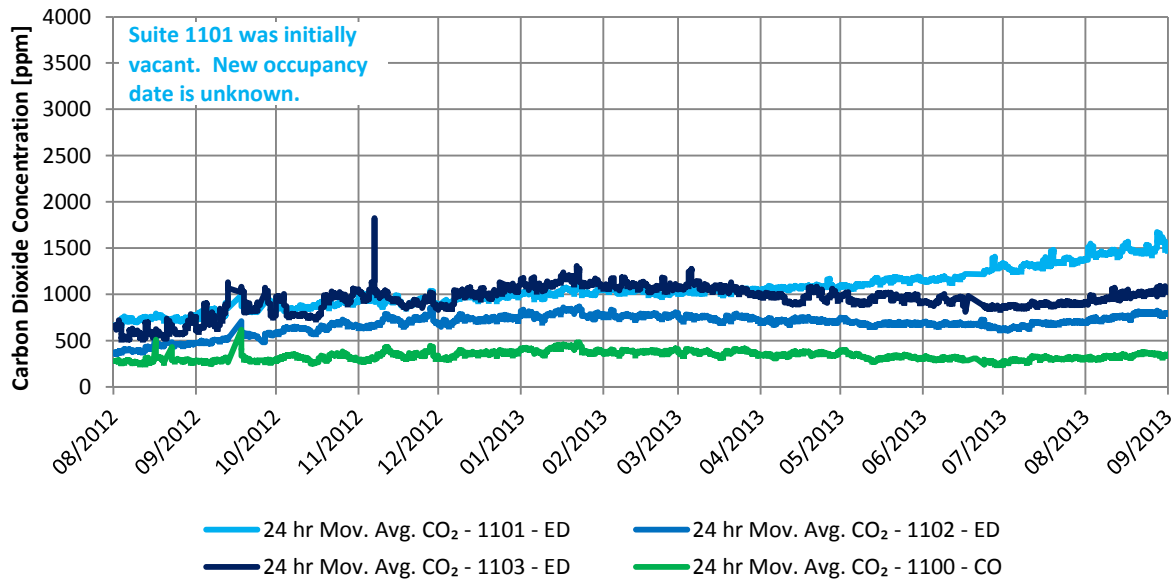


Figure 12-7: Graph of 24 hour moving average suite and corridor CO₂ concentration on Floor 11

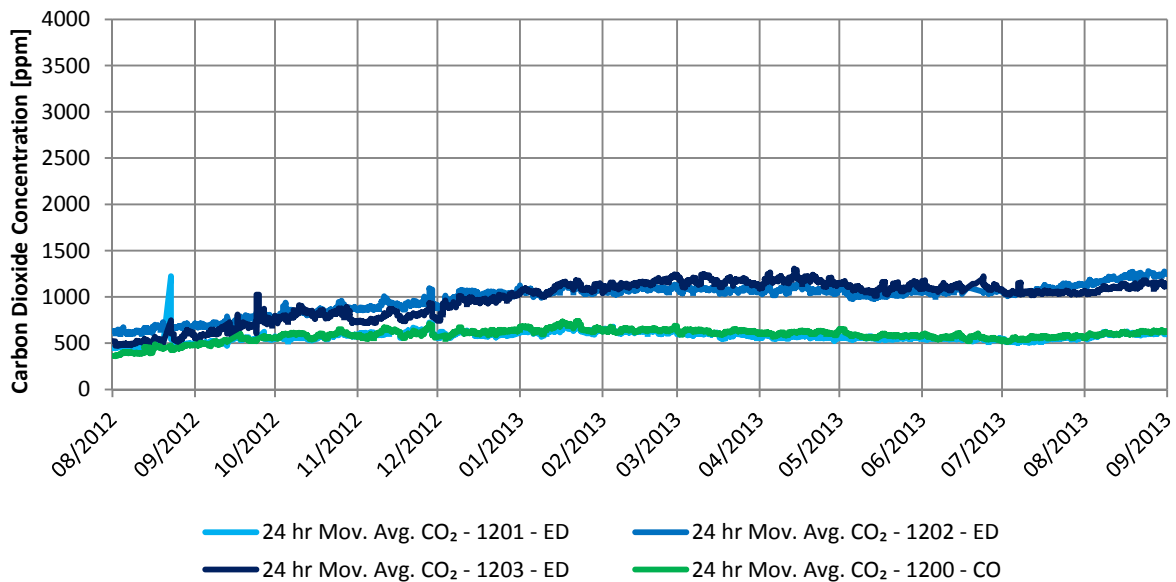


Figure 12-8: Graph of 24 hour moving average suite and corridor CO₂ concentration on Floor 12

Comparison of the preceding figures with the measured total air change rates for the suites presented in Chapter 8 shows a strong correlation between measured air change rates and carbon dioxide concentrations. Typically suites with higher air change rates have lower concentrations. This is noticeable in the difference between upper and lower floors, but also in the difference between suites on a given floor. For example, Suite 302 typically has higher carbon dioxide concentrations during the monitoring period than do Suite 301 and Suite 303, and Suite 302 also had a measured total air change rate of approximately 0.06 ACH versus Suite 301 and Suite 303

which measured 0.15 and 0.14 ACH respectively. Figure 12-9 shows the average carbon dioxide concentrations measured in the suites (by the sensors near the suite entrance doors) during the PFT testing period from April 10th to April 17th, 2013 plotted versus the measured air change rates in those suites determined by the PFT testing (thus measured in the same period). Figure 12-10 shows the same carbon dioxide concentration plotted against the airflow rates instead of air change rates. The air change rates and airflow rates are shown for suite total from all air sources (i.e. from the exterior, the corridor, and adjacent suites) and for just air from the corridor and the exterior as this air would be considered ventilation air. The equations for trend lines are provided in the figures, and the form of these equations corresponds to the theoretical equation relating outdoor air supply flow rate with the concentration of contaminant produced in the zone, Eq. 12.1.

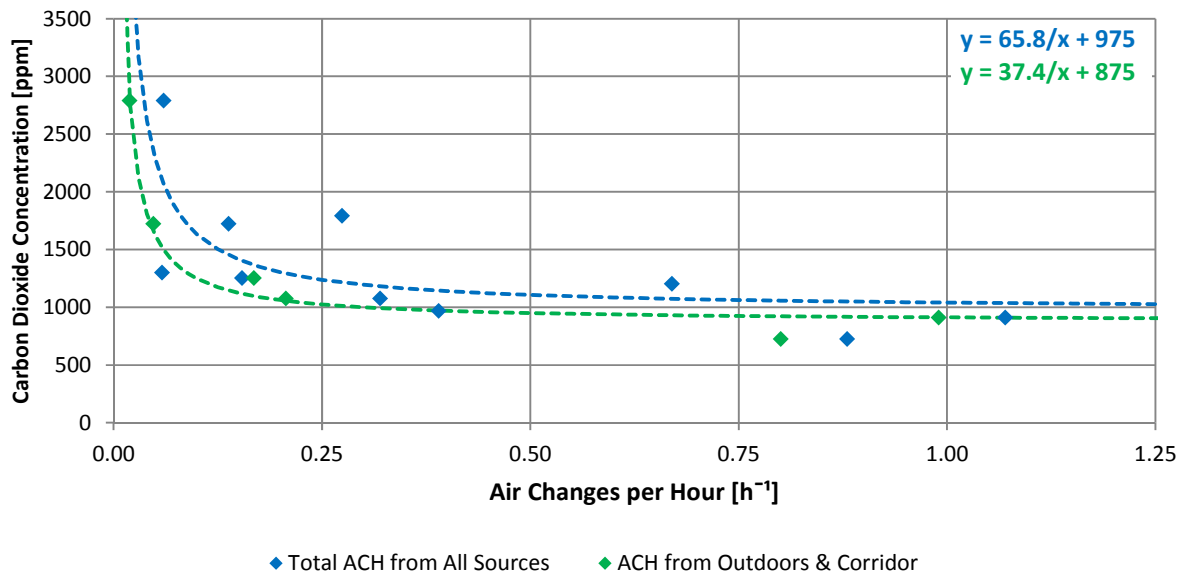
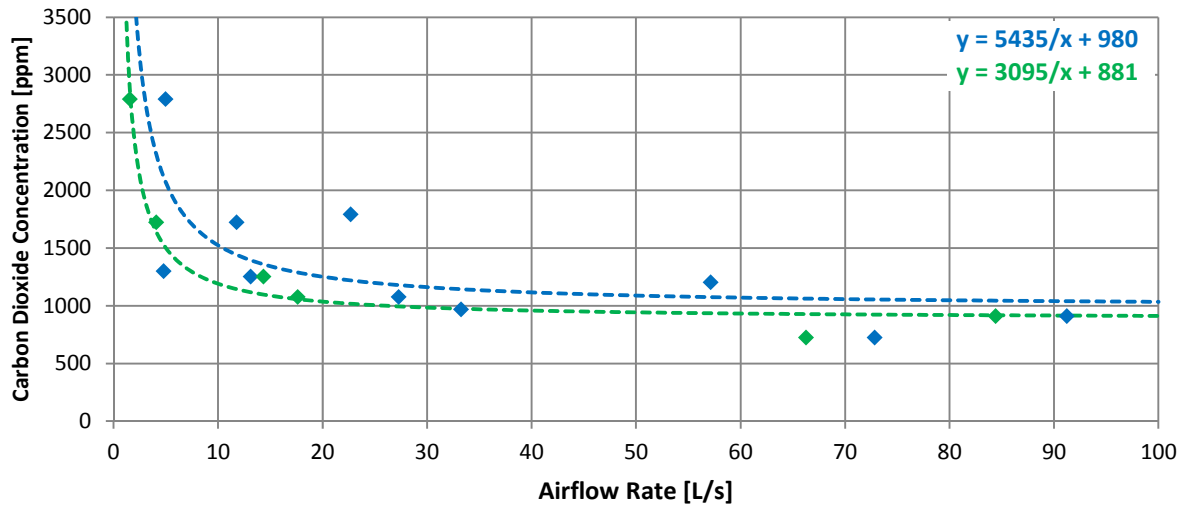


Figure 12-9: Graph of suite air changes rates versus average carbon dioxide concentrations during the PFT testing period



◆ Total Airflow Into Suite from All Sources [L/s] ◆ Ventilation Airflow Into Suite from Outdoor and Corridor [L/s]

Figure 12-10: Graph of airflow rates into suites versus average carbon dioxide concentrations during the PFT testing period

$$C_i = \frac{G}{Q_o} + C_o \tag{Eq. 12.1}$$

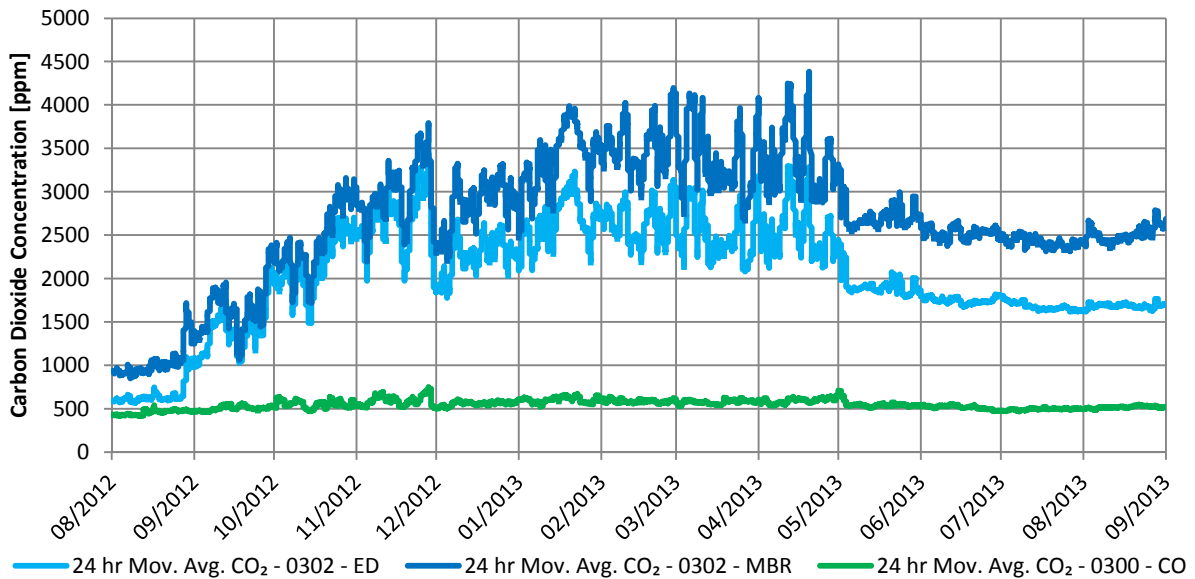
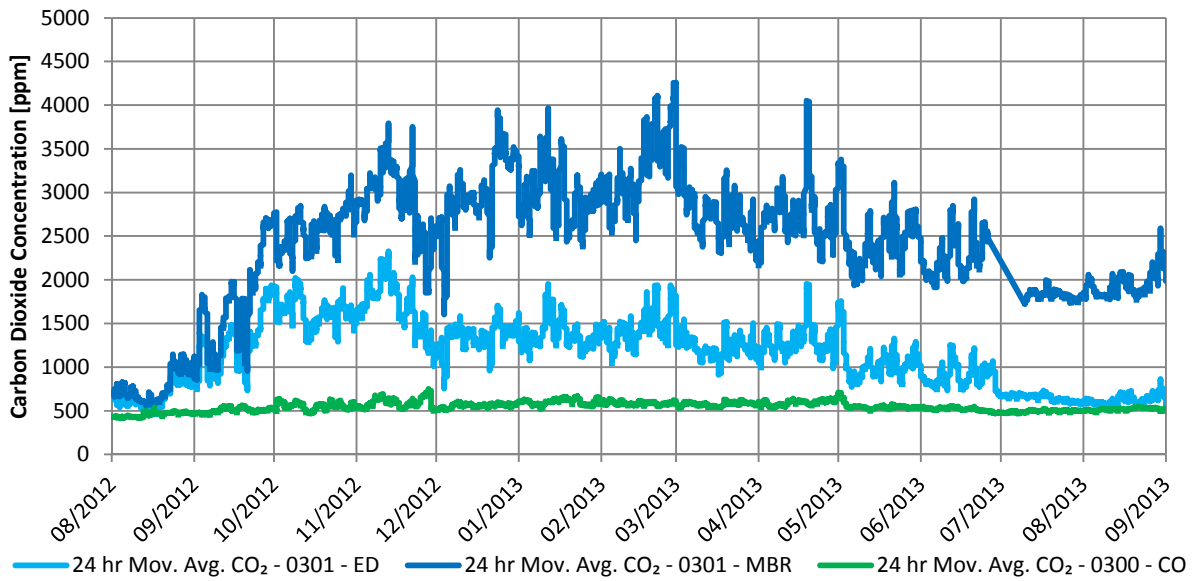
Where: C_i = Concentration of Contaminant in Zone (i.e. carbon dioxide) [ppm]
 G = Contaminant Generation Rate [ppm·m³/s]
 Q_o = Outdoor Airflow into Zone [m³/s]
 C_o = Concentration of Contaminant in Outdoor Air [ppm]

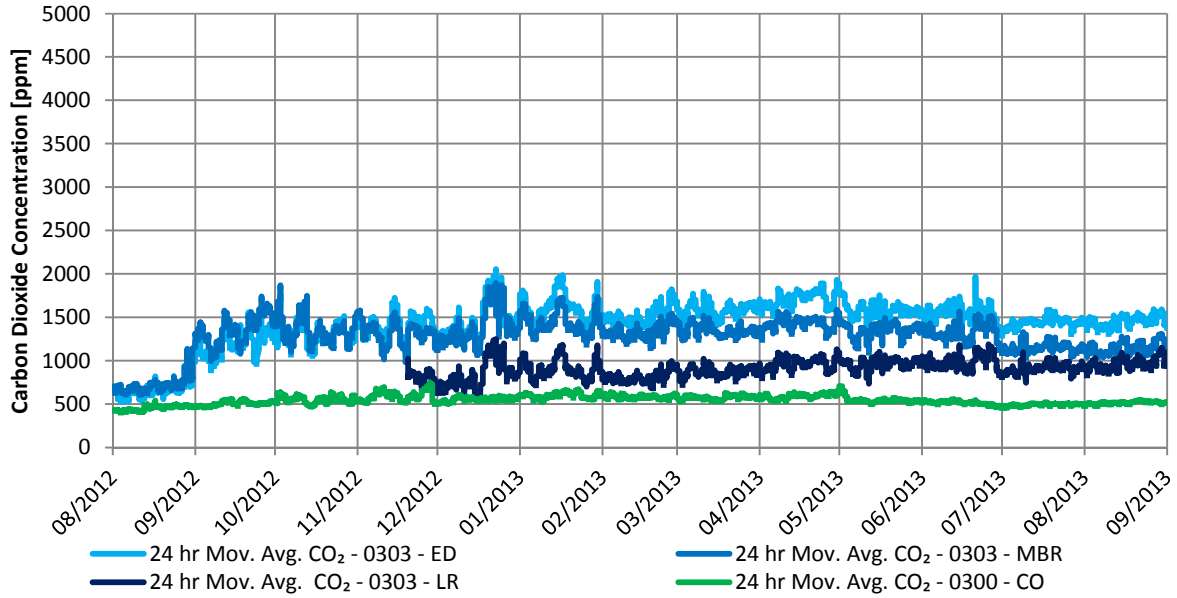
(ASHRAE 2010)

The preceding figures illustrate the correlation between carbon dioxide concentration and air change rates and airflow rates for these suites. The correlation is stronger with the airflow rates only from the exterior and the corridor, which is likely because these sources of air typically have more consistent and lower carbon dioxide concentration than do other sources such as adjacent suites.

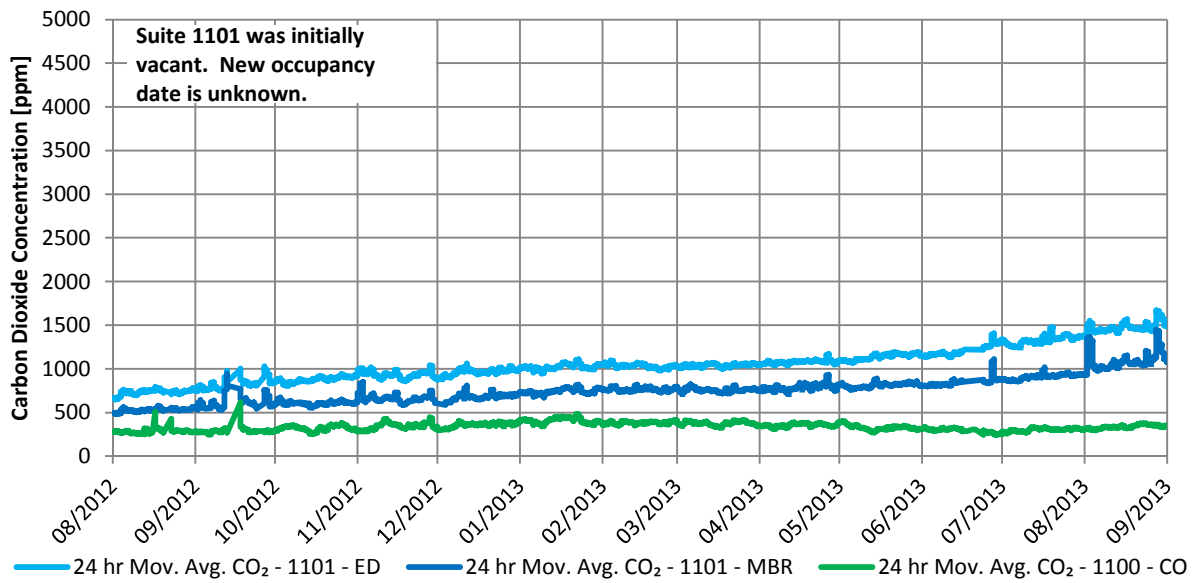
The suite carbon dioxide concentrations presented to this point were measured by sensors located in the suites but near the suite entrance doors. As the suite entrance door is a primary location for ventilation air to enter the suite, the carbon dioxide concentrations at these locations may not be representative of the average carbon dioxide concentration of the suite, and likely are instead provide an approximate lower bound on concentrations in the suite. In suites on Floor 3 and Floor 11, carbon dioxide sensors were also installed in the master bedroom (and in one case in the living room) to allow for comparison of carbon dioxide concentration distribution within the suites. Distributions of carbon dioxide within suites provide an indication of how well the air is mixed within the suites and how well ventilation air is distributed within the suites. The results of this monitoring are provided in Figure 12-11 to Figure 12-16. Note that in these figures “ED”, “MBR”,

“LR”, and “CO” indicate sensors located near the suite entrance door, in the master bedroom, in the living room, or in the corridor, respectively.





24 Hour Moving Average Carbon Dioxide Concentrations - Suite 1101



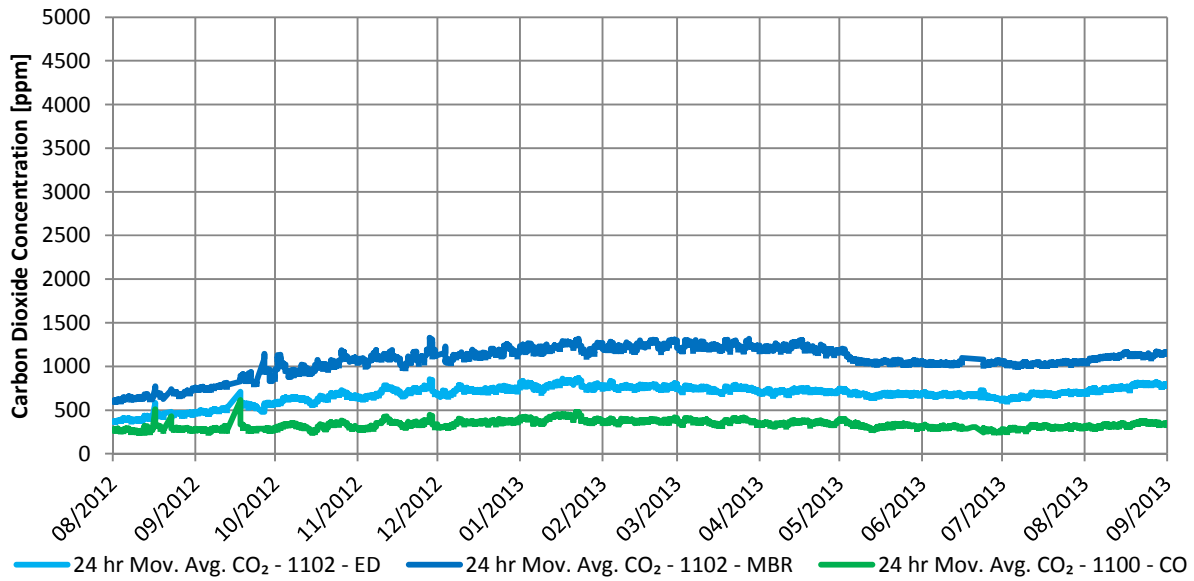


Figure 12-15: Graph of 24 hour moving average CO₂ concentration in Suite 1102

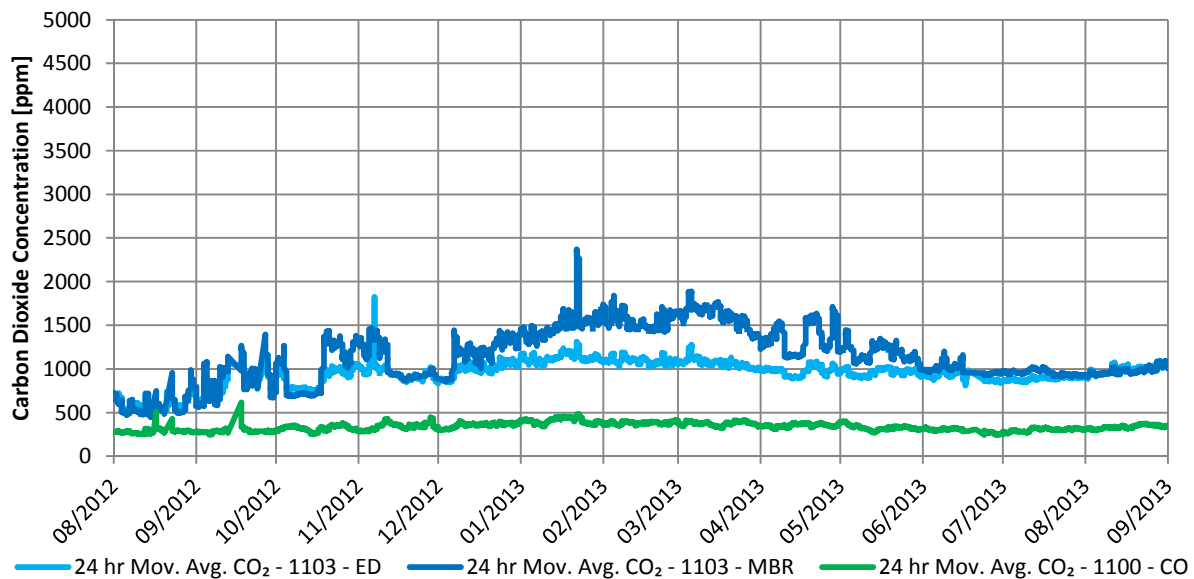


Figure 12-16: Graph of 24 hour moving average CO₂ concentration in Suite 1103

Higher carbon dioxide concentrations were measured in master bedrooms than near the suite entrance doors. This may indicate that ventilation air that enters the suite at the entrance door is not evenly distributed to all areas of the suite. Alternatively, higher concentrations in the master bedrooms could be caused by increased carbon dioxide generation rates in the master bedrooms as compared to the rest of the suites because occupants typically spend extended periods of time in master bedrooms at night while sleeping.

In some suites the master bedroom and entrance door concentrations were similar. This finding indicates that the air is better mixed in these suites, sufficient ventilation air is being provided to these suites to moderate carbon dioxide concentrations regardless of suite air being poorly mixed, or both. Concentrations in the master bedrooms are typically closer to the concentrations at the suite entrance doors on Floor 11 than on Floor 3. This likely indicates that either the higher ventilation rates in these suites (as discussed in Chapter 8) are decreasing the carbon dioxide concentrations in the master bedrooms, or that the forces causing these higher ventilation rates are also increasing the mixing of air within the suites thereby providing better ventilation of the master bedroom. It is likely combination of these factors. The even distribution of carbon dioxide concentrations in these suites may also be a result of occupants not sleeping in the master bedroom.

A number of instances of lower and more consistent carbon dioxide concentrations are apparent in these figures. These periods are most often during periods of vacancy and are discussed in more detail in Section 12.1.1.

No significant correlation was found between wind (speed and direction) and carbon dioxide concentrations. This is likely because wind typically acts over relatively short time periods, thus not acting long enough to develop patterns in carbon dioxide concentration. It was not possible to separate potential long-term effects of wind on ventilation from other influences such as stack effect and the mechanical ventilation system; however, increased wind exposure and wind speeds at the upper levels of the building likely contribute to the lower carbon dioxide concentrations measured in these suites.

Overall, suite carbon dioxide concentrations were often measured to be significantly higher than both outdoor and corridor concentrations, and frequently exceed the guideline concentrations of ASHRAE 62.1-2010. Typically suites which receive less ventilation air (lower suites) also had higher carbon dioxide concentrations. Higher carbon dioxide concentrations were often measured in master bedrooms than in other areas of the suites. This indicates that the suites are inadequately ventilated, that ventilation air is inadequate distributed within the suites, or both. This uneven distribution of carbon dioxide concentrations within the suites was more pronounced on lower floors.

12.1.1 Periods of Vacancy

During the monitoring period a number of suites were unoccupied for extended lengths of time usually due to occupants going on vacation or a gap in occupancy during a change in suite ownership. These periods of vacancy are often readily apparent in the carbon dioxide concentrations of the suites, since when there are no occupants, there is little to no generation of carbon dioxide within the suite.

It is easier to identify these extended periods of vacancy in lower suites because they typically have higher carbon dioxide concentration when occupied. As an example of the decrease in carbon dioxide concentration during vacancy, Figure 12-17 provides a graph of the carbon dioxide concentration of Suite 201 near the entrance door showing the three identified periods of vacancy. The carbon dioxide concentration of the corridor is also provided for reference.

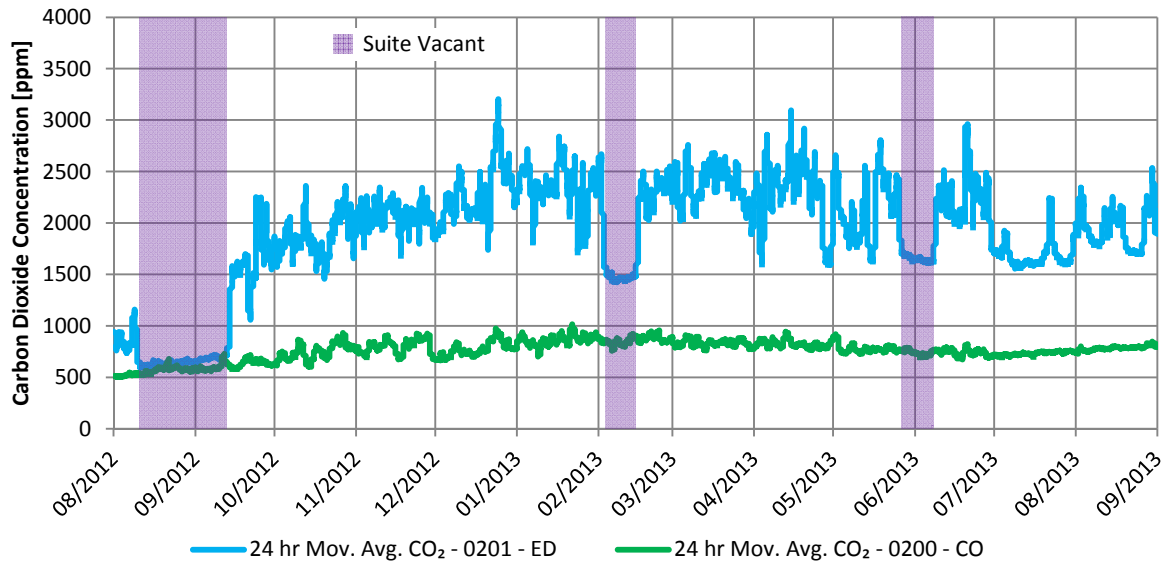


Figure 12-17: Graph of 24 hour moving average CO₂ concentration in Suite 201 showing periods of vacancy

Notably the carbon dioxide concentration in Suite 201 does not always reach same level as the corridor during vacancy. This likely indicates that there is significant transfer airflow into the suite from adjacent suites. This was also found during periods of vacancy in other suites.

12.2 Dew Point Temperature

As part of the monitoring program, temperature and relative humidity were measured at various locations throughout the case study building. These measurements were then used to calculate the dew point temperature which is the maximum temperature at which water vapour in the air will condense, and provides a measure of the amount of water vapour in the air. Sources of moisture in the air include occupant perspiration, pets, cooking, showers, indoor plants, and potentially combustion if fumes are not exhausted. The determined dew point temperatures provide an indication of the ability of the ventilation system to adequately remove and dilute moisture in the air.

In general, the measured dew point temperatures in corridors follow closely with dew point temperature of the MAU intake air as shown in Figure 12-18. This indicates that in general the corridors are relatively well ventilated with outdoor air compared to the amount of moisture released in to the air in the corridors (which is very little). In some cases lower corridors, and in particular Corridor 2, had dew points higher than the MAU intake air dew point by up to approximately 10°C. These conditions primarily occurred during colder months of the year which supports the findings from the carbon dioxide measurements that there is likely significant flow of air from the suites to the corridor on the second floor as a result of stack effect.

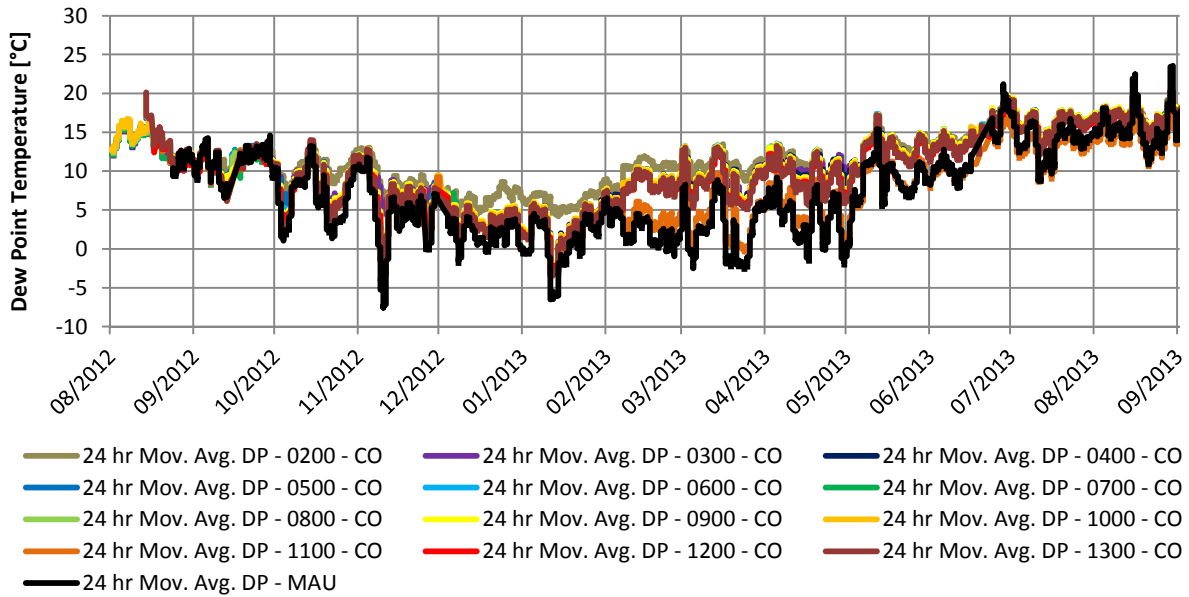


Figure 12-18: Graph of 24 hour moving average corridor and MAU intake air dew point temperatures

The dew point temperatures of the suites (near the suite entrance door) are similar to corridor dew point temperatures as shown in Figure 12-19 to Figure 12-24.

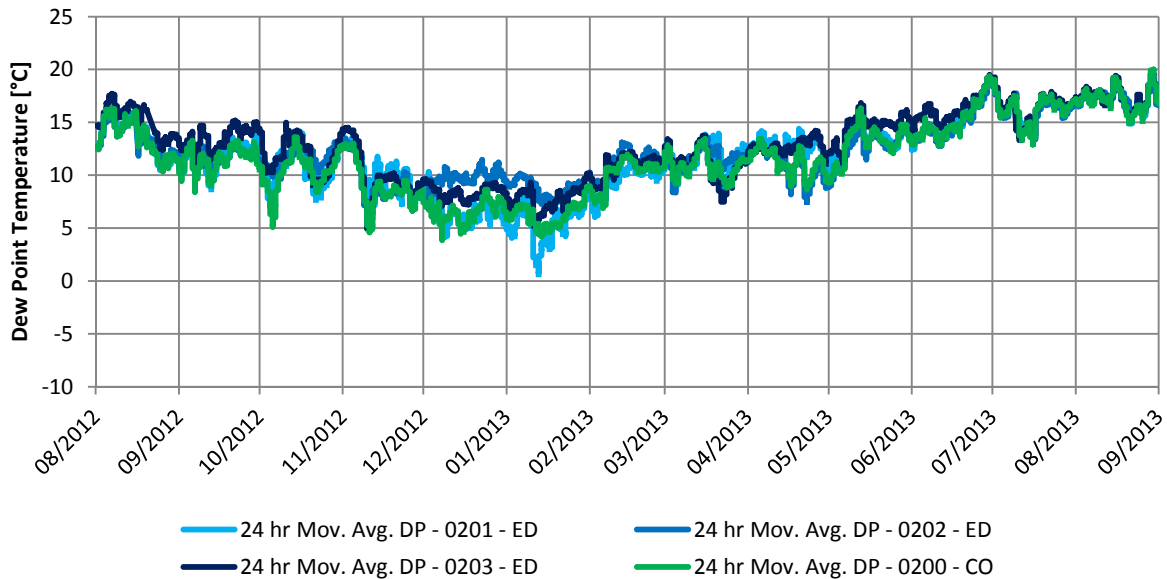


Figure 12-19: Graph of 24 hour moving average suite and corridor dew point temperature on Floor 2

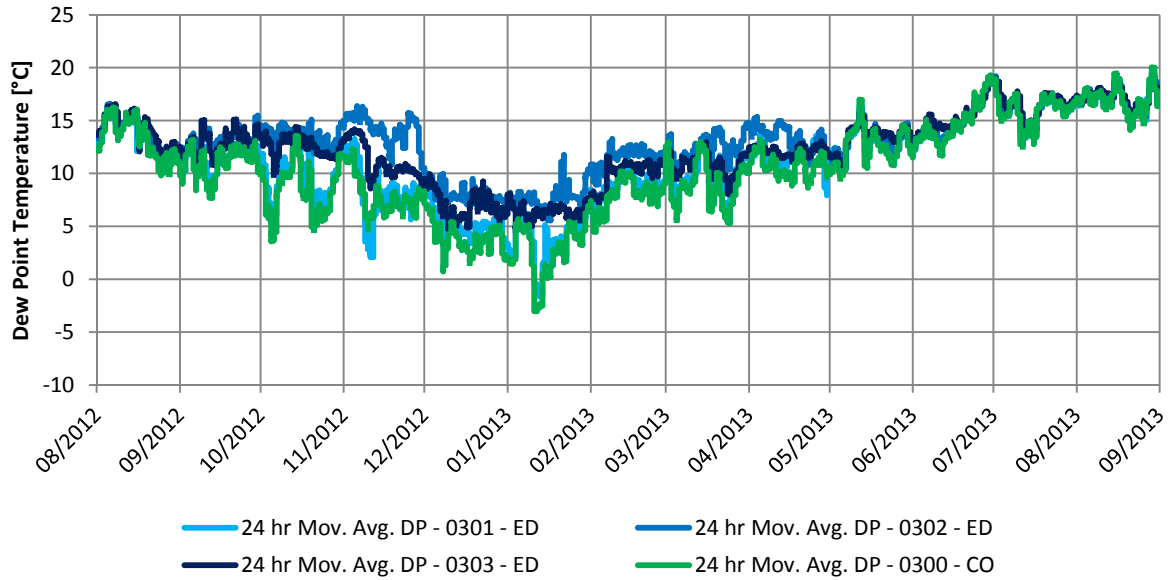


Figure 12-20: Graph of 24 hour moving average suite and corridor dew point temperature on Floor 3

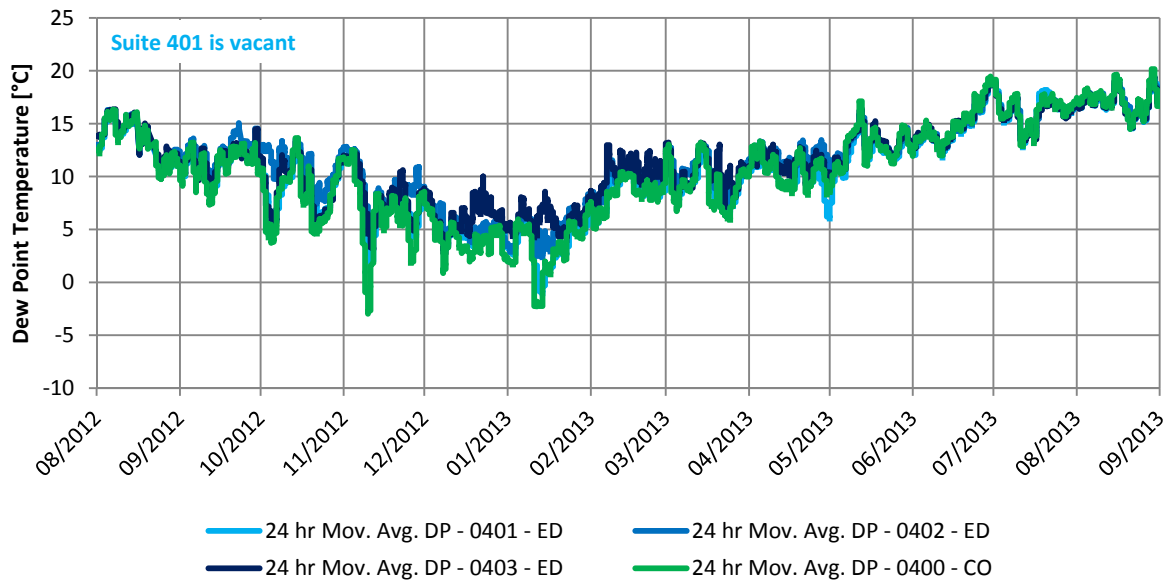


Figure 12-21: Graph of 24 hour moving average suite and corridor dew point temperature on Floor 4

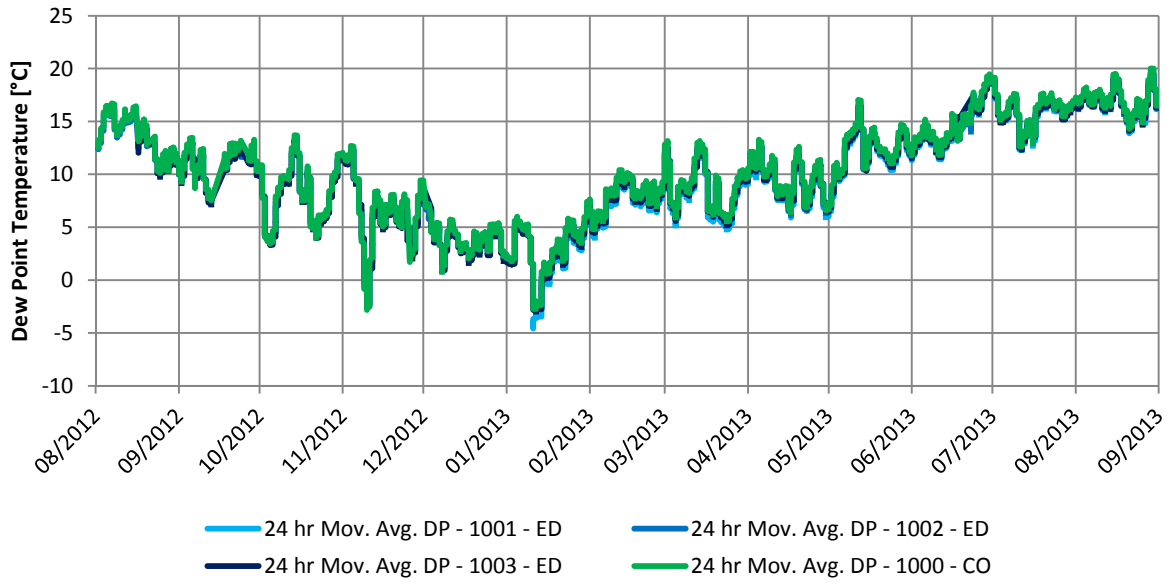


Figure 12-22: Graph of 24 hour moving average suite and corridor dew point temperature on Floor 10

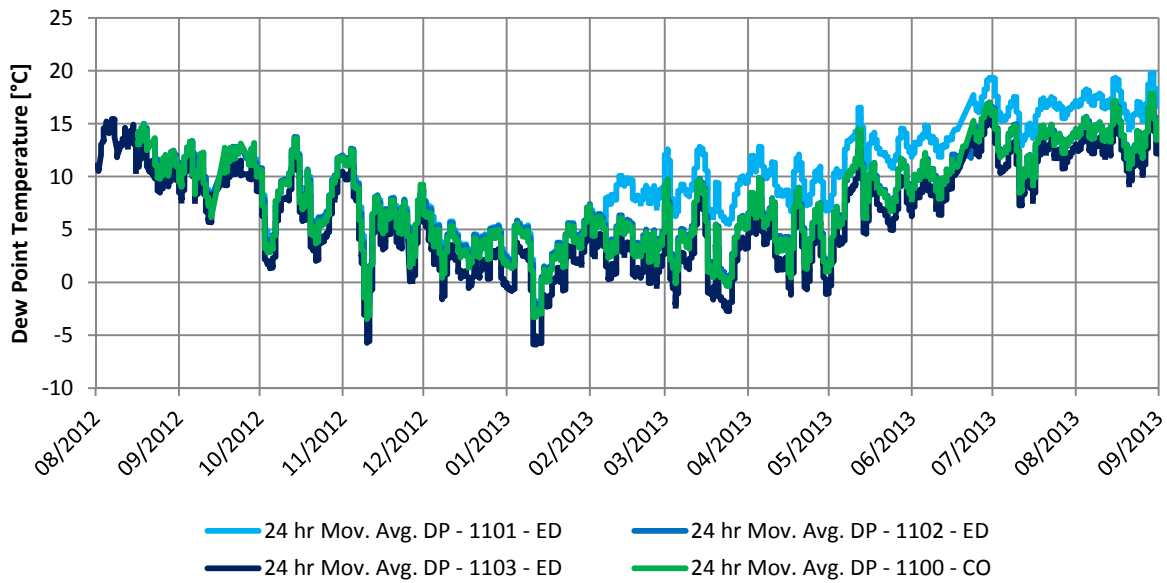


Figure 12-23: Graph of 24 hour moving average suite and corridor dew point temperature on Floor 11

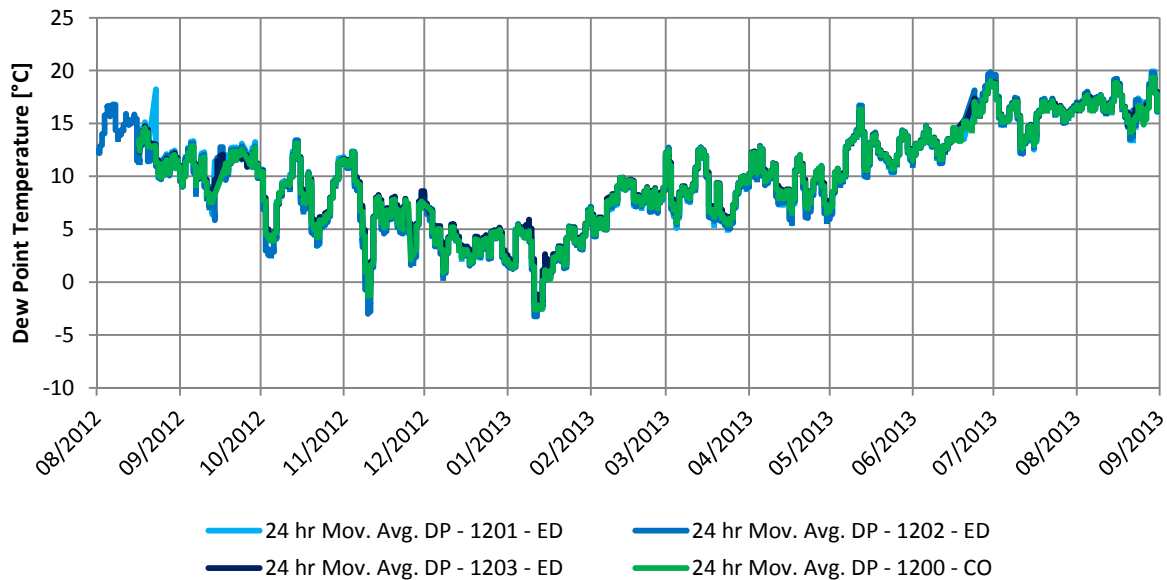


Figure 12-24: Graph of 24 hour moving average suite and corridor dew point temperature on Floor 12

While dew point temperatures of the suites and corridors on the upper floors are similar, on lower floors there are a number of suites with higher dew point temperatures than the corridors. While it is difficult to assign a value to acceptable increase in dew point, based on experience, a rise of approximately 5°C is often associated with indoor air quality issues. A number of suites have dew point temperatures approximately 3 to 6°C higher than outdoors which indicates that the combination of supply and exhaust ventilation in these suites is not sufficient to remove and dilute moisture released in to the air as a result of the occupants..

Note that there is a distinct change in the operation of Suite 1101 near the beginning of February 2013. This suite was unoccupied during this time, so it is not clear what would have caused this difference in operation.

Like carbon dioxide concentrations, dew point temperature can also be used to assess distribution of air within the suites. The dew point temperatures measured near the entrance door and in the master bedroom (and in one case in the living room) for the six suites on Floor 3 and Floor 11 are provided in Figure 12-25 to Figure 12-30.

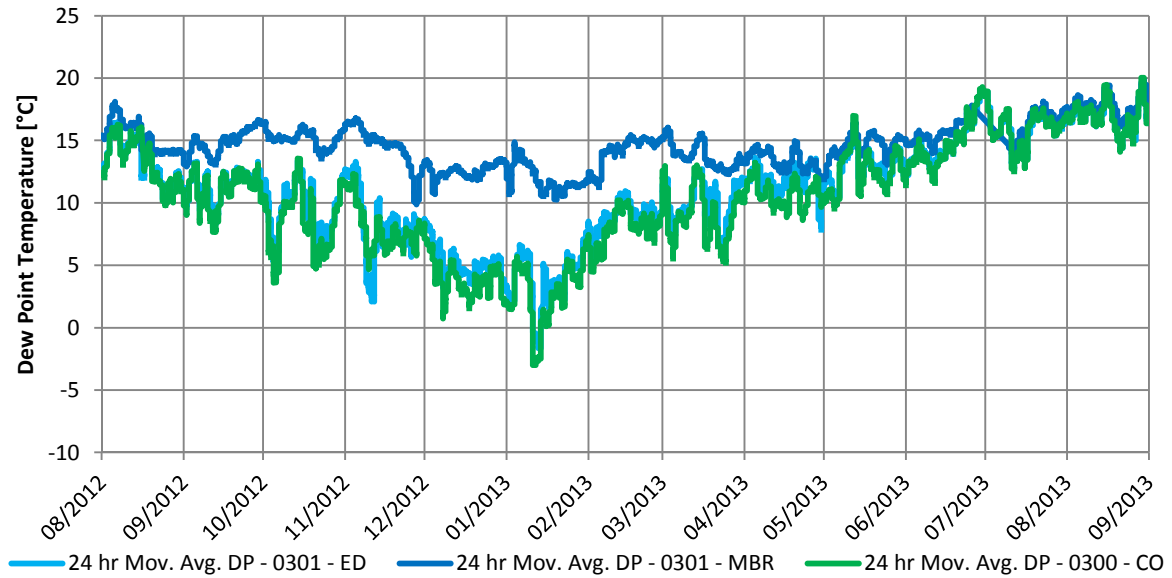


Figure 12-25: Graph of 24 hour moving average dew point temperatures in Suite 301

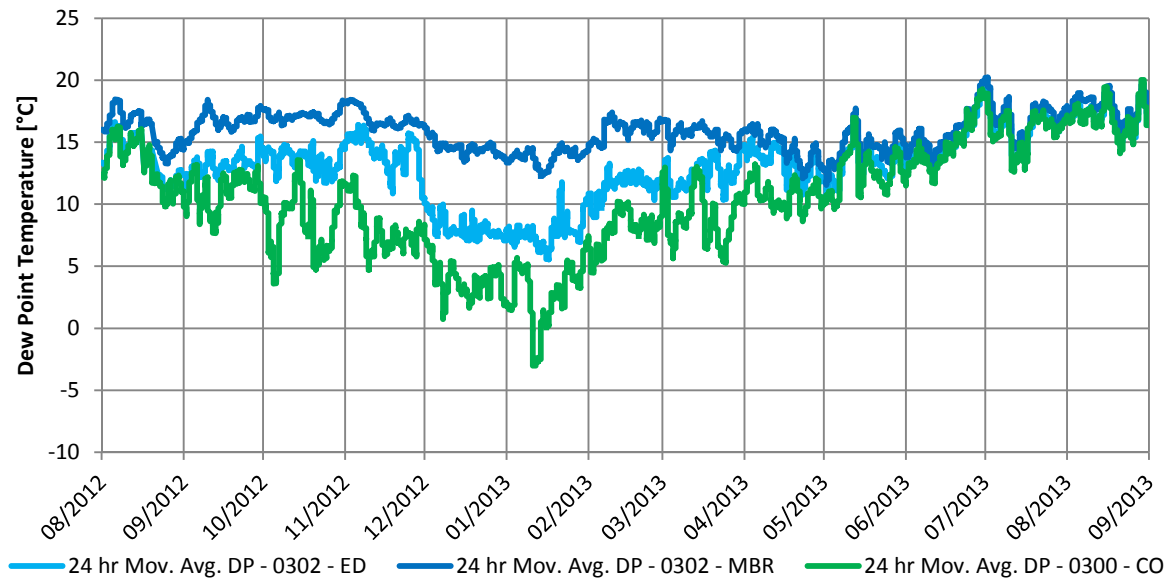


Figure 12-26: Graph of 24 hour moving average dew point temperatures in Suite 302

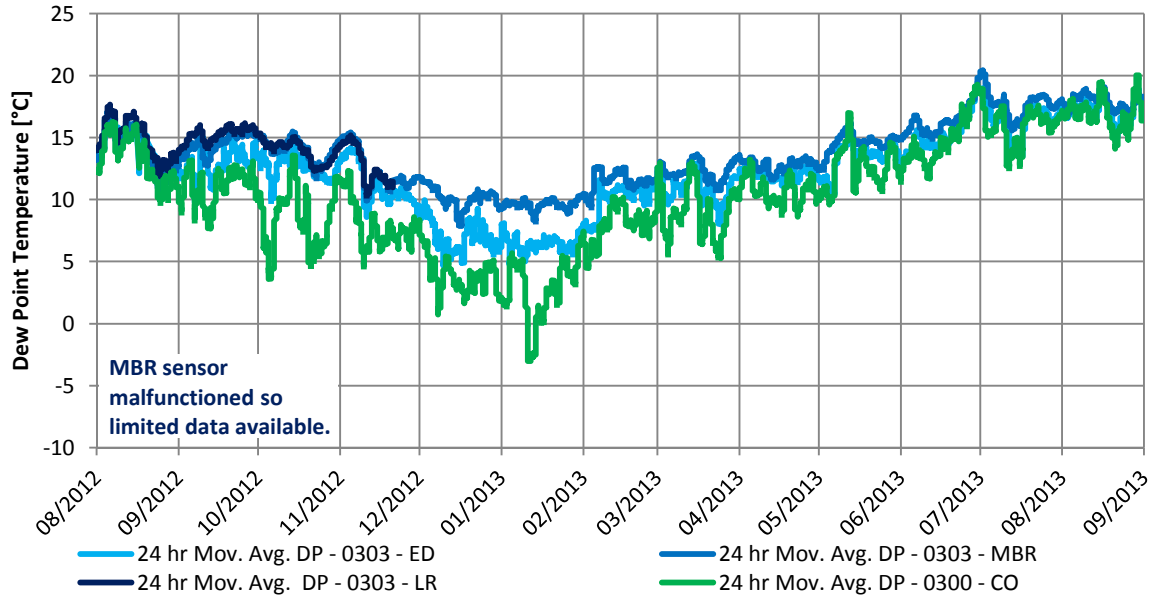


Figure 12-27: Graph of 24 hour moving average dew point temperatures in Suite 303

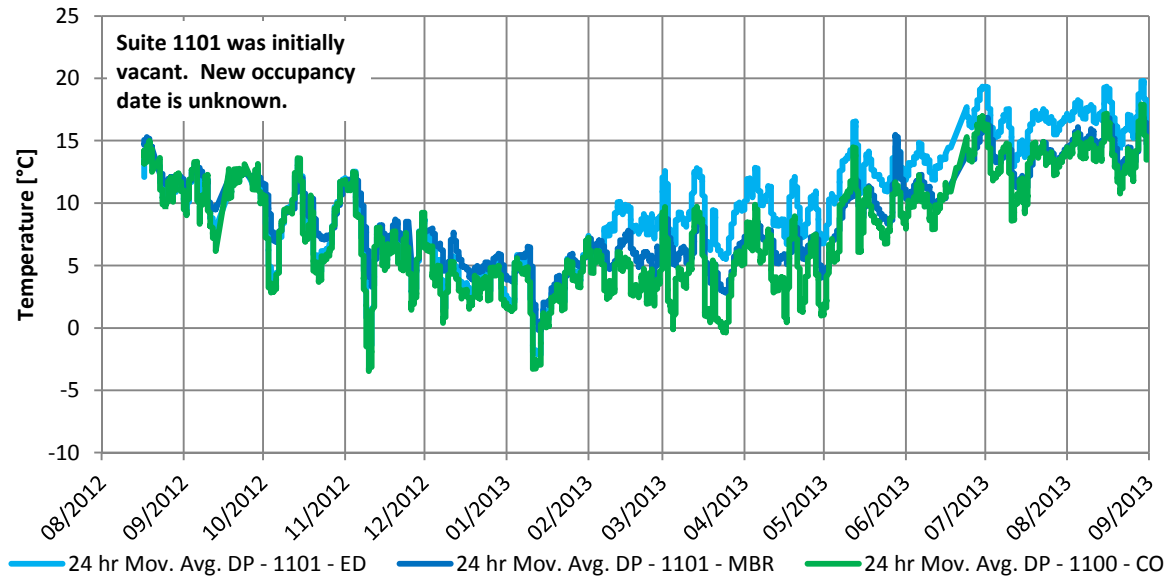


Figure 12-28: Graph of 24 hour moving average dew point temperatures in Suite 1101

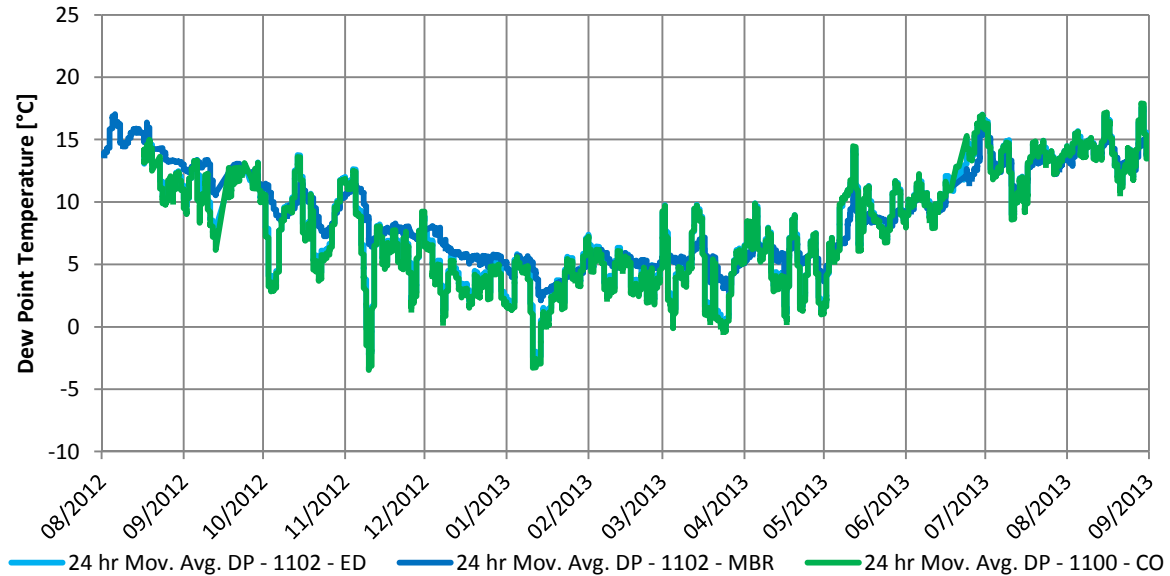


Figure 12-29: Graph of 24 hour moving average dew point temperatures in Suite 1102

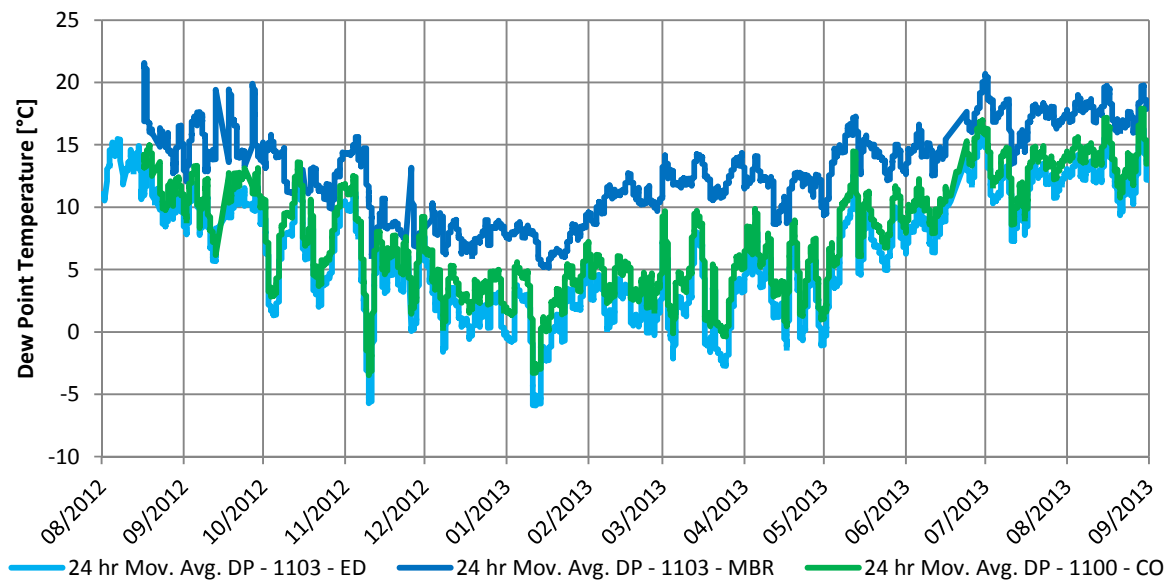


Figure 12-30: Graph of 24 hour moving average dew point temperatures in Suite 1103

The distribution of dew point temperatures generally shows patterns similar to those observed with respect to carbon dioxide concentrations. Suites on lower floors often have higher dew point temperatures in the master bedroom than near the entrance door by up to approximately 10 to 15°C. The maximum difference in dew point temperature within the suites usually occurs during the colder periods of the year which is partly because of lower exterior dew point temperatures that are typical during these periods, but may also indicate that less ventilation air is being provided to lower suites during cold periods of the year, and that the ventilation air that does enter

these suites is not well mixed with areas further from the entrance door such as the master bedroom. The difference in dew point temperature between the entrance door areas and the master bedrooms is larger in suites on Floor 3 than on Floor 11. This again indicates that either higher ventilation rates are causing dilution of the moisture in the air, or that the driving forces are facilitating better distribution (i.e. mixing) of ventilation air within the suites on the upper floors.

No significant correlation was found between wind (speed and direction) and dew point temperature, which is consistent with the findings with respect to carbon dioxide concentrations. This lack of correlation is likely because wind typically acts over relatively short time periods and may not act long enough to develop patterns in dew point temperatures. However, the increased exposure to wind and higher wind speeds at upper floors may contribute to the ventilation of these suites and distribution of air within the suites on a longer term basis. It is difficult to separate the long-term effect of wind from the influence of stack effect and mechanical ventilation systems.

12.3 Summary of Results

Overall, the carbon dioxide concentration and dew point measurements indicate that the corridors are well ventilated with outdoor air relative to the contaminant generation rate in these zones. However, the contaminant generation rates in the corridors are low, so this finding does not indicate even distribution of ventilation air and thus does not conflict with findings with respect to airflow measurements which were presented in Chapter 8.

Suites on lower floors typically had higher carbon dioxide concentration and dew point than the corridor, while suites on upper floors typically had levels similar to the levels in the corridors. These levels correlated well with the measured air change rates for these suites. Frequently the measured carbon dioxide concentrations in lower suites were above recommended levels. This finding reinforces the measured airflow results which found that suites on the upper floors of the building receive significantly more ventilation than do suites on the lower floors of the building.

The master bedrooms were typically measured to have higher carbon dioxide concentrations and dew point temperatures than near the suite entrance doors. This finding is partly due to increased contaminant generation rates in master bedrooms compared to other rooms, and also indicates insufficient supply of ventilation air the suites, insufficient distribution of ventilation air within the suites, or both.

Chapter 13

Conclusions and Recommendations

The conclusions of this research are provided in this chapter. In particular, conclusions are presented regarding corridor pressurization based ventilation systems for high-rise multi-unit residential buildings. These conclusions and the experience gained by conducting this research are used to develop general recommendations for industry and future research.

13.1 Conclusions

The results of the work performed at the case study building support the simplistic yet important conclusion that airflow in high-rise multi-unit residential buildings is complex and difficult to predict despite a relatively strong understanding of the relevant physics.

Pressure differences created by the natural driving forces of airflow are typically of similar magnitude to pressure differences created by mechanical systems, and corridor pressurization based ventilation systems do not provide the temporally or spatially dynamic response necessary to overcome these pressures.

The pressurized corridor based ventilation system at the case study building was found to unevenly distribute ventilation air to both the corridors and suites of the building with upper zones receiving significantly higher ventilation rates than lower zones, and many suites either being significantly over ventilated or under ventilated compared to modern ventilation rates such as ASHRAE-62.1 (2010). These low ventilation rates were unlikely due to poor performance of the make-up air unit as it was both designed and measured to bring air in to the building at nearly modern standards. Instead the low flow rates measured are due to a combination of a lack of control of the ventilation air once brought in to the building and the inability of the ventilation system to overcome stack effect pressures.

Significant leakage was measured from the make-up air unit duct with only approximately 40% of the intake ventilation air reaching the corridors directly. Once the air was supplied to the corridors, only 20% of the flow paths are to the suites through the entrance doors which creates a significant opportunity for ventilation air to instead flow to other adjacent zones such as the elevator shaft and stairwells. This lack of control of the ventilation airflow path creates a significant inefficiency in the corridor pressurization ventilation system and contributes to the low ventilation rates.

Stack effect also influences the ventilation rates at the case study building and contributes to the low ventilation rates measured for lower suites. Pressure differences due to stack effect were found to act primarily across the corridor to suite pressure boundaries instead of the exterior enclosure, likely due to the opening of windows significantly reducing the effective airtightness of the exterior enclosure. This is of particular importance because this is the same pressure boundary across which the corridor pressurization system is intended to control pressure differences to provide ventilation air to the suites and to control the transfer of air contaminants. Because the ventilation system and stack effect are acting to create pressure difference at the same location, it is difficult for the ventilation system to maintain the intended pressure regime and thus difficult for it to perform its intended function. As the climate at the case study building is relatively mild, for

buildings located in climates with more extreme temperatures the pressure differences due to stack effect would be of higher magnitude and thus even more difficult to overcome.

The low ventilation rates, particularly on lower floors, lead to elevated carbon dioxide concentrations and dew point temperatures in the suites indicating potential indoor air quality concerns. In many cases carbon dioxide concentrations were more than double recommended levels. Additionally, these indicators of indoor air quality were found to be higher in the master bedrooms than near suite entrance doors which is part due to increased carbon dioxide generation in master bedrooms due to increased occupancy, and also indicates that suite ventilation rates are insufficient, that distribution of ventilation air within the suites is insufficient, or both.

The inability of the corridor pressurization system to compensate for the natural driving forces of airflow also leads to significant potential for the flow of contaminants between building zones. At the case study building, flow of transfer air between suites was measured and could facilitate this flow of contaminants. While highly variable, wind pressures were found to distribute partially across interior pressure boundaries of the building and were typically the cause of peak pressure differences. The high variability and magnitude of these wind pressures makes it very difficult for any mechanical system to adequately compensate, and thus unintentional airflows can occur. Stack effect pressures were also found to drive flow between building zones, particularly from the parking garage into the occupied spaces of the building. Airflow from the parking garage into the building is of particular concern as it is a strong source of harmful air contaminants.

Overall, the results of the experimental program at the case study building indicate that in a typical high-rise multi-unit residential building the corridor pressurization based ventilation system does not effectively or efficiently ventilate the building and also does not provide reliable control of air contaminants. Furthermore, despite the extensive experimental program measuring airflow and various factors which affect airflow on a much finer scale than is typical, the knowledge of and prediction of airflows is still difficult. Consequently, design and operation measures that increase the predictability and reliability of ventilation systems provide a substantial benefit to system performance

13.2 Recommendations

A number of the problems regarding ventilation and air contaminant control originate with the inability of the corridor pressurization system to overcome the pressure differences created by wind and stack effect. One might suggest that operating the mechanical ventilation system to create higher pressure differences may be a potential solution to this problem; however, this is unlikely to be a practical or effective method for application in most high-rise multi-unit residential buildings as the pressure differences that must be developed to do so would be excessively high such that they would be problematic with respect to window and door operation, whistling noises at air leaks, and drafts. (Morrison Hershfield Ltd, 1996) It may be possible to use pressure differences to provide airflow control if real-time monitoring of pressure differences is used to control the ventilation system and the ventilation system has the ability to dynamically adapt temporally and spatially. This type of system, however, is not typically implemented and would be relatively complicated to design, operate, and maintain.

As the control of airflow patterns in high-rise multi-unit residential buildings by use of mechanically created pressure differences alone has limited potential, other methods for control of airflow must be used. The other factor that can be used to control airflow is the airflow resistance of the pressure boundaries. This parameter can be used to both limit the amount of airflow into, out of, and within buildings, to change the distribution of pressure differences, and to limit the development of pressure differences due to stack effect by reducing the effective stack height. In using airflow resistance to control airflows in high-rise multi-unit residential buildings, it is important to consider that a fundamental difference between these buildings and other types of high-rise buildings is the presence of operable windows and doors that are distributed throughout the building enclosure. The operation of these building components provides the ability for building occupants to significantly alter the airflow resistance of the exterior enclosure and consequently the airflow into, out, of and within a building as well as the associated building pressure regime. As the elimination of operable windows and doors is not a practical or desirable option, buildings must be designed to accommodate this dynamism.

To effectively accommodate the changing airtightness of the exterior enclosure, suites would need to be compartmentalized relative to one another so that the operation of one suite does not significantly impact the operation of adjacent suites. Suites must also be compartmentalized relative to the corridor so that opening exterior windows and doors in a suite or operating exhaust fans does not create the potential to significantly alter the airflow and pressure regime of the floor or building. This would also address current fire and smoke control issues due to the suite entrance door undercut requirement, and have the additional benefit of reducing sound transfer from the corridor to suites. To limit the development of pressure differences due to stack effect, the compartmentalization of vertical shafts, such as elevators and stairwells, from adjacent zones is also necessary.

If suites are to be compartmentalized relative to adjacent zones, the corridor pressurization based ventilation system is no longer a feasible option for ventilation of the suites, and the ventilation air would need to be ducted directly to each suite or supplied by in-suite systems. A directly ducted system or in-suite system would also likely provide significantly more reliable ventilation along known flow paths as compared to the pressurized corridor system. A significantly smaller corridor pressurization system could potentially still be used to ventilate the corridors and could also help control contaminant transfer by pressurizing the corridors. This system would require significantly less airflow than current systems and be more predictable due to the compartmentalized nature of the corridors.

If the pressure boundaries of a building are made more airtight to better control airflows, the exhaust of air from zones has an increased potential to develop significant pressure differences as the provision of make-up air through zone pressure boundaries is more limited. This effect could also make the supply of ventilation air to a suite more difficult. Consequently, while generally beneficial, when relatively airtight pressure boundaries are implemented, the use of ventilation systems which do not impose a pressure difference across building pressure boundaries (i.e. balanced ventilation systems) strongly recommended. These systems may have balanced mechanical supply and exhaust, or may use alternative provisions to mitigate the development or

pressure differences such as barometric dampers or trickle vents. The latter, however, provide less predictable airflow rates than does a mechanically balanced system.

Overall, typical corridor pressurization based ventilation systems do not provide the necessary dynamic response to effectively and efficiently ventilate and control airflow in high-rise multi-unit residential buildings, and furthermore do not likely provide the potential to do so due to the significant pressure differences that would be required. Consequently, alternative ventilation designs should be used for these types of buildings and these systems would likely require the compartmentalization of suites, the direct supply of ventilation air to each suite, and some allowance for balanced ventilation.

13.2.1 Recommendations for the Building Industry

As a result of this thesis work, recommendations can be made for the building industry with regards to airflow into, out of, and within multi-unit residential buildings.

1. **Airtightness of Pressure Boundaries** – The airtightness of building pressure boundaries including the exterior enclosure and interior compartmentalizing elements should be considered a fundamental parameter for the design of building ventilation systems.
2. **Compartmentalization of Suites** – To accommodate the occupant controlled nature of exterior windows and exhaust fans in high-rise multi-unit residential buildings, suites should be compartmentalized from each other and from the corridor.
3. **Compartmentalization of Vertical Shafts** – To control the development of pressures due to stack affect and the migration of air contaminants, vertical shafts should be compartmentalized from adjacent zones.
4. **Direct Supply of Ventilation Air to Suites** – Given the relatively uncontrolled, unpredictable, and inefficient nature of the corridor pressurization based ventilation in combination with the recommendation for compartmentalization of suites, ventilation systems for multi-unit residential building should provide ventilation air directly to each suite by either ducting or in-suite systems.
5. **Balanced Ventilation** – To limit the development of pressure difference which may affect mechanical system performance and create unintentional airflows, multi-unit residential ventilation systems should not impose pressure differences across building pressure boundaries.

13.2.2 Recommendations for Further Research

The results of this thesis help to identify the need for additional continuing research in this area.

1. **Evaluation of Alternative Ventilation Strategies** – Similar experimental work to that performed for this thesis should be conducted to evaluate the performance of alternative high-rise multi-unit residential building ventilation design strategies. This work may also include computational modeling of different ventilation strategies.
2. **Evaluation of Compartmentalization Strategies** – Similar field experimental work to that performed for this thesis should be conducted to evaluate the performance of different compartmentalization strategies including compartmentalization of suites and

compartmentalization of vertical shafts. This work may also include computational modeling of different compartmentalization strategies.

3. Determination of Appropriate Ventilation Rates – This thesis work focuses on understanding airflow patterns and development of the understanding necessary for design of effective and efficient ventilation systems in high-rise multi-unit residential buildings; however, further work is also required to determine appropriate ventilation rates for both supply and exhaust as industry has not yet reached consensus. (Holladay, 2013) Without ventilation and airflow control systems that perform as intended, the determination of appropriate ventilation rates is of limited value.

13.2.3 Recommendations for Implementation of Future Studies

As a result of the experience gained through this research, a number of recommendations for the implementation of future studies can be made.

1. Auto-zeroing Pressure Sensors – While the long-term drift of pressure sensors used for this work appears to be minimal and not to significantly influence the determined results, auto-zeroing pressure sensors are recommended for future studies to provide increased accuracy and reliability of the pressure measurement results. These types of sensors typically use a small valve to permit zeroing, and power consumption can be problematic when using battery powered data acquisition units.
2. Pressure Measurement Frequency – Pressure measurements were taken hourly at the same time as the other measurements made by the monitoring equipment; however, this frequency of measurement is not sufficient to capture peak pressures due to wind and also makes it difficult to identify short-term influences such as exhaust fan operation. This hourly measurement rate was selected in part because long-term average pressures are of most importance for this study, and in part due to limitations of the monitoring equipment used (battery life). An increased measurement rate is recommended for future studies, especially if more refined data regarding wind is necessary. Also, independent of the measurement rate, it would also be useful take multiple measurements over a short time period and average them to determine the recorded pressure difference. There are significant high frequency pressure spikes caused by wind which, if coincidentally captured by the pressure measurement, can be misleading.
3. Carbon Dioxide Sensors – The monitoring equipment provider for this study chose to calibrate the carbon dioxide sensors using the outdoor air concentration as a reference; however, more accurate calibration could be achieved using calibration gases of known carbon dioxide concentration. Additionally, if using the same carbon dioxide sensors for future studies, measures to mitigate sensor drift should be implemented.
4. Additional Pressure Measurements – Pressure differences between the parking garage and the building, between corridors and the elevator shaft, and between corridors and the stairwell shafts were not measured due to budget restriction, but could provide useful information.
5. Pre-Retrofit Monitoring Period – Due to logistical issues primarily associated with securing project funding, the monitoring program was not implemented as early as desired to fully capture pre-retrofit conditions which makes it difficult to draw conclusions regarding the

effect of the retrofit. Future studies assessing the impacts of retrofits should be sure to install the monitoring equipment well in advance of the retrofit to fully capture the pre-retrofit performance.

References

2009. 2009 Seattle Energy Code. Seattle: Seattle Department of Planning and Development.
- AAMA/WDMA/CSA. 2008. NAFS - North American Fenestration Standard/Specification for windows, doors, and skylights. Mississauga: Canadian Standards Association.
- ABAA. 2011. Air Barrier Materials, Accessories & Components, Assemblies and Systems. http://www.airbarrier.org/materials/index_e.php.
- Achakji, G, and G Tamura. 1988. "Pressure Drop Characteristics of Typical Stairshafts in High-Rise Buildings." ASHRAE Transactions, Vol. 94, Pt. 1 1223-1237.
- Air Solutions Inc. 2005. Assessment of Suite Compartmentalization and Depressurization in New High Rise Residential Buildings. Ottawa: Canadian Housing and Mortgage Corporation.
- AIR-INS Inc. 1988. Air Permeance of Building Materials. Ottawa: Canada Mortgage and Housing Corporation.
- ASHRAE. 2009. ASHRAE Handbook - Fundamentals. Atlanta: American Society of Heating, Refrigeration and Air-Conditioning Engineers Inc.
- . 2010. ASHRAE Standard 62.1-2010 Ventilation for Acceptable Indoor Air Quality. Atlanta: American Society of Heating, Refrigerating and Air-Conditioning Engineers Inc.
- . 2010. ASHRAE Standard 62.2-2010 Ventilation and Acceptable Air Quality in Low-Rise Residential Buildings. Atlanta: American Society of Heating, Refrigerating and Air-Conditioning Engineers Inc.
- . 2010. ASHRAE Standard 90.1-2010 Energy Standard for Buildings Except Low-Rise Residential Buildings. Atlanta: American Society of Heating, Refrigerating and Air-Conditioning Engineers Inc.
- . 2011. *ASRAE 189.1-2011 Standard for the Design of High-Performance Green Buildings*. Atlanta: American Society of Heating, Refrigerating, and Air Conditioning Engineers.
- ASTM. 2000. ASTM D3154-00 Standard Test Method for Average Velocity in a Duct (Pitot Tube Method). West Conshohocken: ASTM International.
- . 2003. ASTM E1186-03 Standard Practices for Air Leakage Site Detection in Building Envelopes and Air Barrier Systems. West Conshohocken: ASTM International.
- . 2007. ASTM E1827-96 Standard Test Methods for Determining Airtightness of Buildings Using an Orifice Blower Door. West Conshohocken: ASTM International.
- . 2006. ASTM E741-00 Standard Test Method for Determining Air Change in a Single Zone by Means of a Tracer Gas Dilution. West Conshohocken: ASTM International.
- . 2010. ASTM E779-10 Standard Test Method for Determining Air Leakage Rate by Fan Pressurization. West Conshokocken: ASTM International.
- ATTMA. 2010. Technical Standard L1. - Measuring Air Permeability of Building Envelopes (Dwellings). Northampton: Air Tightness Testing & Measurement Association.

- Baker, P, S Sharples, and I Ward. 1987. "Air Flow Through Cracks." *Building and Environment Vol. 22* 293-304.
- Bohac, D, M Hewett, J Fitzgerald, and D Grimsrud. 2007. "Measured Change in Multifamily Unit Air Leakage and Airflow Due to Air Sealing and Ventilation Treatments." *Proceedings from ASHRAE/DOE Buildings X*. Clearwater: American Society of Heating, Refrigerating, and Air Conditioning Engineers.
- Brundrett, E. 1991. *Fluids Engineering - A Selection of Applied Procedures and Principles for the Analysis and Design of Fluid Flows Systems*. Waterloo: University of Waterloo.
- Building Science Corporation. 2009. *Info-401: Air Barriers - Airtight Drywall Approach*. Somerville: Building Science Press.
- CaGBC. 2009. *LEED Canada for New Construction and Major Renovations 2009*. Ottawa: Canada Green Building Council.
- CGSB. 1986. *CAN/CGSB - 149.10-M86*. Ottawa: Canadian General Standards Board.
- . 1986. *CAN/CGSB-149.10-M86 Determination of the Airtightness of Building Envelopes by the Fan Depressurization Method*. Ottawa: Canadian General Standards Board.
- . 1996. *CAN/CGSB-149.15-96 Determination of the Overall Envelope Airtightness of Buildings by the Fan Pressurization Method Using the Building's Air Handling Systems*. Ottawa: Canadian General Standards Board.
- CO2Meter.com. 2013. *CO2 Sensor Calibration: What You Need to Know*. March 15. <http://www.co2meter.com/blogs/news/7512282-co2-sensor-calibration-what-you-need-to-know>.
- Colliver, D, W Murphy, and W Sun. 1994. "Development of A Building Component Air Leakage Data Base." *ASHRAE Transactions Vol. 100, Part 1*. American Society of Heating, REfrigerating and Air-Conditioning Engineers . 292-305.
- Colliver, D, W Murphy, and W Sun. 1992. *Evaluation of the Techniques for the Measurement of Air Leakage of Building Components*. Atlanta: American Society of Heating, Refrigerating, and Air-Conditioning Engineers Inc.
- Cooke, G. 2005. *Assessment of Suite Compartmentalization and Depressurization in New High-Rise Residential Buildings*. Ottawa: Canada Mortgage and Housing Corporation.
- Cooke, G, J Kokko, and T Greene. 2005. "Airtightness and Ventilation System Performance of Apartments in New Multi-Unit Residnetial Buildings." *Proceedings of the 10th Canadian Conference on Building Science and Technology*. Ottawa: Building Envelope Council Ottawa Region. 94-103.
- Cóstola, D, B Blocken, and J Hensen. 2009. "Overview of pressure coefficient data in building energy simulatoin and airflow network programs." *Building and Environment, Vol. 4, Issue 10* 2027-2036.
- Dalgliesh, W, and D Boyd. 1962. "Wind on Buildings." *Canadian Building Digest No. 28*. National Research Council Canada.

Chapter 13 Conclusions and Recommendations

- Dalglish, W, and W Schriever. 1968. "Wind Pressure On Buildings." *Canadian Building Digest No. 34*. National Research Council Canada.
- DePani, S, and P Fazio. 2001. "Airtightness Testing and Air Flow Modelling of Two and Three-Unit Multifamily Building." *eSim 2011: Canadian Conference on Building Energy Simulation*. Ottawa.
- Diamond, R, F Helmut, and D Dickerhoff. 1996. *Ventilation and Infiltration in High-Rise Apartment Buildings*. Berkeley: Lawrence Berkley Laboratory.
- Diamond, R, M Modera, and H Feustel. 1986. "Ventilation and Occupant Behaviour in Two Apartment Buildings." *Proceedings of 7th AIC Conference*. Stratford-upon-Avon. 6.1-6.18.
- D'Ottavio, T, G Senum, and R Dietz. 1988. "Error Analysis ." *Building and Environment, Vol. 23, No. 3* 187-194.
- Edwards, C. 1999. Modelling of Ventilation and Infiltration Energy Impacts in Mid and High-Rise Apartment Buildings. Ottawa: Canada Mortgage and Housing Corporation.
- Energy Star. 2012. "Energy Star Multifamily High Rise National Prescriptive Path Requirements, Version 1.0." US Environmental Protection Agency, June.
- Environment Canada. 2013. *Accessing the Data*. July 10. <http://climate.weather.gc.ca/>.
- Etheridge, D. 1977. "Crack Flow Equations and Scale Effect." *Building and Enviroment Vol. 12* Pergamon Press.
- Fang, J, and A Persily. 1995. "Airflow and Radon Transport Modeling in Four Large Buildings." *ASHRAE Transactions, Vol. 101, Pt. 1*.
- Feustel, H. 1998. COMIS - An International Multizone Air-Flow and Contaminant Transport Model. Berkeley: Lawrence Berkeley National Laboratory.
- Finch, G. 2007. *The Performance of Rainscreen Walls in Coastal British Columbia*. Masters Thesis, Waterloo: University of Waterloo.
- Finch, G, J Straube, and C Genge. 2009. "Air Leakage Within Multi-Unit Residential Buildings: Testing and Implications for Building Performance." *Proceedings of the 12th Canadian Conference on Building Science and Technology*. Montreal: National Building Envelope Council of Canada. 529-538.
- Flanders, S, and B-H Song. 1989. *Passive Tracer Gas Measurement of Air Exchange in a Large Multi-Celled Building in Alaska*. U.S Army Cold Regions Research and Engineering Laboratory and National Association of Home Builders National Research Center.
- Genge, C. 2011. Modernizing ISO, EN and ASTM Air Leakage Standards. Everson: Retrotec Inc.
- Gulay, B, C Stewart, and G Foley. 1993. Field Investgiation Survey of Airtightness, Air Movement and Indoor Air Quality in High Rise Apartment Buildings Summary Report. Ottawa: Canada Mortgage and Housing Corpotation.
- Heiser, J, and T Sullivan. 2002. The Brookhaven National Laboratory Perfluorocarbon Tracer Technology: A Proven and Cost-Effective Method to Verify Integrity and Monitor Long-Term

- Performance of Walls, Floors, Caps, and Cover Systems. Upton: Brookhaven National Laboratory.
- Hill, D. 1999. Modelling of Ventilation and Infiltration Energy Impacts in Mid and High-Rise Apartment Buildings. Ottawa: Canada Mortgage and Housing Corporation.
- Holladay, M. 2013. *Green Building Advisor*. June 28.
<http://www.greenbuildingadvisor.com/blogs/dept/musings/how-much-fresh-air-does-your-home-need>.
- ICC. 2012. *International Building Code*. International Code Council Inc.
- . 2012. *International Energy Conservation Code*. International Code Council.
- . 2012. *International Mechanical Code*. Country Club Hills: International Code Council Inc.
- ISO. 2006. ISO 9972:2006 Thermal performance of buildings - Determination of air permeability of buildings - Fan pressurization method. Geneva: International Organization for Standardization.
- Klepeis, N, W Nelson, W Ott, J Robinson, A Tsang, P Switzer, J Behar, S Hern, and W Engelmann. 2001. "The National Human Activity Pattern Survey (NHAPS): a resource for assessing exposure to environmental pollutants." *Journal of Exposure Analysis and Environmental Epidemiology* 231-252.
- Klote, J, and G Tamura. 1986. "Elevator Piston Effect and the Smoke Problem." *Fire Safety Journal* 227-233.
- Kronvall, J. 1991. "Crack flow. A power law estimation technique." *12th AIVC Conference Air Movement and Ventilation Control Within Buildings*. Ottawa: Air Infiltration and Ventilation Centre. 261-269.
- Liu, H. 1975. *Wind Pressures and Forces on buildings*. Columbia: University of Missouri-Columbia.
- Loss, W, and R Dietz. 1991. Locating of Leaks in Water-Cooled Generator Stator Bars Using Perfluorocarbon Tracers. Upton: Brookhaven National Laboratory.
- Lstiburek, J. 2013. "Unintended Consequences Suck." *ASHRAE Journal*, June: 52-56.
- Lstiburek, J. 2011. *Insight: Just Right and Airtight*. buildingscience.com.
- Lstiburek, J. 2000. *Toward an Understanding and Prediction of Air Flow in Buildings*. PhD Thesis, Toronto: University of Toronto.
- Matson, N, and M Sherman. 2004. "Why We Ventilate Our Houses - An Historical Look." *2004 ACEEE Summer Study on Energy Efficiency in Buildings*. Washington: American Council for an Energy Efficient Economy. 241-250.
- McWilliams, J. 2002. *Review of Airflow Measurement Techniques*. Berkeley: Lawrence Berkeley National Laboratory.
- Modera, M, R Diamond, and J Brunsell. 1985. "Improving Diagnostics and Energy Analysis for Multifamily Buildings: A Case Study." *Proceedings of the Thermal Performance of the*

- Exterior Envelops of Buildings III*. Clearwater: American Society of Heating, Refrigerating, and Air-Conditioning Engineers. 689-706.
- Moffat, P, I Theaker, and C Wray. 1998. Field Testing to Characterize Suite Ventilation in Recently Constructed Mid- and High-Rise Residential Buildings. Ottawa: Canada Mortgage and Housing Corporation.
- Morrison Hershfield Ltd. 1996. Controlling Stack Pressure in High-Rise Buildings by Compartmenting the Building. Ottawa: Canada Mortgage and Housing Corporation.
- NFPA. 2013. NFPA 105 Standard for Smoke Door Assemblies and Other Opening Protectives. Quincy: National Fire Protection Association.
- . 2013. NPFA 80 Standard for Fire Doors and Other Opening Protectives. Quincy: National Fire Protection Association.
- NFRC. 2004. *NFRC 400-2004*. Silver Spring: National Fenestration Rating Council, Inc.
- NIST. 2013. *Airflow Elements Chart*. January 20.
<http://www.bfrl.nist.gov/IAQanalysis/CONTAM/aechart.htm>.
- NRC. 2010. *National Building Code of Canada 2010*. Ottawa: National Research Council of Canada.
- . 2011. *National Energy Code of Canada for Buildings 2011*. Ottawa: National Research Council Canada.
- Orne, M, M Liddament, and A Wilson. 1998. *Numerical Data for Air Infiltration & Natural Ventilation Calculations*. Coventry: Oscar Faber Group Ltd.
- Passive House Institute. 2012. *Passive House Requirements*.
http://passiv.de/en/02_informations/02_passive-house-requirements/02_passive-house-requirements.htm.
- Persily, A. 1997. "Evaluating Building IAQ and Ventilation with Indoor Carbon Dioxide." *ASHRAE Transactions, Vol. 103, Pt. 2*.
- Persily, A, and E Ivy. 2001. *Input Data for Multizone Airflow and IAQ Analysis*. National Institute of Standards and Technology.
- Proskiw, G, and A Parekh. 2001. "A Proposed Test Procedure for Separating Exterior Envelope Air Leakage from interior Partition Air Leakage." *Conference Proceedings - Performance of Exterior Envelopes of Whole Buildings VIII*. Atlanta: American Society of Heating, Refrigerating and Air-Conditioning Engineers Inc. 1-7.
- Proskiw, G, and B Phillips. 2001. *Air Leakage Characteristics, Test Methods, and Specifications for Large Buildings*. Ottawa: Canada Mortgage and Housing Corporation.
- . 2008. "An Examination of Air Pressure and Air Movement Patterns in Multi-Unit Residential Buildings." *Proceedings of the Building Enclosure Science & Technology 1 Conference*. Minneapolis: National Institute of Building Sciences.
- . 2006. *Characterizing Air Pressure/Air Movement Patterns in Multi-Unit Residential Buildings*. Ottawa: Canada Mortgage and Housing Corporation.

Chapter 13 Conclusions and Recommendations

- RDH Building Engineering Ltd. & FPInnovations. 2013. Guide for Designing Energy-Efficient Building Enclosures for Wood-Frame Multi-Unit Residential Buildings in Marine to Cold Climate Zones in North America. Vancouver: FPInnovations.
- Reardon, J, A Kim, and C Shaw. 1987. "Balanced Fan Depressurization Method for Measuring Component and Overall Air Leakage in Single- and Multifamily Dwellings." *ASHRAE Transactions Volume 93, Pt. 2* 137-152.
- Retech. n.d. *Air Flow in Buildings*. Toronto: Retech Restoration Company Ltd.
- Retrotec. 2012. *Door Fan Operation Manual*. Everson: Retrotec Inc.
- . 2012. *DucTester Operation and Testing Manual*. Everson: Retrotec Inc.
- Shaw, C. 1980. "Methods for Conducting Small-Scale Pressurization Tests and Air Leakage Data of Multi-Storey Buildings." *ASHRAE Transactions, Vol. 86, Part 1* 241-250.
- Shaw, C, and G Tamura. 1977. "The Calculation of Air Infiltration Rates Caused by Wind and Stack Action for Tall Buildings." *ASHRAE Transactions Vol. 83, Part 2* 145-158.
- Shaw, C, M Reardon, M Said, and R Magee. 1991. "Airflow Patterns in a Five-Storey Apartment Building." *Proceedings of the 12th AIVC Conference*. Ottawa: Air Infiltration and Ventilation Centre. 359-374.
- Sherman, M, and M Modera. 1986. "Comparison of Measured and Predicted Infiltration Using the LBL Infiltration Model." *Measured Air Leakage of Buildings, ASTM STP 904* 325-347.
- Sherman, M, and R Chan. 2004. *Building Airtightness: Research and Practice*. Report No. LBNL-53356, Berkley: Lawrence Berkley National Laboratory.
- Solinst Canada Ltd. 2012. *Solinst Technical Bulletin - Understanding Pressure Sensor Drift*. <http://www.solinst.com/Prod/3001/technical-bulletins/Understanding-Pressure-Sensor-Drift.html>.
- Steffen, M. 2012. "Towards Airtightness - The Contractor's Role in Designing and Constructing the Air Barrier System." *Building Enclosure Science & Technology 3 Conference Proceedings*. Atlanta: Omnipress.
- Straube, J, and E Burnett. 2005. *Building Science for Building Enclosures*. Westford: Building Science Press inc.
- Sullivan, T, J Heiser, T Watson, K Allwine, and J Flaherty. 2006. Perfluorocarbon Gas Tracer Studies to Support Risk Assessment Modeling of Critical Infrastructure Subjected to Terrorist Attacks. Upton: Brookhaven National Laboratory.
- Tamura, G. 1969. "Computer Analysis of Smoke Movement in Tall Buildings." *ASHRAE Transactions Vol. 75, Part II* 81-92.
- Tamura, G. 1980. "The Performance of Vestibule Pressurization System for the Protection of Escape Routes of a 17-Story Hotel." *ASHRAE Transactions, Vol. 86, Part 1* 593-603.
- Tamura, G, and C Shaw. 1976. "Air leakage data for the design of elevator and stair shaft pressurization systems." *ASHRAE Transactions, Vol. 82, Pt. 2* 179-190.

- . 1976. "Studies on Exterior Wall Air Tightness and Air Infiltration of Tall Buildings." *ASHRAE Transactions Vol. 82 Part 1* 122-134.
- Tamura, G.T., and C.Y. Shaw. 1976. "Studies on Exterior Wall Air Tightness and Air Infiltration of Tall Buildings." *ASHRAE Transactions* (National Research Council of Canada) 122-134.
- The Energy Conservatory. 2009. *Minneapolis Blower Door Operation Manual for Model 3 and Model 4 Systems*. Minneapolis: The Energy Conservatory.
- The Energy Conservatory. 2012. *Minneapolis Duct Blaster*. Minneapolis: The Energy Conservatory.
- The Sheltair Group. 2003. *Ventilation Systems for Multi-unit Residential Buildings - Performance Requirements and Alternative Approaches*. Ottawa: Canada Mortgage and Housing Corporation.
- Thorogood, R. 1979. *Building Research Establishment Information Paper: Resistance to air flow through external walls*. Watford: Building Research Establishment, Department of the Environment.
- U.S. Department of Energy. 2013. *Weather Data*. July 16.
http://apps1.eere.energy.gov/buildings/energyplus/weatherdata_about.cfm?CFID=42965&CFTOKEN=5d547fb5455516fc-80C83DB8-9849-98DB-7B66E1F8615F64C0&jsessionid=3DE2B95201EAD29A9A6A6CD70F591DB8.eere.
- Ueno, K, J Lstiburek, and D Bergey. 2012. *Multifamily Ventilation Retrofit Strategies*. Somerville: Building Science Press.
- US Army Corps of Engineers. 2012. *U.S. Army Corps of Engineers Air Leakage Test Protocol for Building Envelopes - Version 3*. Champaign: U.S Army Corps of Engineers.
- Walke, Rich. 2012. "Smoke and Draft Control Door Assemblies." *The Code Authority 2012 Issue 2*, 4-5.
- Walker, I, and D Wilson. 1998. "Field Validation of Algebraic Equations for Stack and Wind Driven Air Infiltration Calculations." *ASHRAE HVAC&R Research Journal, Vol. 4, No.2*.
- Walton, G, and S Dols. 2010. *CONTAM A User Guide and Program Documentation*. Gaithersburg: National Institute of Standards and Technology.
2011. *Washington State Energy Code 2009*. Olympia: Washington State Building Code Council.
- Weisstein, E. 2013. *Weibull Distribution*. <http://mathworld.wolfram.com/WeibullDistribution.html>.
- Wilson, A, and G Tamura. 1968. "Stack Effect in Buildings." *Canadian Building Digest No. 104*. National Research Council Canada, August.
- Wray, C, I Walker, and M Sherman. 2002. *Accuarcy of Flow Hoods in residential Applications*. Berkeley: Lawrence Berkeley National Laboratory.
- Yeatts, B. 1992. *Internal Pressure for Buildings*. Lubbock: Texas Tech University.
- Yilmax, V, and H Çelik. 2008. "A Statistical Approach to Estimate the Wind Speed Distribution: The Case of Gelibolu Region." *Doğuş Üniversitesi Dergisi* 122-132.

Appendices

Appendix A

Airflow Resistance of Building Elements

The airflow resistance of various building elements as compiled from literature are provided in Table A-1 to Table A-5 from Murphy, & Sun (1994), Fang & Persily (1995), Gulay, Stewart, & Foley (1993), Moffat, Theaker, & Wray (1998), Tamura & Shaw (1976), and Edwards (1999). Orne et al (1998) also conducted a review of available airtightness data for various building components and provided lower, upper, and median flow exponent and flow coefficient data. This is more detailed information than most sources provide, so excerpts of that data are presented separately in Table A-6 to Table A-9. Morrison Hershfield (1996) also presents useful data for doors based on crack size which is reproduced in Table A-10. Much of the available data has been developed based on testing of houses, commercial buildings, and institutional buildings; however, these many of these values can applied to multi-unit residential buildings.

It should be noted that in many cases these references are in themselves compilations of data available in literature, and in some cases their data sets overlap. Data was provided in a variety of different metrics, commonly in equivalent or effective leakage areas, and was converted to flow rates at 75 Pa, flow coefficients, and flow exponents to allow for comparison. When necessary, flow exponent values were assumed and are provided.

Table A-1: Airflow Characteristics of Windows

Component	Flow Exponent, n	Best Estimate or Mean Average						Minimum			Maximum			Reference
		Flow Coefficient, C [L/s-Pa ⁿ]	Linear Normalized Flow Coefficient, C _l [L/s-Pa ⁿ -m]	Normalized Flow Coefficient, C _n [L/s-Pa ⁿ -m ²]	Q ₇₅ [L/s]	Q ₅₀ /m [L/s-m]	q ₇₅ [L/s-m ²]	Q ₇₅ [L/s]	Q ₅₀ /m [L/s-m]	q ₇₅ [L/s-m ²]	Q ₇₅ [L/s]	Q ₅₀ /m [L/s-m]	q ₇₅ [L/s-m ²]	
Windows: Awning NonWS	0.65*	-	-	0.166	-	-	2.75	-	-	1.38	-	-	4.13	(Colliver, Murphy, & Sun, 1994)
Windows: Awning with weatherstripping	0.65*	-	-	0.083	-	-	1.38	-	-	0.69	-	-	2.07	(Colliver, Murphy, & Sun, 1994)
Windows: Casement with weatherstripping	0.65*	0.025	-	-	0.41	-	-	-	-	-	-	-	-	(Colliver, Murphy, & Sun, 1994)
Windows: Casement w/o WS	0.65*	0.029	-	-	0.48	-	-	-	-	-	-	-	-	(Colliver, Murphy, & Sun, 1994)
Windows: Double Horizontal Slider w/o WS	0.65*	0.114	-	-	1.89	-	-	-	-	-	-	-	-	(Colliver, Murphy, & Sun, 1994)
Windows: Double Horizontal Slider - wood with WS	0.65*	0.057	-	-	0.95	-	-	-	-	-	-	-	-	(Colliver, Murphy, & Sun, 1994)
Windows: Double Horizontal Slider - aluminum with WS	0.65*	0.075	-	-	1.24	-	-	-	-	-	-	-	-	(Colliver, Murphy, & Sun, 1994)
Windows: Double Hung w/o WS	0.65*	0.260	-	-	4.30	-	-	-	-	-	-	-	-	(Colliver, Murphy, & Sun, 1994)
Windows: Double Hung with WS	0.65*	0.068	-	-	1.12	-	-	-	-	-	-	-	-	(Colliver, Murphy, & Sun, 1994)
Windows: Double Hung w/o WS, with storm	0.65*	0.101	-	-	1.67	-	-	-	-	-	-	-	-	(Colliver, Murphy, & Sun, 1994)
Windows: Double Hung w WS, with storm	0.65*	0.082	-	-	1.36	-	-	-	-	-	-	-	-	(Colliver, Murphy, & Sun, 1994)
Windows: Double Hung w WS, with pressurized track system	0.65*	0.050	-	-	0.83	-	-	-	-	-	-	-	-	(Colliver, Murphy, & Sun, 1994)
Windows: Framing - Masonry - uncaulked	0.65*	-	-	-	0.624	-	-	-	-	-	-	-	-	(Colliver, Murphy, & Sun, 1994)
Windows: Framing - Masonry - caulked	0.65*	-	-	-	0.135	-	-	-	-	-	-	-	-	(Colliver, Murphy, & Sun, 1994)
Windows: Framing - Wood - uncaulked	0.65*	-	-	-	0.177	-	-	-	-	-	-	-	-	(Colliver, Murphy, & Sun, 1994)
Windows: Framing - Wood - caulked	0.65*	-	-	-	0.031	-	-	-	-	-	-	-	-	(Colliver, Murphy, & Sun, 1994)
Windows: Jalousie (perlouvre)	0.65*	0.352	-	-	5.82	-	-	-	-	-	-	-	-	(Colliver, Murphy, & Sun, 1994)
Windows: Lumped	0.65*	-	-	-	-	-	-	-	-	-	-	-	-	(Colliver, Murphy, & Sun, 1994)
Windows: Single Horizontal Slider	0.65*	-	0.049	-	-	-	-	-	-	-	-	-	-	(Colliver, Murphy, & Sun, 1994)
Windows: Single Horizontal Slider - aluminum	0.65*	-	0.070	-	-	-	-	-	-	-	-	-	-	(Colliver, Murphy, & Sun, 1994)
Windows: Single Horizontal Slider - wood	0.65*	-	0.083	-	-	-	-	-	-	-	-	-	-	(Colliver, Murphy, & Sun, 1994)
Windows: Single Horizontal Slider - wood clad	0.65*	-	0.046	-	-	-	-	-	-	-	-	-	-	(Colliver, Murphy, & Sun, 1994)
Windows: Storm Inside - Heat Shrink	0.65*	-	0.067	-	-	-	-	-	-	-	-	-	-	(Colliver, Murphy, & Sun, 1994)
Windows: Storm Inside - rigid with magnetic seals	0.65*	-	0.090	-	-	-	-	-	-	-	-	-	-	(Colliver, Murphy, & Sun, 1994)
Windows: Storm Inside - flex sheets with mechanical seals	0.65*	-	0.022	-	-	-	-	-	-	-	-	-	-	(Colliver, Murphy, & Sun, 1994)
Windows: Storm Inside - rigid with mechanical seals	0.65*	-	0.012	-	-	-	-	-	-	-	-	-	-	(Colliver, Murphy, & Sun, 1994)
Windows: Storm Outside - pressurized track	0.65*	-	0.042	-	-	-	-	-	-	-	-	-	-	(Colliver, Murphy, & Sun, 1994)
Windows: Storm Outside - 2 track	0.65*	-	0.055	-	-	-	-	-	-	-	-	-	-	(Colliver, Murphy, & Sun, 1994)
Windows: Storm Outside - 3 track	0.65*	-	0.128	-	-	-	-	-	-	-	-	-	-	(Colliver, Murphy, & Sun, 1994)
Windows: Storm Outside - 2 track	0.65*	-	0.256	-	-	-	-	-	-	-	-	-	-	(Colliver, Murphy, & Sun, 1994)

*Assumed n when unknown to compare values; WS = Weather Stripped; Per meter is per meter of sash

Table A-2: Airflow Characteristics of Doors

Component	Flow Exponent, n	Best Estimate or Mean Average						Minimum			Maximum			Reference
		Flow Coefficient, C [L/s-Pa ⁿ]	Linear Normalized Flow Coefficient, C _{lin} [L/s-Pa ^{n-m}]	Normalized Flow Coefficient, C _n [L/s-Pa ^{n-m²}]	Q ₂₅ [L/s]	Q ₂₅ /m [L/s-m]	q ₂₅ [L/s-m ²]	Q ₂₅ [L/s]	Q ₂₅ /m [L/s-m]	q ₂₅ [L/s-m ²]	Q ₂₅ [L/s]	Q ₂₅ /m [L/s-m]	q ₂₅ [L/s-m ²]	
Doors - Attic/Crawl Space - NonWS	0.65*	3.120	-	-	51.6	-	17.2	-	-	63.7	-	-	(Colliver, Murphy, & Sun, 1994)	
Doors - Attic/Crawl Space - WS	0.65*	1.872	-	-	31.0	-	13.8	-	-	31.8	-	-	(Colliver, Murphy, & Sun, 1994)	
Door - Attic/Fold Down - NonWS	0.65*	4.576	-	-	75.7	-	39.6	-	-	148.0	-	-	(Colliver, Murphy, & Sun, 1994)	
Door - Attic/Fold Down - WS	0.65*	2.288	-	-	37.9	-	24.1	-	-	74.0	-	-	(Colliver, Murphy, & Sun, 1994)	
Door - Attic/Fold Down - with insulated box	0.65*	0.416	-	-	6.9	-	-	-	-	-	-	-	(Colliver, Murphy, & Sun, 1994)	
Doors - Double - Not WS	0.65*	-	-	1.144	-	18.9	-	12.0	-	-	37.9	-	(Colliver, Murphy, & Sun, 1994)	
Doors - Double - WS	0.65*	-	-	0.832	-	13.8	-	5.2	-	-	39.6	-	(Colliver, Murphy, & Sun, 1994)	
Door Frame - General	0.65*	1.248	-	-	20.7	-	4.1	-	-	43.0	-	-	(Colliver, Murphy, & Sun, 1994)	
Door Frame - Masonry - Not Caulked	0.65*	-	-	0.520	-	8.6	-	2.9	-	-	8.6	-	(Colliver, Murphy, & Sun, 1994)	
Door Frame - Masonry - Caulked	0.65*	-	-	0.104	-	1.7	-	0.5	-	-	1.7	-	(Colliver, Murphy, & Sun, 1994)	
Door Frame - Wood - Not Caulked	0.65*	-	-	0.177	-	2.9	-	1.0	-	-	2.9	-	(Colliver, Murphy, & Sun, 1994)	
Door Frame - Wood - Caulked	0.65*	-	-	0.031	-	0.5	-	0.2	-	-	0.5	-	(Colliver, Murphy, & Sun, 1994)	
Door Frame - trim	0.65*	-	0.832	-	-	13.8	-	-	-	-	-	-	(Colliver, Murphy, & Sun, 1994)	
Door Frame - jamb	0.65*	-	0.208	-	-	3.4	-	12.0	-	-	17.2	-	(Colliver, Murphy, & Sun, 1994)	
Door Frame - threshold	0.65*	-	0.208	-	-	3.4	-	2.1	-	-	41.3	-	(Colliver, Murphy, & Sun, 1994)	
Doors - General - average	0.65*	-	0.032	-	-	0.5	-	0.4	-	-	0.8	-	(Colliver, Murphy, & Sun, 1994)	
Doors - Interior (pocket) (on top floor)	0.65*	1.456	-	-	24.1	-	-	-	-	-	-	-	(Colliver, Murphy, & Sun, 1994)	
Doors - Interior (stairs)	0.65*	-	0.094	-	-	1.5	-	0.4	-	-	2.6	-	(Colliver, Murphy, & Sun, 1994)	
Doors - Mail Slot	0.65*	-	0.416	-	-	6.9	-	-	-	-	-	-	(Colliver, Murphy, & Sun, 1994)	
Doors - Sliding Exterior Glass Patio	0.65*	-	2.288	-	-	37.9	-	5.2	-	-	103.3	-	(Colliver, Murphy, & Sun, 1994)	
Doors - Sliding Exterior Glass Patio	0.65*	-	-	0.572	-	-	9.5	-	1.0	-	25.8	-	(Colliver, Murphy, & Sun, 1994)	
Doors - Storm (diff. between with/without)	0.65*	0.624	-	-	10.3	-	5.2	-	-	10.7	-	-	(Colliver, Murphy, & Sun, 1994)	
Doors - Single - Not Weatherstripped	0.65*	2.184	-	-	36.1	-	20.7	-	-	91.2	-	-	(Colliver, Murphy, & Sun, 1994)	
Doors - Single - Weatherstripped	0.65*	1.248	-	-	20.7	-	6.9	-	-	46.5	-	-	(Colliver, Murphy, & Sun, 1994)	
Doors - Vestibule (subtract per each location)	0.65*	1.040	-	-	17.2	-	-	-	-	-	-	-	(Colliver, Murphy, & Sun, 1994)	
Stairwell Doors - Office Buildings (cracks from 2.0 to 4.6 mm)	0.55	16.0	-	-	172	-	113	-	-	271	-	-	(Tamura & Shaw, 1976)	
Suite Entrance Doors - All (85 to 91 cm wide; 200 to 221 cm tall)	0.55*	18.2	-	-	196	-	109	-	-	278	-	-	(Moffat, Theaker, & Wray, 1998)	
Suite Entrance Doors - WS (86 to 90 cm wide; 201 to 221 cm tall)	0.55*	14.0	-	-	151	-	109	-	-	188	-	-	(Moffat, Theaker, & Wray, 1998)	
Suite Entrance Doors - Not WS (excludes one high value) (85 to 91 cm wide; 200 to 206 cm tall)	0.55*	21.3	-	-	229	-	189	-	-	278	-	-	(Moffat, Theaker, & Wray, 1998)	

*Assumed n when unknown to compare values; WS = Weather-Stripped; Per meter is per meter of sash

Table A-3: Airflow Characteristics of Miscellaneous Components Including Mechanical, Electrical, and Plumbing Penetrations

Component	Flow Exponent, n	Best Estimate or Mean Average				Minimum			Maximum			Reference	
		Flow Coefficient, C [L/s-Pa ⁿ]	Linear Normalized Flow Coefficient, C _{lin} [L/s-Pa ⁿ /m]	Normalized Flow Coefficient, C _n [L/s-Pa ⁿ /m ²]	Q ₂₅ [L/s]	Q ₅₀ /m [L/s-m]	q ₇₅ [L/s-m ²]	Q ₂₅ [L/s]	Q ₅₀ /m [L/s-m]	q ₇₅ [L/s-m ²]			
Chimney	0.65*	3.016	-	-	49.91	-	-	36.14	-	-	61.96	-	(Colliver, Murphy, & Sun, 1994)
Ceiling Penetrations - whole house fans	0.65*	2.080	-	-	34.42	-	-	2.75	-	-	36.14	-	(Colliver, Murphy, & Sun, 1994)
Ceiling Penetrations - recessed lights	0.65*	1.040	-	-	17.21	-	-	2.58	-	-	36.14	-	(Colliver, Murphy, & Sun, 1994)
Ceiling Penetrations - ceiling/flue vent	0.65*	3.224	-	-	53.36	-	-	48.19	-	-	53.36	-	(Colliver, Murphy, & Sun, 1994)
Ceiling Penetrations - surface mounted lights	0.65*	0.085	-	-	1.41	-	-	-	-	-	-	-	(Colliver, Murphy, & Sun, 1994)
Crawl Space	0.65*	-	-	1.040	-	-	17.21	-	-	13.77	-	29.26	(Colliver, Murphy, & Sun, 1994)
Crawl Space - 8x16" vents	0.65*	13.416	-	-	222.03	-	-	-	-	-	-	-	(Colliver, Murphy, & Sun, 1994)
Electrical Outlets/Switches (no Gaskets)	0.65*	0.260	-	-	4.30	-	-	0.86	-	-	10.67	-	(Colliver, Murphy, & Sun, 1994)
Electrical Outlets/Switches (with gaskets)	0.65*	0.016	-	-	0.26	-	-	0.14	-	-	6.02	-	(Colliver, Murphy, & Sun, 1994)
Furnace - Sealed (orno) combustion	0.65*	0.000	-	-	0.00	-	-	0.00	-	-	0.00	-	(Colliver, Murphy, & Sun, 1994)
Furnace - Retention head or stack damper	0.65*	3.120	-	-	51.63	-	-	34.42	-	-	51.63	-	(Colliver, Murphy, & Sun, 1994)
Furnace - Retention head & stack damper	0.65*	2.496	-	-	41.31	-	-	30.98	-	-	51.63	-	(Colliver, Murphy, & Sun, 1994)
Fireplace with Damper Closed	0.65*	-	-	4.472	-	-	74.01	-	-	17.21	-	158.34	(Colliver, Murphy, & Sun, 1994)
Fireplace with Damper Open	0.65*	-	-	36.399	-	-	602.40	-	-	249.57	-	654.03	(Colliver, Murphy, & Sun, 1994)
Fireplace with Glass Doors	0.65*	-	-	4.160	-	-	68.85	-	-	6.88	-	68.85	(Colliver, Murphy, & Sun, 1994)
Fireplace with Insert & Damper Closed	0.65*	-	-	3.744	-	-	61.96	-	-	44.75	-	79.17	(Colliver, Murphy, & Sun, 1994)
Fireplace with Insert & Damper Open	0.65*	-	-	6.760	-	-	111.87	-	-	68.85	-	154.90	(Colliver, Murphy, & Sun, 1994)
Gas Water Heater	0.65*	2.080	-	-	34.42	-	-	25.82	-	-	43.03	-	(Colliver, Murphy, & Sun, 1994)
Joints: Ceiling-Wall	0.65*	-	0.156	-	-	2.58	-	0.28	-	-	4.30	-	(Colliver, Murphy, & Sun, 1994)
Joints: Sole Plate, floor/wall - uncaulked	0.65*	-	0.416	-	-	6.88	-	0.65	-	-	9.64	-	(Colliver, Murphy, & Sun, 1994)
Joints: Sole Plate, floor/wall - caulked	0.65*	-	0.083	-	-	1.38	-	0.13	-	-	2.07	-	(Colliver, Murphy, & Sun, 1994)
Joints: Top Plate - Band Joist	0.65*	-	0.010	-	-	0.17	-	0.13	-	-	0.65	-	(Colliver, Murphy, & Sun, 1994)
Piping/Plumbing/Wiring Penetrations Uncaulked	0.65*	0.624	-	-	10.33	-	-	3.44	-	-	41.31	-	(Colliver, Murphy, & Sun, 1994)
Piping/Plumbing/Wiring Penetrations Caulked	0.65*	0.208	-	-	3.44	-	-	1.72	-	-	3.44	-	(Colliver, Murphy, & Sun, 1994)
Vents: Bathroom with Damper Closed	0.65*	1.040	-	-	17.21	-	-	4.30	-	-	34.42	-	(Colliver, Murphy, & Sun, 1994)
Vents: Bathroom with Damper Open	0.65*	2.080	-	-	34.42	-	-	10.50	-	-	37.87	-	(Colliver, Murphy, & Sun, 1994)
Vents: Dryer with Damper	0.65*	0.312	-	-	5.16	-	-	4.99	-	-	12.05	-	(Colliver, Murphy, & Sun, 1994)
Vents: Dryer With out Damper	0.65*	1.560	-	-	25.82	-	-	20.65	-	-	58.52	-	(Colliver, Murphy, & Sun, 1994)
Vents: Kitchen With Damper Open	0.65*	4.160	-	-	68.85	-	-	24.10	-	-	123.92	-	(Colliver, Murphy, & Sun, 1994)
Vents: Kitchen With Damper Closed	0.65*	0.520	-	-	8.61	-	-	1.72	-	-	12.05	-	(Colliver, Murphy, & Sun, 1994)
Vents: Kitchen With Tight Gasket	0.65*	0.104	-	-	1.72	-	-	-	-	-	-	-	(Colliver, Murphy, & Sun, 1994)

Table A-4: Airflow Characteristics of Elevator Doors

Component	Flow Exponent, n	Best Estimate or Mean Average			Reference
		Flow Coefficient, C [L/s·Pa ⁿ]	Q ₇₅ [L/s]	Minimum Q ₇₅ [L/s]	
Doors - Elevator (passenger)	0.55*	0.031	0.33	0.18	(Colliver, Murphy, & Sun, 1994)
Elevator Doors - Office Buildings (1.07m x 2.13m) (cracks from 4.8 to 6.8mm)	0.55	33.5	360	307	(Tamura & Shaw, 1976)

*Assumed n when unknown to compare values

Table A-5: Airflow Characteristics of Shaft Walls

Component	Flow Exponent, n	Best Estimate or Mean Average			Reference
		Normalized Flow Coefficient, C _n [L/s·Pa ⁿ ·m ²]	q ₇₅ [L/s·m ²]	Minimum q ₇₅ [L/s·m ²]	
Elevator Shaft Walls - Office Buildings: Concrete Block	0.65*	0.5	9.00	8.50	(Tamura & Shaw, 1976)
Elevator Shaft Walls - Office Buildings: Cast-in-Place Concrete (front concrete block in some cases)	0.65*	0.2	3.20	1.30	(Tamura & Shaw, 1976)
Stairwell Shaft Walls - Office Buildings: Concrete Block or Cast-In-Place Concrete	0.65*	0.0	0.80	0.13	(Tamura & Shaw, 1976)

*Assumed n when unknown to compare values

Table A-6: Airflow Characteristics of Windows – Orne et al (1998)

Component	Median			Lower Quartile			Upper Quartile			Sample Size
	Flow Exponent, n	Linear Normalized Flow Coefficient, C _{NL} [L/s·Pa ⁿ ·m]	Q ₇₅ /m [L/s·m]	Flow Exponent, n	Linear Normalized Flow Coefficient, C _{NL} [L/s·Pa ⁿ ·m]	Q ₇₅ /m [L/s·m]	Flow Exponent, n	Linear Normalized Flow Coefficient, C _{NL} [L/s·Pa ⁿ ·m]	Q ₇₅ /m [L/s·m]	
Windows: Hinged - WS	0.60	0.13	1.73	0.60	0.09	1.15	0.60	0.41	5.47	29
Windows: Sliding - WS	0.60	0.15	2.00	0.60	0.08	1.05	0.60	0.21	2.80	19
Windows: Hinged - Not WS	0.60	0.74	9.87	0.60	0.39	5.20	0.60	1.10	14.67	42
Windows: Sliding - Not WS	0.60	0.23	3.07	0.60	0.18	2.40	0.60	0.37	4.93	36
Windows: Louvre (per louvre)	0.60	0.34	4.53	0.60	-	-	0.60	-	-	1

Table A-7: Airflow Characteristics of Doors – Orne et al (1998)

Component	Median			Lower Quartile			Upper Quartile			Sample Size
	Flow Exponent, n	Linear Normalized Flow Coefficient, C _{NL} [L/s·Pa ⁿ ·m]	Q ₇₅ /m [L/s·m]	Flow Exponent, n	Linear Normalized Flow Coefficient, C _{NL} [L/s·Pa ⁿ ·m]	Q ₇₅ /m [L/s·m]	Flow Exponent, n	Linear Normalized Flow Coefficient, C _{NL} [L/s·Pa ⁿ ·m]	Q ₇₅ /m [L/s·m]	
Doors: Exterior - Hinged WS	0.60	0.27	3.60	0.60	0.082	1.09	0.60	0.84	11.2	15
Doors: Exterior - Revolving WS (Laboratory test)	0.60	1.50	20.0	0.60	1.0	13.3	0.60	2.0	26.7	4
Doors: Exterior - Hinged Not WS	0.60	1.20	16.0	0.60	1.1	14.7	0.60	1.4	18.7	17
Doors: Exterior - Sliding Not WS	0.60	0.20	2.7	0.60	-	-	0.60	-	-	1
Doors: Interior - Not WS	0.60	1.30	17.3	0.60	1.1	14.7	0.60	2.0	26.7	84
Doors: Loft Hatches - Not WS	0.60	0.68	9.07	0.60	0.64	8.54	0.60	0.75	10.0	4

Table A-8: Airflow Characteristics of Door/Window Interface with Wall – Orne et al (1998)

Component	Median			Lower Quartile			Upper Quartile			Sample Size
	Flow Exponent, n	Linear Normalized Flow Coefficient, C _{NL} [L/s·Pa ⁿ ·m]	Q ₇₅ /m [L/s·m]	Flow Exponent, n	Linear Normalized Flow Coefficient, C _{NL} [L/s·Pa ⁿ ·m]	Q ₇₅ /m [L/s·m]	Flow Exponent, n	Linear Normalized Flow Coefficient, C _{NL} [L/s·Pa ⁿ ·m]	Q ₇₅ /m [L/s·m]	
Caulked Joint (Lab and Field Tests)	0.60	0.0025	0.03	0.60	0.00033	0.00	0.60	0.01	0.2	7
Uncaulked Joint (Lab and Field Tests)	0.60	0.061	0.8	0.60	0.053	0.7	0.60	0.067	0.9	5

Table A-9: Airflow Characteristics of Door/Window Interface with Wall – Orne et al (1998)

Component	Median			Lower Quartile			Upper Quartile			Sample Size
	Flow Exponent, n	Linear Normalized Flow Coefficient, C _{NL} [L/s·Pa ⁿ ·m]	Q ₇₅ /m [L/s·m]	Flow Exponent, n	Linear Normalized Flow Coefficient, C _{NL} [L/s·Pa ⁿ ·m]	Q ₇₅ /m [L/s·m]	Flow Exponent, n	Linear Normalized Flow Coefficient, C _{NL} [L/s·Pa ⁿ ·m]	Q ₇₅ /m [L/s·m]	
Discharge Pipts	0.60	1.2	16.00	0.60	1.1	14.67	0.60	1.4	18.7	2
Sealed Spiral Ducts	0.60	0.14	1.9	0.60	0.027	0.4	0.60	0.78	10.4	2
Vent	0.60	0.80	10.7	0.60	-	-	0.60	-	-	1
Pipes (Laboratory Test)	0.60	0.74	9.9	0.60	0.63	8.4	0.60	0.84	11.2	3

Table A-10: Airflow Characteristics of Doors – Morrison Hershfield (1996)

Category	Q ₇₅ [L/s]	Flow Exponent, n	Flow Coefficient, C [L/s·Pa ⁿ]
Weatherstripped	100	0.55*	9.3
Tight	130	0.55*	12.1
Standard	180	0.55*	16.7
Leaky	240	0.55*	22.3

*Assumed n when unknown to compare values

A-1 References

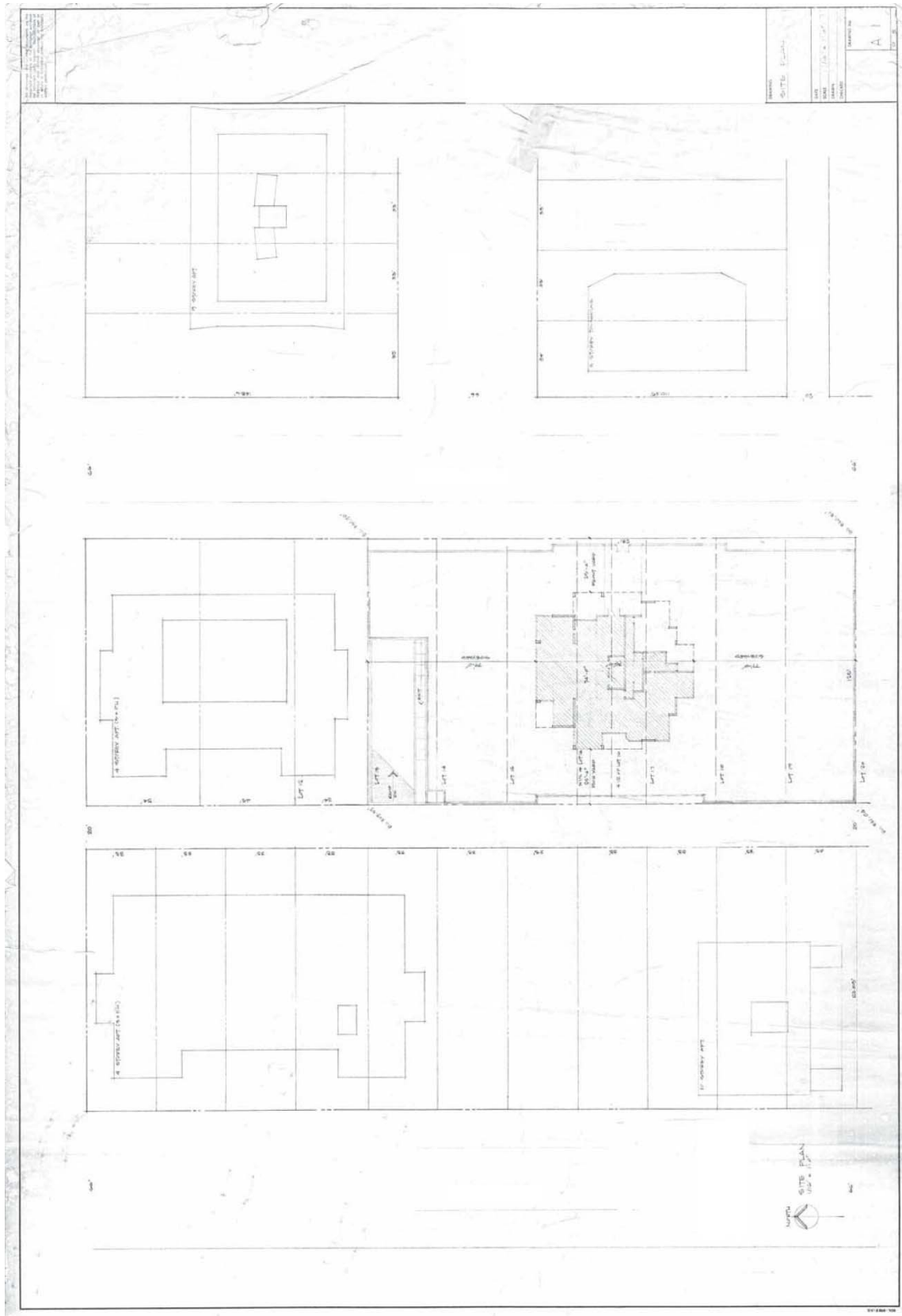
- Colliver, D., Murphy, W., & Sun, W. (1994). Development of A Building Component Air Leakage Data Base. *ASHRAE Transactions Vol. 100, Part 1* (pp. 292-305). American Society of Heating, Refrigerating and Air-Conditioning Engineers .
- Edwards, C. (1999). Modelling of Ventilation and Infiltration Energy Impacts in Mid and High-Rise Apartment Buildings. Ottawa: Canada Mortgage and Housing Corporation.
- Fang, J., & Persily, A. (1995). Airflow and Radon Transport Modeling in Four Large Buildings. *ASHRAE Transactions, Vol. 101, Pt. 1*.
- Gulay, B., Stewart, C., & Foley, G. (1993). Field Investigation Survey of Airtightness, Air Movement and Indoor Air Quality in High Rise Apartment Buildings Summary Report. Ottawa: Canada Mortgage and Housing Corporation.
- Moffat, P., Theaker, I., & Wray, C. (1998). Field Testing to Characterize Suite Ventilation in Recently Constructed Mid- and High-Rise Residential Buildings. Ottawa: Canada Mortgage and Housing Corporation.
- Morrison Hershfield Ltd. (1996). *Controlling Stack Pressure in High-Rise Buildings by Compartmenting the Building*. Ottawa: Canada Mortgage and Housing Corporation.
- Orne, M., Liddament, M., & Wilson, A. (1998). *Numerical Data for Air Infiltration & Natural Ventilation Calculations*. Coventry: Oscar Faber Group Ltd.
- Tamura, G., & Shaw, C. (1976). Air leakage data for the design of elevator and stair shaft pressurization systems. *ASHRAE Transactions, Vol. 82, Pt. 2*, 179-190.

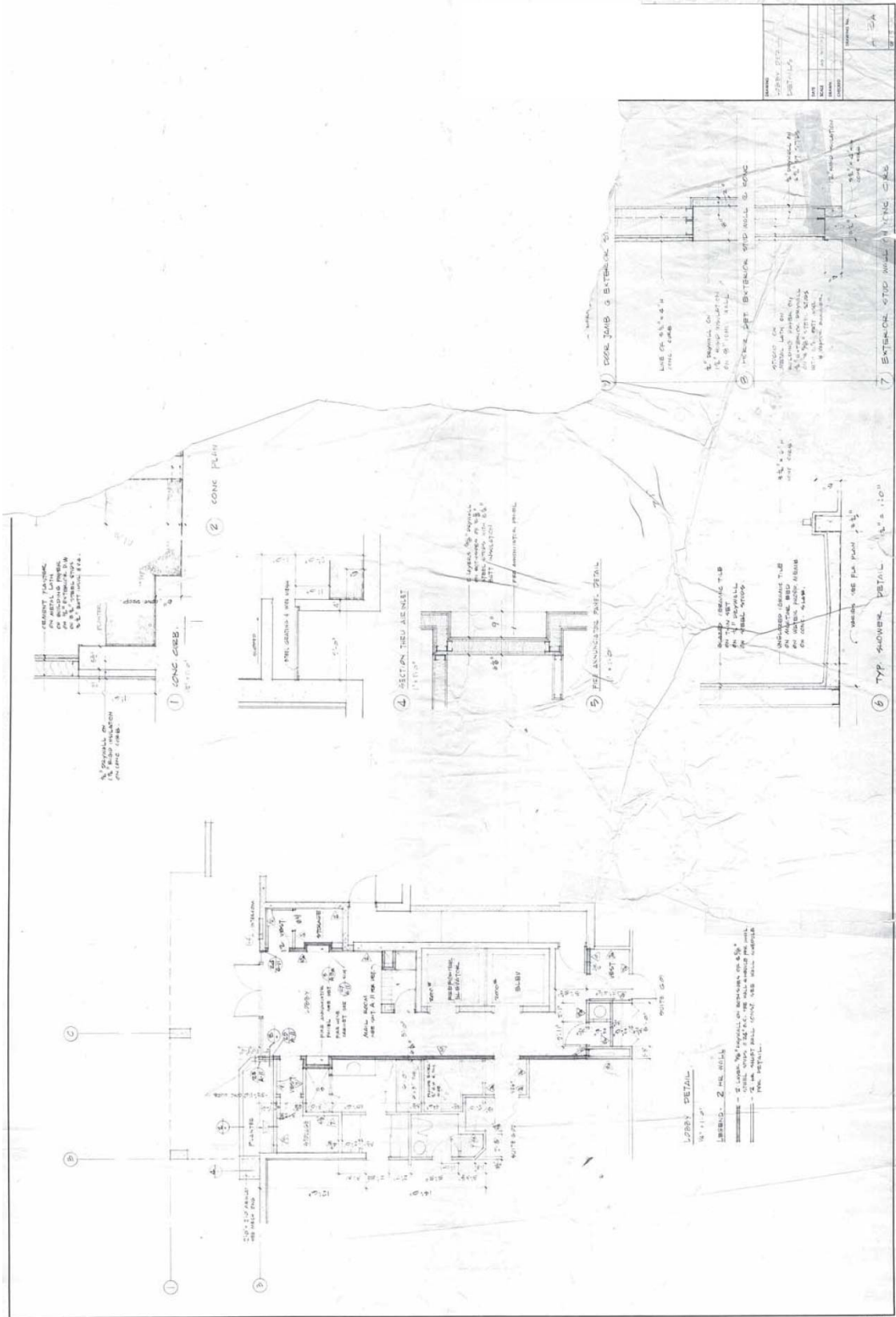
Appendix B

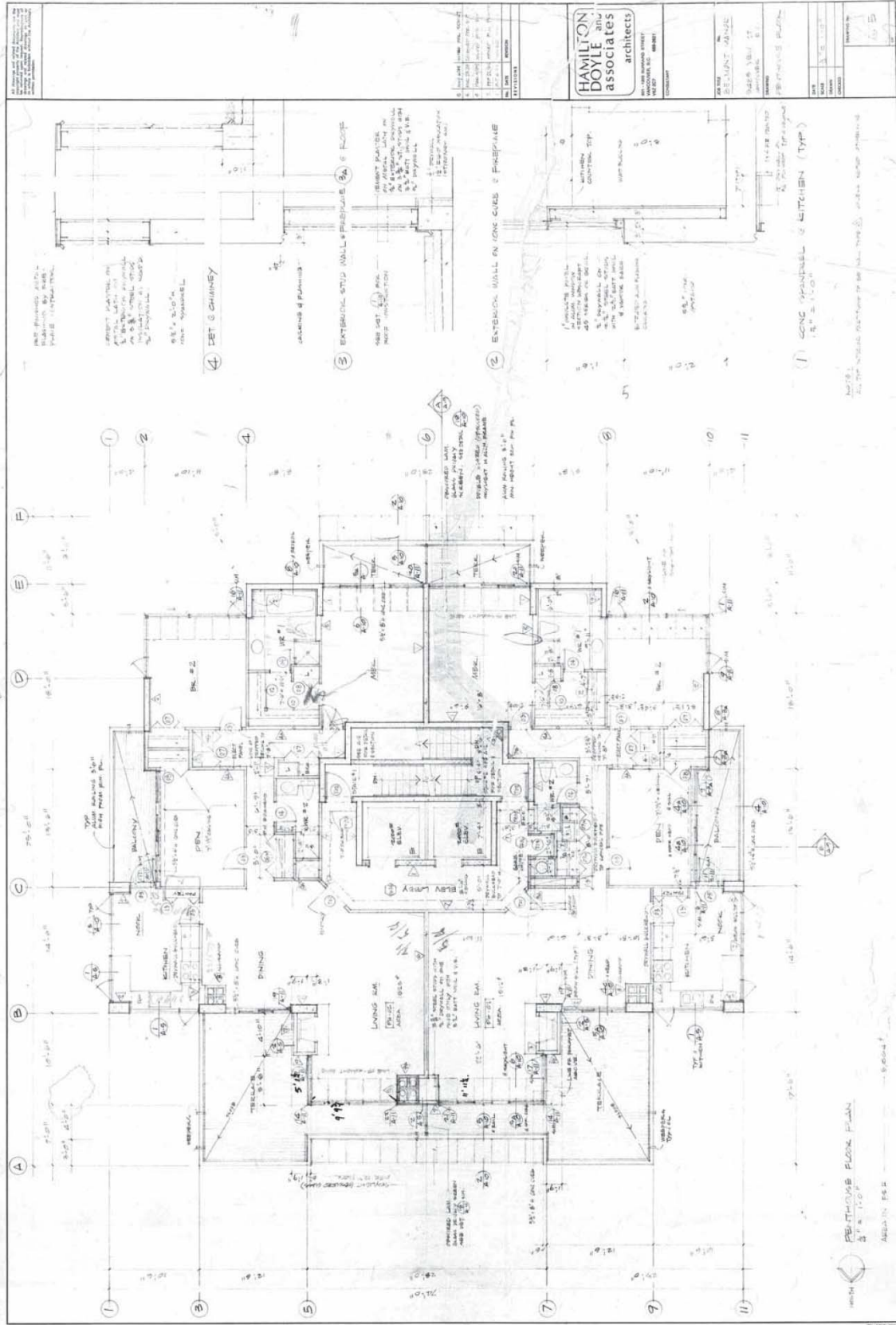
Case Study Building Original Architectural and Mechanical Drawings

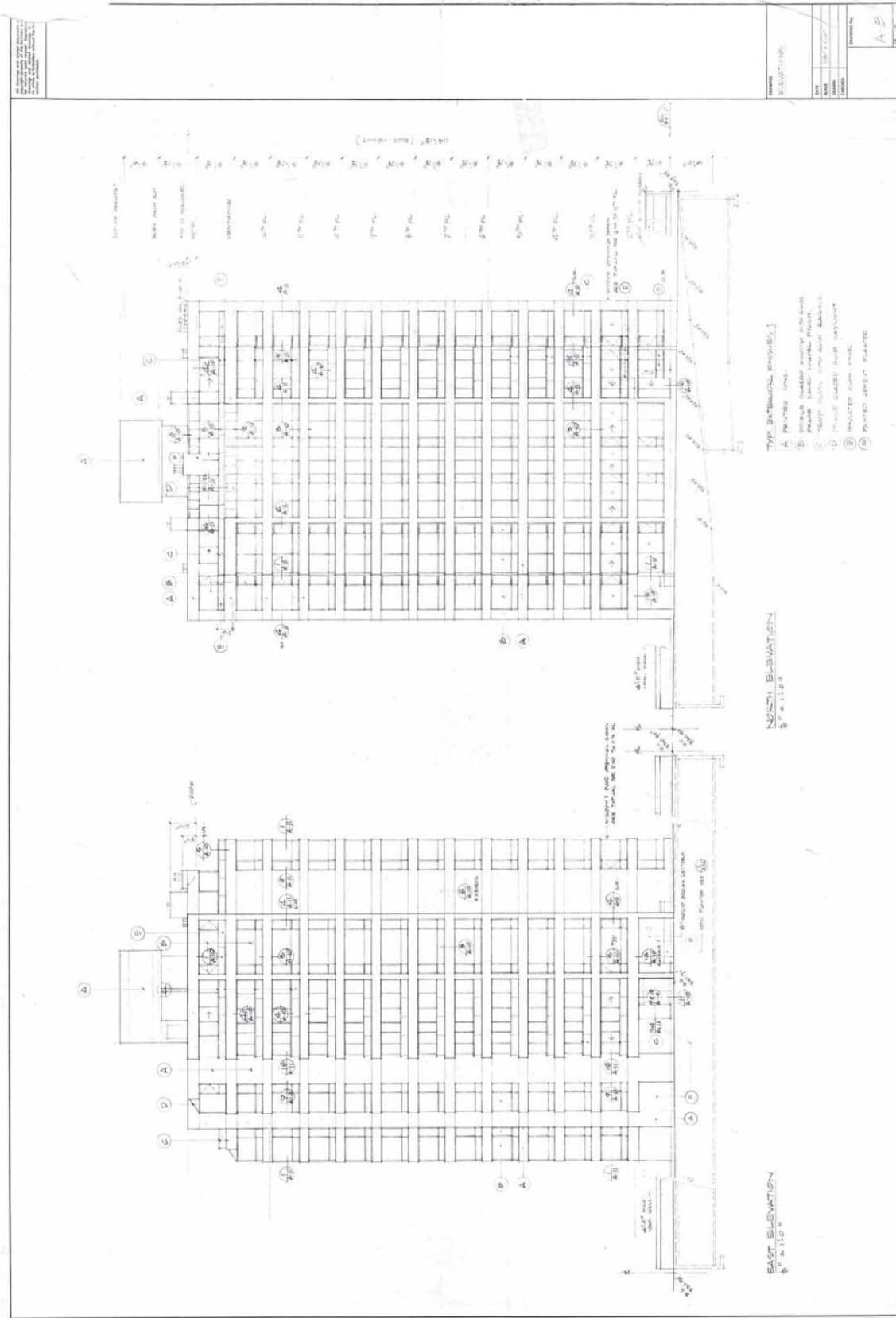
Original architectural and mechanical drawings for the case study building are provided in this appendix. Note that identifying factors such as the address, building name, and adjacent streets have been removed.

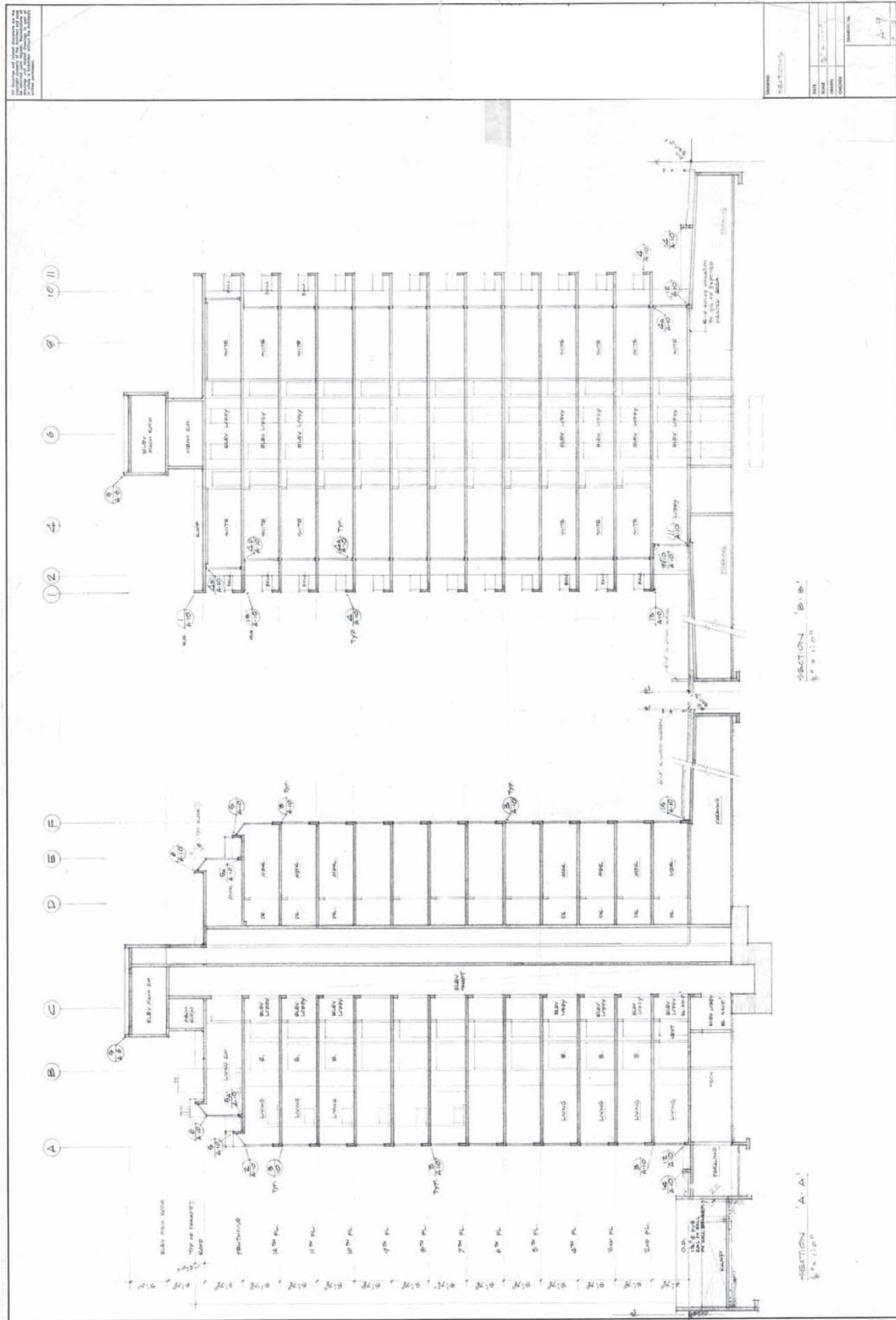
Appendix B Case Study Building Original Architectural and Mechanical Drawings

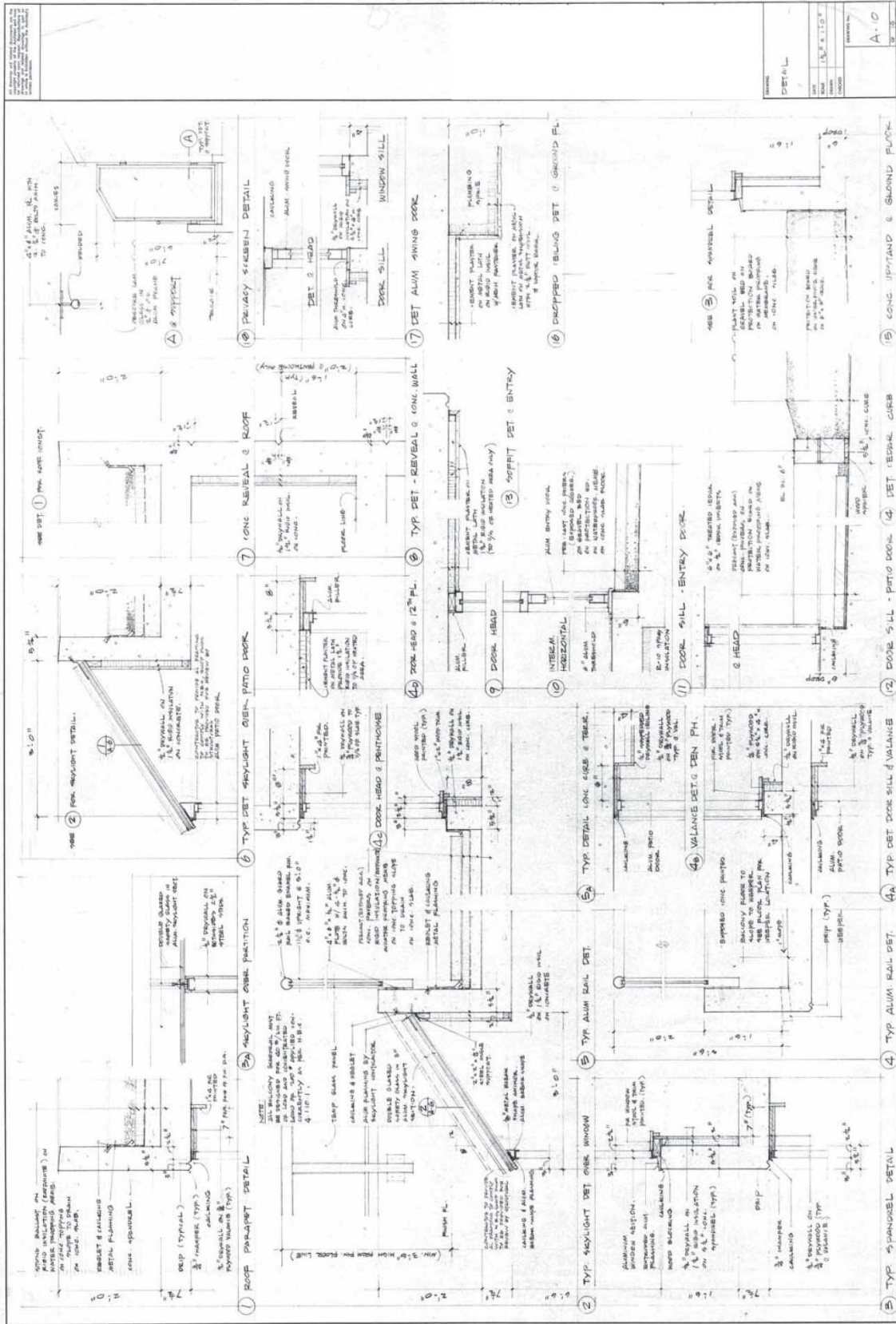


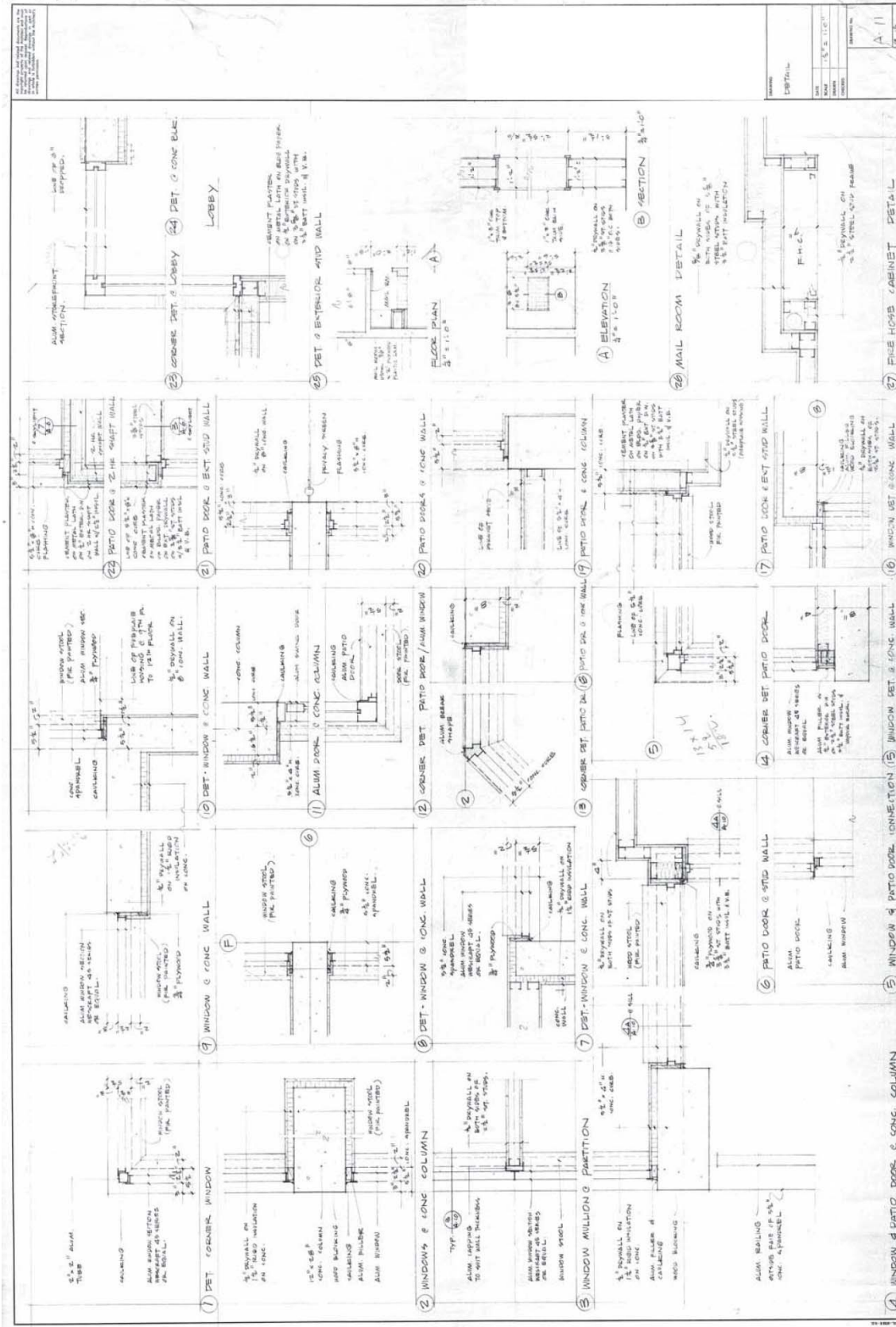


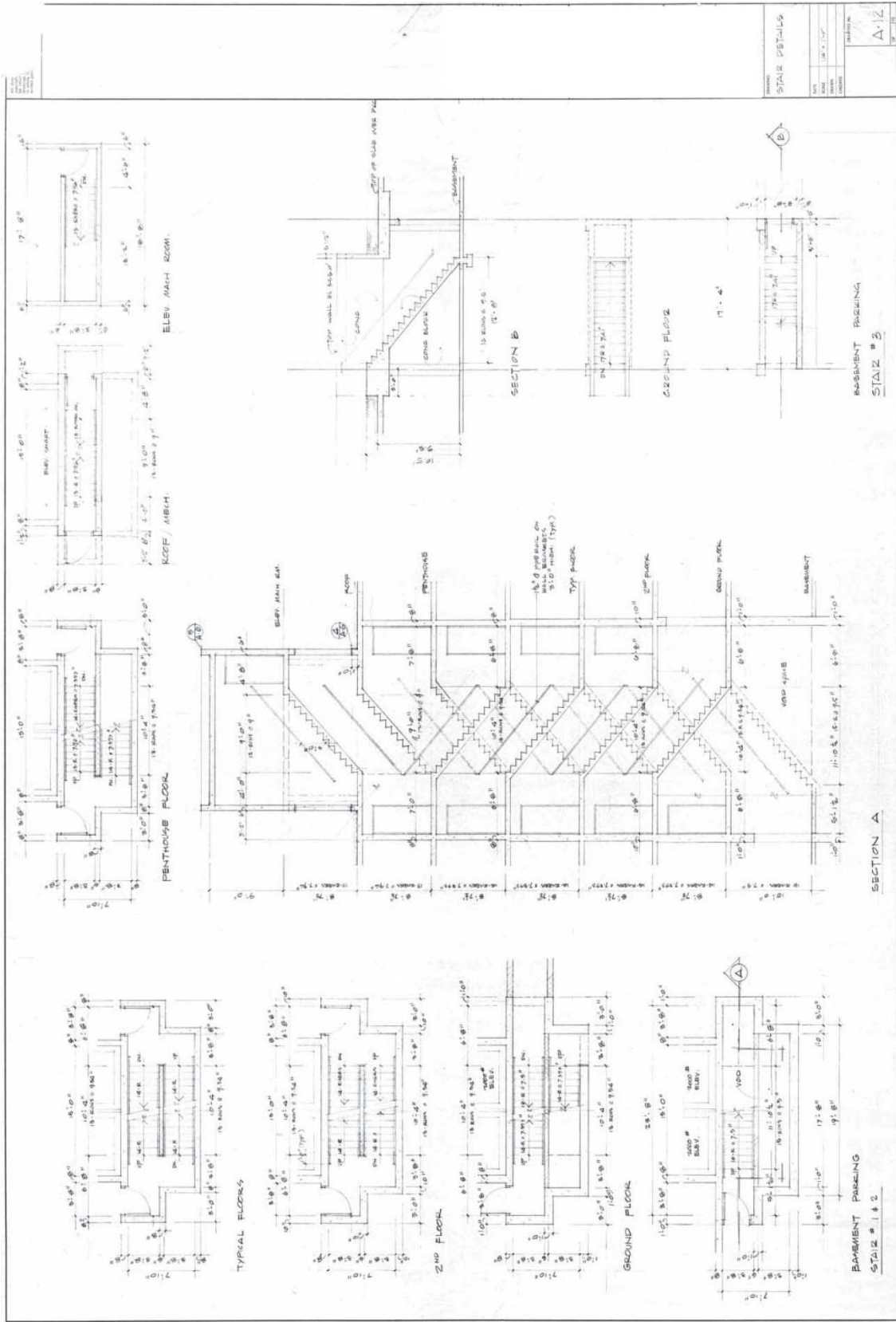




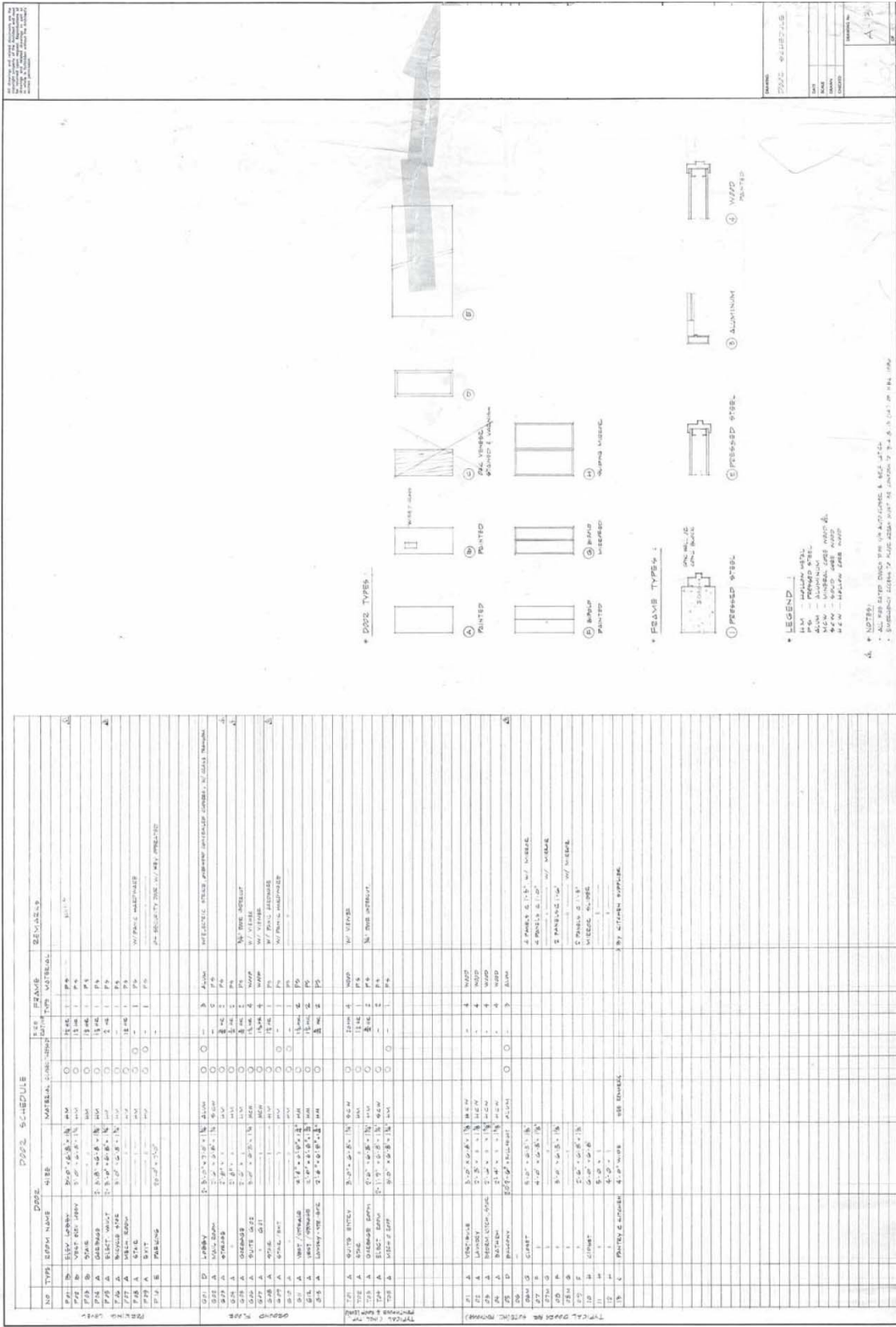


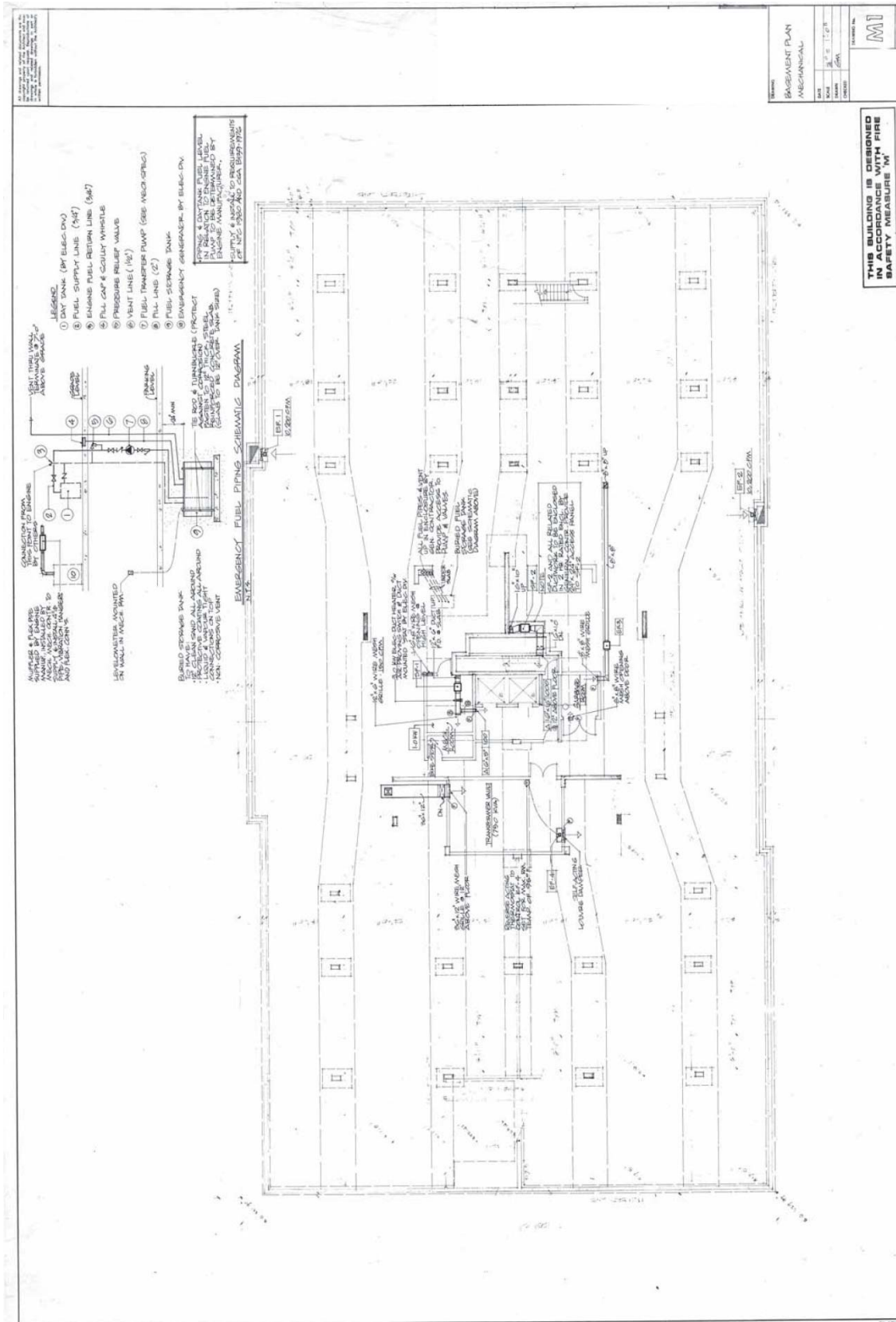


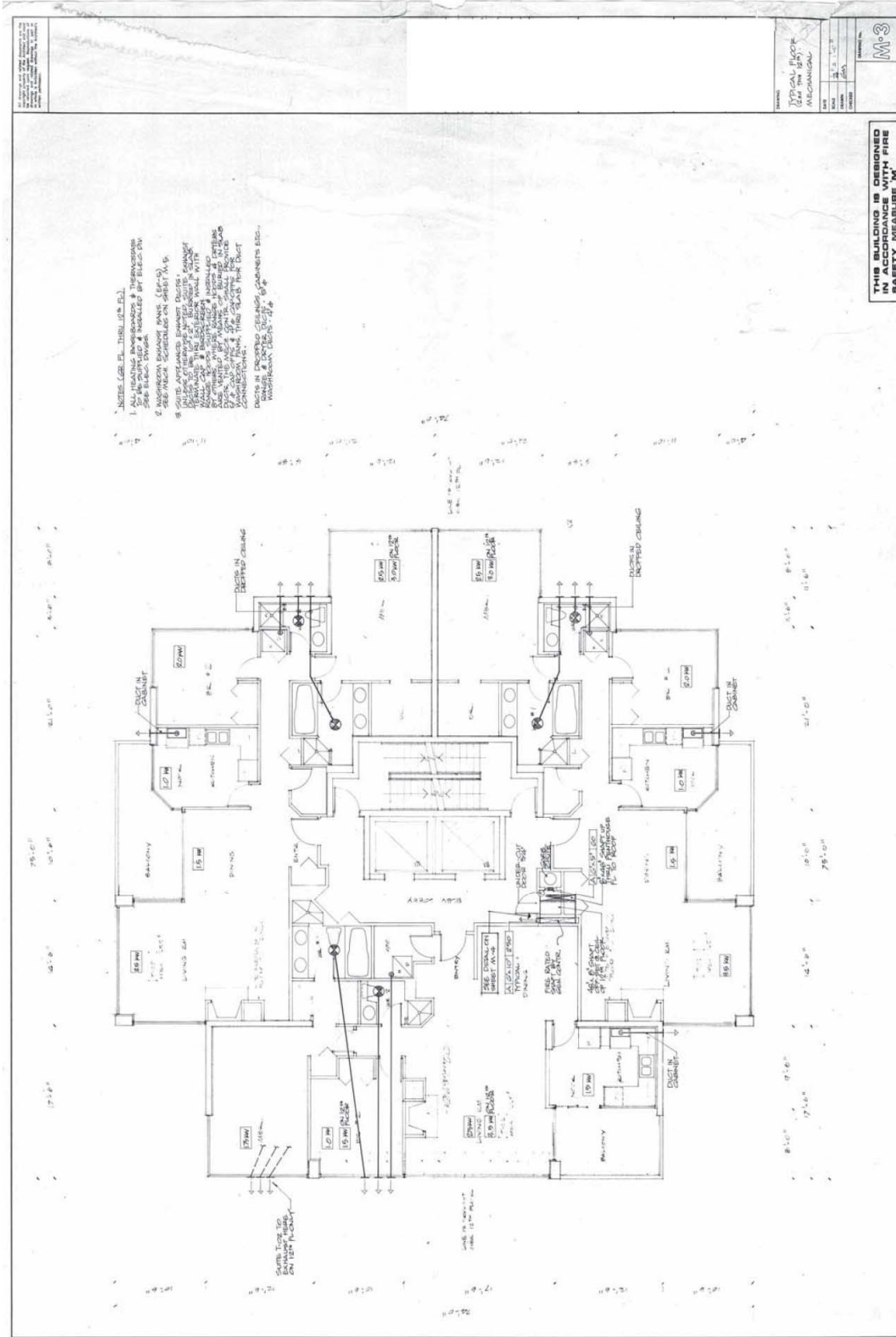


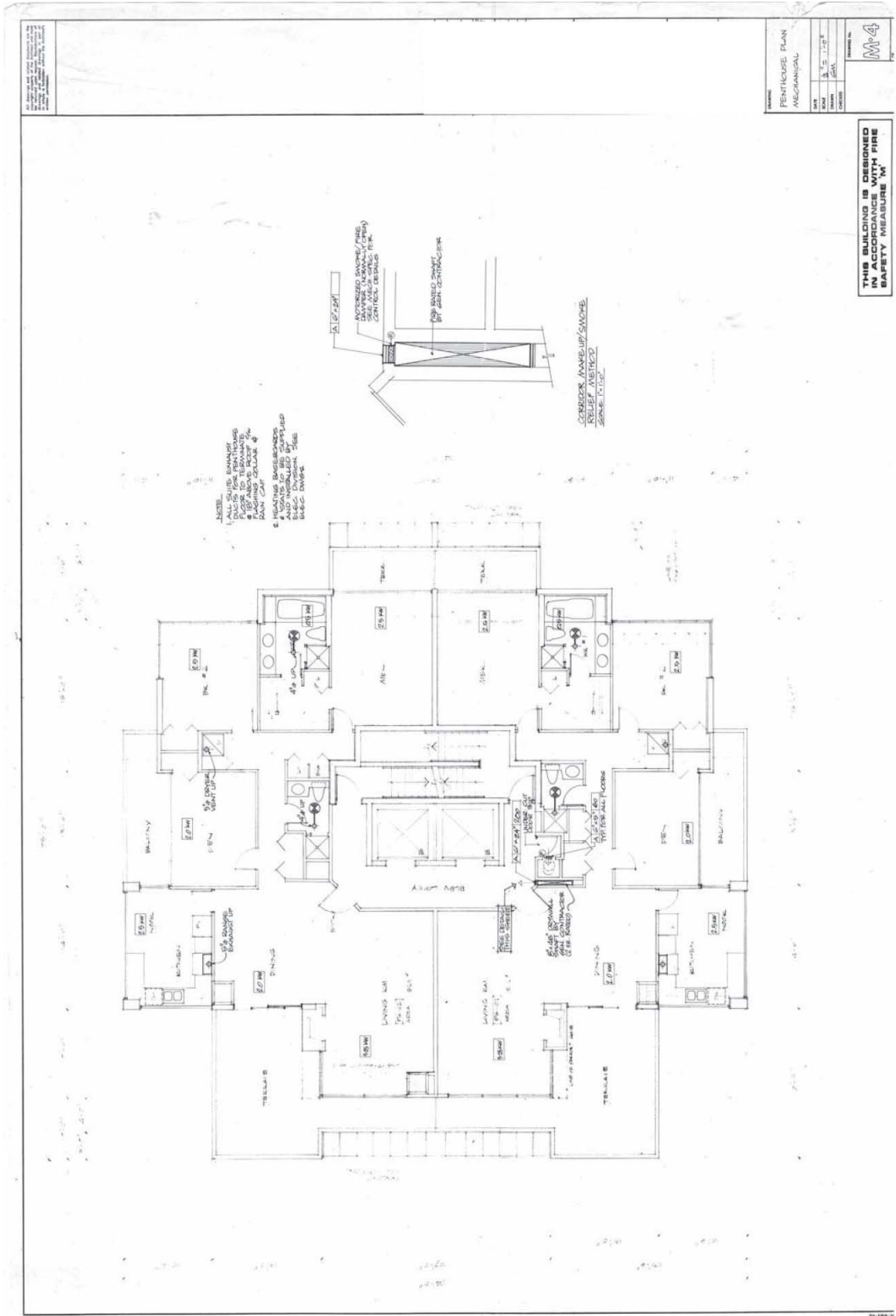


PROJECT	STAIR DETAILS
DATE	12.1.1977
SCALE	1/8" = 1'-0"
NO.	A-12









Appendix C

Supplementary Airflow Measurement Information

Airtightness Airflow measurements were performed at the case study building using a variety of techniques. The test procedures for these techniques were discussed in Section 7.2 and Section 7.3. This appendix provides supplementary airflow testing information including detailed layouts of the perfluorocarbon tracer (PFT) testing equipment.

C-1 PFT Testing

Seven types of PFT were used for the testing at the case study building. The abbreviation, full name, and chemical formula for each of these tracers are provided in Table C- 1. (Heiser and Sullivan, The Brookhaven National Laboratory Perfluorocarbon Tracer Technology: A Proven and Cost-Effective Method to Verify Integrity and Monitor Long-Term Performance of Walls, Floors, Caps, and Cover Systems 2002) (Sullivan, Heiser, Watson, Allwine, & Flaherty, 2006)

Table C- 1: PFT Types Used in Testing at Case Study Building

Abbreviation	Full Name	Chemical Formula
PMCP	Perfluoromethylcyclopentane	C ₆ F ₁₂
ocPDCH	Ortho-cis-perfluorodimethylcyclohexane	C ₈ F ₁₆
PMCH	Perfluotomethylcyclohexane	C ₇ F ₁₄
iPPCH	Perfluoro-isopropylcyclohexane	C ₉ F ₁₈
ptPDCH	Perfluorotrans 1,4 dimethylcyclohexane	C ₈ F ₁₆
PTCH	Perfluorotrimethylcyclohexane	C ₉ F ₁₈
PDCB	Perfluorodimethylcyclobutane	C ₆ F ₁₂

The procedure followed for installation of the PFT sources and CATS at the case study building is provided below. This procedure was developed based on guidance provided by Brookhaven National Laboratory (BNL) through Meadowbrook Partners Inc. (MPI)

1. Store sources and CATS in different buildings prior to testing.
2. Transport the sources and CATS to the test site in difference vehicles.
3. Once at case study building, store sources and CATS in separate locations and keep source outside of the building prior to installation in testing locations.
4. Open sealed plastic bags containing sources away from the building and allow them to air out for at least one minute to remove buildup of PFT within the bags that would create a pulse of PFT if opened in the building. Once aired out, reseal the sources in the bags.
5. Install the sources and CATS in the locations within the building taking care to only open the sealed plastic bags containing the source in the zone of its final location, and to only uncap the numbered (barcode) end of each CATS once in its final position. Both sources and CATS should be carried as directly as possible to their final locations to avoid potential for contamination. Record time when source removed from sealed bag and when caps removed from CATS.
 - a. Sources are installed vertically with the open end (rubber stopper) of the metal vial up on interior walls using standoff as marked on the layout drawings.

Appendix C Supplementary Airflow Measurement Information

- i. Sources are temperature sensitive. Do not install near heat sources such as baseboard heaters, fireplaces, lamps, refrigerators, or below a cooling source such as an AC unit.
 - ii. Do not install sources in direct sunlight.
 - iii. Sources must be at least 1 inch off the wall.
 - iv. Do not install sources in a location where a draft or ventilation air could take the tracer out of the zone prior to mixing. (Not near windows, exhaust fans, et cetera)
 - v. Can also install sources on table legs et cetera as appropriate.
 - vi. Sources should be placed at approximately mid-height of the zone.
 - vii. Sources should be shielded from high velocity air flow. (e.g. place inside a cylinder with one end closed or behind a flat buffer)
- b. CATS are installed vertically with the numbered (barcode) side down using a standoff. Once in position, the cap on the numbered side is removed.
- i. CATS must be at least 1 inch off the wall and 2 meters from any source.
 - ii. CATS should be at least 2 meters from any stream of air that is not representative of the zone air. (e.g. incoming ventilation air, so do not install near suite entrance door or windows)
 - iii. CATS should be at least 6 inches above any horizontal surface
 - iv. CATS should not be located in areas of extreme temperature
 - v. CATS should be shielded from high velocity air flow. (e.g. place inside a cylinder with one end closed or behind a flat buffer)

Generally the PFT testing equipment was uninstalled at the case study building starting at the bottom of the building and working up to the top of the building.

At the case study building, extruded polystyrene blocks were used to space the sources and CATS off the wall as shown in Figure C-1 and Figure C-2. The CATS located in the MAU duct on the roof was shielded as shown in Figure C-3, and the mega sources located in the MAU duct were shielded as shown in Figure C-4.

Appendix C Supplementary Airflow Measurement Information



Figure C-1: Photo of typical source installation using an extruded polystyrene block to space off the wall with a label to identify the source



Figure C-2: Photo of typical CATS installation using extruded polystyrene block to space off of the wall with a label to identify the CATS



Figure C-3: Photo showing cylindrical type airflow shield containing mega sources located in the MAU duct on the roof



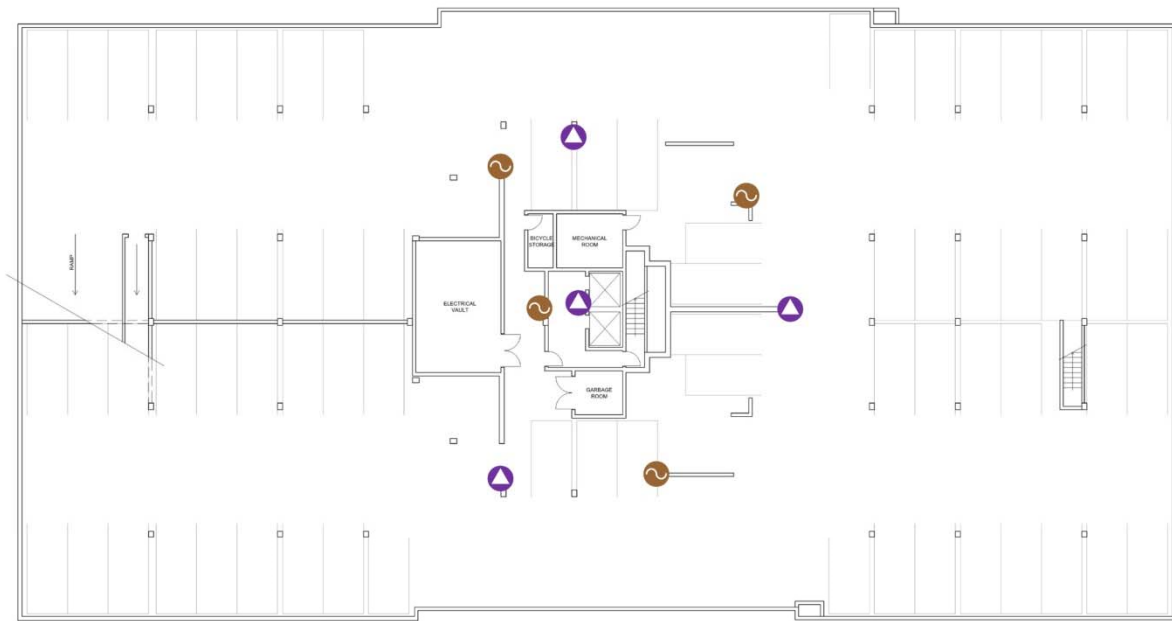
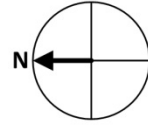
Figure C-4: Photo showing cylindrical type airflow shield containing a CATS located in the MAU duct on the roof downstream of the mega sources

The sources and CATS were installed according to the layouts provided in Figure C-5 to Figure C-17.

Appendix C Supplementary Airflow Measurement Information

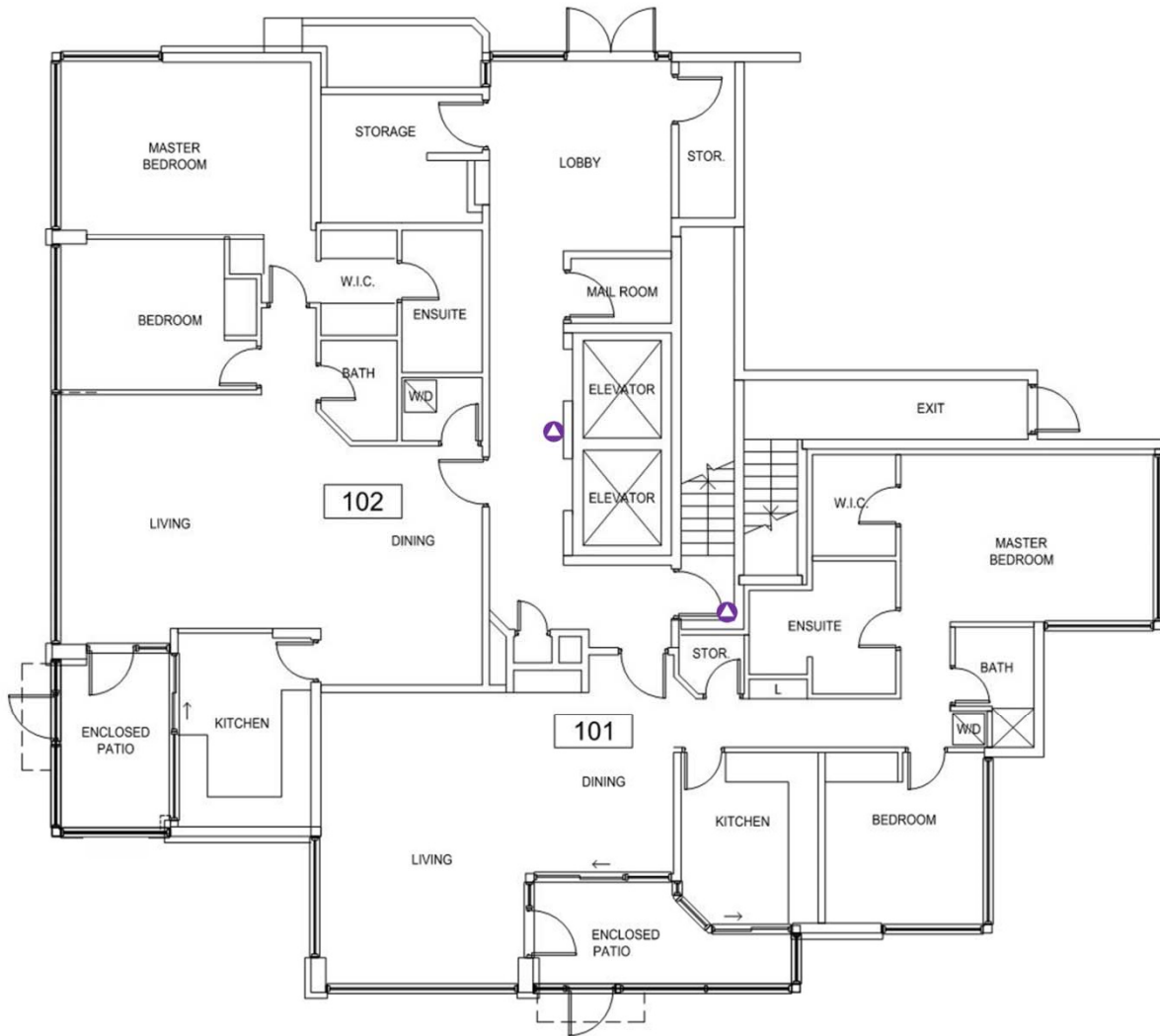
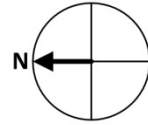
	PMCP
	ocPDCH
	PMCH
	iPPCH
	ptPDCH
	PTCH
	PDCB
	CATS

Figure C-5: Legend for interpretation of PFT layouts



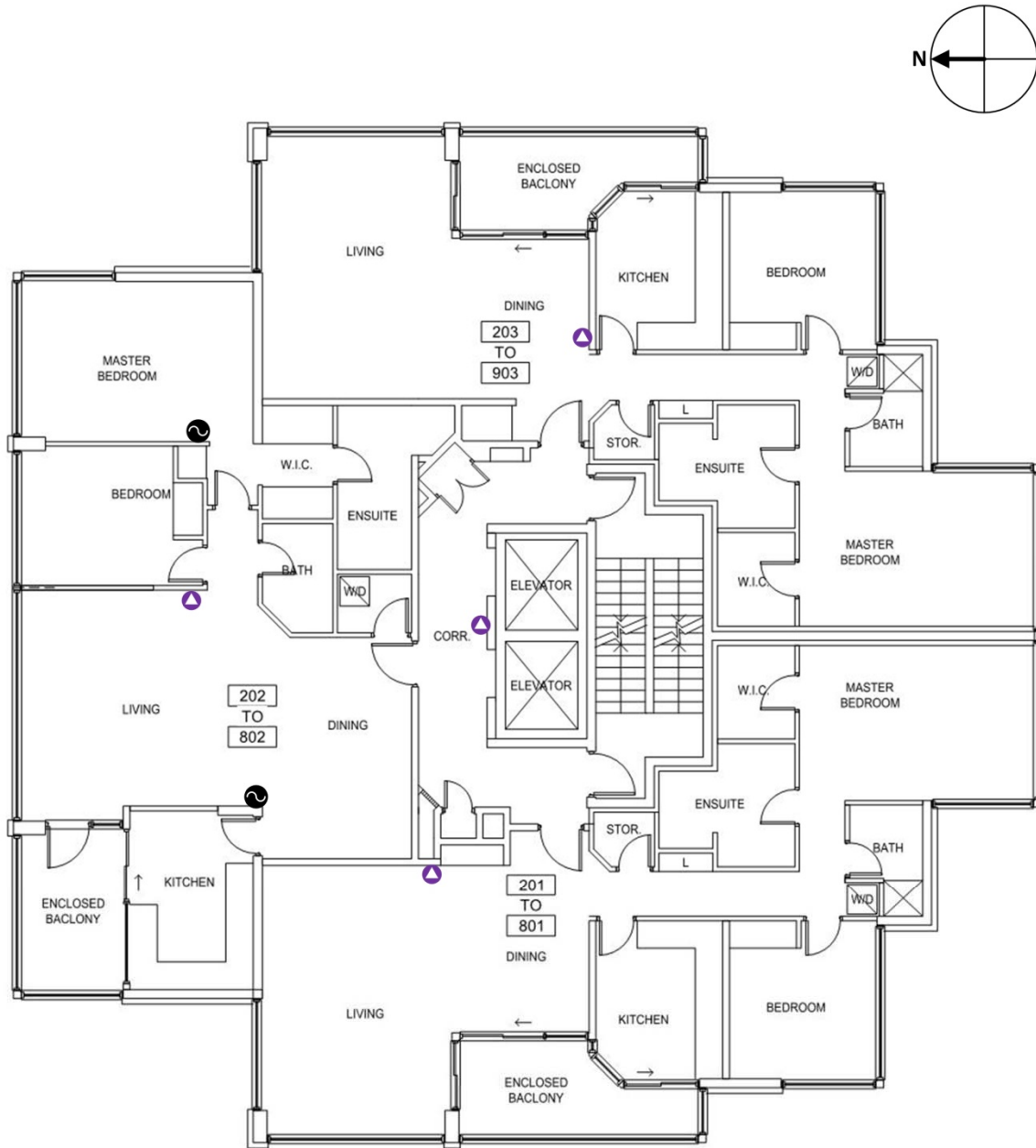
Parking Garage

Figure C-6: Plan of the parking garage at the case study building showing the location of PFT equipment



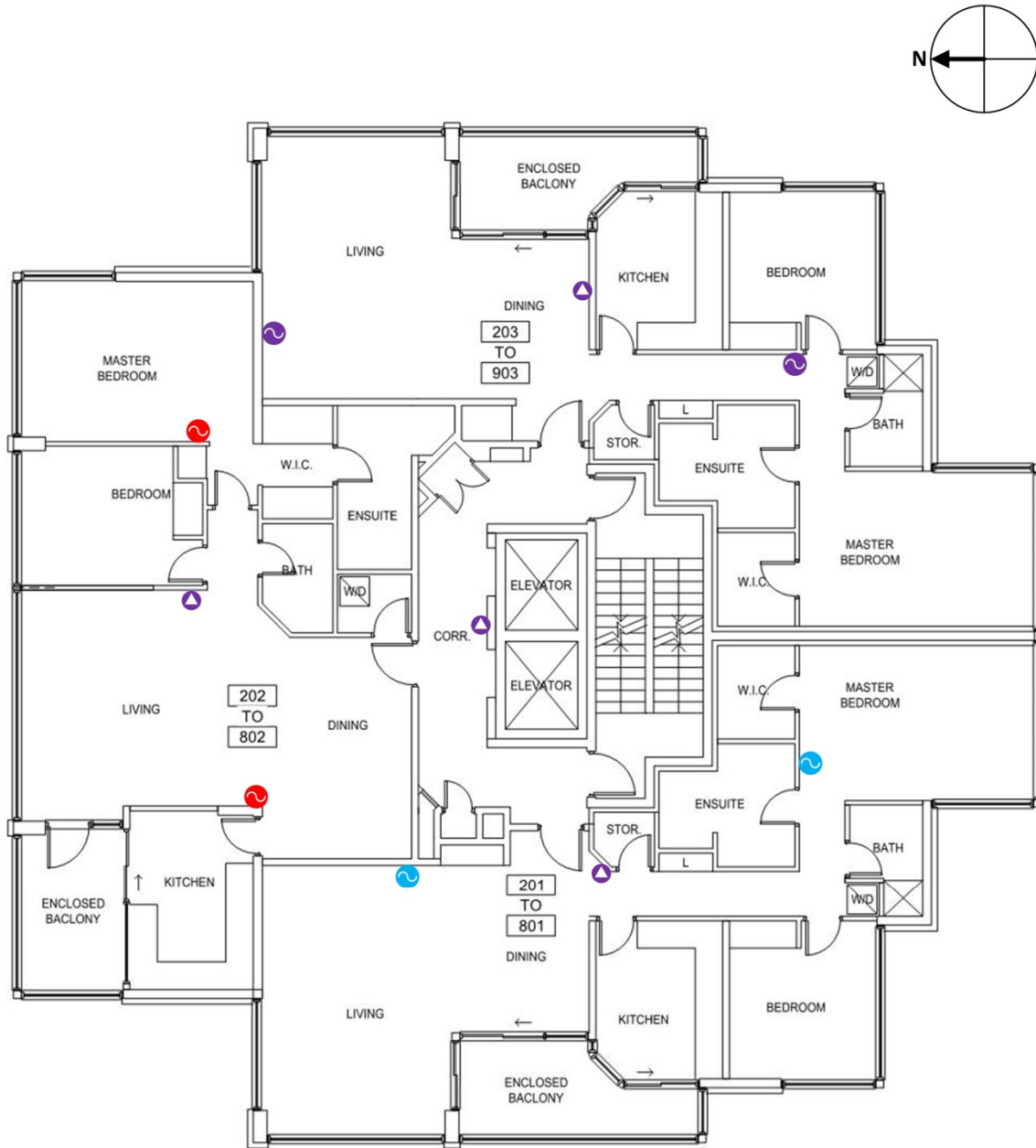
Floor 1

Figure C-7: Plan of the first floor of the case study building showing the location of PFT equipment



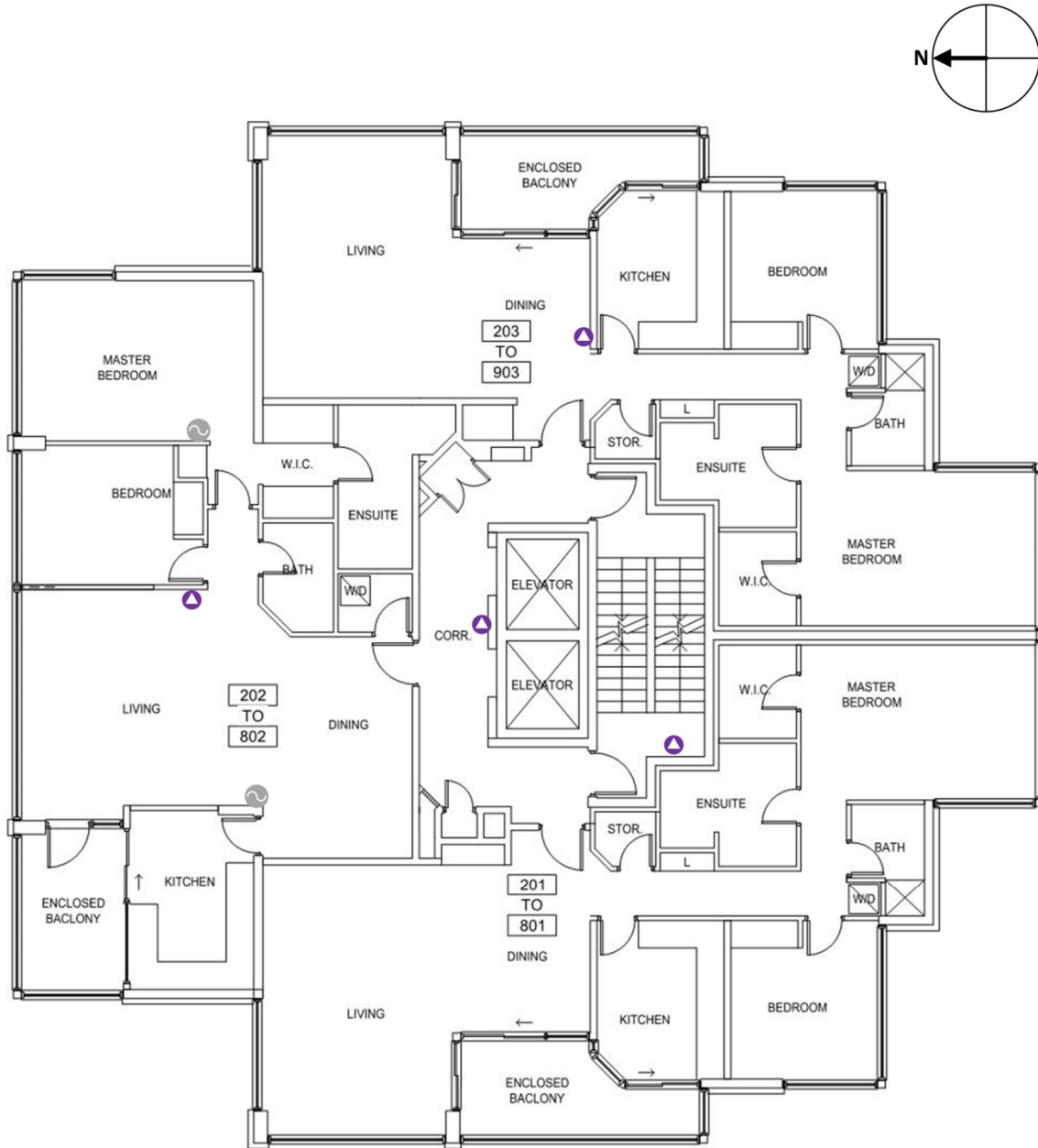
Floor 2

Figure C-8: Plan of the second floor of the case study building showing the location of PFT equipment



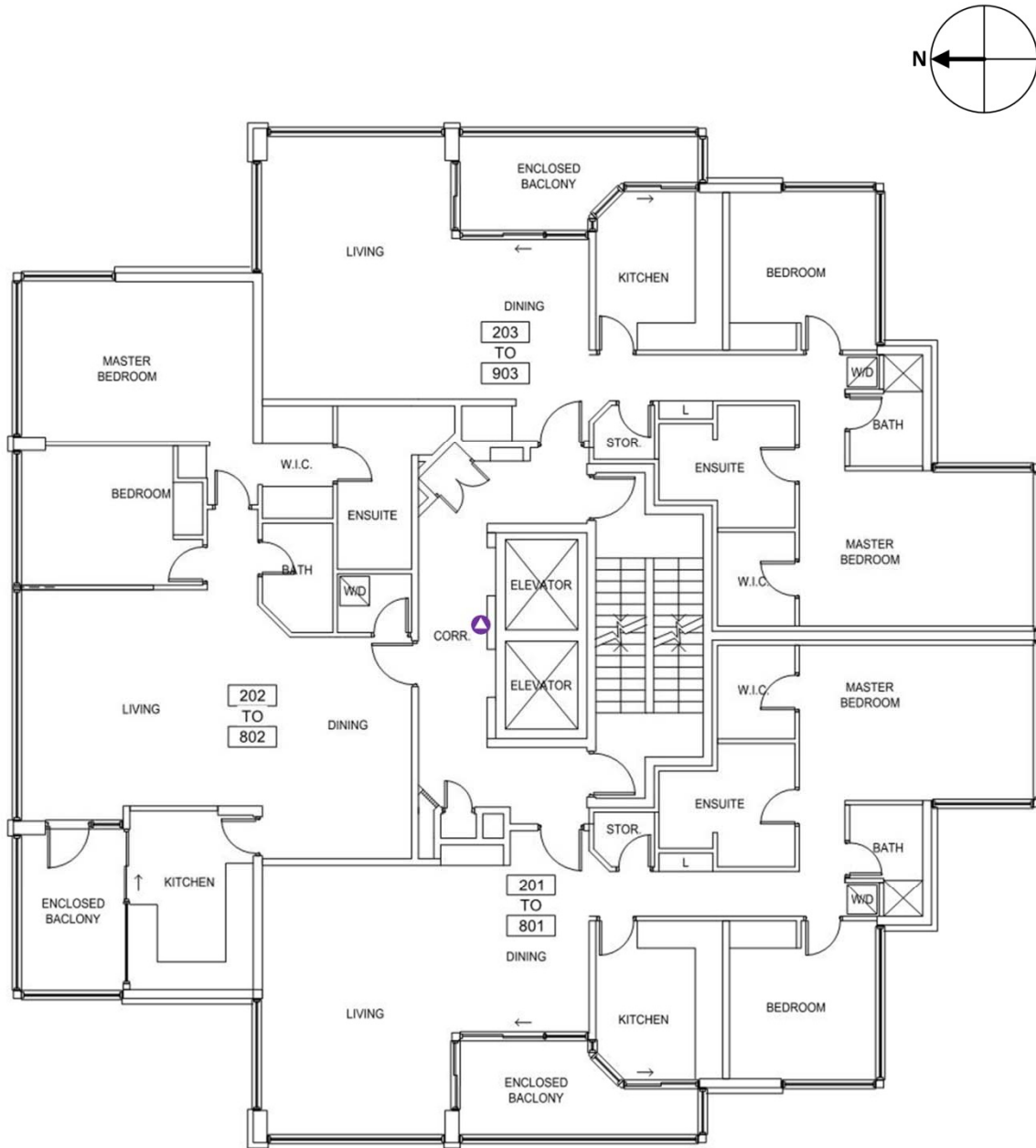
Floor 3

Figure C-9: Plan of the third floor of the case study building showing the location of PFT equipment



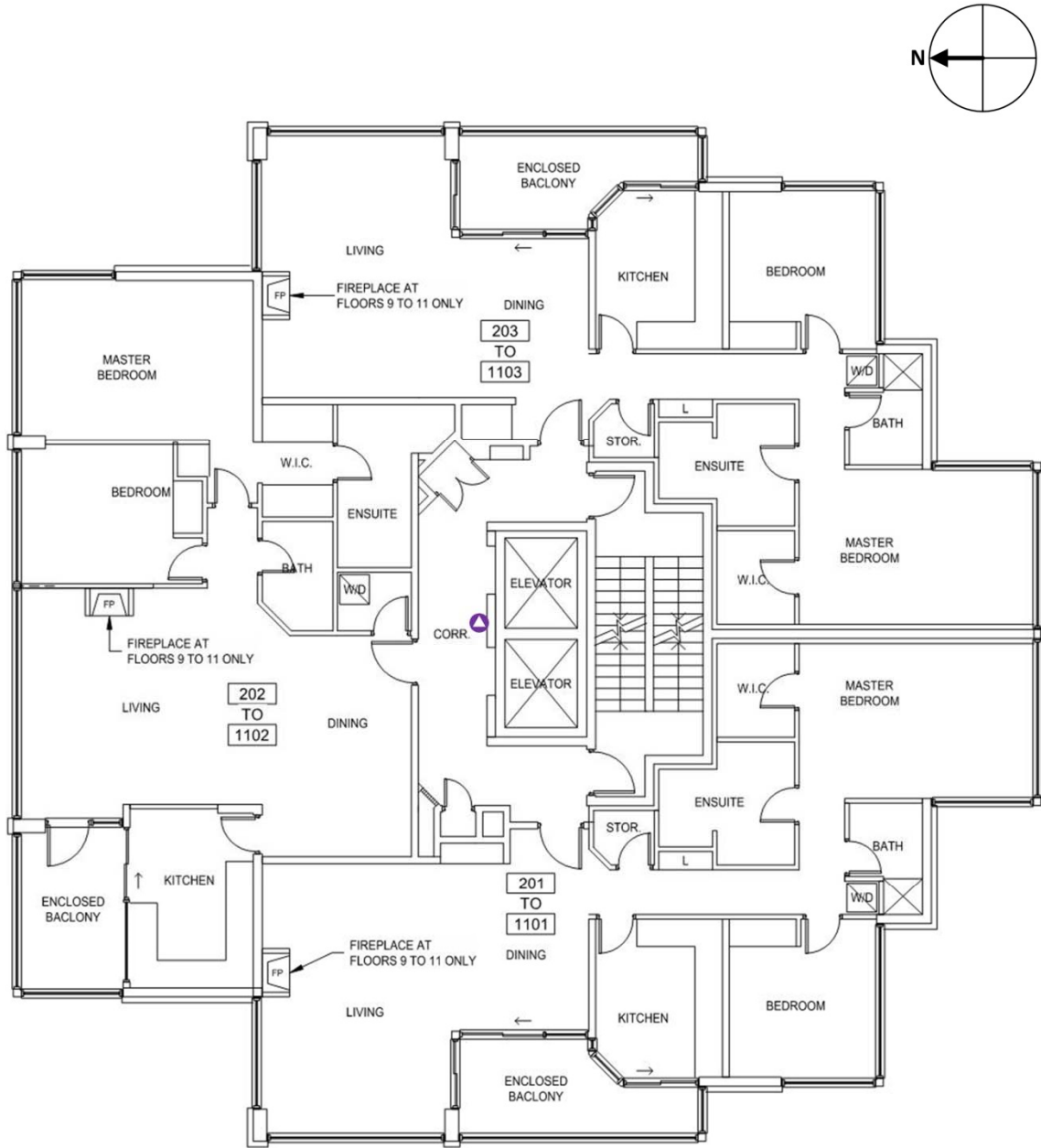
Floor 4

Figure C-10: Plan of the fourth floor of the case study building showing the location of PFT equipment



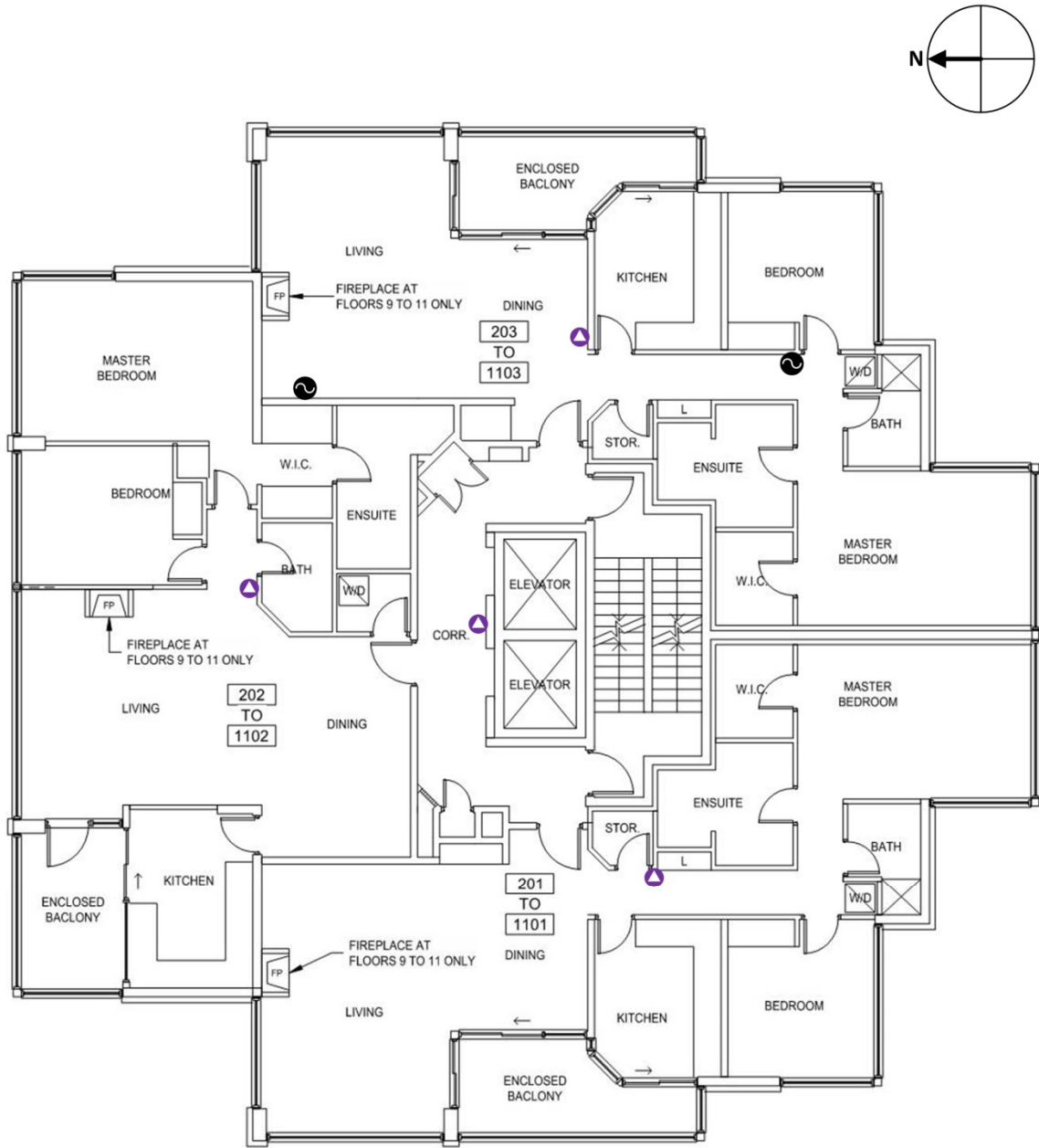
Floors 5 to 8

Figure C-11: Plan of the fifth to eighth floors of the case study building showing the location of PFT equipment



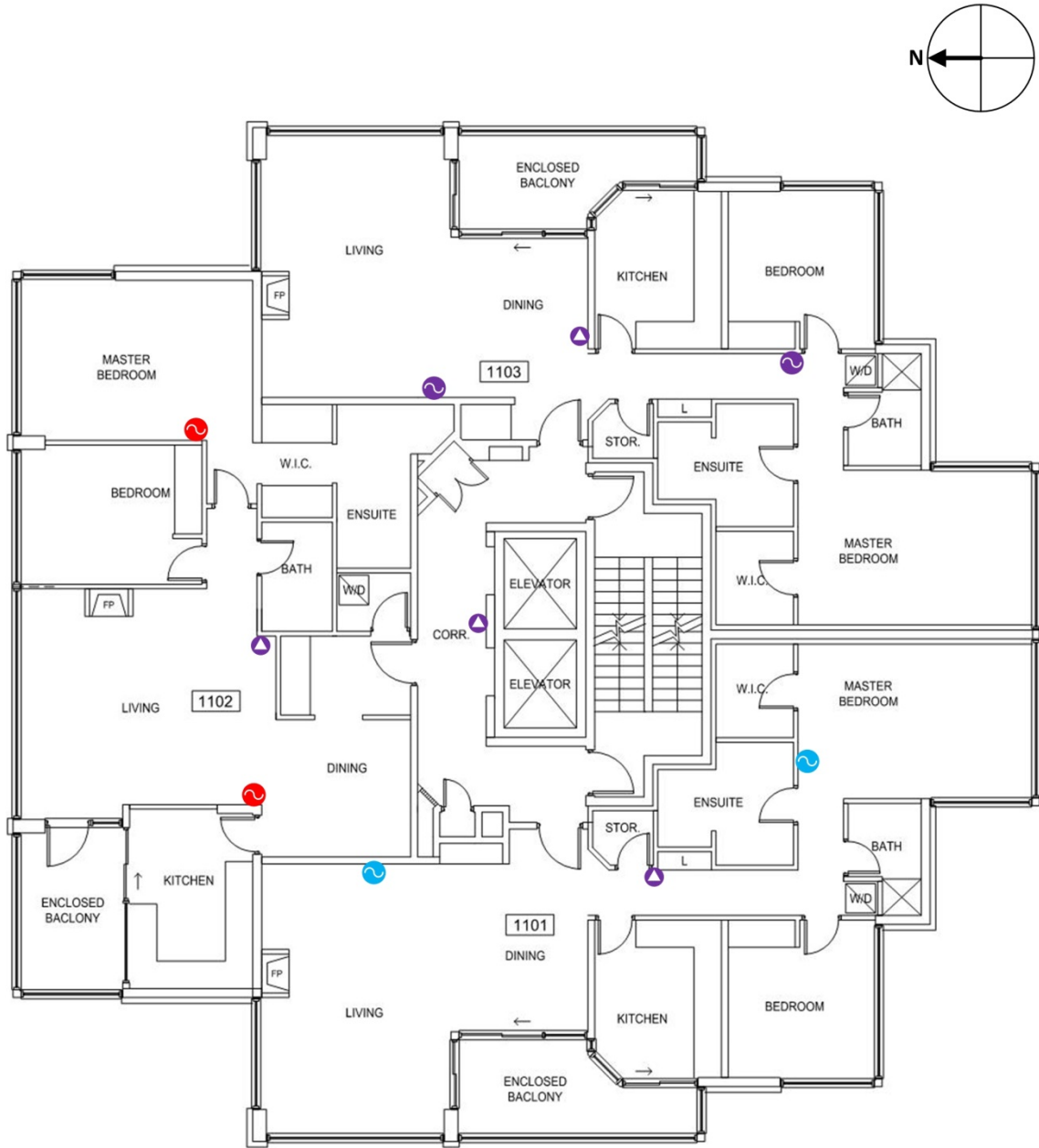
Floor 9

Figure C-12: Plan of the ninth floor of the case study building showing the location of PFT equipment



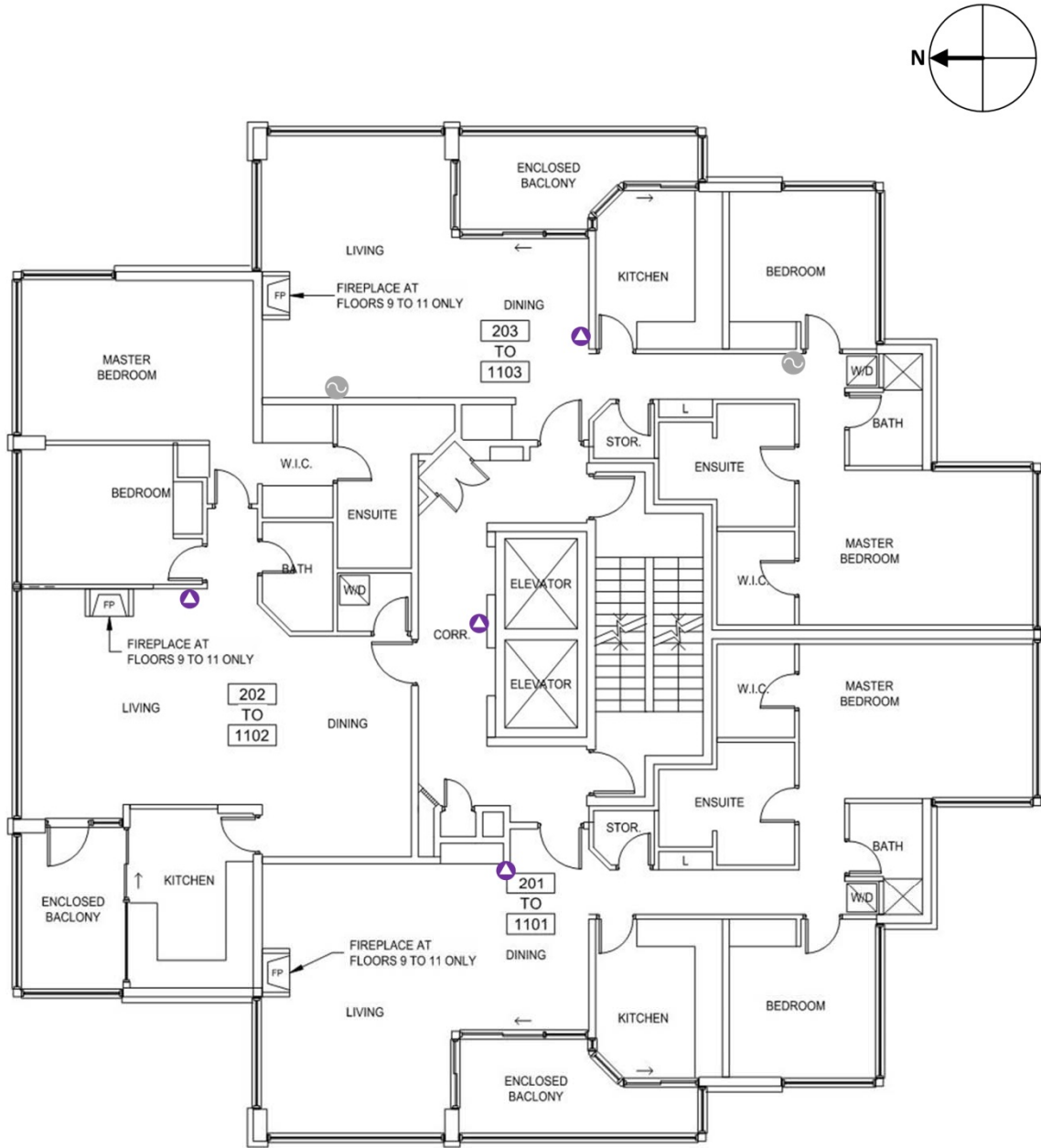
Floor 10

Figure C-13: Plan of the tenth floor of the case study building showing the location of PFT equipment



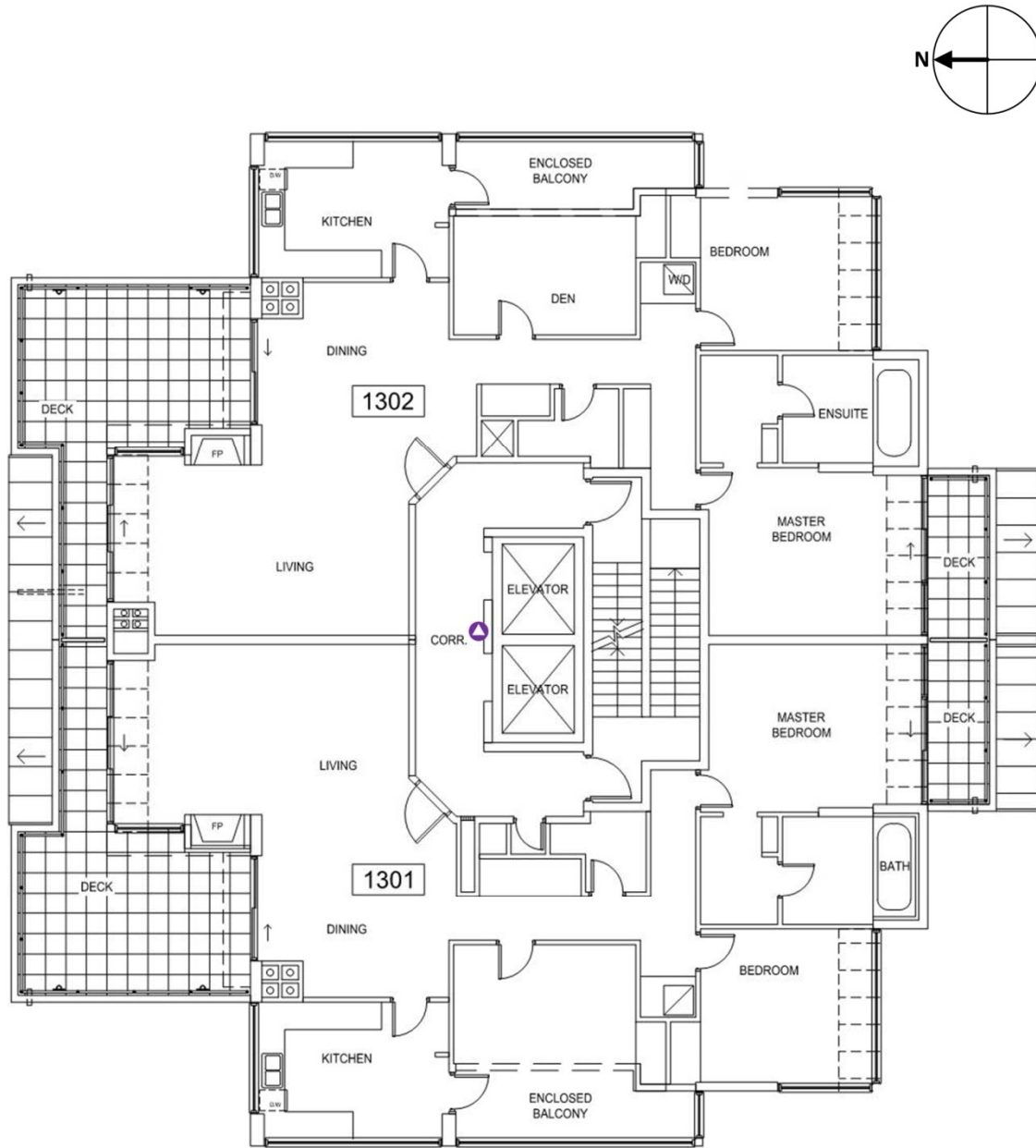
Floor 11

Figure C-14: Plan of the eleventh floor of the case study building showing the location of PFT equipment



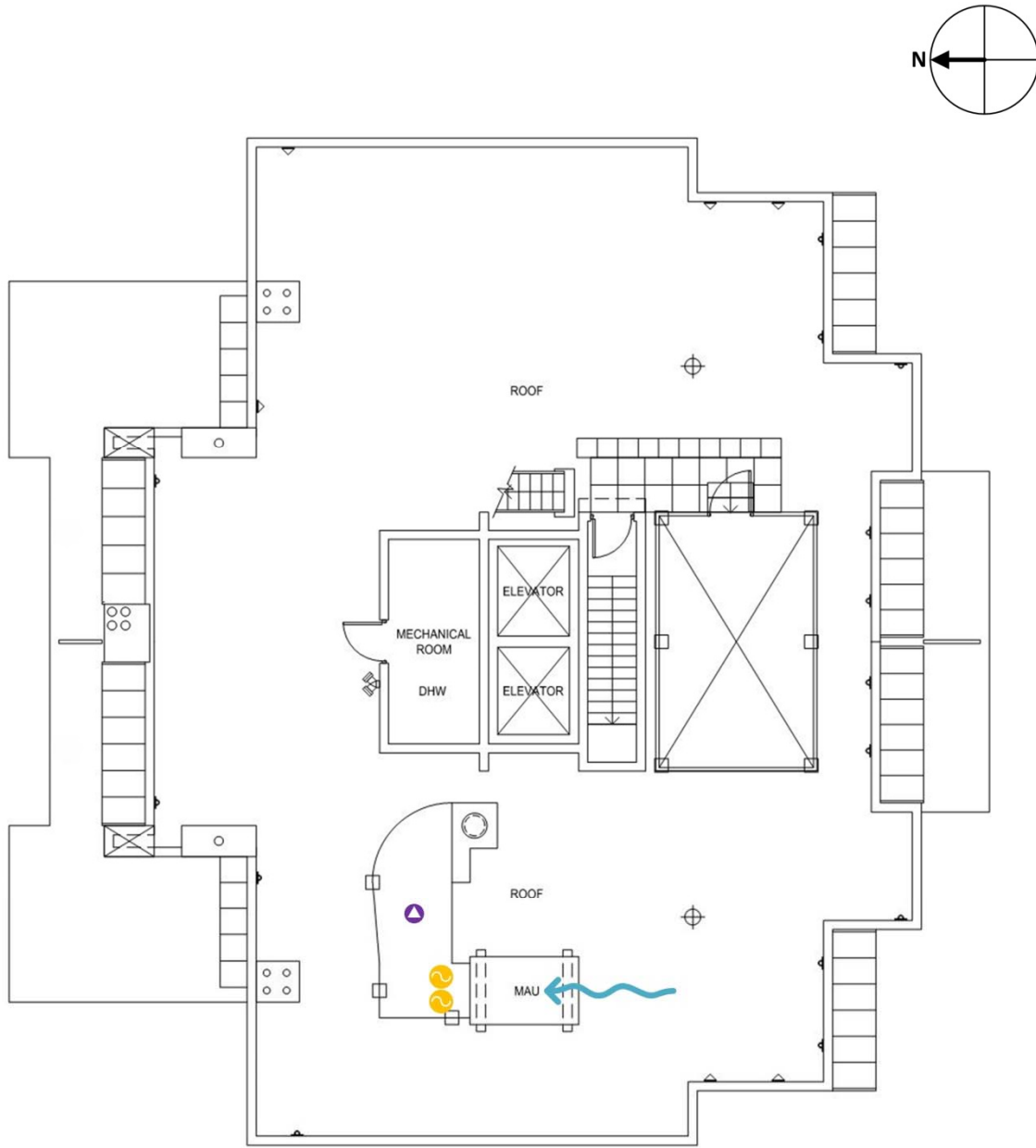
Floor 12

Figure C-15: Plan of the twelfth floor of the case study building showing the location of PFT equipment



Floor 13

Figure C-16: Plan of the thirteenth floor of the case study building showing the location of PFT equipment



Roof

Figure C-17: Plan of the roof of the case study building showing the location of PFT equipment

Four CATS were also used for calibration. These CATS were transported and stored with the other CATS except during the PFT testing period, and remained sealed at all times. Measurement of any PFT absorbed by these CATS would indicate potential unintentional contamination of the CATS.

Appendix C Supplementary Airflow Measurement Information

The procedure followed for uninstalling the PFT sources and CATS at the case study building is provided below. This procedure was developed based on guidance provided by BNL through MPI.

1. Replace stopper on open end of CATS and record time.
2. Remove source, place in double sealed plastic bags, and record time.
3. Take CATS and sources as directly as possible from the test locations to their storage locations near the test building. CATS and sources should be stored and transported separately.
4. Once all CATS and sources are removed, transport them separately to storage locations in separate buildings prior to shipment to MPI.

Generally the PFT testing equipment was uninstalled at the case study building starting at the bottom of the building and working up to the top of the building.

CATS and sources were shipped from and to MPI in separate shipments on different days to avoid close proximity of the CATS and sources during transport. The CATS were stored at the RDH Vancouver office prior to and after testing, and the sources were stored approximately 500m away in a different building and were in two sealed plastic bags, except for the mega sources which were stored in a sealed glass jar inside a sealed plastic bag. The CATS were stored and shipped in foam labelled trays as shown in Figure C-18 to facilitate ease of analysis and to protect from breaking.



Figure C-18: Photos of CATS in one of the two labelled foam trays used for storage and shipping

The information for each source and CATS including install time, uninstall time, average temperature during testing period (from monitoring data), and location are provided in Table C-2 and Table C-3. This information was used to determine the source rates and testing duration for use in the calculation of airflow rates.

Appendix C Supplementary Airflow Measurement Information

Table C-2: PFT Testing Source Information

Name	Type	Colour	Zone	Location	Start Time [yyyy/mm/dd hh:mm]	End Time [yyyy/mm/dd hh:mm]
SOURCE - PARK01	PDCB	Brown	Parkade	See drawing	2013/04/10 1:30 PM	2013/04/17 10:27 AM
SOURCE - PARK02	PDCB	Brown	Parkade	See drawing	2013/04/10 1:30 PM	2013/04/17 10:27 AM
SOURCE - PARK03	PDCB	Brown	Parkade	See drawing	2013/04/10 1:30 PM	2013/04/17 10:27 AM
SOURCE - PARK04	PDCB	Brown	Parkade	See drawing	2013/04/10 1:30 PM	2013/04/17 10:27 AM
SOURCE - 0202 A	ptPDCH	Black	Suite 0202	See drawing	2013/04/10 10:05 AM	2013/04/17 8:43 AM
SOURCE - 0202 B	ptPDCH	Black	Suite 0202	See drawing	2013/04/10 10:05 AM	2013/04/17 8:43 AM
SOURCE - 0301 A	ocPDCH	Blue	Suite 0301	See drawing	2013/04/10 10:28 AM	2013/04/17 8:52 AM
SOURCE - 0301 B	ocPDCH	Blue	Suite 0301	See drawing	2013/04/10 10:28 AM	2013/04/17 8:52 AM
SOURCE - 0302 A	PMCH	Red	Suite 0302	See drawing	2013/04/10 10:40 AM	2013/04/17 8:58 AM
SOURCE - 0302 B	PMCH	Red	Suite 0302	See drawing	2013/04/10 10:40 AM	2013/04/17 8:58 AM
SOURCE - 0303 A	iPPCH	Purple	Suite 0303	See drawing	2013/04/10 9:40 AM	2013/04/17 9:00 AM
SOURCE - 0303 B	iPPCH	Purple	Suite 0303	See drawing	2013/04/10 9:40 AM	2013/04/17 9:00 AM
SOURCE - 0402 A	PTCH	Silver	Suite 0402	See drawing	2013/04/10 10:55 AM	2013/04/17 9:10 AM
SOURCE - 0402 B	PTCH	Silver	Suite 0402	See drawing	2013/04/10 10:55 AM	2013/04/17 9:10 AM
SOURCE - 1003 A	ptPDCH	Black	Suite 1003	See drawing	2013/04/10 11:46 AM	2013/04/17 9:35 AM
SOURCE - 1003 B	ptPDCH	Black	Suite 1003	See drawing	2013/04/10 11:46 AM	2013/04/17 9:35 AM
SOURCE - 1101 A	ocPDCH	Blue	Suite 1101	See drawing	2013/04/10 12:27 AM	2013/04/17 9:44 AM
SOURCE - 1101 B	ocPDCH	Blue	Suite 1101	See drawing	2013/04/10 12:27 PM	2013/04/17 9:44 AM
SOURCE - 1102 A	PMCH	Red	Suite 1102	See drawing	2013/04/10 12:15 PM	2013/04/17 8:27 AM
SOURCE - 1102 B	PMCH	Red	Suite 1102	See drawing	2013/04/10 12:15 PM	2013/04/17 8:27 AM
SOURCE - 1103 A	iPPCH	Purple	Suite 1103	See drawing	2013/04/10 12:06 PM	2013/04/17 9:48 AM
SOURCE - 1103 B	iPPCH	Purple	Suite 1103	See drawing	2013/04/10 12:06 PM	2013/04/17 9:48 AM
SOURCE - 1203 A	PTCH	Silver	Suite 1203	See drawing	2013/04/10 1:00 PM	2013/04/17 8:34 AM
SOURCE - 1203 B	PTCH	Silver	Suite 1203	See drawing	2013/04/10 1:00 PM	2013/04/17 8:34 AM
SOURCE - MAU A	PMCP	MEGA	MAU	See drawing	2013/04/10 2:39 PM	2013/04/17 10:06 AM
SOURCE - MAU B	PMCP	MEGA	MAU	See drawing	2013/04/10 2:39 PM	2013/04/17 10:06 AM

Appendix C Supplementary Airflow Measurement Information

Table C-3: PFT Testing CATS Information

CATS Number	Name	Zone	Location	Start Time [yyyy/mm/dd hh:mm]	End Time [yyyy/mm/dd hh:mm]	Zone Volume [m ³]	Average Temperature [°C]
02721	CATS - PARK01	Parkade	East of core in parkade (see drawing)	2013/04/10 1:32 PM	2013/04/17 10:20 AM	6449	16.3
00469	CATS - 0000	Corridor 00	Elevator lobby at parkade level (see drawing)	2013/04/10 1:41 PM	2013/04/17 10:23 AM	42	16.3
09638	CATS - PARK03	Parkade	South-west of core in parkade (see drawing)	2013/04/10 1:47 PM	2013/04/17 10:18 AM	6449	16.3
04155	CATS - PARK04	Parkade	North of core in parkade (see drawing)	2013/04/10 1:57 PM	2013/04/17 10:19 AM	6449	16.3
03857	CATS - STAIR01	Stairwell at Floor 1 to Upstairs	See drawing	2013/04/10 1:22 PM	2013/04/17 8:14 AM	20	19.7
09296	CATS - 0100	Corridor 01	See drawing	2013/04/10 1:17 PM	2013/04/17 8:13 AM	129	19.7
06605	CATS - 0200	Corridor 02	See drawing	2013/04/10 10:11 AM	2013/04/17 8:46 AM	59	22.8
08751	CATS - 0201	Suite 0201	See drawing	2013/04/10 9:54 AM	2013/04/17 8:40 AM	307	22.8
09046	CATS - 0202	Suite 0202	See drawing	2013/04/10 10:05 AM	2013/04/17 8:43 AM	298	23.0
06110	CATS - 0203	Suite 0203	See drawing	2013/04/10 10:15 AM	2013/04/17 8:48 AM	307	20.7
02463	CATS - 0300	Corridor 03	See drawing	2013/04/10 10:42 AM	2013/04/17 9:03 AM	59	22.7
08559	CATS - 0301	Suite 0301	See drawing	2013/04/10 10:28 AM	2013/04/17 8:52 AM	307	21.6
09137	CATS - 0302	Suite 0302	See drawing	2013/04/10 10:40 AM	2013/04/17 8:58 AM	298	22.0
02935	CATS - 0303	Suite 0303	See drawing	2013/04/10 9:42 AM	2013/04/17 9:00 AM	307	22.9
00424	CATS - 0400	Corridor 04	See drawing	2013/04/10 10:48 AM	2013/04/17 9:14 AM	59	22.6
03931	CATS - STAIR04	Stairwell at Floor 4	See drawing	2013/04/10 10:59 AM	2013/04/17 9:09 AM	40	21.3
07111	CATS - 0402	Suite 0402	See drawing	2013/04/10 10:55 AM	2013/04/17 9:10 AM	298	22.2
08354	CATS - 0403	Suite 0403	See drawing	2013/04/10 11:03 AM	2013/04/17 9:13 AM	307	22.3
04462	CATS - 0500	Corridor 05	See drawing	2013/04/10 11:09 AM	2013/04/17 9:19 AM	59	22.7
08312	CATS - 0600	Corridor 06	See drawing	2013/04/10 11:11 AM	2013/04/17 9:21 AM	59	23.3
04325	CATS - 0700	Corridor 07	See drawing	2013/04/10 11:13 AM	2013/04/17 9:22 AM	59	22.9
05341	CATS - 0800	Corridor 08	See drawing	2013/04/10 11:15 AM	2013/04/17 9:22 AM	59	22.5
05480	CATS - 0900	Corridor 09	See drawing	2013/04/10 11:18 AM	2013/04/17 9:23 AM	59	22.7
00006	CATS - 1000	Corridor 10	See drawing	2013/04/10 11:25 AM	2013/04/17 9:38 AM	59	22.7
00384	CATS - 1001	Suite 1001	See drawing	2013/04/10 11:30 AM	2013/04/17 9:29 AM	307	22.3
06387	CATS - 1002	Suite 1002	See drawing	2013/04/10 11:36 AM	2013/04/17 9:33 AM	298	22.2
03124	CATS - 1003	Suite 1003	See drawing	2013/04/10 11:43 AM	2013/04/17 9:35 AM	307	22.1
04837	CATS - 1100	Corridor 11	See drawing	2013/04/10 12:32 PM	2013/04/17 9:51 AM	59	22.6
02437	CATS - 1101	Suite 1101	See drawing	2013/04/10 12:27 PM	2013/04/17 9:44 AM	307	21.9
07700	CATS - 1102	Suite 1102	See drawing	2013/04/10 12:15 PM	2013/04/17 8:27 AM	298	22.4
01247	CATS - 1103	Suite 1103	See drawing	2013/04/10 12:06 PM	2013/04/17 9:48 AM	307	21.9
07361	CATS - 1200	Corridor 12	See drawing	2013/04/10 12:54 PM	2013/04/17 10:34 AM	59	22.2
07140	CATS - 1201	Suite 1201	See drawing	2013/04/10 12:45 PM	2013/04/17 8:18 AM	307	21.6
00496	CATS - 1202	Suite 1202	See drawing	2013/04/10 12:38 PM	2013/04/17 10:32 AM	298	22.2
08083	CATS - 1203	Suite 1203	See drawing	2013/04/10 1:00 PM	2013/04/17 8:34 AM	307	22.2
06120	CATS - 1300	Corridor 13	See drawing	2013/04/10 1:03 PM	2013/04/17 8:11 AM	59	22.3
09607	CATS - MAU	Make-up Air Unit Intake	In make-up air unit duct downstream of source (See drawing)	2013/04/10 2:39 PM	2013/04/17 10:05 AM	n/a	20.7
06179	CATS - CALIB01	Calibration	n/a	n/a	n/a	n/a	21.0
01929	CATS - CALIB02	Calibration	n/a	n/a	n/a	n/a	
05242	CATS - CALIB03	Calibration	n/a	n/a	n/a	n/a	
01698	CATS - CALIB04	Calibration	n/a	n/a	n/a	n/a	

C-2 Make-Up Air Unit Intake Measurements

The make-up air unit intake flow rate was measured according to the procedure provided in Section 7.3.2. The 15 measurements of flow rate and flow resistance added by the test apparatus that were made during the course of the test are provided in Table C-4. These measurements were averaged to determine the flow rate presented in Section 8.1.

Table C-4: MAU Intake Airflow Rate Measurements

Flow Resistance of Test Apparatus [Pa]	Airflow [L/s]
-0.6	1345
-0.5	1340
-0.2	1357
-0.5	1359
-0.1	1380
0	1397
0.5	1376
0.4	1369
-0.6	1333
-0.6	1336
0.6	1350
0.6	1354
0.5	1359
0.8	1354
0.4	1354
-0.5	1340
0.5	1359

C-3 Bathroom Exhaust Fan Measurements

The bathroom exhaust fan flow rates and flow resistance characteristics were measured using a Retrotec DU200 DucTester, flex-duct, and flow hood as discussed in Section 7.5.1. This fan has a maximum flow rate of 283 L/s at 50 Pa pressure difference. The flow accuracy is $\pm 3\%$. The test fan was controlled using a Retrotec DM-2 gauge, the specifications of which are provided in Appendix C. The results of the bathroom exhaust fan measurements are provided in Table C-5 to Table C-8.

Table C-5: Bathroom Exhaust Fan Testing and Measurement Results – Floor 1 to 4

Suite	Fan Location	Measurement Made With	Flow Rate at Given Pressure Difference [cfm]			Flow Exponent, n [dimensionless]	log (C)	Flow Coefficient, C [ft ³ /min-Pa ⁿ]	R-Squared	Fan Flow Rate - DucTester [cfm]	Fan Flow Rate - Balometer [cfm]	Notes
			Pressure [Pa]									
			25	50	75							
101	Main Bathroom	DucTester	36	60	82	97	0.72	0.55	3.52	0.990	65	
	Ensuite Bathroom	DucTester	24	44	59	75	0.82	0.24	1.75	0.996	11	
102	Main Bathroom	DucTester	43	67	86	101	0.62	0.77	5.90	0.989	62	
	Ensuite Bathroom	DucTester	27	41	53	63	0.61	0.57	3.75	0.994	43	
201	Main Bathroom	DucTester	42	58	73	87	0.52	0.89	7.71	0.999	66	
	Ensuite Bathroom	DucTester	38	55	73	90	0.62	0.71	5.07	1.000	50	
202	Main Bathroom	DucTester	34	54	72	90	0.70	0.55	3.56	0.999	57	
	Ensuite Bathroom	DucTester	38	57	76	93	0.65	0.67	4.70	0.999	55	
203	Main Bathroom	DucTester	40	60	79	98	0.64	0.70	4.99	1.000	60	
	Ensuite Bathroom	DucTester	43	67	90	106	0.66	0.71	5.16	0.992	53	
301	Main Bathroom	DucTester	38	58	78	93	0.65	0.67	4.64	0.996	50	
	Ensuite Bathroom	DucTester	39	60	80	96	0.65	0.68	4.74	0.996	61	
302	Main Bathroom	DucTester	34	53	71	89	0.69	0.56	3.64	1.000	66	
	Ensuite Bathroom	DucTester	32	48	64	78	0.64	0.60	3.99	0.999	63	
303	Main Bathroom	DucTester	66	97	118	139	0.53	1.08	11.90	0.990	63	
	Ensuite Bathroom	DucTester	36	54	69	82	0.59	0.73	5.31	0.995	51	
401	Main Bathroom	DucTester	38	61	81	94	0.66	0.66	4.54	0.986	Negligible	Fan not operating correctly.
	Ensuite Bathroom	DucTester	35	56	76	100	0.75	0.49	3.10	0.998	62	
402	Main Bathroom	DucTester	31	47	61	76	0.64	0.59	3.90	0.999	61	
	Ensuite Bathroom	DucTester	32	51	68	86	0.71	0.51	3.25	1.000	71	
403	Main Bathroom	DucTester	39	63	87	105	0.72	0.58	3.81	0.996	65	
	Ensuite Bathroom	DucTester	38	60	81	98	0.69	0.62	4.15	0.997	67	

Table C-6: Bathroom Exhaust Fan Testing and Measurement Results – Floor 5 to 8

Suite	Fan Location	Measurement Made With	Flow Rate at Given Pressure Difference [cfm]				Flow Exponent, n [dimensionless]	log (C)	Flow Coefficient, C [ft ³ /min-Pa ⁿ]	R-Squared	Fan Flow Rate - DucTester [cfm]	Fan Flow Rate - Balometer [cfm]	Notes
			Pressure [Pa]										
			25	50	75	100							
501	Main Bathroom	DucTester	43	63	78	94	0.56	0.85	0.996	60	-		
	Ensuite Bathroom	DucTester	32	51	68	83	0.69	0.54	0.997	57	-		
502	Main Bathroom	DucTester	34	54	72	87	0.68	0.58	0.996	57	-		
	Ensuite Bathroom	DucTester	29	47	60	73	0.66	0.54	0.993	56	-		
503	Main Bathroom	DucTester	32	50	68	80	0.67	0.57	0.992	57	-		
	Ensuite Bathroom	DucTester	32	50	69	86	0.71	0.50	1.000	61	-		
601	Main Bathroom	DucTester	36	59	82	98	0.73	0.53	0.993	60	-		
	Ensuite Bathroom	DucTester	33	52	67	80	0.64	0.63	0.992	60	-		
602	Main Bathroom	DucTester	33	48	65	82	0.65	0.60	0.999	56	-		
	Ensuite Bathroom	DucTester	28	42	56	70	0.66	0.52	1.000	61	-		
603	Main Bathroom	DucTester	34	53	72	88	0.69	0.57	0.998	67	-		
	Ensuite Bathroom	DucTester	34	53	70	87	0.67	0.59	0.999	12	-		
701	Main Bathroom	DucTester	38	57	74	86	0.59	0.75	0.990	67	-		
	Ensuite Bathroom	DucTester	29	44	58	72	0.65	0.55	1.000	65	-		
702	Main Bathroom	DucTester	31	48	64	78	0.67	0.56	0.998	60	-		
	Ensuite Bathroom	DucTester	36	50	65	77	0.55	0.78	0.998	57	-		
703	Main Bathroom	DucTester	34	55	72	86	0.67	0.59	0.992	45	-		
	Ensuite Bathroom	DucTester	30	48	64	78	0.69	0.51	0.997	65	-		
801	Main Bathroom	DucTester	35	61	80	96	0.73	0.53	0.988	66	-		
	Ensuite Bathroom	DucTester	39	66	87	123	0.80	0.46	0.989	61	-		
802	Main Bathroom	DucTester	36	56	79	98	0.73	0.53	0.999	58	-		
	Ensuite Bathroom	DucTester	40	61	78	93	0.61	0.75	0.994	51	-		
803	Main Bathroom	DucTester	33	50	68	84	0.67	0.57	1.000	67	-		
	Ensuite Bathroom	DucTester	32	51	71	91	0.75	0.45	1.000	36	-		

Table C-7: Bathroom Exhaust Fan Testing and Measurement Results – Floor 9 to 11

Suite	Fan Location	Measurement Made With	Flow Rate at Given Pressure Difference [cfm]			Flow Exponent, n [dimensionless]	log (C)	Flow Coefficient, C [ft ³ /min-Pa ⁿ]	R-Squared	Fan Flow Rate - DucTester [cfm]	Fan Flow Rate - Balometer [cfm]	Notes
			Pressure [Pa]									
			25	50	75							
901	Main Bathroom	DucTester	42	59	74	87	0.52	0.89	7.70	0.996	77	-
	Ensuite Bathroom	DucTester	41	59	77	92	0.58	0.79	6.18	0.998	61	-
902	Main Bathroom	DucTester	33	50	66	78	0.63	0.64	4.39	0.994	60	-
	Ensuite Bathroom	DucTester	29	44	59	72	0.66	0.54	3.46	0.999	42	-
903	Main Bathroom	DucTester	38	57	80	96	0.68	0.63	4.22	0.996	65	-
	Ensuite Bathroom	DucTester	35	52	72	89	0.67	0.59	3.90	0.999	Negligible	Ensuite fan broken.
1001	Main Bathroom	DucTester	32	50	69	82	0.69	0.54	3.48	0.994	68	-
	Ensuite Bathroom	DucTester	34	46	60	71	0.53	0.78	5.98	0.998	65	-
1002	Main Bathroom	DucTester	55	95	130	166	0.79	0.63	4.27	0.999	14	-
	Ensuite Bathroom	DucTester	21	35	46	53	0.68	0.38	2.41	0.979	41	-
1003	Main Bathroom	DucTester	48	70	84	106	0.55	0.90	8.00	0.993	70	-
	Ensuite Bathroom	DucTester	38	53	67	79	0.53	0.84	6.88	0.998	61	-
1101	Main Bathroom	DucTester	36	56	74	86	0.64	0.67	4.66	0.988	65	65
		Balometer	28	40	48	55	-	-	-	-	-	-
	Ensuite Bathroom	DucTester	33	47	58	69	0.53	0.78	6.00	0.996	65	50
		Balometer	24	28	40	44	-	-	-	-	-	-
1102	Main Bathroom	DucTester	28	41	57	67	0.64	0.55	3.51	0.993	63	63
		Balometer	25	38	39	51	-	-	-	-	-	-
	Ensuite Bathroom	DucTester	27	42	52	65	0.62	0.56	3.64	0.995	42	41
		Balometer	21	30	38	44	-	-	-	-	-	-
1103	Main Bathroom	DucTester	31	47	65	78	0.67	0.55	3.51	0.996	12	-
	Ensuite Bathroom	DucTester	33	51	73	94	0.75	0.45	2.84	0.998	60	Very low fan flow

Table C-8: Bathroom Exhaust Fan Testing and Measurement Results – Floor 12 to 13

Suite	Fan Location	Measurement Made With	Flow Rate at Given Pressure Difference [cfm]				Flow Exponent, n [dimensionless]	log (C)	Flow Coefficient, C [ft ³ /min-Pa ⁿ]	R-Squared	Fan Flow Rate - DucTester [cfm]	Fan Flow Rate - Balometer [cfm]	Notes
			Pressure [Pa]										
			25	50	75	100							
1201	Main Bathroom	DucTester	35	55	72	86	0.65	0.63	4.31	0.994	60	73	
		Balometer	27	42	62	75	-	-	-	-	-	-	
	Ensuite Bathroom	DucTester	40	60	78	92	0.60	0.76	5.70	0.994	62	85	
		Balometer	40	55	66	72	-	-	-	-	-	-	
1202	Main Bathroom	DucTester	-	40	56	68	0.77	0.30	1.98	0.993	54	48	
		Balometer	-	30	43	50	-	-	-	-	-	-	
	Ensuite Bathroom	DucTester	37	64	84	102	0.73	0.55	3.55	0.991	51	50	
		Balometer	30	35	40	46	-	-	-	-	-	-	
1203	Main Bathroom	DucTester	55	83	100	118	0.55	0.98	9.58	0.985	100	-	
	Ensuite Bathroom	DucTester	70	102	128	151	0.55	1.07	11.75	0.994	105	-	
1301	Main Bathroom	DucTester	32	50	66	80	0.66	0.58	3.79	0.997	60	-	Occupant reports ensuite fan works worse than main fan.
	Ensuite Bathroom	DucTester	31	48	64	78	0.67	0.56	3.60	0.998	36.5	-	
1302	Main Bathroom	DucTester	38	63	83	98	0.69	0.62	4.18	0.988	-	-	
	Ensuite Bathroom	DucTester	41	64	81	96	0.61	0.76	5.72	0.990	-	-	

C-4 Make-Up Air Unit Corridor Supply Measurements

Corridor supply airflow measurements were made using a balometer as described in Section 7.3.3. The balometer used was an Alnor LoFlo Balometer Capture Hood Model 6200D and the specifications for this device are provided below.



Air Volume Instruments



Shown: LoFlo Balometer® Capture Hood Model 6200D

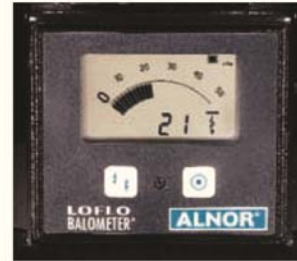
LoFlo Balometer® Capture Hoods Models 6200, 6200D, 6200E, and 6200F

The LoFlo Balometer® Capture Hood is the ideal way to measure very low volumetric flow. Measure confidently and accurately supply or return flows from 10 to 500 cfm (17 to 850 m³/h). This light weight instrument is great for residential or light commercial use.

Features and Benefits

- Uses 4 C-size alkaline batteries
- Weighs only 6.5 lb (3 kg) with 2 ft x 2 ft (610 mm x 610 mm) hood attached
- Simulated analog display shows air trends and digital readings
- Use with or without a hood

Easily observed trend values and fast meter response make the LoFlo Balometer® Capture Hood the preferred tool of residential air balancers.



Rugged. Reliable. Professional.



Balometer®

Capture Hoods

LoFlo Models

Specifications

Range
10 to 500 cfm (17 to 850 m³/h) (4.7 to 236 l/s)

Accuracy
±(3% + 5 cfm) [±(3% + 8.5 m³/h, 2.4 l/s)]

Height
Model 6200 22 in. (559 mm)
Model 6200D 34.5 in. (876 mm)
Model 6200E or base only 15.5 in. (394 mm)
Model 6200F 32 in. (813 mm)

Weight
 about 6 lbs (2.7 kg) with hood
 4.6 lbs (2.1 kg) base only

Base Diameter
Opening 13.3 in. (338 mm) diameter
Hood sizes 16 in. x 16 in., 2 ft x 2 ft, or 26 in. x 26 in.
 (406 mm x 406 mm, 610 mm x 610 mm, or 650 mm x 650 mm)
Display 3.5 digit, .44 in. (11 mm) high, digital display with 26 segment simulated analog display
Resolution 1 cfm from 10 to 500 cfm (0.1 l/s from 4.7 to 9.9) (1 l/s from 10 to 236 l/s)

Power Source
4C 1.5V alkaline batteries (optional Nickel Cadmium)

Battery Life
10 hrs. minimum with continuous use

Model Description

Model 6200 with 16 in. x 16 in. (406 mm x 406 mm), 8 in. (200 mm) tall hood
Model 6200D with 2 ft x 2 ft (610 mm x 610 mm) hood
Model 6200E with base only, metric
Model 6200F with 16 in. x 16 in. (406 mm x 406 mm), 18 in. (457 mm) tall hood

Optional Accessories

634620110 2 ft x 2 ft (610 mm x 610 mm) hood and frame kit
634620085 16 in. x 16 in. (406 mm x 406 mm), 18 in. (457 mm) tall hood and frame kit
634620120 16 in. x 16 in. (406 mm x 406 mm), 8 in. (200 mm) tall hood and frame kit
634620130 26 in. x 26 in. (650 mm x 650 mm) hood and frame kit



The LoFlo Balometer® Capture Hood is mainly used in residential or light commercial applications for taking measurements from 10 to 500 cfm (17 to 850 m³/h). The compact size allows them to be used where full size hoods would not fit such as over bathroom stalls or filing cabinets.

Specifications subject to change without notice.
 TSI, the TSI logo, Alnor, and Balometer are trademarks of TSI Incorporated.
 U.S. Patent 4,548,076

Alnor Products, TSI Incorporated - 500 Cardigan Road Shoreview, MN 55126-3996 USA

USA	Tel: +1 800 424 7427	E-mail: customerservice@alnor.com	Website: www.tsi.com
UK	Tel: +44 149 4 459200	E-mail: tsiuk@tsi.com	Website: www.tsiinc.co.uk
France	Tel: +33 491 11 87 64	E-mail: tsifrance@tsi.com	Website: www.tsiinc.fr
Germany	Tel: +49 241 523030	E-mail: tsigmbh@tsi.com	Website: www.tsiinc.de
India	Tel: +91 80 41132470	E-mail: tsi-india@tsi.com	
China	Tel: +86 10 8260 1595	E-mail: tsibeijing@tsi.com	
Singapore	Tel: +65 6595 6388	E-mail: tsi-singapore@tsi.com	



Contact your local Alnor Distributor or visit our website www.alnor.com for more detailed specifications.

Appendix D

Supplementary Airtightness Testing Information

Airtightness testing was conducted at the case study building to measure the air permeance of the exterior building enclosure and of interior compartmentalizing elements. Section 7.4 presents the general methodology for this testing and Chapter 8 presents the general results. This appendix provides a more detailed description of the test procedure, testing equipment information, and the results of each individual test.

D-1 Supplementary Airtightness Testing Procedure

As discussed in Section 7.4, sequentially neutralized pressurization/depressurization testing was used to determine the airtightness characteristics of suites, whole floors, and corridors. The steps for testing of a typical suite are provided in Section 7.2, and the steps for testing of a corridor or floor are provided below.

Airtightness testing of the corridors was performed in the following 20 steps:

- Step 1 – Pressurize – All 6 Sides: Pressurize the corridor relative to adjacent zones.
- Step 2 – Depressurize – All 6 Sides: Depressurize the corridor relative to adjacent zones.
- Step 3 – Pressurize – Door -01: Pressurize the corridor relative to adjacent zones with door -01 sealed.
- Step 4 – Depressurize – Door -01: Depressurize the corridor relative to adjacent zones with door -01 sealed.
- Step 5 – Pressurize – Door -02: Pressurize the corridor relative to adjacent zones with door -02 sealed.
- Step 6 – Depressurize – Door -02: Depressurize the corridor relative to adjacent zones with door -02 sealed.
- Step 7 – Pressurize – Door -03: Pressurize the corridor relative to adjacent zones with door -03 sealed.
- Step 8 – Depressurize – Door -03: Depressurize the corridor relative to adjacent zones with door -03 sealed.
- Step 9 – Pressurize – Elevator Door: Pressurize the corridor relative to adjacent zones with elevator doors (2) sealed.
- Step 10 – Depressurize – Elevator Door: Depressurize the corridor relative to adjacent zones with elevator doors (2) sealed.
- Step 11 – Pressurize – Stairwell Door: Pressurize the corridor relative to adjacent zones with east stairwell door sealed.
- Step 12 – Depressurize – Stairwell Door: Depressurize the corridor relative to adjacent zones with east stairwell door sealed.
- Step 13 – Pressurize – Electrical Closet Door: Pressurize the corridor relative to adjacent zones with electrical closet doors sealed.
- Step 14 – Depressurize – Electrical Closet Door: Depressurize the corridor relative to adjacent zones with electrical closet doors sealed.

Appendix D Supplementary Airtightness Testing Information

- Step 15 – Pressurize – Garbage Chute Door: Pressurize the corridor relative to adjacent zones with garbage chute door sealed.
- Step 16 – Depressurize – Garbage Chute Door: Depressurize the corridor relative to adjacent zones with garbage chute door sealed.
- Step 17 – Pressurize – Floor Above: Pressurize the corridor relative to adjacent zones while pressure neutralizing the floor above.
- Step 18 – Depressurize – Floor Above: Pressurize the corridor relative to adjacent zones while pressure neutralizing the floor above.
- Step 19 – Pressurize – Floor Below: Pressurize the corridor relative to adjacent zones while pressure neutralizing the floor below.
- Step 20 – Depressurize – Floor Below: Pressurize the corridor relative to adjacent zones while pressure neutralizing the floor below.

Airtightness testing of only the exterior enclosure of a suite or floor was performed using only Step 6 of the procedure for testing a typical suite.

As an example, Figure D-2 and Figure D-3 graphically illustrate the steps for testing a typical -01 type suite by pressurization. Testing of other suite types and testing by depressurization are similar. Figure D-4 to Figure D-10 graphically illustrates the steps for testing a corridor. Figure D-1 provides a legend for interpretation of these schematics.

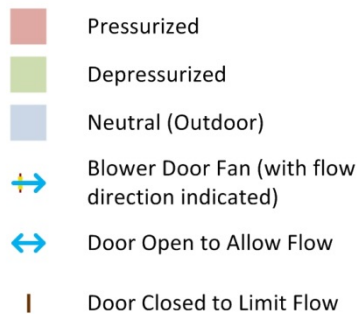


Figure D-1: Legend for interpretation of Figure D-2 to Figure D-10

Appendix D Supplementary Airtightness Testing Information

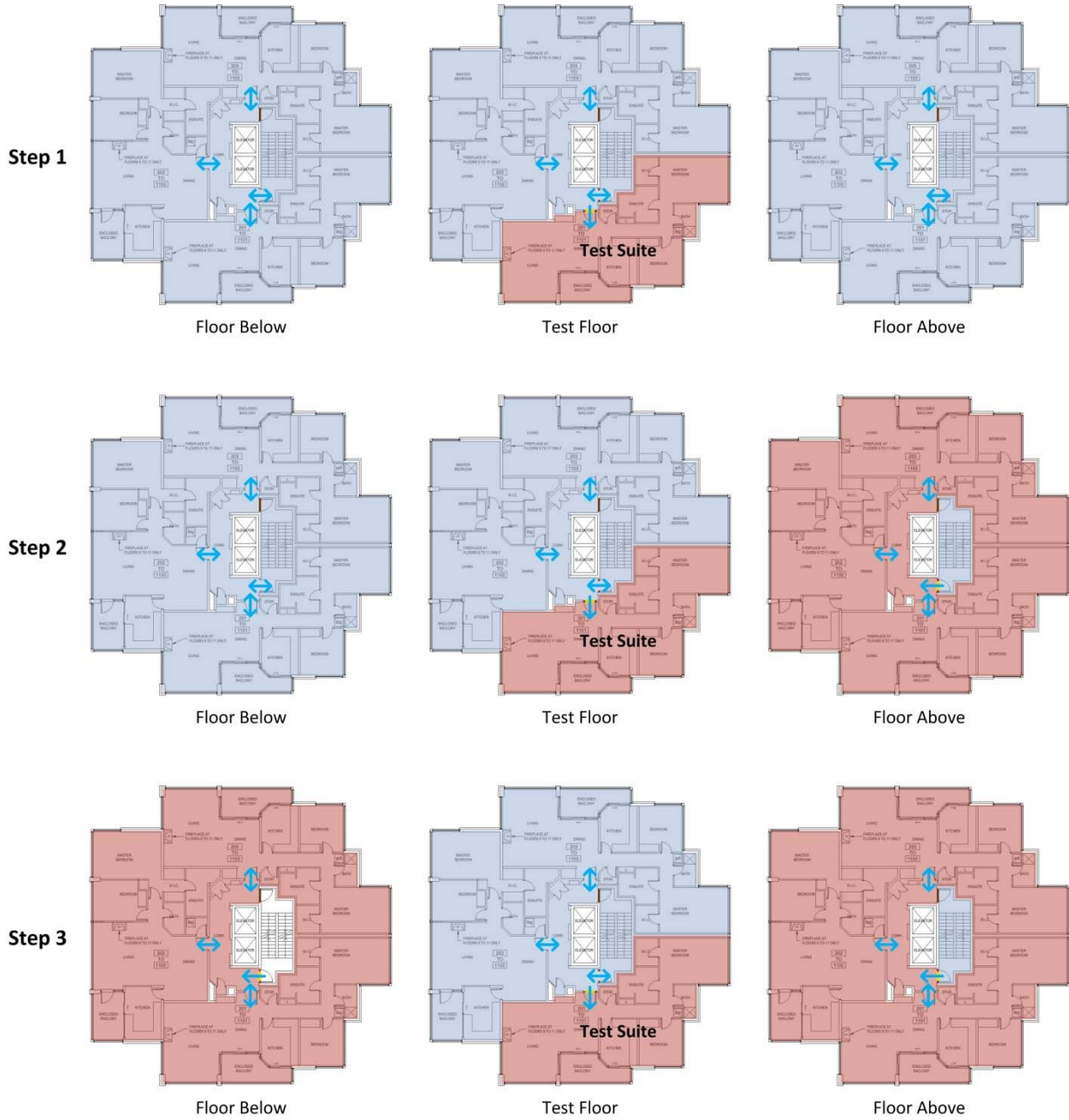


Figure D-2: Schematic illustrating test Steps 1 to 3 of pressurization airtightness testing of a typical -01 type suite

Appendix D Supplementary Airtightness Testing Information

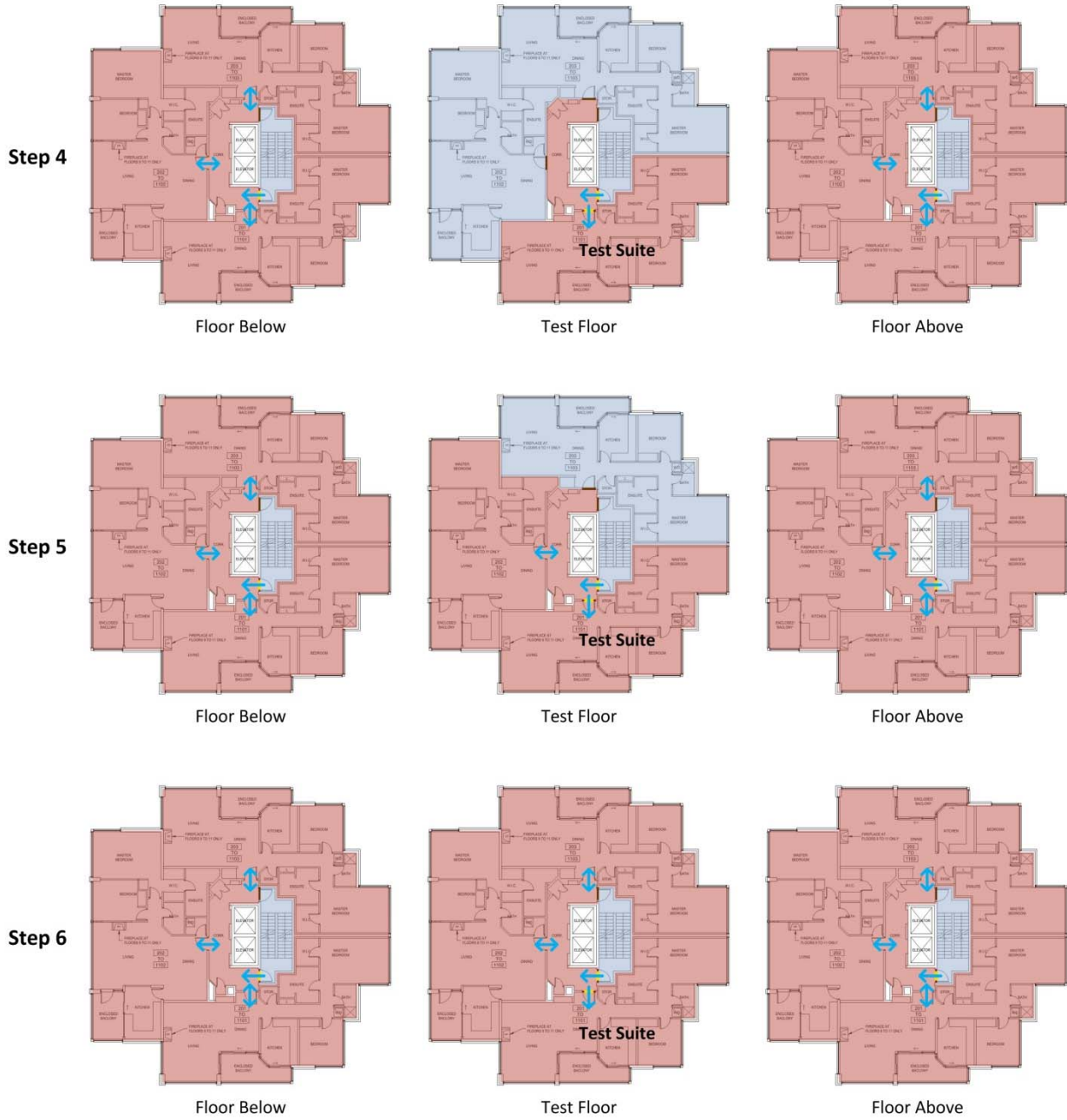


Figure D-3: Schematic illustrating test Steps 4 to 6 of pressurization airtightness testing of a typical -01 type suite

Appendix D Supplementary Airtightness Testing Information

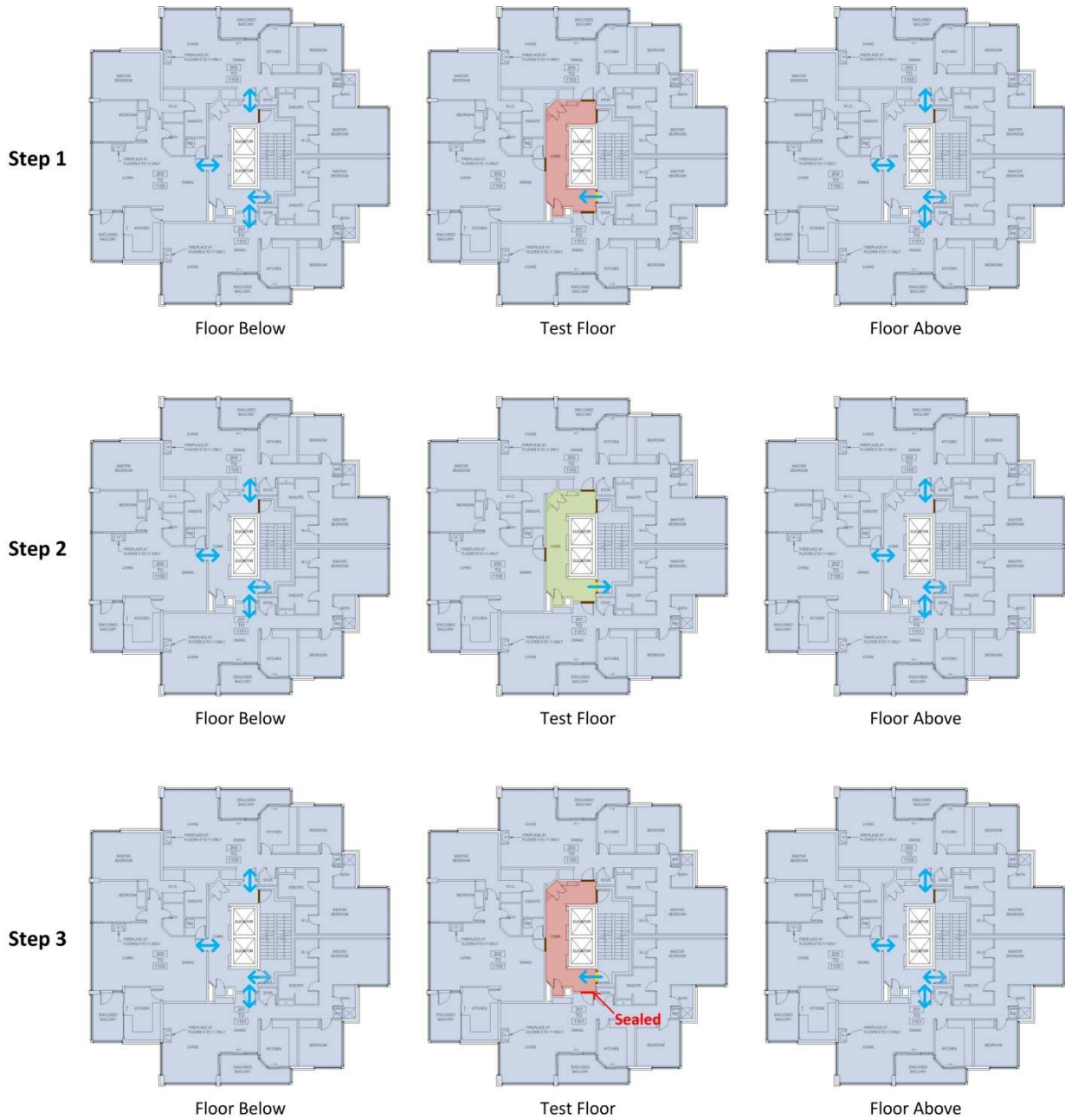


Figure D-4: Schematic illustrating test Steps 1 to 3 of airtightness testing of a typical corridor

Appendix D Supplementary Airtightness Testing Information

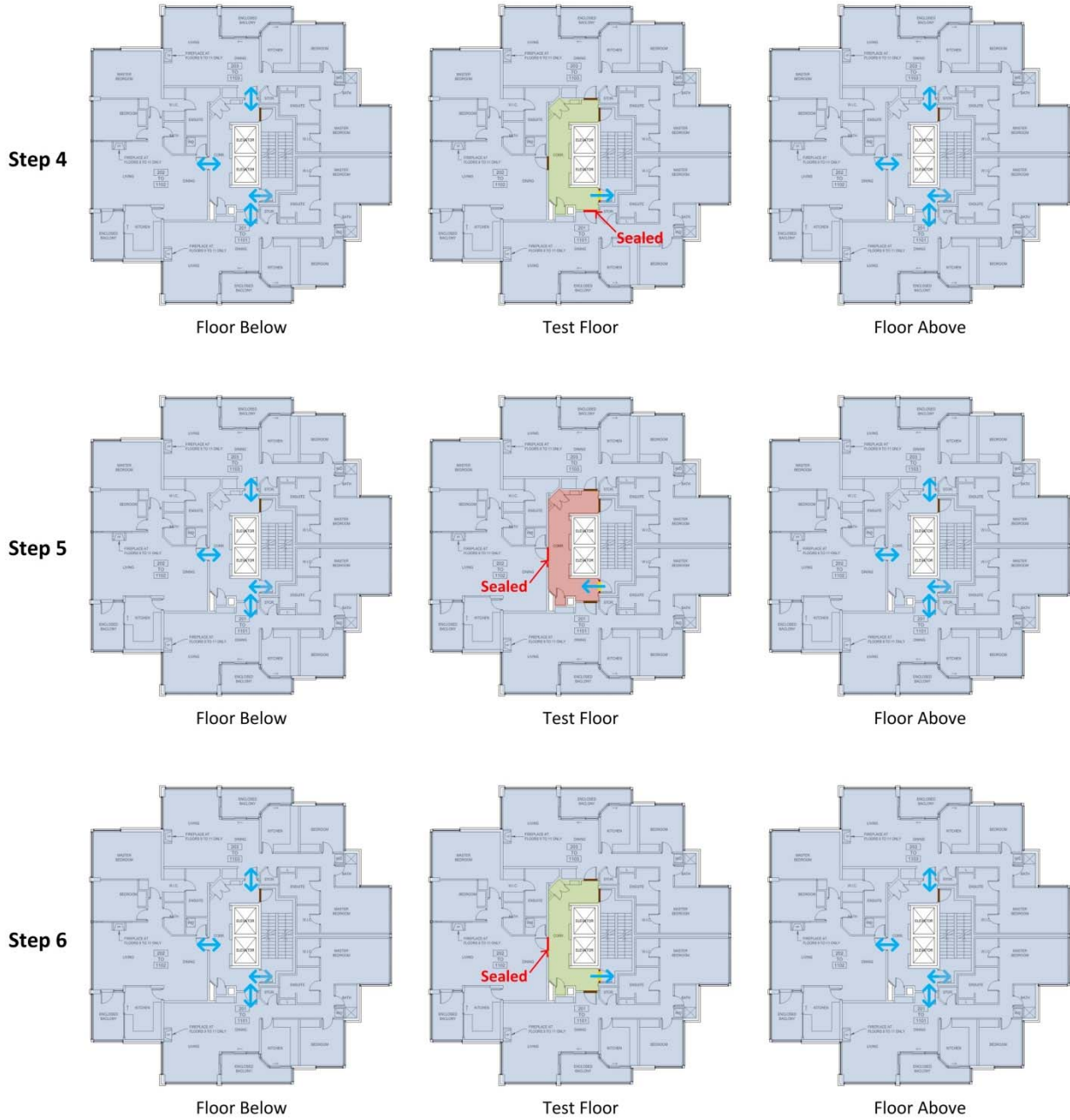


Figure D-5: Schematic illustrating test Steps 4 to 6 of airtightness testing of a typical corridor

Appendix D Supplementary Airtightness Testing Information

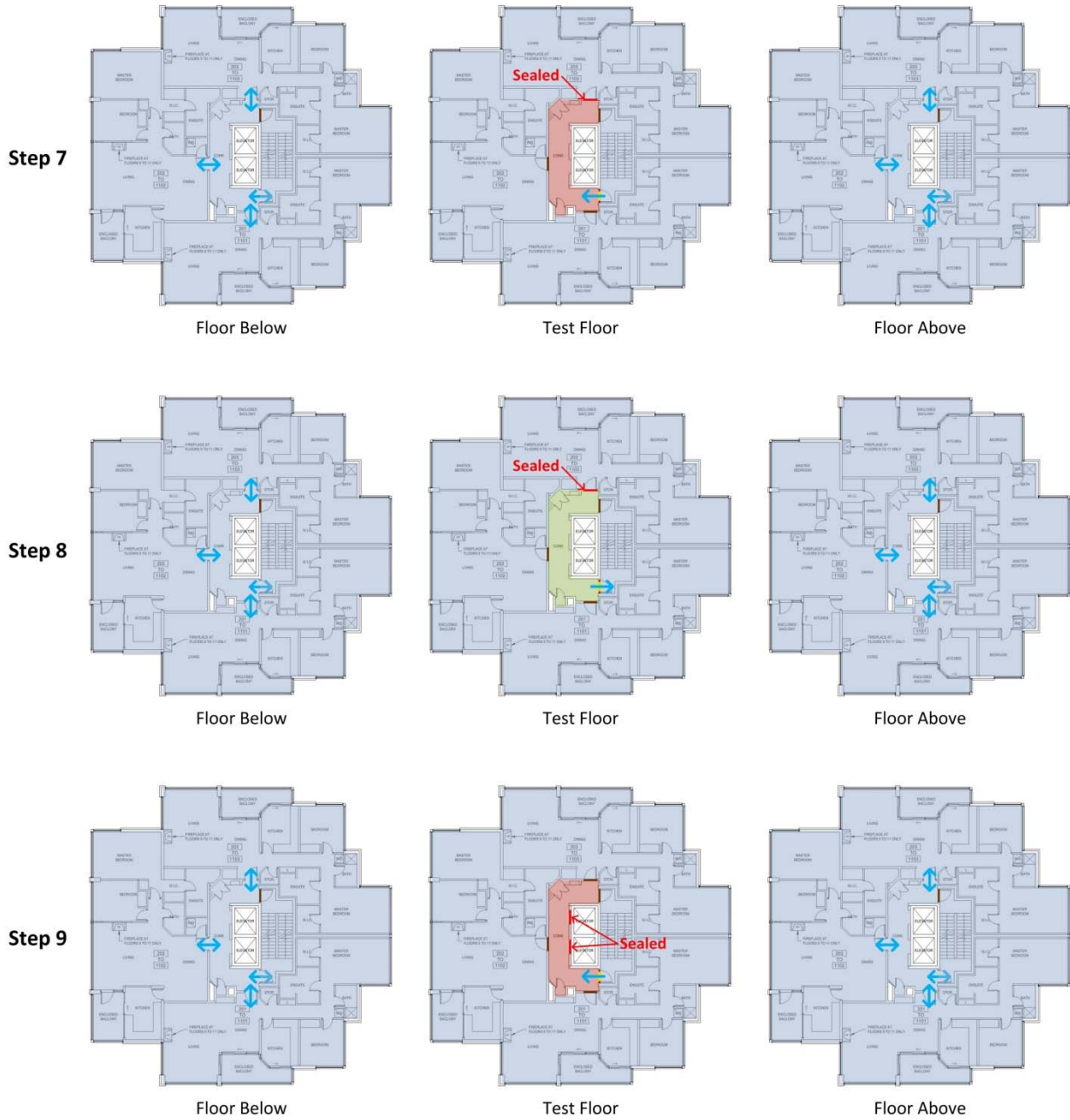


Figure D-6: Schematic illustrating test Steps 7 to 9 of airtightness testing of a typical corridor

Appendix D Supplementary Airtightness Testing Information

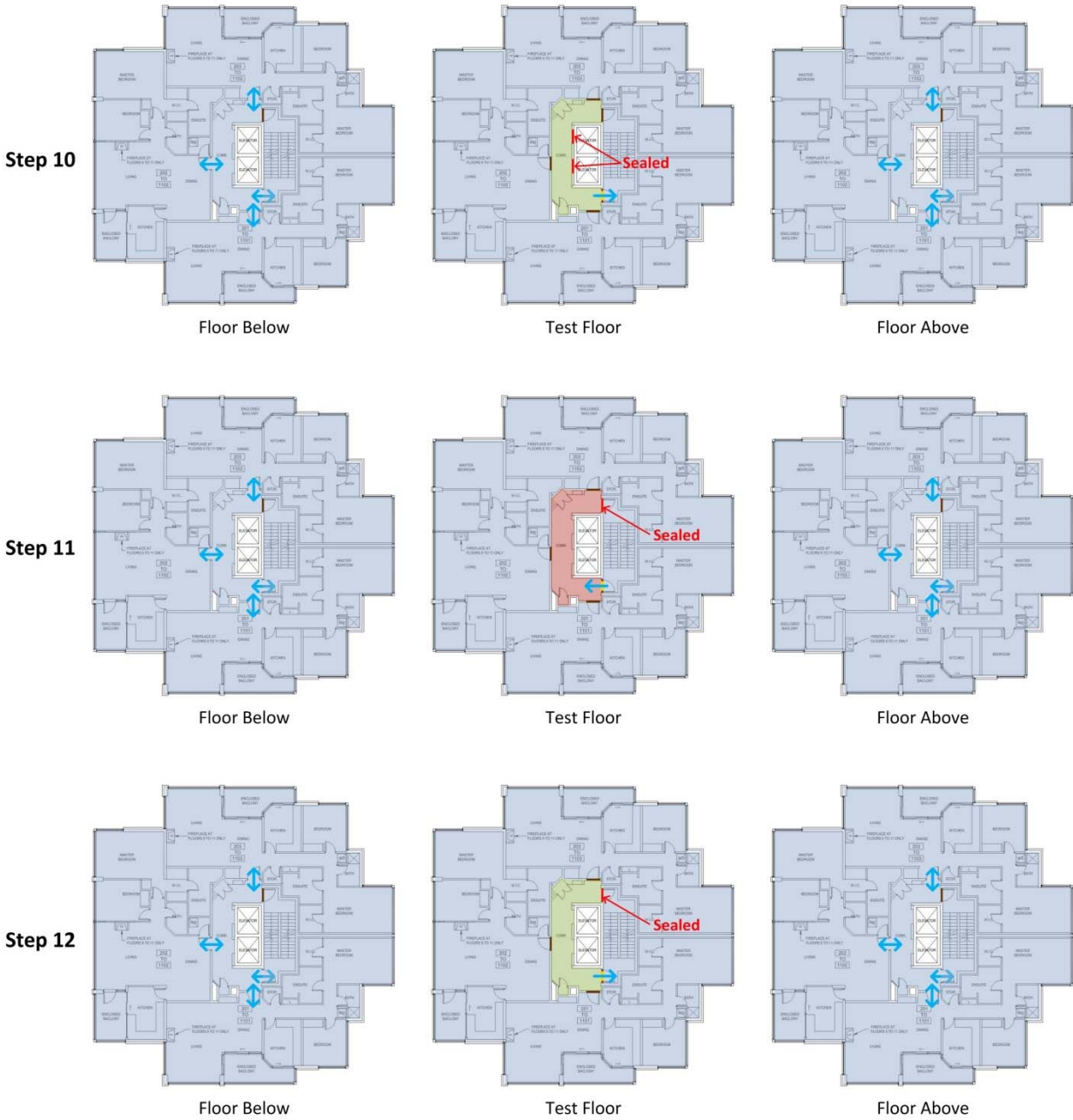


Figure D-7: Schematic illustrating test Steps 10 to 12 of airtightness testing of a typical corridor

Appendix D Supplementary Airtightness Testing Information

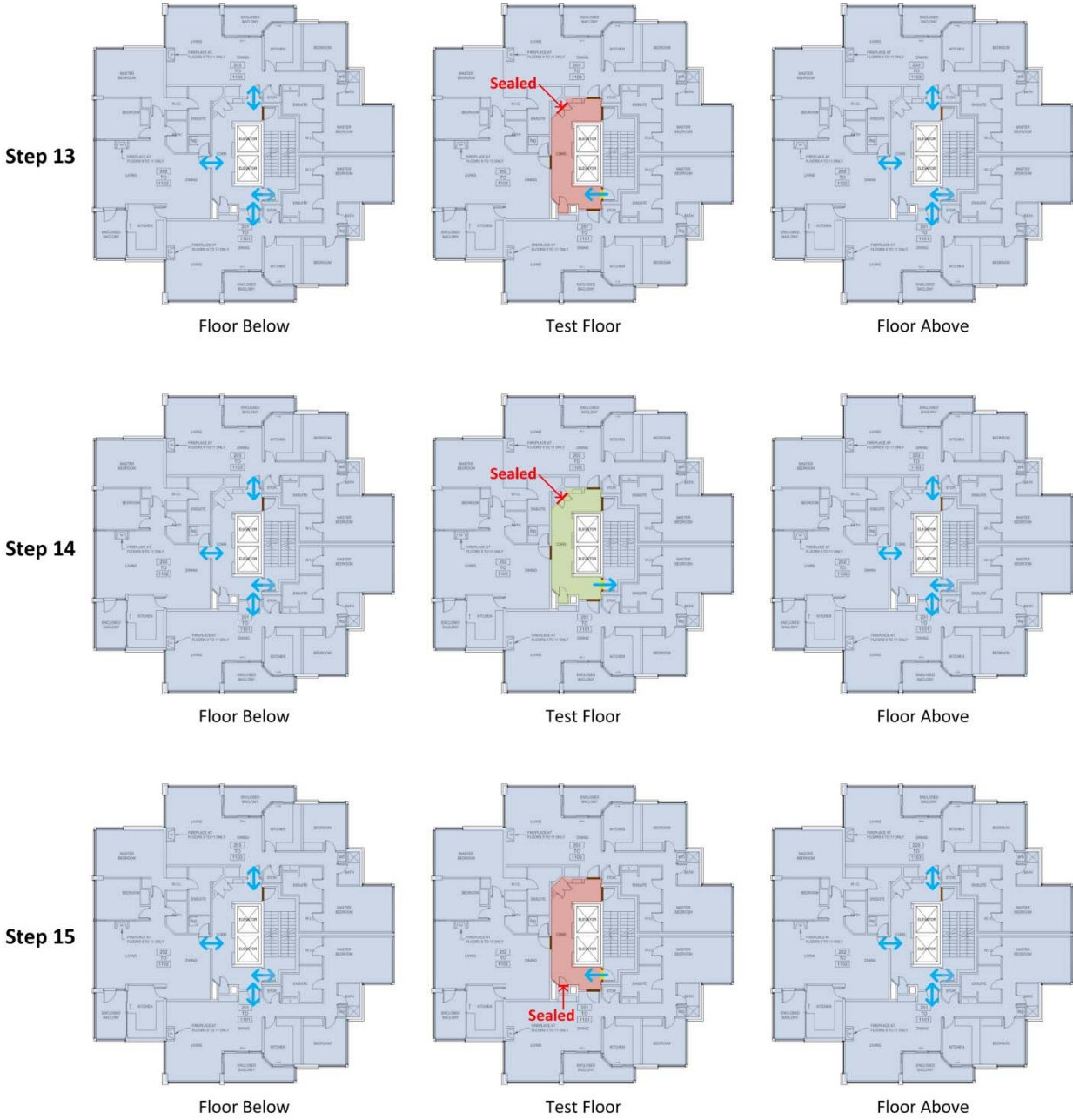


Figure D-8: Schematic illustrating test Steps 13 to 15 of airtightness testing of a typical corridor

Appendix D Supplementary Airtightness Testing Information

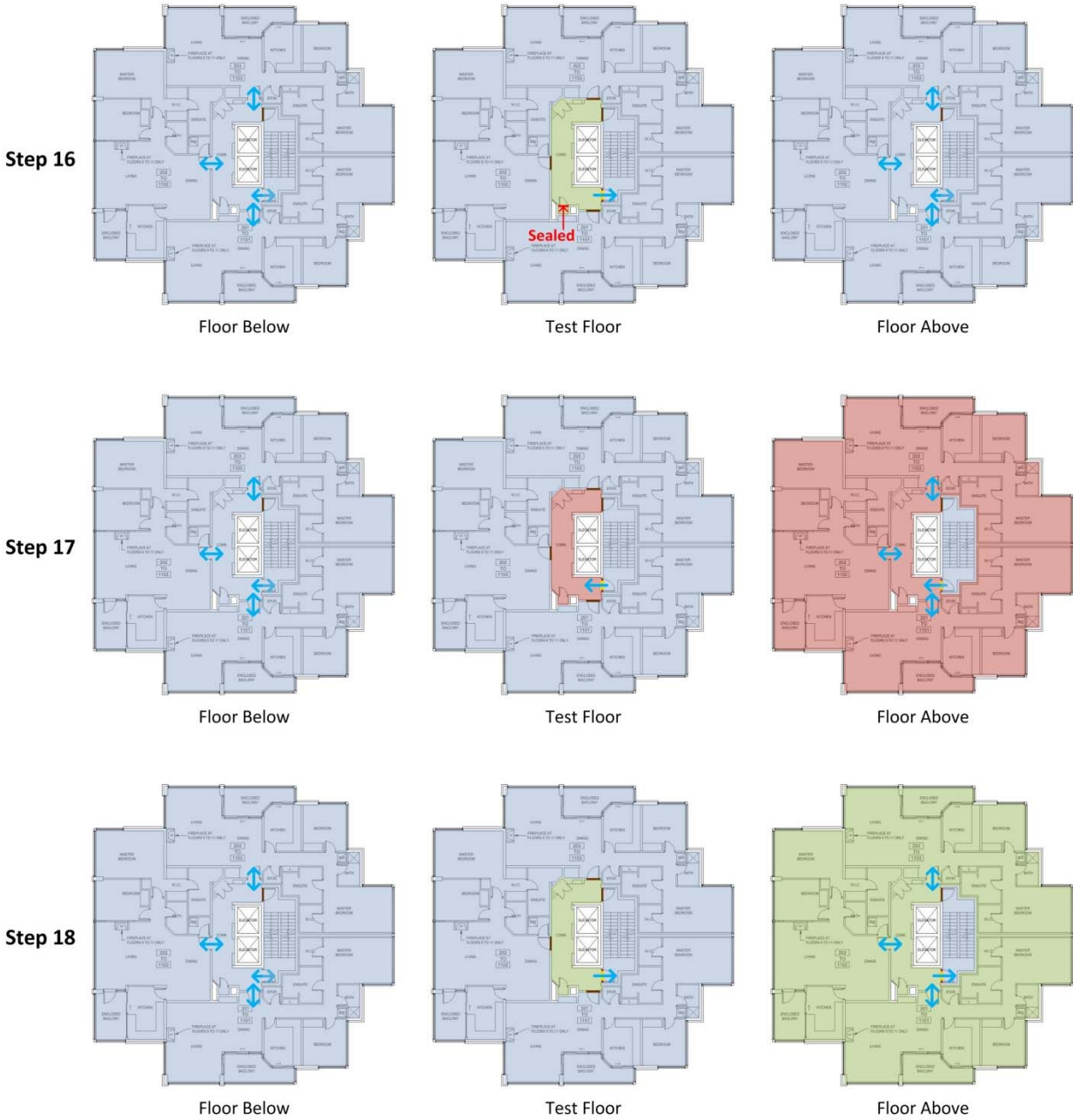


Figure D-9: Schematic illustrating test Steps 16 to 18 of airtightness testing of a typical corridor

Appendix D Supplementary Airtightness Testing Information

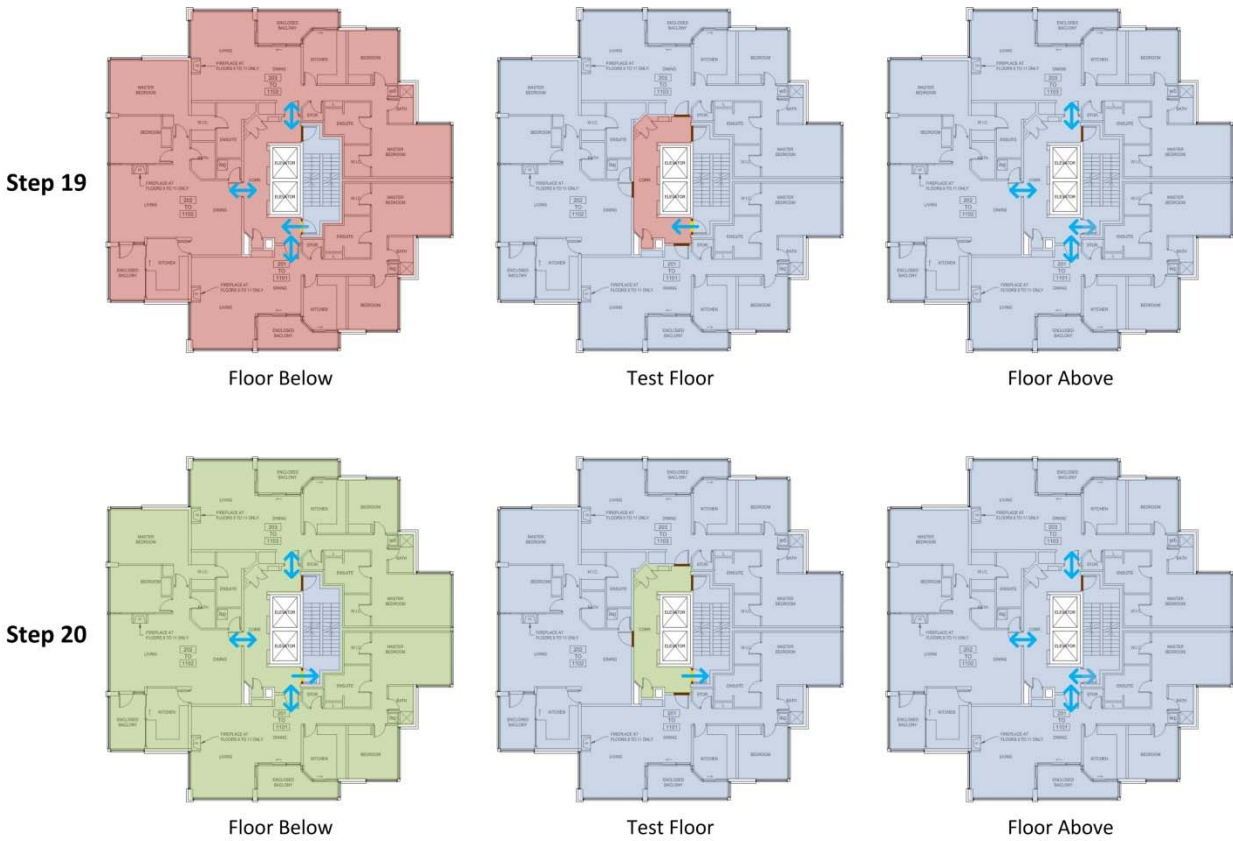


Figure D-10: Schematic illustrating test Steps 19 to 20 of airtightness testing of a typical corridor

Table D-1, Table D-2, and Table D-3 provide comments on each of the tests performed and identify any deviation from the standard test procedure discussed in Section 7.2 and above. These deviations occurred primarily to accommodate the uniqueness of each floor and access considerations (when certain doors could be sealed, et cetera), and in some cases are due to tester error. These deviations are not anticipated to have a significant impact on the test results.

Table D-1: Pre-Retrofit Airtightness Testing Comments

Test Zone	Comments
Suite 101 - Exterior Enclosure	Standard procedure was followed.
Suite 102 - Exterior Enclosure	Standard procedure was followed.
Suite 301	No baseline pressure measurement was made at the end of this test.
Suite 302	No baseline pressure measurement was made at the end of this test.
Suite 303	Standard procedure was followed.
Suite 1101	Steps 1 to 4 for pressurization were conducted at pressure differentials of 10, 20, 30, 40, 50, 60, 70, and 75 Pa. This was one of the first tests and the procedure was revised from this to reduce the time needed for testing. Also, it was difficult to achieve the larger pressure differentials with tripping circuit breakers within the building.
Suite 1102	Step 1 for pressurization was also performed at 20 Pa. No baseline pressure measurement was made at the end of this test.
Suite 1103	Step 6 for depressurization was not performed at 60 Pa.
Suite 1301	Standard procedure was followed.
Suite 1302	10 Pa pressure could not be maintained stably, so the lowest pressure that could be maintained stably was used instead, 16 Pa.
Floor 1 - Exterior Enclosure	Standard procedure was followed.

Table D-2: Post-Retrofit Airtightness Testing Comments

Test Zone	Comments
Suite 101 - Exterior Enclosure	Standard procedure was followed.
Suite 102 - Exterior Enclosure	Standard procedure was followed.
Suite 301	Standard procedure was followed.
Suite 302	Standard procedure was followed.
Suite 303	Standard procedure was followed.
Suite 1101	Standard procedure was followed.
Suite 1102	Standard procedure was followed.
Suite 1103	Standard procedure was followed.
Suite 1301	Standard procedure was followed.
Suite 1302	Standard procedure was followed.
Floor 1 - Exterior Enclosure	Standard procedure was followed.
Floor 13 - Exterior Enclosure	Standard procedure was followed.

Table D-3: Corridor Airtightness Testing Comments

Test Zone	Comments
Corridor 3	Steps 1 and 2 were repeated at the end of the test and an average result of these tests used for analysis.
Corridor 9	Steps 17 through 20 were performed after Step 2 to facilitate access. There is no electrical closet on this floor, so Steps 13 and 14 were not conducted.
Corridor 11	The lowest test pressure was adjusted to 15 Pa to allow for more stability. Steps 17 through 20 were performed after Step 2 to facilitate access. Steps 1 and 2 were repeated at the end of the test because during the test a suite occupant left and at the end of the test it was noticed that the door was left slightly ajar. The repeated Steps 1 and 2 completed with the door ajar were used to determine the airtightness of components tested after the occupant left. This may have caused some inaccuracy in the result, the quantity of which is unknown.

D-2 Equipment Information

The airtightness testing equipment used for this work was manufactured by Retrotec Inc. One Retrotec Q4E Door Fan System was used as the test fan, and three Retrotec Q5E Door Fan Systems were used as the pressure neutralizing fans. Both of these door fan set-ups use the same Retrotec 3000SR fans which are rated at a maximum flow rate of 3776 L/s at a 50 Pa pressure difference. The minimum flow rate for these fans within the calibrated range is 18 L/s. The accuracy of the fans is specified as $\pm 5\%$ of the flow rate, or $\pm 3\%$ if Retrotec software is used, which it was for this testing. The difference between the Q4E system and the Q5E system is that they use a fabric and hard-panel door respectively. The fabric door provides a better seal within the door frame so was selected for the testing fan; however, the hard panel door is easier to set-up and move so was used for the neutralizing fans where leakage through the fan-door would not impact the test results.

These fans were controlled using Retrotec DM-2 Series 2 Channel Digital Pressure Gauges which have two auto-zeroing digital micromanometers built in to measure the fan flow pressure (used to determine flow rate) and the pressure difference between the test zone and adjacent zones. These gauges are designed for use with the Retrotec fans and are preprogrammed with the calibration equations to determine flow rates through the fans. The gauges also provide the ability to use time averaging over various different periods to overcome fluctuations in pressure measurements. The relevant specifications of these gauges are:

- Range: -1250 Pa to +1250 Pa
- Resolution: 0.1 Pa
- Accuracy: 1% of pressure reading or 0.15 Pa (whichever is greater)

The measurement data from the test fan was recorded using Retrotec’s testing software, Fantestic 5.2.115. This software allows for recording of the readings made by the DM-2 gauge over user specified time periods.

D-3 Test Conditions

Airtightness testing was performed on the following days:

- Pre-Retrofit
 - July 4, 2013 – Floor 11 Suites
 - July 5, 2013 – Floor 3 Suites
 - July 6, 2013 – Corridor 11, and Floor 13 Suite
 - July 9, 2013 – Corridor 3, Floor 1 Suites, and Floor 1 Whole Floor
- Post-Retrofit
 - February 4, 2013 – Floor 11 Suites, Floor 13 Suites, and Floor 13 Whole Floor
 - February 5, 2013 – Floor 3 Suites, Floor 1 Suites, and Floor 1 Whole Floor
 - February 6, 2013 – Corridor 9

The exterior conditions on these days are summarized in Table D-4.

Table D-4: Exterior Conditions during Airtightness Testing

Date [yyyy/mm/dd]	Temperature [°C]	Wind Speed [km/hr]	Wind Direction [°, 0 is North]
2012/07/04	17	9	270
2012/07/05	18	7	270
2012/07/06	21	7	250
2012/07/09	13	9	180
2013/02/04	7	10	130
2013/02/05	7	12	140
2013/02/06	7	14	120

D-4 Door Undercut Measurements

Door undercut measurements and observations of weather stripping were made at a variety of doors throughout the case study building to gain an understanding of the typical door conditions in the building and to allow for comparison with airtightness testing results. The results of this survey are provided graphically in Figure D-11 and Figure D-12, and are also tabulated in Table D-5 and Table D-6.

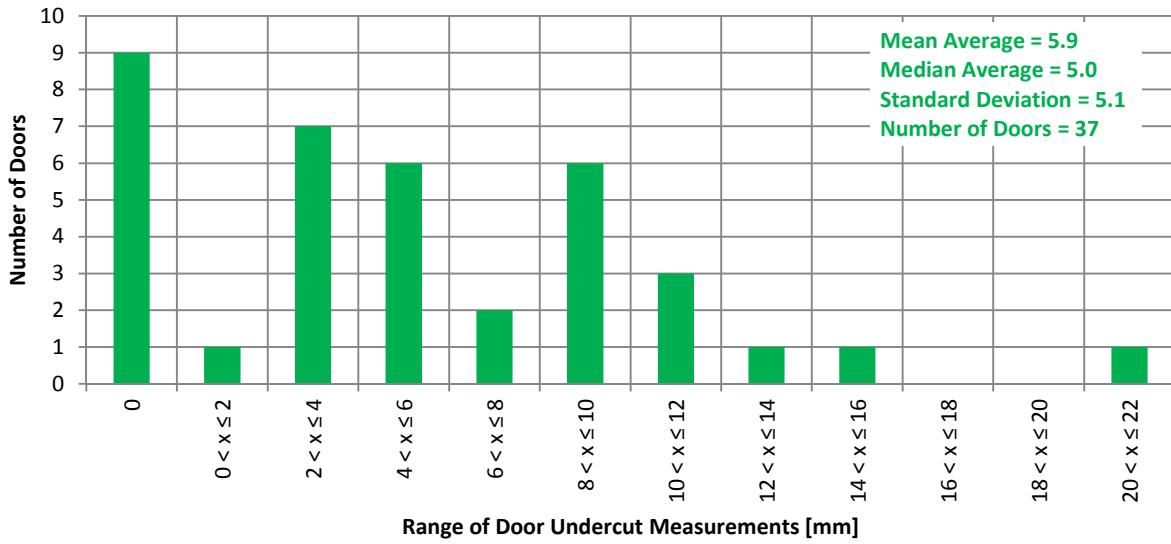


Figure D-11: Chart of distribution of suite entrance door undercut measurements

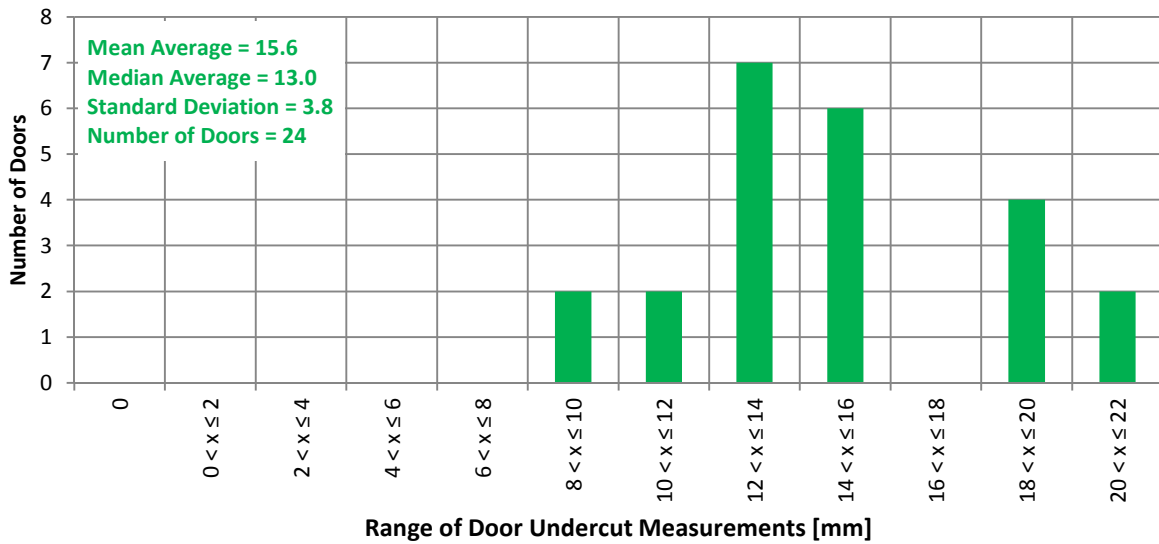


Figure D-12: Chart of distribution of stairwell door undercut measurements

Appendix D Supplementary Airtightness Testing Information

Table D-5: Results of Suite Entrance Door Undercut and Weather Stripping Survey

Suite	Door Undercut [mm]	Notes
101	14	Weather stripped on sides and top, but falling off on top. No weather stripping on bottom.
102	5	Weather stripped on sides and top. Maybe weather stripped on bottom.
201	8	Maybe weather stripped bottom. No weather stripping on sides and top.
202	4	No weather stripping.
203	0	All sides weather stripped.
301	11	No weather stripping.
302	4	No weather stripping.
303	9	No weather stripping.
401	5	No weather stripping.
402	6	No weather stripping.
403	10	No weather stripping.
501	10	No weather stripping.
502	10	No weather stripping.
503	6	No weather stripping.
601	0	Weather stripping on bottom.
602	3	No weather stripping.
603	2	No weather stripping.
701	0	Weather stripping on bottom.
702	10	No weather stripping. Carpet in undercut reducing effectiveness.
703	15	No weather stripping. Rubber piece in sill reducing effectiveness.
801	0	Weather stripping on bottom.
802	0	No weather stripping, but door fits snug.
803	6	No weather stripping.
901	22	No weather stripping.
902	3	Weather stripping on left jamb from door handle to ground.
903	3	Weather stripping on bottom.
1001	0	Weather stripping on bottom.
1002	5	No weather stripping.
1003	3	No weather stripping.
1101	0	Weather stripping on bottom.
1102	9	No weather stripping.
1103	4	No weather stripping.
1201	12	No weather stripping.
1202	0	Weather stripping on bottom.
1203	12	No weather stripping.
1301	0	No weather stripping, but door fits snug.
1302	8	No weather stripping.

Table D-6: Results Stairwell Door Undercut and Weather Stripping Survey

Stairwell	Door Undercut [mm]	Notes
1st Stair - West	19	No weather stripping.
2nd Stair - East	21	No weather stripping.
2nd Stair - West	10	No weather stripping.
3rd Stair - East	14	No weather stripping.
3rd Stair - West	15	No weather stripping.
4th Stair - East	25	No weather stripping.
4th Stair - West	13	No weather stripping.
5th Stair - East	16	No weather stripping.
5th Stair - West	13	No weather stripping.
6th Stair - East	13	No weather stripping.
6th Stair - West	19	No weather stripping.
7th Stair - East	13	No weather stripping.
7th Stair - West	10	No weather stripping.
8th Stair - East	19	No weather stripping.
8th Stair - West	16	No weather stripping.
9th Stair - East	19	No weather stripping.
9th Stair - West	13	No weather stripping.
10th Stair - East	16	No weather stripping.
10th Stair - West	19	No weather stripping.
11th Stair - East	16	No weather stripping.
11th Stair - West	22	No weather stripping.
12th Stair - West	14	No weather stripping.
12th Stair - East	16	No weather stripping.
13th Stair - East	11	No weather stripping.
13th Stair - West	12	No weather stripping.

D-5 Comparison of Demising Wall Tests

Each of the demising walls was tested twice (once for each suite bounded by the wall), it is possible to compare the results for each wall. The results of the different tests are provided Figure D-11 and Figure D-12.

Appendix D Supplementary Airtightness Testing Information

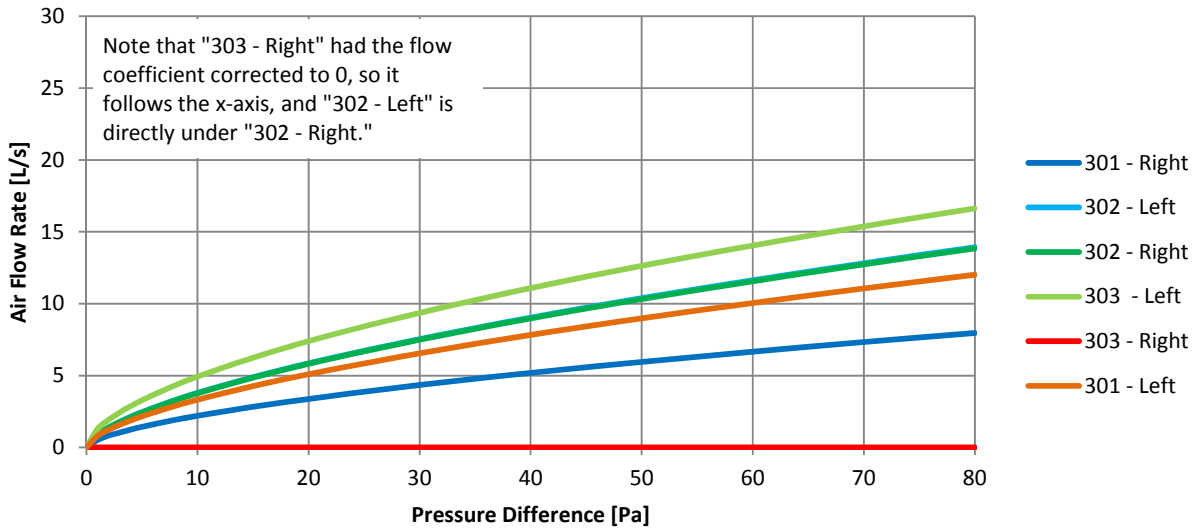


Figure D-13: Graph of airflow versus pressure difference relationships for the suite demising wall airtightness testing on Floor 3

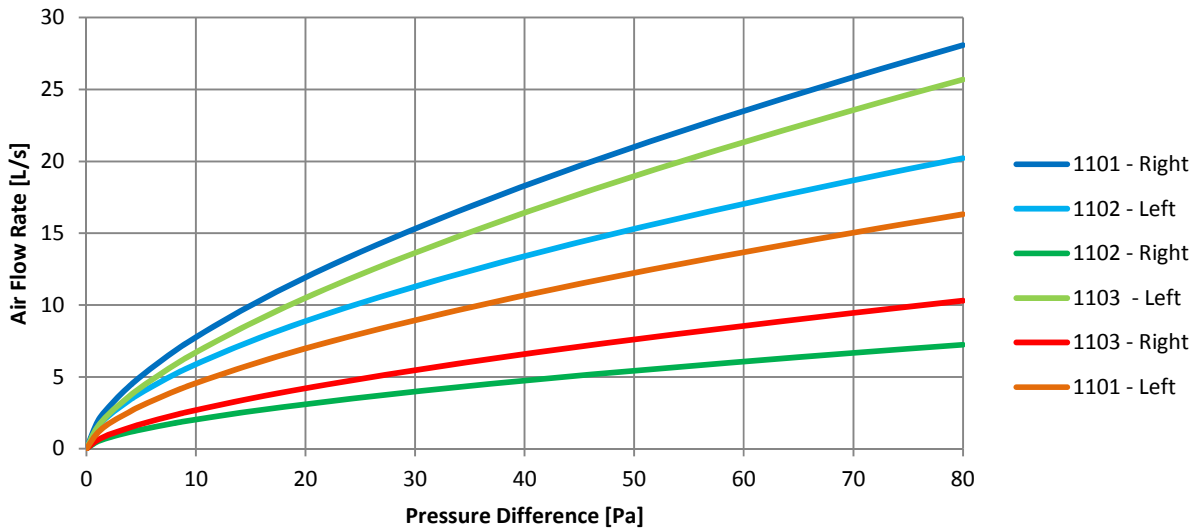


Figure D-14: Graph of airflow versus pressure difference relationships for the suite demising wall airtightness testing on Floor 11

These figures show a discrepancy in the results of the different tests; however, it is important to note the quantities of airflow are relatively low. Consequently, even what appears to be a fairly large difference between tests is actually relatively small compared the total measured airflow in to or out of the suite during testing. The largest difference between the testing pairs is between "1102-Right" and "1103-Left" and is approximately 17 L/s at 75 Pa. For reference, the total average

airflow rate of the typical suite when pressurized by 75 Pa relative to adjacent zones and the exterior was determined to be 564 L/s and 391 L/s pre- and post-retrofit respectively.

Likely the observed discrepancies are because these measurements are determined by the difference between two airtightness tests which measure much higher flow rates, so even a relatively minor error in those measurements could create an error that is significant to the demising wall airflow measurements. This is a noteworthy limitation of the sequentially neutralized airtightness testing technique. These potential errors are somewhat mitigated by using averages of the results of multiple different tests.

Note that the flow coefficient of “303 – Right” was determined to be negative which is not possible, so it was manually corrected to zero, which is also unlikely to be correct. The important finding for this and other demising wall measurements is that the flow rate through these boundaries are relatively low.

D-6 Detailed Results

Correlations were developed based on the airtightness testing data to determine the flow coefficient and flow exponent for each of the testing steps. By rearranging Eq. 3.2, Eq. 2.5 can be developed which shows a linear relationship between $\log(\Delta P)$ and $\log(Q_{\Delta P})$. The slope of this line is the flow exponent and the intercept is $\log(C)$.

$$\log Q_{\Delta P} = n \cdot \log \Delta P + \log C \quad \text{Eq. C-1}$$

Where: $Q_{\Delta P}$ = Airflow at ΔP [m^3/s]
C = Flow Coefficient [$\text{m}^3/\text{s} \cdot \text{Pa}^n$]
 ΔP = Pressure Difference [Pa]
n = Flow Exponent [dimensionless]

Using this linear relationship, correlations were developed for each test step, and thus the flow exponent and flow coefficient were determined. The quality of the fit between the linear equation and the test data is measured using R-squared where unity indicates an exact correlation. The flow coefficient, flow exponent, and R-squared determined from each set of test data are provided in Table D-7, Table D-8, and Table D-9.

Table D-7: Airtightness Testing Results from Correlation for Typical Suites

Test Zone	Pressurize/ Depressurize	Step 1						Step 2						Step 3						Step 4						Step 5						Step 6					
		Flow Coefficient, C [L/s-Pa ⁿ]	Flow Exponent, n	R ²	Flow Coefficient, C [L/s-Pa ⁿ]	Flow Exponent, n	R ²	Flow Coefficient, C [L/s-Pa ⁿ]	Flow Exponent, n	R ²	Flow Coefficient, C [L/s-Pa ⁿ]	Flow Exponent, n	R ²	Flow Coefficient, C [L/s-Pa ⁿ]	Flow Exponent, n	R ²	Flow Coefficient, C [L/s-Pa ⁿ]	Flow Exponent, n	R ²	Flow Coefficient, C [L/s-Pa ⁿ]	Flow Exponent, n	R ²	Flow Coefficient, C [L/s-Pa ⁿ]	Flow Exponent, n	R ²	Flow Coefficient, C [L/s-Pa ⁿ]	Flow Exponent, n	R ²	Flow Coefficient, C [L/s-Pa ⁿ]	Flow Exponent, n	R ²						
Pre-Retrofit	Suite 301	28.6	0.62	1.000	26.1	0.62	1.000	22.2	0.64	1.000	20.3	0.62	0.999	20.3	0.62	0.999	20.3	0.62	0.999	20.3	0.62	0.999	20.3	0.62	0.999	20.3	0.62	0.999	24.0	0.57	0.999						
	Depressurized	25.8	0.62	1.000	26.1	0.60	1.000	23.8	0.58	0.999	19.8	0.60	1.000	19.8	0.60	1.000	21.6	0.57	1.000	21.6	0.57	1.000	21.6	0.57	1.000	21.6	0.57	1.000	27.2	0.50	0.998						
	Pressurized	27.9	0.64	0.996	21.9	0.68	0.998	19.3	0.69	0.999	15.3	0.68	1.000	15.3	0.68	1.000	12.5	0.72	0.992	12.5	0.72	0.992	12.5	0.72	0.992	12.5	0.72	0.992	13.8	0.68	0.995						
	Depressurized	27.1	0.61	1.000	21.4	0.69	0.996	24.9	0.59	0.999	14.6	0.63	0.999	14.6	0.63	0.999	12.4	0.66	0.999	12.4	0.66	0.999	12.4	0.66	0.999	12.4	0.66	0.999	13.6	0.62	0.999						
	Pressurized	38.7	0.56	1.000	43.9	0.52	0.996	33.1	0.57	1.000	30.5	0.56	0.999	30.5	0.56	0.999	28.6	0.57	1.000	28.6	0.57	1.000	28.6	0.57	1.000	28.6	0.57	1.000	30.8	0.54	1.000						
	Depressurized	31.1	0.61	1.000	34.0	0.58	0.998	24.9	0.62	1.000	24.4	0.58	1.000	24.4	0.58	1.000	20.8	0.62	1.000	20.8	0.62	1.000	20.8	0.62	1.000	20.8	0.62	1.000	21.0	0.61	1.000						
	Pressurized	33.6	0.60	0.998	28.1	0.61	1.000	22.8	0.64	0.998	22.6	0.62	0.999	22.6	0.62	0.999	27.5	0.54	0.998	27.5	0.54	0.998	27.5	0.54	0.998	27.5	0.54	0.998	29.7	0.52	0.999						
	Depressurized	28.0	0.63	0.999	36.0	0.55	1.000	36.1	0.52	0.999	36.1	0.52	0.999	36.1	0.52	0.999	32.5	0.50	0.988	32.5	0.50	0.988	32.5	0.50	0.988	32.5	0.50	0.988	31.4	0.49*	0.996						
	Pressurized	62.7	0.61	0.999	56.6	0.60	0.999	49.2	0.62	1.000	54.4	0.52	0.996	54.4	0.52	0.996	57.8	0.50	0.996	57.8	0.50	0.996	57.8	0.50	0.996	57.8	0.50	0.996	56.2	0.49*	0.996						
	Depressurized	54.5	0.61	1.000	50.7	0.60	1.000	51.8	0.57	1.000	51.8	0.48*	0.980	51.8	0.48*	0.980	45.0	0.50	0.990	45.0	0.50	0.990	45.0	0.50	0.990	45.0	0.50	0.990	42.6	0.48*	0.979						
	Pressurized	34.3	0.64	1.000	30.3	0.65	1.000	26.9	0.68	1.000	43.9	0.53	0.998	43.9	0.53	0.998	45.0	0.52	1.000	45.0	0.52	1.000	45.0	0.52	1.000	45.0	0.52	1.000	42.6	0.53	0.999						
	Depressurized	30.2	0.65	1.000	34.9	0.57	0.992	19.6	0.67	0.999	19.6	0.64	0.996	19.6	0.64	0.996	21.0	0.67	0.997	21.0	0.67	0.997	21.0	0.67	0.997	21.0	0.67	0.997	25.0	0.55	1.000						
Suite 301	Pressurized	-	-	-	-	-	-	-	-	-	-	-	-	-	-	-	-	-	-	-	-	-	-	-	-	-	-	-	-	-							
Suite 302	Pressurized	-	-	-	-	-	-	-	-	-	-	-	-	-	-	-	-	-	-	-	-	-	-	-	-	-	-	-	-	-	-						
Suite 303	Pressurized	-	-	-	-	-	-	-	-	-	-	-	-	-	-	-	-	-	-	-	-	-	-	-	-	-	-	-	-	-	-						
Suite 1101	Pressurized	-	-	-	-	-	-	-	-	-	-	-	-	-	-	-	-	-	-	-	-	-	-	-	-	-	-	-	-	-	-						
Suite 1102	Pressurized	-	-	-	-	-	-	-	-	-	-	-	-	-	-	-	-	-	-	-	-	-	-	-	-	-	-	-	-	-	-						
Suite 1103	Pressurized	-	-	-	-	-	-	-	-	-	-	-	-	-	-	-	-	-	-	-	-	-	-	-	-	-	-	-	-	-	-						
Suite 1103	Depressurized	-	-	-	-	-	-	-	-	-	-	-	-	-	-	-	-	-	-	-	-	-	-	-	-	-	-	-	-	-	-						

*Flow exponents less than 0.5 are theoretically impossible and may indicate an error in the test.

Table D-8: Airtightness Testing Results from Correlation for Atypical Suites and Floors

Atypical Suite and Floor Airtightness Testing Results					
	Test Zone	Pressurize/ Depressurize	Step 1		
			Flow Coefficient, C [L/s·Pa ⁿ]	Flow Exponent, n	R ²
Pre-Retrofit	Suite 101	Pressurized	30.0	0.59	0.999
		Depressurized	23.2	0.65	1.000
	Suite 102	Pressurized	29.0	0.56	0.992
		Depressurized	20.9	0.63	0.994
	Suite 1301	Pressurized	36.6	0.74	1.000
		Depressurized	90.3	0.56	1.000
	Suite 1302	Pressurized	133.8	0.52	1.000
		Depressurized	70.1	0.63	1.000
	Floor 01	Pressurized	97.7	0.72	0.999
		Depressurized	185.8	0.53	1.000
Floor 13	Pressurized	-	-	-	
	Depressurized	-	-	-	
Post-Retrofit	Suite 101	Pressurized	23.9	0.56	1.000
		Depressurized	7.8	0.79	0.993
	Suite 102	Pressurized	9.9	0.67	0.998
		Depressurized	6.0	0.69	0.993
	Suite 1301	Pressurized	14.8	0.77	0.991
		Depressurized	42.7	0.57	0.977
	Suite 1302	Pressurized	15.8	0.72	0.972
		Depressurized	40.6	0.47	0.993
	Floor 01	Pressurized	118.7	0.59	1.000
		Depressurized	79.2	0.62	1.000
Floor 13	Pressurized	27.5	0.95	0.999	
	Depressurized	247.4	0.47*	0.993	

*Flow exponents less than 0.5 are theoretically impossible and may indicate an error in the test.

Table D-9: Airtightness Testing Results from Correlation for Corridor

Corridor Compartmentalizing Elements Airtightness Testing Results									
Testing Step	Corridor 03			Corridor 09			Corridor 11		
	Flow Coefficient, C [L/s·Pa ⁿ]	Flow Exponent, n	R ²	Flow Coefficient, C [L/s·Pa ⁿ]	Flow Exponent, n	R ²	Flow Coefficient, C [L/s·Pa ⁿ]	Flow Exponent, n	R ²
Step 1	137.2	0.52	0.998	78.9	0.67	0.999	86.2	0.65	1.000
Step 2	81.6	0.60	1.000	191.9	0.44*	0.999	120.4	0.53	0.999
Step 3	130.4	0.51	0.999	32.2	0.85	0.996	100.3	0.61	0.999
Step 4	77.3	0.60	1.000	130.5	0.50	0.999	147.4	0.49*	1.000
Step 5	145.7	0.50	0.999	57.7	0.73	0.998	98.7	0.60	1.000
Step 6	91.7	0.57	1.000	184.4	0.43*	0.983	132.5	0.50	0.999
Step 7	110.3	0.56	0.999	62.5	0.70	1.000	133.6	0.54	0.997
Step 8	92.0	0.56	0.999	160.4	0.47*	0.999	119.5	0.55	1.000
Step 9	47.9	0.59	0.999	26.0	0.83	0.999	46.6	0.66	1.000
Step 10	46.4	0.58	1.000	74.9	0.54	0.999	68.3	0.57	1.000
Step 11	82.0	0.60	1.000	65.6	0.69	0.997	102.1	0.59	1.000
Step 12	72.7	0.58	1.000	128.4	0.48*	0.995	110.8	0.55	1.000
Step 13	110.7	0.56	1.000	-	-	-	112.9	0.58	0.998
Step 14	97.0	0.56	1.000	-	-	-	138.4	0.50	0.996
Step 15	104.6	0.57	1.000	88.6	0.64	0.999	96.0	0.63	1.000
Step 16	99.8	0.55	1.000	145.9	0.48*	0.998	137.4	0.50	1.000
Step 17	100.4	0.59	0.999	69.7	0.68	0.996	138.5	0.51	1.000
Step 18	106.8	0.54	0.999	168.3	0.47*	1.000	89.2	0.64	0.999
Step 19	93.9	0.61	0.999	52.9	0.76	0.992	137.9	0.50	0.999
Step 20	107.4	0.54	1.000	159.3	0.48	0.998	105.4	0.60	0.998
Step 1'	102.5	0.59	1.000	-	-	-	116.4	0.60	0.999
Step 2'	106.4	0.54	0.999	-	-	-	134.8	0.54	1.000

*Flow exponents less than 0.5 are theoretically impossible and may indicate an error in the test.

In some cases flow exponents less than 0.5 were determined. Theoretically these values are impossible as they are below the value for completely turbulent flow used in Eq. 2.1 as discussed in Section 2.4. At this point, these results will be accepted and used for determination of the flow characteristics for each compartmentalizing element.

In some cases points that were readily identifiable as errors were removed from the data set during analysis. These were often the result of occupant behaviour during the tests such as elevator use or opening/closing suite entrance doors. While effort was made during testing to avoid these disturbances, it was not possible to control all parameters at all times, and in some cases this variability is apparent in the results, and these points were removed.

The flow characteristics for each compartmentalizing element were determined by finding the difference in flow rates between the various steps. Once the difference in flow rate was determined, a flow coefficient and flow exponent value for each compartmentalizing element was determined. In cases where the flow exponent was determined to be less than 0.5 or greater than 1.0, it was adjusted to the value of the flow exponent for the "All 6 Sides" test since this is the average for the zone pressure boundary as a whole. This adjusted flow exponent was then used to manually calculate the flow coefficient so that it would create the same flow rate at 75 Pa. This procedure was selected because generally the flow measurements were most consistent at higher

pressure differences, while at lower pressure differences the results were more variable. In some cases the measurement made at the lowest test pressure appeared anomalous and was removed. This is likely because the pressure difference at these low levels may not be sufficient to significantly outweigh any natural variability in pressure differences due to wind and stack effect.

In general, the adjustment of these flow exponents does create some error in the testing results; however, generally flow exponents outside of the theoretically possible range were determined when the difference in flow rates between steps was very low relative to the total flow rate being measured. This is because even a slight error in the measurements would significantly alter the difference between measurements and cause errors in the flow exponent. The important conclusion of these tests is that the flow rate is low compared to flow through other elements, and the adjustment of the flow exponent does not substantially impact the magnitude of the determined flow. The flow coefficient, flow exponent, and a variety of other common metrics are provided for each compartmentalizing element and exterior enclosure section that was tested in Table D-10 to Table D-14. Note that values provided for the stairwell doors and elevator doors are for two doors each.

Table D-10: Airtightness Testing Results – Floor 3 Suites

Airtightness Testing Results - Floor 3 Suites																		
Suite Type	Suite	Adjacent Zone	Flow Coefficient, C [L/s·Pa ^{0.5}]	Flow Exponent, n	Area [m ²]	Volume [m ³]	Q ₅₀ [L/s]	Q ₇₅ [L/s]	Normalized Flow Coefficient, C _N [L/s·Pa ^{0.5} ·m ²]	q ₅₀ [L/s·m ²]	q ₇₅ [L/s·m ²]	EQLA (Cd = 0.61 ΔP _{ref} = 10 Pa) [cm ²]	EFLA (Cd = 1.0 ΔP _{ref} = 4 Pa) [cm ²]	SLA _{eq} (Cd = 0.61 ΔP _{ref} = 10 Pa) [cm ² /100 m ²]	SLA _{ref} (Cd = 1.0 ΔP _{ref} = 4 Pa) [cm ² /100 m ²]	ACH ₅₀ [1/h]	ACH ₇₅ [1/h]	
Suite 301		Suite Above	1.6	0.75	126	307	30	40	0.012	0.24	0.32	35	17	28	14	0.35	0.47	
		Suite Below	3.2	0.60	126	307	34	43	0.025	0.27	0.34	52	29	41	23	0.40	0.51	
		Corridor	2.1	0.69	14	307	31	41	0.151	2.22	2.93	41	21	295	152	0.36	0.48	
		Suite to Right	0.5	0.62	18	307	6	8	0.030	0.33	0.43	9	5	50	27	0.07	0.09	
		Suite to Left	0.8	0.62	19	307	9	12	0.04	0.46	0.60	13	7	69	38	0.11	0.14	
		Exterior Enclosure - Pre-Retrofit	24.3	0.55	84	307	209	261	0.29	2.47	3.09	346	201	410	239	2.45	3.06	
		Exterior Enclosure - Post-Retrofit	6.9	0.67	84	307	97	127	0.08	1.15	1.51	132	68	156	81	1.14	1.49	
	Suite 302		Suite Above	1.5	0.64	122	298	19	24	0.01	0.15	0.20	27	14	22	12	0.23	0.29
			Suite Below	5.1	0.59	122	298	51	65	0.04	0.42	0.53	80	45	65	37	0.62	0.79
			Corridor	5.2	0.67	26	298	72	95	0.20	2.78	3.65	98	51	378	197	0.87	1.15
		Suite to Right	0.9	0.63	18	298	10	13	0.05	0.58	0.75	15	8	85	46	0.12	0.16	
		Suite to Left	0.9	0.63	18	298	10	13	0.05	0.58	0.75	15	8	86	47	0.13	0.16	
		Exterior Enclosure - Pre-Retrofit	13.7	0.65	71	298	175	228	0.19	2.48	3.23	247	131	350	186	2.12	2.75	
		Exterior Enclosure - Post-Retrofit	6.8	0.71	71	298	108	144	0.10	1.53	2.04	139	70	197	99	1.30	1.74	
Suite 303			Suite Above	1.5	0.59	126	307	14	18	0.01	0.11	0.14	22	13	18	10	0.17	0.21
			Suite Below	3.5	0.59	126	307	34	44	0.03	0.27	0.35	54	30	43	24	0.40	0.51
			Corridor	2.1	0.76	14	307	41	57	0.15	2.98	4.07	49	23	351	168	0.49	0.66
		Suite to Right	0.0	0.59	19	307	0	0	0.00	0.00	0.00	0	0	0	0	0.00	0.00	
		Suite to Left	1.3	0.59	18	307	13	16	0.07	0.71	0.90	20	11	111	63	0.15	0.19	
		Exterior Enclosure - Pre-Retrofit	25.9	0.58	84	307	248	313	0.31	2.94	3.71	393	223	466	265	2.91	3.67	
	Exterior Enclosure - Post-Retrofit	7.6	0.61	84	307	83	106	0.09	0.98	1.26	125	69	148	81	0.97	1.25		

Table D-11: Airtightness Testing Results – Floor 11 Suites

Airtightness Testing Results - Floor 11 Suites																	
Suite Type	Suite	Adjacent Zone	Flow Coefficient, C [L/s·Pa ^{1/n}]	Flow Exponent, n	Area [m ²]	Volume [m ³]	Q ₅₀ [L/s]	Q ₇₅ [L/s]	Normalized Flow Coefficient, C _n [L/s·Pa ⁿ ·m ²]	q ₅₀ [L/s·m ²]	q ₇₅ [L/s·m ²]	E _{qLA} (Cd = 0.61 ΔP _{ref} = 10 Pa) [cm ²]	E _{FLA} (Cd = 1.0 ΔP _{ref} = 4 Pa) [cm ²]	SLA _{req} (Cd = 0.61 ΔP _{ref} = 10 Pa) [cm ² /100 m ²]	SLA _{def} (Cd = 1.0 ΔP _{ref} = 4 Pa) [cm ² /100 m ²]	ACH ₅₀ [1/h]	ACH ₇₅ [1/h]
Floor 11 Suites	Suite 1101	Suite Above	4.6	0.58	126	307	44	56	0.04	0.35	0.45	70	40	56	32	0.52	0.66
		Suite Below	2.0	0.73	126	307	34	46	0.02	0.27	0.37	43	21	34	17	0.40	0.54
		Corridor	1.7	0.76	14	307	34	46	0.12	2.42	3.29	40	19	285	137	0.39	0.54
		Suite to Right	1.9	0.62	18	307	21	27	0.11	1.18	1.52	31	17	175	96	0.25	0.32
		Suite to Left	1.1	0.61	19	307	12	16	0.06	0.63	0.81	18	10	95	52	0.14	0.18
		Exterior Enclosure - Pre-Retrofit	23.2	0.57	84	307	220	277	0.28	2.61	3.29	350	199	415	236	2.58	3.25
	Suite 1102	Exterior Enclosure - Post-Retrofit	9.6	0.66	84	307	127	165	0.11	1.50	1.96	176	93	209	110	1.48	1.94
		Suite Above	5.1	0.69	122	298	76	100	0.04	0.62	0.82	100	51	82	42	0.91	1.21
		Suite Below	2.5	0.79	122	298	56	77	0.02	0.46	0.63	62	29	51	24	0.67	0.93
		Corridor	12.5	0.61	26	298	136	175	0.48	5.25	6.72	205	113	789	435	1.65	2.11
		Suite to Right	0.5	0.61	18	298	5	7	0.03	0.31	0.39	8	5	46	25	0.07	0.08
		Suite to Left	1.5	0.59	18	298	15	19	0.08	0.86	1.09	24	13	133	74	0.18	0.24
	Suite 1103	Exterior Enclosure - Pre-Retrofit	32.5	0.61	71	298	354	453	0.46	5.02	6.43	532	293	754	416	4.28	5.48
		Exterior Enclosure - Post-Retrofit	17.8	0.50	71	298	124	151	0.25	1.75	2.14	224	137	317	194	1.49	1.83
		Suite Above	4.8	0.59	126	307	48	61	0.04	0.38	0.49	75	42	60	33	0.56	0.72
		Suite Below	1.7	0.65	126	307	21	27	0.01	0.17	0.22	30	16	24	13	0.25	0.32
		Corridor	2.6	0.80	14	307	59	82	0.18	4.26	5.91	65	30	469	217	0.70	0.96
		Suite to Right	0.6	0.65	19	307	8	10	0.03	0.39	0.51	11	6	56	30	0.09	0.12
Exterior Enclosure - Pre-Retrofit	Suite to Left	1.5	0.65	18	307	19	25	0.09	1.07	1.38	27	14	151	81	0.22	0.29	
	Exterior Enclosure - Post-Retrofit	33.8	0.54	84	307	276	343	0.40	3.27	4.07	467	275	554	327	3.24	4.03	
Exterior Enclosure - Post-Retrofit	11.2	0.62	84	307	126	162	0.13	1.49	1.92	187	102	222	121	1.48	1.90		

Table D-12: Airtightness Testing Results – Floor 1 and Floor 13 Suites

Airtightness Testing Results - Floor 1 and Floor 13 Suites																	
Suite Type	Suite	Adjacent Zone	Flow Coefficient, C [L/s·Pa ⁿ]	Flow Exponent, n	Area [m ²]	Volume [m ³]	Q ₅₀ [L/s]	Q ₇₅ [L/s]	Normalized Flow Coefficient, C _N [L/s·Pa ⁿ ·m ²]	q ₅₀ [L/s·m ²]	q ₇₅ [L/s·m ²]	EQLA (Cd = 0.61 ΔP _{ref} = 10 Pa) [cm ²]	EFLA (Cd = 1.0 ΔP _{ref} = 4 Pa) [cm ²]	SLA _{req} (Cd = 0.61 ΔP _{ref} = 10 Pa) [cm ² /100 m ²]	SLA _{ref} (Cd = 1.0 ΔP _{ref} = 4 Pa) [cm ² /100 m ²]	ACH ₅₀ [1/h]	ACH ₇₅ [1/h]
1st Floor Suites	Suite 101	Exterior Enclosure - Pre-Retrofit	26.6	0.62	217	307	299	384	0.12	1.38	1.77	444	243	205	112	3.51	4.51
		Exterior Enclosure - Post-Retrofit	15.8	0.67	217	307	219	288	0.07	1.01	1.33	299	156	138	72	2.57	3.38
	Suite 102	Exterior Enclosure - Pre-Retrofit	25.0	0.60	195	298	259	329	0.13	1.33	1.69	397	221	204	114	3.13	3.98
		Exterior Enclosure - Post-Retrofit	8.0	0.68	195	298	112	147	0.04	0.58	0.76	152	79	78	40	1.35	1.78
13th Floor Suites	Suite 1301	Exterior Enclosure - Pre-Retrofit	63.4	0.65	260	371	802	1043	0.24	3.09	4.02	1134	604	437	233	7.78	10.12
		Exterior Enclosure - Post-Retrofit	28.7	0.67	260	371	399	523	0.11	1.54	2.02	542	283	209	109	3.87	5.08
	Suite 1302	Exterior Enclosure - Pre-Retrofit	102.0	0.58	260	371	968	1223	0.39	3.73	4.71	1540	877	593	338	9.40	11.87
		Exterior Enclosure - Post-Retrofit	28.17	0.60	260	371	291	371	0.11	1.12	1.43	447	250	172	96	2.82	3.60

Table D-13: Airtightness Testing Results – Average of Typical Suites (Floors 3 and 11)

Airtightness Testing Results - Average of Typical Suites																	
Suite Type	Suite	Adjacent Zone	Flow Coefficient, C [L/s·Pa ⁿ]	Flow Exponent, n	Area [m ²]	Volume [m ³]	Q ₅₀ [L/s]	Q ₇₅ [L/s]	Normalized Flow Coefficient, C _N [L/s·Pa ⁿ ·m ²]	q ₅₀ [L/s·m ²]	q ₇₅ [L/s·m ²]	EQLA (Cd = 0.61 ΔP _{ref} = 10 Pa) [cm ²]	EFLA (Cd = 1.0 ΔP _{ref} = 4 Pa) [cm ²]	SLA _{req} (Cd = 0.61 ΔP _{ref} = 10 Pa) [cm ² /100 m ²]	SLA _{ref} (Cd = 1.0 ΔP _{ref} = 4 Pa) [cm ² /100 m ²]	ACH ₅₀ [1/h]	ACH ₇₅ [1/h]
Typical Suites	Average	Suite Above	3.18	0.64	125	304	38	50	0.026	0.31	0.40	55	30	44	24	0.46	0.59
		Suite Below	2.99	0.66	125	304	38	50	0.024	0.31	0.41	53	28	43	23	0.46	0.60
		Corridor	4.36	0.72	18	304	62	82	0.215	3.32	4.43	83	43	428	217	0.74	0.98
		Suite to Right	0.73	0.62	18	304	8	11	0.041	0.47	0.60	12	7	69	37	0.10	0.13
		Suite to Left	1.19	0.61	18	304	13	17	0.065	0.72	0.92	20	11	107	59	0.16	0.20
		Exterior Enclosure - Pre-Retrofit	25.56	0.58	80	304	247	312	312	0.321	3.13	3.97	389	221	492	278	2.93
Exterior Enclosure - Post-Retrofit	9.99	0.63	80	304	111	143	143	0.128	1.40	1.81	164	90	208	115	1.31	1.69	

Table D-14: Airtightness Testing Results - Corridors

Corridor Airtightness Testing			
Zone	Adjacent Zone	Flow Coefficient, C [L/s·Pa ⁿ]	Flow Exponent, n
Corridor 03	Door 301	7.9	0.56
	Door 302	3.4	0.58
	Door 303	4.2	0.64
	Elevator Doors (2)	59.6	0.54
	Stairwell Doors (2)	42.5	0.53
	Electrical Closet Door	2.0	0.56
	Garbage Chute Door	4.7	0.56
	Floor Above	1.7	0.56
	Floor Below	0.0	0.56
	Remaining	8.1	0.56
	Corridor 09	Door 901	16.8
Door 902		6.4	0.61
Door 903		8.6	0.55
Elevator Doors (2)		51.8	0.55
Stairwell Doors (2)		47.3	0.55
Electrical Closet Door		0.0	n/a
Garbage Chute Door		10.9	0.55
Floor Above		6.5	0.50
Floor Below		2.2	0.55
Remaining		-10.3	0.55
Corridor 11		Door 1101	2.4
	Door 1102	9.5	0.72
	Door 1103	8.0	0.58
	Elevator Doors (2)	54.0	0.58
	Stairwell Doors (2)	32.8	0.58
	Electrical Closet Door	4.0	0.73
	Garbage Chute Door	1.3	0.68
	Floor Above	1.4	0.68
	Floor Below	3.1	0.58
	Remaining	-4.2	0.58
	Average	Suite Doors (3)	22.4
Elevator Doors (2)		55.2	0.56
Stairwell Doors (2)		40.9	0.55
Electrical Closet Door		3.0	0.64
Garbage Chute Door		5.6	0.60
Floor Above		3.2	0.58
Floor Below		1.8	0.56
Remaining		-2.2	0.57

Appendix E Supplementary Monitoring Information

Long-term monitoring of the case study building was implemented to quantify in service performance characteristics including pressure differences, temperature, relative humidity, carbon dioxide concentrations, and exterior environmental conditions as discussed in Section 7.5. The sensor types used are listed in Table E-1. The naming convention for each sensor is provided in Table E-2. In some limited cases the sensors and data acquisition units do not follow this convention, and in these cases the meaning of the names are readily apparent. The name, location, and attached sensors for each data acquisition unit are provided in Table E-3. The specifications for the data acquisition units and sensors are provided in Section E-2. Note that the dew point temperature sensors are virtual sensors calculated from temperature and relative humidity.

Table E-1: Sensor Types

Sensor Type	Type
CO ₂	COZIR 5000PPM
Pressure	All Sensor 0.25" DS 0032
SMT-A2 & SMT-A3 Built-in Temperature	Cantherm MF58
SMT-A2 & SMT-A3 Built-in Relative Humidity	Honeywell HIH-4000-001
External Temperature Sensors on Leads	Cantherm MF52 Thermistor
Temperature and Relative Humidity	Measurement Specialties HTM25X0LF
Weather Station	Davis Vantage Pro2 with Solar Radiation Sensor

Table E-2: Sensor Naming Convention

"Sensor Type"		-	"Zone"		-	"Location in Zone"	
TEMP	Temperature		####	Suite Number as #### or Corridor Number as ##00		ED	Near Entrance Door
RH	Relative Humidity					LR	Living Room
CO2	Carbon Dioxide Concentration		WS	Weather Station		MBR	Master Bedroom
PRES	Relative Pressure Difference					CO	Corridor
DP	Dew Point Temperature						

Table E-3: Index of Data Acquisition Units

Name	Location	Measurements
0201 - ED	Suite 201 - Near Entrance Door	Temperature, Relative Humidity, Carbon dioxide, Pressure to Corridor
0202 - ED	Suite 202 - Near Entrance Door	Temperature, Relative Humidity, Carbon dioxide, Pressure to Corridor
0203 - ED	Suite 203 - Near Entrance Door	Temperature, Relative Humidity, Carbon dioxide, Pressure to Corridor
0200 - CO	Corridor 02	Temperature, Relative Humidity, Carbon dioxide, Pressure to Corridor Above
0301 - ED	Suite 301 - Near Entrance Door	Temperature, Relative Humidity, Carbon dioxide, Pressure to Corridor
0301 - LR	Suite 301 - Living Room	Temperature, Relative Humidity, Pressure to Exterior
0301 - MBR	Suite 301 - Master Bedroom	Temperature, Relative Humidity, Carbon dioxide
0302 - ED	Suite 302 - Near Entrance Door	Temperature, Relative Humidity, Carbon dioxide, Pressure to Corridor
0302 - LR	Suite 302 - Living Room	Temperature, Relative Humidity, Pressure to Exterior
0302 - MBR	Suite 302 - Master Bedroom	Temperature, Relative Humidity, Carbon dioxide
0303 - ED	Suite 303 - Near Entrance Door	Temperature, Relative Humidity, Carbon dioxide, Pressure to Corridor
0303 - LR	Suite 303 - Living Room	Temperature, Relative Humidity, Carbon dioxide, Pressure to Exterior
0303 - MBR	Suite 303 - Master Bedroom	Temperature, Relative Humidity, Carbon dioxide, Pressure to Exterior
0300 - CO	Corridor 03	Temperature, Relative Humidity, Carbon dioxide, Pressure to Corridor Above
0401 - ED	Suite 401 - Near Entrance Door	Temperature, Relative Humidity, Carbon dioxide, Pressure to Corridor
0402 - ED	Suite 402 - Near Entrance Door	Temperature, Relative Humidity, Carbon dioxide, Pressure to Corridor
0403 - ED	Suite 403 - Near Entrance Door	Temperature, Relative Humidity, Carbon dioxide, Pressure to Corridor
0400 - CO	Corridor 04	Temperature, Relative Humidity, Carbon dioxide, Pressure to Corridor Above
0500 - CO	Corridor 05	Temperature, Relative Humidity, Carbon dioxide, Pressure to Corridor Above
0600 - CO	Corridor 06	Temperature, Relative Humidity, Carbon dioxide, Pressure to Corridor Above
0700 - CO	Corridor 07	Temperature, Relative Humidity, Carbon dioxide, Pressure to Corridor Above
0800 - CO	Corridor 08	Temperature, Relative Humidity, Carbon dioxide, Pressure to Corridor Above
0900 - CO	Corridor 09	Temperature, Relative Humidity, Carbon dioxide, Pressure to Corridor Above
1001 - ED	Suite 1001 - Near Entrance Door	Temperature, Relative Humidity, Carbon dioxide, Pressure to Corridor
1002 - ED	Suite 1002 - Near Entrance Door	Temperature, Relative Humidity, Carbon dioxide, Pressure to Corridor
1003 - ED	Suite 1003 - Near Entrance Door	Temperature, Relative Humidity, Carbon dioxide, Pressure to Corridor
1000 - CO	Corridor 10	Temperature, Relative Humidity, Carbon dioxide, Pressure to Corridor Above
1101 - ED	Suite 1101 - Near Entrance Door	Temperature, Relative Humidity, Carbon dioxide, Pressure to Corridor
1101 - LR	Suite 1101 - Living Room	Temperature, Relative Humidity, Pressure to Exterior
1101 - MBR	Suite 1101 - Master Bedroom	Temperature, Relative Humidity, Carbon dioxide
1102 - ED	Suite 1102 - Near Entrance Door	Temperature, Relative Humidity, Carbon dioxide, Pressure to Corridor
1102 - LR	Suite 1102 - Living Room	Temperature, Relative Humidity, Pressure to Exterior
1102 - MBR	Suite 1102 - Master Bedroom	Temperature, Relative Humidity, Carbon dioxide
1103 - ED	Suite 1103 - Near Entrance Door	Temperature, Relative Humidity, Carbon dioxide, Pressure to Corridor
1103 - LR	Suite 1103 - Living Room	Temperature, Relative Humidity, Pressure to Exterior
1103 - MBR	Suite 1103 - Master Bedroom	Temperature, Relative Humidity, Carbon dioxide, Pressure to Exterior
1100 - CO	Corridor 11	Temperature, Relative Humidity, Carbon dioxide, Pressure to Corridor Above
1201 - ED	Suite 1201 - Near Entrance Door	Temperature, Relative Humidity, Carbon dioxide, Pressure to Corridor
1202 - ED	Suite 1202 - Near Entrance Door	Temperature, Relative Humidity, Carbon dioxide, Pressure to Corridor
1203 - ED	Suite 1203 - Near Entrance Door	Temperature, Relative Humidity, Carbon dioxide, Pressure to Corridor
1200 - CO	Corridor 12	Temperature, Relative Humidity, Carbon dioxide, Pressure to Corridor Above
1300 - CO	Corridor 13	Temperature, Relative Humidity, Carbon dioxide, Pressure to Corridor Above
FLOAT01	As specified	Temperature, Relative Humidity
FLOAT02	Mail Room	Temperature, Relative Humidity
FLOAT03	As specified	Temperature, Relative Humidity
FLOAT04	As specified	Temperature, Relative Humidity
FLOAT05	As specified	Temperature, Temperature, Relative Humidity, Carbon dioxide, Pressure to exterior
FLOAT06	As specified	Temperature, Temperature, Relative Humidity, Carbon dioxide, Pressure to exterior
ROOF	Roof on Mechanical Penthouse Wall	Temperature, Relative Humidity, Carbon dioxide
MAU	Inside Make Up Air Unit	Temperature, Relative Humidity, Carbon dioxide, Pressure
GROUND	On wall near front entrance door	Temperature, Relative Humidity, Carbon dioxide
WS	On top of mechanical penthouse	Temperature, Relative Humidity, Precipitation, Wind Direction, Wind Speed, Solar Radiation, Barometric Pressure (Sensors of different type than on other units.)

The pressure sensors that measure pressures across the exterior enclosure are in some cases also referred to by the floor and elevation at which they are installed for convenience, and the name pairs are provided in Table E-4.

Table E-4: Exterior Enclosure Pressure Sensor Name Pairs

Standard Name	Name by Elevation
PRES - 0301 - LR	PRES - 0301 - WEST
PRES - 0302 - LR	PRES - 0302 - NORTH
PRES - 0303 - LR	PRES - 0303 - EAST
PRES - 0303 - MBR	PRES - 0303 - SOUTH
PRES - 1101 - LR	PRES - 1101 - WEST
PRES - 1102 - LR	PRES - 1102 - NORTH
PRES - 1103 - LR	PRES - 1103 - EAST
PRES - 1103 - MBR	PRES - 1103 - SOUTH

Pressure measurement data is also in some cases presented as referenced to the Corridor 13. These pressures are calculated by adding the pressure differences of multiple sensors so that the pressure difference between a given zone and Corridor 13 can be determined. In these cases the name “RPRES” is used to indicated that the pressure measurement is referenced to Corridor 13.

The standard wall mounted SMT-A3 type data acquisition units with attached sensors are shown in Section 7.3. In some cases other arrangements of these units were used; however, the electronics are the same. Different arrangements of the SMT-A3 units are shown in Figure E-1 and Figure E-2 for different applications.



Figure E-1: Photo of SMT-A3 unit in a waterproof exterior enclosure for use outside as the ROOF and GROUND units which include a shroud on top containing the temperature, relative humidity, and CO2 sensors.



Figure E-2: Photo of SMT-A3 unit installed in a waterproof outdoor case for use as FLOAT05 and FLOAT06 units with sensors attached via leads.

SMT-A2 units were also used as floaters. These units are essentially the same electronically as the SMT-A3 units, except can accommodate less inputs. A typical SMT-A2 is shown in Figure E-3.

Appendix E Supplementary Monitoring Information

These units contain built in temperature and relative humidity sensors, and additional sensors can be attached via leads.



Figure E-3: Photo of typical SMT-A2 unit used for FLOAT01, FLOAT02, FLOAT03, and FLOAT 04

The Dwyer A-306 exterior pressure tap is used for the roof exterior pressure pick-up and is mounted on the weather station tripod as shown in Figure E-4.



Figure E-4: Photo of exterior pressure for roof mounted on weather station tripod

E-1 Monitoring Equipment Layout

The monitoring equipment was installed at the case study building in accordance with the layouts provided in Figure E-5 to Figure E-12.

Appendix E Supplementary Monitoring Information










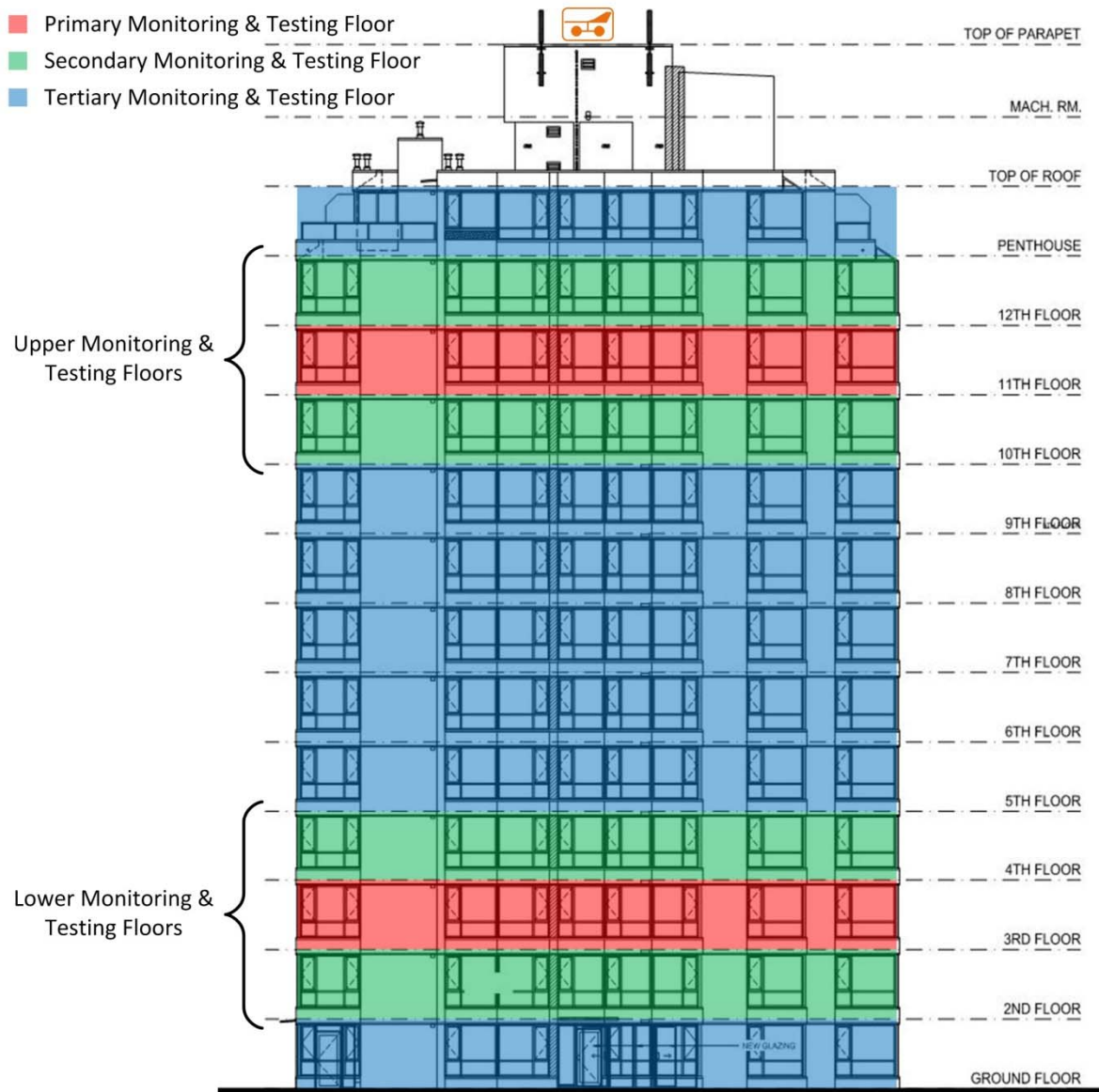
	SMT-A2
	SMT-A3
	SMT-BiG
	Differential pressure sensor with tube ends indicated
	Carbon dioxide sensor
	Relative humidity sensor
	Temperature sensor
	Pitot tube for connection to pressure sensor
	Weather Station

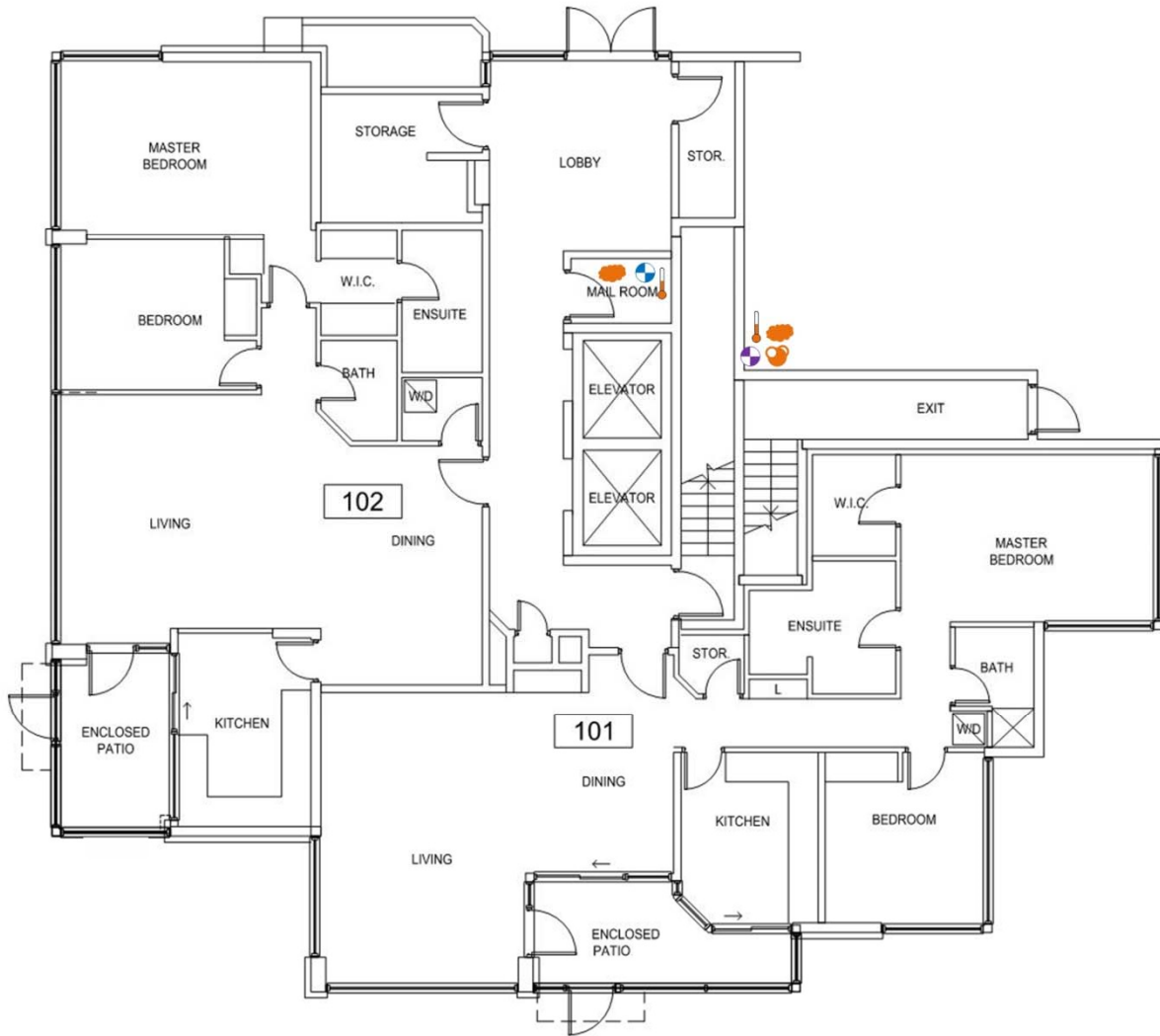
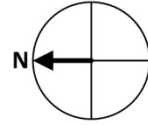
Figure E-5: Legend of symbols used for interpretation of Figure E-6 to Figure E-12

Appendix E Supplementary Monitoring Information



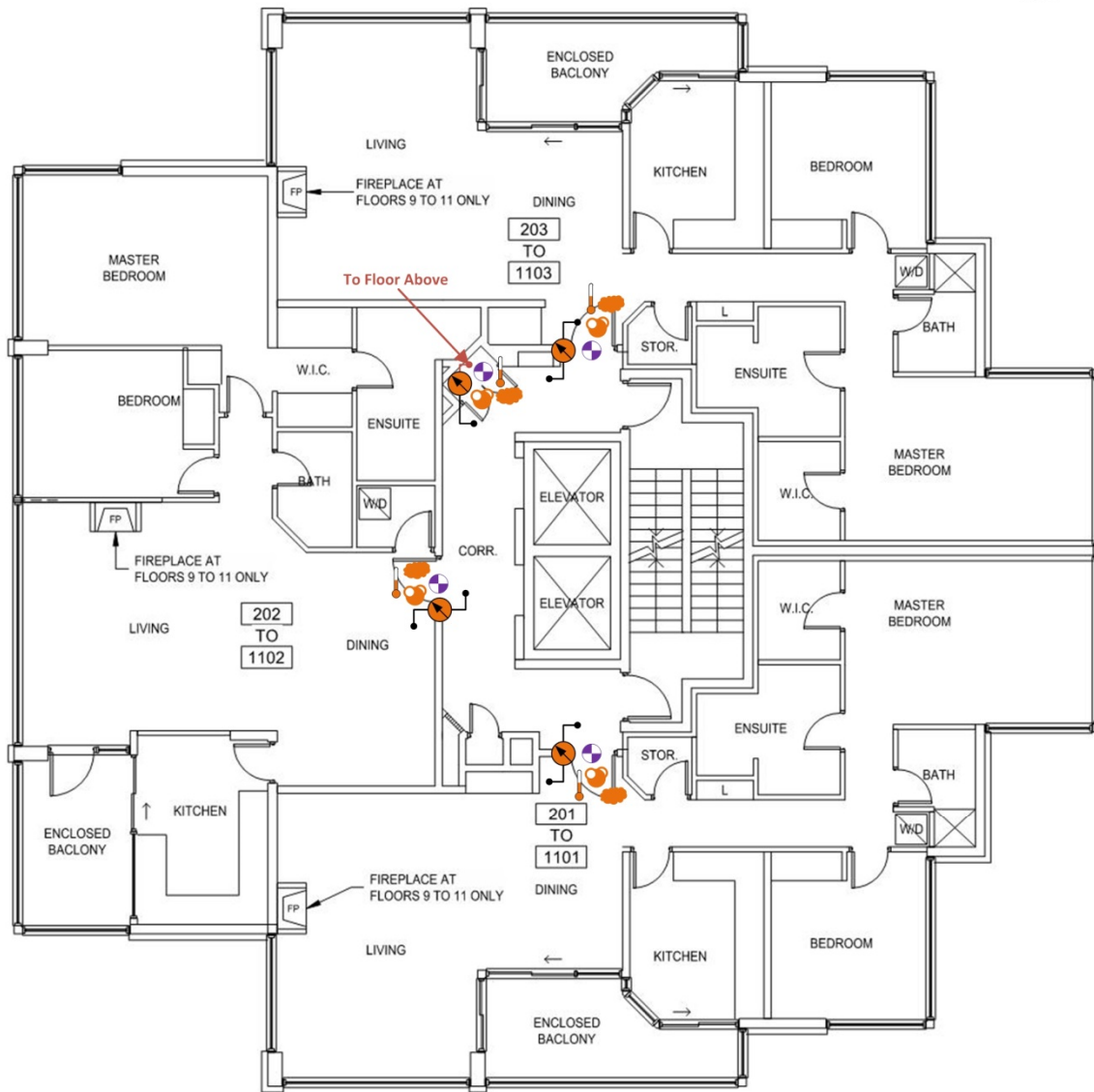
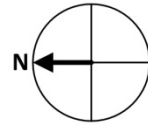
West Elevation

Figure E-6: West elevation of case study building showing primary, secondary, and tertiary monitoring floors and location of the weather station



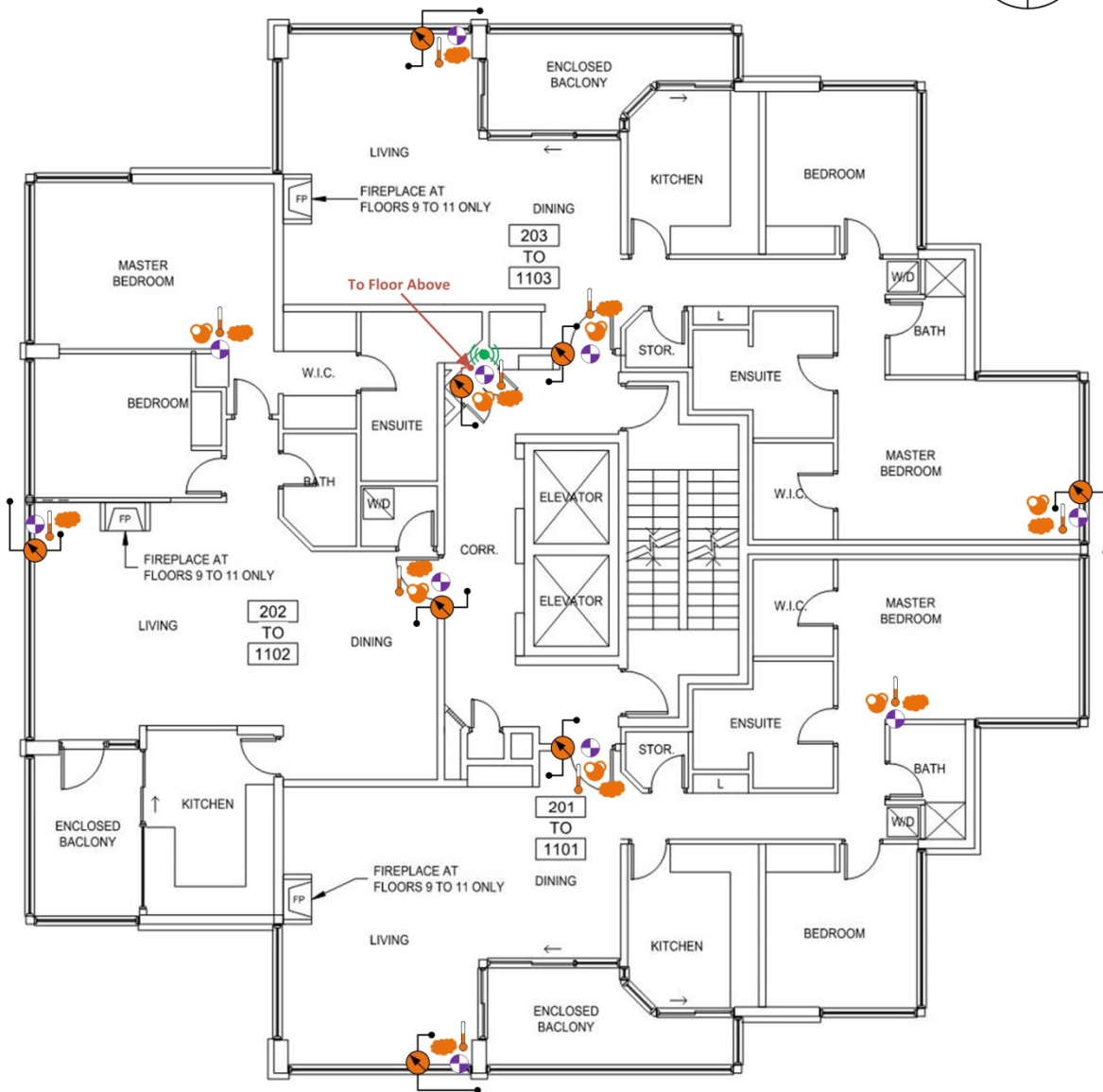
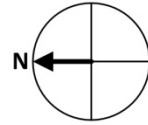
Floor 1

Figure E-7: Floor plan showing layout of monitoring equipment for Floor 1



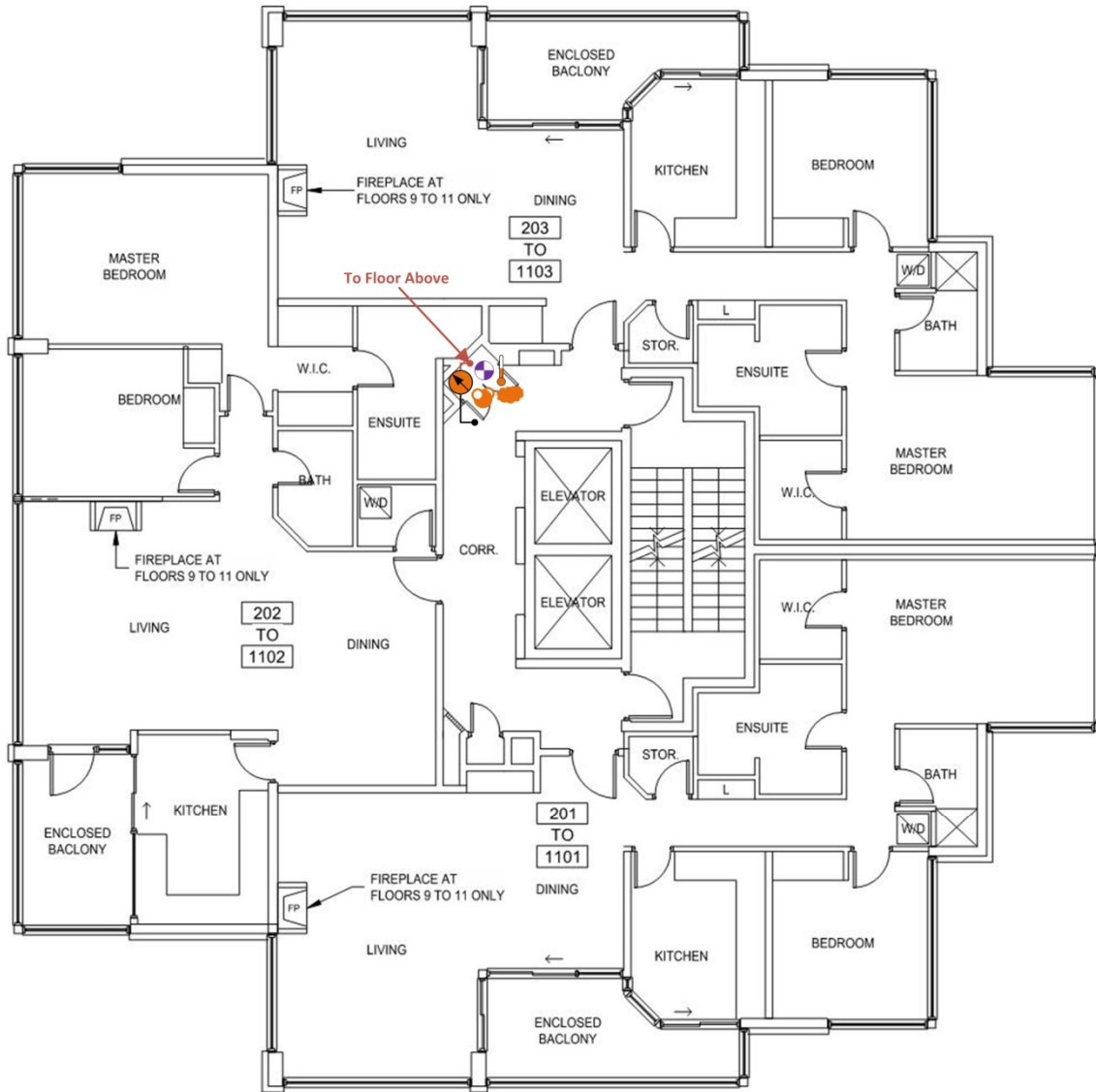
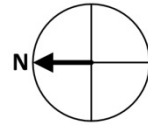
Floors 2, 4, 10 & 12

Figure E-8: Floor plan showing layout of monitoring equipment for Floors 2, 4, 10 and 12



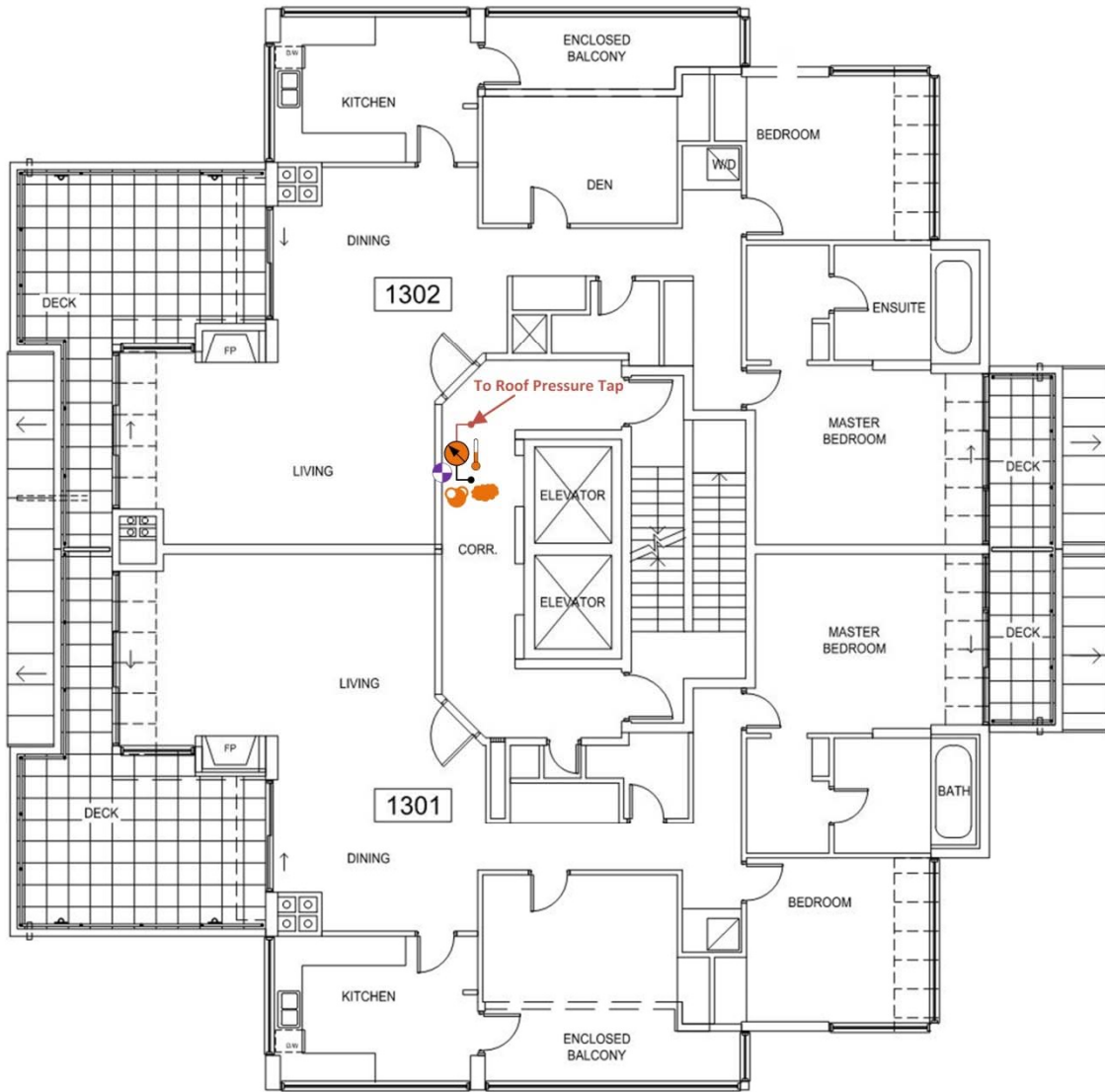
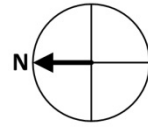
Floors 3 & 11

Figure E-9: Floor plan showing layout of monitoring equipment for Floors 3 and 11



Floors 5 to 9

Figure E-10: Floor plan showing layout of monitoring equipment for Floors 5 to 9



Floor 13

Figure E-11: Floor plan showing layout of monitoring equipment for Floor 13

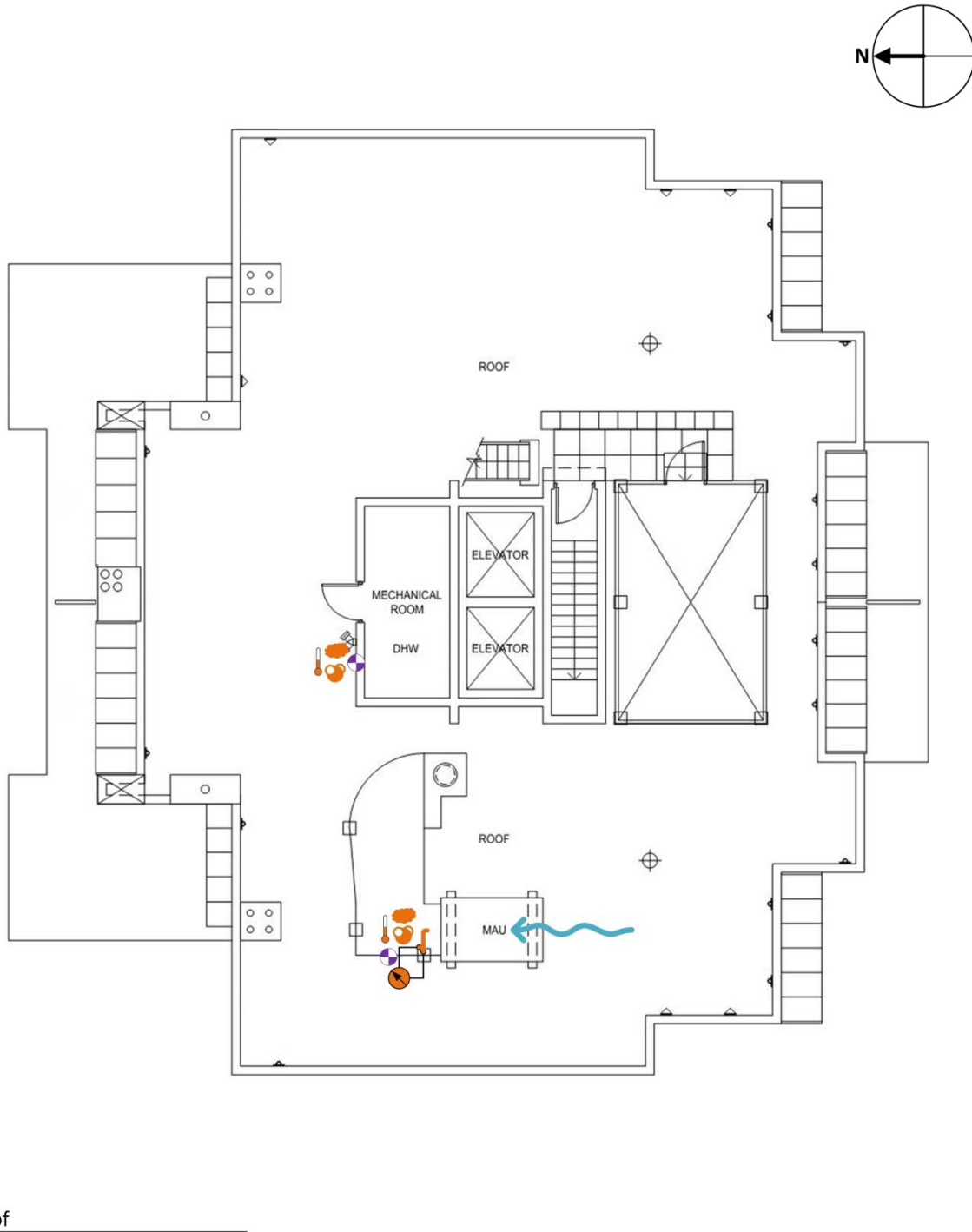


Figure E-12: Floor plan showing layout of monitoring equipment for the roof

E-2 Monitoring Equipment Malfunctions

A variety of sensors and data acquisition units were noted to be malfunctioning during the monitoring period. Individual data points or small sections of data that were readily identifiable as

errors were removed from the data sets used for analysis; however, in some cases data that may potentially be incorrect was not removed. This section provides descriptions of these sensors and the potential errors.

Sensor “PRES-1201-ED” is likely malfunctioning as it provides a nearly steady reading; however, the data from this unit has not been removed to allow for comparison. Any findings based on measurements using this sensor should be considered cautiously. It is important to note that in cases where measurements from this sensor have been included in averages (e.g. average suite to corridor pressures for Floor 12) then the malfunctioning of this sensor acts to dampen any pressure changes observed. Generally, this pressure sensor has been removed from averages and this is noted where applicable.

Sensor “PRES-1300-CO” measures the pressure difference from Corridor 13 across the roof. Initially the outdoor pressure tap of this sensor could not be connected due to ongoing construction on the roof. Consequently, the exterior pressure tap prior to March 8th, 2013 was simply the end of a tube which was located on a west facing wall of the mechanical penthouse and pointed approximately perpendicularly to the wall surface. Generally this was noted to have a significant impact on pressure readings, particularly during westerly winds which would create positive pressure on this pressure tap (higher outside pressure than inside). When the effect of this incomplete installation affects the results, the effect is discussed in the relevant section.

Sensors “CO2-0500-CO” and “CO2-1100-CO” appear to have been miscalibrated by the sensor supplier so measure higher and lower than actual concentration respectively. Assessment of the initial data shows that these sensors were initially offset from the other sensors which suggests this is calibration issue rather than a sensor drift issue. The calibration of these sensors was performed by SMT using outdoor air concentrations as a reference. Calibration gasses were not used which may limit the accuracy of these sensors. This miscalibration and any offsets of other carbon dioxide concentration sensors due to the limited accuracy of this calibration procedure do not have a significant influence on the results of this thesis.

As discussed in Chapter 12, apparent drift of the carbon dioxide sensor was measured near the end of the monitoring period. While this drift was consistently upward (sensors measure higher than actual concentration) the magnitude of the drift was variable. The typical drift was measured to be approximately 450 ppm which is significant in comparison to measured concentrations; however, typically concentrations in the poorly ventilated suites were much higher than this value, so it was still possible to use the measured carbon dioxide concentrations qualitatively.

The weather station was installed by a third party, and the initial installation was noted to be incorrectly installed in various ways leading to errors with the temperature, relative humidity, wind direction, and wind speed sensors. Unfortunately, the incorrect data recorded by these sensors was not noticed immediately. The temperature sensor was corrected on January 11, 2013, the relative humidity sensor was correct on February 25th, 2013, and the wind sensors were corrected April 8th, 2013. Prior to these dates, data collected by Environment Canada at Vancouver International Airport (YVR) was used instead by using correlations developed in Section E-3.

E-3 Weather Monitoring Data

Due to incorrect or incomplete installation of the weather station at the case study building, a significant amount of weather data was lost. To provide weather data for use in analysis, the available weather data from monitoring at the case study building was correlated with weather data from the Vancouver International Airport (YVR) weather station. These correlations were then used during periods when monitoring data at the building was not available to determine conditions at the case study building based on the YVR data. These correlations are shown in Figure E-13 to Figure E-18.

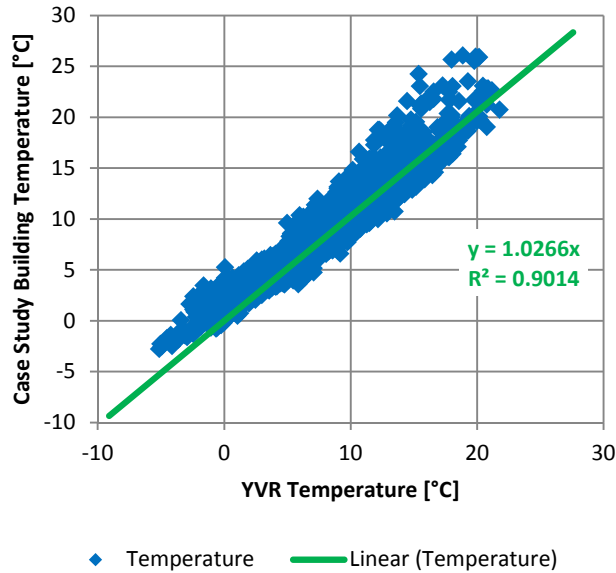


Figure E-13: Graph showing correlation of temperature at YVR and at case study building

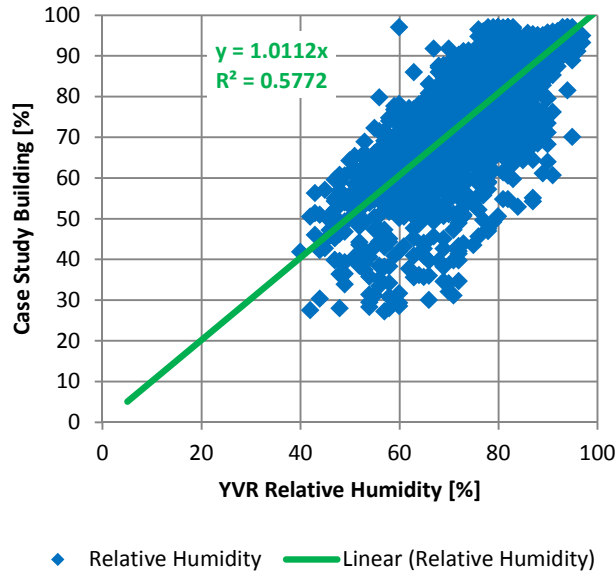


Figure E-14: Graph showing correlation of relative humidity at YVR and at case study building

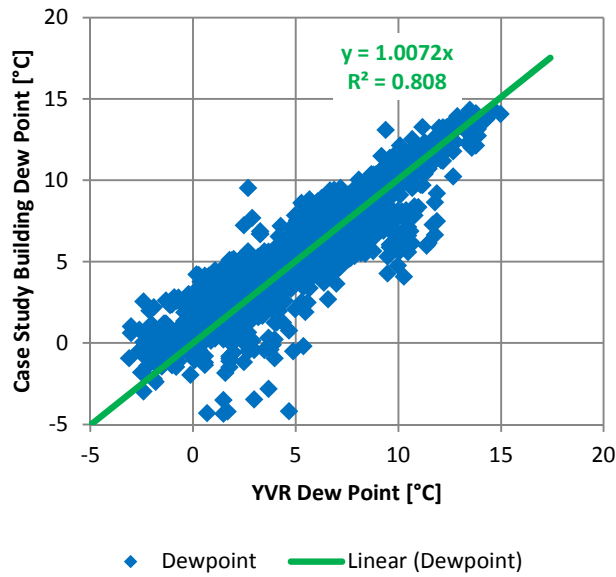


Figure E-15: Graph showing correlation of dew point temperature YVR and at case study building

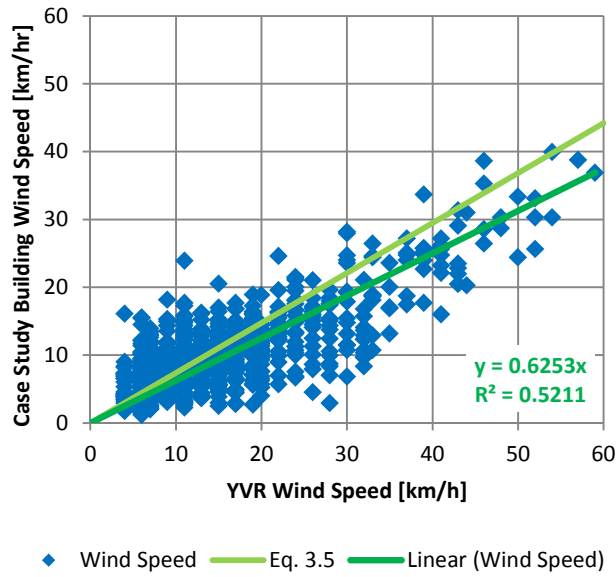


Figure E-16: Graph showing correlation of wind speed at YVR and at case study building

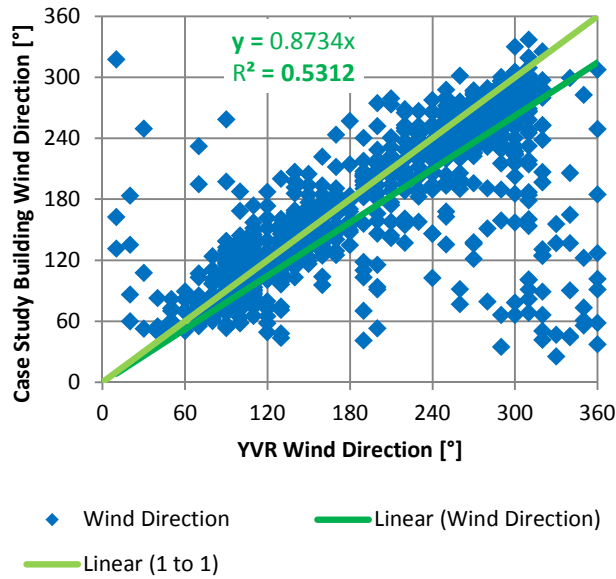


Figure E-17: Graph showing correlation of wind direction at YVR and at case study building

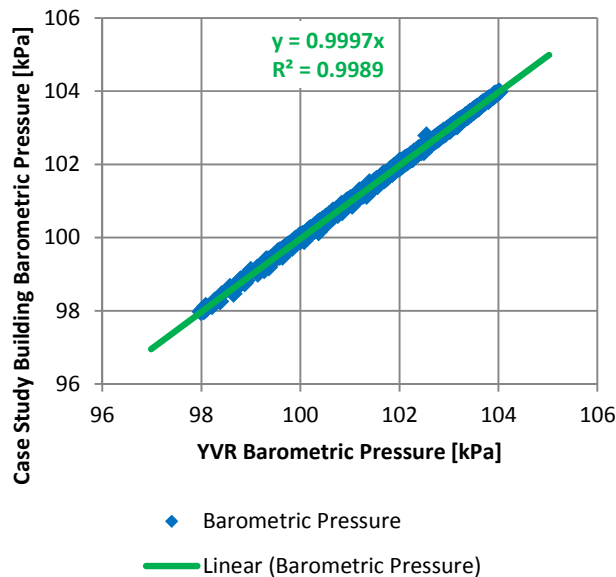


Figure E-18: Graph showing correlation of barometric pressure at YVR and at case study building

In all cases other than wind speed, the relationship between the measured exterior environmental conditions at YVR and at the case study building was acceptably close to a one to one relationship that no conversion was necessary. For wind speed, it is possible to use the atmospheric boundary layer wind speed formula (Eq. 3.5) to estimate the wind speed at the case study building based on the measured wind speed at YVR. While this method was found to predict the wind speed at the case study building relatively well, a linear relationship was also found to predict the wind speed well. For simplicity, the linear relationship was used to estimate the wind speed at the case study building based on the measurements at YVR.

Weather data collected during the monitoring period was presented in Section 7.6.

E-4 Case Study Building Construction Timeline

The case study building underwent a major exterior enclosure during the monitoring and testing phase of this thesis work. While specific testing was organized to avoid interference by the construction process, the monitoring period includes the construction period.

Construction work at the case study building began in July 2012. From July 9th, to September 27th, 2012 significant modifications were made to the exterior enclosure air barrier in the form of replacement of the windows as discussed in Section 7.1.1.3. The periods during which these windows were being replaced are provided in Table E-5. In general, the window replacement started with windows in -02 and -03 types suites and then with windows in -01 type suites working from the top of the building down.

Table E-5: Window Replacement Dates

Suite	Dates of Window Replacement
101	September 24 to 25
102	September 6
201	September 21
202	September 4
203	September 5
301	September 20
302	August 31
303	August 30
401	September 19
402	August 28
403	August 29
501	September 18
502	August 24
503	August 27
601	September 17
602	August 22
603	August 23
701	Septemeber 14
702	August 17
703	August 21
801	September 13
802	August 16
803	August 20
901	September 12
902	August 8 to 15
903	August 14
1001	September 11
1002	July 26 to August 3
1003	July 26 to August 3
1101	September 10
1102	July 9 to 13, and reinstalled July 23
1103	July 11 to 16
1201	September 7, skylights September 26 to 27
1202	July 17, skylights August 28 to September 27
1203	July 17 to 18 and reinstalled July 23, skylights September 18 to 27
1301	July 19 to 20, skylights September 12 to 27
1302	August 10 to 13, skylights September 13 to 27

To facilitate construction, scaffolding was erected around the building and is of importance to the airflow patterns primarily due to the inclusion of protective netting which could provide significant shielding to wind pressures. This scaffolding was fully installed at the start of the testing and

monitoring program. The scaffolding on the north and east elevations of the building was removed from the top down relatively consistently from December 12th, 2012 to January 8th, 2013. The scaffolding on the south and west elevations was removed from January 14th, 2013 to February 4th, 2013.

The construction process also changes the operational characteristics of the building. Due to the increase in exterior noise, the presence of dust and debris from exterior work, and the blocking of views by the scaffolding, occupants reported being less likely to open their windows during the construction period than during normal operation. Additionally, construction workers also change the operational behavior of the building directly by opening and closing exterior doors more often than during typical building operation.

Once the scaffolding was removal was completed on February 4th, 2013, the construction process at the case study building was complete and the building was no longer be impacted by ongoing construction.

E-5 Supplementary MAU Off Pressure Measurements

Section 10.9 discusses the pressures created by the MAU based on the changes in pressure due to turning the MAU off. These measurements were made on three different occasions: February 6, July 11, and July 26, 2013. The February measurements were presented in Section 10.9, and the July measurements are provided here for reference in Figure E-19 to Figure E-28. Note that the cause of the significant drop in pressure in Corridor 6 for the July 11th measurements is unknown but likely due to a factor other than the MAU operation. The timing is thought to be simply coincidental.

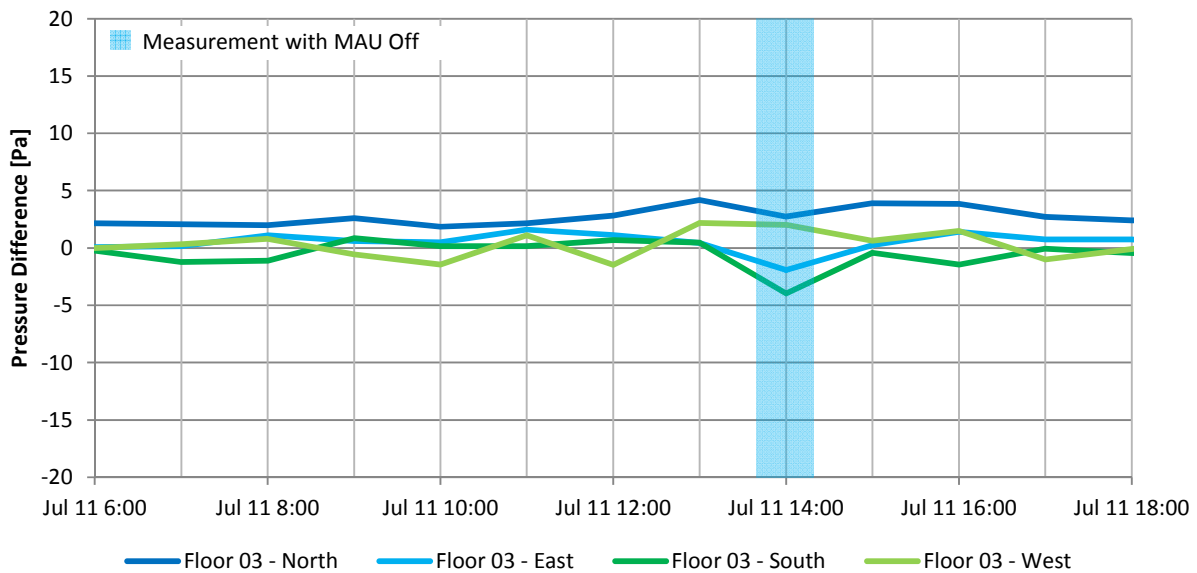


Figure E-19: Graph of hourly exterior enclosure pressure differences on Floor 3 when MAU off on July 11th, 2013

Appendix E Supplementary Monitoring Information

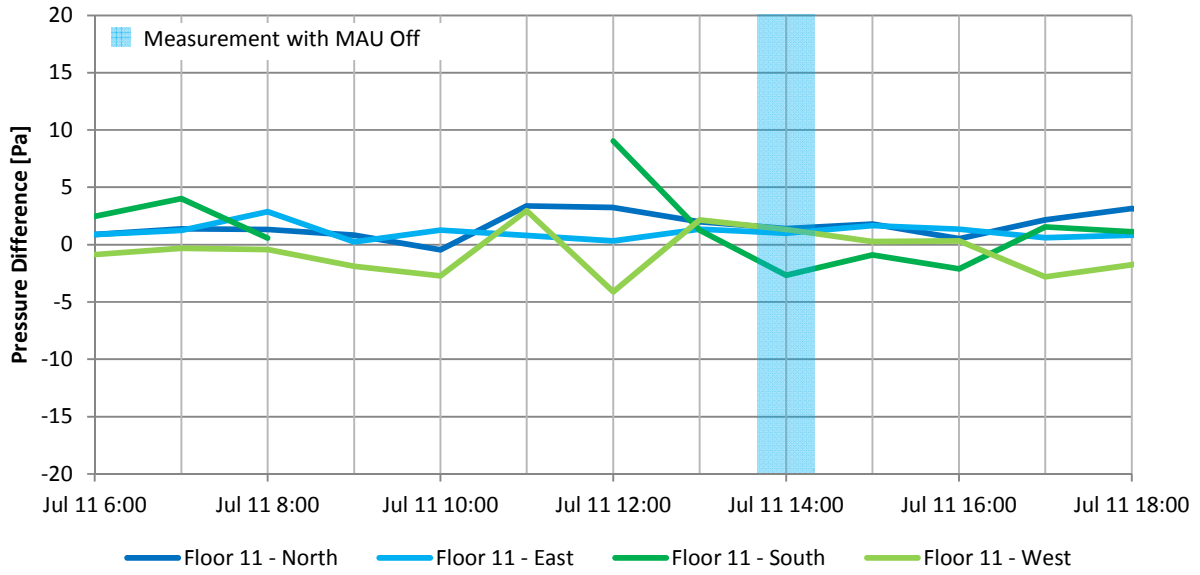


Figure E-20: Graph of hourly exterior enclosure pressure differences on Floor 11 when MAU off on July 11th, 2013

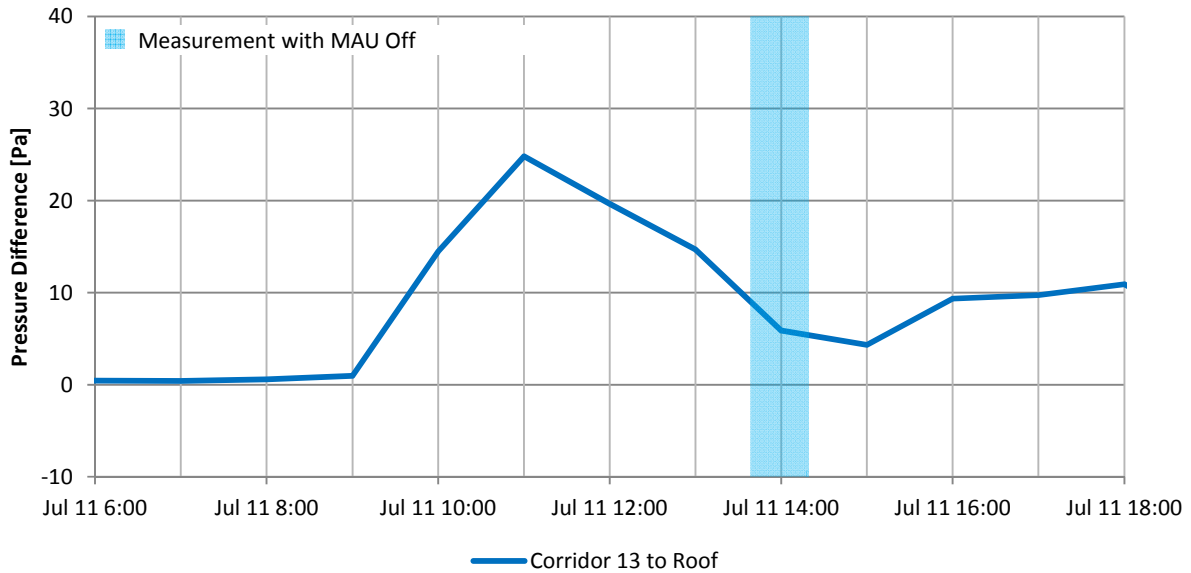


Figure E-21: Graph of hourly exterior enclosure pressure differences from Floor 13 to the roof when MAU off on July 11th, 2013

Appendix E Supplementary Monitoring Information

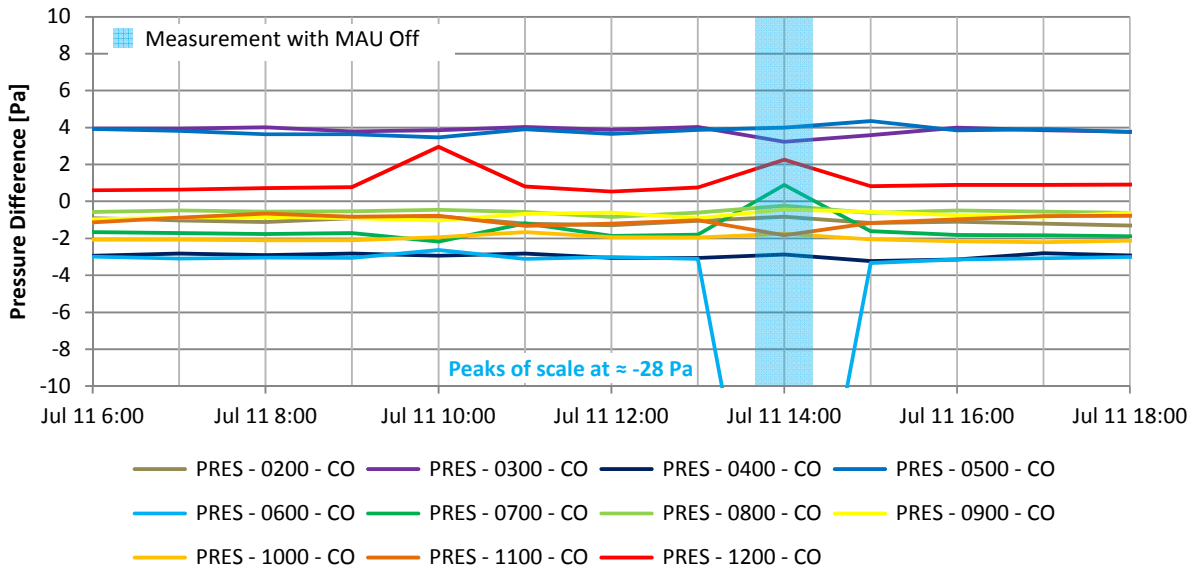


Figure E-22: Graph of hourly corridor-to-corridor pressure differences when MAU off on July 11th, 2013

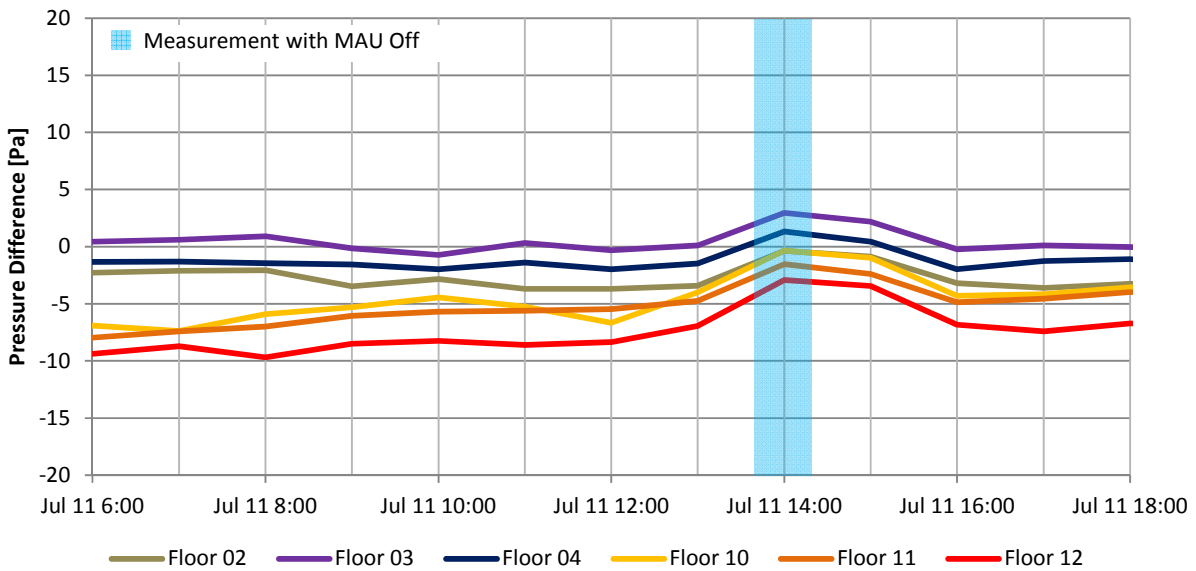


Figure E-23: Graph of hourly suite-to-corridor pressure differences when MAU off on July 11th, 2013

Appendix E Supplementary Monitoring Information

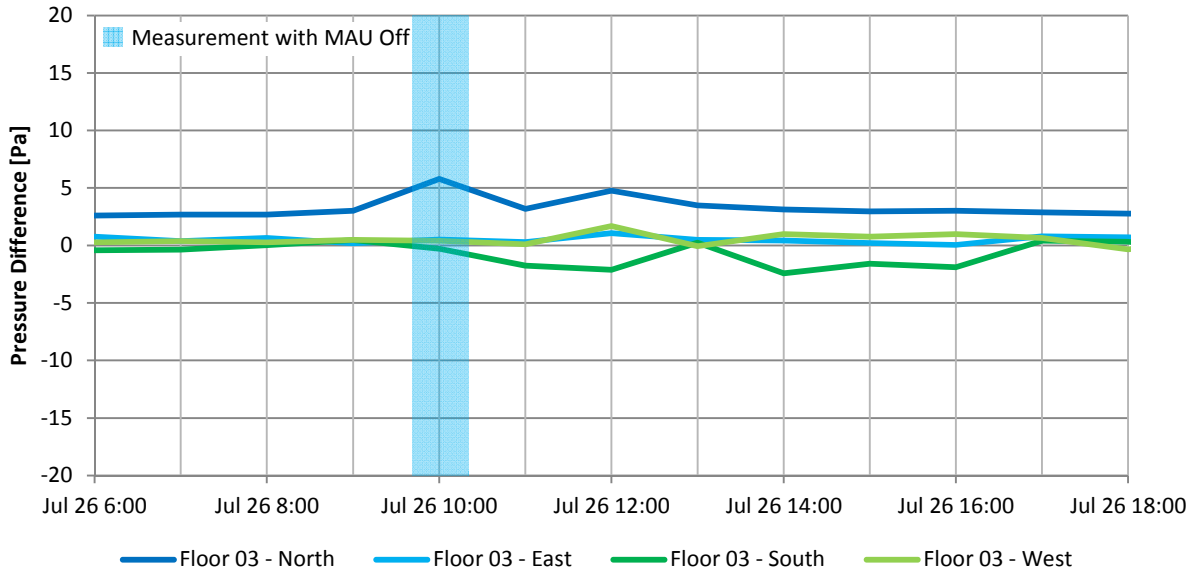


Figure E-24: Graph of hourly exterior enclosure pressure differences on Floor 3 when MAU off on July 26th, 2013

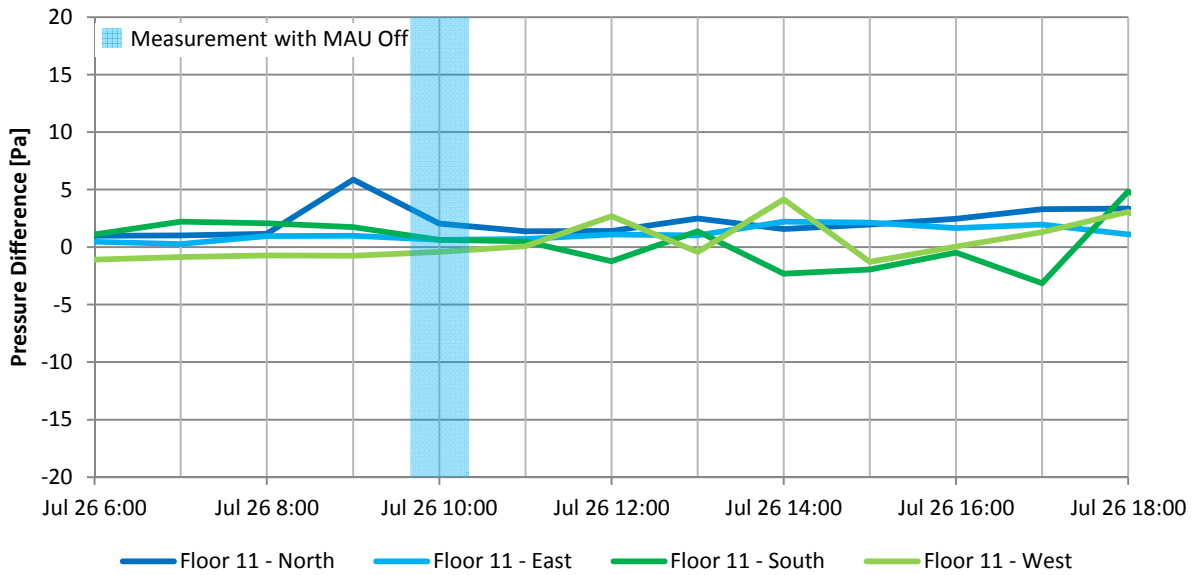


Figure E-25: Graph of hourly exterior enclosure pressure differences on Floor 11 when MAU off on July 26th, 2013

Appendix E Supplementary Monitoring Information

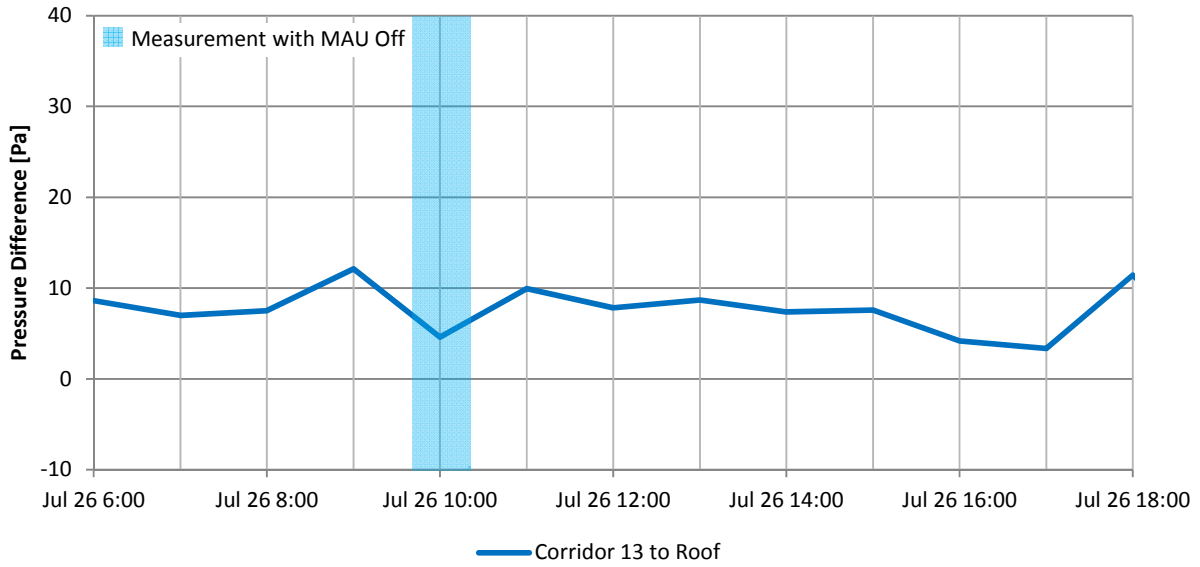


Figure E-26: Graph of hourly exterior enclosure pressure difference from Floor 13 to the roof when MAU off on July 26th, 2013

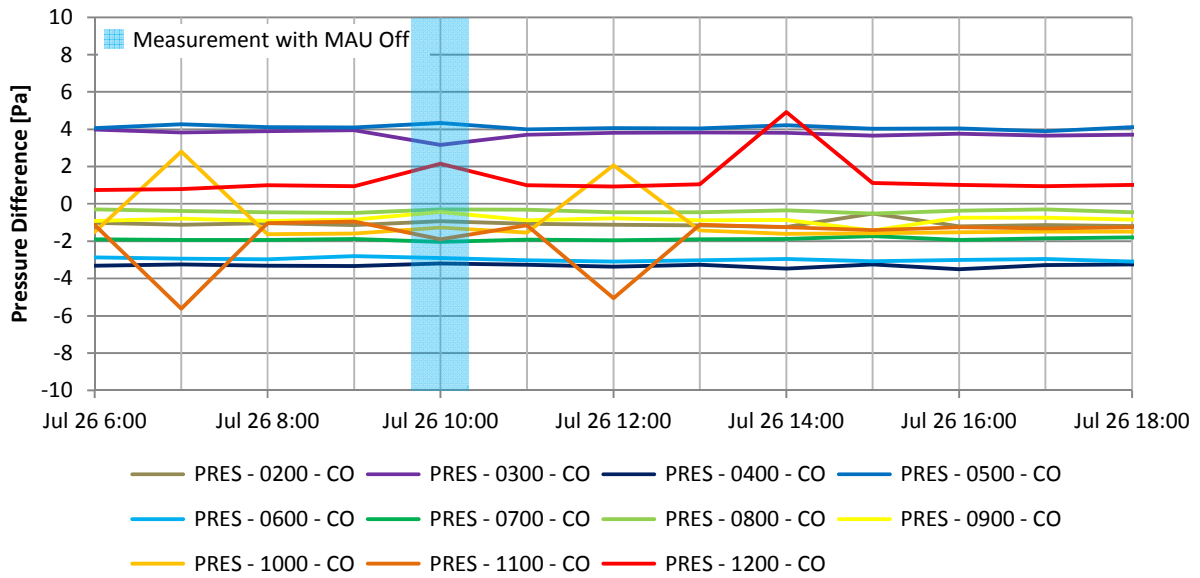


Figure E-27: Graph of hourly corridor-to-corridor pressure differences when MAU off on July 26th, 2013

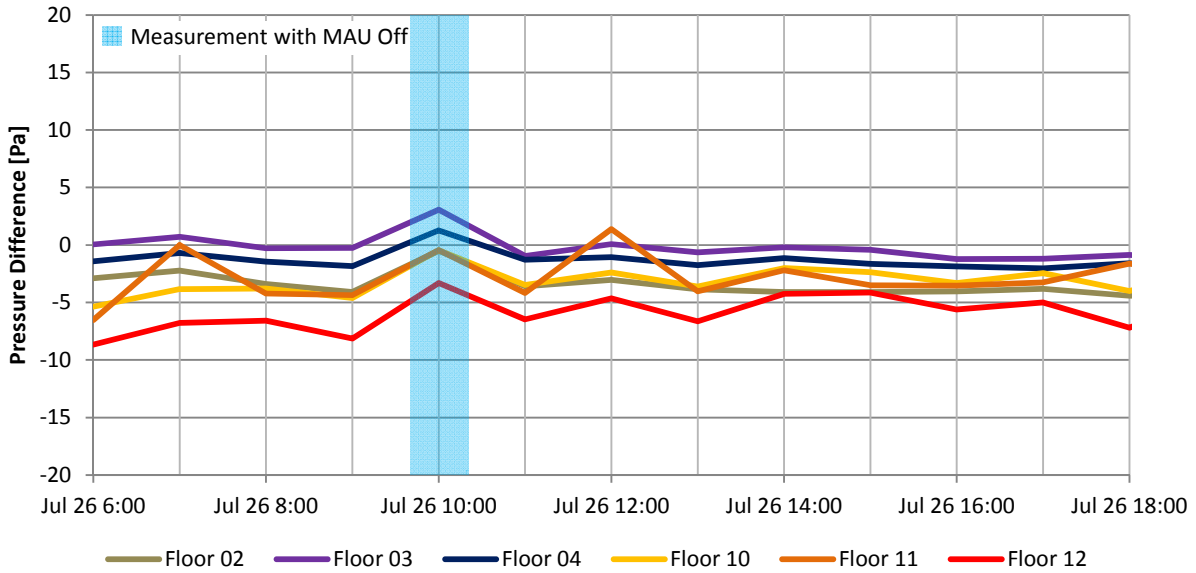


Figure E-28: Graph of hourly suite-to-corridor pressure differences when MAU off on July 26th, 2013

E-6 Suite 1103 Pressure Anomaly

On five weekdays in January 2013 a significant pressure anomaly was measured in Suite 1103. This pressure anomaly was a consistent pressurization of the suite relative to adjacent zones and the exterior by approximately 15 Pa compared to its usual operating pressure, and also depressurized the corridor relative to adjacent zones. The pressure differences from the suites to the corridor on Floor 11 are provided in Figure E-29 and illustrate this anomaly.

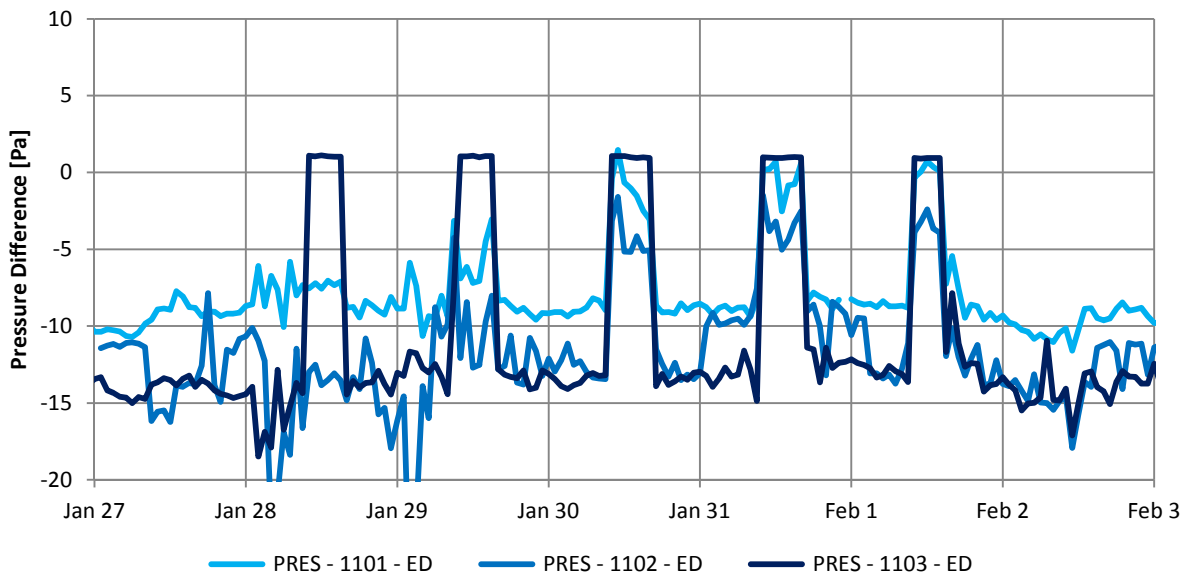


Figure E-29: Graph of suite-to-corridor pressure difference on Floor 11 showing Suite 1103 anomaly

Appendix E Supplementary Monitoring Information

In general, Suite 1103 was consistently pressurized relative the corridor, but the distribution of pressure difference across other building pressure boundaries varied throughout the week. The pressure difference from the corridor to the suites for Suite 1101 and Suite 1102 due to the anomaly increases throughout the week; consequently, the pressure difference between Suite 1103 and adjacent suites decreases throughout the week as shown in Figure E-30. The pressure differences from Corridor 11 to adjacent corridors increases throughout the week, and the pressure difference across the exterior enclosure of Suite 1103 decrease throughout the week, as shown in Figure E-31 and Figure E-32 respectively.

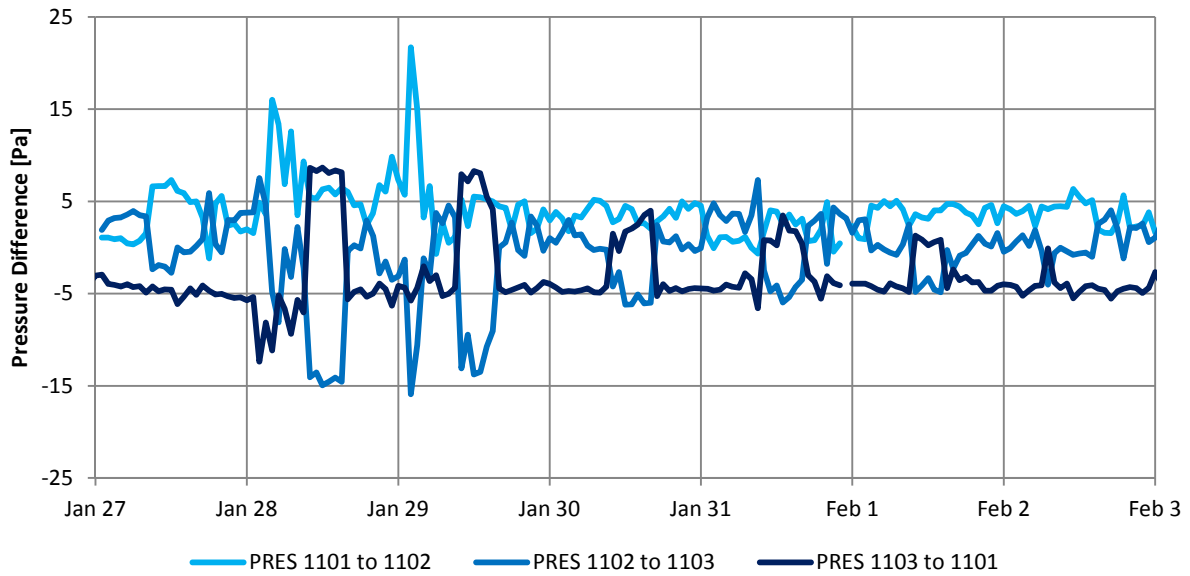


Figure E-30: Graph of suite-to-suite pressure differences on Floor 11 showing Suite 1103 anomaly

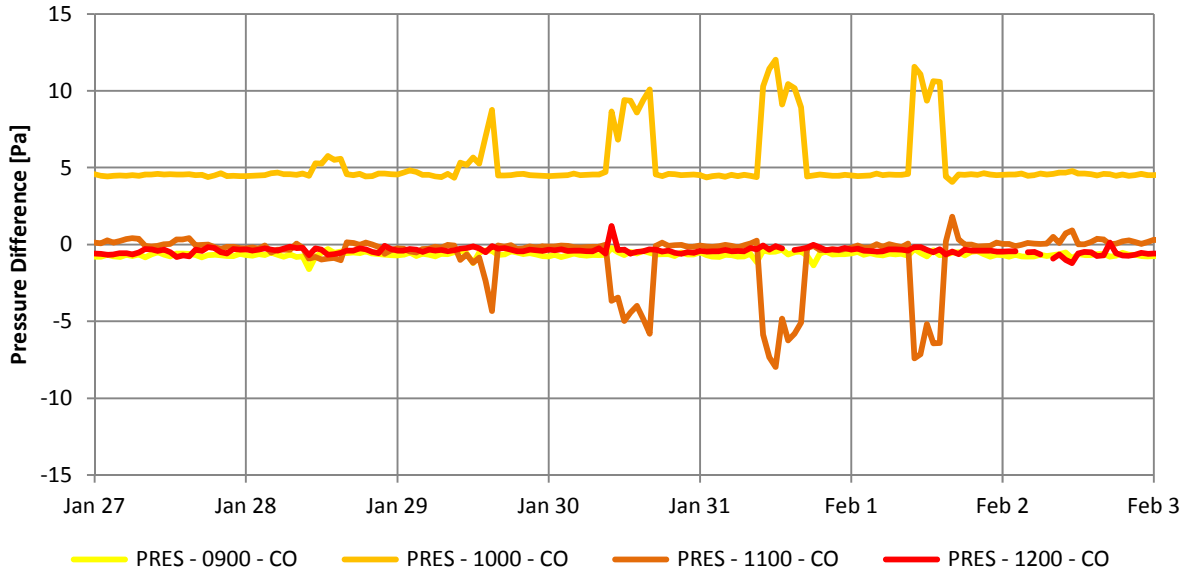


Figure E-31: Graph of corridor-to-corridor pressure differences for corridors near Corridor 11 showing Suite 1103 anomaly

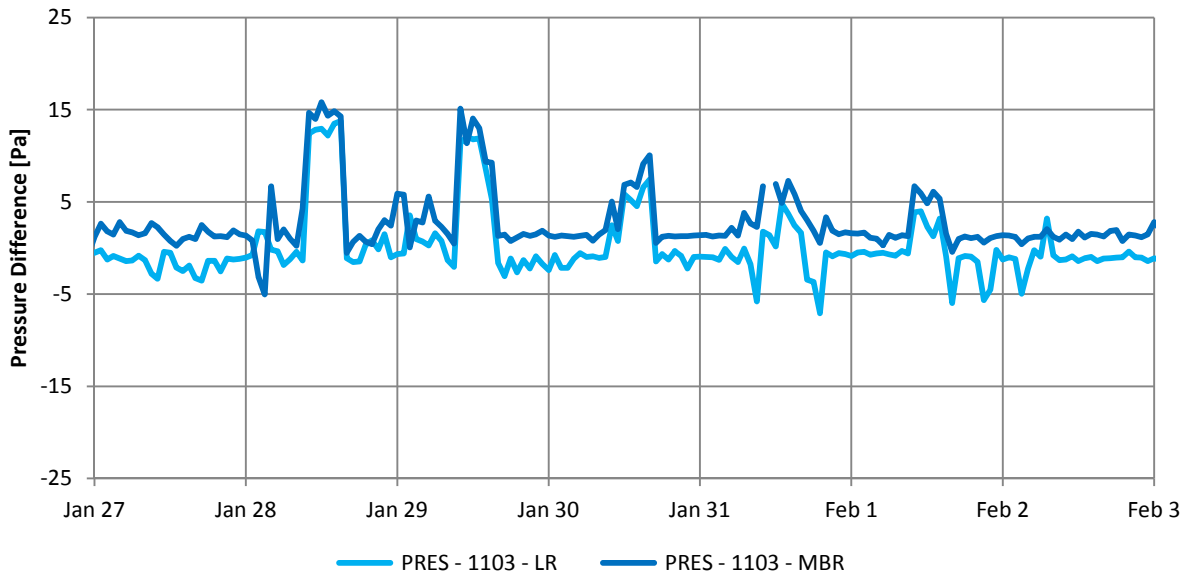


Figure E-32: Graph of exterior enclosure pressure differences for Suite 1103 showing anomaly

The cause of this anomaly is unknown; however, the relatively steady pressurization of Suite 1103 relative to the corridor suggests that a mechanical ventilation system (fan) was used to intentionally pressurize or ventilate this suite. The observed pressure patterns suggest that likely this fan was installed in the doorway of Suite 1103 drawing air from Corridor 11 and forcing it in to Suite 1103.

The pressure of Suite 1103 decreases over the course of the week relative to the exterior pressure. It is theorized that this is a result of opening windows in the suite which would significantly mitigate the developed pressure difference between the suite and the exterior. As the pressure difference across the suite entrance doors of Suites 1101 and 1102 were observed to increase following a similar pattern to the increase in pressures between Corridor 11 and adjacent corridors, it is theorized that initially some measure was implemented to mitigate the development of negative pressures from the corridor to adjacent zones such as opening of stairwell doors or opening of adjacent suite doors, but that later in the week these measures were not implemented.

E-7 Carbon Dioxide Sensor Checking

As discussed in Chapter 12, a hand held carbon dioxide sensor was used to check the accuracy of the installed carbon dioxide sensors. The handheld unit was a Telaire 7001 type unit and the specifications for this unit are provided below. These units were calibrated according the manufacturers calibration instructions on September 16th, 2013, and used to make measurement from September to October 2013.



Telaire® 7001



Telaire® 7001

Carbon Dioxide and Temperature Monitor with Ventilation Rate Displayed in CFM/Person



Equipped with Telaire's patented dual beam Absorption Infrared™ technology, the TELAIRE® 7001 is an easy-to-use CO₂/temperature monitor designed for use in residential or commercial applications. With the ability to display CO₂ readings and calculate outside air ventilation rates in cfm/person the monitor is an ideal tool for: identifying energy saving opportunities in over-venti-

lated spaces, determining if air quality complaints are due to insufficient ventilation, or locating the presence of combustion fumes generated from vehicles and appliances. If you wish to record CO₂ concentration for further analysis TELAIRE® offers CO₂View™ software that allows you to log concentrations directly to a PC. For remote monitoring TELAIRE® offers a Datalogging Kit that easily attaches to the back of the 7001.

Specifications	Applications	Features/Benefits
<p>Method Dual Beam Absorption Infrared™</p> <p>Sample Method Diffusion or flow through (50 - 100 ml/min)</p> <p>Warranty 18 months parts and labor</p> <p>Performance</p> <p>CO₂ Channel</p> <p>Measurement Range 0-4,000 ppm voltage output 0-10,000 ppm display</p> <p>Sensitivity ± 1 ppm</p> <p>Accuracy ±50 ppm or ±5% of reading (up to 1.5% or 15,000 ppm), whichever is greater</p> <p>Repeatability ±20 ppm</p> <p>Temperature Dependence ±0.1% of reading per °C or ±2 ppm per °C, whichever is greater, referenced to 25°C</p> <p>Pressure Dependence: 0.13% of reading per mm Hg (Corrected via user input for elevation)</p> <p>Annual Drift ± 20 ppm typical</p> <p>Response Time <60 seconds for 90% of step change</p> <p>Warm-Up Time <60 seconds at 22°C</p> <p>Operating Conditions 32-122°F (0-50°C) 0-95% RH, non-condensing</p> <p>Storage Temperatures -40 to 140°F (-40 to 60°C)</p> <p>Calibration Interval 12 months, offset adjustment using single gas at 0-1000 ppm CO₂. Full factory calibration available</p> <p>Temperature Channel</p> <p>Temperature Range Voltage output 32 to 104°F (0 to 40°C) Display 32 to 122°F (0 to 50°C)</p> <p>Display Resolution 0.1°F (0.1°C)</p> <p>Display Options °F, °C, or Off. Set with panel button.</p> <p>Accuracy ±2°F (±1°C)</p> <p>Response Time 20-30 minutes (case must equilibrate with environment)</p> <p>Calibration Interval 12 months, offset adjustment using temperature standard at 50 to 86°F (10 to 30°C). Full factory calibration available</p> <p>Output - Analog</p> <p>CO₂ 0-4 VDC, 1mV/ppm (4,000 ppm max)</p> <p>Temperature 0-4 VDC linear, 32-104°F (0-40°C)</p> <p>Output Impedance 100 Ohms</p> <p>Wiring Connection Via RJ-45 to DB9 serial port cable (for use with CO₂View™ PC Graphing Software)</p>	<p>■ Identify areas with low or substandard ventilation.</p> <p>■ Identify hidden energy savings in over-ventilated spaces.</p> <p>■ Determine if ventilation is a factor in air quality complaints.</p> <p>■ Locate the presence of combustion fumes from vehicles and appliances.</p> <p>■ Use as a reference to calibrate wall mounted CO₂ sensors.</p>	<p>■ Patented dual beam, Absorption Infrared™ gas sensor ensures long term stability and durability.</p> <p>■ Large, easy to read display. Temperature displayed in °F or °C. CO₂ displayed in ppm. Easily adjusted for altitude changes.</p> <p>■ Fast, simple calibration using external port and display. Calibrate with ambient air or bottled gas.</p> <p>■ Calibrate, set elevation, change °F or °C using on-board controls or optional computer interface (UIP Kit model 2072)</p> <p>■ Flip out stand for desktop monitoring.</p> <p>■ Voltage output via RJ45 connector provides easy interface to most dataloggers.</p> <p>■ Plug In AC power adaptor.</p> <p>■ Operates for up to 80 hours on 4 AA alkaline batteries. (not included).</p> <p>■ Displays cfm-per-person ventilation rate based on CO₂ inside outside differential reading.</p>
		
	<p>Accessories/Ordering Information</p> <p>62933 International Power Supply</p> <p>62285 Cable -RJ-45 to DB-9</p> <p>Factory Calibration Call 805-685-4000 for a RMA number</p> <p>2070 Cable Voltage Output cable, includes 2 pigtail leads for connecting to 3rd party devices</p> <p>2075 Calibration Kit Regulator, tubing and gas. Perform up to 20 calibrations.</p> <p>2080 CO₂View™ Graphing Software for logging CO₂ concentrations directly to a PC.</p> <p>2077 Hobo Datalogger Kit Small Datalogger that velcro's to the back of the 7001. Includes CO₂ input with additional temp and relative humidity measurement, graphing software and all necessary connection cables.</p>	<p>About the CFM/Person Ventilation Rate Measurement</p> <p>The 7001 will calculate the outside air ventilation rate to a space based on the inside/outside CO₂ differential readings. Outside readings can be established by measuring outside levels and holding the "enter" button on the sensor for 5 seconds. The outside reading can also be manually set using the on-board keypad and display (default 400 ppm).</p> <p>Accurate interpretation of the Ventilation Rate indicator requires a measuring 2 to 3 hours after occupancy has stabilized in a space or at a peak in daily CO₂ concentrations. In other conditions the indicator may tend to over estimate ventilation rates.</p> <p>The Ventilation Rate display assumes a people activity level in the measured space similar to an office type environment (1.2, MET). If higher levels of activity are present the indicator may tend to under estimate ventilation levels.</p>
	<p>Specifications (cont)</p> <p>Display LCD with independent CO₂/Temperature readings (panel buttons set elevation, °F/°C, calibration functions)</p> <p>Power Supply</p> <p>Battery Type Four AA batteries, not included</p> <p>Battery Operation 80 hours (alkaline)</p> <p>External 6 VDC from external AC/DC adapter, included</p> <p>Power Requirements 100 mA Peak, 20 mA average from 6V</p> <p>Certification FCC Class 15 Part B</p>	<p>TELAIRE</p> <p>8660 Cortona Drive, Suite B, Goleta, CA 93117 P- 805-685-4000 F- 805-685-0015 www.telaire.com</p> <p>It is our intention to keep the product information current and accurate. We can not cover specific applications or anticipate all requirements. All specifications are subject to change without notice. For more information or questions relative to this Specification Sheet, contact Telaire.</p> <p>Covered by United States Patents: 5,060,508 / 5,163,332 / 6,255,653 Other Patents Pending</p> <p>©Copyright 1998-2004 Telaire®</p>

E-8 Monitoring Equipment Specifications

The monitoring equipment specifications are provided in this section.

Amplified Very Low Pressure Sensors

AMPLIFIED Pressure Sensors



Features

- 0.25 and 0.50 In H₂O Pressure Ranges
- Ratiometric 4V Output
- Temperature Compensated
- Calibrated Zero and Span

Applications

- Medical Breathing
- HVAC

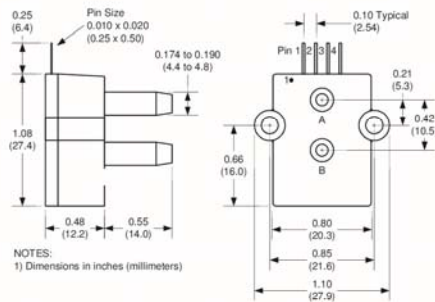
General Description (generic product)

The Amplified line of low pressure sensors is based upon a proprietary technology to reduce all output offset or common mode errors. This model provides a ratiometric 4-volt output with superior output offset characteristics. Output offset errors due to change in temperature, stability to warm-up, stability to long time period, and position sensitivity are all significantly reduced when compared to conventional compensation methods. In addition the sensor utilizes a silicon, micromachined, stress concentration enhanced structure to provide a very linear output to measured pressure.

These calibrated and temperature compensated sensors give an accurate and stable output over a wide temperature range. This series is intended for use with non-corrosive, non-ionic working fluids such as air, dry gases and the like.

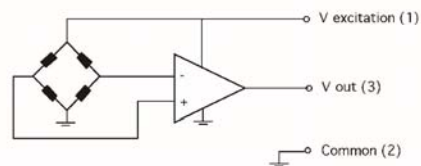
The output of the device is ratiometric to the supply voltage over a supply voltage range of 4.5 to 5.5 volts.

Physical Dimensions



- pin 1: Vsupply
- pin 2: Common
- pin 3: Voutput
- pin 4: do not connect

Equivalent Circuit



All Sensors

DS-0032 Rev A

all sensors

www.allsensors.com

408 225 2079

408 225 4314

16035 Vineyard Blvd. Morgan Hill, CA 95037

408 225 4314

16035 Vineyard Blvd. Morgan Hill, CA 95037

Appendix E Supplementary Monitoring Information

Pressure Sensor Ratings

Supply Voltage, V_s	+4.5 to +5.5 Vdc
Common-mode pressure	-10 to +10 psig
Lead Temperature, max (soldering 2-4 sec.)	250°C

Environmental Specifications

Temperature Ranges	
Compensated	5 to 50° C
Operating	-25 to 85° C
Storage	-40 to 125° C
Humidity Limits	0 to 95% RH (non condensing)

Performance Characteristics for: 0.25 INCH-D-4V

Parameter, NOTE 1	Minimum	Nominal	Maximum	Units
Operating Range, differential pressure		±0.25		"H ₂ O
Output Span, NOTE 5	±1.80	±2.0	±2.20	volt
Offset Voltage @ zero differential pressure	2.00	2.25	2.50	volt
Offset Temperature Shift (5°C-50°C), NOTE 2			±50	mvolt
Offset Warm-up Shift, NOTE 3		±20	±50	mvolt
Offset Position Sensitivity (±1g)		±40	±100	mvolt
Offset Long Term Drift (one year)		±20	±50	mvolt
Linearity, hysteresis error, NOTE 4		0.05	0.25	%fs
Span Shift (5°C-50°C), NOTE 2			±4	%span

Performance Characteristics for: 0.5 INCH-G-4V

Parameter, NOTE 1	Minimum	Nominal	Maximum	Units
Operating Range, gage pressure		0.5		"H ₂ O
Output Span, NOTE 5	3.80	4.0	4.20	volt
Offset Voltage @ zero gage pressure	0.10	0.25	0.40	volt
Offset Temperature Shift (5°C-50°C), NOTE 2			±50	mvolt
Offset Warm-up Shift, NOTE 3		±20	±50	mvolt
Offset Position Sensitivity (±1g)		±40	±100	mvolt
Offset Long Term Drift (one year)		±20	±50	mvolt
Linearity, hysteresis error, NOTE 4		0.05	0.25	%fs
Span Shift (5°C-50°C), NOTE 2			±4	%span

Specification Notes

NOTE 1: ALL PARAMETERS ARE MEASURED AT 5.0 VOLT EXCITATION, FOR THE NOMINAL FULL SCALE PRESSURE AND ROOM TEMPERATURE UNLESS OTHERWISE SPECIFIED. **PRESSURE MEASUREMENTS ARE WITH POSITIVE PRESSURE APPLIED TO PORT B.**

NOTE 2: SHIFT IS RELATIVE TO 25°C.

NOTE 3: SHIFT IS WITHIN THE FIRST HOUR OF EXCITATION APPLIED TO THE DEVICE.

NOTE 4: MEASURED AT ONE-HALF FULL SCALE RATED PRESSURE USING BEST STRAIGHT LINE CURVE FIT.

NOTE 5: THE VOLTAGE ADDED TO THE OFFSET VOLTAGE AT FULL SCALE PRESSURE. NOMINALLY THE OUTPUT VOLTAGE RANGE IS 0.25 TO 4.25 VOLTS FOR MINUS TO PLUS FULL SCALE PRESSURE.

All Sensors reserves the right to make changes to any products herein. All Sensors does not assume any liability arising out of the application or use of any product or circuit described herein, neither does it convey any license under its patent rights nor the rights of others.

Amplified VeryLow Pressure Sensors



CANTHERM
Supplying high-quality bimetal and thermal sensor products.

MF52 Pearl-Shaped Precision NTC Thermistor for Temperature Measurement

The MF52 series of Pearl-Shaped NTC Thermistors is ethoxyline resin coated. The small size is made possible by new materials and manufacturing methods which provide the benefit of close tolerances and fast response. MF52 thermistors are available with 5 lead styles in standard or custom lengths.



Application

- Heating, Ventilation & Air Conditioning
- Temperature Regulation and Measurement
- Electronic Thermometers
- Liquid Level Sensing
- Automotive Electronics
- Medical Equipment and Apparatus
- Battery Packs and Portable Electronics

Characteristics

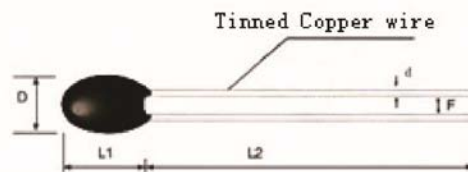
- Small Size and fast response
- Available tolerances: $\pm 1\%$, $\pm 2\%$, $\pm 3\%$ and $\pm 5\%$
- Long-term Stability and Reliability
- Excellent Tolerance and Interchangeability
- Available in all popular resistance values
- Dissipation Constant $\geq 2.0 \text{ mW}/^\circ\text{C}$
- Time Constant of ≤ 7 seconds in still air
- Available in custom probes
- UL Listed E240991

Dimensions(mm)

Code	D max	L ₁ max	L ₂ min	d +/- 0.05	F +/- 0.05
A1	2	3	25	0.3	2.0
A2	3	4	25	0.45	2.5



UL 1434
(File E240991)



A: Tin. Ag. nickel plated cu wire



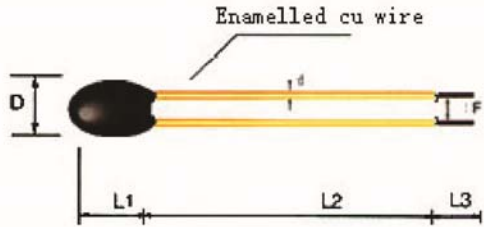
CANTHERM

8415 Mountain Sights Avenue • Montreal (Quebec), H4P 2B8, Canada
Tel: (514) 739-3274 • 1-800-561-7207 • Fax: (514) 739-2902
E-mail: sales@cantherm.com • Website: www.cantherm.com

2006/Mar

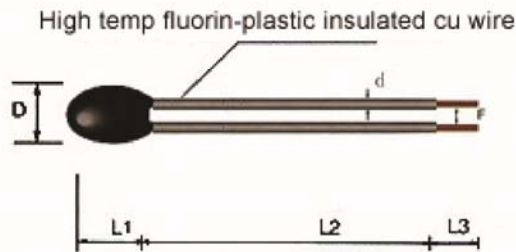


CANTHERM
Supplying high-quality bimetal and thermal sensor products.



B: Enamelled cu wire

Code	D max	L ₁ max	L ₂ min	L ₃ +/- 1	d +/- 0.05	F +/- 0.05
B1	2	3.5	Customer Specified	5	0.2	2.0
B2	3	4	Customer Specified	5	0.3	2.5



C: High temp fluorin-plastic wire

Code	D max	L ₁ max	L ₂ min	L ₃ +/- 1	d +/- 0.05	F +/- 0.05
C1	2	3.5	Customer Specified	5	0.4	2.0
C2	3	4	Customer Specified	5	0.5	2.5

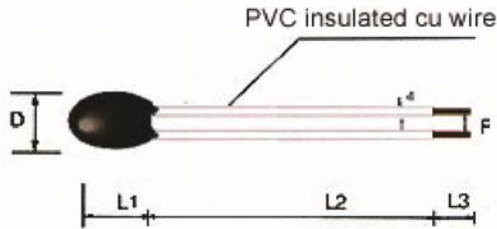


CANTHERM

8415 Mountain Sights Avenue • Montreal (Quebec), H4P 2B8, Canada
Tel: (514) 739-3274 • 1-800-561-7207 • Fax: (514) 739-2902
E-mail: sales@cantherm.com • Website: www.cantherm.com

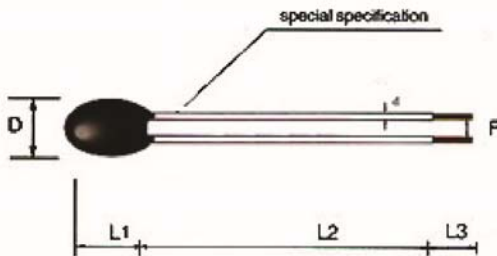


CANTHERM
Supplying high-quality bimetal and thermal sensor products.



D: PVC wire

Code	D max	L ₁ max	L ₂ min	L ₃ +/-1	d +/- 0.05	F +/- 0.05
D1	2	3.5	Customer Specified	5	0.26	2.5
D2	3	4	Customer Specified	5	0.32	2.5



E: Lead and head according to specification

Code	D max	L ₁ max	L ₂ min	L ₃ +/- 1	d +/- 0.05	F +/- 0.05
E1	Customer Specified	Customer Specified	Customer Specified	5	Customer Specified	2.5
E2	Customer Specified	Customer Specified	Customer Specified	5	Customer Specified	2.5

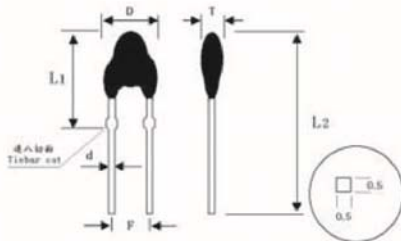


CANTHERM

8415 Mountain Sights Avenue • Montreal (Quebec), H4P 2B8, Canada
Tel: (514) 739-3274 • 1-800-561-7207 • Fax: (514) 739-2902
E-mail: sales@cantherm.com • Website: www.cantherm.com



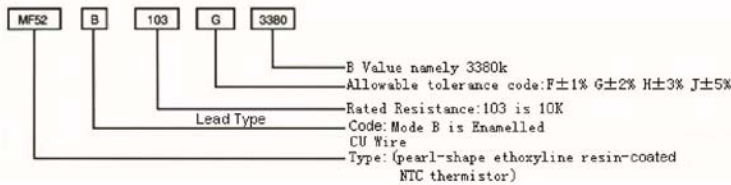
CANTHERM
Supplying high-quality bimetal and thermal sensor products.



F: Tinned Lead-Frame Style

Code	D max	L ₁ max	L ₂ +/- 1.5	d max	F +/- 0.5	Tmax
F	3.8	9.5	17	5.0	2.5	3.5

➤ Specification



➤ Main Techno-Parameter

Part No.	Rated Resistance R ₂₅ (KΩ)	B Value (25/50°C) (K)	Rated Power(mw)	Dissi. Coef. (mW/°C)	Thermal time Constant(S)	Operating Temp.(°C)
MF52□□□3100	0.1-20	3100	≤ 50	≥ 2.0 In Still Air	≤ 7 In Still Air	-55° - +125°C
MF52□□□3270	0.2-20	3270				
MF52□□□3380	0.5-50	3380				
MF52□□□3470	0.5-50	3470				
MF52□□□3600	1-100	3600				
MF52□□□3950	5-100	3950				
MF52□□□4000	5-100	4000				
MF52□□□4050	5-200	4050				
MF52□□□4150	10-250	4150				
MF52□□□4300	20-1000	4300				
MF52□□□4500	20-1000	4500				

Remark:

* B Value (25/50C) error is ±1% for components with rated resistance tolerance of ±1% and ±2% for all others.

Notice:

* The two ends of the lead wire cannot endure too big pull because of the small size and soldered spot in series of MF52.

* Solder at least 5mm from the bottom of wire.



CANTHERM

8415 Mountain Sights Avenue • Montreal (Quebec), H4P 2B8, Canada
Tel: (514) 739-3274 • 1-800-561-7207 • Fax: (514) 739-2902
E-mail: sales@cantherm.com • Website: www.cantherm.com



CANTHERM
Supplying high-quality bimetal and thermal sensor products.

MF58 Glass Shell Precision NTC Thermistors

The MF58 is a NTC thermistor which is manufactured using a combination of ceramic and semiconductor techniques. It is equipped with tinned axial leads and then wrapped with purified glass.



Applications

Temperature compensation and detection for:

- Household appliances (air conditioners, microwave ovens, electric fans, electric heaters etc.)
- Office equipment (copiers, printers etc.)
- Industrial, medical, environmental, weather and food processing equipment
- Liquid level detection and flow rate measurement
- Mobile phone battery
- Apparatus coils, integrated circuits, quartz crystal oscillators and thermocouples.

Features

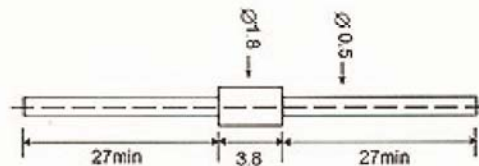
- Good stability and repeatability
- High reliability
- Wide range of resistance: 0.1~1000K Ω
- Tight tolerance on resistance and Beta values
- Usable in high-temperature and high-moisture environments
- Small, light, strong package,
- Suitable for automatic insertion on thru-hole PCBs
- Rapid response
- High sensitivity

Specifications



- B Value: 3650 namely 3650k
- The Allowable Tolerance Of Rated Resistance F is $\pm 1\%$
- Rated Resistance 502 namely 5k Ω
- Type: Glass Shell Precision NTC Thermistor

Dimensions(mm)



Main Techno-Parameter

- Zero power resistance range (R25): 0.1~1000K Ω
- Available tolerances of R25:
F= $\pm 1\%$ G= $\pm 2\%$ H= $\pm 3\%$ J= $\pm 5\%$ K= $\pm 10\%$
- B value (B25/50 $^{\circ}$ C) range: 3100~4500K
- Available tolerances of B value: $\pm 0.5\%$, $\pm 1\%$, $\pm 2\%$
- Dissipation factor: $\geq 2\text{mW}/^{\circ}\text{C}$ (In Still Air)
- Thermal time constant: $\leq 20\text{S}$ (In Still Air)
- Operating temperature range: $-55^{\circ}\text{C} \sim +200^{\circ}\text{C}$
- Rated Power: $\leq 50\text{mW}$



CANTHERM

8415 Mountain Sights Avenue • Montreal (Quebec), H4P 2B8, Canada
Tel: (514) 739-3274 • 1-800-561-7207 • Fax: (514) 739-2902
E-mail: sales@cantherm.com • Website: www.cantherm.com

2008/Feb



COZIR™

Ultra Low Power Carbon Dioxide Sensor

COZIR is an ultra low power (3.5mW^4), high performance CO_2 sensor, ideally suited for battery operation, portable instruments and HVAC. Based on GSS IR LED and Detector technology, and innovative optical designs, the COZIR offers the lowest power NDIR sensor available. Optional temperature, humidity and light sensing are available. COZIR is a third generation product from GSS – leaders in IR LED CO_2 sensing.



- Ultra-low Power 3.5mW
- Measurement ranges from 2000ppm to 2%
- Low noise measurement (<10ppm)
- 3.3V supply.
- Peak current only 33mA.
- Optional Temperature and Humidity Output



Specifications

General Performance

Warm-up Time

- < 10s

Operating Conditions

- 0°C to 50°C (standard)
- -25°C to 55°C (extended range)
- 0 to 95% RH, non-condensing

Recommended Storage

- -30°C to +70°C

CO2 Measurement

Sensing Method

- Non-dispersive infrared (NDIR) absorption
- Patented Gold-plated optics
- Patented Solid-state source and detector

Sample Method

- Diffusion

Measurement Range

- 0-2,000ppm, 0-5,000ppm, 0-10,000ppm (1%) CO₂
- Extended range (up to 100%) available

Accuracy

- ± 50 ppm +/- 3% of reading¹

Non Linearity

- < 1% of FS

Pressure Dependence

- 0.13% of reading per mm Hg



131 Business Center Drive, Suite A-3
Ormond Beach, FL 32174
877.678.4259 Toll Free
866.422.2356 Fax
www.co2meter.com
info@co2meter.com



Operating Pressure Range

- 950 to 1050 bar²

Response Time

- 30 secs to 2 mins (user Configurable)³
- Reading refreshed twice per second.³

Electrical/Mechanical

Power Input

- 3.25V to 5.5V DC
- Peak Current 33mA⁴.
- Average Current <1.5mA⁴.

Power Consumption

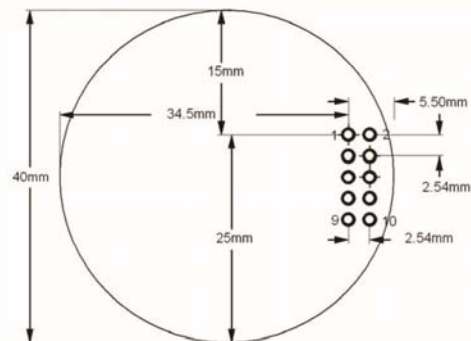
- 3.5 mW⁴

Wiring Connections

- 2x5 0.1" header.

view from underside (connector side)

1	GND	2	N/C
3	3.3V (nominal)	4	N/C
5	Rx	6	N/C
7	Tx	8	Nitrogen Zero
9	Analog (0.1 to 3.3V)	10	Fresh Air Zero



Note that the drawing shows details of the PCB inside the sensor casing. The outside dimension of the sensor casing is 43mm.

Pin 2 should not be connected. Pins 4 and 6 do not require connection and are internally connected to GND.



The zeroing options are for hardware zeroing (both active low). These functions can also be implemented by sending a serial command (recommended).

Typical connections for digital interface are GND, 3.3V, Rx and Tx.

The analog (voltage) output is available only when specified. Otherwise, N/C.

The serial connection is 9600baud, 8 bit, no parity, one stop bit. There is no hardware flow control. Note that Vh for the serial Rx and Tx lines will be 3V regardless on the supply voltage.

Temperature & Humidity Measurement⁵

Optional Temperature and Humidity sensor (only available as digital output)

Sensing Method

Humidity: Capacitive
Temperature: Bandgap

Measurement Range

- -25 to +55 °C
- 0 to 95% RH

Resolution

- 0.08 °C , 0.08% RH

Absolute Accuracy⁵

- +/- 1 °C 0°C to 55°C.
- +/- 3% RH 20°C to 55°C.
- +/- 2 °C over the full temperature range.
- +/- 5% RH over the full temperature range.

Repeatability

- +/- 0.1 °C
- +/- 0.1 % RH

Note 1: All measurements are at STP unless otherwise stated.

Note 2: External Pressure calibration required to eliminate pressure dependence.

Note 3: User Configurable Filter Response.

Note 4: Power measurements for standard CO2 sensor with 2 readings/second. Temp. and humidity measurements increase power consumption.

Note 5: Temperature and Humidity derived from Sensirion SHT21 chip. See Sensirion data sheet for full details.



131 Business Center Drive, Suite A-3
Ormond Beach, FL 32174
877.678.4259 Toll Free
866.422.2356 Fax
www.co2meter.com
info@co2meter.com

**Wireless Vantage Pro2™ &
Vantage Pro2™ Plus Stations**
(Including Fan-Aspirated Models)



6152 6162
6153 6163

VANTAGE PRO2™

Vantage Pro2™ (6152, 6153) and Vantage Pro2™ Plus (6162, 6163) Wireless Weather Stations include two components: the Integrated Sensor Suite (ISS) which houses and manages the external sensor array, and the console which provides the user interface, data display, and calculations. The ISS and Vantage Pro2 console communicate via an FCC-certified, license-free, spread-spectrum frequency-hopping (FHSS) transmitter and receiver. User-selectable transmitter ID codes allow up to eight stations to coexist in the same geographic area. The frequency hopping spread spectrum technology provides greater communication strength over longer distances and areas of weaker reception. The Wireless Vantage Pro2™ Plus weather station includes two additional sensors that are optional on the Vantage Pro2: the UV sensor and the solar radiation sensor. The console may be powered by batteries or by the included AC-power adapter. The wireless ISS is solar powered with a battery backup. Use WeatherLink™ for Vantage Pro and Vantage Pro2 to let your weather station interface with a computer, to log weather data, and to upload weather information to the internet.

The 6152 and 6162 rely on passive shielding to reduce solar-radiation induced temperature errors in the outside temperature sensor readings. The Fan-aspirated 6153 and 6163 combine passive shielding with a solar-powered fan that draws outside air in over the temperature and humidity sensors, providing a much more accurate temperature reading than that available using passive shielding alone.

Integrated Sensor Suite (ISS)

Operating Temperature	-40° to +150°F (-40° to +65°C)
Non-operating Temperature	-40° to +158°F (-40° to +70°C)
Current Draw (ISS SIM only)	0.14 mA (average), 30 mA (peak) at 4 to 6 VDC
Solar Power Panel	0.5 Watts (ISS SIM), plus 0.75 Watts (Fan-Aspirated)
Battery (ISS SIM /Fan-Aspirated)	CR-123 3-Volt Lithium cell / 2 - 1.2 Volt NiCad C-cells
Battery Life (3-Volt Lithium cell)	8 months without sunlight - greater than 2 years depending on solar charging
Battery Life (NiCad C-cells)	1 year
Fan Aspiration Rate (Fan-Aspirated Only)	190 feet/min. (0.9 m/s) (full sun), 80 feet/min. (0.4 m/s) (battery only) (intake flow rate) 500 feet/min. (2.5 m/s) (full sun), 280 feet/min. (1.4 m/s) (battery only) (sensor chamber flow rate)
Connectors, Sensor	Modular RJ-11
Cable Type	4-conductor, 26 AWG
Cable Length, Anemometer	40' (12 m) (included) 540' (165 m) (maximum recommended)
Wind Speed Sensor	Wind cups with magnetic switch
Wind Direction Sensor	Wind vane with potentiometer
Rain Collector Type	Tipping bucket, 0.01" per tip (0.2 mm with metric rain adapter), 33.2 in ² (214 cm ²) collection area
Temperature Sensor Type	PN Junction Silicon Diode
Relative Humidity Sensor Type	Film capacitor element
Housing Material	UV-resistant ABS, ASA plastic

ISS Dimensions:

Product #	(Length x Width x Height)	Package Weight
6152	11.00" x 9.38" x 14.00"	5.7 lbs. (2.6 kg)
6162	(279 mm x 238 mm x 355 mm)	6.1 lbs. (2.6 kg)
6153	11.00" x 9.38" x 21.00"	8.6 lbs. (3.9 kg)
6163	(279 mm x 238 mm x 533 mm)	9 lbs. (4.1 kg)

2

Vantage Pro2™

Console

Console Operating Temperature	+32° to +140°F (0° to +60°C)
Non-Operating (Storage) Temperature	+14° to +158°F (-10° to +70°C)
Current Draw	0.9 mA average, 30 mA peak, (add 120 mA for display lamps, add 0.125 mA for each optional wireless transmitter received by the console) at 4 - 6 VDC
AC Power Adapter	5 VDC, 300 mA, regulated
Batteries	3 C-cells
Battery Life	up to 9 months
Connectors	Modular RJ-11
Housing Material	UV-resistant ABS plastic
Console Display Type	LCD Transflective
Display Backlight	LEDs
Dimensions (console: length x width x height, display length x height)	
Console with antenna down	10.625" x 6.125" x 1.625" (270 mm x 156 mm x 41 mm)
Console with antenna extended up	10.625" x 9.625" x 1.625" (270 mm x 245 mm x 41 mm)
Display	5.94" x 3.375" (151 mm x 86 mm)
Weight (with batteries)	1.88 lbs. (.85 kg)

Data Displayed on Console

Data display categories are listed with General first, then in alphabetical order.

General

Historical Data	Includes the past 24 values listed unless otherwise noted; all can be cleared and all totals reset
Daily Data	Includes the earliest time of occurrence of highs and lows; period begins/ends at 12:00 am
Monthly Data	Period begins/ends at 12:00 am on the first of the month
Yearly Data	Period begins/ends at 12:00 am on the first of January unless otherwise noted
Current Display Data	Current display data describes the current reading for each weather variable. In most cases, the variable lists the most recently updated reading or calculation. Some current variable displays can be adjusted so there is an offset for the reading
Current Graph Data	Current graph data appears in the right-most column in the console graph and represents the latest value within the last period on the graph; totals can be set or reset. Display intervals vary. Examples include: Instant, 15-min., and Hourly Reading; Daily, Monthly, High and Low
Graph Time Interval	1 min., 10 min., 15 min., 1 hour, 1 day, 1 month, 1 year (user-selectable, availability depends upon variable selected)
Graph Time Span	24 Intervals + Current Interval (see Graph Intervals to determine time span)
Graph Variable Span (Vertical Scale)	Automatic (varies depending upon data range); Maximum and Minimum value in range appear in ticker
Alarm Indication	Alarms sound for only 2 minutes (time alarm is always 1 minute) if operating on battery power. Alarm message is displayed in ticker as long as threshold is met or exceeded. Alarms can be silenced (but not cleared) by pressing the DONE key.
Transmission Interval	Varies with transmitter ID code from 2.25 seconds (#1=shortest), to 3 seconds (#8=longest)
Update Interval	Varies with sensor - see individual sensor specs

Barometric Pressure

Resolution and Units	0.01" Hg, 0.1 mm Hg, 0.1 hPa/mb (user-selectable)
Range	16.00" to 32.50" Hg, 410 to 820 mm Hg, 540 to 1100 hPa/mb
Elevation Range	-999' to +15,000' (-600 m to 4570 m) (Note that console screen limits entry of lower elevation to -999' when using feet as elevation unit.)
Uncorrected Reading Accuracy	±0.03" Hg (±0.8 mm Hg, ±1.0 hPa/mb) (at room temperature)
Sea-Level Reduction Equation Used	United States Method employed prior to use of current "R Factor" method

Equation Source	Smithsonian Meteorological Tables
Equation Accuracy	±0.01" Hg (±0.3 mm Hg, ±0.3 hPa/mb)
Elevation Accuracy Required	±10' (3m) to meet equation accuracy specification
Overall Accuracy	±0.03" Hg (±0.8 mm Hg, ±1.0 hPa/mb)
Trend (change in 3 hours).....	Change 0.06" (2 hPa/mb, 1.5 mm Hg) = Rapidly Change 0.02" (.7hPa/mb, .5 mm Hg)= Slowly
Trend Indication	5 position arrow: Rising (rapidly or slowly), Steady, or Falling (rapidly or slowly)
Update Interval	1 minute or when console BAR key is pressed twice
Current Display	Instant
Current Graph Data	Instant, 15-min., and Hourly Reading; Daily, Monthly, High and Low
Historical Graph Data	15-min. and Hourly Reading; Daily, Monthly Highs and Lows
Alarms	High Threshold from Current Trend for Storm Clearing (Rising Trend) Low Threshold from Current Trend for Storm Warning (Falling Trend)
Range for Rising and Falling Trend Alarms	0.01 to 0.25" Hg (0.1 to 6.4 mm Hg, 0.1 to 8.5 hPa/mb)

Clock

Resolution	1 minute
Units	Time: 12 or 24 hour format (user-selectable)
Date	US or International format (user-selectable)
Accuracy	±8 seconds/month
Adjustments	Time: Automatic Daylight Savings Time (for users in North America and Europe that observe it in AUTO mode, MANUAL setting available for all other areas) Date: Automatic Leap Year
Alarms	Once per day at set time when active

Dewpoint (calculated)

Resolution and Units	1°F or 1°C (user-selectable) °C is converted from °F rounded to the nearest 1°C
Range	-105° to +130°F (-76° to +54°C)
Accuracy	±3°F (±1.5°C) (typical)
Update Interval	10 to 12 seconds
Source	World Meteorological Organization (WMO)
Equation Used	WMO Equation with respect to saturation of moist air over water
Variables Used	Instant Outside Temperature and Instant Outside Relative Humidity
Current Display Data	Instant Calculation
Current Graph Data	Instant Calculation; Daily, Monthly High and Low
Historical Graph Data	Hourly Calculations; Daily, Monthly Highs and Lows
Alarms	High and Low Threshold from Instant Calculation

Evapotranspiration (calculated, requires solar radiation sensor)

Resolution and Units	0.01" or 0.1 mm (user-selectable)
Range	Daily to 32.67" (832.1 mm); Monthly & Yearly to 199.99" (1999.9 mm)
Accuracy	Greater of 0.01" (0.25 mm) or ±5%, Reference: side-by-side comparison against a CIMIS ET weather station
Update Interval	1 hour
Calculation and Source	Modified Penman Equation as implemented by CIMIS (California Irrigation Management Information System) including Net Radiation calculation
Current Display Data	Latest Hourly Total Calculation
Current Graph Data	Latest Hourly Total Calculation, Daily, Monthly, Yearly Total
Historical Graph Data	Hourly, Daily, Monthly, Yearly Totals
Alarm	High Threshold from Latest Daily Total Calculation

4

Vantage Pro2™

Forecast

Variables Used	Barometric Reading & Trend, Wind Speed & Direction, Rainfall, Temperature, Humidity, Latitude & Longitude, Time of Year
Update Interval	1 hour
Display Format	Icons on top center of display; detailed message in ticker at bottom
Variables Predicted	Sky Condition, Precipitation, Temperature Changes, Wind Direction and Speed

Heat Index (calculated)

Resolution and Units	1°F or 1°C (user-selectable) °C is converted from °F rounded to the nearest 1°C
Range	-40° to +165°F (-40° to +74°C)
Accuracy	±3°F (±1.5°C) (typical)
Update Interval	10 to 12 seconds
Source	United States National Weather Service (NWS)/NOAA
Formulation Used	Steadman (1979) modified by US NWS/NOAA and Davis Instruments to increase range of use
Variables Used	Instant Outside Temperature and Instant Outside Relative Humidity
Current Display Data	Instant Calculation
Current Graph Data	Instant Calculation; Daily, Monthly High
Historical Graph Data	Hourly Calculations; Daily, Monthly Highs
Alarm	High Threshold from Instant Calculation

Humidity

Inside Relative Humidity (sensor located in console)

Resolution and Units	1%
Range	1 to 100% RH
Accuracy	±3% (0 to 90% RH), ±4% (90 to 100% RH)
Update Interval	1 minute
Current Display Data	Instant (user-adjustable offset available)
Current Graph Data	Instant; Hourly Reading; Daily, Monthly High and Low
Historical Graph Data	Hourly Readings; Daily, Monthly Highs and Lows
Alarms	High and Low Threshold from Instant Reading

Outside Relative Humidity (sensor located in ISS)

Resolution and Units	1%
Range	1 to 100% RH
Accuracy	±3% (0 to 90% RH), ±4% (90 to 100% RH)
Temperature Coefficient	0.03% per °F (0.05% per °C), reference 68°F (20°C)
Drift	±0.5% per year
Update Interval	50 seconds to 1 minute
Current Display Data	Instant (user-adjustable offset available)
Current Graph Data	Instant; Hourly Reading; Daily, Monthly High and Low
Historical Graph Data	Hourly Readings; Daily, Monthly Highs and Lows
Alarms	High and Low Threshold from Instant Reading

Extra Outside Relative Humidity (sensor located inside Temperature/Humidity Station)

Resolution and Units	1%
Range	1 to 100% RH
Accuracy	±3% (0 to 90% RH), ±4% (90 to 100% RH)
Temperature Coefficient	0.03% per °F (0.05% per °C), reference 68°F (20°C)
Drift	±0.5% per year
Update Interval	50 seconds to 1 minute
Current Display Data	Instant Reading (user adjustable)
Alarms	High and Low Threshold from Instant Reading

Leaf Wetness (requires leaf wetness sensor)

Resolution	1
Range	0 to 15
Dry/Wet Threshold	User-selectable
Accuracy	±0.5
Update Interval	15 to 18 seconds
Current Graph Data	Instant Reading; Daily High and Low; Monthly High
Historical Graph Data	Hourly Readings; Daily Highs and Lows; Monthly Highs
Alarms	High and Low Thresholds from Instant Reading

Moon Phase

Console Resolution	1/8 (12.5%) of a lunar cycle, 1/4 (25%) of lighted face on console
WeatherLink Resolution	0.09% of a lunar cycle, 0.18% of lighted face maximum (depends on screen resolution)
Range	New Moon, Waxing Crescent, First Quarter, Waxing Gibbous, Full Moon, Waning Gibbous, Last Quarter, Waning Crescent
Accuracy	±38 minutes

Rainfall

Resolution and Units	0.01" or 0.2 mm (user-selectable) (1 mm at totals ≥ 2000 mm)
Daily/Storm Rainfall Range	0 to 99.99" (0 to 999.8 mm)
Monthly/Yearly/Total Rainfall Range	0 to 199.99" (0 to 6553 mm)
Rain Rate	0 to 96" (0 to 2438 mm)
Accuracy	For rain rates up to 2"/hr (50 mm/hr): ±4% of total or +0.01" (0.2mm) (0.01" = one tip of the bucket), whichever is greater. For rain rates from 2"/hr (50 mm/hr) to 4"/hr (100 mm/hr): ±4% of total or +0.01" (0.25 mm) (0.01" = one tip of the bucket), whichever is greater
Update Interval	20 to 24 seconds
Storm Determination Method	0.02" (0.5 mm) begins a storm event, 24 hours without further accumulation ends a storm event
Current Display Data	Totals for Past 15-min
Current Graph Data	Totals for Past 15-min, Past 24-hour, Daily, Monthly, Yearly (start date user-selectable) and Storm (with begin date); Umbrella is displayed when 15-minute total exceeds zero
Historical Graph Data	Totals for 15-min, Daily, Monthly, Yearly (start date user-selectable) and Storm (with begin and end dates)
Alarms	High Threshold from Latest Flash Flood (15-min. total, default is 0.50", 12.7 mm), 24-Hour Total, Storm Total,
Range for Rain Alarms	0 to 99.99" (0 to 999.7 mm)

Rain Rate

Resolution and Units	0.01" or 0.1 mm (user-selectable) at typical rates (see Fig. 3 and 4)
Range	0, 0.04"/hr (1 mm/hr) to 96"/hr (0 to 2438 mm/hr)
Accuracy	±5% for rates less than 5" per hour (127 mm/hr)
Update Interval	20 to 24 seconds
Calculation Method	Measures time between successive tips of tipping bucket. Elapsed time greater than 15 minutes or only one tip of the rain collector constitutes a rain rate of zero.
Current Display Data	Instant
Current Graph Data	Instant and 1-min. Reading; Hourly, Daily, Monthly and Yearly High
Historical Graph Data	1-min Reading; Hourly, Daily, Monthly and Yearly Highs
Alarm	High Threshold from Instant Reading

6

Vantage Pro2™

Soil Moisture (requires soil moisture Sensor)

Resolution	.1 cb
Range	.0 to 200 cb
Update Interval	.75 to 90 seconds
Current Graph Data	Instant Reading; Daily and Monthly High and Low
Historical Graph Data	Hourly Readings; Daily and Monthly Highs and Lows
Alarms	High and Low Thresholds from Instant Reading

Solar Radiation (requires solar radiation sensor)

Resolution and Units	.1 W/m ²
Range	.0 to 1800 W/m ²
Accuracy	±5% of full scale (Reference: Eppley PSP at 1000 W/m ²)
Drift	up to ±2% per year
Cosine Response	±3% for angle of incidence from 0° to 75°
Temperature Coefficient	-0.067% per °F (-0.12% per °C); reference temperature = 77°F (25 °C)
Update Interval	.50 seconds to 1 minute (5 minutes when dark)
Current Graph Data	Instant Reading and Hourly Average; Daily, Monthly High
Historical Graph Data	Hourly Average, Daily, Monthly Highs
Alarm	High Threshold from Instant Reading

Sunrise and Sunset

Resolution	.1 minute
Accuracy	±1 minute
Reference	United States Naval Observatory

Temperature

Inside Temperature (sensor located in console)

Resolution and Units	Current Data: 0.1°F or 1°F or 0.1°C or 1°C (user-selectable) °C is converted from °F rounded to the nearest 1°C Historical Data and Alarms: 1°F or 1°C (user-selectable)
Range	+32° to +140°F (0° to +60°C)
Sensor Accuracy	±1°F (±0.5°C)
Update Interval	.1 minute
Current Display Data	Instant (user-adjustable offset available)
Current Graph Data	Instant Reading; Daily and Monthly High and Low
Historical Graph Data	Hourly Readings; Daily and Monthly Highs and Lows
Alarms	High and Low Thresholds from Instant Reading

Outside Temperature (sensor located in ISS)

Resolution and Units	Current Data: 0.1°F or 1°F or 0.1°C or 1°C (user-selectable) nominal (see Fig. 1) °C is converted from °F rounded to the nearest 1°C Historical Data and Alarms: 1°F or 1°C (user-selectable)
Range	-40° to +150°F (-40° to +65°C)
Sensor Accuracy	±1°F (±0.5°C) above 20°F (-7°C), ±2°F (±1°C) under 20°F (-7°C) (see Fig. 2)
Radiation Induced Error (Passive Shield)	+4°F (2°C) at solar noon (insolation = 1040 W/m ² , avg. wind speed ≤ 2 mph (1 m/s)) (reference: RM Young Model 43408 Fan-Aspirated Radiation Shield)
Radiation Induced Error (Fan-Aspirated Shield)	+0.6°F (0.3°C) at solar noon (insolation = 1040 W/m ² , avg. wind speed ≤ 2 mph (1 m/s)) (reference: RM Young Model 43408 Fan-Aspirated Radiation Shield)
Update Interval	.10 to .12 seconds
Current Display Data	Instant (user-adjustable offset available)
Current Graph Data	Instant Reading; Daily, Monthly, Yearly High and Low
Historical Graph Data	Hourly Readings; Daily, Monthly, Yearly Highs and Lows
Alarms	High and Low Thresholds from Instant Reading

Extra Temperature Sensors or Probes

Resolution and Units	Current Data: 1°F or 1°C (user-selectable) °C is converted from °F rounded to the nearest 1°C Historical Data and Alarms: 1°F or 1°C (user-selectable)
----------------------	---

Range	-40° to +150°F (-40° to +65°C)
Sensor Accuracy	±1°F (±0.5°C) above 20°F (-7°C), ±2°F (±1°C) under 20°F (-7°C) (see Fig. 2)
Update Interval	10 to 12 seconds (40 to 48 seconds for Leaf Wetness/Temperature and Soil Moisture/Temperature Stations)
Current Display Data	Instant Reading (user-adjustable offset available)
Alarms	High and Low Thresholds from Instant Reading

Temperature Humidity Sun Wind Index (requires solar radiation sensor)

Resolution and Units	1°F or 1°C (user-selectable) °C is converted from °F rounded to the nearest 1°C
Range	-90° to +165°F (-68° to +74°C)
Accuracy	±4°F (±2°C) (typical)
Update Interval	10 to 12 seconds
Sources and Formulation Used	United States National Weather Service (NWS)/NOAA Steadman (1979) modified by US NWS/NOAA and Davis Instruments to increase range of use and allow for cold weather use
Variables Used	Instant Outside Temperature, Instant Outside Relative Humidity, 10-minute Average Wind Speed, 10-minute Average Solar Radiation
Formulation Description	Uses Heat Index as base temperature, affects of wind and solar radiation are either added or subtracted from this base to give an overall effective temperature
Current Graph Data	Instant and Hourly Calculation; Daily, Monthly High
Historical Graph Data	Hourly Calculation; Daily, Monthly Highs
Alarm	High Threshold from Instant Reading

Ultra Violet (UV) Radiation Dose (requires UV sensor)

Resolution and Units	0.1 MEDs to 19.9 MEDs; 1 MED above 19.9 MEDs
Range	0 to 199 MEDs
Accuracy	±5% of daily total
Drift	up to ±2% per year
Update Interval	50 seconds to 1 minute (5 minutes when dark)
Current Graph Data	Latest Daily Total (user resetable at any time from Current Screen)
Historical Graph Data	Hourly, Daily Totals (user reset from Current Screen does not affect these values)
Alarm	High Threshold from Daily Total
Alarm Range	0 to 19.9 MEDs

Ultra Violet (UV) Radiation Index (requires UV sensor)

Resolution and Units	0.1 Index
Range	0 to 16 Index
Accuracy	±5% of full scale (Reference: Yankee UVB-1 at UV index 10 (Extremely High))
Cosine Response	±4% (0° to 65° incident angle); 9% (65° to 85° incident angle)
Update Interval	50 seconds to 1 minute (5 minutes when dark)
Current Graph Data	Instant Reading and Hourly Average; Daily, Monthly High
Historical Graph Data	Hourly Average, Daily, Monthly Highs
Alarm	High Threshold from Instant Calculation

Wind

Wind Chill (Calculated)	
Resolution and Units	1°F or 1°C (user-selectable) °C is converted from °F and rounded to the nearest 1°C
Range	-110° to +135°F (-79° to +57°C)
Accuracy	±2°F (±1°C) (typical)
Update Interval	10 to 12 seconds
Source	United States National Weather Service (NWS)/NOAA
Equation Used	Osczevski (1995) (adopted by US NWS in 2001)
Variables Used	Instant Outside Temperature and 10-min. Avg. Wind Speed
Current Display Data	Instant Calculation

8

Vantage Pro2™

Current Graph Data	Instant Calculation; Hourly, Daily and Monthly Low
Historical Graph Data	Hourly, Daily and Monthly Lows
Alarm	Low Threshold from Instant Calculation
Wind Direction	
Range	0 - 360°
Display Resolution	16 points (22.5°) on compass rose, 1° in numeric display
Accuracy	±3°
Update Interval	2.5 to 3 seconds
Current Display Data	Instant (user-adjustable offset available)
Current Graph Data	Instant; 10-min. Dominant; Hourly, Daily, Monthly Dominant
Historical Graph Data	Past 6 10-min. Dominants on compass rose only; Hourly, Daily, Monthly Dominants
Wind Speed	
Resolution and Units	1 mph, 1 km/h, 0.4 m/s, or 1 knot (user-selectable). Measured in mph, other units are converted from mph and rounded to nearest 1 km/hr, 0.1 m/s, or 1 knot.
Range	2 to 180 mph, 2 to 156 knots, 1 to 80 m/s, 3 to 290 km/h
Update Interval	Instant Reading: 2.5 to 3 seconds, 10-minute Average: 1 minute
Accuracy	±2 mph (2 kts, 3 km/h, 1 m/s) or ±5%, whichever is greater
Maximum Cable Length	540' (165 m)
Current Display Data	Instant
Current Graph Data	Instant; 10-minute and Hourly Average; Hourly High; Daily, Monthly and Yearly High with Direction of High
Historical Graph Data	10-min. and Hourly Averages; Hourly Highs; Daily, Monthly and Yearly Highs with Direction of Highs
Alarms	High Thresholds from Instant Reading and 10-minute Average

Wireless Communications

Transmit/Receive Frequency	US Models: 902-928 MHz FHSS. Overseas Models: 868.0 - 868.6 MHz FHSS
ID Codes Available	8
Output Power	902-928 MHz FHSS: FCC-certified low power, less than 8 mW, no license required 868.0 - 868.6 MHz FHSS: CE-certified, less than 8 mW, no license required
Range	
Line of Sight	up to 1000 feet (300 m)
Through Walls	200 to 400 feet (60 to 120 m)
Sensor Inputs	
RF Filtering	RC low-pass filter on each signal line

Sensor Charts

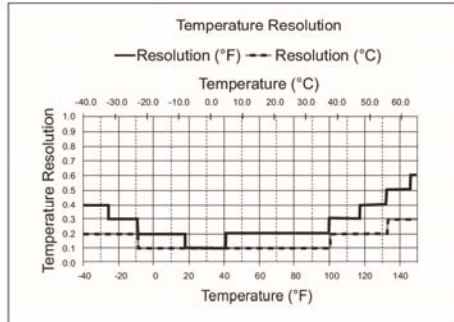


Figure 1. Temperature Resolution

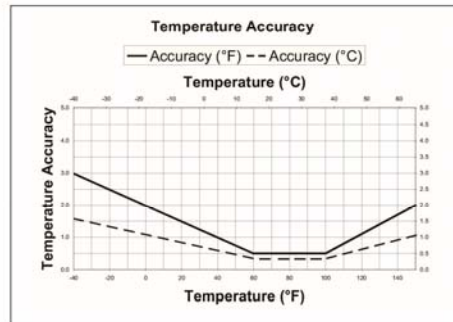


Figure 2. Temperature Accuracy

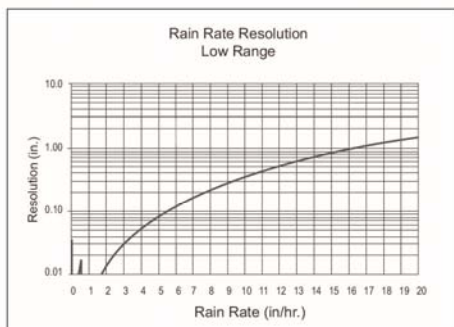


Figure 3. Low Range Rain Rate Resolution

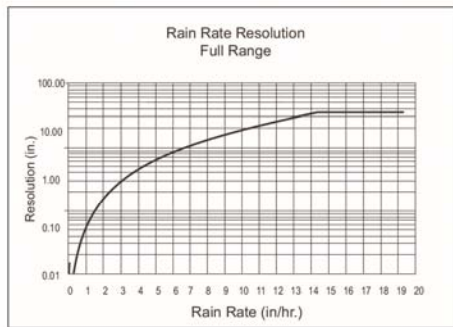


Figure 4. Full Range Rain Rate Resolution

Package Dimensions

Product #	Package Dimensions (Length x Width x Height)	Package Weight	UPC Codes
6152 6152EU 6152UK	17.0" x 11.0" x 13.0" (410 mm x 264 mm x 330 mm)	12.8 lbs. (5.8 kg)	011698 00229 0
			011698 00347 1 011698 00348 8
6162 6162EU 6162UK	15.0" x 13.0" x 24.0" (378 mm x 327 mm x 594 mm)	13.3 lbs. (6.0 kg)	011698 00306 8
			011698 00307 5 001698 00308 2
6153 6153EU 6153UK	15.0" x 13.0" x 24.0" (378 mm x 327 mm x 594 mm)	12.8 lbs. (5.8 kg)	011698 00335 8
			011698 00336 5 001698 00337 2
6163 6163EU 6163UK	15.0" x 13.0" x 24.0" (378 mm x 327 mm x 594 mm)	13.3 lbs. (6.0 kg)	011698 00341 9
			011698 00342 6 001698 00342 3

Honeywell



Representative photograph, actual product appearance may vary.

Due to regional agency approval requirements, some products may not be available in your area. Please contact your regional Honeywell office regarding your product of choice.

HIH-4000-001

HIH-4000 Series Integrated Circuitry Humidity Sensor, 2,54 mm (0.100 in) Lead Pitch SIP

Features

- Molded thermoset plastic housing with cover
- Linear voltage output vs %RH
- Laser trimmed interchangeability
- Low power design
- High accuracy
- Fast response time
- Stable, low drift performance
- Chemically resistant

Typical Applications

- Refrigeration
- Drying
- Meteorology
- Battery-powered systems
- OEM assemblies

Description

The HIH-4000 Series Humidity Sensors are designed specifically for high volume OEM (Original Equipment Manufacturer) users. Direct input to a controller or other device is made possible by this sensor's linear voltage output. With a typical current draw of only 200 μ A, the HIH-4000 Series is ideally suited for low drain, battery operated systems. Tight sensor interchangeability reduces or eliminates OEM production calibration costs. Individual sensor calibration data is available.

The HIH-4000 Series delivers instrumentation-quality RH (Relative Humidity) sensing performance in a low cost, solderable SIP (Single In-line Package). Available in two lead spacing configurations, the RH sensor is a laser trimmed, thermoset polymer capacitive sensing element with on-chip integrated signal conditioning. The sensing element's multilayer construction provides excellent resistance to most application hazards such as wetting, dust, dirt, oils and common environmental chemicals.



HIH-4000-001

HIH-4000 Series Integrated Circuitry Humidity Sensor, 2,54 mm (0.100 in) Lead Pitch SIP

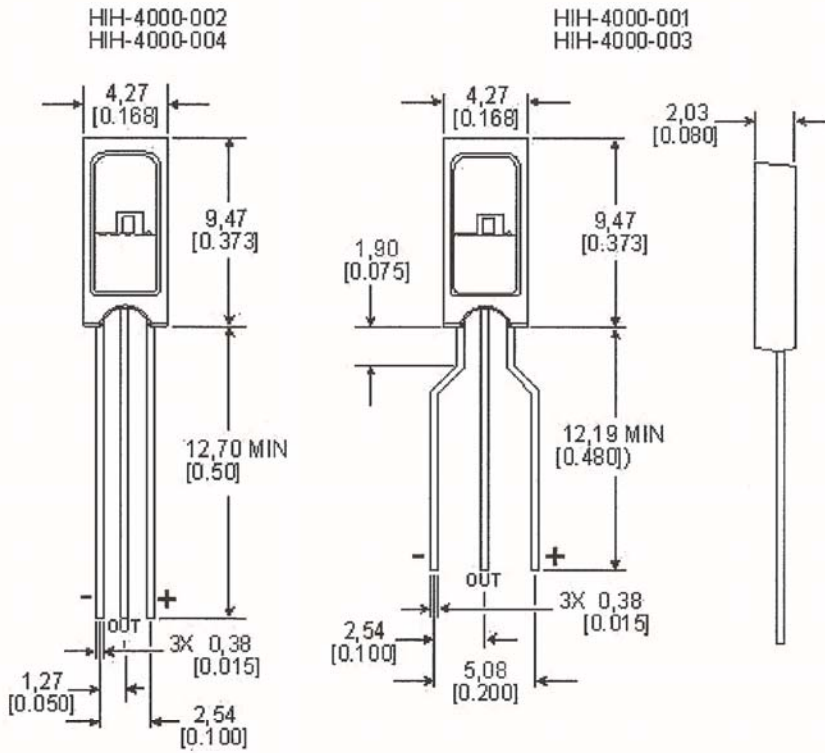
Product Specifications	
Package Style	Solderable SIP
Termination Details	2,54 mm [0.100 in] Lead Pitch
Series Name	HIH-4000 Series
RH Accuracy	± 3.5% RH, 0-100 % RH non-condensing, 25 °C, 5 Vdc supply
RH Interchangeability	± 5% RH, 0-60% RH; ± 8% @ 60-100% RH Typical
RH Hysteresis	± 3% of RH Span Maximum
RH Repeatability	± 0.5% RH
RH response time, 1/e	15 s in slowly moving air @ 25 °C
RH Stability	± 0.2% RH Typical at 50% RH in 1 Year
Supply Voltage	4.0 Vdc to 5.8 Vdc
Supply Current	500 µA Max.
Operating Humidity Range	0 to 100% RH, non-condensing
Operating Temperature Range	-40 °C to 85 °C (-40 °F to 185 °F)
Temperature Compensation	True RH = Sensor RH/(1.0305+0.000044T-0.0000011T ²) T in °C (True RH = Sensor RH/(0.9237-0.0041T+0.000040T ²) T in °C)
Availability	Global
Comment	Light sensitive, shield from bright light.
UNSPSC Code	411121
UNSPSC Commodity	411121 Transducers



HIH-4000-001

HIH-4000 Series Integrated Circuitry Humidity Sensor, 2,54 mm (0.100 in) Lead Pitch SIP

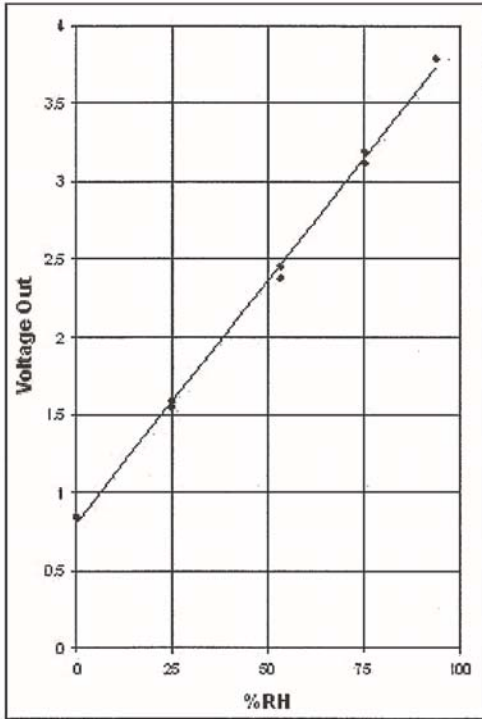
Mounting Dimensions
For Reference Only [mm/in]



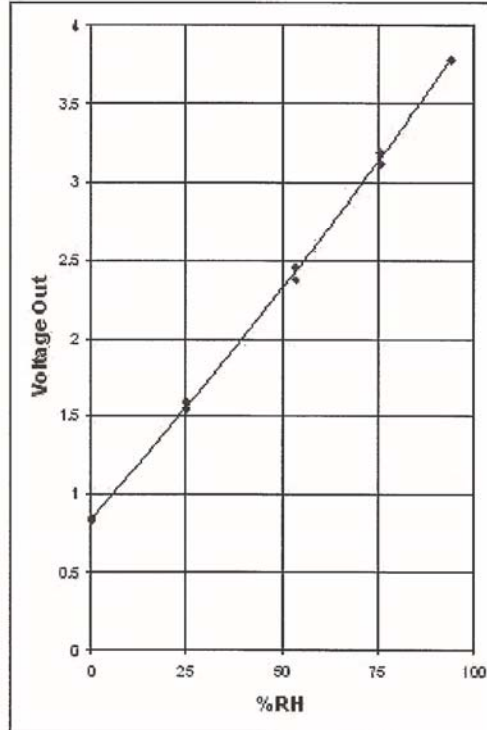
HIH-4000-001

HIH-4000 Series Integrated Circuitry Humidity Sensor, 2,54 mm (0.100 in) Lead Pitch SIP

TYPICAL BEST FIT STRAIGHT LINE



TYPICAL 2nd ORDER CURVE FIT

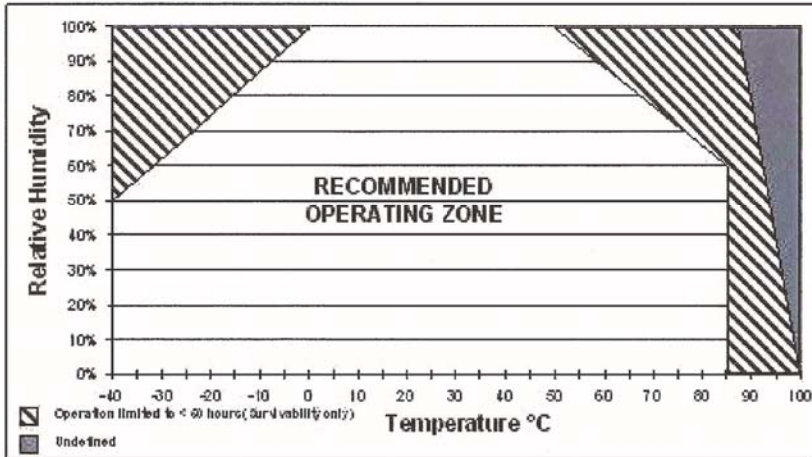


Honeywell

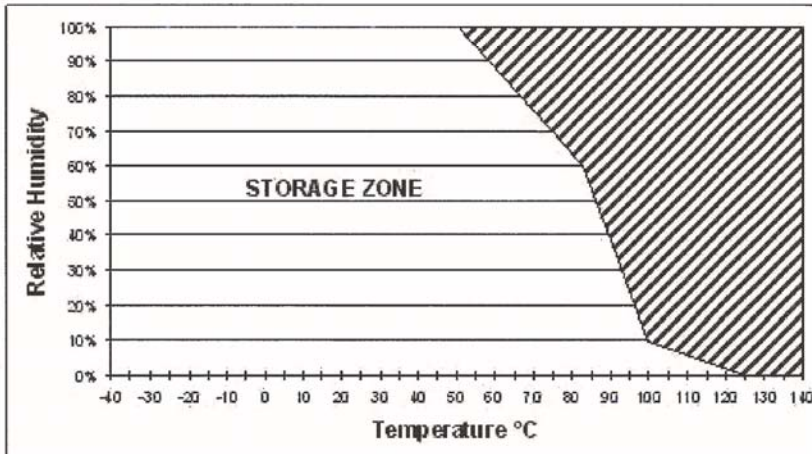
HIH-4000-001

HIH-4000 Series Integrated Circuitry Humidity Sensor, 2,54 mm (0.100 in) Lead Pitch SIP

Recommended Operating Conditions



Storage Environment



Honeywell

HIH-4000-001

HIH-4000 Series Integrated Circuitry Humidity Sensor, 2,54 mm (0.100 in) Lead Pitch SIP

⚠ WARNING

PERSONAL INJURY

DO NOT USE these products as safety or emergency stop devices, or in any other application where failure of the product could result in personal injury.

Failure to comply with these instructions could result in death or serious injury.

⚠ WARNING

MISUSE OF DOCUMENTATION

- The information presented in this product sheet (or catalog) is for reference only. DO NOT USE this document as product installation information.
- Complete installation, operation and maintenance information is provided in the instructions supplied with each product.

Failure to comply with these instructions could result in death or serious injury.

© Copyright Honeywell Inc. 1998-2004 All rights reserved.

HTM25X0LF – Temperature and Relative Humidity Module



- Hermetic Housing
- Humidity calibrated within +/-2% @55%RH
- Temperature measurement through NTC 10kOhms +/-1% direct output
- Small size product
- Typical 1 to 4 Volt DC output for 0 to 100%RH at 5Vdc



DESCRIPTION

Based on the rugged HTS2230 humidity / temperature sensor, HTM25X0LF is a dedicated humidity and temperature transducer designed for OEM applications where a reliable and accurate measurement is needed. Direct interface with a micro-controller is made possible with the module's humidity linear voltage output.

FEATURES

- | | |
|--|--|
| <ul style="list-style-type: none"> • Full interchangeability • High reliability and long term stability • Not affected by water immersion • Ratiometric to voltage supply • Suitable for 3 to 10 Vdc supply voltage | <p>Humidity Sensor Specific Features</p> <ul style="list-style-type: none"> • Instantaneous de-saturation after long periods in saturation phase • Fast response time • High resistance to chemicals • Patented solid polymer structure <p>Temperature Sensor Specific Features</p> <ul style="list-style-type: none"> • Stable • High sensitivity |
|--|--|

APPLICATIONS

- Industrial
- Process control
- Hygrostat
- Data logger
- ...



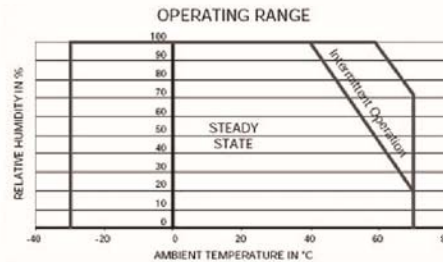
HTM25X0LF – Temperature and Relative Humidity Module

PERFORMANCE SPECS

MAXIMUM RATINGS

Ratings	Symbol	Value	Unit
Storage Temperature	Tstg	-40 to 125	°C
Storage Humidity	RHstg	0 to 100	% RH
Supply Voltage (Peak)	Vs	12	Vdc
Humidity Operating Range	RH	0 to 100	% RH
Temperature Operating Range	Ta	-40 to 125	°C

Peak conditions: less than 10% of the operating time



NOMENCLATURE

HTM25X0LF

Output Temperature Sensor:
 X = 0 – Direct NTC Output
 X = 3 – Voltage Output

ELECTRICAL CHARACTERISTICS

(Ta=23°C, Vs=5Vdc +/-5%, RL>1MΩ unless otherwise stated)

Humidity Characteristics	Symbol	Min	Typ	Max	Unit
Humidity Measuring Range	RH	1		99	%RH
Relative Humidity Accuracy (10 to 95% RH)	RH		+/-3	+/-5	%RH
Supply Voltage	Vs	4.75	5.00	5.25	Vdc
Nominal Output @55%RH (at 5Vdc)	Vout	2.42	2.48	2.54	V
Current consumption (HTM2500LF)	Ic		1.0	1.2	mA
Current consumption (HTM2530LF)	Ic		3.4	3.6	mA
Temperature Coefficient (10 to 50°C)	Tcc		+0.1		%RH/°C
Average Sensitivity from 33% to 75%RH	$\Delta V_{out}/\Delta RH$		+26		mV/%RH
Sink Current Capability (RL=15kΩ)	Is			300	μA
Recovery time after 150 hours of condensation	tr		10		s
Humidity Hysteresis			+/-1.5		%RH
Long term stability	T		+/-0.5		%RH/yr
Time Constant (at 63% of signal, static) 33% to 76%RH ⁽¹⁾	τ		5		s
Output Impedance	Z		70		Ω

(1) At 1m/s air flow

(Ta=25°C)

Temperature Characteristics	Symbol	Min	Typ	Max	Unit
Nominal Resistance @25°C	R		10		kΩ
Beta value: B25/50	β	3347	3380	3413	K
Temperature Measuring Range*	Ta	-40		125	°C
Nominal Resistance Tolerance @25°C	R _N			1	%
Beta Value Tolerance	β		1		%
Response Time	τ		10		s

* For temperature upper than 85°C, specific cable is required: HTM25X0LF-L products



HTM25X0LF – Temperature and Relative Humidity Module

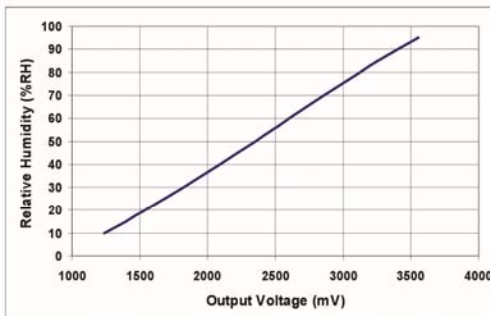
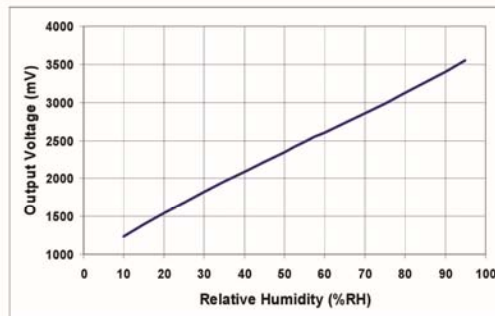
TYPICAL PERFORMANCE CURVES

HUMIDITY SENSOR

- Typical response look-up table

RH (%)	Vout (mV)	RH (%)	Vout (mV)
10	1235	55	2480
15	1390	60	2605
20	1540	65	2730
25	1685	70	2860
30	1825	75	2990
35	1960	80	3125
40	2090	85	3260
45	2220	90	3405
50	2350	95	3555

- Modeled linear voltage output ($V_s = 5V$)



- Linear Equations

$$V_{out} = 26.65 RH + 1006$$

$$RH = 0.0375 V_{out} - 37.7$$

with V_{out} in mV and RH in %

- Polynomial Equations

$$V_{out} = 1.05E^{-3}RH^3 - 1.76E^{-1}RH^2 + 35.2RH + 898.6$$

$$RH = -1.92E^{-9}V_{out}^3 + 1.44E^{-5}V_{out}^2 + 3.4V_{out} - 1.2$$

with V_{out} in mV and RH in %

- Measurement Conditions

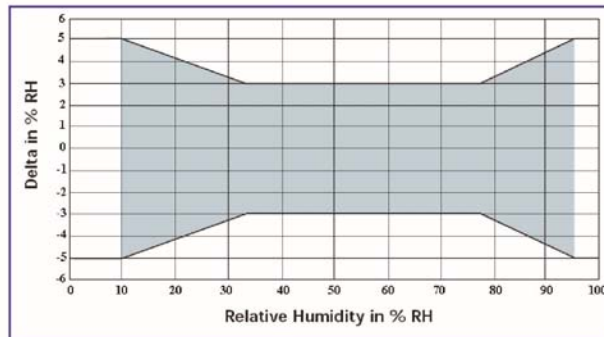
HTM25X0LF is specified for accurate measurements within 10 to 95% RH.

Excursion out of this range (<10% or >95% RH, including condensation) does not affect the reliability of HTM25X0LF characteristics.

HTM25X0LF – Temperature and Relative Humidity Module

- Error Budget at 23°C

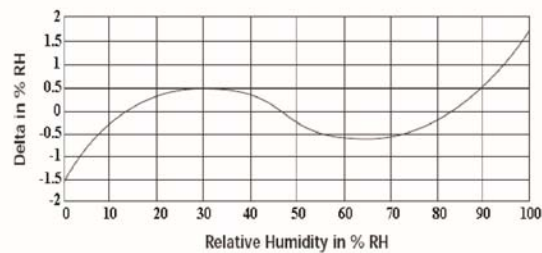
HTM25X0LF Error Limits:



Temperature coefficient compensation:

$$RH_{Cor} \% = RH_{read} \% \times (1 - (T_a - 23) \times 2.4 E^{-3})$$

HTM25X0LF Linearity Error:



Non-linearity and temperature compensation:

$$RH\% = \frac{-1.9206 E^{-9} V_{out}^3 + 1.437 E^{-5} V_{out}^2 + 3.421 E^{-3} V_{out} - 12.4}{1 + (T_a - 23) \times 2.4 E^{-3}}$$

All equations Vout in mV, RH in % and Ta in °C



HTM25X0LF – Temperature and Relative Humidity Module

HTM2500LF TEMPERATURE SENSOR: DIRECT NTC OUTPUT

- Typical temperature output

Depending on the needed temperature measurement range and associated accuracy, we suggest two methods to access to the NTC resistance values.

$$R_T = R_N \times e^{\beta \left(\frac{1}{T} - \frac{1}{T_N} \right)}$$

- R_T NTC resistance in Ω at temperature T in K
- R_N NTC resistance in Ω at rated temperature T in K
- T, T_N Temperature in K
- β Beta value, material specific constant of NTC
- e Base of natural logarithm (e=2.71828)

① The exponential relation only roughly describes the actual characteristic of an NTC thermistor can, however, as the material parameter β in reality also depend on temperature. So this approach is suitable for describing a restricted range around the rated temperature or resistance with sufficient accuracy.

② For practical applications, a more precise description of the real R/T curve may be required. Either more complicated approaches (e.g. the Steinhart-Hart equation) are used or the resistance/temperature relation as given in tabulation form. The below table has been experimentally determined with utmost accuracy for temperature increments of 1 degree.

Actual values may also be influenced by inherent self-heating properties of NTCs. Please refer to MEAS-France Application Note HPC106 “Low power NTC measurement”.

- Temperature look-up table

Temp (°C)	R (Ω)	Temp (°C)	R (Ω)
-40	195652	25	10000
-35	148171	30	8315
-30	113347	35	6948
-25	87559	40	5834
-20	68237	45	4917
-15	53650	50	4161
-10	42506	55	3535
-5	33892	60	3014
0	27219	65	2586
5	22021	70	2228
10	17926	75	1925
15	14674	80	1669
20	12081	85	1452

HTM25X0LF – Temperature and Relative Humidity Module

- Steinhart-Hart coefficients

According to the equation below, the Steinhart-Hart coefficients for the operating temperature range for HTM2500LF thermistor are:

$$\frac{1}{T} = a + b * \ln(R) + C * \ln(R) * \ln(R) * \ln(R)$$

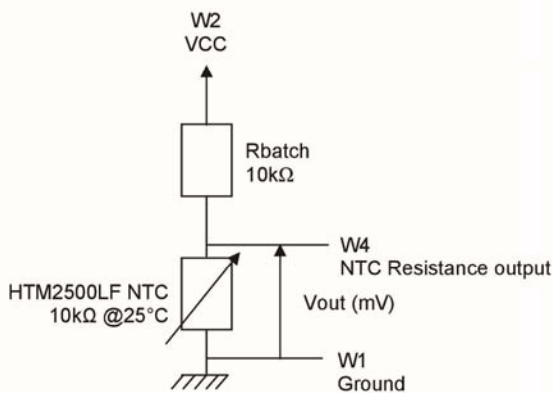
- R NTC resistance in Ω at temperature T in K
- T Temperature in K
- a Constant value (a = 8.54942E-04)
- b Constant value (b = 2.57305E-04)
- c Constant value (c = 1.65368E-07)

- Temperature Interface Circuit

Concerning the temperature sensor of the HTM2500LF, the following measuring method described below is based on a voltage bridge divider circuit. It uses only one resistor component (Rbatch) at 1% to design HTM2500LF temperature sensor interfacing circuit.

Rbatch is chosen to be equal to NTC @25°C to get: $V_{out} = V_{cc}/2$ @25°C.

The proposal method connects Rbatch to Vcc (5Vdc) and NTC to Ground. It leads to a negative slope characteristic (Pull-Up Configuration).



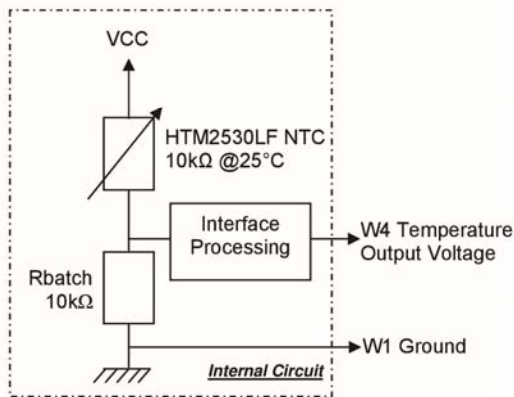
$$V_{OUT} (mV) = \frac{V_{cc}(mV) * NTC_{HTM 2500LF} (\Omega)}{R_{batch} (\Omega) + NTC_{HTM 2500LF} (\Omega)}$$

Temp (°C)	R (Ω)	Pull-up Configuration Vout (mV)
-40	195652	4757
-30	113347	4595
-20	68237	4361
-10	42506	4048
0	27219	3657
10	17926	3210
20	12081	2736
25	10000	2500
30	8315	2270
40	5834	1842
50	4161	1469
60	3014	1158
70	2228	911
80	1669	715

HTM25X0LF – Temperature and Relative Humidity Module

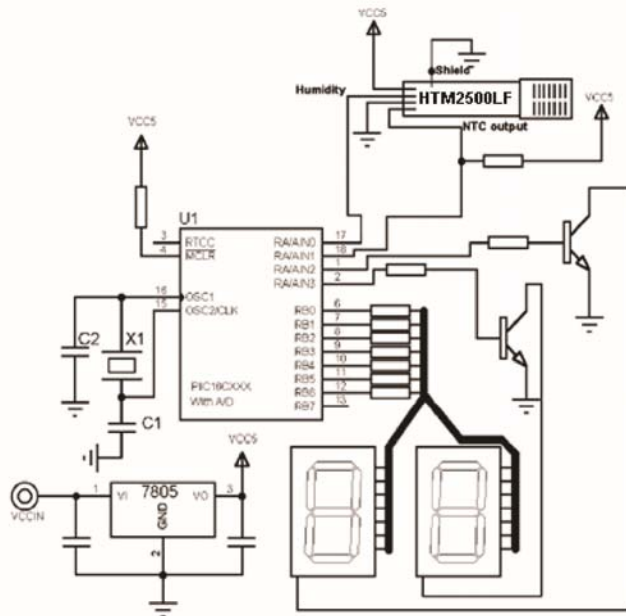
HTM2530LF TEMPERATURE SENSOR: VOLTAGE OUTPUT

Concerning the temperature sensor of the HTM2530LF, it is built as the HTM2500LF temperature sensor interface circuit. The voltage bridge divider circuit is internal. It uses only one resistor component (Rbatch) at 1% to design HTM2530LF temperature sensor interfacing circuit. Rbatch is chosen to be equal to NTC @25°C to get: $V_{out} = V_{cc}/2$ @25°C. The difference is based on internal connections: Rbatch connected to Ground and NTC to Vcc (5Vdc). It leads to a positive slope characteristic (Pull-Down Configuration).

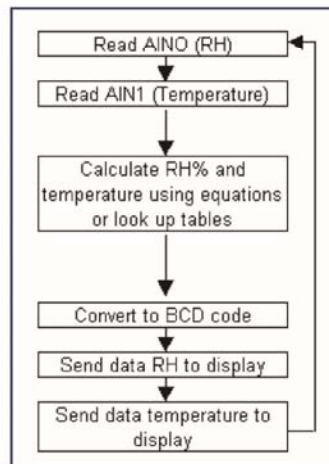


Temp (°C)	R (Ω)	Pull-Down Configuration Vout (mV)
-20	68237	1280
-10	42506	1515
0	27219	1775
10	17926	2050
20	12081	2330
25	10000	2470
30	8315	2600
40	5834	2850
50	4161	3070
60	3014	3240
70	2228	3360

SUGGESTED APPLICATION



Steps of 1% RH are achievable by using 8-bit A/D. If more resolution is required, a 10-bit A/D needs to be used and a third display will be added, giving steps of 0.2% RH.



HTM25X0LF – Temperature and Relative Humidity Module

QUALIFICATION PROCESS

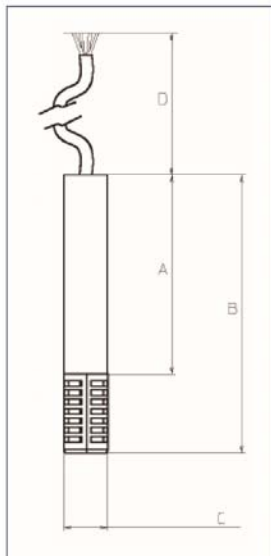
RESISTANCE TO PHYSICAL AND CHEMICAL STRESSES

- HTM25X0LF has passed through qualification processes of MEAS-France including vibration, shock, storage, high temperature and humidity, ESD.
- Additional tests under harsh chemical conditions demonstrate good operation in presence of salt atmosphere, SO₂ (0.5%), H₂S (0.5%), O₃, NO_x, NO, CO, CO₂, Softener, Soap, Toluene, acids (H₂SO₄, HNO₃, HCl), HMDS, Insecticide, Cigarette smoke, this is not an exhaustive list.
- HTM25X0LF is not light sensitive.

SPECIFIC PRECAUTIONS

- HTM25X0LF is not protected against reversed polarity - Check carefully when connecting the device.
- If you wish to use HTM25X0LF in a chemical atmosphere not listed above, consult us.

PACKAGE OUTLINE



Dim	Min (mm)	Max (mm)
A	53	55
B	74.3	76.3
C	11.2	11.6
D*	200	250

* Specific length available on request

For operating temperature upper than 85°C, specific cable is required (1500mm long)

Wire	Color	Function
W1	Brown	Ground
W2	White	Supply Voltage
W3	Yellow	Humidity Voltage Output
W4	Green	Temperature Output (NTC Direct or Voltage)
W5	Black	Shield

Weight: 17.5g

Wire characteristics: AWG 24 for W1, W2, W3 and W4 / AWG 22 for W5



HTM25X0LF – Temperature and Relative Humidity Module

ORDERING INFORMATION

HPP809A031 : HTM2500LF

HUMIDITY VOLTAGE OUTPUT + NTC (TEMPERATURE DIRECT OUTPUT)

HPP809A032 : HTM2530LF

VOLTAGE OUTPUT FOR HUMIDITY AND TEMPERATURE

HPP809A033 : HTM2500LFL

HUMIDITY VOLTAGE OUTPUT + NTC (TEMPERATURE DIRECT OUTPUT) WITH LONG CABLE

HPP809A034 : HTM2530LFL

VOLTAGE OUTPUT FOR HUMIDITY AND TEMPERATURE WITH LONG CABLE

(MULTIPLE PACKAGE QUANTITY OF 10 PIECES)

Customer Service contact details

Measurement Specialties, Inc.
 105 av. du Général Eisenhower
 BP 23705 31037 TOULOUSE CEDEX 1
 FRANCE
 Tél: +33 (0) 561 194 848
 Fax: +33 (0) 561 194 553
 Sales: humidity.sales@meas-spec.com

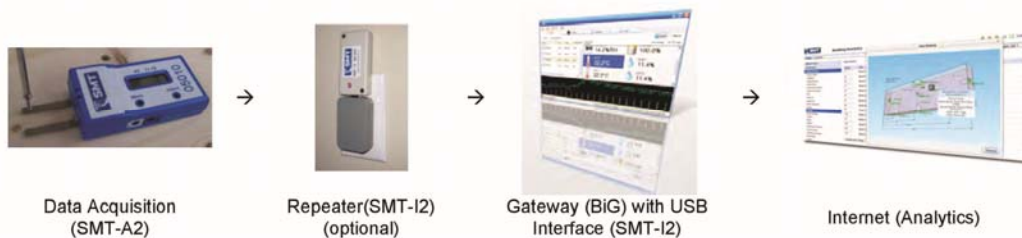
Revision	Comments	Who	Date
0	Document creation	D. LE GALL	July 09
A	Temperature operating range updated, HTM25X0LFL references added	D. LE GALL	December 09

The information in this sheet has been carefully reviewed and is believed to be accurate; however, no responsibility is assumed for inaccuracies. Furthermore, this information does not convey to the purchaser of such devices any license under the patent rights to the manufacturer. Measurement Specialties, Inc. reserves the right to make changes without further notice to any product herein. Measurement Specialties, Inc. makes no warranty, representation or guarantee regarding the suitability of its product for any particular purpose, nor does Measurement Specialties, Inc. assume any liability arising out of the application or use of any product or circuit and specifically disclaims any and all liability, including without limitation consequential or incidental damages. Typical parameters can and do vary in different applications. All operating parameters must be validated for each customer application by customer's technical experts. Measurement Specialties, Inc. does not convey any license under its patent rights nor the rights of others.



SMT-A2 – Wireless Data Acquisition Unit

General Description	Features
<p>The SMT-A2 Wireless Data Acquisition unit is a high precision measurement device designed for distributed remote sensor data acquisition. The built-in 24-bit A/D converter and low noise high precision measurement circuitry facilitates data acquisition from a wide variety of sensors.</p> <p>Integrated Moisture Content, RH and temperature sensors make the SMT-A2 suitable for building monitoring applications.</p> <p>External sensor inputs, LCD display, large memory capacity and extended wireless range gives the SMT-A2 flexibility in a wide range of applications.</p> <p>The SMT-A2 unit communicates wireless sensor readings to the SMT Building Intelligence gateway. Optional powered repeaters can be used to extend the wireless range.</p> <p>Applications</p> <ul style="list-style-type: none"> • Remote sensor analysis and data collection • High precision data acquisition • Building science research • Targeted repair monitoring • Restoration monitoring 	<ul style="list-style-type: none"> • Integrated moisture content sensing elements. • Integrated relative humidity and temperature sensors. • Two external resistance channels capable of reading wide moisture content ranges and precision thermistors. • Sensor inputs use compact audio jacks for quick and simple connectivity. • Internal memory capable of logging 340,000 data points. • Auxiliary input for voltage measurement capable of reading 0-5V sensors. • Wireless transceiver with 1000m line of sight communication. • Communicates to SMT Building Intelligence Gateway (BiG) via USB to Wireless device; SMT-I2. • Extreme low power device suitable for long term battery operation. • USB connectivity supports data downloads and firmware upgrades. • Backlit LCD user interface for easy network and sensor verification • Rechargeable batteries via USB port.






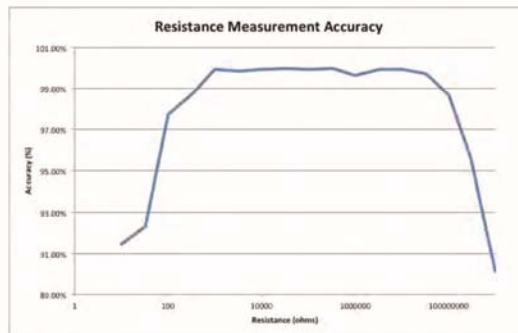
Performance/Functional Specifications

Electrical Performance	
<u>Wireless</u>	
Specification	IEEE 802.15.4
Max Distance from coordinator	1000m line of site. Powered repeaters can be added to extend range.
Max Nodes per coordinator	32 (dependent on application density and acquisition speed)
<u>Battery</u>	
Life	1000 hours (dependent on sample frequency)
Type	Ni-MH Rechargeable Eneloop HR-4UTGA
Voltage	1.2V
Capacity	Typical: 800 mAh Minimum 750 mAh
Self Discharge	75% after 3 years
Charging Cycles	Up to 1500
Charger	USB 5V
<u>Memory and USB</u>	
Memory	16 Mbit EEPROM for data storage Stores 340,000 samples.
USB	USB 1.0 Interface

Environmental	
Operating Temperature	0° to 40°C / 32° to 104°F
Storage Temperature	-25° to 70°C / -13° to 158°F
Humidity	5% to 100% RH non-condensing
Electrostatic Discharge (ESD)	8kVdc air, 4 kVDC contact (exposed inputs)

Safety/Regulatory	
Safety Requirements	SELV Separated Extra Low Voltage
Regulatory	Contains FCC ID: OA3MRF24J40MA
	This device complies with Part 15 of the FCC Rules. Operation is subject to the following two conditions: (1) this device may not cause harmful interference, and (2) this device must accept any interference received, including interference that may cause undesired operation.

Measurement Specifications	
<u>Internal Temperature</u>	
Sensor	Cantherm MF58104F3950 Beta 4390K
Range	-40°C to +70°C
Resolution	0.1°C
Accuracy	±1°C
<u>Internal Relative Humidity</u>	
Sensor	Honeywell HCH-1000-001
Accuracy Range	10-95% RH
Resolution	±0.5%
Accuracy	±5%
<u>Resistance</u>	
Range	10Ω to 100Ω
Resolution	1Ω
Accuracy	±5%
Range	100Ω to 100KΩ
Resolution	10Ω
Accuracy	±1%
Range	100KΩ to 1GΩ
Resolution	1KΩ
Accuracy	±5%



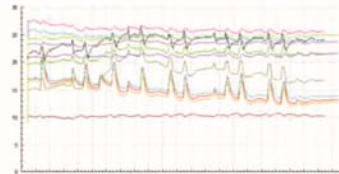
Specifications are subject to change without notice



Building Intelligence Gateway

Name	Node	Input	Type	Last Reading	Reading Date
Temperature Sensor	5006	1	Temper.	23.94 °C	12/01/04-20:03:32
Speed Switch	5006	2	Other	0.00	12/01/04-20:03:32
Temperature Sensor	5006	3	Temper.	22.18 °C	12/01/04-20:03:32
Differential Pressure	5006	4	Custom	-0.55	12/01/04-20:03:32
Internal Temperature	5006	5	Temper.	23.99 °C	12/01/04-20:03:32
RH	5006	6	Custom	41.61	12/01/04-20:03:32
Battery	5006	7	Power	2.81 V	12/01/04-20:03:32
Diagnostic Codes	5006	256		5.863.00	12/01/04-19:28:47

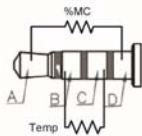
Building Analytics



Mechanical	
Standard Enclosure	
Dimensions	100mm (L) x 50 mm (W) x 24mm(H)
Weight	150g
Connections	
Port A Resistance	Two channels Resistance 100Ω to 1GΩ
Port B Voltage	5V, GND, Vin Or Differential voltage
Interface	
LCD	Network join/rejoin Display measurements
LEDs	Green – USB Power Red - Charging
Buttons	Menu/Select buttons

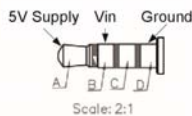
External Port Connectivity

Resistance based and voltage based sensors can be connected to the external audio jack ports:



Resistance Based Sensors

Plug resistance based sensors into the blue audio jack port (input 1/2)



0-5V Sensors

Plug 0-5V Sensors into the white audio jack port. (input 3/4)

Thermistor or short must be connected between C and D to signal port is active.

BiG and Analytics Input Configuration

Inputs appear in the Building Intelligence Gateway (BiG) as *Autonomous* nodes with default values in resistance (Ω) or voltage (mV) depending on the sensor. Select the appropriate sensor type and temperature sensor for compensation (if applicable) to have the desired unit of measurement displayed. Refer to the BiG User Manual for further instructions on programming the sensor inputs.

Restoration Model Configuration:

Input	Function	Sensor Type
1	Internal Temperature	1-04JT (°C)
2 Probes	Moisture Content	Moisture (%)
3 White	RH Temperature	Temperature HTM2500 (°C)
4 White	RH (%RH)	HTM2500
5	Internal Temperature	1-04JT (°C)
6	Integrated RH (%RH)	Custom x=.01
7	Battery	Battery (V)

Research Model Configuration:

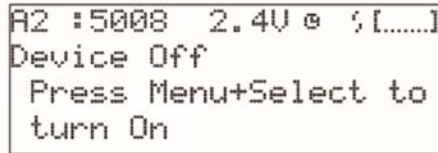
Input	Function	Sensor Type
1 Blue	Resistance (ohms)	
2 Blue	Resistance (ohms)	
3 White	Resistance (ohms)	
4 White	Voltage (mV)	
5	Integrated Temperature	1-04JT (°C)
6	Integrated RH (%RH)	Custom x=.01
7	Battery	Battery (V)



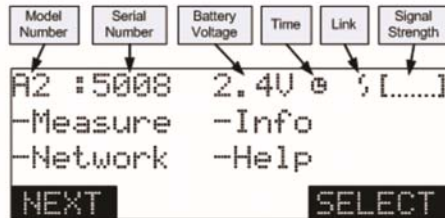
User Interface

If the A2 is OFF, press Menu followed by Select to turn the unit ON. You will be prompted to turn the unit ON.

To turn the unit OFF at anytime, press Menu followed by Select.



The main menu contains links to the submenus as shown below. The header reports the immediate status of the unit.

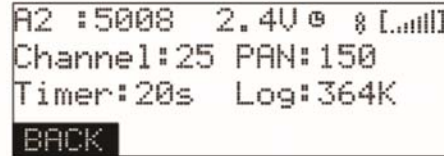


Status Menu	Description
Serial Number	Unique identifier of this unit used in BiG and Analytics
Battery Voltage	Unit should be recharged or batteries changed at 2V (this is dependent on sample frequency) . The unit will stop functioning if the battery is less than 1.8V.
Time	⊕ Indicates A2 has time ⊘ Indicates A2 does not have time. Join network with BiG to establish time.
Link	⊘ No link established ⊕ Link established. Message transmit successful
Signal Strength	[.....] No signal. Ensure connectivity to network. [.....] Full signal strength

To join the network ensure BiG is running with an SMT-I2 USB to Wireless interface and select Network.

Joining network will be displayed, if joining was successful Joining Network on 25 will be displayed where 25 is the wireless channel, otherwise No Network will be displayed.

To rejoin the network select Join. To see the status of the network select Info from the main menu.

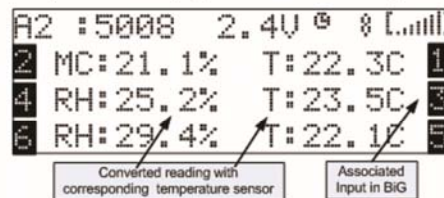


Function	Description
Channel	Channel is autoselected by the SMT-A2
PAN	Personalized Area Network (PAN) is specific to all A2 and I2 devices on the network.
Timer	Sample/Log frequency. This is inherited from the SMT-I2 setting in BiG. All units on the network will have the same timer.
Log	Number of samples in memory.
Nwk ID	Unique network ID identifier

Measurements can be taken at anytime regardless of the network status. If a network is available, a reading will be displayed and transmitted. If not, the readings will be logged and transmitted later when the network becomes available.

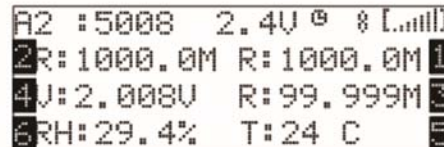
Measure Display - Restoration:

Values are converted to moisture content, temperature and relative humidity. The associated temperature sensor used for temperature compensation is displayed next to each reading.



Measure Display - Research:

Resistance is in ohms and voltage in volts. Range will be adjusted automatically. Full values will be transmitted and stored in BiG.



The display will time out after 10 seconds. Press SELECT to keep it from timing out.



Battery Charging



The SMT-A2 is equipped with a rechargeable battery. To recharge the battery, power the unit using a USB 2.0 A Male to Mini-B Male cable from a standard computer USB port or wall adaptor.

The *USB Connected* (Green LED) indicates that USB power is available and that charging circuitry is enabled.

The *Charging* (Red LED) indicates that the batteries are being charged. The Red LED will turn off when charging is complete. A flashing LED indicates that USB power is insufficient.

The SMT-A2 will continue to take readings when powered over USB. If it is plugged into a USB port on a computer with BiG running data will be communicated via USB to BiG.

Depending on the application, different batteries may be used and charging may not be available.

Installation



The SMT-A2 can be housed in a mobile unit used for indoor applications, sealed in an IP67 enclosure or mounted on a double gang face plate.

Consult Application Notes and specific installation instructions for further details.

Data collection and analysis

Data is collected by the *Building Intelligence Gateway* (BiG) and forwarded to the *Building Analytics* server database for further analysis and user access. See the BiG and Analytics user manuals for sensor configuration and data analysis capabilities.

Troubleshooting

Unit appears to be frozen or has difficulty turning on:

- Battery power may be too low. Charge the batteries until the Charge LED is off.
- If the screen appears to be frozen wait 10 seconds and then reattempt. The A2 periodically handles critical tasks and could take up to 10 seconds to timeout or complete the task.
- Reset the unit: Hold down Menu and Select for 5+ seconds. Do not do this while USB is plugged in.

RH readings are not accurate:

- RH sensor may have been wet and requires recalibration. The unit will need to be sent back to SMT for recalibration.
- Make sure audio jacks are firmly plugged in.

SMT-A2 does not appear in BiG

- Ensure the I2 and A2 are on the same PAN. The PAN on the I2 can be queried by double clicking on the BiN serial number in BiG. Select *Get* under PAN to view the PAN. To query the PAN on the A2 select *Info* from the main screen on the unit.

Ordering Information	
Restoration SMT-A2 w/ moisture probes, RH/T	SMT-A2-M12-R21-L
Research SMT-A2 External sensors inputs, RH/T	SMT-A2-M12-H21-L
External RH Sensor	HTM2500-01-006
Point Moisture Measurement w/ thermistor	PMM-02-006
Thermistor	104JT-01-006



SMT-A3 – 8 Channel Wireless Data Acquisition Unit

General Description

The SMT-A3 Wireless Data Acquisition unit is a multi-channel high precision measurement device designed to interface with a variety of different building sensors.

The sleek design of the SMT-A3 allows it to be installed in occupied spaces in building units and homes. The SMT-A3 seamlessly attaches to a double junction box and supports up to eight external sensors with optional integrated sensors.

The 24-bit A/D and long range wireless proven on the SMT-A2 platform is duplicated on the SMT-A3 making it ideal for building monitoring in both new construction and retrofit work.

Options for integrated CO₂, RH, temperature and differential pressure are available upon request.

The SMT-A3 communicates wireless sensor readings to the SMT Building Intelligence gateway. Optional powered repeaters can be used to extend the wireless range.

Applications

- Permanent monitoring solutions
- Remote sensor analysis and data collection
- High precision data acquisition
- Building science research
- Targeted repair monitoring

Features

- Supports up to 8 external resistance channels capable of reading wide moisture content ranges and precision thermistors.
- Supports up to 8 0-5V sensors such as RH, pressure differential, LVDT, displacement, light sensors and more.
- Supports up to 4 differential voltage inputs capable of reading sensors such as thermocouples, heat flux and more. Gain amplification boost circuitry is available to measure very small voltage differentials.
- Optional integrated relative humidity and temperature sensors.
- Sensors are installed using a two part terminal block permitting sensor lengths to be cut to their appropriate lengths and terminated prior to installing electronics.
- Large internal memory allows an 8 channel unit to log hourly data for up to 3 years without extracting data.
- Wireless transceiver with 1000m line of sight communication. Optional repeaters can be used to extend the wireless range.
- Communicates to SMT Building Intelligence Gateway (BiG) via USB to Wireless device; SMT-I2.
- Extreme low power device and 3 AA battery pack makes the SMT-A3 suitable for long term battery operation.
- USB connectivity supports data downloads, configuration and firmware upgrades.
- Backlit LCD user interface for easy network and sensor verification



Data Acquisition (SMT-A3)



Gateway (BiG) with USB Interface (SMT-I2)



Internet (Analytics)



Electrical Performance	
<u>Wireless</u>	
Specification	IEEE 802.15.4
Working Frequency	2.4 GHz – 2.4835 GHz
Power	20dBm (100mW)
Output Range (free air)	1000m. Powered repeaters can be added to extend range.
Max Nodes per coordinator	32 (dependent on application density and acquisition speed)
<u>Battery</u>	
Life	3 - 5 years (depending on sample rate)
Type	3 AA Alkaline Battery Pack
<u>Memory and USB</u>	
Memory	16 Mbit EEPROM for data storage Stores 340,000 data points.
USB	USB 1.0 Interface

Environmental	
Operating Temperature	0° to 40°C / 32° to 104°F
Storage Temperature	-25° to 70°C / -13° to 158°F
Humidity	5% to 100% RH non-condensing
Electrostatic Discharge (ESD)	8kVdc air, 4 kVDC contact (exposed inputs)
Enclosure	The enclosure is designed for indoor use only. Consult SMT for outdoor rated units.

Regulatory	
Regulatory	Contains FCC ID: OA3MRF24J40MB
	This device complies with Part 15 of the FCC Rules. Operation is subject to the following two conditions: (1) this device may not cause harmful interference, and (2) this device must accept any interference received, including interference that may cause undesired operation.
	Contains IC: 7693A-24J40MB

Specifications are subject to change without notice

Measurement Specifications	
<u>Internal Temperature</u>	
Sensor	Cantherm MF58104F3950 Beta 4390K
Range	-40°C to +70°C
Resolution	0.1°C
Accuracy	±1°C
<u>Internal Relative Humidity (optional)</u>	
Sensor	Honeywell HIH-4000-001
Interchangeability	0-59% RH ±5% 60-100% RH ±8%
Resolution	0.5% RH
Accuracy	±5% RH
Hysteresis	3% RH
Repeatability	±0.5% RH
<u>Resistance</u>	
Range	10Ω to 100Ω
Resolution	1Ω
Accuracy	±5%
Range	100Ω to 100KΩ
Resolution	10Ω
Accuracy	±1%
Range	100KΩ to 1GΩ
Resolution	1KΩ
Accuracy	±5%
<u>Voltage</u>	
Range	0V to 5V
Resolution	100mV
Accuracy	±5%

Mechanical	
<u>Standard Enclosure</u>	
Dimensions	
Weight	
<u>Connections</u>	
Resistance Ports	4 to 8 channels Resistance 100Ω to 1GΩ
Voltage Ports	4 to 8 channels 5V, GND, Vin Or Differential voltage
<u>Interface</u>	
LCD	Network join/rejoin Display measurements
Buttons	Menu/Select buttons



Input Port Connectivity

A3's can be configured to have 8 resistance inputs, 8 voltage inputs or 4 resistance and 4 voltage inputs.

In addition to the sensor inputs, the A3 has a variety of optional integrated sensors.

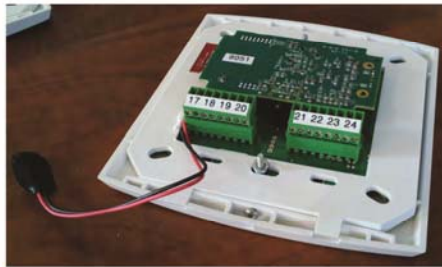
Integrated Sensors

A variety of sensors are available to measure parameters at the installed location of the A3. Faceplates are vented accordingly to allow the sensor to access the parameter being sensed.

Optional sensors that can be included are as follows:

1. Relative Humidity sensor
2. Temperature sensor
3. CO2 sensor (5000 ppm range)
4. Differential pressure sensor

Resistance Based Sensors



Resistance based sensors such as PMM's, EMS sensors thermistors and linear displacement potentiometers can be used.

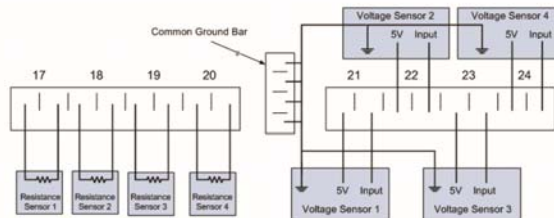
Connect sensors to ports 17 to 24. Polarity is not important unless specified by the sensor. Unused ports can be left open or factory negated. Sensors that require temperature compensation should have the temperature inserted into the lower number (so it is recorded first). For example, a PMM should connect temperature to port 17 and moisture content to port 18.

0-5V Sensors

0-5V sensors such as RH sensors, differential pressure sensors and solar radiation sensors can be connected to the A3. The A3 can be configured to have 8 voltage ports (8R) or 4 resistance ports and 4 voltage ports (4R4V) as shown in the diagram below. Power is switched on individually to all connected sensors, each sensor is permitted to draw a maximum current of 50mA. Sensors have a warm up time of 3 seconds.



4R4V unit with CO2. Install resistance sensors in 17-20 and voltage sensors in 21 to 24 using the centre connector as a ground bar. Connect the CO2 sensor to input 24.



Typical sensor connectivity for 4R4V model. Grounds are interconnected on ground bar located in the center between the two 8 pin terminal blocks.



Installation

Install a non-metallic double gang mounting box at the desired location. Ensure the junction box has clearance for the center mounting screw on the A3.



Double gang low voltage bracket used in existing construction:

Manufacturer: Arlington LV2
Distribution: MCM Model: 28-6356



Double gang plastic junction box used in new construction:

Manufacturer: T&B NuTek 2FWSW-CRT
Distributor: Home Depot Model: 2WSW-UPC



Affix battery back to rear or side of junction box.

Route sensor wires into junction box and terminate on provided terminal block headers.



Secure the A3 to a double gang junction box.



A3 with integrated RH/T, Differential Pressure and CO2 sensors.

Configuration

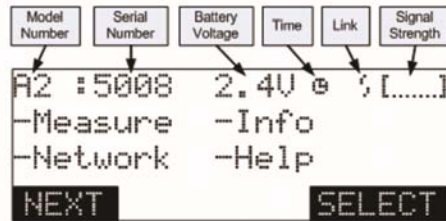
Use the LCD display and menu buttons to verify the operation of the A3. It is recommended to place the Building Intelligence Gateway (BiG) in its desired location so wireless signal strength and communication could be verified. Refer to the BiG Quick Reference Guide and Manual for further setup and configuration options.

User Interface

If the A3 is OFF, press Menu followed by Select to turn the unit ON. You will be prompted to turn the unit ON.

To turn the unit OFF at anytime, press Menu followed by Select.

The main menu contains links to the submenus as shown below. The header reports the immediate status of the unit.



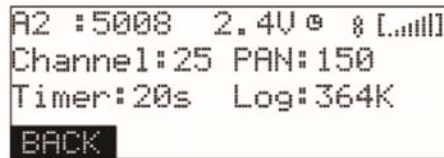
Status Menu	Description
Serial Number	Unique identifier of this unit used in BiG and Analytics
Battery Voltage	Replace batteries if the voltage is less than 2.4V. The unit will stop functioning if the battery voltage is less than 1.8V.
Time	☉ Indicates A3 has time ☾ Indicates A3 does not have time. Join network with BiG to establish time. You may need to wait up to 5 minutes for the unit to establish time.
Link	⌘ No link established ⌘ Link established. Message transmit successful
Signal Strength	[.....] No signal. Ensure connectivity to network. Ensure PAN is correct and there are no range/obstacle issues. [] Full signal strength



To join the network, ensure BiG is running with an SMT-I2 USB to Wireless interface and select Network.

Joining Network will be displayed, if joining was successful Joining Network on 25 will be displayed where 25 is the wireless channel, otherwise No Network will be displayed.

To rejoin the network select Join. To see the status of the network select Info from the main menu.



Function	Description
Channel	Channel is autoselected by the SMT-A3
PAN	Personalized Area Network (PAN) is specific to all A3 and I2 devices on the network.
Timer	Sample/Log frequency. This is inherited from the SMT-I2 setting in BiG. All units on the network will have the same timer.
Log	Number of samples in memory. To clear the log hold Menu and press Select 5 times. Select Erase Log.
Nwk ID	Unique network ID identifier

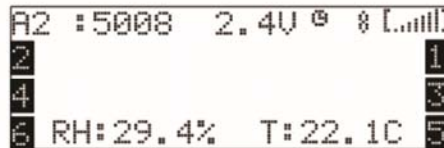
Measurements can be taken at anytime regardless of the network status. If a network is available, a reading will be displayed and transmitted. If not, the readings will be logged and transmitted later when the network becomes available.

The A3 MUST have time in order to log a reading.

Measure

Select Measure to force a reading.

Values for internal sensors will be displayed.

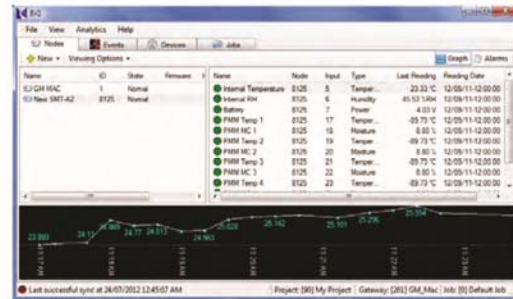


The display and backlight will time out after 10 seconds. Press SELECT to keep it from timing out.

The display is normally OFF for power savings.

Building Intelligence Gateway Configuration

Inputs appear in the Building Intelligence Gateway (BiG) as New SMT-A2 with default values in resistance (Ω) or voltage (mV) depending on the sensor. Select the appropriate sensor type and identify the temperature sensor for compensation (if applicable) to have the desired unit of measurement displayed. Refer to the BiG User Manual for further instructions on programming the sensor inputs, creating jobs and synchronizing with Analytics.



A list of the various inputs and sensor types is listed in the table below:

Input	Function	Sensor Type
5	Internal Temperature	1-04JT (°C)
6	Integrated RH	HIH-4000 (%RH)
7	Battery	Battery (V)
17	Resistance	
18	Resistance	
19	Resistance	
20	Resistance	
21	Resistance/Voltage	
22	Resistance/Voltage	
23	Resistance/Voltage Pressure if included	All Sensors .25"
24	Resistance/Voltage CO2 if included	COZIR 5000 PPM

Inputs 21 to 24 can be either configured as resistance based or voltage based sensors depending on the configuration selected. If Pressure is included it will be allocated to input 23 and if CO2 is included it will be allocated to input 24. Specific delays and warm up times are included to support these sensors.



USB Interface

The USB port can be used for data collection, unit configuration and firmware upgrades.



If an SMT-I2 isn't available to facilitate a wireless data download to BiG, data can be collected using the onboard USB port.

Connect the SMT-A3 mini USB port to a computer running the Building Intelligence Gateway software. The A3 serial number should show up under the Devices tab. If there are readings the data will automatically be transferred into the BiG database.

Configuration settings can be changed by selecting Device ID under the devices tab. Do not change settings here if you are unsure what you are doing.

The A3 will continue to take readings and transmit to BiG when powered over USB.

Data collection and analysis

Data is collected by the *Building Intelligence Gateway* (BiG) and forwarded to the *Building Analytics* server database for further analysis and user access. See the BiG and Analytics user manuals for sensor configuration and data analysis capabilities.

Faceplate Installation

After the inputs on the A3 are confirmed and data is being transmitted, slide the faceplate on by hooking it to the top and then pushing firmly on the bottom.



Hook faceplate on top and push down.



Push CO2 unit up while pushing down on faceplate



A3 with RH/T, CO2 and pressure port.



A3 installed in living space

Troubleshooting

Unit appears to be frozen or will not turn on:

- Battery power may be too low. Check the battery voltage and change the batteries if they are less than 2.4v
- If the screen appears to be frozen wait 10 seconds and then reattempt. The A3 periodically handles critical tasks and could take up to 10 seconds to timeout or complete a task.
- Reset the unit: Make sure A2 is not plugged into USB. Hold down Menu and Select for 5+ seconds.

Internal RH/T readings are not accurate:

- RH sensor may have been wet and requires recalibration. The unit will need to be sent back to SMT for recalibration.
- Ensure the RH sensor has good venting out the front face plate.
- Unplug the A3 from USB as the unit heats up while charging.

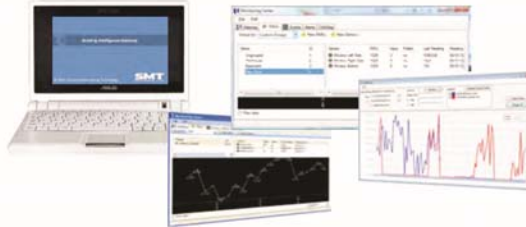
A3 does not appear in BiG

- Ensure the I2 and A3 are on the same PAN. The PAN on the I2 can be queried by double clicking on the serial number under Devices in BiG. Select *Get* next to PAN. To query the PAN on the A3 select *Info* from the main screen on the unit.

Ordering Information	
A3 8 Resistance Channels with RH/T	A3-J22-H00-8R
A3 4 Resistance 4 Voltage Channels with RH/T	A3-J22-H00-4R4V
A3 4 Resistance 4 Voltage Channels with RH/T and CO2	A3-J22-H00-4R3V-CO2
A3 4 Resistance Channel with RH/T, Differential Pressure	A3-J22-H00-4R-P
A3 4 Resistance Channel with RH/T Pressure and CO2	A3-J22-H00-4R-P-CO2
Industrial NEMA IP66 Hammond Weatherproof Case with 2 cinch connectors and desiccant	A3-1554N2
Double gang low voltage bracket	A3-LV2
Double gang plastic junction box	A3-2FWSW



Building Intelligence Gateway[®]



General Description

The Building Intelligence Gateway[®] (BiG) is a compact yet powerful computer system used to provide continuous monitoring and data collection of distributed sensors used for automated structure monitoring.

The BiG system collects data from a variety of different sensors located within the monitored structure and provides local analysis of data as well as synchronization with SMT's on-line monitoring and reporting system, Analytics[®].

The BiG system uses the Windows platform to provide a familiar and user friendly interface for configuration and local data viewing. The software can communicate with wireless and wired sensors and is capable of scaling for large sensor networks, where real-time data of hundreds of sensors is required.

BiG can monitor sensors using configurable thresholds and can be setup to react to threshold violations with a variety of built-in actions including e-mail, pager, and triggering an electrical relay.

Applications

Building Science Research

- Window and wall module evaluation
- External façade sensing
- Moisture, RH and temperature sensing
- Pressure, solar radiation and displacement

Field Applications/Research

- Long term structure monitoring
- Targeted repair monitoring
- Restoration Monitoring

Flood Monitoring

- Flood detection and alarm forwarding

Roof Monitoring

- Automated leak detection

Features

- Compact design. Fits in standard wall mount cabinets.
- Rugged and portable. Rugged case available for portable and outdoor applications.
- Local Windows user interface displayed on 7 inch backlit LCD display.
- Simple configuration. Keyboard and touchpad used for local configuration.
- Solid state storage permits rugged installations and is expandable using the local MMC/SD interface.
- Standard 10/100 Mbit Ethernet and 802.11 b/g wireless.
- USB ports permit expansion and compatibility to 3rd party systems.
- Optional GSM interface to cellular network for installations where internet is not available.
- Interface to 802.15.4 wireless and Controller Area Network wired sensor units.
- Multithreaded communication permits communication to large sensor networks.
- Event handling and alarm processing allows system to be used as a stand-alone monitoring center.
- Displays sensor data in real-time.
- Unique graph manipulation tools available for viewing and scanning large data sets. Advanced graphing functions permit detailed analysis of sensor data.
- Synchronizes sensor configurations and recorded data with SMT Analytics[®].
- Facilitates data set groupings per job and synchronizes with Analytics server.
- Unique sensor groupings and mass configuration schemes available.
- Real time clock and built in battery backup.



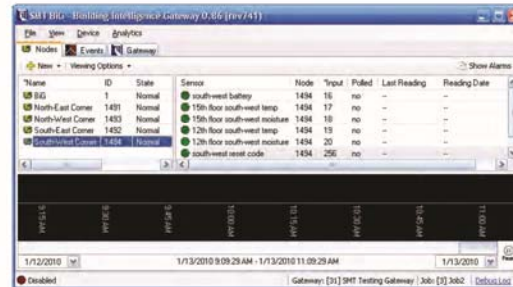
Hardware Specifications	
Operating System	Microsoft® Windows XP/Vista/7
Display	7" with LED backlight
Memory	512MB
Storage	Solid State 4GB. Expansion SD cards available.
Local Input	Keyboard/Touchpad
User Connectivity	10/100 Mbit Ethernet 802.11 b/g wireless LAN GSM cell network
Expansion	3 USB 2.0 ports MMC/SD card reader
Sensor Connectivity	Wireless 802.15.4 Wired CAN 2.0
Max Distance from coordinator node	Wireless 30m (IEEE 802.15.4) Wired 300m (CAN)
Power	5200 mAh battery backup 120VAC
Dimension	225mm (L) x 165mm (D) x 35mm(H)
Weight	1 kg (2.2 lb)

Sensor Monitoring Performance
See specific sensor datasheets

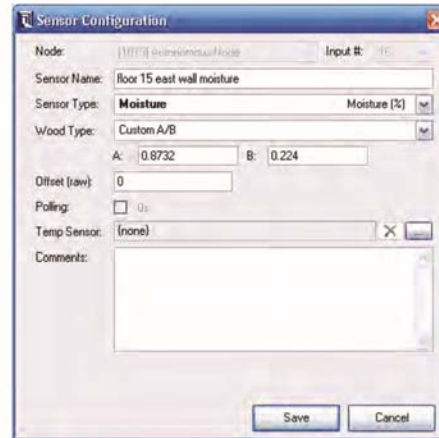
Regulatory	
EMC Radiated and Conducted Emissions	FCC Part 15 Class B Industry Canada ICES 003
Safety Requirements	cULus and CE



BIG General Configuration



- Compatible sensors on network are automatically discovered.
- Sensors are grouped by hardware by default. Custom groupings can be defined.
- Ascending or descending sort can be applied to any column.



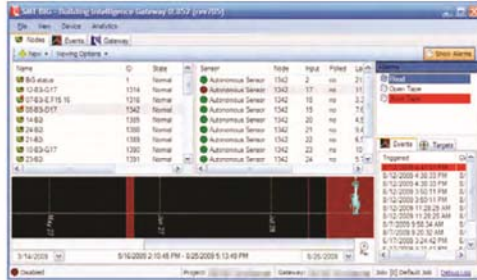
Parameters of each sensor can be easily modified. Batch modifications are possible for applying changes to more than one sensor. BIG comes with a large library of built-in sensor conversions. Sensor conversion formulas can also be manually entered with a custom quadratic equation.



Structure Monitoring Technology

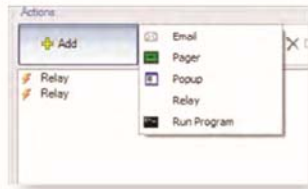
Building Intelligence Gateway

Alarm Handling



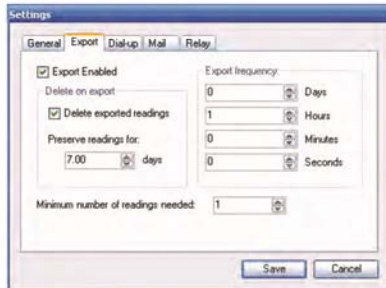
- Thresholds can be defined with configurable durations. Any number of alarms can be linked to a sensor.
- Nodes and sensors in alarm are logged along with details on the alarm.

Targets



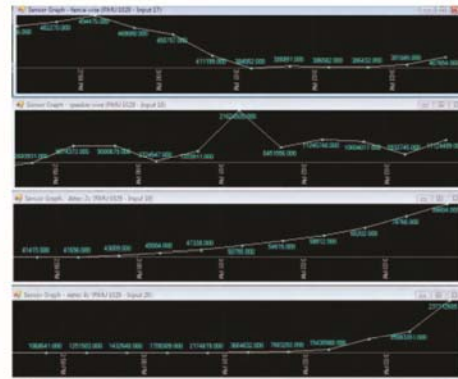
Alarms can be forwarded via Email, Pager, Relay contact or custom actions can be defined.

Export Functionality



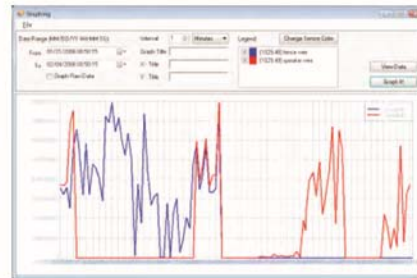
- Specific interval can be defined for forwarding data to Analytics[®].
- All data can be easily exported for analysis in custom tools if desired.

Real Time Data Analysis



Sensor data is recorded and graphed in real-time. Using simple mouse controls the view can be panned forward/backward and zoomed in/out on the time axis.

Advanced Graphing



Sensor inputs can be analyzed using an advanced graphing feature. Graphs can be customized, compared and printed.

Ordering Information

Standard Gateway BIG-001
 (6 months monitoring)
 CAN and Wireless
 interfaces sold separately.

Specifications are subject to change without notice

Appendix F Supplementary Calculated Airflow Graphs

Average calculated airflows for the suites based on the monitored pressure differences and measured airtightness of the pressure boundaries were discussed in Section 11.2. For reference, graphs showing the average airflow rates under various wind conditions are provided here in Figure F-1 to Figure F-24. The wind conditions are the same as those discussed with respect to pressure monitoring in Chapter 10 and in some cases charts are repeated from Section 11.2.

Appendix F Supplementary Calculated Airflow Graphs

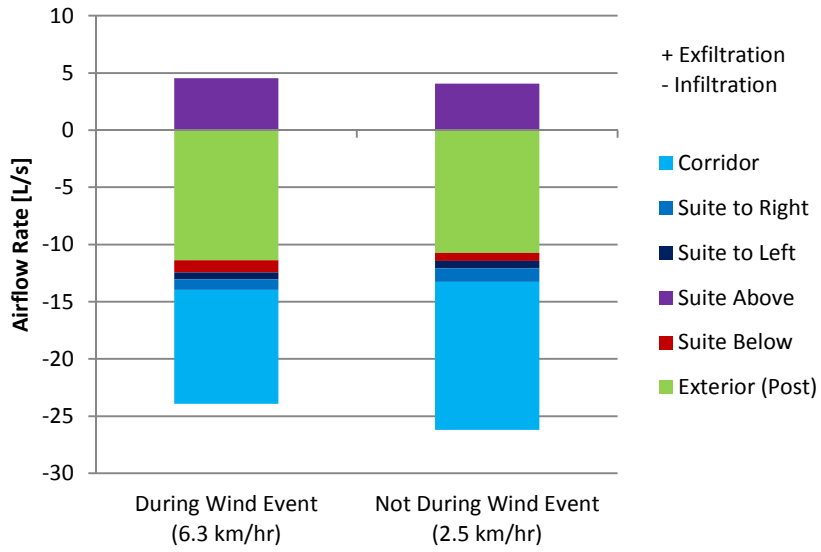


Figure F-1: Chart of the average flow into and out of Suite 301 during a light east wind

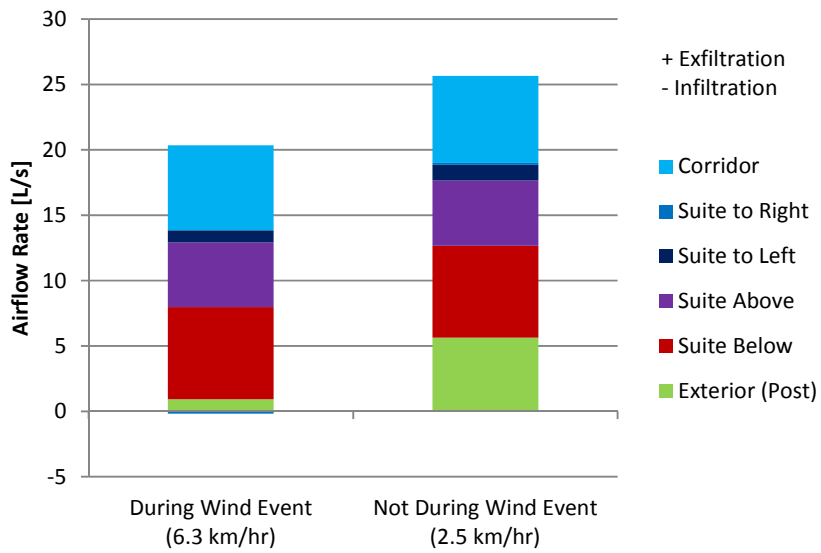


Figure F-2: Chart of the average flow into and out of Suite 302 during a light east wind

Appendix F Supplementary Calculated Airflow Graphs

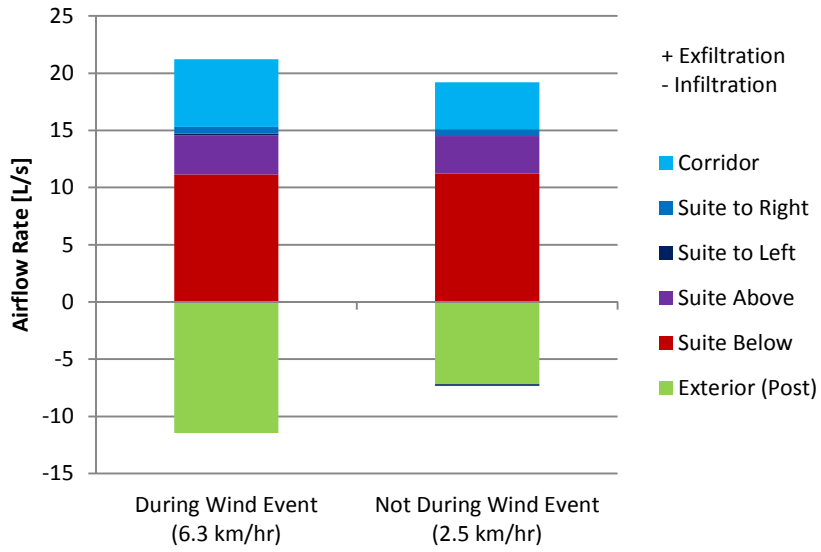


Figure F-3: Chart of the average flow into and out of Suite 303 during a light east wind

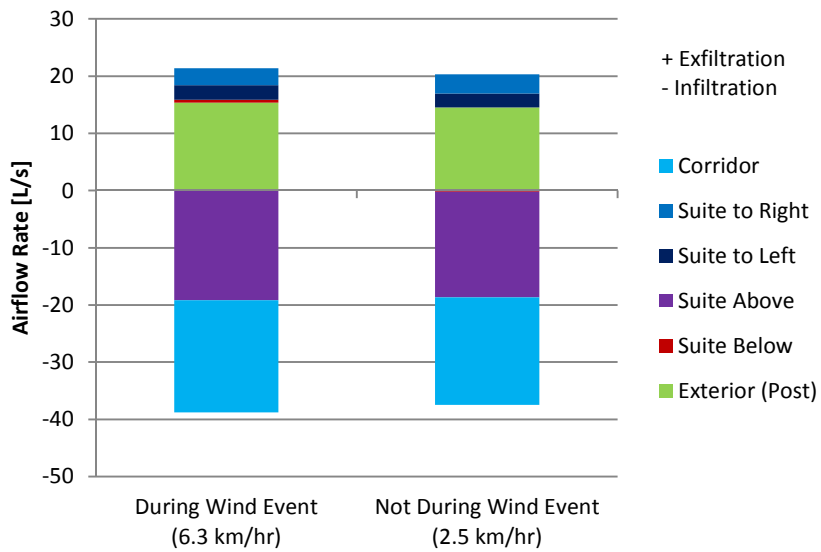


Figure F-4: Chart of the average flow into and out of Suite 1101 during a light east wind

Appendix F Supplementary Calculated Airflow Graphs

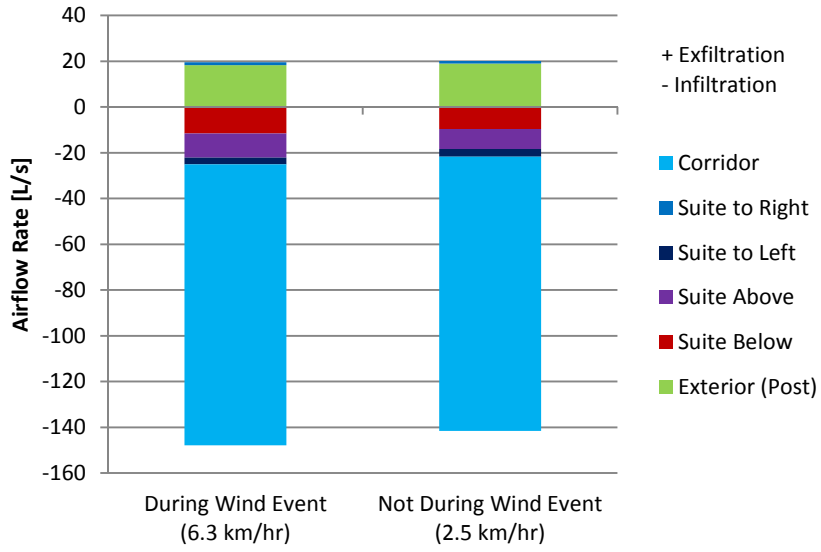


Figure F-5: Chart of the average flow into and out of Suite 1102 during a light east wind

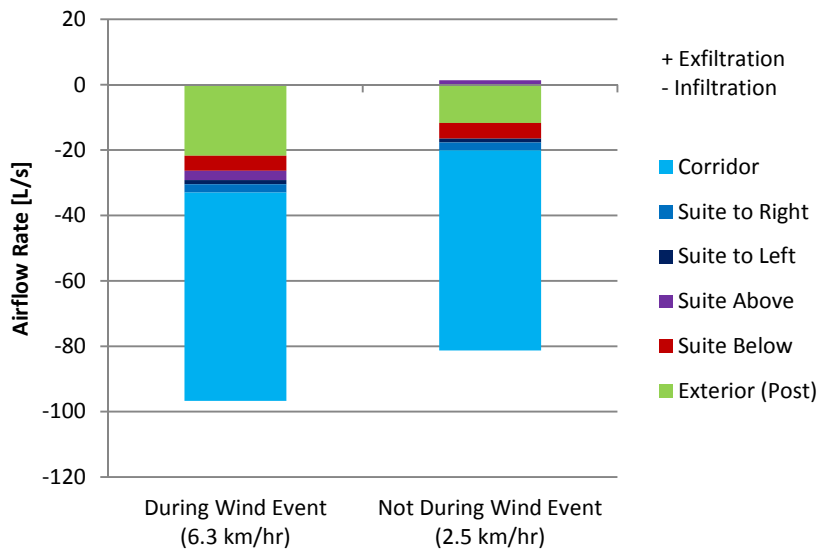


Figure F-6: Chart of the average flow into and out of Suite 1103 during a light east wind

Appendix F Supplementary Calculated Airflow Graphs

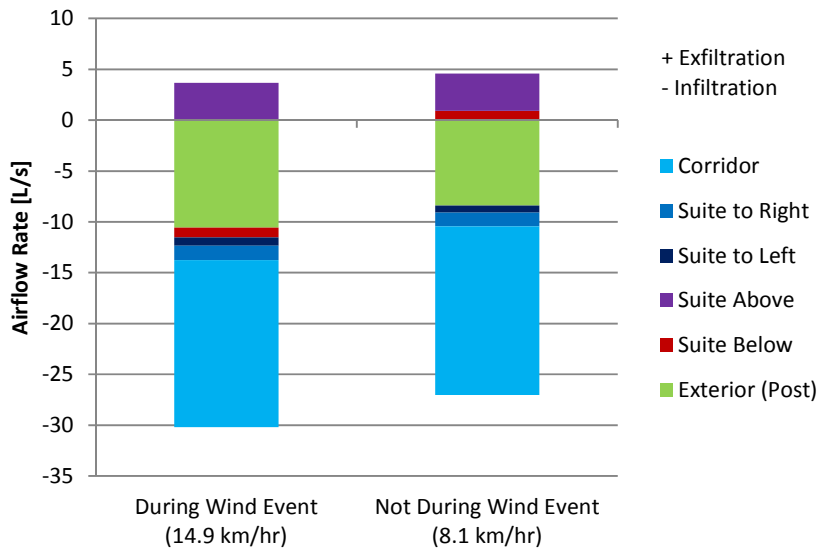


Figure F-7: Chart of the average flow into and out of Suite 301 during a moderate east wind

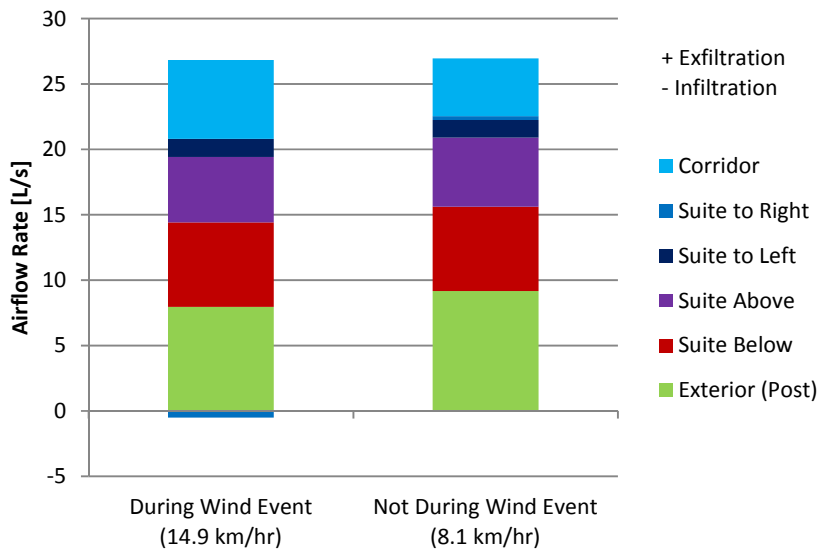


Figure F-8: Chart of the average flow into and out of Suite 302 during a light moderate wind

Appendix F Supplementary Calculated Airflow Graphs

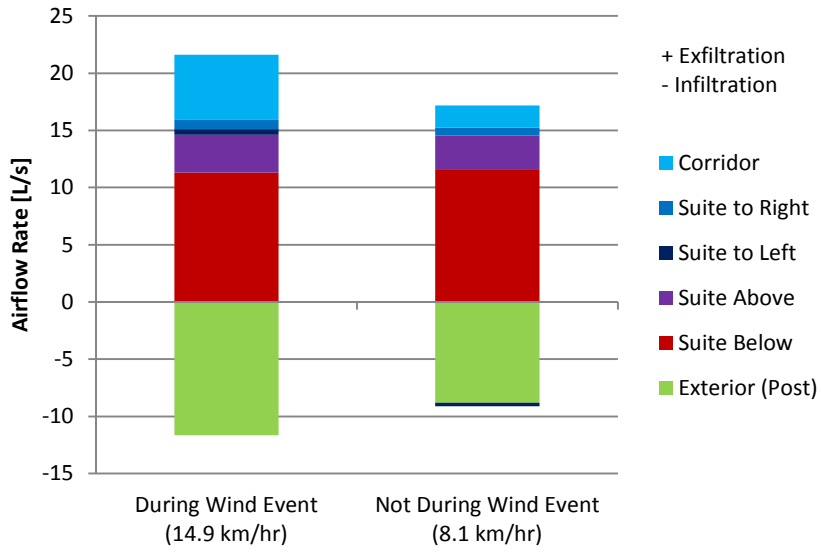


Figure F-9: Chart of the average flow into and out of Suite 303 during a light moderate wind

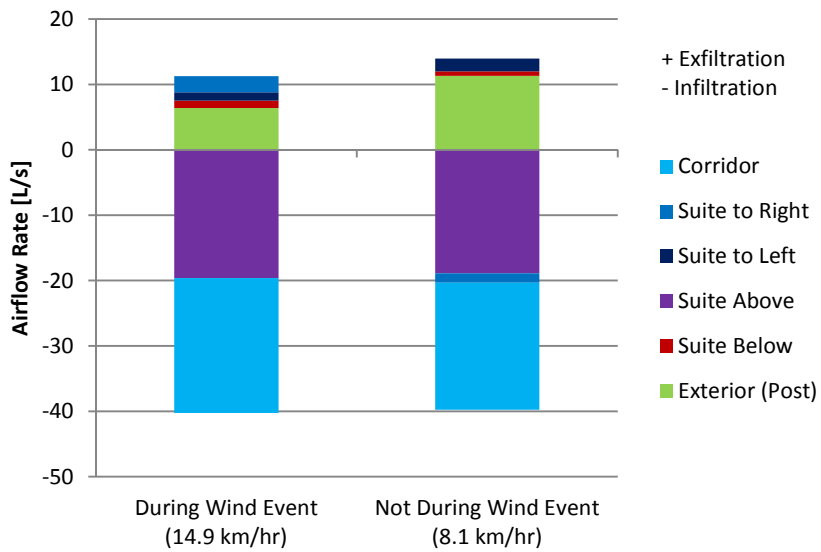


Figure F-10: Chart of the average flow into and out of Suite 1101 during a light moderate wind

Appendix F Supplementary Calculated Airflow Graphs

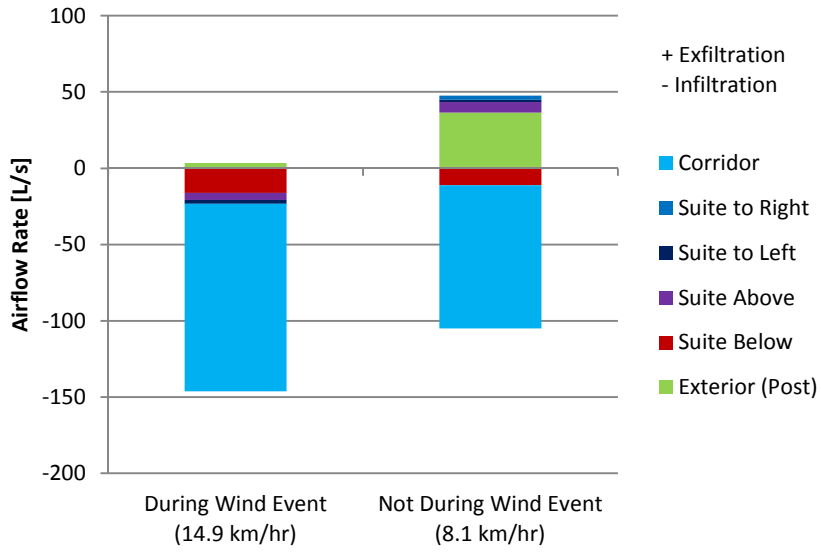


Figure F-11: Chart of the average flow into and out of Suite 1102 during a light moderate wind

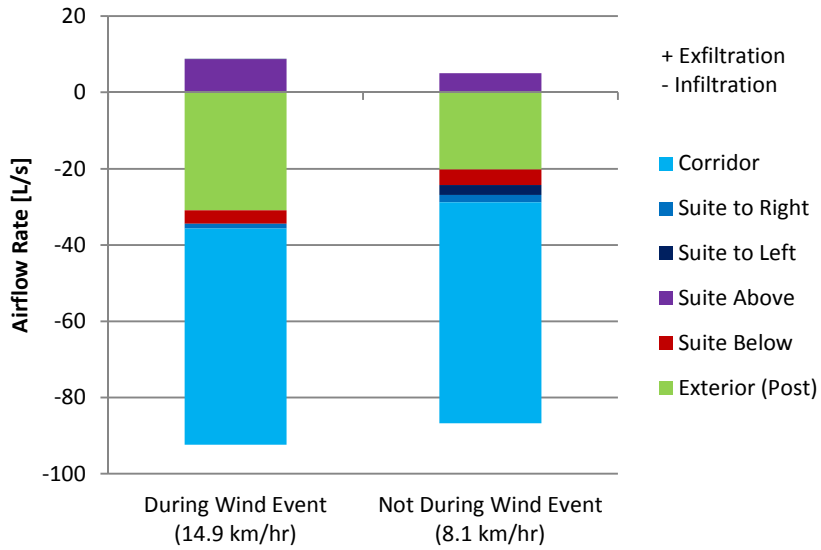


Figure F-12: Chart of the average flow into and out of Suite 1103 during a moderate east wind

Appendix F Supplementary Calculated Airflow Graphs

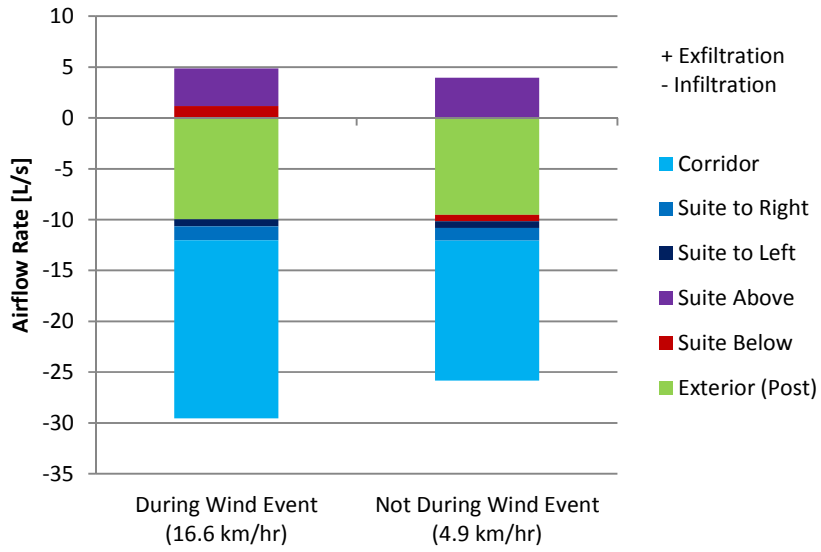


Figure F-13: Chart of the average flow into and out of Suite 301 during a moderate west wind

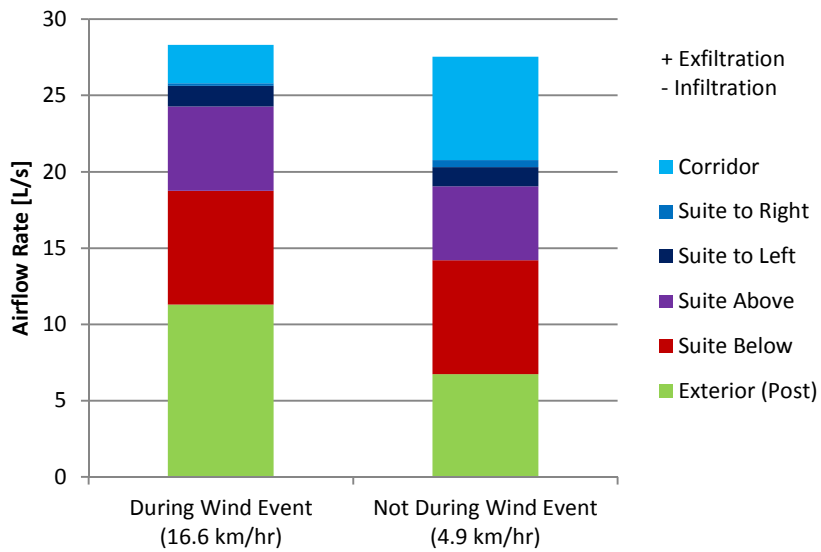


Figure F-14: Chart of the average flow into and out of Suite 302 during a moderate west wind

Appendix F Supplementary Calculated Airflow Graphs

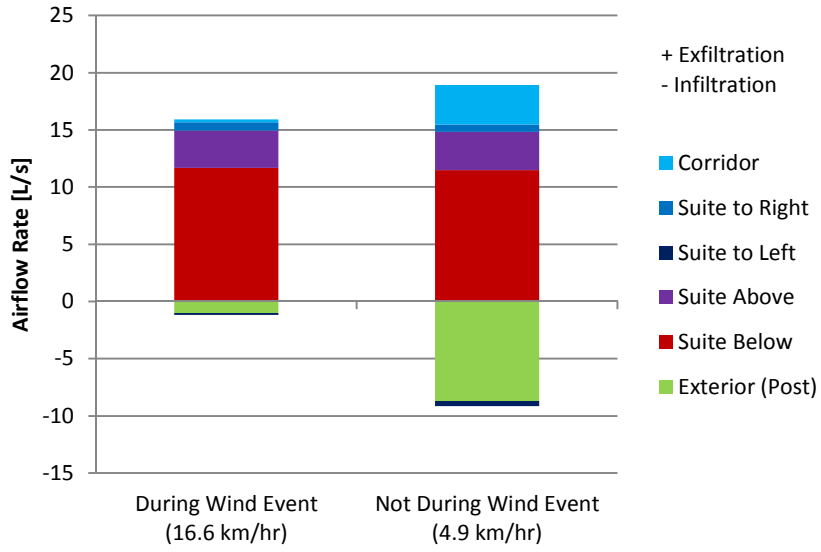


Figure F-15: Chart of the average flow into and out of Suite 303 during a moderate west wind

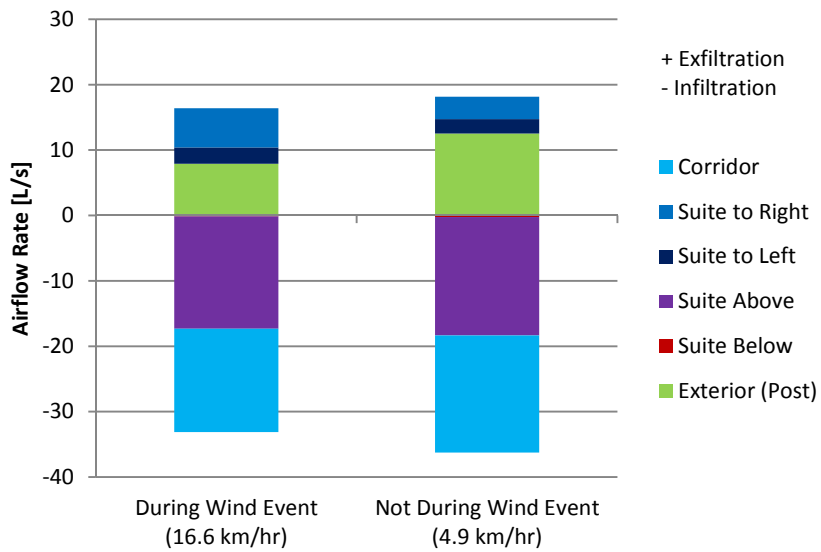


Figure F-16: Chart of the average flow into and out of Suite 1101 during a moderate west wind

Appendix F Supplementary Calculated Airflow Graphs

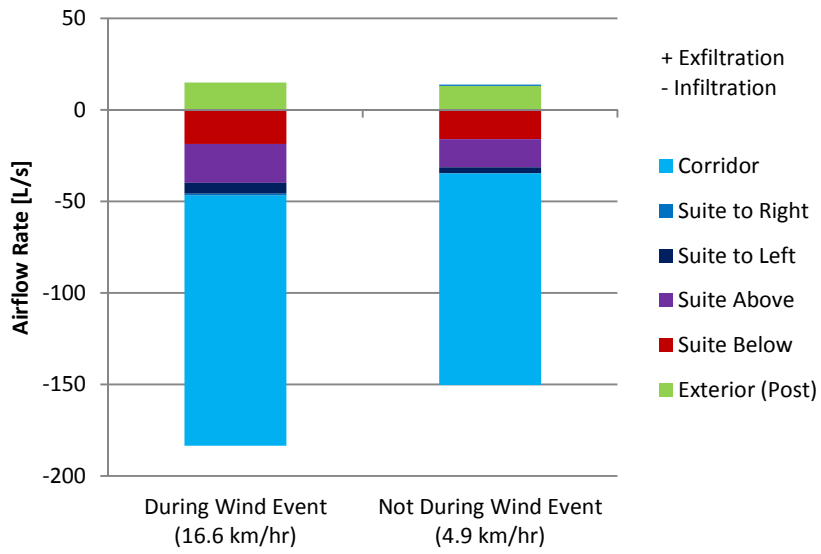


Figure F-17: Chart of the average flow into and out of Suite 1102 during a moderate west wind

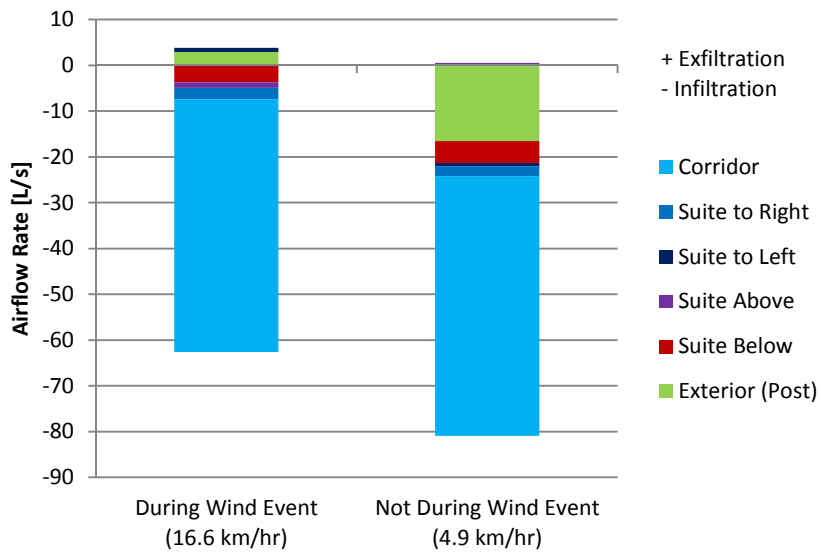


Figure F-18: Chart of the average flow into and out of Suite 1103 during a moderate west wind

Appendix F Supplementary Calculated Airflow Graphs

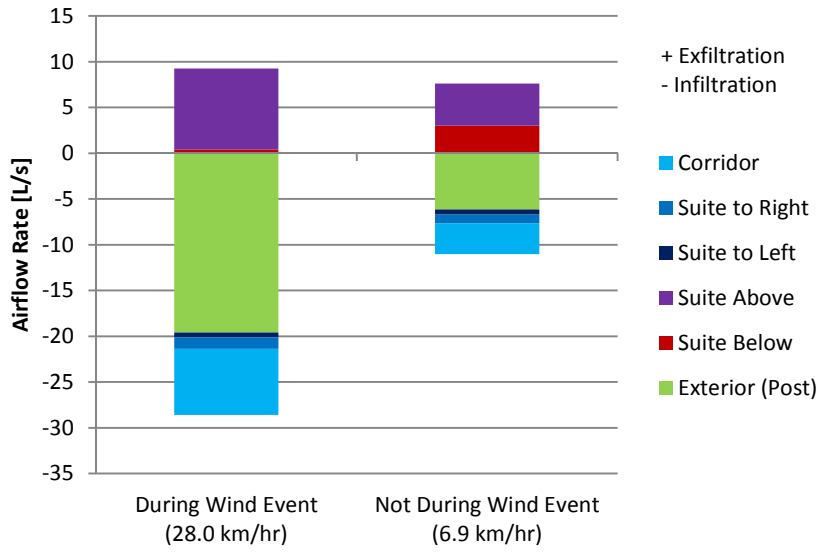


Figure F-19: Chart of the average flow into and out of Suite 301 during a strong west wind

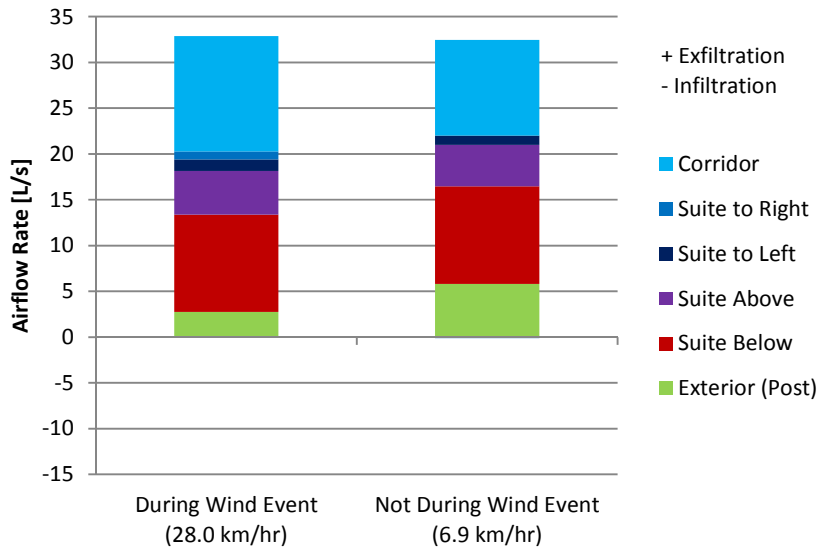


Figure F-20: Chart of the average flow into and out of Suite 302 during a strong west wind

Appendix F Supplementary Calculated Airflow Graphs

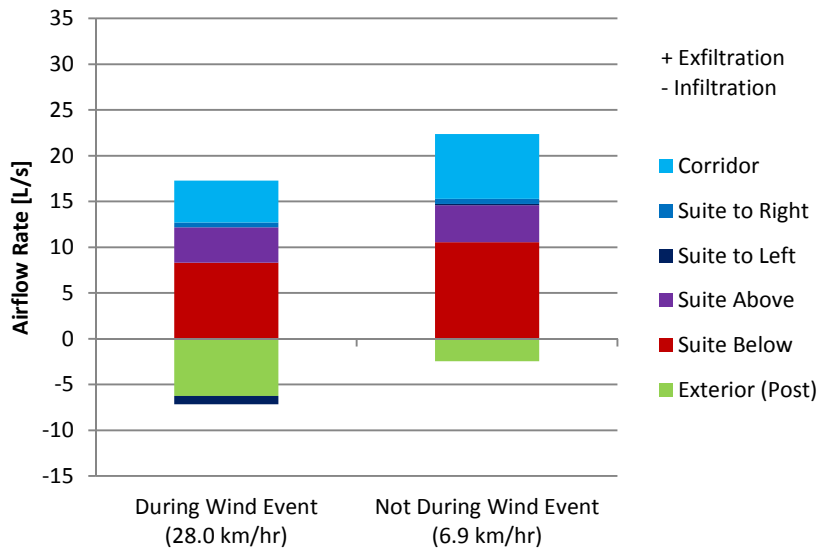


Figure F-21: Chart of the average flow into and out of Suite 303 during a strong west wind

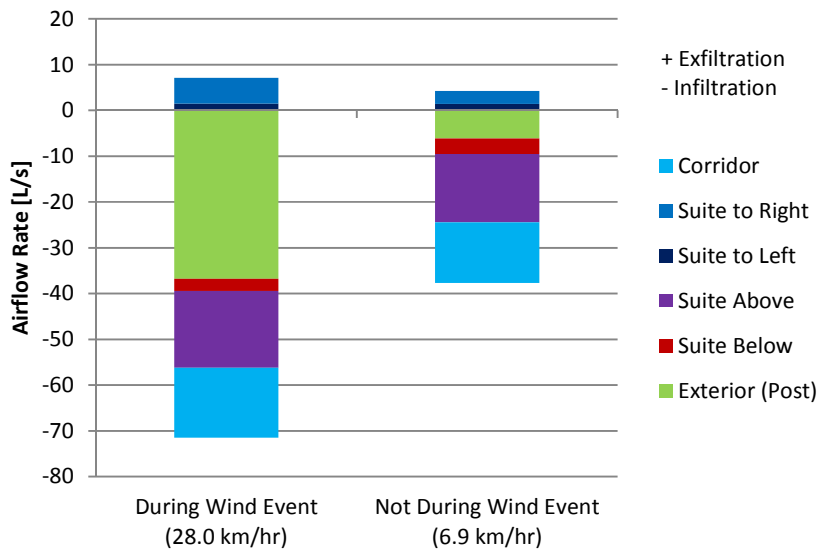


Figure F-22: Chart of the average flow into and out of Suite 1101 during a strong west wind

Appendix F Supplementary Calculated Airflow Graphs

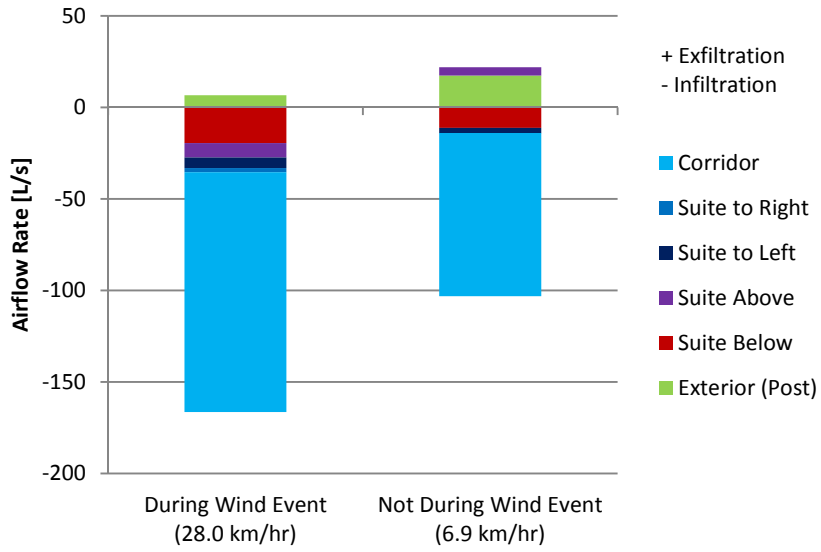


Figure F-23: Chart of the average flow into and out of Suite 1102 during a strong west wind

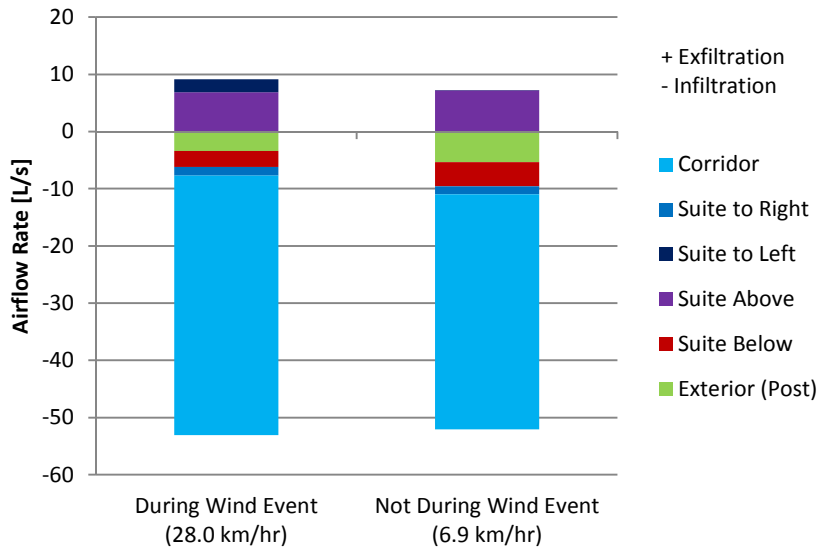


Figure F-24: Chart of the average flow into and out of Suite 1103 during a strong west wind

Appendix G PFT Testing Report

Brookhaven Nation Laboratory provided the analysis of the PFT testing conducted at the case study building through Meadowbrook Partners Inc, including measurement of the concentrations of the tracers measured and the subsequent calculations to determine the airflow rates. The results of this analysis are provided in the report provided in this appendix. For privacy, this report has been modified from its original version to conceal the name of the case study building.

PFT Housing Study “Case Study Building” Apartment Study

Terry Sullivan
Brookhaven National Laboratory
May 28, 2013

Introduction

The “Case Study Building” Apartment Building is a 13 story building with a Parkade beneath the first floor. Each floor contains 3 suites and the associated hallways, stairwell, and elevator. Perfluorocarbon Tracer (PFT) Testing was performed the week of April 10 – 17th. Two concurrent tests were performed during the week long testing period. In these tests several suites were tagged with a unique PFT tracer and sample measurements were collected through passive sampling in a Capillary Absorption Tube Sampler (CATS). Two regions of the building were tested the Parkade and Floors 1 – 4, lower region, and Floors 10 – 12, upper region.

Test Layout

The test used seven unique PFT tracers in the lower region (Parkade, Main Building and Five Suites) and six PFT tracers in the upper region (Main Building and Five Suites). In the first region, sources were placed in the Parkade and Suites 202, 301, 302, 303, and 402. The building supply air was tagged with the tracer PMCP. An objective of this test was to determine the amount of air entering the building from the parking garage beneath the first floor. The second test also relied on PMCP to interpret building flows and placed sources in Suites 1003, 1101, 1102, 1103, and 1203. There is wide enough separation between the lower and upper regions to permit re-using the PFTs in the suites.

Sampling was performed in all source zones and in the hallway on every floor. Samples were also collected in all three suites on floors that had a source. Four samples were collected in the Parkade due to its large size. One sample was collected in the supply air vent immediately downstream of the PMCP source in the vent. In total, 37 samples were collected. All samples were approximately one week in duration. The sample collection points and the sampler ID (CATS number) are provided in Table 1.

Table 1 Sample Locations and CATS ID

CATS Number	Name	Zone
2721	CATS - PARK01	Parkade
00469	CATS - 0000	Corridor 00
9638	CATS - PARK03	Parkade
4155	CATS - PARK04	Parkade
3857	CATS - STAIR01	Stairwell at Floor 1 to Upstairs
9296	CATS - 0100	Corridor 01
6605	CATS - 0200	Corridor 02
8751	CATS - 0201	Suite 0201
9046	CATS - 0202	Suite 0202
6110	CATS - 0203	Suite 0203
2463	CATS - 0300	Corridor 03
8559	CATS - 0301	Suite 0301
9137	CATS - 0302	Suite 0302
2935	CATS - 0303	Suite 0303
00424	CATS - 0400	Corridor 04
3931	CATS - STAIR04	Stairwell at Floor 4
7111	CATS - 0402	Suite 0402
8354	CATS - 0403	Suite 0403
4462	CATS - 0500	Corridor 05
8312	CATS - 0600	Corridor 06
4325	CATS - 0700	Corridor 07
5341	CATS - 0800	Corridor 08
5480	CATS - 0900	Corridor 09
00006	CATS - 1000	Corridor 10
00384	CATS - 1001	Suite 1001
6387	CATS - 1002	Suite 1002
3124	CATS - 1003	Suite 1003
4837	CATS - 1100	Corridor 11
2437	CATS - 1101	Suite 1101
7700	CATS - 1102	Suite 1102
1247	CATS - 1103	Suite 1103
7361	CATS - 1200	Corridor 12
7140	CATS - 1201	Suite 1201
00496	CATS - 1202	Suite 1202
8083	CATS - 1203	Suite 1203
6120	CATS - 1300	Corridor 13
9607	CATS - MAU	Make-up Air Unit Intake

Sources

The source layout is provided in Table 2. PMCH was added to the supply air (MAU – make up air) to the entire building and is in both zones. It is assumed that the supply air is equally distributed to all floors and this would provide a uniform source of PMCH to the building. Table 2 provides the source type, number of sources used, location, zone number, and nominal source rate for all sources used in the analysis.

Table 2 Source Type and

Source Type	Number	Location	Zone Number	Nominal Source Rate (nL/h) at 21.5 °C
Lower Region				
PMCP	2	MAU	1	6035
ptPDCH	2	Suite 0202	2	8.3
ocPDCH	2	Suite 0301	3	6.66
PMCH	2	Suite 0302	4	22
iPPCH	2	Suite 0303	5	7.55
PTCH	2	Suite 0402	6	5.62
PDCB	4	Parkade	7	41.11
Upper Region				
PMCP	2	MAU	1	6035
ptPDCH	2	Suite 1003	2	8.3
ocPDCH	2	Suite 1101	3	6.66
PMCH	2	Suite 1102	4	22
iPPCH	2	Suite 1103	5	7.55
PTCH	2	Suite 1203	6	5.62

The PMCP source was provided in a small glass bottle with a thin rubber cover which allowed diffusion out of the vial. The initial amount of PFT in the source was approximately 12 g. These sources typically last only a few months and are prepared individually for each test. Due to time constraints, six PMCP sources were prepared and two were sent as part of the test. The four that remained at BNL were used to determine the release rate, which was measured as 3800 ± 500 nL/h. The intent was to measure the source rates of the PMCP vials used in the test when they were returned. However, one vial was returned empty having released its entire inventory. The

other PMCP source was measured at 3900 ± 200 nL/h, consistent with the other PMCP sources. Inspecting the empty vial showed a defect in the formation of the seal which would allow the higher release rates. A picture of the PMCP source taken just before the test showed that about 85 -90% of the inventory had been released. The field crew did not notice that the vial was empty upon testing. Using this information it was assumed that 10% of the inventory was released over the test duration. This gave a release rate approximately double from the other source and the combined effective release rate was 6035 nL/h. For the error analysis it was assumed that this could be $\pm 18\%$ (1100 nL/h). The other sources were provided in metal cases with rubber stoppers. These have a measured variation in release rate at room temperature of 7%. All source release rates were adjusted to the measured release temperature.

The PMCP sources have trace amounts of PMCH (0.67%) and ocPDCH (0.17%) as measured at BNL. For all analysis the PMCH and ocPDCH concentrations were corrected to account for this by multiplying the PMCP concentration by the fraction of PMCH (ocPDCH) and subtracting that value from the measured PMCH (ocPDCH).

Results

The PFT volumes (pL) as measured are presented in Table 3 for the lower zone (Table 3) and upper zone (Table 4). These tables include the CATS ID, Zone, Location of the sampler, and volumes of PFT measured in pL. The values for PMCH and ocPDCH have been corrected to account for the impurities in the PMCP source used in the supply air. Measured values are presented in the file “GC10 “Case Study Building” Summary.xls.’ Highlighted values correspond to the source in the suite.

Table 3 Measured PFT levels (pL) in the lower zone.

CATSID	Zone	Location	PMCH	ocPDCH	PDCB	ptPDCH	PMCP	PTCH	iPPCH
		El Lobby							
469	7	Parkade	0.05	0.02	0.09	0.000	2.45	0.06	0.09
2721	7	East Parkade	0.00	0.00	2.02	0.017	0.63	0.02	0.00
4155	7	North Parkade	0.08	2.63	2.64	0.022	0.93	0.05	0.06
9638	7	SW Parkade	0.07	0.03	2.32	0.013	0.65	0.06	0.06
3857	1	Stairwell at 1	0.05	0.01	0.86	0.102	82.04	0.03	0.04
9296	1	1 Hall	0.06	0.02	0.77	0.112	165.32	0.02	0.02
6605	1	2 Hall	0.90	0.28	1.02	4.805	172.42	0.15	0.21
8751	1	Suite 201	0.21	0.09	0.12	0.399	12.69	0.03	0.04
9046	2	Suite 202	5.48	1.23	1.87	80.247	8.76	0.89	1.41
6110	1	Suite 203	0.19	0.04	0.09	0.754	3.12	0.04	0.11
2463	1	3 Hall	3.41	1.21	1.28	0.228	298.35	0.08	1.17
8559	3	Suite 301	3.80	22.63	1.32	1.455	55.02	0.79	1.60
9137	4	Suite 302	212.37	2.57	3.91	2.794	55.70	2.07	3.25
2935	5	Suite 303	4.73	1.13	1.58	1.203	45.96	1.01	28.19
424	1	4 Hall	0.62	0.36	0.88	0.275	171.96	0.63	0.21
3931	1	stairwell ar 4	1.14	0.38	1.28	0.814	137.66	0.09	1.29
7111	6	Suite 402	7.46	0.77	1.21	0.897	78.05	10.62	0.93
8354	1	Suite 403	0.47	0.33	0.34	0.535	42.52	0.38	0.42

Table 4 Measured PFT levels (pL) in the lower zone.

CATSID	Zone	Location	PMCH	ocPDCH	PDCB	ptPDCH	PMCP	PTCH	iPPCH
4462	1	Hall 5	0.77	3.04	0.00	0.06	329.02	0.02	0.03
8312	1	Hall 6	0.82	3.26	0.00	0.04	342.69	0.00	0.02
4325	1	Hall 7	0.88	3.17	0.00	0.08	339.84	0.00	0.03
5341	1	Hall 8	0.74	1.51	0.00	0.53	173.86	0.06	0.22
5480	1	Hall 9	1.43	2.23	0.00	10.78	264.19	0.05	0.31
6	1	Hall 10	0.76	2.72	0.00	0.22	323.94	0.02	0.09
384	1	Suite 1001	0.47	1.61	0.00	0.16	193.14	0.02	0.11
6387	1	Suite 1002	0.80	2.04	0.00	0.33	259.91	0.04	0.12
3124	2	Suite 1003	2.08	1.98	0.00	11.34	209.06	0.25	0.47
4837	1	Hall 11	0.81	2.88	0.00	0.25	336.80	0.02	0.07
2437	3	Suite 1101	2.18	13.44	0.00	0.89	308.08	0.36	0.70
7700	4	Suite 1102	15.23	2.42	0.00	0.38	264.90	0.11	0.25
1247	5	Suite 1103	0.69	1.31	0.00	0.31	137.48	0.13	3.50
7361	1	Hall 12	0.75	1.67	0.00	0.50	209.53	0.05	0.27
7140	1	Suite 1201	0.62	2.29	0.00	0.39	262.32	0.03	0.11
496	1	Suite 1202	0.82	2.67	0.00	0.46	310.10	0.03	0.12
8083	6	Suite 1203	1.26	1.94	0.00	0.81	200.67	4.04	0.47
6120	1	Hall 13	0.82	3.40	0.00	0.10	390.56	0.00	0.06

The supply air (MAU) showed a measured value of 851 pL for PMCP, 8.8 pL for PMCH, and 2.5 pL for ocPDCH. This is consistent with the measured impurity fraction.

Examining tables 3 and 4 provides several key insights into the flow behavior within the building. These include:

- With the exception of the elevator lobby in the Parkade, the air in the Parkade is well mixed with the other 3 CATS samplers providing similar values for PDCB, the tracer released in the Parkade. The elevator lobby showed much lower values of PDCB.
- Very low amounts of any of the tracers released in the building appeared in the Parkade. This suggests there is very little flow from the building to the Parkade.
- PDCB released in the Parkade was not detected above the 4th floor. The measured value of 3.9 pL in Suite 302 (CATS 9137) is an outlier as the concentration cannot be higher than in the Parkade where the tracer is released. Other values do suggest some air flow from the Parkade into the building.
- Much higher measured concentrations in the source suites in the lower level (highlighted in yellow) as compared to the upper level. This suggests that the air exchange rate is much lower in the lower level suites.
- There is a clear distinction in the PMCP levels on Floors 1 – 4 and Floors 5 – 12. PMCP, the tracer used throughout the entire building, is much lower in the lower zone as compared to the higher zone. The average in the lower zone is 95 pL and in the upper zone the average is 270 pL. The dramatic change in PMCP levels is the basis for dividing the zones between the 4th and 5th floor.

- Much lower PMCP concentrations in the suites of the lower zone as compared to the halls of the lower zone. The average lower zone PMCH value in the source suites was 49 pL while in the hall it was 202 pL. This effect was not as pronounced in the upper zone where the average source suite PMCH value was 224 pL while in the upper halls it was 301 pL. The factor of 4 differences in PMCH levels in the hall as compared to the suites in the lower region also suggests very little air exchange with the suites in this region.
- All of the above observations are consistent with a chimney effect occurring in the building. In the chimney effect cold air is drawn in from the lower levels and rises through the building where it exfiltrates from the roof and top floors. This would explain the lower PMCH values on floors 1 – 4 and the higher concentrations in the suites in this region.
- One of the assumptions in the calculation of flows is that within a zone the air is well mixed and the concentrations are uniform. This is clearly not the case for PMCP in the lower zone where PMCP levels range from 82 to 300 pL in the hall data. There is also substantial variability in the hall PMCP levels in the upper region. This variability will be reflected in the uncertainty in the flow estimates.

Multi-zone Calculations

The volume of PFT measured on each sampler is presented in the file: “A – “Case Study Building” Apartment Data – CATS data.xls” which contains a summary of the measured PFT values in pL and the values for each test on a separate spreadsheet. The sources used in each zone for the tests are listed in the file “A- “Case Study Building” Data – Sources.xls.” This file provides the nominal source rate, number of sources for each zone, zone volume, zone temperature used to adjust the source rate, and sampling time. These values are used as input to calculate the flows between the different zones.

Air Flow Rate Calculations

Lower Region

The data in these two EXCEL files were used in the MATLAB program AIMS that calculates the overall air change rate for the system as well as the flow rates between different zones in the system. Six cases were analyzed. As previously mentioned, there was a great discrepancy between the suite level PMCP and the hallway level. For this reason, simulations were performed for the upper and lower region using a) all of the data in the non-source zones to represent the building and b) using only the hall data to represent the building. The Parkade was found to be a supply of air to the building and a simulation was performed omitting the Parkade from the lower zone to see the impact. The AIMS calculation generates a report that includes the infiltration and exfiltration from each zone, the air exchange rate between zones (e.g. from Suite 201 to the Building and from the Building to Suite 201) for each zone, and the overall flow rate in each zone. These are reported in ““Case Study Building” Summary.xls.”

Table 5 shows the ACH (air changes per hour) for each test for the modeled system. Hall data refers to the cases where only Hall data was used to represent the building. Using only the hall

data reduced the ACH as this led to higher building PMCH concentrations. Removing the Parkade from the lower region analysis increased the ACH

Table 5 Air Changes per hour for each test.

System	All data	Hall Data
Lower-All Zones	0.49	0.39
Lower -No Parkade	0.73	0.28
Upper – All Zones	0.33	0.23

Table 6 shows the infiltration flow rate (m^3/h), exfiltration flow rate (m^3/h) and ACH (h^{-1}) along with the standard deviation of each in the estimate for the lower region with all seven zones using the Hall data to represent the building. The standard deviation in the flow rates for exfiltration, and infiltration to a lesser extent are large, often exceeding the estimate for the rate in the case of exfiltration. This is due to the variability in PMCH throughout the hall in the lower region. Adding the additional suite data adds more variability and increases the uncertainty. In general, the infiltration and exfiltration into the suites is small.

Table 6 Infiltration, Exfiltration, and air changes per hour for lower region all seven zones using hall data to represent the building.

Z	ZONE	EXFILTRATION		INFILTRATION		ACH	SD
N	LOCATION	RATE	SD	RATE	SD	(1/h)	
E		(m^3/h)		(m^3/h)			
1	Building	3484	1311	1903	802	0.19	0.08
2	Suite 202	-39	103	2.5	2.2	0.01	0.01
3	Suite 301	-229	186	12.1	4.9	0.04	0.02
4	Suite 302	-5	28	2.8	1.6	0.01	0.01
5	Suite 303	2	67	7.1	4.6	0.02	0.02
6	Suite 402	14	97	20.5	9.3	0.07	0.03
7	Parkade	3723	1181	5002	1124	0.77	0.18

The total flow for this case and number of air changes per hour for each zone is provided in Table 7. The data show that with the exception of Suite 402 the flow rates in the suites are low with less than 0.2 ACH. The Parkade has the highest exchange rate with an ACH near 0.8.

Table 7 Total flow rate through each of the seven zones in the lower region.

Zone	Location	RATE (m ³ /h)	SD ± (m ³ /h)	ACH (1/h)	SD ± (1/h)
1	Building	3544.8	1327.9	0.352	0.133
2	Suite 202	17.3	3.6	0.058	0.012
3	Suite 301	47.4	9.8	0.154	0.033
4	Suite 302	18	3.7	0.06	0.013
5	Suite 303	42.2	8.7	0.138	0.029
6	Suite 402	81.6	16.9	0.274	0.058
7	Parkade	5039.4	1132.2	0.775	0.178

The predicted flows shown in table 6 and 7 summarize the flow in the zones. The AIMS calculation also predicts the flow rate between zones, Table 8. Table 8 includes the flow rate between zones (e.g. from the Building to Suite 202) and an estimate of the error in the calculation. For the most part, there is very little flow between Suites. The major flow is from the Parkade to the Building. There is very little flow in the reverse direction.

Table 8 Flow rate between zones in the lower region.

ZONE	-	ZONE	RATE	±SD (m ³ /h)	ZONE	-	ZONE	RATE	±SD (m ³ /h)
Building	-	Suite 202	-0.3	0.2	Suite 202	-	Building	53.4	104.4
Building	-	Suite 301	11	4.5	Suite 301	-	Building	270.5	189.4
Building	-	Suite 302	2.9	1.2	Suite 302	-	Building	18.2	28.2
Building	-	Suite 303	7.6	3.1	Suite 303	-	Building	27.7	67.5
Building	-	Suite 402	30.3	12.2	Suite 402	-	Building	37.8	96.9
Building	-	Parkade	9.2	6.8	Parkade	-	Building	1233.9	599.2
Suite 202	-	Suite 301	0.6	0.4	Suite 301	-	Suite 202	0.8	0.2
Suite 202	-	Suite 302	0.5	0.2	Suite 302	-	Suite 202	0.4	0.1
Suite 202	-	Suite 303	0.4	0.3	Suite 303	-	Suite 202	0.7	0.2
Suite 202	-	Suite 402	0.3	0.9	Suite 402	-	Suite 202	1.2	0.3
Suite 202	-	Parkade	0.6	0.4	Parkade	-	Suite 202	11.9	3.2
Suite 301	-	Suite 302	1.6	0.4	Suite 302	-	Suite 301	0.6	0.2
Suite 301	-	Suite 303	1.3	0.5	Suite 303	-	Suite 301	2.3	0.6
Suite 301	-	Suite 402	0	1.6	Suite 402	-	Suite 301	2.8	0.8
Suite 301	-	Parkade	2.4	4.7	Parkade	-	Suite 301	17.9	5.4
Suite 302	-	Suite 303	0.7	0.2	Suite 303	-	Suite 302	1.8	0.5
Suite 302	-	Suite 402	2.6	0.7	Suite 402	-	Suite 302	3.1	0.8
Suite 302	-	Parkade	0.3	1.1	Parkade	-	Suite 302	5.4	1.8
Suite 303	-	Suite 402	1.9	0.8	Suite 402	-	Suite 303	3.5	0.9
Suite 303	-	Parkade	5.8	6.2	Parkade	-	Suite 303	21.7	6.2
Suite 402	-	Parkade	19.3	9.9	Parkade	-	Suite 402	26.1	9

Upper Region

The upper region is characterized by much lower concentrations within the source suites, suggesting more flow through the suites and much higher concentrations in the building zone suggesting less flow in this area. Table 9 shows the exfiltration, infiltration, and the air changes per hour for infiltration for the six zones in this region.

Table 9 Infiltration and exfiltration in the upper region

Z	ZONE	EXFILTRATION		INFILTRATION		ACH	SD
N	LOCATION	RATE	SD	RATE	SD	(1/h)	
E		(m ³ /h)		(m ³ /h)			
1	Bldg	2006	709	2354	751	0.234	0.075
2	Suite 1003	56	43	27	18	0.089	0.058
3	Suite 1101	-55	65	-14	21	-0.05	0.069
4	Suite 1102	200	54	24	56	0.08	0.189
5	Suite 1103	229	85	174	50	0.568	0.165
6	Suite 1203	180	43	51	31	0.166	0.101

It is noted that the exfiltration and infiltration are negative for Suite 1101. This is not physically possible. However, the average estimated error is greater than the estimated flow rate, suggesting that the flow rates are actually near zero. A partial cause for this is the PMCP level in suite 1101 is slightly greater than the average in the building. It is not physically possible to have a concentration in an adjacent zone greater than in the source zone. The fact that the concentration of PMCP in suite 1101 being greater than the average PMCP level reflects the variability in PMCP within the building. The PMCP concentration in the upper region halls is 205 ± 50 pL/L while the measured concentration is 207 ± 21 pL/L. Inspecting the data carefully, the PMCP level in the hall on floor 11 is about 10% greater than the value in suite 1101. This suggests that there is substantial air flow from the hall to suite 1101.

Table 10 shows the overall air flow rate and number of air changes per hour (ACH) through each zone. The flow rates and ACH are much higher through the suites than in the lower zone. This is consistent with a chimney effect where air enters the lower portion of the building and rises and exits from the upper part of the building.

Table 11 includes the flow rate between zones (e.g. from the Building to Suite 1003) and an estimate of the error in the calculation. For the most part, there is very little flow between Suites. There is some flow from the corridor (Building) to the suites in both directions.

Table 10 Total flow and Air Changes per hour in each zone in the upper region.

Zone	Location	RATE	±	SD (m ³ /h)	ACH (1/h)	±	SD (1/h)
1	Bldg	3938		1093	0.39		0.11
2	Suite 1003	120		17	0.39		0.06
3	Suite 1101	98		15	0.32		0.05
4	Suite 1102	260		37	0.88		0.13
5	Suite 1103	328		47	1.07		0.16
6	Suite 1203	204		29	0.67		0.10

Table 11 Flow rate between zones in the Upper Region

ZONE	-	ZONE	RATE ±	SD (m ³ /h)	ZONE	-	ZONE	RATE ±	SD (m ³ /h)
Bldg	-	Suite 1003	60.8	22.4	Suite 1003	-	Bldg	37.7	47.3
Bldg	-	Suite 1101	77.5	28.3	Suite 1101	-	Bldg	145.2	78.9
Bldg	-	Suite 1102	214.6	76.1	Suite 1102	-	Bldg	26.2	21
Bldg	-	Suite 1103	129.9	46.5	Suite 1103	-	Bldg	37	73.1
Bldg	-	Suite 1203	108	39.2	Suite 1203	-	Bldg	-3.3	15
Suite 1003	-	Suite 1101	5	2	Suite 1101	-	Suite 1003	1.2	1.9
Suite 1003	-	Suite 1102	3.8	4.1	Suite 1102	-	Suite 1003	11.8	3.1
Suite 1003	-	Suite 1103	5.5	2.8	Suite 1103	-	Suite 1003	12.5	3.7
Suite 1003	-	Suite 1203	11.5	3.6	Suite 1203	-	Suite 1003	6.3	1.7
Suite 1101	-	Suite 1102	1.7	6.4	Suite 1102	-	Suite 1101	8.1	2.3
Suite 1101	-	Suite 1103	2.7	4	Suite 1103	-	Suite 1101	15.2	4.6
Suite 1101	-	Suite 1203	2.8	3.4	Suite 1203	-	Suite 1101	7.2	1.9
Suite 1102	-	Suite 1103	6.2	2	Suite 1103	-	Suite 1102	11.3	6.8
Suite 1102	-	Suite 1203	8.5	2.5	Suite 1203	-	Suite 1102	5.1	1.9
Suite 1103	-	Suite 1203	22.2	6.6	Suite 1203	-	Suite 1103	9	2.4

Summary

Perfluorocarbon Tracer (PFT) Testing was performed the week of April 10 – 17th at the “Case Study Building” Apartments. Two concurrent tests were performed during the week long testing period. In these tests several suites were tagged with a unique PFT tracer and sample measurements were collected through passive sampling in a Capillary Absorption Tube Sampler (CATS). Two regions of the building were tested the Parkade and Floors 1 – 4, lower region, and Floors 10 – 12, upper region.

The data suggest that the building exhibited a chimney effect with cold air drawn in from the outside or Parkade at the lower levels and exfiltrating at the top. PMCP was added to the make-up air used to supply the building. It was expected that PMCP should have a relatively uniform concentration throughout the corridors of the building. The fact that PMCP was much lower in the lower region as compared to the upper region supports the hypothesis of a chimney effect. The Parkade supplied a substantial amount of air to the building, while little air from the building entered the Parkade, also supporting the chimney effect interpretation.

In the lower level the suites had relatively low rates of air change per hour and there was little flow from the hall corridors into the suites as determined by the low concentrations of PMCP in the suites. In the upper level the suite concentrations were much closer to the corridor concentrations of PMCP showing substantial air exchange between these regions. The concentrations of the source in the suite were substantially lower than on the lower level indicating much higher rates of air exchange.

+

Appendix A. Example output file from Lower Region using the corridor data to represent the building.

BNL - AIMS

Project Title: "Case Study Building" Start
 4/10/2013
 House Description Lower Stop 4/17/2013
 Project ID: "Case Study Building" Apt-7 Analyzed
 5/10/2013

*****RATES*****
 OVERALL INFILTRATION RATE = 6911.2 ± 1288.9 (m³/h)
 OVERALL INFILTRATION RATE = 4065.4 ± 758.2 cfm
 OVERALL AIR EXCHANGE RATE = 0.382 ± 0.019 (1/h)

Z	O	ZONE	SOURCE RATE	EXFILTRATION	-INFILTRATION--
N	E	LOCATION	@21.5C QTY @T	RATE RATE SD	RATE SD ACH SD
			(nL/m)	(nL/h) (m ³ /h)	(m ³ /h) (1/h)
1		Building	3991.002 464113	3519.4 1317.8	1915.9 803.2 0.190 0.080
2		Suite 20	8.30 2 1055.9	-36.6 103.7	2.6 2.2 0.009 0.007
3		Suite 30	6.66 2 802.3	-380.7 328.3	12.3 5.0 0.040 0.016
4		Suite 30	22.00 2 2692.1	-2.9 28.5	2.8 1.6 0.010 0.005
5		Suite 30	7.55 2 956.8	9.3 68.9	7.3 4.6 0.024 0.015
6		Suite 40	5.62 2 693.1	22.9 99.0	20.7 9.4 0.070 0.032
7		Parkade	41.11 4 8019.7	3779.8 1209.5	4949.4 1122.1 0.761 0.177

ZONE	-	ZONE	RATE	±SD (m ³ /h)	ZONE	-	ZONE	RATE	±SD (m ³ /h)
Building	-	Suite 202	-0.3	0.2	Suite 202	-	Building	53.4	104.4
Building	-	Suite 301	11	4.5	Suite 301	-	Building	270.5	189.4
Building	-	Suite 302	2.9	1.2	Suite 302	-	Building	18.2	28.2
Building	-	Suite 303	7.6	3.1	Suite 303	-	Building	27.7	67.5
Building	-	Suite 402	30.3	12.2	Suite 402	-	Building	37.8	96.9
Building	-	Parkade	9.2	6.8	Parkade	-	Building	1233.9	599.2
Suite 202	-	Suite 301	0.6	0.4	Suite 301	-	Suite 202	0.8	0.2
Suite 202	-	Suite 302	0.5	0.2	Suite 302	-	Suite 202	0.4	0.1
Suite 202	-	Suite 303	0.4	0.3	Suite 303	-	Suite 202	0.7	0.2
Suite 202	-	Suite 402	0.3	0.9	Suite 402	-	Suite 202	1.2	0.3
Suite 202	-	Parkade	0.6	0.4	Parkade	-	Suite 202	11.9	3.2
Suite 301	-	Suite 302	1.6	0.4	Suite 302	-	Suite 301	0.6	0.2
Suite 301	-	Suite 303	1.3	0.5	Suite 303	-	Suite 301	2.3	0.6
Suite 301	-	Suite 402	0	1.6	Suite 402	-	Suite 301	2.8	0.8
Suite 301	-	Parkade	2.4	4.7	Parkade	-	Suite 301	17.9	5.4
Suite 302	-	Suite 303	0.7	0.2	Suite 303	-	Suite 302	1.8	0.5
Suite 302	-	Suite 402	2.6	0.7	Suite 402	-	Suite 302	3.1	0.8

Appendix G PFT Testing Report

Suite 302	-	Parkade	0.3	1.1	Parkade	-	Suite 302	5.4	1.8
Suite 303	-	Suite 402	1.9	0.8	Suite 402	-	Suite 303	3.5	0.9
Suite 303	-	Parkade	5.8	6.2	Parkade	-	Suite 303	21.7	6.2
Suite 402	-	Parkade	19.3	9.9	Parkade	-	Suite 402	26.1	9

```

|-----TOTAL FLOW IN OR OUT-----|
Zone  RATE      ±      SD (m^3/h)      ACH (1/h)  ±      SD (1/h)
1      3533.1      ±      1320.4      0.351      ±      0.132
2      17.3         ±      3.6         0.058      ±      0.012
3      48.1         ±      10.1        0.157      ±      0.034
4      18.0         ±      3.7         0.060      ±      0.013
5      42.2         ±      8.7         0.137      ±      0.029
6      81.5         ±      16.9        0.274      ±      0.058
7      5117.0        ±      1164.2     0.787      ±      0.183
    
```

***** Zone Average Concentration (pL/L) and Standard Deviation *****

Z	0 VOL	Source	PMCP		ptPDCH		ocPDCH		PMCH		iPPCH		PTCH		PDCB	
N	m^3	Type	Avg	Stdev	Avg	Stdev	Avg	Stdev	Avg	Stdev	Avg	Stdev	Avg	Stdev	Avg	Stdev
1	10073.7	PMCP	135.0	42.97	1.0	1.77	1.4	0.75	1.1	1.14	0.3	0.42	0.2	0.23	0.7	0.15
2	297.7	ptPDCH	5.8	0.58	61.3	6.13	0.9	0.09	3.9	0.39	1.1	0.11	0.7	0.07	1.3	0.13
3	306.8	ocPDCH	36.8	3.68	1.1	0.11	17.4	1.74	2.7	0.27	1.3	0.13	0.6	0.06	0.9	0.09
4	297.7	PMCH	37.0	3.70	2.1	0.21	2.0	0.20	151.3	15.13	2.6	0.26	1.7	0.17	0.9	0.09
5	306.8	iPPCH	30.6	3.06	0.9	0.09	0.9	0.09	3.4	0.34	22.9	2.29	0.8	0.08	1.1	0.11
6	297.7	PTCH	52.1	5.21	0.7	0.07	0.6	0.06	5.3	0.53	0.8	0.08	8.6	0.86	0.8	0.08
7	6500.0	PDCB	0.5	0.11	0.0	0.00	0.7	1.18	0.0	0.03	0.0	0.03	0.0	0.01	1.6	0.21

*****		Concentration (pL/L)		*****												
CATSID	Zone	PMCP	ptPDCH	ocPDCH	PMCH	iPPCH	PTCH	PDCB								
9296	1	110.47	0.09	0.74	0.25	0.02	0.02	0.52								
6605	1	115.21	3.69	1.10	0.86	0.17	0.12	0.69								
2463	1	199.35	0.18	2.46	2.80	0.95	0.06	0.86								
424	1	114.90	0.21	1.16	0.65	0.17	0.51	0.59								
9046	2	5.83	61.33	0.94	3.91	1.14	0.72	1.26								
8559	3	36.77	1.12	17.37	2.72	1.30	0.64	0.89								
9137	4	36.98	2.13	1.96	151.28	2.63	1.67	0.94								
2935	5	30.63	0.92	0.87	3.38	22.89	0.82	1.06								
7111	6	52.15	0.69	0.59	5.34	0.76	8.65	0.82								
2721	7	0.43	0.01	-0.00	0.00	0.00	0.02	1.39								
4155	7	0.63	0.02	2.06	0.06	0.05	0.04	1.81								
9638	7	0.44	0.01	0.02	0.05	0.05	0.05	1.59								

*****NOTE*****

All gas volumes are reported at 21.5 C. and 1 atm.
 The standard deviation in the source strength has been set at 18.0 %
 The standard deviation in the volume measurement has been set at 5.0 %
 The overall normalized condition number (K(C) /N^1.5 = 0.5
 K(DC) /N = 1.3

Zonal condition numbers are:
 Zone 1 2 3 4 5 6 7
 Condition Number 1.3 1.2 1.2 1.1 1.2 1.2 1.8

Header File :A - "Case Study Building" Apartment Headers.xlsx
 Data File :A- "Case Study Building" Apartment -CATS concentrations.xlsx
 Source File :A - "Case Study Building" Apartment - Sources.xlsx

Appendix G PFT Testing Report

Suite 302	-	Parkade	0.3	1.1	Parkade	-	Suite 302	5.4	1.8
Suite 303	-	Suite 402	1.9	0.8	Suite 402	-	Suite 303	3.5	0.9
Suite 303	-	Parkade	5.8	6.2	Parkade	-	Suite 303	21.7	6.2
Suite 402	-	Parkade	19.3	9.9	Parkade	-	Suite 402	26.1	9

-----TOTAL FLOW IN OR OUT-----						
Zone	RATE	±	SD (m ³ /h)	ACH (1/h)	±	SD (1/h)
1	3533.1		1320.4	0.351		0.132
2	17.3		3.6	0.058		0.012
3	48.1		10.1	0.157		0.034
4	18.0		3.7	0.060		0.013
5	42.2		8.7	0.137		0.029
6	81.5		16.9	0.274		0.058
7	5117.0		1164.2	0.787		0.183

***** Zone Average Concentration (pL/L) and Standard Deviation *****

Z	N	Source	PMCP	ptPDCH	ocPDCH	PMCH	iPPCH	PTCH	PDCB							
	m ³	Type	Avg	Stdev	Avg	Stdev	Avg	Stdev	Avg	Stdev						
1	10073.7	PMCP	135.0	42.97	1.0	1.77	1.4	0.75	1.1	1.14	0.3	0.42	0.2	0.23	0.7	0.15
2	297.7	ptPDCH	5.8	0.58	61.3	6.13	0.9	0.09	3.9	0.39	1.1	0.11	0.7	0.07	1.3	0.13
3	306.8	ocPDCH	36.8	3.68	1.1	0.11	17.4	1.74	2.7	0.27	1.3	0.13	0.6	0.06	0.9	0.09
4	297.7	PMCH	37.0	3.70	2.1	0.21	2.0	0.20	151.3	15.13	2.6	0.26	1.7	0.17	0.9	0.09
5	306.8	iPPCH	30.6	3.06	0.9	0.09	0.9	0.09	3.4	0.34	22.9	2.29	0.8	0.08	1.1	0.11
6	297.7	PTCH	52.1	5.21	0.7	0.07	0.6	0.06	5.3	0.53	0.8	0.08	8.6	0.86	0.8	0.08
7	6500.0	PDCB	0.5	0.11	0.0	0.00	0.7	1.18	0.0	0.03	0.0	0.03	0.0	0.01	1.6	0.21

CATSID	Zone	PMCP	ptPDCH	ocPDCH	PMCH	iPPCH	PTCH	PDCB
9296	1	110.47	0.09	0.74	0.25	0.02	0.02	0.52
6605	1	115.21	3.69	1.10	0.86	0.17	0.12	0.69
2463	1	199.35	0.18	2.46	2.80	0.95	0.06	0.86
424	1	114.90	0.21	1.16	0.65	0.17	0.51	0.59
9046	2	5.83	61.33	0.94	3.91	1.14	0.72	1.26
8559	3	36.77	1.12	17.37	2.72	1.30	0.64	0.89
9137	4	36.98	2.13	1.96	151.28	2.63	1.67	0.94
2935	5	30.63	0.92	0.87	3.38	22.89	0.82	1.06
7111	6	52.15	0.69	0.59	5.34	0.76	8.65	0.82
2721	7	0.43	0.01	-0.00	0.00	0.00	0.02	1.39
4155	7	0.63	0.02	2.06	0.06	0.05	0.04	1.81
9638	7	0.44	0.01	0.02	0.05	0.05	0.05	1.59

*****NOTE*****

All gas volumes are reported at 21.5 C. and 1 atm.
 The standard deviation in the source strength has been set at 18.0 %
 The standard deviation in the volume measurement has been set at 5.0 %
 The overall normalized condition number (K(C) /N^{1.5} = 0.5
 K(DC) /N = 1.3
 Zonal condition numbers are:
 Zone 1 2 3 4 5 6 7
 Condition Number 1.3 1.2 1.2 1.1 1.2 1.2 1.8

Header File :A - "Case Study Building" Apartment Headers.xlsx
 Data File :A- "Case Study Building" Apartment -CATS concentrations.xlsx
 Source File :A - "Case Study Building" Apartment - Sources.xlsx

Appendix G PFT Testing Report

CATS Exposure Time (hrs) :166.6